frontiers | Research Topics

Rising stars in comparative and clinical medicine 2021

Edited by
Fazul Nabi and Muhammad Asif Arain

Published in
Frontiers in Veterinary Science

ISSN 1664-8714
ISBN 978-2-8325-1154-1
DOI 10.3389/978-2-8325-1154-1

About Frontiers

Frontiers is more than just an open access publisher of scholarly articles: it is a pioneering approach to the world of academia, radically improving the way scholarly research is managed. The grand vision of Frontiers is a world where all people have an equal opportunity to seek, share and generate knowledge. Frontiers provides immediate and permanent online open access to all its publications, but this alone is not enough to realize our grand goals.

Frontiers journal series

The Frontiers journal series is a multi-tier and interdisciplinary set of open-access, online journals, promising a paradigm shift from the current review, selection and dissemination processes in academic publishing. All Frontiers journals are driven by researchers for researchers; therefore, they constitute a service to the scholarly community. At the same time, the *Frontiers journal series* operates on a revolutionary invention, the tiered publishing system, initially addressing specific communities of scholars, and gradually climbing up to broader public understanding, thus serving the interests of the lay society, too.

Dedication to quality

Each Frontiers article is a landmark of the highest quality, thanks to genuinely collaborative interactions between authors and review editors, who include some of the world's best academicians. Research must be certified by peers before entering a stream of knowledge that may eventually reach the public - and shape society; therefore, Frontiers only applies the most rigorous and unbiased reviews. Frontiers revolutionizes research publishing by freely delivering the most outstanding research, evaluated with no bias from both the academic and social point of view. By applying the most advanced information technologies, Frontiers is catapulting scholarly publishing into a new generation.

What are Frontiers Research Topics?

Frontiers Research Topics are very popular trademarks of the *Frontiers journals series*: they are collections of at least ten articles, all centered on a particular subject. With their unique mix of varied contributions from Original Research to Review Articles, Frontiers Research Topics unify the most influential researchers, the latest key findings and historical advances in a hot research area.

Find out more on how to host your own Frontiers Research Topic or contribute to one as an author by contacting the Frontiers editorial office: frontiersin.org/about/contact

Rising stars in comparative and clinical medicine: 2021

Topic editors

Fazul Nabi — Lasbela University of Agriculture, Water and Marine Sciences, Pakistan

Muhammad Asif Arain — Lasbela University of Agriculture, Water and Marine Sciences, Pakistan

Citation

Nabi, F., Arain, M. A., eds. (2023). *Rising stars in comparative and clinical medicine: 2021*. Lausanne: Frontiers Media SA. doi: 10.3389/978-2-8325-1154-1

Table of contents

frontiers | Frontiers in Veterinary Science

TYPE Editorial
PUBLISHED 13 December 2022
DOI 10.3389/fvets.2022.1030960

OPEN ACCESS

EDITED AND REVIEWED BY
Isaac Karimi,
Razi University, Iran

*CORRESPONDENCE
Fazul Nabi
✉ fazulnabishar@yahoo.com

SPECIALTY SECTION
This article was submitted to Comparative and Clinical Medicine, a section of the journal Frontiers in Veterinary Science

RECEIVED 29 August 2022
ACCEPTED 28 November 2022
PUBLISHED 13 December 2022

CITATION
Nabi F and Arain MA (2022) Editorial: Rising stars in comparative and clinical medicine: 2021. *Front. Vet. Sci.* 9:1030960. doi: 10.3389/fvets.2022.1030960

Editorial: Rising stars in comparative and clinical medicine: 2021

Fazul Nabi[1,2]* and Muhammad Asif Arain[1]

[1]Faculty of Veterinary and Animal Science, Lasbela University of Agriculture, Water and Marine Science, Uthal, Balochistan, Pakistan, [2]Department of Traditional Chinese Veterinary Medicine, College of Veterinary Medicine, Southwest University, Chongqing, China

KEYWORDS

gene expression, animal nutrition, poultry, microbiota, animal health, microbiology

Editorial on the Research Topic
Rising stars in comparative and clinical medicine: 2021

The authors have been invited to serve as guest editors for this Research Topic. In this capacity, it was our pleasure to review a wide range of fascinating manuscripts and reviews within the field. In this editorial, we summarize the key findings presented in the Research Topic. The primary objective of this Research Topic is to provide a platform to share current research findings in the domain of comparative and clinical medicine. In the current era of emerging drug resistance and incalculable side effects of synthetic medicines (particularly antibiotics), this topic has been attracting increasing attention among researchers and the scientific community, who have been engaging in efforts to identify alternative biological compounds or drugs with the potential to promote health in multiple ways alongside limited side effects. Therefore, the researchers who have published articles under this Research Topic summarize a range of new evidence regarding the use of natural compounds with medicinal properties as an alternative to antibiotics in various species of livestock in order to improve the productive performance, immune functioning, and health status of animals. Numerous research questions and suggestions have thus been proposed as part of this Research Topic by rising stars in clinical medicine. The majority of studies published in this collection can be categorized into the following research areas: (1) animal health and management; (2) genetics and gene regulation; (3) microbiota in health and disease; and (4) poultry nutrition and morphology.

Animal health and management

The livestock sector plays a vital role in providing animal food containing high-quality protein, essential nutrients, minerals, vitamins, and biological compounds to fulfill the physiological and nutritional requirements of the ever-rising population of human beings. Generally, a healthy animal can be defined as one that shows normal physiological behavior and is free from abiotic and biotic forms of infection that may

alter the normal maintenance of homeostasis and normal physiology (1). Recently, the livestock and poultry sector has faced numerous challenges related to the input costs of production, global warming, heat stress, drug resistance, and the emergence of associated health problems (2, 3). A variety of nutritional strategies have been applied in animal feeding practices in domestic animals to optimize productive performance, improve health status, stimulate immune functions, and reduce the chances of infection (4). Infectious diseases and global warming are the major obstacles threatening the health and welfare of animals throughout the world. In the current era of modern science, several strategies have been developed to overcome these challenges, such as dietary supplementation of nutraceuticals, use of natural antioxidants in feeding practices, mineral supplementation, application of medicinal plants, derivatives, and genetic improvements (5, 6). The livestock sector is a subsector of agriculture that has not only played a central role in fulfilling the nutritional needs of the growing human population, but also contributed significantly to the economic growth of rural communities in general and national economies in particular (2). Recent development and growth in the livestock sector, particularly in developing countries, has been driven by several factors, including the growing human population, urbanization, its role as a source of employment and income, and the increasing availability of resource-efficient technology for modern farming systems. Over the last few decades, the potential productivity of livestock has been constantly improved by genetic modulation, nutritional management, environmentally controlled farming practices, disease prevention practices, and the use of antibiotic growth promoters. Moreover, future improvement of productive performance in this sector will require in-depth molecular research to explore the genetic potential of animals in terms of immunization and disease prevention. Additionally, further *in vitro* and *in vivo* research into alternative treatment options is needed in order to validate existing results on the use of these approaches for the treatment of infectious disease, with limited side effects, in order to resolve the emerging issue of antibiotic resistance. In this special issue, several of the researchers introduce novel research proposals in field of clinical and comparative medicine that might hold future benefits for researchers, scientists, and livestock farmers.

Genetics and gene regulation

Recently, researchers have focused on gene therapy, in the process of which they have discovered novel pharmacotherapeutic targets in domains including gene cloning, identification, and expression, as well as the molecular signaling pathways controlling gene expression and functionality. The study of nutrigenomics has recently become an emerging area of research among the scientific community for exploration of the biological role of nutrients and other biological compounds in triggering or downregulating the functions of particular genes, leading to enhancements to immunological function in animals (7). Various nutrients have been incorporated into animal and poultry feed to promote the health status of the animals and of gene-related food products (meat, eggs, and milk). Niu et al. provide an overview of drug resistance mechanisms of the *Mycoplasma bovis* (M. bovis) pathogen in yaks that have arisen due to indiscriminate use of antibiotics, resulting in base mutations in drug target genes. Their results indicate that *M. bovis* in yaks exhibits single-site base mutations and two-base mutations leading to the production of strains highly resistant to aminoglycosides (genes rrs3 and rrs4) and fluoroquinolones (genes gyrA and parC). Furthermore, Wei et al. present an excellent review summarizing the underlying mechanism of cytotoxicity caused by fluoride poisoning. Their result suggest that fluorosis causes a series of changes associated with mitochondrial dysfunction, such as the generation of reactive oxygen species (ROS), cessation of the mitochondrial respiratory chain, mitochondrial fission, autophagy apoptosis, and mitochondrial calcium regulation. Gong et al. screened out the fat deposition genes in pigs and discovered that back fat deposition and thickness are associated with the expression of genes ACACA, SLC_2A_4, and THRSP in Tibetan pigs, while in the case of Yorkshire pigs, the genes associated with fat deposition are IDL_1, ACACA, $ELOVL_5$, $PLAC_8$, SLC_2A_4, and THRSP. They conclude that signaling pathways and gene expression significantly affect fat deposition in both species of pig. Furthermore, several molecular techniques have been employed in clinical and comparative medicine for the diagnosis and treatment of diseases, and for drug and vaccine production, in order to improve animal productivity. Nabi et al. (8) suggest that the genotype and phenotype structures of all domestic animals can be impaired by continuous exposure to certain toxins, pathogens, and a variety of other compounds; these contribute to the liberation of certain enzymes and the production of free radicals of ROS, leading to oxidative stress and initiation of an inflammatory process alongside the development of pathological conditions. Meanwhile, the utilization of emerging technology for the development of alternative diagnostic and treatment options has been proposed, as a way to target the particular genes relevant to a given pathogen to improve the potential productivity of livestock animals.

Microbiota in health and disease

The gastrointestinal tract (GIT) of animals is occupied by millions of microorganisms; these are collectively known as the gut microbiota and play a pivotal role in the animal body under normal circumstances. Several types of gut microbiota are found in the animal body, such as bacteria, fungi, protozoa, viruses,

parasites, and archaea (Chen et al.). The animal body serves as a home for numerous microorganisms that may contribute to the function of communication between external and internal environments. Interestingly, one study published in this special issue reveals the involvement of the gut microbiota community in the development of mastitis in buffalo (Chen et al.). The authors of this article characterize the various bacterial and fungal communities in healthy and mastitis-affected animals and suggest that neither fungal nor bacterial activity is influenced by mastitis, with exceptions for a few bacteria and fungi. Similarly, Li et al. investigated the microbial diversity of the GIT in healthy and diarrheic horses. The findings of this study reveal that alpha diversity among GIT microorganisms declines significantly in diseased horses; however, several genera are dominant in the microbial community of both healthy and diseased animals.

Recent developments in the field of biotechnology and molecular biology have introduced numerous novel techniques such as gene sequencing and gene regulation, which support researchers in moving toward an in-depth understanding of the complexity and diversity of microbial populations in the animal body. Molecular phylogenetic analysis also provides details on the microbial community present in the GIT (9). It has been proven that the gut microbiota plays a significant role in several biological processes, such as stimulation of the metabolism, maintenance of energy balance, triggering of immunological responses, control of inflammatory processes, involvement in systemic diseases, initiation of neurological disorders, and making a contribution to obesity and host life processes (10). In conclusion, further research is needed to explore the connections between the host and the gut microbiota for treatment and disease prevention.

Poultry nutrition and morphology

Poultry farming has expanded continuously over the last three decades, owing to its ability to supply protein-rich, high-quality meat and eggs at cheap prices to satisfy the growing demands of the human population. The poultry sector constitutes 37% of the world meat industry according to an OECD/FAO survey (2019), and there has been speculation that this sector will grow sharply in the coming years to produce about 331 million tons of meat in 2028 (4). This remarkable progress could be achieved through the application of advanced management practices, use of sub-therapeutic doses of AGPs (antibiotic growth promoters), control of infections, genetic improvement, and utilization of resource-efficient technologies (11). Currently, several nutritional strategies have been adopted to increase the production performance of egg- and meat-type poultry; these include nutritional manipulation with a number of anti-antibiotic feed additives, such as herbs and their extracts, and the use of nutraceuticals, probiotics, prebiotics, and immunostimulants, which are regarded as efficient and safe for use in poultry production systems (12).

In modern livestock and poultry farming practices, the extensive use of AGPs has been banned in several countries due to the emergence of antibiotic resistance and the transfer of this issue from the animal to the human domain. Therefore, research attention has been diverted to the identification of alternative compounds derived from natural sources that yield similar benefits with minimal side effects. In this context, medicinal plants and their biological compounds are of interest as a replacement for AGPs (13). In this Research Topic, Li et al. investigated the health-promoting potential in poultry birds of capsaicin alkaloid derived from capsicum fruit. The results of this study suggest that capsaicin alkaloid significantly improves the production performance of poultry birds by improving their metabolic efficiency, leading to greater organ weight and higher organoleptic quality of the broiler meat.

On this Research Topic, another study reveals the effect of capsaicin on the production performance of poultry. Similarly, another study also reports on the beneficial application of glycyrrhiza polysaccharide (GPS) in a poultry model, observing improved performance in terms of gut development and disease prevention (Wu et al.). The results show that dietary supplementation of GPS significantly enhances gut health by upregulating the expression of genes and cytokine production, leading to activation of T cells (CD4 and CD8) that may contribute to the maintenance of immune functions and the gut microbial community. Interestingly, Zhu et al. studied the role of telocyte cells (TCs) in the regulatory functions of the utero–vaginal junction (UVJ) and in intercellular communication in chickens. The authors of this study successfully demonstrate the presence of TCs at the UVJ of egg-laying chickens and speculate that these cells might play a role in maintaining the animals' physiological functions *via* intracellular communication and transfer of information related to sperm storage and oviduct infections. Overall, it can be concluded that the use of alternative nutritional strategies, in the form of dietary supplementation of phytobiotics, nutraceuticals, and immunostimulants, could be a preferable option to enhance the productive performance of various poultry species.

Conclusion

Taken together, the articles published in this Research Topic make important contributions to our understanding of how livestock production can be improved with the application of various diagnostic and treatment options in clinical and comparative veterinary medicine. A plethora of future studies are proposed, suggesting that precision medicine, treatments with novel compounds, genetic

improvement, nutritional manipulation, and adoption of advanced management practices could all be used to enhance the health status and productive performance of various livestock species in future. However, further research on these topics is required to develop an improved understanding of the use of alternative strategies for the treatment of various pathological disorders. The authors would like to thank all the contributors who participated in this Research Topic for their unwavering support.

Author contributions

Both authors listed have made a substantial, direct, and intellectual contribution to the work and approved it for publication.

Funding

This work was supported by Department of Traditional Chinese Veterinary Medicine, College of Veterinary Medicine, Southwest University, Chongqing, China for supporting the author's research and for the special funding for Chongqing Postdoctoral Research project 2020, number 7820100603.

Acknowledgments

FN would like to extend special thanks to Professor Juan Liu, Department of Traditional Chinese Veterinary Medicine, College of Veterinary Medicine, Southwest University, Chongqing, China, for acknowledging the support with technical revision of this editorial. Furthermore, both the authors of this editorial thank and acknowledge their respective universities and institutions.

Conflict of interest

The authors declare that the research was conducted in the absence of any commercial or financial relationships that could be construed as a potential conflict of interest.

Publisher's note

References

1. Ducrot C, Bed'Hom B, Béringue V, Coulon JB, Fourichon C, Guérin JL, et al. Issues and special features of animal health research. *Veter Res.* (2011) 42:1–10. doi: 10.1186/1297-9716-42-96

2. Arain MA, Nabi F, Marghazani IB, Hassan FU, Soomro H, Kalhoro H, et al. In ovo delivery of nutraceuticals improves health status and production performance of poultry birds: a review. *World's Poultry Sci J.* (2022) 78:765–88. doi: 10.1080/00439339.2022.2091501

3. Nabi F, Arain MA, Rajput N, Alagawany M, Soomro J, Umer M, et al. Health benefits of carotenoids and potential application in poultry industry: A review. *J Anim Physiol Anim Nutr.* (2020) 104:1809–18. doi: 10.1111/jpn.13375

4. Arain MA, Nabi F, Shah QA, Alagawany M, Fazlani SA, Khalid M, et al. The role of early feeding in improving performance and health of poultry: herbs and their derivatives. *World's Poultry Sci J.* (2022) 78:499–513. doi: 10.1080/00439339.2022.2043133

5. Nabi F, Arain M, Hassan F, Umar M, Rajput N, Alagawany M, et al. Nutraceutical role of selenium nanoparticles in poultry nutrition: a review. *World's Poultry Sci J.* (2020) 76:459–71. doi: 10.1080/00439339.2020.1789535

6. Pirzado SA, Hassan FU, Arain MA, Zhengke W, Huiyi C, Haile TH, et al. Effect of azomite on growth performance, nutrient utilization, serum biochemical index and bone mineralization of broilers fed low protein diet. *Italian J Animal Sci.* (2021) 20:1282–91. doi: 10.1080/1828051X.2021.1953409

7. Arain MA, Mei Z, Hassan F, Saeed M, Alagawany M, Shar A, et al. Lycopene: a natural antioxidant for prevention of heat-induced oxidative stress in poultry. *World's Poultry Sci J.* (2018) 74:89–100. doi: 10.1017/S0043933917001040

8. Nabi F, Tao W, Ye R, Li Z, Lu Q, Shang Y, et al. Penthorum chinense pursh extract alleviates aflatoxin b1-induced liver injury and oxidative stress through mitochondrial pathways in broilers. *Front Veter Sci.* (2022) 9:822259. doi: 10.3389/fvets.2022.822259

9. Zhu XY, Zhong T, Pandya Y, Joerger RD. 16S rRNA-based analysis of microbiota from the cecum of broiler chickens. *Appl Environ Microbiol.* (2002) 68:124–37. doi: 10.1128/AEM.68.1.124-137.2002

10. Durack J, Lynch SV. The gut microbiome: relationships with disease and opportunities for therapy. *J Exp Med.* (2019) 216:20–40. doi: 10.1084/jem.20180448

11. Saeed M, Arain MA, Naveed M, Alagawany M, El-Hack A, Ezzat M, et al. Yucca schidigera can mitigate ammonia emissions from manure and promote poultry health and production. *Environ Sci Pollut Res.* (2018) 25:35027–33. doi: 10.1007/s11356-018-3546-1

12. Alagawany M, Abd El-Hack ME, Saeed M, Naveed M, Arain MA, Arif M, et al. Nutritional applications and beneficial health applications of green tea and l-theanine in some animal species: a review. *J Anim Physiol Anim Nutr.* (2020) 104:245–56. doi: 10.1111/jpn.13219

13. Saeed M, Arain MA, Ali Fazlani S, Marghazani IB, Umar M, Soomro J, et al. A comprehensive review on the health benefits and nutritional significance of fucoidan polysaccharide derived from brown seaweeds in human, animals and aquatic organisms. *Aquac Nutr.* (2021) 27:633–54. doi: 10.1111/anu.13233

frontiers in Veterinary Science

ORIGINAL RESEARCH
published: 21 February 2022
doi: 10.3389/fvets.2022.841231

Effects of Capsaicin on Growth Performance, Meat Quality, Digestive Enzyme Activities, Intestinal Morphology, and Organ Indexes of Broilers

*Zhihua Li, Jiaqi Zhang, Ting Wang, Jingfei Zhang, Lili Zhang and Tian Wang**

College of Animal Science and Technology, Nanjing Agricultural University, Nanjing, China

This experiment was conducted to investigate the effects of capsaicin (CAP) on growth performance, meat quality, digestive enzyme activities, intestinal morphology, and organ indexes of broilers. A total of 256 one-day-old Arbor Acre male broilers were randomly allocated into four treatments with eight replicates of eight birds, feeding a basal diet (control group), a basal diet supplemented with 2, 4, and 6 mg/kg CAP for 42 d, respectively. The growth performance, digestive enzyme activities of intestinal contents, small intestinal morphology, and organ indexes were measured at 21 and 42 d. The meat quality traits of breast muscles were determined at 42 d. The results showed dietary 4 mg/kg CAP supplementation decreased ($P < 0.05$) the feed to gain ratio (F/G) in the grower phase (22–42 d) and overall (1–42 d) compared with the control group, and 2 mg/kg CAP group also decreased ($P < 0.05$) the F/G from 1 to 42 d. Dietary 4 mg/kg CAP supplementation decreased ($P < 0.05$) the drip loss at 48 h and the pH_{24h} of breast muscles relative to the control group. Some digestive enzymes activities of jejunal and ileal contents were increased in the 2 and 4 mg/kg CAP groups compared with the control group both at 21 and 42 d. In addition, dietary 2 mg/kg CAP supplementation increased ($P < 0.05$) the relative weight of liver, jejunal villus height, villus width, and villous surface area at 21 d; The length of the jejunum segment and the relative weight of Bursa of Fabricius at 42 d in the 4 mg/kg CAP group were higher ($P < 0.05$) than the control group. In conclusion, dietary 2 or 4 mg/kg CAP supplementation decreased the F/G, improved meat quality, enhanced digestive enzyme activities, improved the jejunal development, and increased the relative liver and Bursa of Fabricius weight in broilers.

Keywords: capsaicin, growth performance, meat quality, intestinal morphology, broiler

OPEN ACCESS

Edited by:
Fazul Nabi,
Lasbela University of Agriculture, Water and Marine Sciences, Pakistan

Reviewed by:
Khalid M. Mahrose,
Zagazig University, Egypt
Ahmed Nisar,
Lasbela University of Agriculture, Water and Marine Sciences, Pakistan

****Correspondence:***
Tian Wang
tianwangnjau@163.com

Specialty section:
This article was submitted to Comparative and Clinical Medicine, a section of the journal Frontiers in Veterinary Science

Received: *22 December 2021*
Accepted: *24 January 2022*
Published: *21 February 2022*

Citation:
Li Z, Zhang J, Wang T, Zhang J, Zhang L and Wang T (2022) Effects of Capsaicin on Growth Performance, Meat Quality, Digestive Enzyme Activities, Intestinal Morphology, and Organ Indexes of Broilers. Front. Vet. Sci. 9:841231. doi: 10.3389/fvets.2022.841231

INTRODUCTION

Poultry meat is in great demand in the global market for its high nutritional values, relatively low fat, and low price (1, 2). The meat quality genetic selection for larger breast muscles, along with increased gross body weight (BW) and rapid growth rate, may make modern chickens' immune function decline and susceptible to various stresses and diseases (3).

Natural plant chemicals (active ingredients of most Chinese herbal medicines) are considered beneficial to organism health possibly through their anti-inflammatory, antioxidant, and prebiotic integration responses (4), thus resisting disease invasion and improving production performance. With the advent of the era of banning the use of antibiotics, research on plant extracts as a class of alternatives is in full swing.

Capsaicin (CAP), named as 8-methyl-N-vanilla base-6-nonene amide ($C_{18}H_{27}NO_3$), is present at the highest level in capsaicinoids extracted from Chilli pepper (5). The transient receptor potential vanilloid 1 (TRPV1) ion channel is the receptor of CAP, whose discovery led to the 2021 Nobel Prize in Physiology or Medicine (6). For decades, CAP has shown the various biological functions through the TRPV1 pathway, including the anti-microbial, anti-obesity, anti-diabetes, anti-hypertension activities (7), anti-oxidation, anti-inflammation (8), and especially beneficial influences on the gastrointestinal system (9). The liver is the largest digestive gland in the body and the intestine is the main digestive tube. The two constitute the main digestive system, which is involved in the digestion of food and providing nutrients to the body for proper maintenance (10, 11). The previous studies demonstrated that dietary CAP supplementation had positive effects on the liver index, small intestinal absolute length, and villus structure (12–14) in rats and hamsters. Meanwhile, CAP could improve growth performance, antioxidant status, immune function, and meat quality in poultry (15, 16). What is more, CAP has a wide range of market sources with relatively low prices. The world's pepper production has increased from more than 12 million tons in 1993 to more than 31 million tons in 2013 (17). Therefore, CAP has clinical value and is a potential functional nutrient supplement for animals.

Previously, the studies mostly focused on the effects of capsicum oleoresin and a mixture of it with other plant extracts on live stocks, or mechanisms of biological functions of CAP (18, 19). However, researches on the application of purified CAP in poultry are still scarce. Besides, the beneficial effects of CAP on animals were related to its dosage and growth stage of animals (20), but the supplementation dosage of CAP was only one level in previous studies (15, 16). Thus, this study was carried out to investigate the effects of different levels of CAP supplementation on growth performance, meat quality, digestive enzyme activities, intestinal morphology, and organ indexes of broilers during the starter and grower stages, which would provide a further theoretical basis for its commercial application in the broiler feed.

MATERIALS AND METHODS

Experimental Animals, Diets, and Design

A total of 256, male, 1-day-old Arbor Acres broilers were selected with 39.78 ± 0.16 g of average BW and randomly divided into four treatment groups including eight replicates with eight broilers per group. Broilers were, respectively, fed with a basal diet (control group) and a basal diet supplemented with either 100, 200, and 300 mg/kg CAP commercial product from the Guangzhou Leader Bio-Technology Co., Ltd., China, which accounts for 98% diluent (stearic acid) and 2% natural extracted CAP until 42 d of age. The dietary levels of CAP are correspondingly 2, 4, and 6 mg/kg diet. The CAP commercial product was mixed into the ingredients during the feed pelleting process. All broilers were provided a starter diet (pelleted and crumbled feed) from 1 to 21 d of age (starter stage) and a grower diet (pelleted feed) from 22 to 42 d of age (grower stage). The composition and nutrient levels of the basal diet for broilers were formulated based on the recommendation by the National Research Council (21), which are shown in **Table 1**. During the whole trial period, broilers were housed in wired cages (120 × 70 × 60 cm; 0.105 m^2 per broiler) and had free access to water and feed. Broilers were kept in an environmentally controlled room at a temperature around 35°C for 5 d, which then gradually decreased to around 22°C and maintained it unchanged until the rest period, and supplied with a 23 h light and 1 h dark daily. Mortalities and healthy status of broilers were observed and recorded daily during the whole experimental time.

TABLE 1 | Composition and nutrient level of the basal diet.

Items	Days 1–21	Days 22–42
Ingredient (%)		
Corn	55.60	55.20
Soybean meal (CP, 44%)	29.00	24.00
Cottonseed meal	2.50	3.00
Wheat flour	4.00	4.00
Hydrolyzed feather meal	1.50	1.50
Dicalcium phosphate (16.5%)	0.90	0.80
Limestone powder	1.50	1.50
Bentonite	1.00	1.00
Soy oil	2.00	7.00
Premix[a]	2.00	2.00
Total	100.00	100.00
Calculation of nutrients[b]		
Metabolizable energy, kcal/kg	2,894	3,212
Crude protein, %	21.50	19.51
Calcium, %	0.96	0.84
Total phosphorus, %	0.66	0.55
Lysine, %	1.45	1.40
Methionine, %	0.54	0.50
Threonine, %	0.91	0.80

[a] *Supplied per kilogram of diet: vitamin A, 11,500 IU; cholecalciferol, 3,500 IU; vitamin E, 30 mg; vitamin K3, 5 mg; thiamin, 3.38 mg; riboflavin, 9.0 mg; pyridoxine, 4.5 mg; vitamin B12, 0.025 mg; choline chloride, 800 mg; calcium pantothenate, 13 mg; niacin, 45 mg; biotin, 0.15 mg; folic acid, 1.20 mg; Mn (from manganese sulfate), 60 mg; Fe (from ferrous sulfate), 66.5 mg; Zn (from zinc sulfate), 88 mg; Cu (from copper sulfate), 8.8 mg; I (from calcium iodate), 0.70 mg; Se (from sodium selenite), 0.3 mg.*

[b] *The nutrient levels were as fed basis.*

Growth Performance

The BW of the broilers was measured at 1, 21, and 42 d. The feed intake of the broilers in each replicate was recorded daily. The average daily gain (ADG), average daily feed intake (ADFI), and feed to BW gain ratio (F/G) were calculated.

Sample Collection, Organ Indexes, and Carcass Traits

After feed deprivation for 12 h, one bird with a BW similar to the mean BW of its replicate was selected, weighed, and euthanized by exsanguination from each replicate of groups for the collection of breast muscle and intestine samples at 21 and 42 d. The left pectoralis major muscle sample was collected and stored at 4°C for the measurement of meat quality. The length of the jejunum (from the pancreatic loop to Meckel's diverticulum) and ileum (between Meckel's diverticulum and the caecal junction) was measured. Then the mid-jejunum and mid-ileum (1 cm) samples were collected and fixed in 4% paraformaldehyde for the morphological analysis. The jejunal and ileal contents samples (middle portion) were collected, snap-frozen in liquid nitrogen, and stored at −80°C for enzyme assays. Meanwhile, the liver, spleen, thymus, and Bursa of Fabricius were stripped and weighed to calculate the organ indexes. Furthermore, items on carcass traits were calculated after removing and weighing entrails and other relevant organs following the Terminology of Poultry Production Performance and Statistical Method of Measurement (NY/T823- 2004, China) at the end of the experiment.

Breast Muscle Quality

The indexes of breast muscle quality were measured by the methods previously published (22, 23). Each index of each muscle sample was measured three times. Briefly, the breast muscle pH was detected at 45 min (pH_{45min}) and 24 h (pH_{24h}) using a pH meter (HI9125 portable waterproof pH/ORP meter, HANNA Instrument, Italy). The color of muscle was detected at 24 h postmortem by a colorimeter (Minolta CR-10, Konica Minolta Sensing, Japan) based on the CIELAB (international commission on illumination) system (L* = lightness, a* = redness, and b* = yellowness). To measure the drip loss, the muscle samples were cut into 3 cm (length) × 2 cm (width) × 1 cm (thickness) sizes, which were weighed after hanging for 0 h (W1), 24 h (W2), and 48 h (W3) at 4°C. Drip loss at 24 h (%) = (W1–W2)/W1 × 100%, Drip loss at 48 h (%) = (W1– W3)/W1 × 100%. About 15 g of each regularly shaped muscle sample was prepared and weighed (W1), then placed at 4°C for 24 h, cooked in a water bath at 80°C until the internal temperature was up to 75°C, cooled, dried, and weighed again (W2). The amount of liquid separating during cooking was measured and calculated as a percentage of cooking loss by the following equation: Cooking loss (%) = (W1–W2)/W1 × 100%. The shearing force of each cooked meat was detected using a Digital Meat Tenderness Meter (C-LM3B, Northeast Agricultural University, Harbin, China) by shearing three different sections, the direction of which is vertical to the myofibers longitudinal axis.

Digestive Enzyme Analysis

The jejunal and ileal contents were homogenized in the ice-cold physiological saline (wt/vol, 1:4) using an Ultra-Turrax homogenizer (Tekmar Co., Cincinnati, OH, USA) and then centrifuged at 3,500 × g for 10 min at 4°C. The supernatant was collected and stored at −80°C for further analysis. The protein concentration and digestive enzymes activities, including the amylase, lipase, and trypsin of the intestinal content homogenates were measured by spectrophotometric methods according to the manufacturers' instructions (Jiancheng Biological Engineering Research Institute, Nanjing, China).

Morphological Measurements of the Small Intestine

The jejunal and ileal samples were fixed in 4% paraformaldehyde for 24 h and dehydrated in graded alcohol series (75, 85, 95, and 100%). Then the samples were immersed in xylene and embedded in paraffin. The tissue blocks were sectioned at 5 μm, dewaxed with xylene, rehydrated with alcohol, and finally stained with hematoxylin and eosin (hematoxylin for 1 min and 1% eosin for 10 s). Villus height and crypt depth of 10 well-oriented villi per segment were determined using an optical binocular microscope (Olympus BX5; Olympus Optical Co. Ltd, Tokyo, Japan) equipped with a digital camera (Nikon H550L; Nikon, Tokyo, Japan). Morphological parameters including villus length, crypt depth, and villus width were measured via the Dotslide software. The villous surface area was calculated following the previous work (24).

Statistical Analysis

All statistical data were analyzed with the SPSS statistical software (Ver.22.0 for windows, SPSS Inc., Chicago, IL). The normality and homogeneity of variances of results were, respectively, evaluated by the Shapiro-Wilk test and Levene's test. The statistical significance of differences among the four groups was determined using a one-way analysis of variance accompanied by Tukey's *post hoc* test. Linear and quadratic effects of CAP supplementation were assessed using the polynomial contrasts. A pen (replicate) was an experimental unit for growth performance, and the individual broiler from each replicate was an experimental unit for other data. Results were shown as means with SEM. *P*-values <0.05 were considered to be significant.

RESULTS

Growth Performance and Carcass Traits

As shown in **Table 2**, dietary CAP supplementation had no significant ($P > 0.05$) impacts on the ADG and ADFI during days 1 to 21, days 22 to 42, and during the whole period (days 1 to 42). Dietary supplementation with 4 mg/kg CAP decreased ($P < 0.05$) the F/G during days 22 to 42, compared with the control group. Dietary supplementation with 2 and 4 mg/kg CAP decreased ($P < 0.05$) the F/G during days 1 to 42, compared with the control group. Dietary CAP supplementation quadratically ($P < 0.05$) decreased the F/G from 22-42 d, and linearly ($P < 0.05$) and quadratically ($P < 0.05$) decreased the F/G from 1 to 42 d. There were no significant differences ($P > 0.05$) in the dressed, semi-eviscerated, eviscerated, breast muscle, and thigh muscle percentage among four treatments (**Table 3**).

Meat Quality of Breast Muscle

As shown in **Table 4**, the pH_{45min} and pH_{24h} in the 6 mg/kg CAP group were lower ($P < 0.05$) than the 2 mg/kg CAP and control group, respectively. Dietary 4 mg/kg CAP supplementation

TABLE 2 | Effects of different levels of capsaicin on the growth performance of broilers.

Item	Control	Dietary capsaicin level (mg/kg)			SEM	*P*-value		
		2	4	6		ANOVA	Linear	Quadratic
Days 1–21								
ADG (g/bird per day)	36.08	35.01	35.36	35.00	0.164	0.060	0.043	0.251
ADFI (g/bird per day)	45.80	44.04	45.33	44.02	0.313	0.091	0.133	0.701
F/G (g/g)	1.27	1.26	1.28	1.26	0.006	0.407	0.786	0.597
Days 22–42								
ADG (g/bird per day)	90.82	92.08	96.81	87.49	1.377	0.111	0.653	0.052
ADFI (g/bird per day)	151.71	144.41	147.80	140.51	1.815	0.156	0.063	0.999
F/G (g/g)	1.68^{a}	1.57^{ab}	1.53^{b}	1.61^{ab}	0.016	0.006	0.057	0.002
Days 1–42								
ADG (g/bird per day)	63.45	63.55	66.07	61.24	0.706	0.112	0.498	0.076
ADFI (g/bird per day)	99.94	95.51	98.07	93.34	1.152	0.194	0.095	0.949
F/G (g/g)	1.57^{a}	1.50^{b}	1.49^{b}	1.52^{ab}	0.010	0.007	0.038	0.004

ADG, average daily gain; ADFI, average daily feed intake; F/G, feed to gain ratio. Values are presented as the mean with SEM (n = 8). Means with unlike superscript letters in the same row are significantly different (P < 0.05).

TABLE 3 | Effects of different levels of capsaicin on carcass traits of broilers at 42 d.

Item	Control	Dietary capsaicin level (mg/kg)			SEM	*P*-value		
		2	4	6		ANOVA	Linear	Quadratic
Dressed percentage (%)	90.35	90.97	90.42	90.70	0.227	0.772	0.806	0.716
Semi-eviscerated percentage (%)	82.55	81.91	82.97	83.20	0.311	0.499	0.293	0.501
Eviscerated percentage (%)	72.83	72.58	73.61	73.37	0.443	0.847	0.523	0.993
Breast muscle percentage (%)	30.07	33.10	31.34	30.44	0.476	0.104	0.875	0.038
Thigh muscle percentage (%)	11.10	10.56	10.22	10.32	0.158	0.201	0.061	0.303

Values are presented as the mean with SEM (n = 8). Dressed percentage, semi-eviscerated percentage, and eviscerated percentage: Calculated as a percentage of live body weight. Breast muscle percentage and thigh muscle percentage: Calculated as a percentage of eviscerated carcass weight.

significantly decreased ($P < 0.05$) pH_{24h} and drip loss at 48 h of breast muscle, compared with the control group. There were no significant differences ($P > 0.05$) in the L*, a*, and b* values, cooking loss, and shearing force of breast muscles of broilers among the four groups. Dietary CAP supplementation linearly ($P < 0.05$) decreased the pH_{45min} and pH_{24h}, and drip loss at 48 h of breast muscle.

Digestive Enzyme Activities

The digestive enzyme activities for the jejunal and ileal contents of broilers were shown in **Tables 5**, **6**. In the jejunal contents (**Table 5**), the lipase activity at 21 d in the broilers fed with the 2 and 4 mg/kg CAP diets was greater ($P < 0.05$) than those fed with the control diet. The trypsin activity of the 4 mg/kg CAP group was higher ($P < 0.05$) than the control group at 42 d. Dietary CAP supplementation linearly ($P < 0.05$) and quadratically ($P < 0.05$) increased the lipase activity at 21 d, as well as quadratically ($P < 0.05$) increased the trypsin activity at 21 and 42 d. In the ileal contents (**Table 6**), dietary 4 mg/kg CAP supplementation increased ($P < 0.05$) the lipase activity at 21 and 42 d compared with the control group. The amylase activity in the 2 mg/kg CAP group was higher ($P < 0.05$) than the control group at 42 d. Dietary CAP supplementation linearly ($P < 0.05$) and quadratically ($P < 0.05$) increased the lipase activity at 21 d, as well as quadratically ($P < 0.05$) increased the amylase and lipase activities at 42 d.

The Liver Index and Length of the Small Intestine

In the present study, dietary 2 mg/kg CAP supplementation increased ($P < 0.05$) the relative liver weight of broilers at 21 d (**Table 7**), compared with the control group. There was no significant difference ($P > 0.05$) in the relative liver weight of broilers among the four groups at 42 d. As presented in **Table 7**, dietary CAP supplementation had no significant effects ($P > 0.05$) on the length of jejunum and ileum in broilers at 21 d. Dietary 4 mg/kg CAP supplementation increased ($P < 0.05$) the length of jejunum and ileum at 42 d, compared with the control group and broilers fed with 6 mg/kg CAP, respectively. Dietary CAP supplementation quadratically ($P < 0.05$) increased the length of jejunum and ileum at 42 d.

TABLE 4 | Effects of different levels of capsaicin on meat quality of breast muscle in broilers at 42 d.

Item	Control	Dietary capsaicin level (mg/kg)			SEM	*P*-value		
		2	4	6		ANOVA	Linear	Quadratic
pH_{45min}	6.52^{ab}	6.73^{a}	6.25^{b}	6.32^{b}	0.048	<0.001	0.002	0.365
pH_{24h}	5.98^{a}	5.91^{ab}	5.88^{bc}	5.82^{c}	0.016	0.001	<0.001	0.966
L*	48.16	47.48	46.65	48.46	0.447	0.506	0.985	0.177
a*	3.51	3.34	3.40	3.37	0.134	0.973	0.768	0.803
b*	9.60	10.68	9.68	9.77	0.244	0.374	0.823	0.316
Drip loss at 24 h (%)	1.88	1.83	1.74	2.18	0.061	0.057	0.122	0.039
Drip loss at 48 h (%)	3.07^{a}	3.12^{a}	2.46^{b}	2.70^{ab}	0.088	0.016	0.016	0.561
Cooking loss (%)	26.00	24.35	27.63	29.78	0.771	0.071	0.031	0.194
Shearing force (N)	27.25	30.53	27.88	23.48	1.185	0.213	0.186	0.107

Values are presented as the mean with SEM (n = 8). Means with unlike superscript letters in the same row are significantly different (P < 0.05). pH_{45min}: pH value at 45 min; pH_{24h}: pH value at 24 h. L, lightness; a*, redness; b*, yellowness.*

TABLE 5 | Effects of different levels of capsaicin on the digestive enzyme activities of jejunal contents of broilers.

Item	Control	Dietary capsaicin level (mg/kg)			SEM	*P*-value		
		2	4	6		ANOVA	Linear	Quadratic
21 d								
Amylase (U/mgprotein)	7.04	9.00	7.58	7.55	0.462	0.497	0.979	0.293
Lipase (U/gprotein)	381.15^{b}	473.33^{a}	472.73^{a}	463.54^{ab}	12.759	0.019	0.021	0.033
Trypsin (U/mgprotein)	4,096.86	4,804.43	4,888.41	4,612.78	119.492	0.077	0.113	0.036
42 d								
Amylase (U/mgprotein)	7.54	9.28	8.60	8.17	0.484	0.658	0.787	0.286
Lipase (U/gprotein)	435.16	502.33	518.63	482.15	14.941	0.226	0.237	0.086
Trypsin (U/mgprotein)	4,104.88^{b}	4,836.4^{ab}	5,023.48^{a}	4,538.53^{ab}	126.873	0.049	0.164	0.014

Values are presented as the mean with SEM (n = 8). Means with unlike superscript letters in the same row are significantly different (P < 0.05).

Small Intestinal Morphology

The morphologic analysis of the small intestine in broilers was shown in **Tables 8**, **9**, and **Figure 1**. Dietary supplementation with 2 mg/kg CAP could increase ($P < 0.05$) the villus height, width, and surface area of jejunum at 21 d, compared with the control group (**Table 8**). Dietary CAP supplementation quadratically ($P < 0.05$) increased the jejunal villus height, villus width, and surface area at 21 d. There were no significant differences ($P > 0.05$) in the villus height, crypt depth, villus width, villus height/crypt depth, and villous surface area of jejunum at 42 d, and ileum at 21 and 42 d (**Tables 8**, **9**). As shown in **Figure 1**, the structure of villi was basically integral in the representative samples of jejunum and ileum in four groups.

The Immune Organ Indexes

There were no significant differences ($P > 0.05$) in the relative spleen and thymus weight of broilers at 21 and 42 d among the four groups (**Table 10**). The relative Bursa of Fabricius weight of broilers at 21 and 42 d fed with 2 mg/kg CAP was higher ($P < 0.05$) than the 6 mg/kg CAP group and other three groups, correspondingly. Dietary CAP supplementation quadratically ($P < 0.05$) increased the relative Bursa of Fabricius weight at 21 and 42 d.

DISCUSSION

CAP, a major pungent hydrophobic alkaloid of capsicum fruits, shows several biological activities, including antimicrobial activity, improving digestive function, antioxidation, anti-inflammation, and so on, which is conducive to livestock production (7, 25). The presented results showed that dietary 2 and 4 mg/kg CAP had more distinct effects than the dietary 6 mg/kg CAP supplementation, possibly due to less irritation. Meanwhile, 2 and 4 mg/kg CAP groups are more cost-effective than the 6 mg/kg CAP group.

In the present study, dietary 2 and 4 mg/kg CAP supplementation could decrease the F/G, which might improve the feed efficiency, thereby reducing the breeding costs. This may be partly because dietary CAP supplementation could increase the digestive enzymes (15, 26, 27), bile acids (14), and endogenous cholecystokinin (28) in the gut, which are required for the efficient digestion of nutrients. In accordance with it, we found that dietary 2 or 4 mg/kg

TABLE 6 | Effects of different levels of capsaicin on the digestive enzyme activities of ileal contents of broilers.

Item	Control	Dietary capsaicin level (mg/kg)			SEM	*P*-value		
		2	4	6		ANOVA	Linear	Quadratic
21 d								
Amylase (U/mgprotein)	8.51	9.30	8.96	7.92	0.535	0.832	0.672	0.416
Lipase (U/gprotein)	394.36^{b}	494.68^{ab}	510.10^{a}	477.69^{ab}	15.000	0.022	0.034	0.019
Trypsin (U/mgprotein)	4,577.07	4,718.93	4,797.96	4,541.24	116.288	0.862	0.979	0.416
42 d								
Amylase (U/mgprotein)	7.19^{b}	11.10^{a}	10.02^{ab}	8.94^{ab}	0.504	0.033	0.315	0.011
Lipase (U/gprotein)	417.69^{b}	505.73^{ab}	520.17^{a}	482.68^{ab}	13.233	0.023	0.057	0.013
Trypsin (U/mgprotein)	4,488.42	5,105.69	4,929.34	4,620.11	130.237	0.329	0.851	0.083

Values are presented as the mean with SEM (n = 8). Means with unlike superscript letters in the same row are significantly different (P < 0.05).

TABLE 7 | Effects of different levels of capsaicin on the liver index and the length of the small intestine of broilers.

Item	Control	Dietary capsaicin level (mg/kg)			SEM	*P*-value		
		2	4	5		ANOVA	Linear	Quadratic
21 d								
Liver weight/BW(g/kg)	25.39^{b}	29.37^{a}	28.21^{ab}	28.49^{ab}	0.524	0.034	0.064	0.060
Length of jejunum (cm)	51.75	53.23	54.76	53.41	0.810	0.650	0.386	0.401
Length of ileum (cm)	40.28	40.10	43.60	42.61	0.905	0.449	0.207	0.825
42 d								
Liver weight/BW(g/kg)	24.56	23.56	25.01	22.94	0.584	0.607	0.527	0.654
Length of jejunum (cm)	65.13^{b}	74.63^{ab}	79.00^{a}	68.88^{ab}	1.659	0.010	0.231	0.002
Length of ileum (cm)	47.00^{ab}	51.50^{ab}	53.00^{a}	45.63^{b}	0.965	0.011	0.728	0.001

Values are presented as the mean with SEM (n = 8). Means with unlike superscript letters in the same row are significantly different (P < 0.05).

CAP supplementation could enhance the lipase activity of jejunal and ileal contents, trypsin activity of jejunal contents, and amylase activity of ileum contents. These endogenous digestive enzymes play important roles in the whole digestion process. The amylase, lipase, and trypsin are good for the decomposition, digestion, and absorption of carbohydrates, protein, and lipid, respectively (29). Similarly, feeding the mixture of 5% carvacrol, 3% cinnamaldehyde, and 2% capsicum oleoresin at 100 mg/kg improved the feed efficiency by 9.8% in Ross 308 male broiler chickens (30). Interestingly, it was reported no differences in feed efficiency were observed in the leghorn chicks fed with diets containing 5 and 20 mg/kg CAP (31). This controversy may be due to the level and composition of capsaicin preparation in the basal diet, diet composition, broiler types, and feeding management. The CAP in the present study was processed by microencapsulation technology which could help to decrease the irritating effect and control its release throughout the gastrointestinal tract (25).

The physical characteristics of meat quality including pH, meat color, water holding capacity, tenderness, and so on determine the acceptability, storage, and processability of meat products. The accumulation of lactic acid in the muscles caused by glycogen degradation leads to a pH decline at 24 h (32). The pH value can be associated with color, cooking loss, tenderness, shelf-life, and other traits (33). In the present study, dietary 4 mg/kg CAP supplementation reduced the pH_{24h} value of muscle within a normal range ($5.7 < pH_{24h}$, not low enough to promote the formation of the pale, soft, and exudative meat), which may be beneficial to prolong the shelf life of muscle (32, 34), as it may retard meat spoilage through inhibiting microbes growth (33). In addition, meat color is the appearance and manifestation of the physiological, biochemical, and microbiological changes of muscle, which can influence consumer acceptance of poultry meat (35). Drip loss and cooking loss reflect the water-holding capacity (WHC). Dietary 4 mg/kg CAP supplementation also decreased the drip loss at 48 h, which may increase the water content of muscles and enhance tenderness and juiciness, thus improving the meat quality (2). The shearing force partly reflects the tenderness of the meat. There were no significant differences in the meat color, cooking loss, and shearing force of breast meat after CAP treatment. Theoretically, the higher light value of meat is accompanied with lower pH, higher moisture, and lower WHC (35). However, the pH value has little relationship to other parameters, such as meat color and drip losses in our study. These irrelevances maybe because the meat quality of breast muscle measured in this trial is within the normal range, or there may be some other factors

TABLE 8 | Effects of different levels of capsaicin on the jejunal morphology of broilers.

Item	Control	Dietary capsaicin level (mg/kg)			SEM	*P*-value		
		2	4	6		ANOVA	Linear	Quadratic
21 d								
Villus height (μm)	988.69^{b}	1,216.87^{a}	1,084.06^{ab}	973.09^{b}	31.696	0.013	0.452	0.004
Crypt depth (μm)	233.18	272.93	241.05	250.58	6.594	0.162	0.720	0.240
Villus width (μm)	122.61^{b}	179.94^{a}	139.43^{b}	142.29^{b}	5.970	0.001	0.640	0.005
Villus height/crypt depth (μm/μm)	4.35	4.46	4.56	3.92	0.149	0.473	0.393	0.227
Villous surface area ($\times 10^3$ μm^2)	191.39^{b}	329.52^{a}	244.84^{ab}	231.71^{ab}	16.115	0.010	0.760	0.009
42 d								
Villus height (μm)	1,622.78	1,685.03	1,750.36	1,558.55	41.445.	0.420	0.735	0.141
Crypt depth (μm)	332.37	328.63	342.16	329.19	9.026	0.885	0.963	0.812
Villus width (μm)	244.02	244.67	211.97	223.23	7.195	0.301	0.148	0.711
Villus height/crypt depth (μm/μm)	4.93	5.29	5.14	4.74	0.147	0.602	0.604	0.222
Villous surface area ($\times 10^3$ μm^2)	622.37	654.65	587.25	555.86	27.993	0.654	0.313	0.587

Values are presented as the mean with SEM (n = 8). Means with unlike superscript letters in the same row are significantly different (P < 0.05).

TABLE 9 | Effects of different levels of capsaicin on the ileal morphology of broilers.

Item	Control	Dietary capsaicin level (mg/kg)			SEM	*P*-value		
		2	4	6		ANOVA	Linear	Quadratic
21 d								
Villus height (μm)	817.14	817.06	810.61	756.84	18.831	0.643	0.293	0.497
Crypt depth (μm)	229.00	217.24	196.36	194.97	6.146	0.136	0.027	0.657
Villus width (μm)	141.09	145.44	141.76	122.33	4.707	0.315	0.163	0.214
Villus height/crypt depth (μm/μm)	3.58	3.78	4.13	3.95	0.090	0.148	0.064	0.268
Villous surface area ($\times 10^3$ μm^2)	182.77	185.05	180.18	146.13	6.778	0.132	0.056	0.167
42 d								
Villus height (μm)	1,250.53	1,141.65	1,242.32	1,060.76	34.650	0.164	0.126	0.586
Crypt depth (μm)	223.17	236.12	250.96	221.05	6.705	0.385	0.889	0.124
Villus width (μm)	170.97	191.91	169.93	170.43	4.349	0.208	0.534	0.235
Villus height/crypt depth (μm/μm)	5.62	4.95	5.00	4.81	0.150	0.237	0.081	0.418
Villous surface area ($\times 10^3$ μm^2)	334.80	342.68	338.95	285.50	13.232	0.399	0.214	0.259

Values are presented as the mean with SEM (n = 8). Means with unlike superscript letters in the same row are significantly different (P < 0.05).

affecting these meat quality traits. The above indicates that dietary MC supplementation could improve the meat quality by decreasing the pH and drop losses. What's more, the main target of commercial broiler chicken production is achieving high-yield and high-quality muscles, especially breast muscle, which is considered the most valuable piece of the chicken carcass and greatly affected by the breed (36). In the present study, dietary MC supplementation had no significant influences on the carcass trait.

To further understand the effects of CAP on modulating nutrient digestion and absorption, we measured the liver and small intestinal development. In the present study, dietary 2 mg/kg CAP supplementation increased the relative liver weight at 21 d, which is beneficial to enhance digestive function. It was also reported that a plant extract mixture including 1.98 mg/kg CAP increased the liver weight of broilers at 42 d (27). In addition, histologically, longer and wider villi, and larger villous surfaces of the small intestine indicate an increase in feed efficiency and growth-promoting efficiency (37). In general, villi are the longest in the jejunum where most nutrients are digested and absorbed. Previous studies have shown that dietary pungent spices supplementation increased the length of the small intestine in rats (38) and the length and perimeter of microvilli, which contributes to an increase in the absorption surface of the small intestine, thereby improving the bioavailability of micronutrients (12). Similarly, in our study, dietary 2 and 4 mg/kg CAP supplementation also increased the length of jejunum and ileum at 42 d and enhanced the villus height, villus width, and villous surface area in the jejunum at 21 d, suggesting CAP could promote small intestine development and improve the utilization

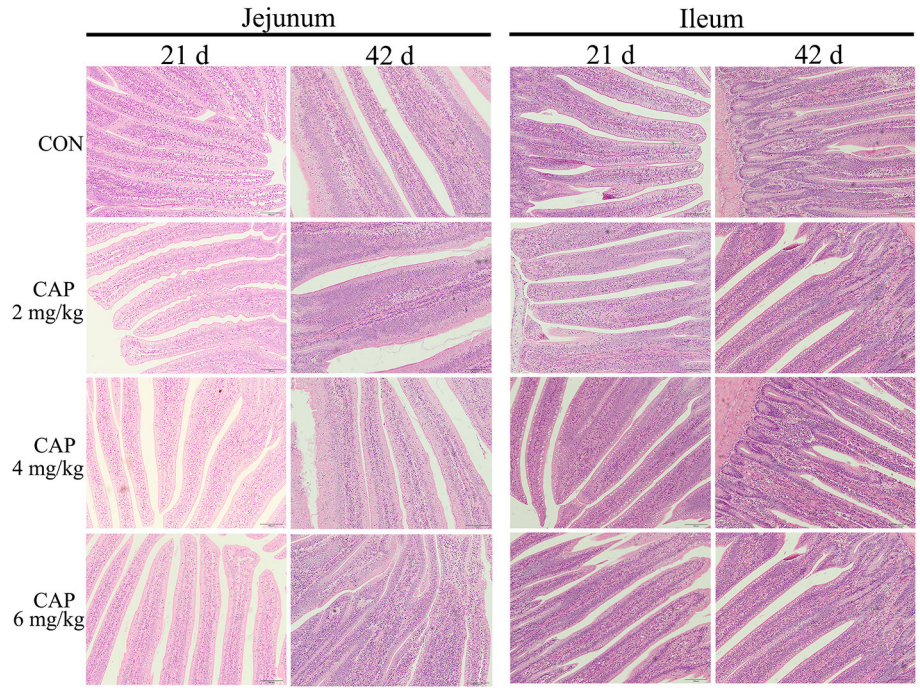

FIGURE 1 | The jejunum and ileum histological morphology of broilers (hematoxylin and eosin). CON, broilers were fed with a basal diet; CAP 2, CAP 4, and CAP 6 mg/kg, broilers were fed with a basal diet supplemented with 2, 4, and 6 mg/kg capsaicin, respectively. Scale bars = 100 μm.

TABLE 10 | Effects of different levels of capsaicin on the immune organ indexes of broilers (g/kg).

Item	Control	Dietary capsaicin level (mg/kg)			SEM	*P*-value		
		2	4	6		ANOVA	Linear	Quadratic
21 d								
Spleen weight/BW	0.84	0.87	0.91	0.86	0.035	0.915	0.754	0.583
Thymus weight/BW	4.33	4.40	4.74	3.82	0.151	0.197	0.368	0.102
Bursa of Fabricius weight/BW	1.92^{ab}	2.40^{a}	2.05^{ab}	1.82^{b}	0.080	0.049	0.325	0.024
42 d								
Spleen weight/BW	0.96	0.96	0.97	0.93	0.031	0.959	0.759	0.743
Thymus weight/BW	2.31	2.51	2.48	2.34	0.061	0.610	0.897	0.190
Bursa of Fabricius weight/BW	0.84^{b}	1.19^{a}	0.93^{b}	0.91^{b}	0.039	0.026	0.856	0.009

BW, body weight. Values are presented as the mean with SEM (n = 8). Means with unlike superscript letters in the same row are significantly different (P < 0.05).

of nutrients in broilers. These positive effects of CAP on the liver and small intestine may be one of the reasons for its reduced F/G.

The immune organ index is commonly measured to assess immunity in poultry (34). The Bursa of Fabricius is vital to the normal development of B lymphocytes and antibody production (39). Furthermore, the Bursa of Fabricius may expand the antibody-producing apparatus by promoting the contact between intestinal antigens and lymphoid tissue of the organ wall (40). Our studies showed dietary 2 mg/kg CAP supplementation increased the relative Bursa of Fabricius weight, which is directly in line with the previous finding (15), suggesting CAP is conducive to the improvement of immune function.

CONCLUSIONS

Dietary 2 or 4 mg/kg CAP supplementation could reduce the F/G, improve meat quality, increase digestive enzymes of small intestinal contents and improve the liver, small intestine, and immune organ development of broilers. Therefore, CAP can be used as a functional additive for broilers.

DATA AVAILABILITY STATEMENT

The original contributions presented in the study are included in the article/supplementary material, further inquiries can be directed to the corresponding author/s.

ETHICS STATEMENT

The animal study was reviewed and approved by Animal Care and Use Committee of Nanjing Agricultural University.

AUTHOR CONTRIBUTIONS

ZL and TiaW conceived and designed the experiment. ZL, JiaZ, and TinW performed the experiment. ZL and JinZ processed the data. ZL prepared and drafted the manuscript. LZ and TiaW revised the manuscript. All authors reviewed the final manuscript.

FUNDING

This work was supported by the National Natural Science Foundation of China (nos. 31772634 and 32172775).

ACKNOWLEDGMENTS

We thank the postgraduate students of The Laboratory of Animal Nutrition Regulation Research for collecting the samples, and the technicians and teachers from the College of Animal Sciences and Technology, National Experimental Teaching Demonstration Centre of Animal Science, Nanjing Agricultural University.

REFERENCES

1. Gratta F, Fasolato L, Birolo M, Zomeno C, Novelli E, Petracci M, et al. Effect of breast myopathies on quality and microbial shelf life of broiler meat. *Poult Sci.* (2019) 98:2641–51. doi: 10.3382/ps/pez001
2. Mir NA, Rafiq A, Kumar F, Singh V, Shukla V. Determinants of broiler chicken meat quality and factors affecting them: a review. *J Food Sci Technol.* (2017) 54:2997–3009. doi: 10.1007/s13197-017-2789-z
3. Guo Y, Balasubramanian B, Zhao ZH, Liu WC. Marine algal polysaccharides alleviate aflatoxin B1-induced bursa of Fabricius injury by regulating redox and apoptotic signaling pathway in broilers. *Poult Sci.* (2021) 100:844–57. doi: 10.1016/j.psj.2020.10.050
4. Xue C, Li Y, Lv H, Zhang L, Bi C, Dong N, et al. Oleanolic acid targets the gut–liver axis to alleviate metabolic 2 disorders and hepatic steatosis. *J Agric Food Chem.* (2021) 69:7884–97. doi: 10.1021/acs.jafc.1c02257
5. Barbero GF, Liazid A, Azaroual L, Palma M, Barroso CG. Capsaicinoid contents in peppers and pepper-related spicy foods. *Int J Food Prop.* (2016) 19:485–93. doi: 10.1080/10942912.2014.968468
6. Caterina MJ, MarkA.Schumacher†k, Tominaga M, A.Rosen T, Levine JD, Julius D. The capsaicin receptor a heat-activated ion channel in the pain pathway. *Nature.* (1997) 389:816–24. doi: 10.1038/39807
7. Wang F, Xue Y, Fu L, Wang Y, He M, Zhao L, et al. Extraction, purification, bioactivity and pharmacological effects of capsaicin: a review. *Crit Rev Food Sci Nutr.* (2021) 1:1–29. doi: 10.1080/10408398.2021.1884840
8. Lv Z, Xu X, Sun Z, Yang YX, Guo H, Li J, et al. TRPV1 alleviates osteoarthritis by inhibiting M1 macrophage polarization via Ca(2+)/CaMKII/Nrf2 signaling pathway. *Cell Death Dis.* (2021) 12:504. doi: 10.1038/s41419-021-03792-8
9. Srinivasan K. Biological activities of red pepper (*Capsicum annuum*) and its pungent principle capsaicin: a review. *Crit Rev Food Sci Nutr.* (2016) 56:1488–0. doi: 10.1080/10408398.2013.772090
10. Trefts E, Gannon M, Wasserman DH. The liver. *Curr Biol.* (2017) 27:R1147–51. doi: 10.1016/j.cub.2017.09.019
11. Paone P, Cani PD. Mucus barrier, mucins and gut microbiota: the expected slimy partners? *Gut.* (2020) 69:2232–43. doi: 10.1136/gutjnl-2020-322260
12. Prakash UN, Srinivasan K. Beneficial influence of dietary spices on the ultrastructure and fluidity of the intestinal brush border in rats. *Br J Nutr.* (2010) 104:31–9. doi: 10.1017/S0007114510000334
13. Zhang L, Fang G, Zheng L, Chen Z, Liu X. The hypocholesterolemic effect of capsaicinoids in ovariectomized rats fed with a cholesterol-free diet was mediated by inhibition of hepatic cholesterol synthesis. *Food Funct.* (2013) 4:738–44. doi: 10.1039/c3fo30321g
14. Liang YT, Tian XY, Chen JN, Peng C, Ma KY, Zuo Y, et al. Capsaicinoids lower plasma cholesterol and improve endothelial function in hamsters. *Eur J Nutr.* (2013) 52:379–88. doi: 10.1007/s00394-012-0344-2
15. Liu SJ, Wang J, He TF, Liu HS, Piao XS. Effects of natural capsicum extract on growth performance, nutrient utilization, antioxidant status, immune function, and meat quality in broilers. *Poult Sci.* (2021) 100:101301. doi: 10.1016/j.psj.2021.101301
16. Liu JG, Xia WG, Chen W, Abouelezz KFM, Ruan D, Wang S, et al. Effects of capsaicin on laying performance, follicle development, and ovarian antioxidant capacity in aged laying ducks. *Poult Sci.* (2021) 100:100901. doi: 10.1016/j.psj.2021.101155
17. Penella C, Calatayud A. Pepper crop under climate change: Grafting as an environmental friendly strategy. In: Shanker A, editor. *Climate Resilient Agriculture-Strategies and Perspectives*. London: IntechOpen (2018) 129–55. doi: 10.5772/intechopen.72361
18. Adaszek L, Gadomska D, Mazurek L, Lyp P, Madany J, Winiarczyk S. Properties of capsaicin and its utility in veterinary and human medicine. *Res Vet Sci.* (2019) 123:14–9. doi: 10.1016/j.rvsc.2018.12.002
19. Baenas N, Belovic M, Ilic N, Moreno DA, Garcia-Viguera C. Industrial use of pepper (*Capsicum annum L.*) derived products: technological benefits and biological advantages. *Food Chem.* (2019) 274:872–85. doi: 10.1016/j.foodchem.2018.09.047
20. Rollyson WD, Stover CA, Brown KC, Perry HE, Stevenson CD, McNees CA, et al. Bioavailability of capsaicin and its implications for drug delivery. *J Control Release.* (2014) 196:96–105. doi: 10.1016/j.jconrel.2014.09.027
21. National Research Council. *Nutrient Requirements of Poultry*. 9th rev ed. Washington, DC: National Academy Press (1994).
22. Zhang J, Hu Z, Lu C, Bai K, Zhang L, Wang T. Effect of various levels of dietary curcumin on meat quality and antioxidant profile of breast muscle in broilers. *J Agric Food Chem.* (2015) 63:3880–6. doi: 10.1021/jf505889b
23. Wan XL, Song ZH, Niu Y, Cheng K, Zhang JF, Ahmad H, et al. Evaluation of enzymatically treated *Artemisia annua* L. on growth performance, meat quality, and oxidative stability of breast and thigh muscles in broilers. *Poult Sci.* (2017) 96:844–50. doi: 10.3382/ps/pew307
24. Dong L, Zhong X, Ahmad H, Li W, Wang Y, Zhang L, et al. Intrauterine growth restriction impairs small intestinal mucosal immunity in neonatal piglets. *J Histochem Cytochem.* (2014) 62:510–8. doi: 10.1369/0022155414532655
25. Meunier JP, Cardot JM, Manzanilla EG, Wysshaar M, Alric M. Use of spray-cooling technology for development of microencapsulated capsicum oleoresin for the growing pig as an alternative to in-feed antibiotics: a study of release using in vitro models. *J Anim Sci.* (2007) 85:2699–710. doi: 10.2527/jas.2007-0027
26. Platel K, Srinivasan K. Influence of dietary spices and their active principles on pancreatic digestive enzymes in albino rats. *Nahrung.* (2000) 44:42–6. doi: 10.1002/(SICI)1521-3803(20000101)44:1<42::AID-FOOD42>3.0.CO;2-D
27. Jamroz D, Wiliczkiewicz A, Wertelecki T, Orda J, Skorupinska J. Use of active substances of plant origin in chicken diets based on maize and locally grown cereals. *Br Poult Sci.* (2005) 46:485–93. doi: 10.1080/00071660500191056
28. Yamamoto M, Otani M, Jia DM, Fukumitsu K, Yoshikawa H, Akiyama T, et al. Differential mechanism and site of action of CCK on the pancreatic secretion and growth in rats. *Am J Physiol Gastrointest Liver Physiol.* (2003) 285:G681–7. doi: 10.1152/ajpgi.00312.2002
29. Long S, Liu S, Wang J, Mahfuz S, Piao X. Natural capsicum extract replacing chlortetracycline enhances performance via improving digestive enzyme activities, antioxidant capacity, anti-inflammatory function, and gut health

in weaned pigs. *Anim Nutr.* (2021) 7:305–14. doi: 10.1016/j.aninu.2020.12.004
30. Bravo D, Pirgozliev V, Rose SP. A mixture of carvacrol, cinnamaldehyde, and capsicum oleoresin improves energy utilization and growth performance of broiler chickens fed maize-based diet. *J Anim Sci.* (2014) 92:1531–6. doi: 10.2527/jas.2013-6244
31. McElroy P, Manning JG, Jaeger LA, Taub M, Williams JD, Hargis BM. Effects of prolonged administration of dietary capsaicin on broiler growth and salmonella enteritidis susceptibility. *Avian Dis.* (1994) 38:329–33. doi: 10.2307/1591958
32. Barbut S, Sosnicki AA, Lonergan SM, Knapp T, Ciobanu DC, Gatcliffe LJ, et al. Progress in reducing the pale, soft and exudative (PSE) problem in pork and poultry meat. *Meat Sci.* (2008) 79:46–63. doi: 10.1016/j.meatsci.2007.07.031
33. Akuru EA, Oyeagu CE, Mpendulo TC, Rautenbach F, Oguntibeju OO. Effect of pomegranate (*Punica granatum* L) peel powder meal dietary supplementation on antioxidant status and quality of breast meat in broilers. *Heliyon.* (2020) 6:e05709. doi: 10.1016/j.heliyon.2020.e05709
34. Tong HB, Lu J, Zou JM, Wang Q, Shi SR. Effects of stocking density on growth performance, carcass yield, and immune status of a local chicken breed. *Poult Sci.* (2012) 91:667–73. doi: 10.3382/ps.2011-01597
35. Qiao M, Fletcher DL, Smith DP, Northcutt JK. The effect of broiler breast meat color on pH, moisture, water-holding capacity, and emulsification capacity. *Poult Sci.* (2001) 80:676–80. doi: 10.1093/ps/80.5.676
36. Nematbakhsh S, Selamat J, Idris LH, Abdull Razis AF. Chicken authentication and discrimination via live weight, body size, carcass traits, and breast muscle fat content clustering as affected by breed and sex varieties in malaysia. *Foods.* (2021) 10:1575. doi: 10.3390/foods10071575
37. Jha R, Das R, Oak S, Mishra P. Probiotics (direct-fed microbials) in poultry nutrition and their effects on nutrient utilization, growth and laying performance, and gut health: a systematic review. *Animals.* (2020) 10:1863. doi: 10.3390/ani10101863
38. Prakash UN, Srinivasan K. Enhanced intestinal uptake of iron, zinc and calcium in rats fed pungent spice principles–piperine, capsaicin and ginger (*Zingiber officinale*). *J Trace Elem Med Biol.* (2013) 27:184–90. doi: 10.1016/j.jtemb.2012.11.003
39. Feng XL, Liu QT, Cao RB, Zhou B, Zhang YP, Liu K, et al. Characterization and immunomodulatory function comparison of various bursal-derived peptides isolated from the humoral central immune organ. *Peptides.* (2012) 33:258–64. doi: 10.1016/j.peptides.2012.01.012
40. Schaffner T, Mueller J, W.Hess M, Cottier H, Sordat B, Ropke C. The bursa of Fabricius a central organ providing for contact between the lymphoid system and intestinal content. *Cell Immunol.* (1974) 13:304–12. doi: 10.1016/0008-8749(74)90247-0

Conflict of Interest: The authors declare that the research was conducted in the absence of any commercial or financial relationships that could be construed as a potential conflict of interest.

frontiers in Veterinary Science

ORIGINAL RESEARCH
published: 24 March 2022
doi: 10.3389/fvets.2022.849500

Seroprevalence of Cystic Echinococcosis in Yaks and Sheep During 2017 on the Qinghai–Tibet Plateau, China

Xing Gao[1†], Luosong Xire[2†], Zhao Zhang[1], Chuxian Quan[1], Shimeng Zhou[1], Kewei Li[1], Rende Song[3], Suonan Zhao[4], Xiangying Kong[4], Cairang Naori[5], Muhammad Fakhar-e-Alam Kulyar[1], Yuhua Bao[2] and Jiakui Li[1,6*]*

[1] College of Veterinary Medicine, Huazhong Agricultural University, Wuhan, China, [2] Veterinary Biological Medicine Manufacturing Factory of Tibet Autonomous Region, Lhasa, China, [3] Qinghai Animal and Veterinary Sciences Work Station, Yushu, China, [4] Haibei Agricultural and Animal Husbandry Sciences Institute, Haibei, China, [5] Animal Husbandry and Veterinary Science Research Institute of Gannan Prefecture, Gannan, China, [6] College of Animals Husbandry and Veterinary Medicine, Tibet Agricultural and Animal Husbandry University, Linzhi, China

OPEN ACCESS

Edited by:
Fazul Nabi,
Lasbela University of Agriculture, Water and Marine Sciences, Pakistan

Reviewed by:
Yung-Fu Chang,
Cornell University, United States
Liu Sidang,
Shandong Agricultural University, China
Bahador Sarkari,
Shiraz University of Medical Sciences, Iran

***Correspondence:**
Jiakui Li
lijk210@sina.com
Yuhua Bao
651320318@qq.com

[†]These authors have contributed equally to this work and share first authorship

Specialty section:
This article was submitted to Comparative and Clinical Medicine, a section of the journal Frontiers in Veterinary Science

Received: 06 January 2022
Accepted: 25 January 2022
Published: 24 March 2022

Citation:
Gao X, Xire L, Zhang Z, Quan C, Zhou S, Li K, Song R, Zhao S, Kong X, Naori C, Kulyar MF-e-A, Bao Y and Li J (2022) Seroprevalence of Cystic Echinococcosis in Yaks and Sheep During 2017 on the Qinghai–Tibet Plateau, China. Front. Vet. Sci. 9:849500. doi: 10.3389/fvets.2022.849500

Cystic echinococcosis (CE) is a livestock disease caused by a parasite known as *Echinococcus granulosus*. It is one of the primary cause for illness and poverty especially for herders on the Qinghai–Tibet plateau, China. Meanwhile, the Qinghai–Tibet plateau has been a key area for echinococcosis control in China. Here in current study, we determined the seroprevalence of *E. granulosus* in ruminants on this region. A total of 2,730 serum samples (1,638 samples from yaks and 1,092 samples from sheep) were collected on the plateau during the period of 2017. The samples were assayed for *E. granulosus* antibodies by commercial enzyme-linked immunosorbent assay kits. Our results exhibited a prevalence percentage of 52.2% in Tibetan yaks and 38.2% in Tibetan sheep. Moreover, there was more chance of being infected with *E. granulosus* infection in old animals due to more exposure to contaminated sources of infection. However, no significant difference was observed. Furthermore, we observed that the rainfall and presence of several lakes has increased the risk of CE infection in yaks and sheep in the Qinghai, Qinglong, and Baingoin areas. Hence, with this investigation, it was possible to determine the frequency and distribution of CE in yaks and Tibetan sheep on the Qinghai-Tibet plateau, that laying the groundwork for its prevention and management.

Keywords: seroprevalence, *Echinococcus granulosus*, risk factors, yaks, Tibetan sheep

INTRODUCTION

Cystic echinococcosis (CE) is a livestock disease caused by a parasite called *Echinococcus granulosus*. It is transmitted by dogs, wolves, and foxes, causing different symptoms in different viscera or brain (1–3). Approximately 30 million livestock are infected with this globally distributed disease every year, causing more than 1.92 billion US dollars loss to the global animal husbandry (4, 5). Moreover, the health of livestock and herders is seriously endangered with the low development of breeding industry under the affect of CE. It is one of the main factors causing illness and making herders poor on the Qinghai–Tibet plateau. The Qinghai–Tibet plateau has been a key area for echinococcosis control in China.

E. granulosus is mainly found in low-lying moist areas and swamps (6, 7). The strategies to control the risk of *E. granulosus* are more important particularly in such areas, where humans and domestic livestock are in the same environment (8–12).

A number of diagnostic tests are available for the detection of *E. granulosus*, such as polymerase chain reaction, enzyme-linked immunosorbent assay (ELISA), indirect ELISA, and colloidal gold method (13–18). The ELISA approach is notable for its inexpensive cost, increased sensitivity, and specificity as compared to other methods, which often overlook infections with low parasitemia (14, 15).

In current research, we determined the seroprevalence of *E. granulosus* in ruminants using ELISA. With the investigation, the prevalence and distribution of CE were basically clarified in yaks and Tibetan sheep on the Qinghai–Tibet plateau, which provided a basis for the prevention and control of the disease.

MATERIALS AND METHODS

Information of Collecting Region

The Qinghai–Tibet plateau is located on the southwestern border of China and south-central Eurasia. It is the largest and highest plateau in China (latitude and longitude, 20°00'−39°47'N and 73°19'−104°47'E, respectively). The average altitude is above 4,000 m with a complex climate, low temperature, and a sufficient sunshine. There were more than 300 lakes within 10 km^2 on the plateau. Also, it is one of the important pastoral areas in China with abundant grassland (19).

Information of Sampled Animals

Yak is a unique bovine species on the Qinghai–Tibet plateau. More than 14 million yaks are mainly distributed on the Qinghai–Tibet plateau in China, while there is a small distribution in Afghanistan, India, and Pakistan. The yaks are necessary for herders because of the milk, wool, and meat (20, 21). Tibetan sheep is one of the three original varieties in China and the biggest proportion in livestock, with more than 30,000,000 sheep on the plateau (22).

Serum Samples

A total of 2,370 blood samples (1,638 samples from yaks, **Figure 1**; 1,092 samples from sheep, **Figure 2**) were collected during 2017 on Qinghai, Gansu, and Tibet, respectively. Age, sex, and region was the information that obtained for each animal, involving this study. Then serum of each animal was separated by centrifugation and stored at −20°C till analysis.

FIGURE 1 | Geographic distribution of yaks enrolled in study.

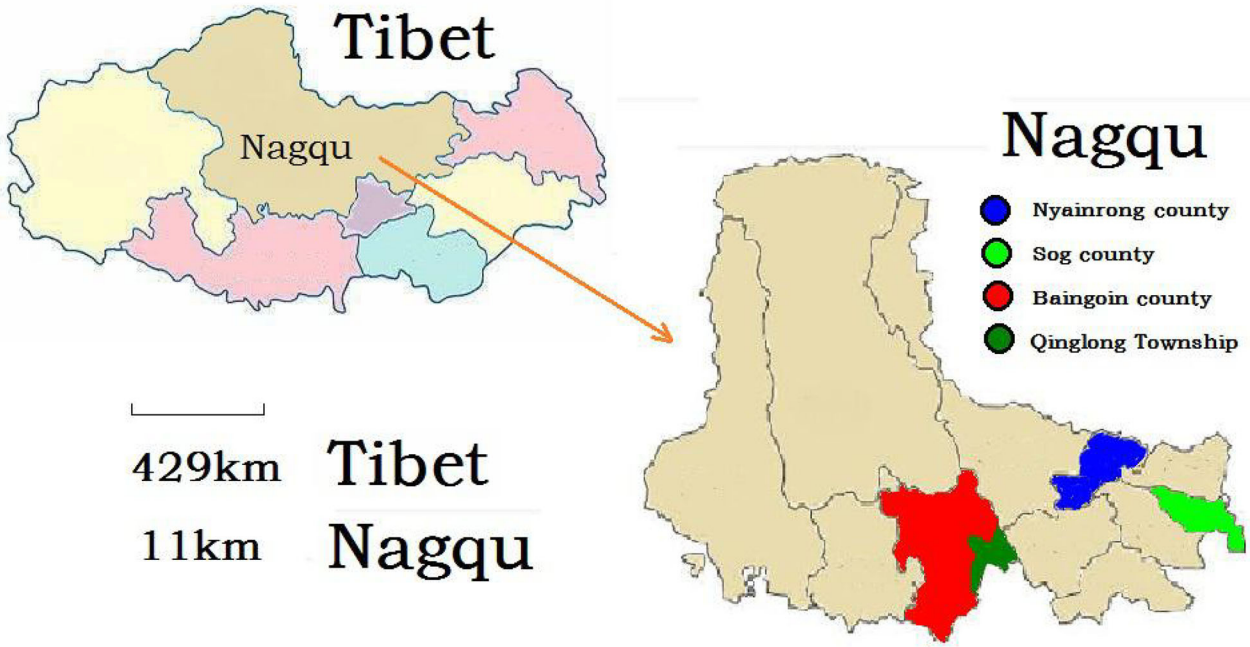

FIGURE 2 | Geographic distribution of Tibetan sheep enrolled in study.

Determination of Antibodies Against *E. granulosus*

All serum had been determined for anti-*E. granulosus* antibodies by using two commercial enzyme-linked immunosorbent kits (Jianlun Biological Pharmaceuticals Co., Ltd., Guangzhou China; Duoyu Biological Pharmaceuticals Co., Ltd., Shanghai, China) according to the manufacturer's instructions. The detailed method was consistent with the previous research (23).

RESULTS

A total of 855 of the 1,638 (52.2%) yaks were detected to have a CE infection, of which 328 (50.2%) were males and 527 (53.6%) were females. The prevalence values were 45.1, 64.3, and 49.5% on Tibet, Qinghai, and Gansu, respectively. While the prevalence ranged from 17.4 to 57.5% in different ages (**Table 1**).

In the current research, the more influencing risk factors were region and age according to logistic regression models. Qinghai yaks were considered to be 2.20 times of higher risk of being positive compared with Tibet yaks, whereas Gansu yaks were considered to be 1.19 times at higher risk of CE infection compared with Tibet yaks (**Table 1**). In different ages, yaks <1 year ≤2 years had 3.46 times higher risk of CE infection compared with yaks <0 years ≤1 year; both yaks of <2 years ≤4 years and >4 years (57.54%) had 5.19 times and 6.42 times higher risk of being positive, respectively, when compared with yaks <0 years ≤1 year (**Table 1**). Also, there was no significant difference between males and females for yaks (**Table 1**).

In our research, 1,092 serum samples of Tibetan sheep were tested, 38.2% were detected to be positive for *E. granulosus*, with the distribution of 25.3% (Sog county), 15.4% (Nyainrong), 54.4% (Qinglong), and 56.8% (Baingoin) (**Table 2**). Tibetan sheep from both Nyainrong and Sog county had a significantly lower risk of CE infection compared with that from Qinglong and Baingoin (**Table 2**). With regard to sex, there was a non-significant difference. However, the seroprevalence values were 25.7% (juveniles), 42.8% (sub-adults), and 50.7% (adults) (**Table 2**). The Tibetan sheep in sub-adults and adults had two times higher risk of CE infection in juveniles (**Table 2**).

DISCUSSION

Parasites have lived on Earth for as long as life has existed, and no species, whether animal or human, is exempt to parasites (24). *E. granulosus* had caused a tremendous economic loss and a severe public health risk in China as a foodborne neglected parasitic disease (25). More than seven million livestock are infected by CE yearly (8).

The seroprevalence of CE infection in yaks was 52.2% in our study, which was higher than the prevalence in the previous research in Turkey (41.1%), Greece (42%), and Ethiopia (27.6%), and significantly higher than the prevalence in Southern Brazil (13.7%) and Pakistan (13.46%) (3). Meanwhile, the previous investigation showed that the average infection rates of sheep decreased from 8.17% in 2012 to 3.68% by 2018 in the Western

TABLE 1 | Prevalence and risk factors of *Echinococcus granulosus* infection in yaks on Qinghai–Tibet plateau.

Variable	Category	No. tested	No. positive	% (95% CI)	*P*-value	OR (95% CI)
Region	Tibet	819	369	45.1 (41.6–48.5)	Reference	
	Qinghai	546	351	64.3 (60.1–68.3)	<0.001	2.20 (1.36–2.75)
	Gansu	273	135	49.5 (43.4–55.5)	0.207	1.19 (0.64–1.92)
Gender	Male	654	328	50.2 (43.6–54.1)	Reference	
	Female	984	527	53.6 (50.4–56.7)	0.177	1.15 (0.72–1.56)
Age	0 < year ≤ 1	109	19	17.4 (10.8–25.9)	Reference	
	1 < year ≤ 2	90	38	42.2 (31.9–53.1)	<0.001	3.46 (1.15–5.55)
	2 < year ≤ 4	570	298	52.3 (48.1–56.4)	<0.001	5.19 (4.11–6.32)
	Year > 4	869	500	57.5 (54.2–60.9)	<0.001	6.42 (4.09–8.26)
Total		1,638	855	52.2 (49.7–54.6)		

TABLE 2 | Prevalence and risk factors of *Echinococcus granulosus* infection in Tibetan sheep on Qinghai–Tibet plateau.

Variable	Category	No. tested	No. positive	% (95% CI)	*P*-value	OR (95% CI)
Region	Sog County	273	69	25.3 (20.2–30.9)	0.004	1.86 (0.35–3.82)
	Nyainrong County	273	42	15.4 (11.3–20.2)	Reference	
	Qinglong Township	171	93	54.4 (46.6–62.0)	<0.001	6.56 (5.10–7.24)
	Baingoin County	375	213	56.8 (51.6–61.9)	<0.001	7.23 (6.09–8.20)
Gender	Male	616	249	40.4 (36.5–44.4)	Reference	
	Female	476	168	35.3 (31.0–39.8)	0.084	1.24 (0.97–1.59)
Age	0 < year ≤ 1	393	101	25.7 (21.4–30.3)	Reference	
	1 < year ≤ 2	484	207	42.8 (38.3–47.3)	<0.001	2.16 (2.35–2.62)
	Year > 2	215	109	50.7 (43.8–57.6)	<0.001	2.97 (2.24–3.48)
Total		1,092	417	38.2 (35.3–41.1)		

Sichuan Plateau (26). It was also significantly lower than the seroprevalence of CE infection in Tibetan sheep in our research (38.2%).

The previous study identified that the prevalence of CE was bound with environment culture, exerting complicated and combined effects (27). Meanwhile, the low temperatures could be a possible reason for the seroprevalence of CE. The Qinghai–Tibet plateau had a low surface temperature for years and has been a suitable place for CE due to its high altitude (28, 29). On the other hand, the stagnant economy is one of the main reason for CE. In rural areas, people had no awareness to undergo a personal medical checkup before the illness. People could be infected easily by echinococcosis due to the lack of education, information, and low sanitation conditions (30–33). A recent study showed that the plateau is the key area of CE in China (3).

In our research, the analysis showed that *E. granulosus* infection is closely related to region and age of animals. Due to the rainfall and many lakes, the ruminants had a higher risk of CE infection in Qinghai province, Qinglong, and Baingoin (23). In addition, the results suggested that old animals had more chances to acquire *E. granulosus* infection due to more exposure to the source of infection. However, no significant difference was observed in sex. Therefore, persons had a much higher risk of *E. granulosus* infection by frequent exposure to infected animals.

CONCLUSION

Our research showed the high seroprevalence rate of *E. granulosus* infection in ruminants on the Qinghai–Tibet plateau in China. It was indicated that *E. granulosus* could cross-transmit between the environment and host, including human beings. Therefore, effective measures must be taken to control the spread of *E. granulosus* by considering the role of various factors. Hence, our study might be useful to wiping off such transmissible disease on Qinghai–Tibet plateau of China.

DATA AVAILABILITY STATEMENT

The original contributions presented in the study are included in the article/supplementary material, further inquiries can be directed to the corresponding author/s.

ETHICS STATEMENT

Blood samples were collected under the permission of the relevant institutions. All procedures were approved and performed by Laboratory Animals Research Centre of Hubei, Qinghai, Gansu and Tibet in China, and the Ethics Committee of Huazhong Agricultural University, China (Permit number: 4200695757). All animal experiments and procedures were conducted under the relevant procedures of Proclamation of

the Standing Committee of Hubei People's Congress (PSCH No.5), China.

AUTHOR CONTRIBUTIONS

XG, YB, and JL conceived and designed the study. LX, RS, SZha, XK, and CN collected the sample. XG, ZZ, and SZho executed the experiment and analyzed the samples. XG, CQ, and KL analyzed the data. XG and LX finished the first draft. MK revised the manuscript. All authors interpreted the data, critically revised the manuscript for important intellectual contents, and approved the final version.

FUNDING

This study was supported by the Chinese Agricultural Research Systems (CARS-37) and the Key Research and Development Program of Tibet Autonomous Region (XZ202001ZY0044N).

REFERENCES

1. Gavidia CM, Gonzalez AE, Barron EA, Ninaquispe B, Llamosas M, Verastegui MR, et al. Evaluation of oxfendazole, praziquantel and albendazole against Cystic Echinococcosis: a randomized clinical trial in naturally infected sheep. *PLoS Negl Trop Dis.* (2010) 4:e616. doi: 10.1371/journal.pntd.0000616
2. Schurer JM, Rafferty E, Farag M, Zeng W, Jenkins EJ. Echinococcosis: an economic evaluation of a veterinary public health intervention in rural Canada. *PLoS Negl Trop Dis.* (2015) 9:e0003883. doi: 10.1371/journal.pntd.0003883
3. Li K, Zhang L, Zhang H, Lei Z, Luo H, Mehmood K, et al. Epidemiological investigation and risk factors of *Echinococcus granulosus* in yaks (*Bos grunniens*), Tibetan pigs and Tibetans on Qinghai Tibetan plateau. *Acta Trop.* (2017) 173:147. doi: 10.1016/j.actatropica.2017.06.019
4. Hélène C, Francisco JBR., José RS, Benner CT, Benito A, Fernández-Crespo JC, et al. Cystic echinococcosis in the province of Álava, North Spain: the monetary burden of a disease no longer under surveillance. *PLoS Negl Trop Dis.* (2014) 8:e3069. doi: 10.1371/journal.pntd.0003069
5. Qian MB, Abelaridder B, Wu WP, Zhou XN. Combating echinococcosis in China: strengthening the research and development. *Infect Dis Poverty.* (2017) 6:161. doi: 10.1186/s40249-017-0374-3
6. Song MX, Zhang LX. *Veterinary Parasitology*. Beijing: Science Press (2009).
7. Maharana BR, Kumar B, Allaie IM. *Veterinary Parasitology: A Complete Objective Type Guide* Kolkata, West Bengal: Kalyani Publisers (2017).
8. Budke CM, Deplazes P, Torgerson PR. Global socioeconomic impact of cystic echinococcosis. *Emerg Infect Dis.* (2006) 12:296–303. doi: 10.3201/eid1202.050499
9. Torgerson PR, Krista K, Mellissa M. The global burden of alveolar echinococcosis. *PLoS Negl Trop Dis.* (2010) 4:e722. doi: 10.1371/journal.pntd.0000722
10. Wang LY, Wu WP, Zhu XH. The endemic status of hydatidosis in China from 2004 to 2008. *Chin J Zoonoses.* (2010) 26:699–702.
11. Wang Q, Huang Y, Huang L, Yu W, He W, Zhong B, et al. Review of risk factors for human echinococcosis prevalence on the Qinghai-Tibet plateau, China: a prospective for control options. *Infect Dis Poverty.* (2014) 3:3. doi: 10.1186/2049-9957-3-3
12. Budke CM, Campos-Ponce M, Qian W, Torgerson PR. A canine purgation study and risk factor analysis for echinococcosis in a high endemic region of the Tibetan plateau. *Vet Parasitol.* (2005) 127:43–9. doi: 10.1016/j.vetpar.2004.08.024
13. Ris DR, Hamel KL, Mackle ZM. Use of two polysaccharide antigens in ELISA for the detection of antibodies to Echinococcus granulosus in sheep sera. *Res Vet Sci.* (1987) 43:257–63. doi: 10.1016/S0034-5288(18)30784-7
14. Simsek S, Balkaya I, Ciftci AT, Utuk AE. Molecular discrimination of sheep and cattle isolates of *Echinococcus granulosus* by SSCP and conventional PCR in Turkey. *Vet Parasitol.* (2011) 178:367–9. doi: 10.1016/j.vetpar.2011.01.033
15. Osman AMA, Aradaib IE, Ashmaig ALK, Gameel AA. Detection and differentiation of *Echinococcus granulosus*-complex using a simple PCR-based assay. *Int J Trop Med.* (2009) 4:21–6. Available online at: http://www.medwelljournals.com/abstract/?doi=ijtmed.2009.21.26
16. Hjalmar V. Double-antibody sandwich ELISA using biotinylated antibodies for the detection of *Echinococcus granulosus*, coproantigens in dogs. *Acta Trop.* (2005) 95:9–15. doi: 10.1016/j.actatropica.2005.03.005
17. Zhuo X, Yu Y, Chen X, Zhang Z, Yang Y, Du A. Development of a colloidal gold immunochromatographic strip based on HSP70 for the rapid detection of *Echinococcus granulosus* in sheep. *Vet Parasitol.* (2017) 240:34. doi: 10.1016/j.vetpar.2017.03.027
18. Gao JS, Zhang XC, Liu Y, Kou JH, Zhang Z, Li JH, et al. Preparation of colloidal gold strip for detection of *Echinococcus granulosus* infection in dogs. *Chin J Biol.* (2018) 31:271–5. doi: 10.13200/j.cnki.cjb.002119
19. Zhang XX, Feng SY, Ma JG, Zheng WB, Yin MY, Qin SY, et al. Seroprevalence and risk factors of fascioliasis in yaks, Bos grunniens, from three counties of Gansu province, China. *Korean J Parasitol.* (2017) 55:89–93. doi: 10.3347/kjp.2017.55.1.89
20. Li K, Gao JF, Shahzad M, Han Z, Nabi F, Liu M, et al. Seroprevalence of *Toxoplasma gondii* infection in yaks (*Bos grunniens*) on the Qinghai-Tibetan Plateau of China. *Vet Parasitol.* (2014) 205:354–6. doi: 10.1016/j.vetpar.2014.07.014
21. Li JK, Li K, Shahzad M, Han Z, Nabi F, Gao J, et al. Seroprevalence of Bluetongue virus in domestic yaks (*Bos grunniens*) in Tibetan regions of China based on circulating antibodies. *Trop Anim Health Prod.* (2015) 47:1221–3. doi: 10.1007/s11250-015-0853-0
22. Xin GS, Long RJ, Guo XS, Irvine J, Ding L. Blood mineral status of grazing Tibetan sheep in the Northeast of the Qinghai–Tibetan plateau. *Livest Sci.* (2011) 136:102–7. doi: 10.1016/j.livsci.2010.08.007
23. Gao X, Zhang L, Tong X, Zhang H, Mehmood K, Jiang X, et al. Epidemiological survey of fasciolosis in yaks and sheep living on the Qinghai-Tibet plateau, China. *Acta Trop.* (2020) 201:105212. doi: 10.1016/j.actatropica.2019.105212
24. Mitchell PD. Human parasites in the Roman World: health consequences of conquering an empire. *Parasitology.* (2016) 144:48–58. doi: 10.1017/S0031182015001651
25. Da SA. Human echinococcosis: a neglected disease. *Gastroenterol Res Pract.* (2010) 2010:583297. doi: 10.1155/2010/583297
26. Yuan DB, Hao L, Yin NC, Zhou MZ, Yang AG, Zeng ZX, et al. Epidemiological survey of hydatid disease of livestock in the western Sichuan Plateau from 2012 to 2018. *Chin Vet J.* (2020) 256:20–21+24.
27. Huang D, Li RD, Qiu J, Sun X, Yuan R, Shi Y, et al. Geographical environment factors and risk mapping of human Cystic Echinococcosis in Western China. *Int J Environ Res Public Health.* (2018) 15:1729. doi: 10.3390/ijerph15081729
28. Eckert J, Gemmell MA, Meslin FX, Pawlowski ZS. *WHO/OIE Manual on Echinococcosis in Humans and Animals: A Public Health Problem of Global Concern.* : Paris: World Organisation for Animal Health; Geneva: World Health Organization (2001). p. 265.
29. Hu HH, Wu PW, Guan YY, Wang LY, Wang Q, Cai HX, et al. Village-based multidisciplinary study on factors affecting the intensity of Cystic *Echinococcosis* in an endemic region of the Tibetan plateau, China. *Epidemiol Infect.* (2014) 142:1214–20. doi: 10.1017/S0950268813002124
30. Yang YR, Craig PS, Sun T. Echinococcosis in Ningxia Hui Autonomous Region, northwest China. *Trans R Soc Trop Med Hyg.* (2008) 102:319–28. doi: 10.1016/j.trstmh.2008.01.007
31. Possenti A, Manzanoromán R, Sánchezovejero C, Boufana B, La Torre G, Siles-Lucas M, et al. Potential risk factors associated with human Cystic *Echinococcosis*: systematic review and meta-analysis.

PLoS Negl Trop Dis. (2016) 10:e0005114. doi: 10.1371/journal.pntd.0005114

32. Merino V, Westgard CM, Bayer AM, García PJ. Knowledge, attitudes, and practices regarding Cystic *Echinococcosis* and sheep herding in Peru: a mixed-methods approach. *BMC Vet Res.* (2017) 13:213. doi: 10.1186/s12917-017-1130-4
33. Ye HE, Yin J. Analysis for epidemiological factors of echinococcosis. *China Tropical Medicine.* (2017) 17:418–20. doi: 10.13604/j.cnki.46-1064/r.2017.04.25

Conflict of Interest: The authors declare that the research was conducted in the absence of any commercial or financial relationships that could be construed as a potential conflict of interest.

Publisher's Note: All claims expressed in this article are solely those of the authors and do not necessarily represent those of their affiliated organizations, or those of the publisher, the editors and the reviewers. Any product that may be evaluated in this article, or claim that may be made by its manufacturer, is not guaranteed or endorsed by the publisher.

frontiers in Veterinary Science

ORIGINAL RESEARCH
published: 24 March 2022
doi: 10.3389/fvets.2022.852407

Telocytes and Their Structural Relationships With the Sperm Storage Tube and Surrounding Cell Types in the Utero-Vaginal Junction of the Chicken

Xudong Zhu[1†], Qi Wang[2†], Piotr Pawlicki[3], Ziyu Wang[4], Bernadetta Pawlicka[5], Xiangfei Meng[2], Yongchao Feng[2] and Ping Yang[2]*

[1] College of Sciences, Nanjing Agricultural University, Nanjing, China, [2] MOE Joint International Research Laboratory of Animal Health and Food Safety, College of Veterinary Medicine, Nanjing Agricultural University, Nanjing, China, [3] Center of Experimental and Innovative Medicine, University of Agriculture in Krakow, Krakow, Poland, [4] College of Animal Science and Technology, Nanjing Agricultural University, Nanjing, China, [5] Laboratory of Genetics and Evolutionism, Institute of Zoology and Biomedical Research, Jagiellonian University, Krakow, Poland

OPEN ACCESS

Edited by:
Fazul Nabi,
Lasbela University of Agriculture, Water and Marine Sciences, Pakistan

Reviewed by:
Abdul Haseeb,
University of Poonch Rawalakot, Pakistan
Haitao Nie,
Anhui Normal University, China

***Correspondence:**
Ping Yang
yangping@njau.edu.cn

[†]These authors have contributed equally to this work

Specialty section:
This article was submitted to Comparative and Clinical Medicine, a section of the journal Frontiers in Veterinary Science

Received: *11 January 2022*
Accepted: *24 January 2022*
Published: *24 March 2022*

Citation:
Zhu X, Wang Q, Pawlicki P, Wang Z, Pawlicka B, Meng X, Feng Y and Yang P (2022) Telocytes and Their Structural Relationships With the Sperm Storage Tube and Surrounding Cell Types in the Utero-Vaginal Junction of the Chicken. Front. Vet. Sci. 9:852407. doi: 10.3389/fvets.2022.852407

Telocytes (TCs) are a new type of mesenchymal cells that have been discovered recently in many organs and tissues. However, studies of TCs in the avian reproductive system are still at the beginning. Chickens are one of the world's most popular domesticated animals, providing inexpensive but valuable proteins and nutrients from chickens and eggs to nourish the human bodies. Chickens have important scientific value; thus, understanding the reproductive system regulations seems to be important. The utero-vaginal junction is involved in the regulation of sperm storage. The sperm storage tube (SST) in the utero-vaginal junction stores sperm. The purpose of this study was to investigate the existence of TCs in the utero-vaginal junction of the chicken, and their structural relationships with the sperm storage tube and surrounding cell types. We studied the morphology, ultrastructure, and immune characterization of TCs.

Methods: The utero-vaginal junction of 4-month-old healthy adult chickens ($n = 10$) were used for Masson's staining, fluorescent *in situ* hybridization technique (FISH), and transmission electron microscopy (TEM) analysis. The results showed that TCs were present in the utero-vaginal junction. TCs appear as CD34 immunopositive and C-kit immunopositive. They were identified especially *via* small-body and long-protrusion telopodes (Tps) containing Podomers (Pm) and Podoms (Pd). The Tps were bent, folded, and intertwined with each other, sometimes in the shape of a labyrinth. The Tps were embedded between collagen fiber bundles, smooth muscle bundles, and around blood vessels and releasing vesicles. TCs surround these glands, forming heteromorphic cell connections with surrounding lymphocytes and plasma cells, smooth muscle cells, blood vessels, collagen fibers, and fibroblast-formed homotypic or allotypic connections in a complex three-dimensional network structure. This study provides a morphological basis for the possible role of TCs in regulating the utero-vaginal junction physiological role and in intercellular communication.

Keywords: telocytes (TCs), chicken, utero-vaginal junction, sperm storage tube, ultrastructure

INTRODUCTION

Telocytes (TCs) are a new type of mesenchymal cells named by Romanian Professor Popescu and Italian Professor Faussone in 2010. This cell type was first discovered in the human pancreas by Popescu and his team in 2005 because its form is similar to the interstitial cells of Cajal (ICCs) in the digestive tract. He speculated that these cells may be a form of ICC, called simple Cajal interstitial cells (interstitial Cajal like cells; ICLCs) (1). In 2008, Pieri et al. reported that ICLCs are completely different from ICCs in morphological structure, immunophenotype, and distribution characteristics by using electron microscopy, immunofluorescence, and immunohistochemistry techniques. Popescu keenly recognized that ICLCs are a new type of mesenchymal cell that had not been discovered. In 2010, Popescu and Faussone reported that TCs have extremely long protrusions, which are important markers to distinguish TCs from ICCs, fibroblasts, and dendritic cells. Because of their special shape, ICLCs were initially renamed to TCs in 2010 (2). Telocytes have a small oval body containing a nucleus surrounded by a small amount of cytoplasm. The nucleus is large and contains clusters of heterochromatins distributed over the nuclear membrane. There are 2–6 extremely long and thin (ranging from tens to hundreds of microns in length with internal diameters $< 0.2\,\mu m$) protrusions showing alternation of expanded segments (Pd) and elongated segments (Pm) in the shape of rosary beads. The enlarged segment contains vesicles, mitochondria, and rough endoplasmic reticulum, while the elongated segment rarely contains organelles (3).

Researchers have studied TCs in various organs of mammals, such as the heart, oviduct, small intestine, skin, myometrium, testis, and esophagus (4–8), but only a few studies have been performed on the chicken oviduct. TCs can be labeled by multiple antibodies, such as CD34, vimentin, c-kit, caveolin-1, and platelet-derived growth factor (PDGFR) receptor (9–17), but their immunophenotypes varied by species and organ. In the heart, TCs express CD34, CD28, vimentin, PDGFR-α, Sca-1, and c-kit but are negative for the hematopoietic marker CD45 (7, 13). As CD28 and vimentin are also expressed by cardiac mesenchymal stem cells, it is speculated that TCs may originate from differentiated cardiac mesenchymal stem cells. In the lungs, TCs are positive for c-kit, CD34, and vascular endothelial growth factor, suggesting that they may be involved in angiogenesis (18). In the female reproductive system, TCs express CD34, c-kit, PDGFR-α, T-type/the Ca^{2+} channel, and estrogen and progesterone receptors (7, 19). However, until today no single marker specific for TCs has been found; the immunophenotype of TCs is heterogeneous and it is generally believed that reliable immune markers for TCs include CD34 and PDGFR-α, double CD34, and PDGFR-α, or a double marker based on CD34 and PDGFR-α (2). The functions of TCs are less understood. TCs extend extremely long protrusions to form multiple junction points through homotypic and heterotypic junctions and a complex three-dimensional (3D) network structure in stromal tissue. Homotypic junctions are contacts between different TC processes, and heterotypic junctions are contacts between TCs and blood vessels and adjacent cells (such as cardiomyocytes, stem cells, fibroblasts, and immune cells) (2, 20). The structure of a cell determines its function, and the unique shape of TCs is linked with a variety of functional roles. TCs play roles in cell signaling, mechanical support, immune surveillance, tissue repair, and regeneration, and are potentially involved in a variety of diseases and physiological processes (21).

However, research on TCs in the female reproductive system of birds is still at the beginning. The utero-vaginal junction is involved in the regulation of sperm storage. The sperm storage tube in the utero-vaginal junction stores sperm. The fowl and mammalian oviducts are similar in that they are divided into a mucous membrane, a muscular layer, and a serosal layer (outer membrane). In contrast, the fowl oviduct is a unilateral organ, coiling in the abdominal cavity on the left side, and composed of the infundibulum, magnum, isthmus, uterine, and vagina. The Japanese scholar Fujii reported in 1963 that the oviduct and uterus and the integration of the vaginal mucosa lamina propria gland can store sperm (22). The oviduct at the front end of the vagina is referred to as the vagina gland and is a fine tubular sperm gland or sperm storage tube (23). The sperm storage tube is a tubular gland surrounded by a single row of columnar epithelial cells and is distributed in the lamina propria of the mucosa. The tubular gland opens on the surface of the longitudinal mucosal folds at the utero-vaginal junction. The opening is surrounded by pseudostratified columnar ciliated epithelium, and the gland is surrounded by loose connective tissue. This study explores the distribution and ultrastructure of TCs in the utero-vaginal junction, as well as the tissue structure and microenvironment of the junction with the participation of TCs and the particular spatial relationships with neighboring cells. This study will fill in the TC gaps in chicken oviduct research and provide a morphological basis for the possible role of TCs in regulating the utero-vaginal junction physiological role and in intercellular communication.

MATERIALS AND METHODS

Animals

Sample

Ten healthy adult laying chickens, 4 months of age, weighing 2.0–2.5 kg per chicken were used in this study. The feed fed was commercial adult broiler feed (Chengdu New Hope Group, China). Healthy adult chickens were kept in a temperature-controlled room with natural light ($20 \pm 1°C$) (light/dark period, 12/12 h), with free access to food and water. The chickens were kept and observed for 7 days. For sample collection, the birds were euthanized by cervical dislocation after intravenous administration of 3% sodium pentobarbital. The left oviduct was extracted immediately. The utero-vaginal junction was taken and fixed in 2.5% glutaraldehyde for transmission electron microscopy method. The utero-vaginal junction was fixed in 4% paraformaldehyde/PBS overnight for Masson staining. The utero-vaginal junction was fixed in the 4% paraformaldehyde/DEPC (G1113, Servicebio, Wuhan, China) above 12 h for fluorescent *in situ* hybridization. Tissue samples were dehydrated in a series of graded concentration ethanol (75, 85, 95, 95, 100, and 100%) (100092683, Sinopharm Chemical

Reagent Co., Ltd., Shanghai, China). Tissue samples were first embedded and made into paraffin wax blocks, and then tissue sections were cut into 5 μm. Sample preparation was conducted according to accepted international standards.

Masson Staining

Tissue sections were dewaxed, stained with Weigert ferroxylin staining solution, and differentiated with acidic ethanol differentiation solution. After sections were washed with water, the Masson blue solution returned to blue, followed by the lichunsin fuchsin staining solution, and then washed with molybdenum phosphomolybdic acid solution and the prepared weak acid working solution. Sections were dyed in aniline blue solution and washed in weak acid working solution. Dehydration was performed in ethanol and xylene (100092683, Sinopharm Chemical Reagent Co., Ltd.) and then cover-slipped (Masson's Trichrome Stain Kit; G1340; Solarbio, Beijing, China). The stained sections were analyzed using a light microscope (BX53; Olympus, Tokyo, Japan) equipped with a camera (DP73; Olympus).

Fluorescent *in situ* Hybridization Technique

For FISH, firstly, the gene sequence of chicken CD34 and C-kit was obtained from GenBank, and the GenBank login number was GI: 2024484067(CD34), 303532(C-kit); the DNA STAR software was used to compare it with CD34 and C-kit gene sequences of other species to find the homologous sequence. BLAST analysis was performed on the NCBI website based on chicken the genome database to confirm the specificity of the homologous sequence, and then a specific reverse-phase three-oligonucleotide probe was designed. Fluorescence probe CD34 and C-Kit were synthesized by Wuhan Servicebio Technology Co., Ltd. The tissue sections were dewaxed, washed in DEPC dilution, followed by retrieval of the antigen epitope, and naturally cooled. Add proteinase K (20 μg/ml) (G1205, Servicebio, Wuhan, China) working solution to cover objectives and incubate at 37°C for 30 min. Wash in pure water, then wash three times in PBS (pH 7.4) (G0002, Servicebio, Wuhan, China) on a Rocker device, 5 min each. Add pre-hybridization solution to each section and incubate for 1 h at 37°C. Remove the pre-hybridization solution, add the fluorescence probe CD34 and C-kit hybridization solution with a concentration of 0.25 μg/ml, and incubate the section in a humidity chamber and hybridize overnight at 42°C. Remove the hybridization solution. Wash sections in 2× SSC (G3016-4, Servicebio, Wuhan, China) for 10 min at 37°C. Wash sections in 1× SSC two times for 5 min each at 37°C, and wash in 0.5× SSC for 10 min at room temperature. Fluorescent staining was protected from light and sections were mounted with a mounting medium with 4′,6-diamidino-2-phenylindole (DAPI) (catalog no. AR1176; Boster Biotechnology, Wuhan, China). The sections were examined using a luminescence microscope (BX53; Olympus, Tokyo, Japan) equipped with a camera (DP73; Olympus).

Transmission Electron Microscopy

Small sections of fresh tissue (1 mm^3) were fixed in 2.5% glutaraldehyde PBS solution pre-cooled overnight at 4°C. Tissue fragments were then rinsed with 0.01 M PBS solution (pH = 7.4) and then post-fixed with 1% osmium tetroxide at room temperature for 1 h (Polysciences Inc., Warrington, PA, USA). Dehydration was done in ethanol; the material was embedded in Epon812 epoxy resin and polymerized at 60°C for 3 days. After the careful orientation of the 1-μm semi-thin section, the ultrathin sections (50 nm) were prepared and attached to the copper net. The ultrathin sections were stained with 1% uranyl acetate for 10 min and Reynold's lead citrate for 5 min. Ultrathin sections were analyzed with a Hitachi H-7650 transmission electron microscope (Japan).

RESULTS

General Histology of the Utero-Vaginal Junction of the Chicken

The collagen fibers were stained in blue, and the muscle fibers were stained in red by Masson's staining. Masson's staining revealed the mucosal, muscular, and serosal layers from inside to outside the utero-vaginal junction. The free surface of the mucosal epithelium had movable and dense cilia, so the mucosal epithelium was a pseudostratified columnar ciliated epithelium. The mucosal epithelial cells were well-developed, consisting of columnar ciliated cells and a large number of secretory cells. A large number of glands were present in the lamina propria of the mucosa. Sparse and scattered collagen fibers were observed in the lamina propria. Collagen fibers are also embedded in smooth muscle (**Figure 1A**). However, the number of collagen fibers in the uterine-vaginal junction is less than in other parts of the chicken oviduct. The blood vessels contained a large number of red blood cells and were surrounded by a large number of collagen fibers (**Figures 1C,D**). The sperm storage tube existed between the collagen fibers, most of which were in the lamina propria, close to the mucosal epithelium (**Figure 1A**, black triangular arrow; **Figure 1B**, wavy arrow). The sperm storage tube was mostly round or oval. They were monolayer tubular glands surrounded by conical cells or monolayer columnar epithelium. The glands opened in the mucosal epithelium and were mainly distributed at the edge of the mucosal fold. Several glandular cells were close by but arranged irregularly. The gland was generally composed of 15–20 glandular cells.

FISH Analysis of Telocytes in Chicken Utero-Vaginal Junction

Chickens' utero-vaginal junction TCs were CD34/C-kit positive (**Figure 2**). The CD34/C-kit-positive reaction was mainly expressed in the lamina propria of the mucosal layer at the junction of the utero-vaginal junction and vagina. CD34/C-kit-positive cells were present around the subepithelial sperm storage tube and were attached to the peripheral glands – prolongations with dichotomous branching that bears spindle-shaped or cone-shaped cells with nucleus (**Figures 2A–C**, a–c). Due to the lack of commercial poultry antibodies on the market, we further identified TCs at the utero-vaginal junction using the "gold standard" (TEM) for identifying TCs.

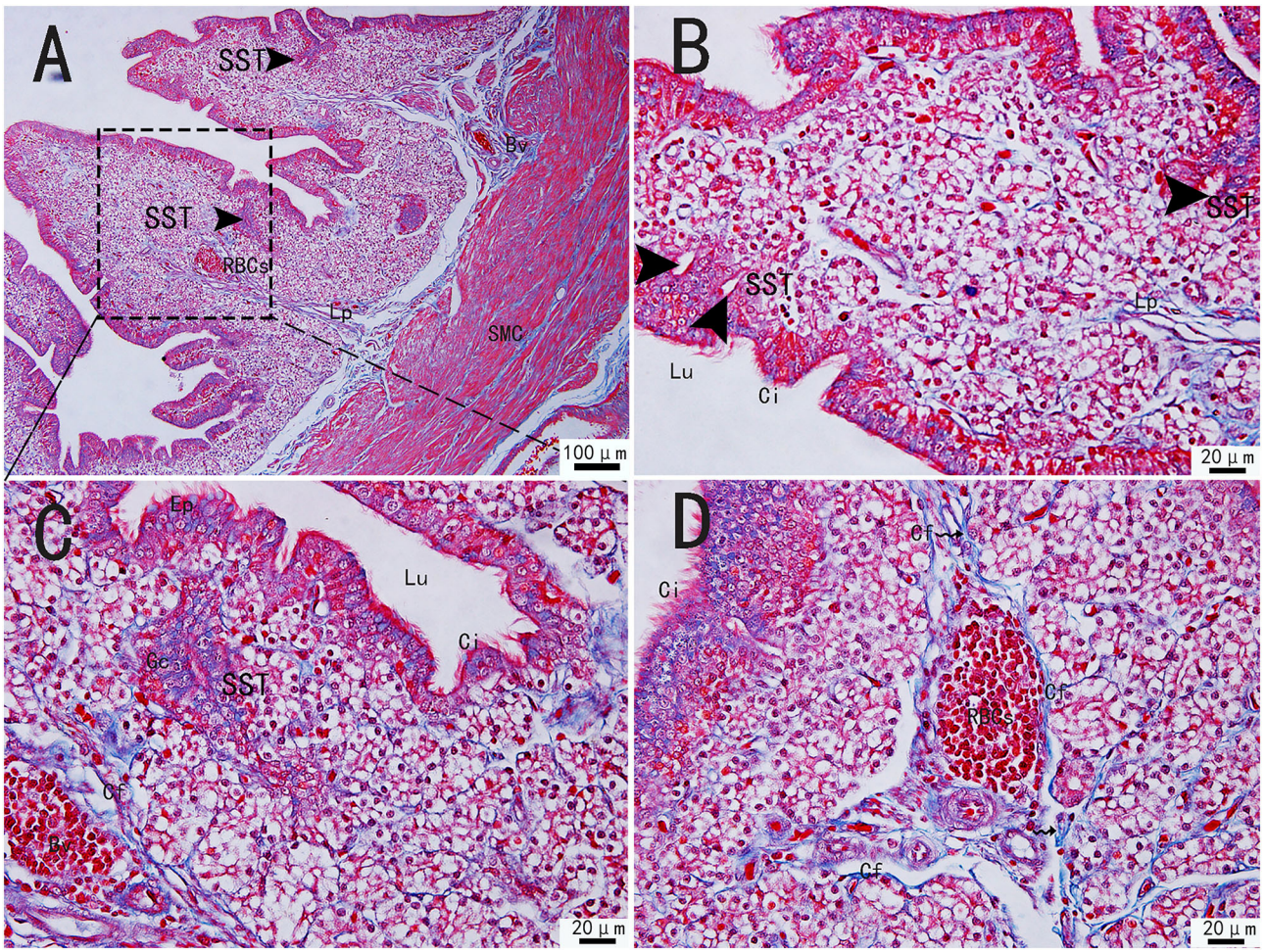

FIGURE 1 | Morphological structure of the uterine-vaginal junction of the oviduct in chicken by Masson's staining. **(C)** The enlargement of the area marked by **(A)** dotted box. The sperm storage tube existed between the collagen fibers **(B)**. The blood vessels contained a large number of red blood cells and were surrounded by a large number of collagen fibers **(D)**. SMC, Smooth muscle; Lp, lamina propria; Ep, Epithelial cells; SST, Sperm storage tube (black triangular arrow); Gc, Gland cell; Bv, blood vessel; Ci, cilia; RBCs, red blood cells; Cf, Collagen fiber; Lu, lumen. Scale bar **(A)** = 100 μm; Scale bar **(B–D)** = 20 μm.

Ultrastructure of Telocytes in the Utero-Vaginal Junction of Chicken

Transmission electron microscopy (TEM) showed that TCs were present in both the muscularis and lamina propria of the utero-vaginal junction and had a typical TCs cell structure (**Figures 3–7**). The muscularis layer of the utero-vaginal junction was well developed, and TCs were observed in the interstitial spaces between the smooth muscle bundles (**Figure 3**). The Tps were slender and rosary shaped with alternating enlarged and elongated segments (**Figure 3A**). The enlarged segments contained abundant mitochondria, rough endoplasmic reticulum, and vesicles, whereas few organelles were present in the elongated segments (**Figures 3B–D**). The TCs cell body is small and spindle-shaped, with a spindle or oval nucleus with protrusions extending tens or even hundreds of microns long (**Figures 3–7**). TCs are located around the gland (**Figures 4A,B**, **6A,B,E**), embedded in collagen fibers (**Figures 4E,F**), with a long fusiform nucleus and a long labyrinth of Tp surrounded by clearly visible vesicles of varying sizes (**Figures 4C,D**), as well as synthetic but unreleased vesicles in Tps. The elongated protrusions allowed the TCs to contact surrounding TCs, sperm storage tube, smooth muscle cells, blood vessels, plasma cells, potential stem cells, and lymphocytes to form homomorphic or heteromorphic connections and a complex 3D network structure, which play a role in information communication and transmission (**Figures 4–7**). TCs form a typical cell connection with surrounding plasma and lymphocyte cells through Tps, and there are a large number of mitochondria in the Podom (**Figures 5B,D**). Around the blood vessels, TCs form homotypic cell connections *via* Tps (**Figures 7B–E**).

DISCUSSION

Since TCs were discovered by Professor Popescu in 2005, they have attracted extensive attention from many researchers. The markers expressed in TCs vary from tissue to tissue, and even

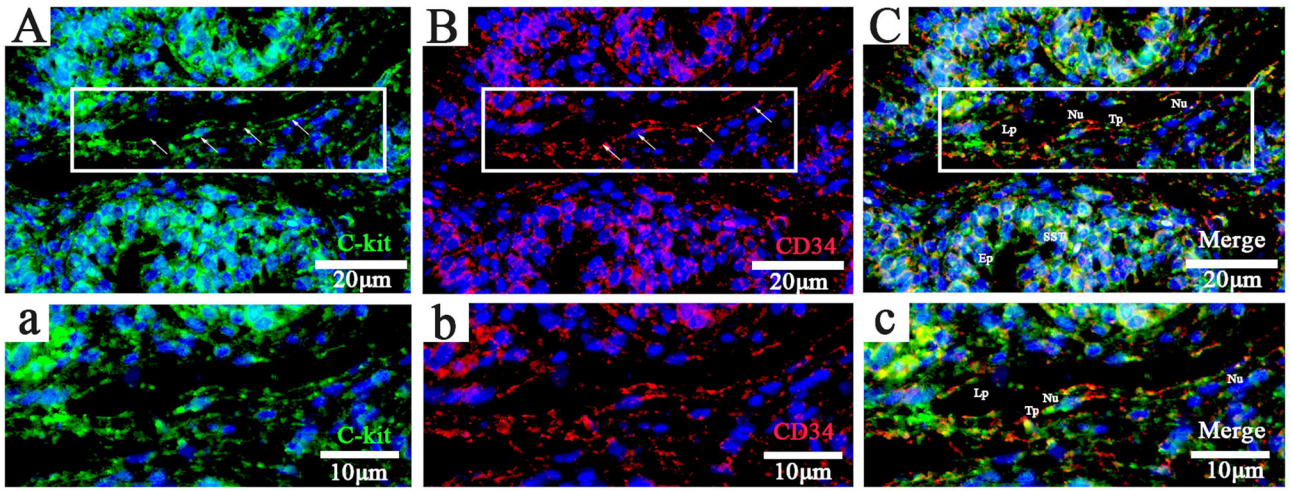

FIGURE 2 | Fluorescence probe CD34/C-kit FISH in the uterine-vaginal junction of the oviduct in chicken. (**A–C**, a-c; Panels a, b, and c are enlarged versions of Panels A, B, and C, respectively: C-kit$^+$, CD34$^+$, and merged). DAPI (blue), C-kit$^+$(green),CD34$^+$(red). Lp, lamina propria; Nu, nuclear; SST, sperm storage tube; Tp, telopode (arrows); Ep, epithelial cells. Scale bar **(A–C)** = 20 μm; Scale bar (a-c) = 10 μm.

from cell to cell within the same tissue (2). It is difficult to observe the typical morphological characteristics of TCs under light microscope. So, TEM is the "gold standard" for identifying TCs and the only accurate method to identify TCs at present (24). Connections between TCs and homotypic or heterotypic cells can also be observed using TEM (25).

In this study, a combination of TEM and FISH (CD34 and C-kit) was used (16, 26) to reveal the existence of TCs at the utero-vaginal junction of the chicken for the first time. TCs at the utero-vaginal junction are consistent with previous studies. Chicken utero-vaginal junction TCs exhibited CD34 and C-kit immunopositive by FISH. TCs express CD34, which is frequently expressed in hematopoietic stem/progenitor cells. It is suggested that TC has the dryness and properties of undifferentiated cells. Morphologically, the TCs in the chicken utero-vaginal junction have a slender Tp and can also secrete vesicles, which is consistent with the structure of typical TCs.

Our TEM results show two or three slender Tps were observed on TEM. The number of Tps depended on the angle and position of the section, as all Tps cannot be completely present on a plane during sectioning (27, 28). These structures can only be observed by TEM, such as the identification criteria proposed by Professors Popescu and Faussone-Pellegrini (29). Masson's staining showed that the utero-vaginal junction was composed of glandular cells, epithelial cells, secretory cells, ciliary cells, collagen fiber bundles, smooth muscle cells, immunoreactive cells, and blood vessels. The secretory and ciliated cells produce tubular fluid and promote gamete transport, respectively (30). Masson's staining showed that the lamina propria of the utero-vaginal junction was thinner and had few collagen fibers. The number of TCs was positively correlated with the number of lamina propria cells, and there were fewer TCs in this part compared with other animals or tissues and organs. There are still some differences between avian and mammalian oviduct TCs. TCs were mainly distributed in the mucosa and muscular layer between smooth muscle fibers in the human oviduct (14), while TCs in the utero-vaginal junction of the chicken existed in the area below the epithelium and lamina propria, between collagen fibers and smooth muscle bundles, and around blood vessels and some glands.

The unique morphology and structure of TCs must allow for unique function. TCs may play a role in signaling between cells. The stroma is composed of cells that integrate all information from the blood vessels, nerves, the immune system, and stem cells through contact with the same or different cells (20). TCs use their elongated protrusions to form homotypic or heterotypic connections with adjacent cells (31) and produce a 3D network structure in the stroma. The blood vessels and glands in the utero-vaginal junction were surrounded by TCs, and also occurred between collagen fiber bundles and smooth muscle. The TCs formed homotypic and heterotypic connections with other TCs, potential stem cells, plasma cells, fibroblasts, and glandular cells. It has been proposed that TCs function in cell-to-cell communication by paracrine secretion of small molecules, or by the release of cellular vesicles that transport important macromolecules (3, 32–34). Cellular vesicles secreted by telocytes contain mainly proteins, lipids, microRNAs, mRNAs, and mitochondrial DNA (mtDNA), indicating a key role of these cells in intercellular signaling of the interstitial compartment, influencing the function and/or modification of post-transcriptional activity of neighboring cells (35, 36). In the heart, TCs release three types of extracellular vesicles, such as exosomes, microvesicles, and polyvesicles (31), but the exact functions of the vesicles after release remain to be determined. Scattered vesicles were detected around the TCs at the utero-vaginal junction, and vesicles used in the process of synthesis and secretion by TCs were also present, providing morphological support for information communication between

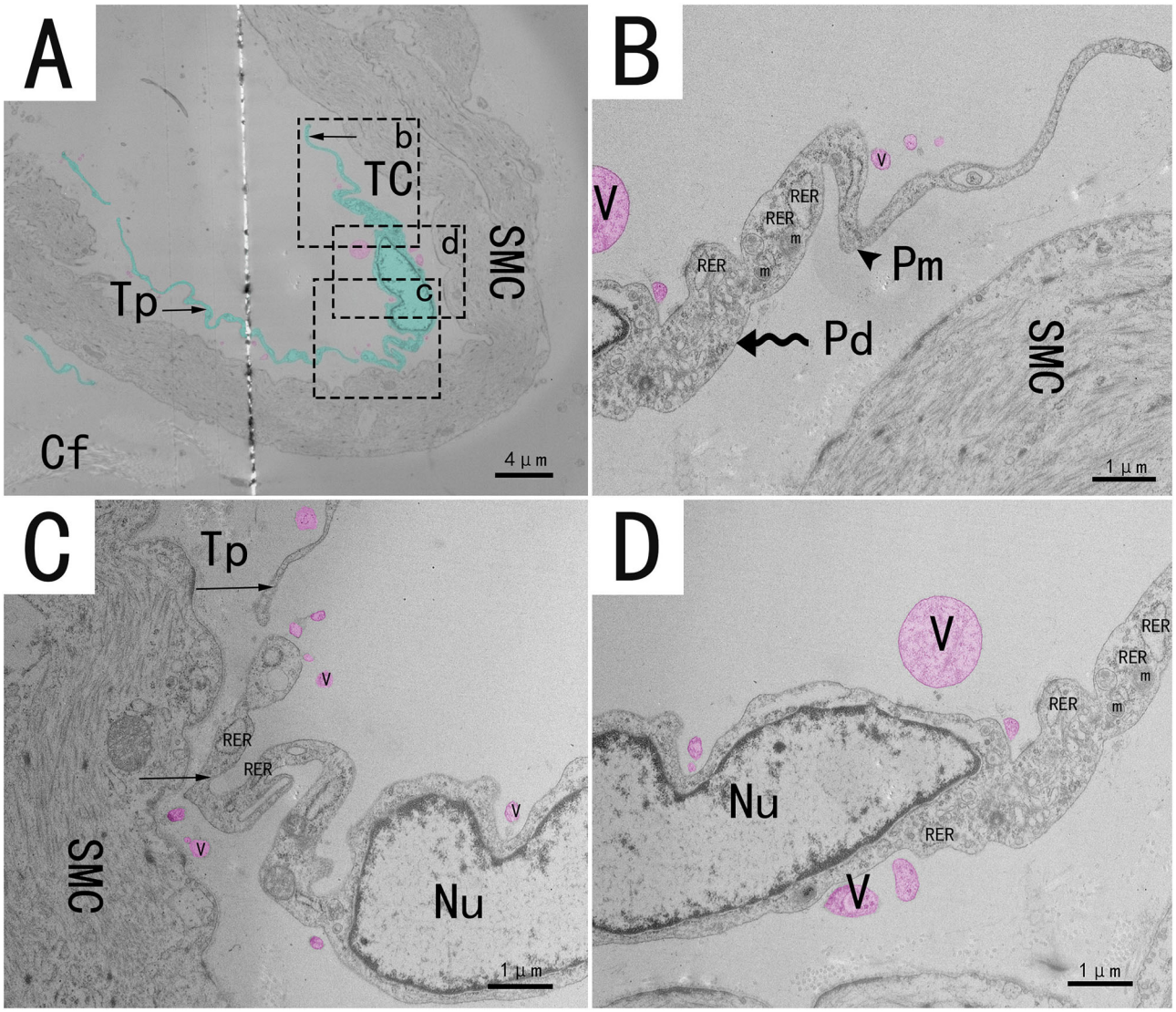

FIGURE 3 | Transmission electron microscope analysis of TCs from the utero-vaginal junction of the chicken **(A)**. **(B–D)** The enlargement of the area marked by the dotted box in panels b–d. Around the smooth muscle, a typical TC has an irregularly fusiform nucleus and two long, curved and folded rosary projections containing alternating bulges (**B**, wavy arrow, Podom) and fine segments (**B**, black triangular arrow, Podomers). Sparsely distributed vesicles of different sizes and shapes can be seen around the protrusion (red mark in this figure). Mitochondria and rough endoplasmic reticulum were abundant in the enlarged region **(B–D)**. TC, telocyte; Tp, telopode (black arrow); Pd, Podom; Pm, Podomer; SMC, Smooth muscle; Cf, Collagen fiber; RER, rough endoplasmic reticulum; m, Mitochondria; V, vesicle. Scale bar **(A)** = 4 μm; Scale bar **(B–D)** = 1 μm.

cells. These results suggest that the vesicles and exosomes released by TCs at the utero-vaginal junction may be involved in intercellular communication.

TCs were located around capillaries and connected with fibroblasts and pericytes. TCs also express growth factor receptors involved in neovascularization (37–39). TCs that make heterocytic contacts with various stromal components in the oviduct may participate in information exchange between various stromal cells or may participate in information exchange through the indirect structure of the TCs-vesicle gap junction-cytoskeleton (40, 41). TCs that function in specific intercellular signaling help regulate the activity of adjacent cells and regulate tissue development, remodeling, metabolism, immune regulation, immune monitoring, and maintenance of gastrointestinal homeostasis (42, 43).

The ICCs in the gastrointestinal tract have the role of slow-wave pacing and conduction (44). TCs form an intercellular 3D network structure in the intestinal muscular layer that resists deformation and thus supports gastrointestinal peristalsis (45). Similarly, the network of TCs creating a 3D scaffold in the human urinary bladder interstitial space provides mechanical support during bladder wall expansion and relaxation and avoids

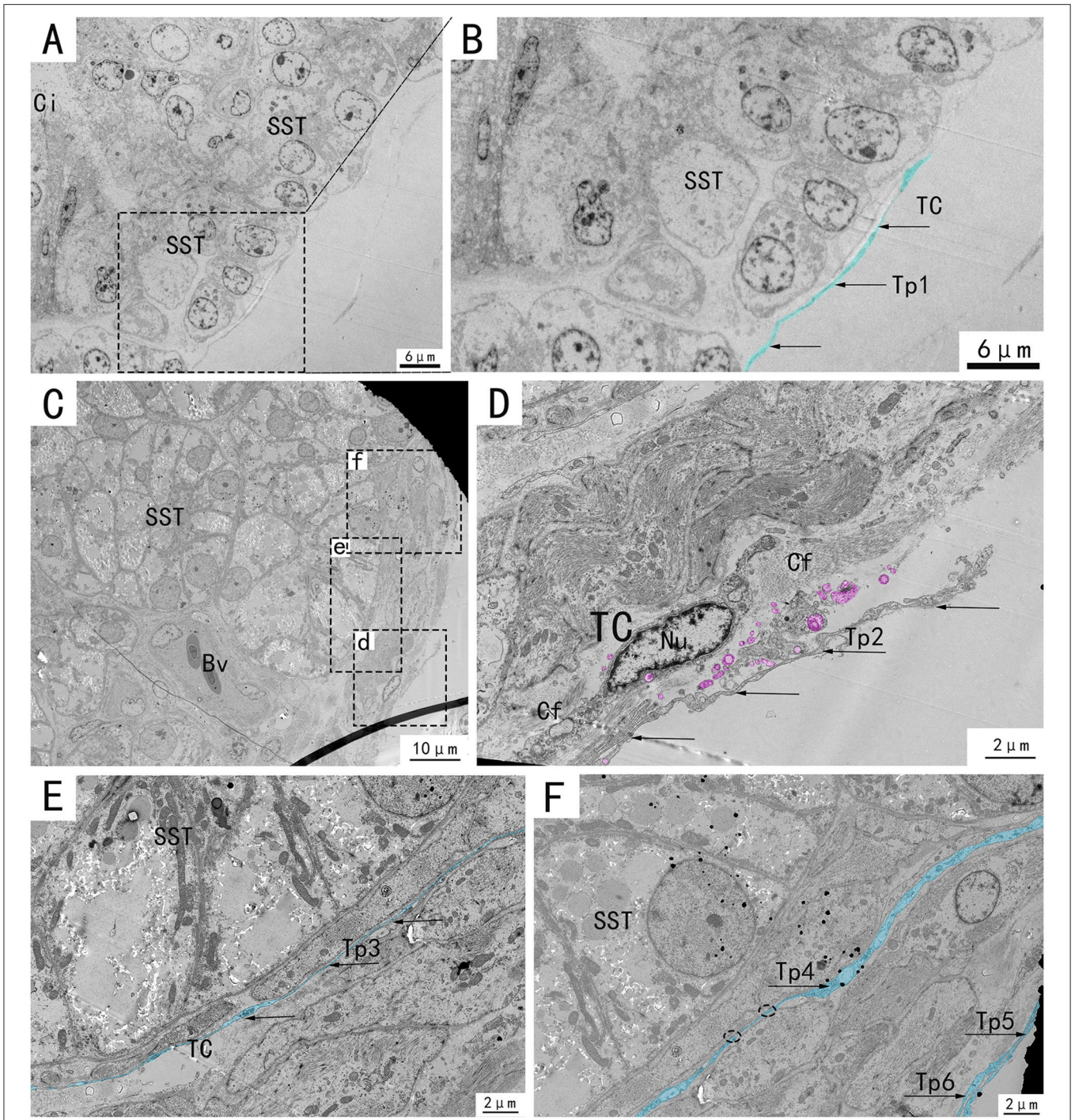

FIGURE 4 | Transmission electron microscope analysis of glands and TCs in the utero-vaginal junction of the chicken. **(B,D–F)** The amplification of the area marked by the dotted box in **(A)**, d–f, respectively. TCs, blood vessels, and collagen fibers are present around the subepithelial glands **(C)**. A typical TC is located around the gland, embedded in collagen fibers, with a long fusiform nucleus and a long labyrinth of Tp surrounded by clearly visible vesicles of varying sizes, as well as synthetic but unreleased vesicles in Tp (**D**, marked pink). Two very elongated, almost parallel Tps surround the glands closely (**E,F**, marked in blue, with black arrows). SST, sperm storage tube; V, vesicle; Bv, blood vessel; telopode, Tp1, Tp2, Tp3, Tp4, Tp5, Tp6; Cf, Collagen fiber. Scale bar **(A,B)** = 6 μm; Scale bar **(C)** = 10 μm; Scale bar **(D–F)** = 2 μm.

abnormal wall deformation (46). Tubal TCs also produce slow waves in the smooth muscle of the oviduct and are considered pacemaker cells of the oviduct (40, 41, 47). TCs express estrogen and progesterone receptors in the human myometrium and act as estrogen sensors to participate in myometrial contraction and movement of substances in the oviduct through gap

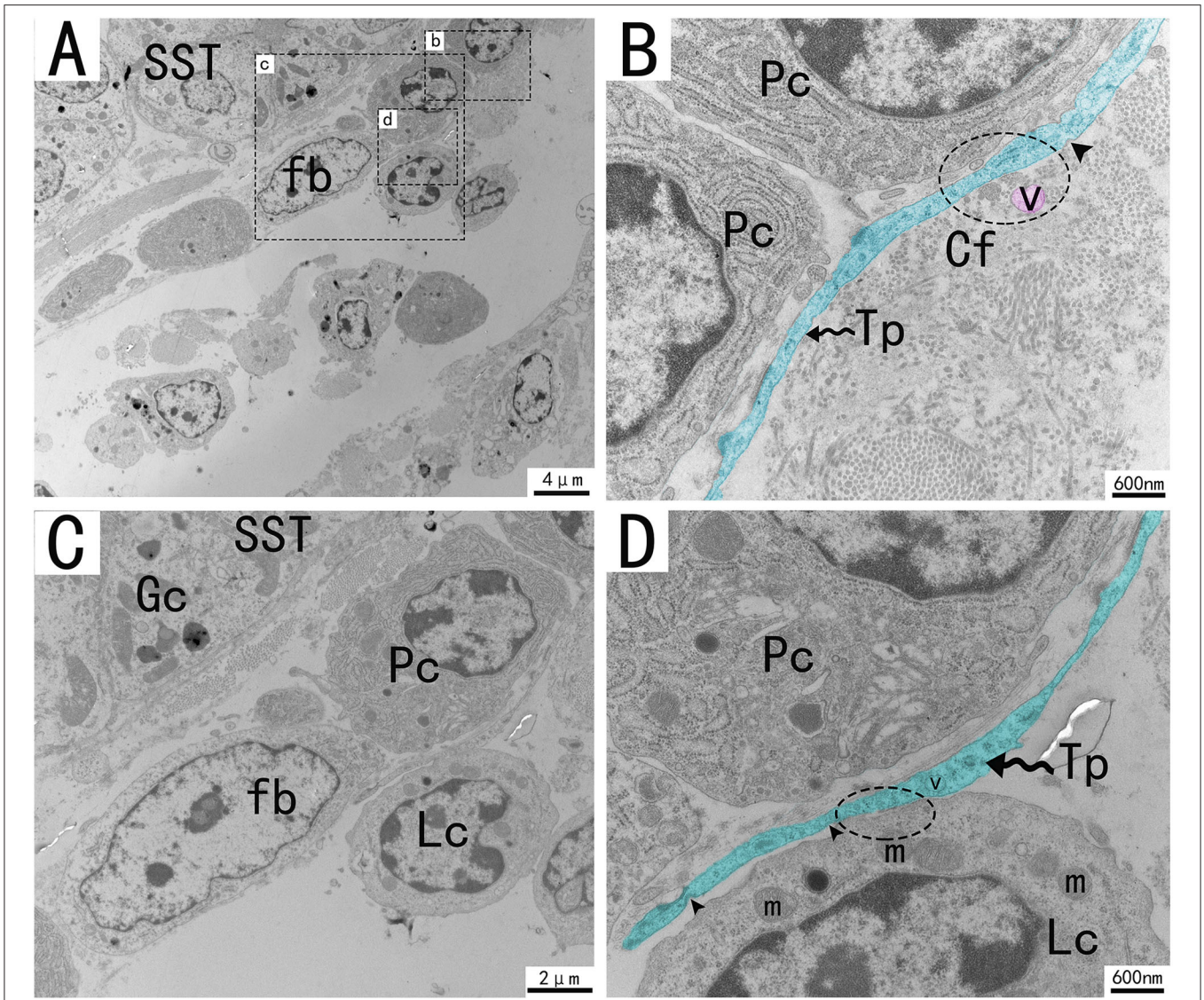

FIGURE 5 | Transmission electron microscope analysis of glands, TCs, and adjacent cells in the utero-vaginal junction of the chicken **(A)**. **(B–D)** The enlargement of the area marked by the dotted box in panels b–d. A typical Tp of TC is surrounded by plasma cells, fibroblast lymphocytes, and collagen fibers. TCs form typical cell connections with surrounding plasma cells and lymphocytes through Tps, and there are a large number of mitochondria in the Podom (**B,D,** dotted ellipse). Around Tps, vesicles of uniform size and different shapes can be clearly seen and are scattered (**B**, marked in red). There were a large number of mitochondria and rough endoplasmic reticulum in the enlargement of Tps, and the unreleased vesicles were also clearly visible **(B,D)**. Several concave pits around the bulge are associated with calcium absorption and release (**D**, black triangular arrow). The gland is surrounded by plasma cells, fibroblasts, etc. The nucleus of the glandular cell is located in the center. Tp, telopodes (black wavy arrow); Cf, Collagen fiber; RER, rough endoplasmic reticulum; m, Mitochondria; Lc, lymphocytes; Pc, plasma cell; Fb, fibroblast; Gc, Gland cell; V, vesicles; SST, sperm storage tube. Scale bar **(A)** = 4 μm; Scale bar **(B,D)** = 600 nm; Scale bar **(C)** = 2 μm.

junction or paracrine mechanisms (47, 48). These results provide morphological evidence for the role of TCs in the contractive motion of smooth muscle at the uterine-vaginal junction and in promoting the transport of sperm and ovum.

TCs have also been found in the intestinal crypt of the exocrine pancreas and intestinal stem cells (49, 50). TCs may be a subpopulation of mesenchymal progenitor/dry cells and thus have the potential to differentiate into other cell types. The formation of heterocellular connections between TCs and potential stem cells around the gland suggests that TCs are involved in epithelial renewal and play an important role in the repair and regeneration of the utero-vaginal junction. Cretoiu and Popescu reported that TCs in the human mammary gland and myometrium, and in the rat stomach, intestine, bladder, and uterus, establish close contacts with various immune cells, including lymphocytes, plasma cells, eosinophils, basophils, macrophages, and mast cells (2, 51–53). A large number of glands and sperm storage glands exist, and TCs surround these glands, forming heteromorphic cell connections with surrounding lymphocytes and plasma cells, and have

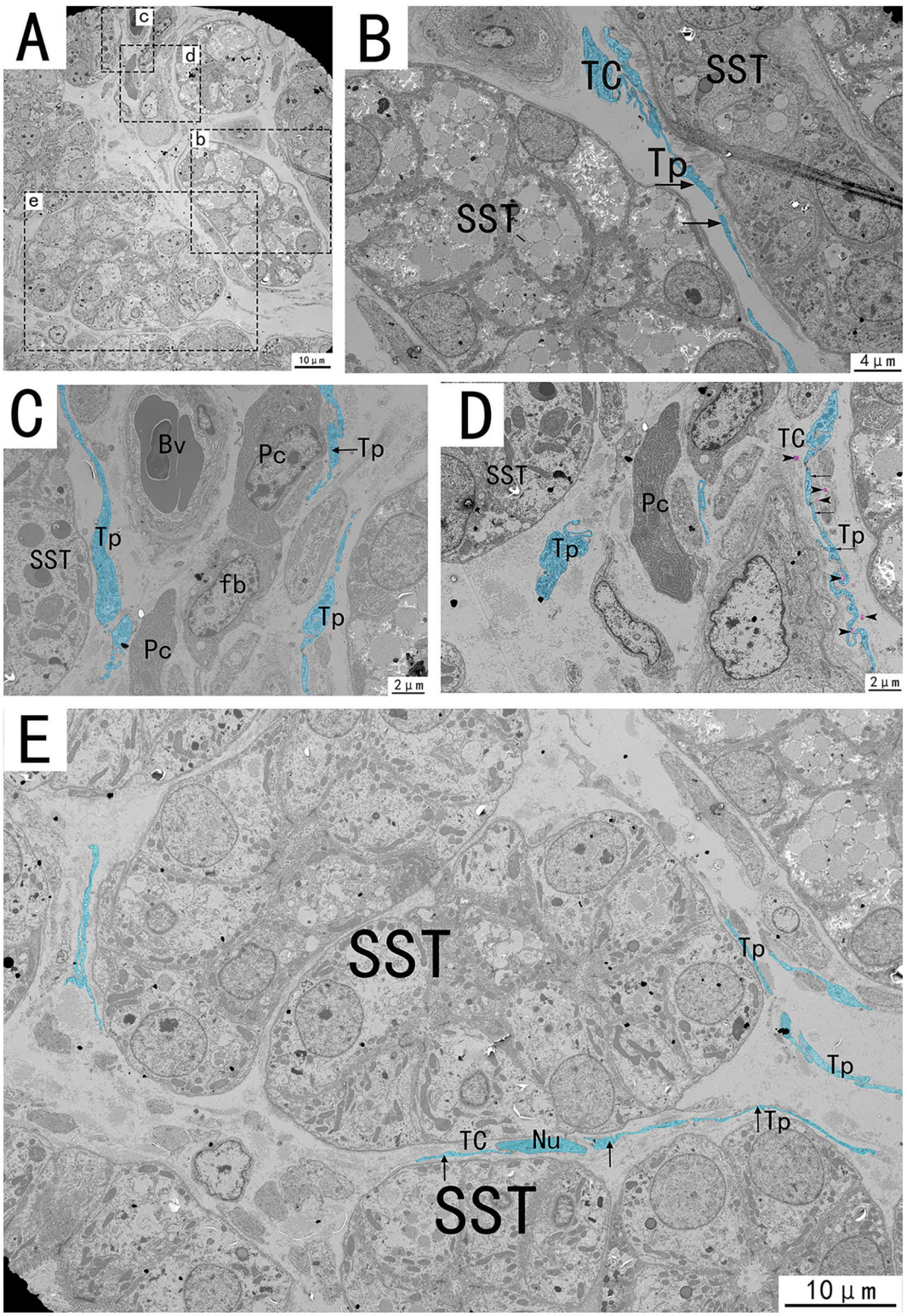

FIGURE 6 | Transmission electron microscope analysis of glands, TCs, vessels, and adjacent cells in the utero-vaginal junction of the chicken **(A)**. **(B–E)** The amplification of the area marked by the dotted box in panels b–e. The typical TCs can be seen between the glands. Tp is curved and folded like a labyrinth, with long fusiform nuclei and long Tp surrounded by vesicles of varying sizes (**B,E**, black arrows). Tp is surrounded by collagen fibers. There is TC between the glands and the blood vessels, forming a SST-TC-Bv positional relationship **(C)**. There is TC between the gland and fibroblasts, forming a SST-TC-fb positional relationship **(D)**. There are also vesicles in the process of synthesis in Tp that have not yet been released (**D**, marked in pink). SST, sperm storage tube; Bv, blood vessel; Cf, Collagen fiber; Pc, plasma cell; Fb, fibroblast; Nu, nuclear. Scale bar **(A,E)** = 10 μm; Scale bar **(B)** = 4 μm; Scale bar **(C,D)** = 2 μm.

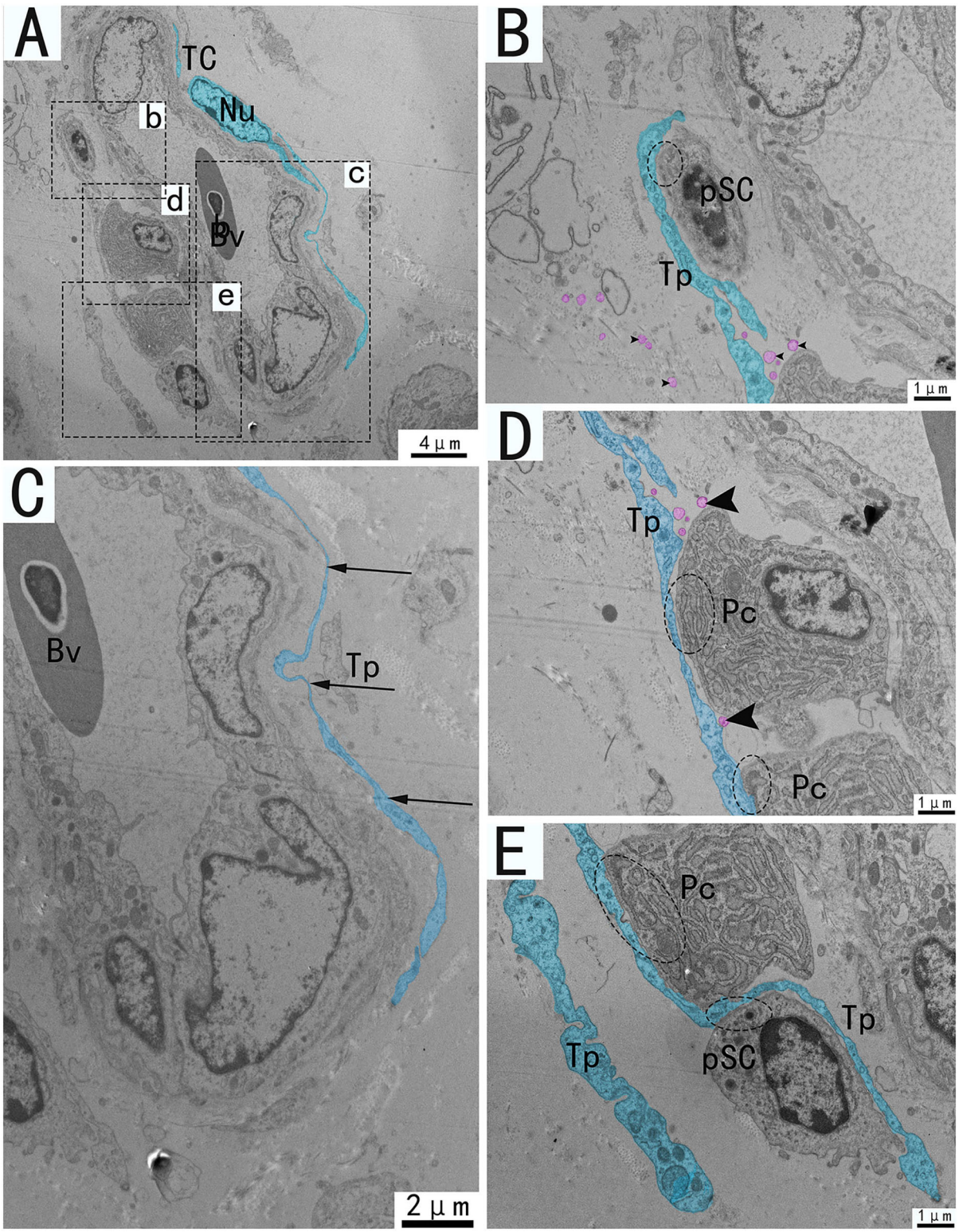

FIGURE 7 | Transmission electron microscope analysis of TCs, vessels, and adjacent cells from the utero-vaginal junction of the chicken **(A)**. **(B–E)** The enlargement of the area of the dotted box in panels b–e. Around the blood vessels, TCs forms homotypic cell connections *via* Tp (**A**, dashed ellipse). The vessels are typically surrounded by TCs and Tp is extremely elongated **(C)**. **(B,D,E)** Tp of the same TC forms heterogeneous cell connections with plasma cells, fibroblasts, stem cells, etc. (**B,D,E**, dotted ellipse), forming a network structure connecting blood vessels and surrounding cells in the stroma. There are vesicles of different sizes scattered around Tp (**B,D**, black triangular arrow), and there are also vesicles in the process of synthesis that have not been released (**D**, pink marks). Bv, blood vessel; Pc, plasma cell; pSC, potential stem cells; Tp, telopode; Nu, nuclear. Scale bar **(A)** = 4 μm; Scale bar **(C)** = 2 μm; Scale bar **(B,D,E)** = 1 μm.

an immune function in the microenvironment of the utero-vaginal junction.

In conclusion, our results confirm the presence of TCs at the utero-vaginal junction in chickens. TCs were CD34/C-kit positive. TCs surrounds glands, forming homogenous or heterogenous connections with lymphocytes, plasma cells, smooth muscle cells, blood vessels, collagen fibers, and fibroblasts around them, forming a complex three-dimensional network structure. This study provides morphological basis for the possible role of TCs in regulating utero-vaginal junction physiological function and intercellular communication.

CONCLUSIONS

This is the first study to confirm the existence of TCs at the utero-vaginal junction of the chicken. In the lamina propria, the TCs were curved and folded, embedded between bundles of collagen fibers and around blood vessels, and released vesicles. In the smooth muscle layer, TCs were mostly distributed around smooth muscle bundles. TCs and their surrounding structures, such as sperm storage tube, smooth muscle cells, blood vessels, collagen fibers, plasma cells, and fibroblasts, formed homotypic and allotypic connections to produce a 3D network structure. We postulate that TCs may play a role in information transmission, which provides a theoretical basis for the relationship between TCs in the utero-vaginal junction and sperm storage, transport, and oviduct disease, and provides a reference for the plasticity of TCs. This study provides morphological basis for the possible role of TCs in regulating the utero-vaginal junction physiological function and intercellular communication.

DATA AVAILABILITY STATEMENT

The original contributions presented in the study are included in the article/supplementary material, further inquiries can be directed to the corresponding author/s.

ETHICS STATEMENT

The animal study was reviewed and approved by the Science and Technology Agency of Jiangsu Province. Written informed consent was obtained from the owners for the participation of their animals in this study.

AUTHOR CONTRIBUTIONS

XZ, QW, PP, and PY: conceptualization, data curation, and writing—review and editing. ZW and BP: formal analysis. ZW, BP, XM, YF, and PY: methodology. XZ, QW, and PP: writing—original draft. All authors have read and agreed to the published version of the manuscript.

FUNDING

This work was supported by the National Natural Science Foundation of China (Grant No. 31772688), and the Priority Academic Program Development of Jiangsu Higher Education Institutions, China.

REFERENCES

1. Faussone PM, Popescu LM. Telocytes. *Biomol Concepts.* (2011) 2:481–9. doi: 10.1515/BMC.2011.039
2. Cretoiu SM, Popescu LM. Telocytes revisited. *Biomol Concepts.* (2014) 5:353–69. doi: 10.1515/bmc-2014-0029
3. Popescu LM, Faussone-Pellegrini M. TELOCYTES - a case of serendipity: the winding way from Interstitial Cells of Cajal (ICC), *via* Interstitial Cajal-Like Cells (ICLC) to TELOCYTES. *J Cell Mol Med.* (2010) 14:729–40. doi: 10.1111/j.1582-4934.2010.01059.x
4. Cretoiu D, Gherghiceanu M, Hummel E, Zimmermann H, Simionescu O, Popescu LM. FIB-SEM tomography of human skin telocytes and their extracellular vesicles. *J Cell Mol Med.* (2015) 19:714–22. doi: 10.1111/jcmm.12578
5. Popescu LM, Curici A, Wang E, Zhang H, Hu S, Gherghiceanu M. Telocytes and putative stem cells in ageing human heart. *J Cell Mol Med.* (2015) 19:31–45. doi: 10.1111/jcmm.12509
6. Cretoiu D, Radu BM, Banciu A, Banciu DD, Cretoiu SM. Telocytes heterogeneity: From cellular morphology to functional evidence. *Semin Cell Dev Biol.* (2017) 64:26–39. doi: 10.1016/j.semcdb.2016.08.023
7. Radu B, Banciu A, Banciu D, Radu M, Cretoiu D, Cretoiu S. Calcium signaling in interstitial cells: focus on telocytes. *Int J Mol Sci.* (2017) 18:397. doi: 10.3390/ijms18020397
8. Haseeb A, Tarique I, Iqbal A, Gandahi NS, Ali Vistro W, Bai X. et al. Characterization of multilamellar bodies and telocytes within the testicular interstitium of naked mole rat Heterocephalus glabe. *Theriogenology.* (2019) 138:111–20. doi: 10.1016/j.theriogenology.2019.07.010
9. Cretoiu SM, Cretoiu D, Marin A, Radu BM, Popescu LM. Telocytes: ultrastructural, immunohistochemical and electrophysiological characteristics in human myometrium. *Reproduction.* (2013) 145:357–70. doi: 10.1530/REP-12-0369
10. Zhang H, Yu P, Zhong S, Ge T, Peng S, Guo X. et al. Telocytes in pancreas of the Chinese giant salamander (Andrias davidianus). *J Cell Mol Med.* (2016) 20:2215–9. doi: 10.1111/jcmm.12948
11. Nizyaeva NV, Sukhacheva TV, Serov RA, Kulikova GV, Nagovitsyna MN, Kan NE. et al. Ultrastructural and immunohistochemical features of telocytes in placental villi in preeclampsia. *Sci Rep.* (2018) 8:3453. doi: 10.1038/s41598-018-21492-w
12. Traini C, Fausssone-Pellegrini M, Guasti D, Del Popolo G, Frizzi J, Serni S. et al. Adaptive changes of telocytes in the urinary bladder of patients affected by neurogenic detrusor overactivity. *J Cell Mol Med.* (2018) 22:195–206. doi: 10.1111/jcmm.13308
13. Xu Y, Tian H, Cheng J, Liang S, Li T, Liu J. Immunohistochemical biomarkers and distribution of telocytes in ApoE–/– mice. *Cell Biol Int.* (2019) 43:1286–95. doi: 10.1002/cbin.11128
14. Vannucchi MG. The telocytes: ten years after their introduction in the scientific literature. An update on their morphology, distribution, and potential roles in the gut. *Int J Mol Sci.* (2020) 21:4478. doi: 10.3390/ijms21124478
15. Creţoiu SM. Telocytes and other interstitial cells: from structure to function. *Int J Mol Sci.* (2021) 22:5271. doi: 10.3390/ijms22105271
16. Díaz-Flores L, Gutiérrez R, González-Gómez M, García MP, Díaz-Flores L, Carrasco JL. et al. CD34+ stromal cells/telocytes as a source of cancer-associated fibroblasts (CAFs) in invasive lobular carcinoma of the breast. *Int J Mol Sci.* (2021) 22:3686. doi: 10.3390/ijms22073686
17. Selviler Sizer S, Kabak YB, Kabak M. Telocytes in the hearts of Saanen goats. *Microsc Res Tech.* (2021) 84:548–54. doi: 10.1002/jemt.23612

18. Ma R, Wu P, Shi Q, Song D, Fang H. Telocytes promote VEGF expression and alleviate ventilator-induced lung injury in mice. *Acta Biochim Biophys Sin.* (2018) 50:817–25. doi: 10.1093/abbs/gmy066
19. Campeanu R, Radu BM, Cretoiu SM, Banciu DD, Banciu A, Cretoiu D. et al. Near-infrared low-level laser stimulation of telocytes from human myometrium. *Lasers Med Sci.* (2014) 29:1867–74. doi: 10.1007/s10103-014-1589-1
20. Mirancea N. Telocyte - a particular cell phenotype. Infrastructure, relationships and putative functions. *Rom J Morphol Embryol.* (2016) 57:7–21.
21. Fu S, Wang F, Cao Y, Huang Q, Xiao J, Yang C. et al. Telocytes in human liver fibrosis. *J Cell Mol Med.* (2015) 19:676–683. doi: 10.1111/jcmm.12542
22. Yang G, Li S, Zhao Q, Chu J, Zhou B, Fan S. et al. Transcriptomic and metabolomic insights into the variety of sperm storage in oviduct of egg layers. *Poult Sci.* (2021) 100:101087. doi: 10.1016/j.psj.2021.101087
23. Han J, Ahmad HI, Jiang X, Liu G. Role of genome-wide mRNA-seq profiling in understanding the long-term sperm maintenance in the storage tubules of laying hens. *Trop Anim Health Prod.* (2019) 51:1441–7. doi: 10.1007/s11250-019-01821-5
24. Kucybala I, Janas P, Ciuk S, Cholopiak W, Klimek-Piotrowska W, Holda MK. A comprehensive guide to telocytes and their great potential in cardiovascular system. *Bratislava Med J.* (2017) 118:302–9. doi: 10.4149/BLL_2017_059
25. Cantarero I, Luesma MJ, Alvarez-Dotu JM, Muñoz E, Junquera C. Transmission electron microscopy as key technique for the characterization of telocytes. *Curr Stem Cell Res Ther.* (2016) 11:410. doi: 10.2174/1574888X10666150306155435
26. Xu Y, Tian H, Qiao G, Zheng W. Telocytes in the atherosclerotic carotid artery: Immunofluorescence and TEM evidence. *Acta Histochem.* (2021) 123:151681. doi: 10.1016/j.acthis.2021.151681
27. Popescu LM, Fertig ET, Gherghiceanu M. Reaching out: junctions between cardiac telocytes and cardiac stem cells in culture. *J Cell Mol Med.* (2016) 20:370–80. doi: 10.1111/jcmm.12719
28. Yang P, Zhu X, Wang L, Ahmed N, Huang Y, Chen H. et al. Cellular evidence of telocytes as novel interstitial cells within the magnum of chicken oviduct. *Cell Transplant.* (2017) 26:135–43. doi: 10.3727/096368916X692942
29. Enciu A, Popescu LM. Telopodes of telocytes are influenced *in vitro* by redox conditions and ageing. *Mol Cell Biochem.* (2015) 410:165–74. doi: 10.1007/s11010-015-2548-2
30. Kessler M, Hoffmann K, Brinkmann V, Thieck O, Jackisch S, Toelle B. et al. The Notch and Wnt pathways regulate stemness and differentiation in human fallopian tube organoids. *Nat Commun.* (2015) 6:8989. doi: 10.1038/ncomms9989
31. Gherghiceanu M, Popescu LM. Cardiac telocytes — their junctions and functional implications. *Cell Tissue Res.* (2012) 348:265–79. doi: 10.1007/s00441-012-1333-8
32. Mandache E, Popescu LM, Gherghiceanu M. Myocardial interstitial Cajal-like cells (ICLC) and their nanostructural relationships with intercalated discs: shed vesicles as intermediates. *J Cell Mol Med.* (2007) 11:1175–84. doi: 10.1111/j.1582-4934.2007.00117.x
33. Manole CG, Cismaşiu V, Gherghiceanu M, Popescu LM. Experimental acute myocardial infarction: telocytes involvement in neo-angiogenesis. *J Cell Mol Med.* (2011) 15:2284–96. doi: 10.1111/j.1582-4934.2011.01449.x
34. Popescu LM, Gherghiceanu M, Suciu LC, Manole CG, Hinescu ME. Telocytes and putative stem cells in the lungs: electron microscopy, electron tomography and laser scanning microscopy. *Cell Tissue Res.* (2011) 345:391–403. doi: 10.1007/s00441-011-1229-z
35. Roatesi I, Radu BM, Cretoiu D, Cretoiu SM. Uterine telocytes: a review of current knowledge. *Biol Reprod.* (2015) 93:10. doi: 10.1095/biolreprod.114.125906
36. Yang R, Tang Y, Chen X, Yang Y. Telocytes-derived extracellular vesicles alleviate aortic valve calcification by carrying miR-30b. *ESC Heart Failure.* (2021) 8:3935–46. doi: 10.1002/ehf2.13460
37. Aleksandrovych V, Bereza T, Sajewicz M, Walocha JA, Gil K. Uterine fibroid: common features of widespread tumor (Review article). *Folia Med Cracov.* (2015) 55:61.
38. Hussein MT, Abdel-Maksoud FM. Structural investigation of epididymal microvasculature and its relation to telocytes and immune cells in camel. *Microscopy Microanalysis.* (2020) 26:1024–34. doi: 10.1017/S1431927620001786
39. Soliman SA. Telocytes are major constituents of the angiogenic apparatus. *Sci Rep.* (2021) 11:5775. doi: 10.1038/s41598-021-85166-w
40. Yang X, Xu J, Shen Z, Zhao J. Immunohistochemical alterations of cajal-like type of tubal interstitial cells in women with endometriosis and tubal ectopic pregnancy. *Arch Gynecol Obstet.* (2013) 288:1295–300. doi: 10.1007/s00404-013-2878-9
41. Yang XJ, Yang J, Liu Z, Yang G, Shen ZJ. Telocytes damage in endometriosis-affected rat oviduct and potential impact on fertility. *J Cell Mol Med.* (2015) 19:452–62. doi: 10.1111/jcmm.12427
42. Ullah S, Yang P, Zhang L, Zhang Q, Liu Y, Chen W. et al. Identification and characterization of telocytes in the uterus of the oviduct in the Chinese soft-shelled turtle,Pelodiscus sinensis:TEM evidence. *J Cell Mol Med.* (2014) 18:2385–92. doi: 10.1111/jcmm.12392
43. Cretoiu D, Roatesi S, Bica I, Plesca C, Stefan A, Bajenaru O. et al. Simulation and modeling of telocytes behavior in signaling and intercellular communication processes. *Int J Mol Sci.* (2020) 21:2615. doi: 10.3390/ijms21072615
44. Popescu LM, Gherghiceanu M, Cretoiu D, Radu E. The connective connection: interstitial cells of Cajal (ICC) and ICC-like cells establish synapses with immunoreactive cells.: Electron microscope study in sity. *J Cell Mol Med.* (2005) 9:714–30. doi: 10.1111/j.1582-4934.2005.tb00502.x
45. Ji S, Traini C, Mischopoulou M, Gibbons SJ, Ligresti G, Faussone Pellegrini MS, et al. Muscularis macrophages establish cell-to-cell contacts with telocytes/PDGFRα-positive cells and smooth muscle cells in the human and mouse gastrointestinal tract. *Neurogastroenterol Motility.* (2021) 33:e13993. doi: 10.1111/nmo.13993
46. Sanches BDA, Tamarindo GH, Maldarine JDS, Da Silva ADT, Dos Santos VA, Góes RM. et al. Telocytes of the male urogenital system: Interrelationships, possible functions, pathological implications. *Cell Biol Int.* (2021) 45:1613–23. doi: 10.1002/cbin.11612
47. Cretoiu SM, Cretoiu D, Suciu L, Popescu LM. Interstitial Cajal-like cells of human Fallopian tube express estrogen and progesterone receptors. *J Mol Histol.* (2009) 40:387–94. doi: 10.1007/s10735-009-9252-z
48. Aleksandrovych V, Wrona A, Bereza T, Pityński K, Gil K. Oviductal telocytes in patients with uterine myoma. *Biomedicines.* (2021) 9:1060. doi: 10.3390/biomedicines9081060
49. Popescu LM, Hinescu ME, Ionescu N, Ciontea SM, Cretoiu D, Ardeleanu C. Interstitial cells of Cajal in pancreas. *J Cell Mol Med.* (2005) 9:169–90. doi: 10.1111/j.1582-4934.2005.tb00347.x
50. Albulescu R, Tanase C, Codrici E, Popescu DI, Cretoiu SM, Popescu LM. The secretome of myocardial telocytes modulates the activity of cardiac stem cells. *J Cell Mol Med.* (2015) 19:1783–94. doi: 10.1111/jcmm.12624
51. Rosa I, Marini M, Manetti M. Telocytes: An Emerging Component of Stem Cell Niche Microenvironment. *J Histochem Cytochem.* (2021) 69:795–818. doi: 10.1369/00221554211025489
52. Cretoiu SM. Immunohistochemistry of telocytes in the uterus and fallopian tubes. *Adv Exp Med Biol.* (2016) 913:335–57. doi: 10.1007/978-981-10-1061-3_22
53. Domino M, Pawlinski B, Zabielski R, Gajewski Z. C-kit receptor immunopositive interstitial cells (Cajal-type) in the porcine reproductive tract. *Acta Vet Scand.* (2017) 59:32. doi: 10.1186/s13028-017-0300-5

Conflict of Interest: The authors declare that the research was conducted in the absence of any commercial or financial relationships that could be construed as a potential conflict of interest.

Publisher's Note: All claims expressed in this article are solely those of the authors and do not necessarily represent those of their affiliated organizations, or those of the publisher, the editors and the reviewers. Any product that may be evaluated in this article, or claim that may be made by its manufacturer, is not guaranteed or endorsed by the publisher.

frontiers | Frontiers in Veterinary Science

ORIGINAL RESEARCH
published: 14 April 2022
doi: 10.3389/fvets.2022.857834

Assessing the Risk of Commercial Vaccines Against Pseudorabies Virus in Cats

Lu Tu[1], *Jingjie Zhao*[1], *Qiuyang Chen*[1], *Shan Zhang*[1], *Lin Liang*[1], *Xinming Tang*[1], *Shaohua Hou*[1], *Weifang Yang*[2] *and Ruiying Liang*[1]*

[1] *Institute of Animal Sciences, Chinese Academy of Agricultural Sciences, Beijing, China,* [2] *Beijing General Station of Animal Husbandry, Beijing, China*

OPEN ACCESS

Edited by:
Fazul Nabi,
Lasbela University of Agriculture, Water and Marine Sciences, Pakistan

Reviewed by:
Lijun Ling,
University of North Carolina at Chapel Hill, United States
Quratulain Hanif,
Pakistan Institute of Engineering and Applied Sciences, Pakistan
Lijun Hu,
United States Food and Drug Administration, United States

***Correspondence:**
Ruiying Liang
liangruiying@caas.cn

Specialty section:
This article was submitted to Comparative and Clinical Medicine, a section of the journal Frontiers in Veterinary Science

Received: *19 January 2022*
Accepted: *03 March 2022*
Published: *14 April 2022*

Citation:
Tu L, Zhao J, Chen Q, Zhang S, Liang L, Tang X, Hou S, Yang W and Liang R (2022) Assessing the Risk of Commercial Vaccines Against Pseudorabies Virus in Cats. Front. Vet. Sci. 9:857834. doi: 10.3389/fvets.2022.857834

Pseudorabies virus (PRV) is a zoonotic agent that causes significant economic losses in animal husbandry worldwide, and *gE*-deleted vaccines play an important role in its treatment in the swine industry. However, the potential risk of attenuated PRV strains in commercial vaccines for other hosts remains unclear. Especially, cats are important companion animals for human beings. In this study, we investigated the prevalence and pathogenicity of the PRV wild strain in the cat population. We found that the occurrence of PR diseases in cats is sporadic, that the attenuated PRV strain causes slight clinical signs in cats, and that the virus is excreted 3 days post-infection. Our findings will be beneficial in furthering our understanding of the epidemiology and pathogenicity of PRV in cats and implying the great risk of RPV transmission from pigs to cats.

Keywords: pseudorabies virus, attenuated vaccine, cat, epidemiology, pathogenicity

INTRODUCTION

Pseudorabies virus (PRV) causes a viral disease of economic significance since it affects animal husbandry worldwide (1). The causative agent of this disease belongs to the genus *Varicellovirus* of the subfamily *Alphaherpesvirinae* of the *Herpesviridae* family (2). Previous reports indicated that pigs are the primary hosts of PRV (3, 4). Clinically, the manifestation of disease in pigs is related to the age of the pig, as young piglets usually present with severe central nervous system symptoms, and the outcome is invariably fatal. In contrast, elderly pigs usually present with mild respiratory signs or subclinical symptoms. Large-scale vaccination with *gE*-deleted vaccines may play an important role in controlling this disease. To date, PR has been eradicated in pigs in several European countries, the USA, and New Zealand (5–7).

Pseudorabies virus has a wide range of hosts, including pigs, cats, rabbits, cows, goats, cattle, sheep, dogs, bats, bears, coyotes, foxes, wolves, horses, deer, panthers, and some avian species (8). Unlike infections in pigs, fatal infections have been reported in several animals (including cats, dogs, and cattle) regardless of age. PRV is considered a zoonotic agent. In 2019, a PRV strain of human origin, hSD-1/2019, was isolated from a diseased human with acute encephalitis (9), providing solid evidence of the public health significance of PRV.

TABLE 1 | Viral detection in a retrospective survey.

Sample	Source	Tissues	*gB*	*gE*
1	Pet cat	Nasal swab	+	+
2	Pet cat	Nasal swab	+	+
3	Pet cat	Nasal swab	+	–
4	Cat on pig farms	Nasal swab	+	–
5	Cat on pig farms	Lung, nasal swab	+	–

Cats have been confirmed as hosts for PRVs (10–12). Generally, cats are infected mainly through the ingestion of PRV-contaminated raw pork, particularly of the lungs and other offal. The virus generally enters through the oral route, replicates in the tonsil and pharynx, and spreads through the cranial nerve and the central nervous system. Cats infected with highly pathogenic PRV strains usually die within 48 h after the onset of the signs of this disease, which can include anorexia, pruritus, self-mutilation, ataxia, and, eventually, paralysis (13). The tolerance to PRV infection and trans-neuronal transport (12) in cats differs according to the neuronal cell types (13). However, the pathogenicity of attenuated PRV strains in cats remains unclear. In this study, we assessed the pathogenicity of attenuated PRV strains in cats and performed a retrospective analysis to monitor their epidemiological status. The results of our study will be beneficial for our understanding of the epidemiology and pathogenicity of PRV in cats.

MATERIALS AND METHODS

Ethics Statement

This study was approved by the Animal Care Committee of the Institute of Animal Sciences of the Chinese Academy of Agricultural Sciences and animal experimental protocols (approval ID: IAS-2021-112). All study procedures and animal care activities were conducted in accordance with the recommendations of the Guide for the Care and Use of Laboratory Animals of the Ministry of Science and Technology of the People's Republic of China.

Viruses and Animals

Attenuated PRV strain Bartha-K61 was purchased from YEBIO Co., Ltd. The pathogenic PRV strain SD18 (Batch No. MN443976), a variant PRV strain circulating in the Chinese swine industry, was isolated in the Shandong province of China in 2018 (14). In total, nine 10-week-old domestic cats were purchased from the Guangdong Research Center of Laboratory Animals (approval ID: SCXK-2013-0007). All animals were negative for PRV, as was detected by ELISA and PCR.

Clinical Samples

From July 2019 to June 2020, a total of 54 feline samples (including nasal swab, heart, lung, liver, and brain) were collected in Guangdong province, China. Among these 54 feline specimens, 14 were collected from diseased cats that exhibited anorexia, pruritus, and ataxia; 9 were collected from diseased homeless cats around pig farms; and the remaining 31 were randomly collected from dead cats in pet hospitals. All samples were stored at −80°C.

Virus Detection

The presence of PRV was detected using real-time quantitative PCR assay as previously described (14). Viral DNA was extracted from clinical samples using TRIzol reagent (Invitrogen). The specific primer pairs 5-TGAAGCGGTTCGTGATGG-3 and 5-CCCCGCACAAGTTCAAGG-3 targeting the PRV *gB* gene and the specific primer pairs 5-CCGCGGGCCGTGTTCTTTGT-3 and 5-GCGCCGGCGAGGTGAAGC-3 targeting the PRV *gE* gene were designed according to previous studies (14). Real-time quantitative PCR was performed as previously described (14). Briefly, the recipe contains 10 μl of a 2 × SYBR Premix ExTaq Green mix (TaKaRa), 1 μl of a template, and 0.5-mm concentration of specific primers. Thermal cycling parameters were as follows: 95°C for 5 min; 40 cycles of 95°C for 10 s, 58°C for 30 s, and 72°C for 30 s; and one cycle of 95°C for 30 s, 60°C for 30 s, and 95°C for 30 s.

Challenge Study

To assess the virulence of different PRV strains in cats, nine 10-week-old cats were randomly divided into three groups (three cats per group). The cats in the first group were infected with the attenuated strain, Bartha-K61, at a dose of $10^{3.0}$ $TCID_{50}$. The cats in the second group were infected with the highly pathogenic strain SD18 at a dose of $10^{3.0}$ $TCID_{50}$. The cats in the third group were infected with phosphate-buffered saline as a negative control. Clinical signs of the disease were observed daily. All the cats were humanely euthanized until one of them presented with signs of disease or sudden death.

Histopathology

Fresh pathological tissues were fixed in 10% neutral-buffered formalin, routinely processed, embedded in paraffin, sectioned (4-μm thick), and stained with hematoxylin and eosin according to standard protocols. Pathological changes were examined using light microscopy.

RESULTS

The Prevalence of PRV in Cats

We collected 54 feline specimens from diseased or dead cats to perform a retrospective investigation. As a result, a total of five specimens were positive for PRV *gB* gene. Among these *gB*-positive samples, three were collected from diseased cats in pet hospitals, and two were collected from diseased homeless cats around pig farms (**Table 1**). Interestingly, all the PRV-positive samples from cats on pig farms were *gB*-positive and *gE*-negative. Among the PRV *gB*-positive samples from pet cats, one sample was negative for the PRV *gE* gene, whereas two samples were positive for PRV gE. These results showed that, of the five PRV-positive specimens, two were infected by wild virus strains, and three were infected by vaccine strains. These data provide clues to PRV infection in cats.

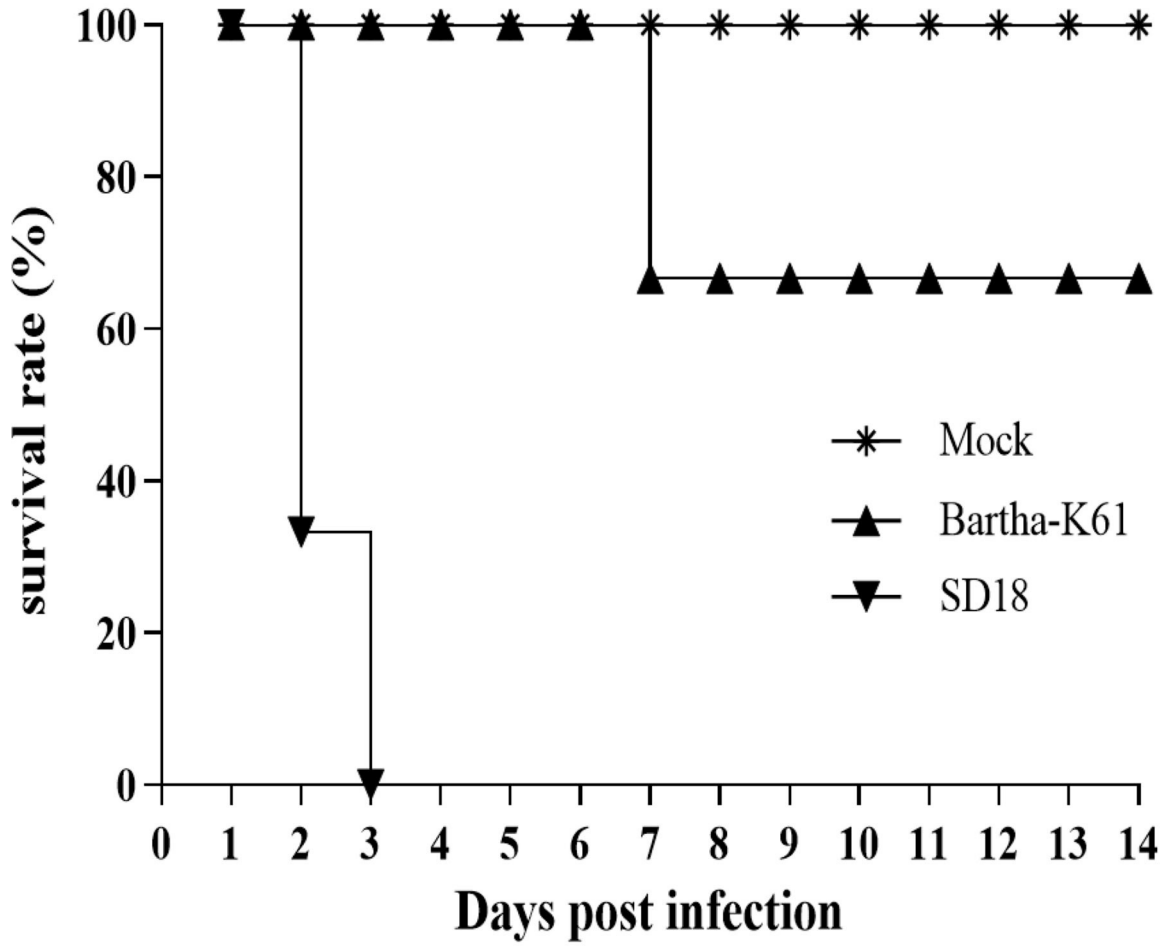

FIGURE 1 | Survival curves of PRV-infected cats. Cats that were 10 weeks old were infected with Bartha-K61, SD18, or PBS. Clinical signs of disease were observed daily. In the Bartha-K61-infected group, one cat exhibited anorexia, anxiety, and crying and euthanized at the end of expeirence. Fourteen days later, the cats were euthanized with sodium nitrite.

PRV Cause Clinical Manifestation in Cats

PRV-infected cats usually present with anorexia and, sometimes, with intense pruritus, but few reports on the clinical signs caused by the attenuated PRV strain in commercial vaccines against cats are available. In this study, we infected 10-week-old domestic short hairs with the Bartha-K61 strain and recorded the clinical manifestations. The experiment was terminated 14 days post-infection (dpi). Compared to the cats in the mock-infected group, the death rate of the cats in the SD18-infected group reached 100%, while no deaths occurred in the Bartha-K61-infected group (**Figure 1**). Generally, all the cats in the SD18-infected group died or were euthanized at 2–3 dpi, following the presentation of nervous signs of disease. In the Bartha-K61-infected group, one cat exhibited anorexia, anxiety, and crying at 7 dpi, whereas the other two cats were euthanized at the end of the experiment. All mock-infected cats, without any signs of disease, were euthanized at 14 dpi.

Clinical observations were monitored during the experimental period. Compared to that of the mock-infected cats, the incubation period of SD18-infected cats was shorter: no longer than 2 days. All the cats presented with anorexia, pruritus, ataxia, and paralysis. The infected cats usually died within 24 h

TABLE 2 | Virus detection in the excretion of challenged cats.

Group	Swab samples	Days post-infection							
		0	1	2	3	4	5	6	7
Mock	Buccal	0/3	0/3	0/3	0/3	0/3	0/3	0/3	0/3
	Nasopharyngeal	0/3	0/3	0/3	0/3	0/3	0/3	0/3	0/3
	Anal	0/3	0/3	0/3	0/3	0/3	0/3	0/3	0/3
Bartha-K61	Buccal	0/3	0/3	2/3	2/3	3/3	3/3	3/3	3/3
	Nasopharyngeal	0/3	0/3	2/3	3/3	3/3	3/3	3/3	3/3
	Anal	0/3	0/3	2/3	3/3	3/3	3/3	3/3	3/3
SD-18	Buccal	0/3	2/3	3/3	/	/	/	/	/
	Nasopharyngeal	0/3	2/3	3/3	/	/	/	/	/
	Anal	0/3	1/3	3/3	/	/	/	/	/

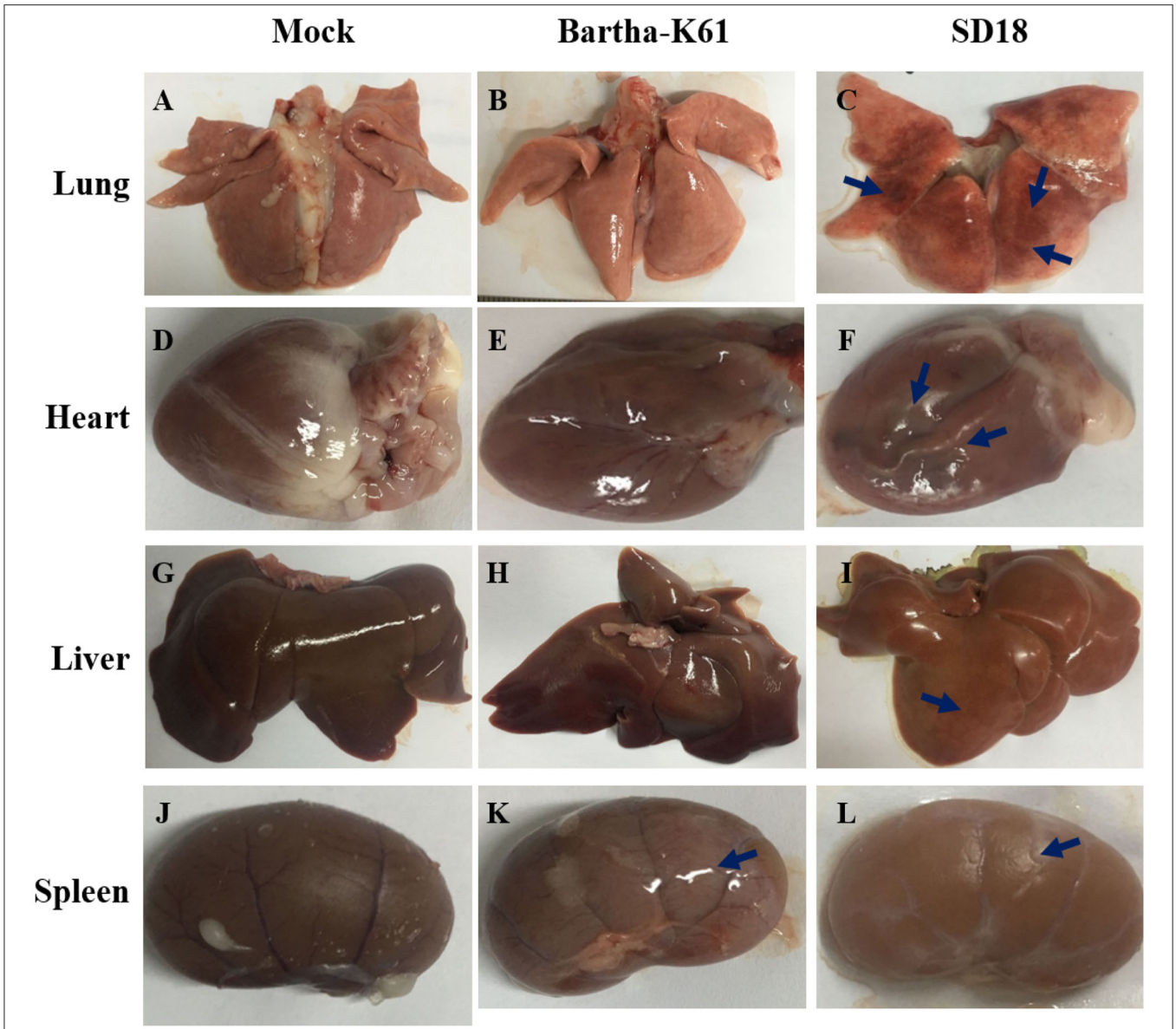

FIGURE 2 | Pathologic changes in PRV-infected cats. Cats that were 10 weeks old were infected with Bartha-K61, SD18, or PBS. All the cats were euthanized at 14 dpi. The autopsy was performed, and the gross abnormalities were recorded at necropsy. **(A–C)** The necropsy symptoms of the lung. **(D–F)** The necropsy symptoms of the heart. **(G–I)** The necropsy symptoms of the liver. **(J–L)** The necropsy symptoms of the kidney.

after the onset of clinical signs. In the Bartha-K61-infected group, the cats exhibited slight symptoms at 6–7 dpi, including anorexia, anxiety, and crying. Additionally, viruses were detected in nasopharyngeal swabs, anal swabs, and buccal swabs of the challenged cats at 1 or 2 dpi (**Table 2**).

PRV Cause Pathological Lesions in Cats

To further assess the pathogenicity of the attenuated PRV strain in cats, we performed an autopsy and recorded gross abnormalities at necropsy. Compared to the mock-infected cats, the SD18-infected cats presented with apparent lesions, while the Bartha-K61-infected cats exhibited slight symptoms of disease at necropsy (**Figure 2**). Generally, SD18-infected cats presented with severe hemorrhages and congestion in the lung (**Figure 2C**), swelling in the kidney and heart (**Figures 2F,L**), and focal hemorrhage in the liver (**Figure 2I**), which is consistent with previous reports (11). Exceeding our expectations, the Bartha-K61-infected cats did not show typical apparent lesions, except for kidney swelling (**Figure 2K**).

Histopathological Analysis of PRV in Cats

To further analyze the pathogenicity of the attenuated PRV strain in cats, histopathological analysis was performed. As a result, compared to the sham-infected cats, the BarthaK61-infected cats

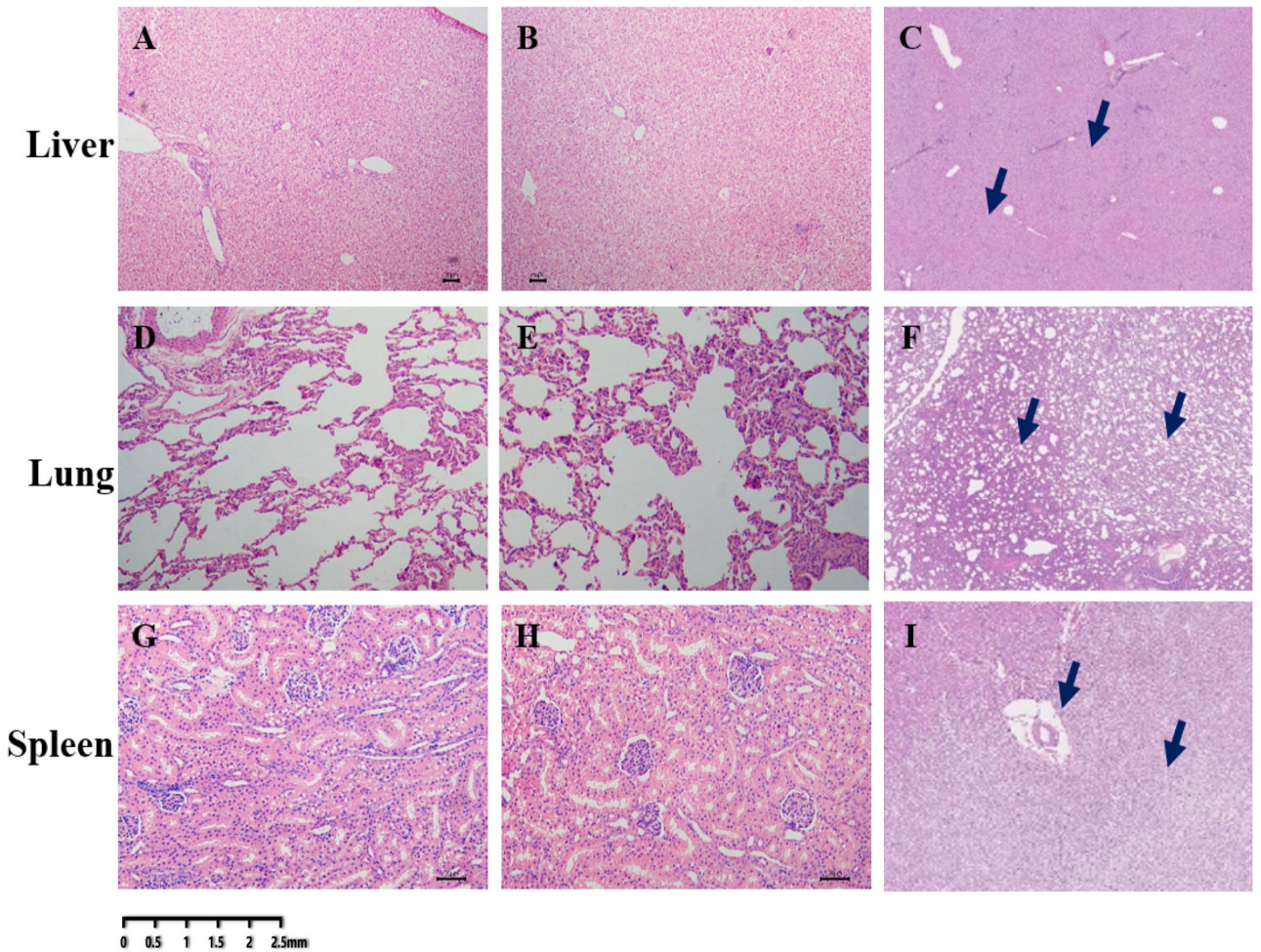

FIGURE 3 | Histological changes in PRV-infected cats. Affected tissues collected from the mock-, BarthaK61, and SD18-infected cats were used for histological analysis. Histological changes were examined by light microscopy. **(A–C)** Histological changes of the liver. **(D–F)** Histological changes of the lung. **(G–I)** Histological changes of the spleen.

only presented with lesions in the kidney (**Figure 3**), which is consistent with the observations at necropsy. However, SD18-infected cats presented with severe multiorgan lesions. Generally, cellular degeneration, as was observed in the liver and kidney of the SD18-infected cats (**Figures 3A–C,G–I**), severe hemorrhage, and congestion were observed in the lungs of the SD18-infected cats (**Figures 3D–F**).

DISCUSSION

PRV was first identified in a cat in China and subsequently isolated from many species of animals (15), including pigs, cattle, cows, goats, dogs, rabbits, some avian species, and humans (16). Pigs are considered the primary hosts and reservoirs of PRVs (3, 4). Interestingly, PRV strains circulating in many animal species may be transmitted from swine because of the high homology of genomic sequences between PRV isolates from these animals and the commercial vaccine strains or swine epidemic strains (14, 17, 18). Our previous studies confirmed the transmission route of PRV from pigs to dogs (14, 18). Cats are usually infected with the PRV through direct contact with PRV-contaminated raw pork (19). Of course, the route of infection may be indirect. Viruses can be transmitted *via* viral excretion or by virally contaminated fomites. A series of case reports on the outbreak of this disease in sheep, cats, and dogs have confirmed this transmission route (20). More efforts are required to monitor viral epidemics and morbidity in cats.

With the presence of companion animals, cats have become increasingly ubiquitous in human life, resulting in a hidden threat to humans due to the susceptibility of cats and humans to PRV. Although the occurrence of this disease in cats is sporadic, PR disease should receive more attention because it is easily mistaken

for rabies, and death occurs rapidly. Thus, it is necessary to investigate the prevalence of PRV in cats, especially pets. Previous reports have indicated that cats can be infected with highly pathogenic PRV mainly through contact with PRV-contaminated raw pork and die within 12–48 h after the onset of clinical signs (13). Considering the widespread use of attenuated PRV strains in commercial vaccines, we speculated that PRV might be widely distributed in cats. To test this hypothesis, we performed a retrospective investigation of PRV infection in cats. Our data provide evidence that *gE*-deleted PRV strains are prevalent in Chinese cats. Unfortunately, no virus was successfully isolated, owing to low viral titers in swab specimens and the long storage time of the samples. More efforts are required to monitor PRV-infected cats for virus identification.

The pathogenicity of highly pathogenic PRV strains in cats was assessed. According to previous publications, the incubation time of PRV in cats is ∼48–72 h, and death mainly occurred within 12–48 h after the onset of typical symptoms of this disease. To date, the pathogenicity of attenuated PRV strains in cats has remained unclear. Therefore, in this study, we infected cats with an attenuated PRV strain to evaluate its pathogenesis. We used the attenuated PRV strain Bartha-K61 as the viral template because Bartha-K61 is widely used in the Chinese swine industry, resulting in relatively favorable control of this disease (16, 21, 22). Similar to previous publications (11), the incubation period of highly virulent PRV infection in cats was ∼24–48 h, and all the cats died within 24 h after the onset of clinical signs. In contrast, the Bartha-K61-infected cats did not present any neurological symptoms, except for anorexia, anxiety, and crying. To confirm the association of signs with Bartha-K61, we performed an autopsy of a Bartha-K61-infected cat and recorded gross abnormalities at necropsy. Interestingly, no pathological changes were observed. It appears that Bartha-K61 is not pathogenic to cats. However, why do Bartha-K61-infected cats present clinical signs? The impaired intra-axonal transport process may affect replication, the spread, and tissue tropism of the Bartha strain *in vivo*. Further effort is required to study the involvement of Bartha-K61 with clinical signs in cats.

DATA AVAILABILITY STATEMENT

The original contributions presented in the study are included in the article/supplementary material, further inquiries can be directed to the corresponding author.

ETHICS STATEMENT

The animal study was reviewed and approved by the Animal Care Committee at the Institute of Animal Sciences of the Chinese Academy of Agricultural Sciences approved the animal experiment protocols (approval ID: IAS-2021-112).

AUTHOR CONTRIBUTIONS

RL and LT designed the study, interpreted the data, and gave final approval of the version to be published. LT, JZ, QC, SZ, LL, XT, and SH performed the experiments. WY mainly responsible for the collection of samples. All authors contributed to the article and approved the submitted version.

FUNDING

This work was supported by the Central Public-Interest Scientific Institution Basal Research Fund (Grant Nos. 2020-YWF-YTS-10 and 2022-YWF-ZYSQ-12) and the Agricultural Science and Technology Innovation Program of China (ASTIP-IAS15).

REFERENCES

1. Mettenleiter TC. Aujeszky's disease (pseudorabies) virus: the virus and molecular pathogenesis–state of the art, June 1999. *Vet Res*. (2000) 31:99–115. doi: 10.1051/vetres:2000110
2. Nauwynck H, Glorieux S, Favoreel H, Pensaert M. Cell biological and molecular characteristics of pseudorabies virus infections in cell cultures and in pigs with emphasis on the respiratory tract. *Vet Res*. (2007) 38:229–41. doi: 10.1051/vetres:200661
3. Mettenleiter TC. Immunobiology of pseudorabies (Aujeszky's disease). *Vet Immunol Immunopathol*. (1996) 54:221–9. doi: 10.1016/S0165-2427(96)05695-4
4. Marcaccini A, Lopez Pena M, Quiroga MI, Bermudez R, Nieto JM, Aleman N. Pseudorabies virus infection in mink: a host-specific pathogenesis. *Vet Immunol Immunopathol*. (2008) 124:264–73. doi: 10.1016/j.vetimm.2008.03.013
5. MacDiarmid SC. Aujeszky's disease eradication in New Zealand. *Aust Vet J*. (2000) 78:470–1. doi: 10.1111/j.1751-0813.2000.tb11862.x
6. Muller T, Batza HJ, Schluter H, Conraths FJ, Mettenleiter TC. Eradication of Aujeszky's disease in Germany. *J Vet Med B Infect Dis Vet Public Health*. (2003) 50:207–13. doi: 10.1046/j.1439-0450.2003.00666.x
7. Hahn EC, Fadl-Alla B, Lichtensteiger CA. Variation of Aujeszky's disease viruses in wild swine in USA. *Vet Microbiol*. (2010) 143:45–51. doi: 10.1016/j.vetmic.2010.02.013
8. Pomeranz LE, Reynolds AE, Hengartner CJ. Molecular biology of pseudorabies virus: impact on neurovirology and veterinary medicine. *Microbiol Mol Biol Rev*. (2005) 69:462–500. doi: 10.1128/MMBR.69.3.462-500.2005
9. Liu Q, Wang X, Xie C, Ding S, Yang H, Guo S, et al. A novel human acute encephalitis caused by pseudorabies virus variant strain. *Clin Infect Dis*. (2021) 73:e3690–700. doi: 10.1093/cid/ciaa987
10. Morest DK. Experimental study of the projections of the nucleus of the tractus solitarius and the area postrema in the cat. *J Comp Neurol*. (1967) 130:277–300. doi: 10.1002/cne.901300402
11. Hagemoser WA, Kluge JP, Hill HT. Studies on the pathogenesis of pseudorabies in domestic cats following oral inoculation. *Can J Comp Med*. (1980) 44:192–202.
12. Card JP, Enquist LW, Miller AD, Yates BJ. Differential tropism of pseudorabies virus for sensory neurons in the cat. *J Neurovirol*. (1997) 3:49–61. doi: 10.3109/13550289709015792
13. Masot AJ, Gil M, Risco D, Jimenez OM, Nunez JI, Redondo E. Pseudorabies virus infection (Aujeszky's disease) in an Iberian lynx (Lynx pardinus) in Spain: a case report. *BMC Vet Res*. (2017) 13:6. doi: 10.1186/s12917-016-0938-7
14. Tu L, Lian J, Pang Y, Liu C, Cui S, Lin W. Retrospective detection and phylogenetic analysis of pseudorabies virus in dogs in China. *Arch Virol*. (2021) 166:91–100. doi: 10.1007/s00705-020-04848-4

15. Wong G, Lu J, Zhang W, Gao GF. Pseudorabies virus: a neglected zoonotic pathogen in humans? Emerg Microbes Infect (2019) 8:150–154. doi: 10.1080/22221751.2018.1563459
16. Sun Y, Luo Y, Wang CH, Yuan J, Li N, Song K, Qiu HJ. Control of swine pseudorabies in China: Opportunities and limitations. *Vet Microbiol*. (2016) 183:119–24. doi: 10.1016/j.vetmic.2015.12.008
17. Quiroga MI, Nieto JM, Sur J, Osorio F. Diagnosis of Aujeszky's disease virus infection in dogs by use of immunohistochemistry and *in-situ* hybridization. *Zentralbl Veterinarmed A*. (1998) 45:75–81. doi: 10.1111/j.1439-0442.1998.tb00803.x
18. Li H, Liang R, Pang Y, Shi L, Cui S, Lin W. Evidence for interspecies transmission route of pseudorabies virus via virally contaminated fomites. *Vet Microbiol*. (2020) 251:108912. doi: 10.1016/j.vetmic.2020.108912
19. Thiry E, Addie D, Belak S, Boucraut-Baralon C, Egberink H, et al. Aujeszky's disease/pseudorabies in cats: ABCD guidelines on prevention and management. *J Feline Med Surg*. (2013) 15:555–6. doi: 10.1177/1098612X13489211
20. Henderson JP, Graham DA, Stewart D. An outbreak of Aujeszky's disease in sheep in Northern Ireland. *Vet Rec*. (1995) 136:555–7. doi: 10.1136/vr.136.22.555
21. Klupp BG, Lomniczi B, Visser N, Fuchs W, Mettenleiter TC. Mutations affecting the UL21 gene contribute to avirulence of pseudorabies virus vaccine strain Bartha. *Virology*. (1995) 212:466–73. doi: 10.1006/viro.1995.1504
22. Muller T, Hahn EC, Tottewitz F, Kramer M, Klupp BG, Mettenleiter TC, Freuling C. Pseudorabies virus in wild swine: a global perspective. *Arch Virol*. (2011) 156:1691–705. doi: 10.1007/s00705-011-1080-2

Conflict of Interest: The authors declare that the research was conducted in the absence of any commercial or financial relationships that could be construed as a potential conflict of interest.

Publisher's Note: All claims expressed in this article are solely those of the authors and do not necessarily represent those of their affiliated organizations, or those of the publisher, the editors and the reviewers. Any product that may be evaluated in this article, or claim that may be made by its manufacturer, is not guaranteed or endorsed by the publisher.

frontiers | Frontiers in Veterinary Science

REVIEW
published: 19 April 2022
doi: 10.3389/fvets.2022.850771

Effect of Fluoride on Cytotoxicity Involved in Mitochondrial Dysfunction: A Review of Mechanism

Mingbang Wei[1,2†], *Yourong Ye*[1,2†], *Muhammad Muddassir Ali*[3], *Yangzom Chamba*[1,2], *Jia Tang*[1,2*] *and Peng Shang*[1,2*]

[1] College of Animal Science, Tibet Agriculture and Animal Husbandry College, Linzhi, China, [2] The Provincial and Ministerial Co-founded Collaborative Innovation Center for R&D in Tibet Characteristic Agricultural and Animal Husbandry Resources, Linzhi, China, [3] Institute of Biochemistry and Biotechnology, University of Veterinary and Animal Sciences, Lahore, Pakistan

OPEN ACCESS

Edited by:
Fazul Nabi,
Lasbela University of Agriculture, Water and Marine Sciences, Pakistan

Reviewed by:
Eman Khalifa,
Faculty of Veterinary Medicine/ Alexandria University Branch (Matrouh University), Egypt
Niharika Sinha,
Michigan State University, United States

***Correspondence:**
Peng Shang
nemoshpmh@126.com
Jia Tang
xztangj@126.com

[†] These authors have contributed equally to this work

Specialty section:
This article was submitted to Comparative and Clinical Medicine, a section of the journal Frontiers in Veterinary Science

Received: 08 January 2022
Accepted: 07 February 2022
Published: 19 April 2022

Citation:
Wei M, Ye Y, Ali MM, Chamba Y, Tang J and Shang P (2022) Effect of Fluoride on Cytotoxicity Involved in Mitochondrial Dysfunction: A Review of Mechanism. Front. Vet. Sci. 9:850771. doi: 10.3389/fvets.2022.850771

Fluoride is commonly found in the soil and water environment and may act as chronic poison. A large amount of fluoride deposition causes serious harm to the ecological environment and human health. Mitochondrial dysfunction is a shared feature of fluorosis, and numerous studies reported this phenomenon in different model systems. More and more evidence shows that the functions of mitochondria play an extremely influential role in the organs and tissues after fluorosis. Fluoride invades into cells and mainly damages mitochondria, resulting in decreased activity of mitochondrial related enzymes, weakening of protein expression, damage of respiratory chain, excessive fission, disturbance of fusion, disorder of calcium regulation, resulting in the decrease of intracellular ATP and the accumulation of Reactive oxygen species. At the same time, the decrease of mitochondrial membrane potential leads to the release of Cyt c, causing a series of caspase cascade reactions and resulting in apoptosis. This article mainly reviews the mechanism of cytotoxicity related to mitochondrial dysfunction after fluorosis. A series of mitochondrial dysfunction caused by fluorosis, such as mitochondrial dynamics, mitochondrial Reactive oxygen species, mitochondrial fission, mitochondrial respiratory chain, mitochondrial autophagy apoptosis, mitochondrial fusion disturbance, mitochondrial calcium regulation are emphasized, and the mechanism of the effect of fluoride on cytotoxicity related to mitochondrial dysfunction are further explored.

Keywords: fluoride, apoptosis, mitochondrial dysfunction, cytotoxicity, ROS

INTRODUCTION

Fluoride is abundantly existing in our environment in different forms and it can cause serious harm to the ecological environment and human health. Worldwide numerous cases of fluorosis have been observed. Especially, in China, the fluorine pollution in soil is of serious concern, as it is causing a greater negative impact on human health and ecological environment (1). The situation of fluorosis in 20 countries showed that about 260 million people suffer from fluorosis caused by various fluorine sources (2). In 1997, fluorosis in China showed that about 31 million people showed signs of fluorosis (3), including about 21 million dental fluorosis patients and 10 million skeletal fluorosis patients (DDCMH, China). A large amount of fluoride is deposited into the environment, which in the long run will lead to excessive fluorine content in the soil and water environment,

which ultimately penetrate into agricultural products, and resulting in excessive fluorine content in crops (4). A survey is shown that most of the fluorine pollution in China comes from iron and steel, phosphate fertilizer and electrolytic aluminum, in which the iron and steel industry is the biggest cause of fluorine pollution (5). He et al. (6) analyzed the fluorine pollution in 122 kinds of vegetables and 36 topsoil samples within 10 kilometers range of the aluminum plant abandoned for 5 years. It was observed that the fluorine content of 89.26% of the agricultural products was beyond maximum permissible level of food pollutants in China.

Fluoride is a necessary element in the normal development and growth of animals, but excessive fluoride will cause damage to the animal body. A large number of phenomena showed that the typical manifestations of fluorosis are; dental fluorosis (7), hypertension (8), skeletal fluorosis (9), reproductive disorders (10) and dementia (11). A large amount of fluoride deposition mainly damages to bones, teeth, and central nervous system via passing through the blood-brain barrier that can lead to insomnia or somnolence and other symptoms (12). There is evidence that excessive fluoride intake can damage various organs including brain (13, 14), liver (15, 16), kidney (17), ovary (18). Fluoride in the environment into the body is mainly absorbed by the stomach and intestines, through the cell membrane, deposited in bone and soft tissue, causing damage to bone and soft tissue. The most important deposition point is in the liver, and the excretion point is mainly the kidney (19). Long-term exposure to fluoride lead to the accumulation of fluoride in liver tissue, affect the activity of antioxidant enzymes and the expression of cyclooxygenase, seriously destroy the ultrastructure of hepatocytes, cause significant pathological changes of liver tissue, and destroy the balance of the body (20). Higher concentration of sodium fluoride increases the expression of phosphorus (P), potassium (K), blood urea nitrogen (BUN), uric acid (UA) and creatinine (CRE), and induce renal histopathological damage and lead to apoptosis (21). It also increased the mRNA and protein expression levels of death receptor (FAS), tumor necrosis factor (TNF), TNF-related apoptosis-inducing ligand (TRAIL), Caspase 8, Caspase 3 and poly (ADP-ribose polymerase) on the cell surface. It has been reported that long-term drinking water with high levels of fluoride has a higher risk of developing dementia than drinking water with relatively low levels of fluoride (6). Moreover, long-term exposure to fluoride can significantly increase the expression of mRNA related to the neurotoxicity of fluoride and down-regulate the pathways related to learning and memory in the hippocampus of their offspring, indicating that long-term exposure to fluoride lead to brain nervous system damage (22). Neurotoxicity caused by fluoride lead to apoptosis, production of reactive oxygen species, impaired mitochondrial dynamics and decreased ability of antioxidant enzymes (23–25). A large number of studies have shown that absorbed fluoride can damage the structure and function of tissues and cells, such as thyroid (26), spleen, cecal tonsilla lymphocytes, human neuroblastoma SH-SY5Y cells, ameloblasts and Leydig cells, resulting in apoptosis (27, 28). At the same time, in recent years, apoptosis induced by fluoride through mitochondria has attracted wide attention.

It is well known that high concentrations of fluoride can lead to a certain degree of toxicity in organs or systems, such as primer oxidative stress, cell cycle arrest and apoptosis, resulting in nuclear condensation, nuclear membrane rupture, mitochondrial vacuolation, fragmentation and mitochondrial fission (as shown in **Table 1**). Fluoride causes cytotoxicity by interfering with the mechanism of enzyme action and calcium metabolism (55). Certain amount (1–2%) of fluoride can cause mucosal inflammation and necrosis (56). In fluoride induced neuronal damage, inhibition of mitochondrial fission is involved in autophagy and excessive apoptosis (57). The cellular damage mechanism of fluoride is usually via protein inhibition, organelle destruction, pH change and electrolyte imbalance (58, 59). Absorption of elevated concentrations of fluoride can lead to strong DNA damage, mainly due to DNA single-strand or double-strand DNA breakage (60) caused by oxidative stress of free radicals. In fewer cases of fluoride-amino acid binding, it is shown that most of the metal protein active sites in related proteins bind to fluoride or fluoride-metal complexes which act as substrate mimics (58, 61). Fluoride inhibits nutrient transport, cell respiration and glycolysis (62, 63) through the inhibition of metalloproteins (64). At the cellular level, long-term exposure to fluoride lead to electrolyte imbalance due to inhibition of transmembrane proteins, mitochondrial abnormalities, metabolic disruption and stress signal induction (65–67). Long-term exposure to fluoride causes the permanent damage of mitochondria and abnormal respiratory chain, mainly due to the reduction of ATP produced by anaerobic glycolysis ($ATP \rightarrow ADP+AMP+H^+$), the release of protons, leading to intracellular acidification, leading to oxidative stress (62, 64, 68). Moreover, fluoride irreversibly destroys cells and organelles via destroying the unfolded protein response pathway of endoparasitic reticulum (69, 70), directly removing Ca^{2+} and ER proteins or stimulating oxidative stress signals, and (71, 72) disturbing Ca^{2+} balance (73) in mitochondria via excessive release of Ca^{2+}. The activation of G protein in the Golgi apparatus (74) by fluoride leads to Ca^{2+}-dependent activation of exocytosis. Long-term exposure of fluoride irreversibly damages the integrity of the mitochondrial membrane (75), resulting in mitochondrial dysfunction. Fluoride can change mitochondrial permeability, consume ATP, inhibit the normal operation of cellular respiratory chain, reduce mitochondrial activity, and release cytochrome C, resulting in oxidative stress (76, 77).

Mitochondria are the main energy-supplying organelles of cells, which are closely related to the regulation of physiological function of eukaryotic cells (78, 79). Mitochondria play an important part in energy metabolism, apoptosis, cell differentiation, cell signal transduction and iron metabolism (10, 80, 81). After long-term exposure to fluoride or absorption of abnormal concentrations of fluoride, the structure of mitochondria in cells and tissues is seriously damaged. This results in decrease of number of mitochondria, abnormal activity of the respiratory chain, increase of oxidative stress, gene damage and biogenic dysfunction. Fluoride can induce the balance between fission and fusion of mitochondria, resulting in abnormal function and morphology of mitochondria. Fluoride

TABLE 1 | Apoptosis mechanism related to mitochondrial disturbance caused by fluorosis.

Pathways of apoptosis	Mechanism	Related factors	References
Energy metabolic pathway	It leads to the inhibition of the expression / activity of respiratory chain complex, the insufficient production of ATP, the accumulation of ROS in cells, and the apoptosis of cells.	NDUFV2, SDHA, CYC1	(29, 30)
	It leads to the decrease of the activity of key enzymes in mitochondrial intima and the production of ATP, which leads to cell apoptosis.	ATP5J, ATP5H, The ATP synthase	(31–34)
Reactive oxygen species pathway	Destroy the oxygen homeostasis, so as to destroy the normal biological process, from the mitochondrial permeability transition pore (mPTP) opening mechanism, increase mmp, resulting in the content of CtyC, caspase 3, caspase 8, caspase 9, RARP, the release of ROS oxidative stress signal, resulting in the increase of ROS and apoptosis.	mmp, Cty C, caspase 3, caspase 8, caspase 9, RARP	(35, 36)
	ROS interacts with purine bases, pyrimidine bases and ribose to increase the content of messenger RNA, destroy single or double strands of DNA, activate DNA-dependent proteases and p53, and cause cell apoptosis.	DNA dependent protease, P53	(37)
	It causes a small amount of electrons to escape from the electron chain, forms peroxides, aggravates oxidative stress, causes mitochondrial complex I to produce ROS and activates NLRP3, ASC and caspase 1.	NLRP3, ASC, caspase 1	(38)
	Cells stop in G0/G1 phase, which aggravates apoptosis.	/	(35)
	The intermembrane gap protein is released after permeating into the outer membrane of the mitochondria, activating cystatin and leading to apoptosis.	Smac, Diabio, Endonuclease G	(39)
Autophagy and apoptosis	Inhibit cell proliferation, induce apoptosis and autophagy. After fluoride invasion, autophagy apoptosis pathway was activated, and apoptosis factor, caspase, ATG protein and p53 regulated autophagy.	BCL-2, Bax, caspase, ATG protein, P53	(40)
	Fluoride invades as long as it attacks the main autophagy pathway of mitochondria	Sirt1/FoxO3a, PINK1/Parkin, Nix/BNIP3L, BNIP3 and FUNDC1, PHB2	(41–45)
	Cause autophagy to accumulate in small volume and induce autophagy injury and inhibit the release of Cyt C.	Cyt C	(46)
Fission and fusion	The synergistic action of fission molecules leads to the breaking of the balance of fission and fusion and the morphological changes of mitochondria.	Drp1, Dyn2	(47, 48)
	Decrease the level of fission protein and increase the level of fusion protein	Cyt C, caspase 3, caspase 9, Mfn1, Mfn2, Fis1, Pro-caspase9	(49, 50)
Calcium pathway	F invasion can combine with Ca^{2+} to form insoluble CaF_2 and reduce F absorption and cytotoxicity.	/	(51, 52)
	Ca^{2+} strictly controls the entry of ATP and ROS, F^- into cells in a simple way. Mitochondria absorb Ca^{2+}, through mitochondrial Ca^{2+} unidirectional receptors and then flow into mitochondria through Ca^{2+} unidirectional transporters (MEU), manipulating energy metabolism, resulting in ROS accumulation and cell apoptosis.	MEU	(53)
	ER- mitochondria-calcium-apoptosis: caspase activation leads to the increase of Ca^{2+} content, which stimulates the release of CytC and pro-apoptotic factors into mitochondria. CytC and APAF-1 form apoptotic bodies, which indirectly act on the upstream signal of apoptosis, leading to downstream caspase 3 and caspase 7 division, resulting in cell apoptosis.	Caspase 3, caspase 7, Cyt C, BcL-2, Bax	(54)

induced mitochondrial kinetic damage and oxidative stress in SH-SY5Y cells revealed that sodium fluoride (NaF) could increase the level of fusion protein and significantly reduce the level of protein fission in rat hippocampus, indicating that fluoride leads to the occurrence of human Alzheimer's disease (10) by inhibiting mitochondrial fission, autophagy and excessive apoptosis. Studies have demonstrated that fluoride enters the body, resulting in the production and accumulation of a large amount of ROS in the brain, an increase in lipid and nucleic acid oxidation, and a decrease in the activity of antioxidant enzymes. Zhou et al. also found that fluoride exposure can lead to mitochondrial damage and ROS accumulation (82–85) in mouse lymphocytes, which further indicates that fluorosis can lead to mitochondrial fission / fusion imbalance and increase of intracellular ROS.

POTENTIAL MOLECULAR MECHANISM OF MITOCHONDRIAL DYSFUNCTION INVOLVED IN CELL DAMAGE INDUCED BY FLUOROSIS

Molecular Mechanisms of Energy Metabolism Involved in Fluoride-Induced Cell Injury

Numerous study states that excessive intake of fluoride lead to cell dysplasia or decrease the ability of cell proliferation and differentiation. The main reason is that, excessive fluoride destroys the ultrastructure of cell mitochondria and interfere with the expression of respiratory chain complex, being expected to result in a decrease in the content of ATP and an increase

in the content of ROS. Some studies have shown that excessive fluoride intake cause mitochondrial dysfunction and reduce the production of ATP in cardiomyopathy (15), hepatocytes (84), kidney cells (86), granuloma cells (85), oocytes (87). Mitochondrial respiratory chain is the principal link of ATP production, and ATP production depends on the mitochondrial respiratory chain complex (88) in the mitochondrial inner membrane. Once the transmission of mitochondrial respiratory chain is blocked, ATP synthesis will be affected, resulting in mitochondrial dysfunction. Mitochondrial respiratory chain complex I (NDUFV2), mitochondrial respiratory chain complex II (SDHA) and mitochondrial respiratory chain complex III (CYC1) play an important role in regulating mitochondrial function and are the key links between ATP production (29, 30). Mitochondrial respiratory chain complex I (NDUFV2) and mitochondrial respiratory chain complex II (SDHA) are the main receptors for electron entry into the mitochondrial electron transfer chain (30, 89, 90), which manage the entry and exit of related ions inside and outside the membrane; mitochondrial respiratory chain complex III (CYC1) is called the gatekeeper of mitochondrial respiratory chain, which maintains the normal production capacity of mitochondria. Mitochondrial respiratory chain complex I (NDUFV2) mainly catalyzes NADH oxidation, while mitochondrial respiratory chain complex II (SDHA) mainly catalyzes succinic acid oxidation to fuming acid (91). Mitochondrial respiratory chain complex III (including CYC1) is an important target of mitochondrial oxidative phosphorylation and the third main source of reactive oxygen species (92). Once the expression or activity of the mitochondrial respiratory chain complex is blocked, it can lead to insufficient production of ATP and accumulation of ROS in mitochondria, resulting in severe mitochondrial dysfunction. Abnormal expression of mitochondrial respiratory chain complex can cause mitochondrial dysfunction. Mitochondrial respiratory chain complexes such as NDUFV2, SDHA and CYC1 are involved in intracellular oxidative phosphorylation and ATP synthesis. The expression of NDUFV2, SDHA and CYC1 in heart increased significantly after excessive fluoride treatment, which may be related to the damage of the mitochondrial respiratory chain. At the same time, change of mitochondrial membrane will affect the transmission of mitochondrial respiratory chain. ATP5J and ATP5H are key enzymes in mitochondrial intima, which can promote the process of oxidative phosphorylation to increase the synthesis of ATP. Ovarian granulose cells were severely damaged after exposure to fluoride, and the content of ATP in the ovary was significantly reduced. The mechanism of this phenomena was mainly due to the damage of its sub cellular organelles (mitochondria, ribosomes, endoparasitic reticulum, geology apparatus, etc.). The mitochondria showed vacuolation, crest fracture, dissolution, etc. It was assumed that mitochondria were destroyed when granulose cells were exposed to fluoride during the development and maturation of follicles and oocytes, resulting in insufficient cell energy supply and massive cell damage. These results further suggest that the normal expression of the mitochondrial respiratory chain complex and ATP5J and ATP5H play a crucial role in the maintenance of mitochondrial function in ovarian granulose cells (93). It has been reported that the content of ATP in liver and kidney decreased after fluoride treatment, and the expression of important ATP synthase ATP5J and ATP5H decreased significantly, which further indicated that fluoride or fluoride could destroy the main synthase of the mitochondrial respiratory chain. Previous studies have shown that fluoride has negative effects on sperm morphology (94), captivation (95), overestimation (96), acrosome reaction and fertilization ability (97, 98). Mammalian sperm need a lot of energy to complete fertilization in the process of energy acquisition and hyperventilation, while glycolysis and mitochondrial respiration are the key links of energy generation (99). Mitochondrial respiration is considered to be the main source of ATP production, and the production efficiency of ATP is higher than that of glycolysis (100, 101), indicating that fluorine's harm to sperm mainly lies in reducing sperm ATP production and vitality. The study reported that in fluorosis areas, the incidence of heart disease is associated with long-term exposure to fluoride; such heart disease symptoms are often characterized by atherosclerosis, myocardial infarction and high blood pressure. The regular contraction and relaxation of the heart are mainly caused by the production of ATP in myocardial fibers and mitochondria of cardiomyopathy. The content of total phosphorus decreased after fluoride-induced cardiomyopathy injury. Mitochondrial ATP synthase plays an important role in the synthesis of ATP in mitochondria, which is mainly composed of two parts: water-soluble protein complex F_1 and hydrophobic part F_0. ATP5J and ATP5H were closely related to ATP synthesis. After fluoride stimulation, the mRNA expression and protein levels of ATP5J and ATP5H increased significantly, but ATP production decreased. Therefore, the increased expression of ATP5J and ATP5H compensates for the mitochondrial dysfunction induced by fluoride, which further lead to the decrease of ATP synthesis. It has been reported that mitochondrial respiratory chain damage can induce a sharp increase of intracellular ROS.

Potential Molecular Mechanisms of Fluoride-Induced Mitochondrial ROS Involved in Cell Damage Induced by Fluorosis

Fluorine is a small molecular element with active polarity and often exists in nature. Some studies have shown that long-term exposure to fluoride and exceeding the threshold of the body will not only cause damage to various tissues of the body (102), but also invade the central nervous system and produce dementia (103). Some studies have also shown that fluoride can lead to fetal mental retardation, mainly because fluoride can break through the placental barrier, enter the fetal brain, and accumulate in the fetal brain (104). Some studies have shown that ROS-mediated dysfunction of mitochondrial respiratory chain can lead to fluoride-induced cell damage (105). Some studies have shown that fluoride may transform the apoptosis pathway into necrosis, which shows the increase of inhibitory apoptosis factors. Mitochondria can cause cell injury or apoptosis by producing ROS, pro-inflammatory signals or through mitochondrial membrane permeability (106).

Excessive ROS can damage the structure and function of mitochondria, and when mitochondrial dysfunction occurs, the oxygen homeostasis in the tissue is destroyed, resulting in the damage of normal cellular biological processes. It is released from mitochondria through the mitochondrial permeability conversion pore (mPTP) opening mechanism (107). When ROS is used as a signal of oxidative stress, the increase of intracellular reactive oxygen species (ROS) can activate the signal pathway of apoptosis. Once the apoptosis stimulus signal is present, excessive ROS production contributes to macromolecular oxidation, leading to free radicals attacking membrane phospholipids, leading to membrane damage by inducing lipid peroxidation, mitochondrial membrane depolarization, and apoptosis (38). Mitochondria is both ROS targets and sources of additional ROS production. Studies have demonstrated that the release of cytochrome C (CytC) may lead to the production of ROS (108). At the same time, previous studies have shown that the formation of reactive oxygen species opens the mitochondrial permeability conversion pore injection (mPTP drug) and increases the destruction of mitochondrial membrane potential (MMP), which then causes the subsequent increase in Cyt C, leading to the reduction of Caspase-3 and eventual apoptosis (36). Studies have shown that ROS can interact with the purine base, pyrimidine base and ribose. At the same time, ROS can destroy a single or double strand of DNA and activate DNA-dependent protein kinases and P53, leading to cell apoptosis (37). Studies confirmed that NaF could improve HL-60 cells (109), testicular interstitial cells (110), H9C2 cardiomyopathy (111), oocytes (112), human lung BeAS-2B cells (113), rat liver and thymocytes (114), CytC, caspase-3, caspase-9 mid or protein levels are associated with apoptosis. After exposure to fluoride, the expression of caspase-3, caspase-9 and caspase-8 in fish kidney and porcine hepatocytes increased in a dose-dependent manner, indicating that fluoride can induce Caspase-dependent apoptosis. In addition, Buckalew detected activated caspase-8, caspase-3, and polyhidrosis diphosphate ribose polymerase (PARP) by western blotting and found induction of apoptosis in ameloblasts (35). Secondly, Apoptosis caused by mitochondrial disorders is caused by oxidative damage (39), and the increase of ROS in cells can make cells stay in the G0/G1 phase, thus aggravating cell death (35). The release of cytomembrane gap proteins such as Smac/Diablo and endonuclease G after permeating the outer membrane of mitochondria can promote cell apoptosis by activating cysteine. Mitochondria continuously reduce oxygen by adding electrons resulting in the formation of many ROS and RNS, including superoxide, hydrogen peroxide, hydroxyl radical, hypochlorous acid, peroxynitrite anion and nitric oxide, which aggravate the oxidative stress of cells and lead to further apoptosis (39). A large number of studies in cell culture and experimental animal models have shown that the accumulation of fluoride in the brain leads to the production of more ROS, increased oxidation of lipids and nucleic acids, and decreased activity of antioxidant enzymes (115). ROS is a by-product of metabolism. A small number of electrons may escape from the mitochondrial electron transport chain, resulting in the production of superoxides. Increased oxidant load also promoted the production of additional ROS from mitochondrial complex I to further enhance cell oxidative stress and promote cell death (116). In addition, ROS produced by mitochondria can activate NLRP3, adaptive proteins ASC and caspase-1 to form inflammatory bodies, and the accumulation of damaged mitochondria aggravates inflammation and leads to cell damage. The change of mitochondrial permeability is another important cause of cell death, which leads to the dissipation of mitochondrial transmembrane potential and the cessation of oxidase (117). In addition, it can lead to rapid apoptosis necrosis (117). When apoptosis was induced by mitochondrial damage, the ATP produced by mitochondria through the respiratory chain decreased or ROS increased (118). Complexes I, II, III and IV from respiratory chains with ubiquinones and Cytc, and their inhibition can reduce the electron transport kinetics and Cytc.

Fluorine-Induced Mitochondrial Ca^{2+} Regulations Are a Potential Molecular Mechanism Involved in Fluoride-Induced Cell Damage

The latest evidence shows that fluoride can lead to soft tissue damage, and the degree of fluoride injury depends on the concentration of fluoride, exposure time and organ type (28). Fluorine has a pronounced effect on the bones of the body. When fluorine is absorbed by the blood, it is rapidly distributed all over the body and finally mainly accumulates in calcium-rich tissues such as bones and teeth. Excessive fluoride will make the collagen fibers of tibia loose, curved and heterogeneous, widen the bone lacuna space, decrease bone plasticity, reduce bone tolerance and increase the probability of fracture; excessive fluoride mainly leads to bone damage. Recently, it has been noted that the right amount of calcium can relieve fluorosis (52). A large number of literature have shown that F and Ca have a strong affinity. Supplementary Ca forms a novel complex, insoluble CaF_2, in the intestine by combining with F, which reduces the absorption and toxicity of fluoride (51). However, a large amount of serum calcium into bone tissue will lead to increasing bone mineral density, hyperosteogeny, hypocalcemia. The proliferation rate of osteoblasts reduced and apoptosis increased in fluorosis. Mitochondrial pathway is part of the most important pathways of apoptosis. Mitochondria are the main energy centers and the main source of ATP and ROS. Their functions are strictly controlled by Ca^{2+}. In the process of fluoride poisoning, mitochondrial Ca^{2+} uptake is needed in order to meet energy supply and demand, while maintaining reduced antioxidant capacity to prevent excessive release of ROS (119). Some studies have concluded that the content of fluoride and the level of Ca^{2+} in cells exposed to fluoride increased. This may be the product of simple diffusion of fluoride into the cell (120). The accumulation of fluoride may increase the release of excess Ca^{2+} from intracellular Ca^{2+} reserve, which makes cells vulnerable to damage. On the other hand, TSCE treatment decreased the fluoride content and Ca^{2+} level of fluoride-exposed cells. Mitochondria absorb Ca^{2+} through mitochondrial Ca^{2+} unidirectional receptor. Mitochondrial calcium unipolar (MCU) is the main mediator of Ca flowing

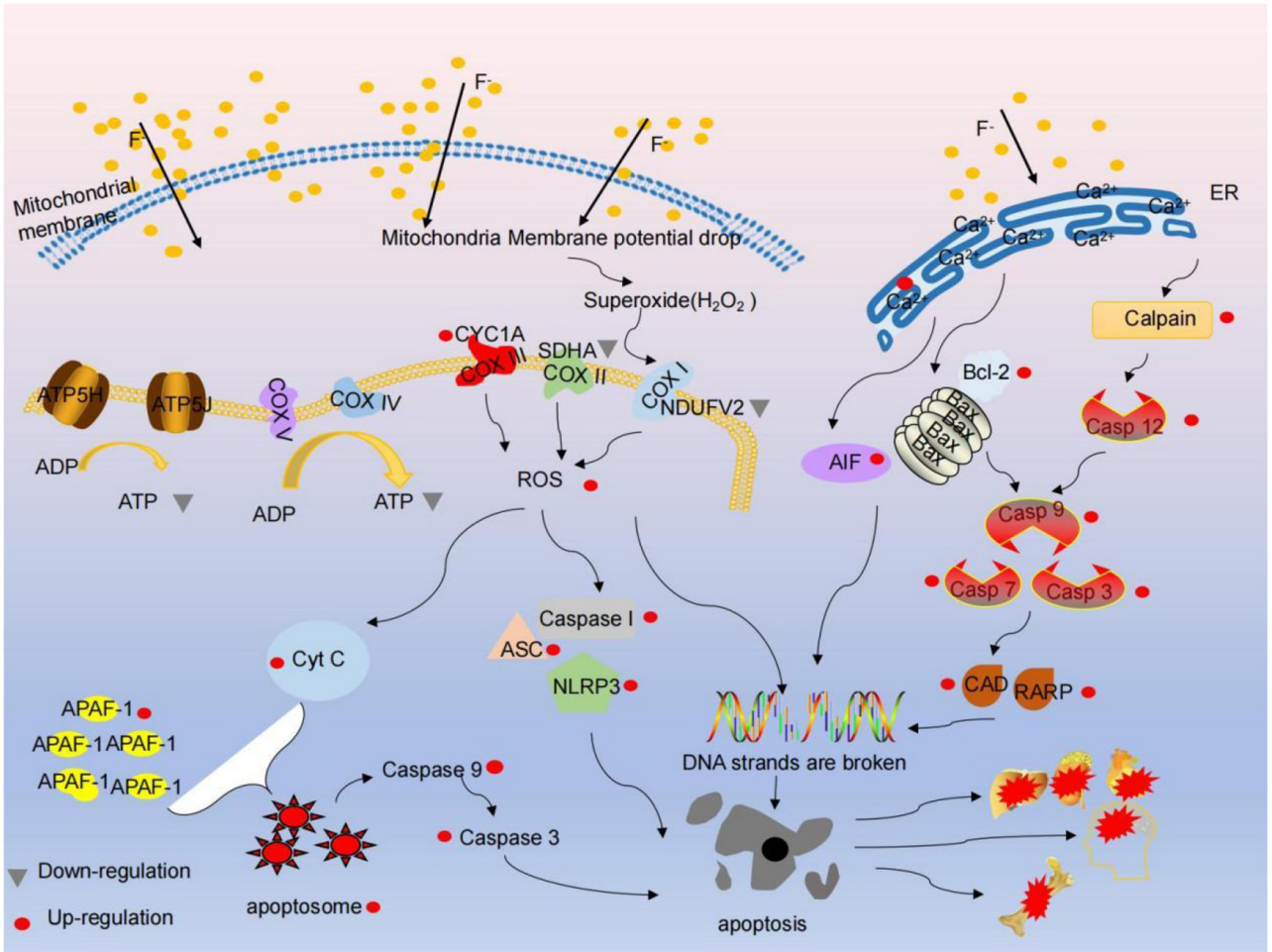

FIGURE 1 | Fluoride cause energy metabolism, mitochondrial respiratory chain damage, ER- mitochondrial-calcium-apoptotic pathway, resulting in apoptosis, resulting in dementia, skeletal fluorosis, hepatomegaly toxicity and other symptoms. (1) F^- entered the mitochondria by free diffusion, the activities of key enzymes of respiratory chain complexes COX I, COX II, Cox III and ATP decreased, protein expression levels of NDUFV2 and SDHA decreased, and ROS increased. At the same time, the decrease of ATP synthesis and the decrease of mitochondrial membrane potential caused the release of Cytc, which further triggered the caspase cascade reaction, which gave rise to cell apoptosis. (2) F^- enters the mitochondria by free diffusion, and a small amount of electrons escape from the respiratory chain to form peroxides (H_2O_2), which act on COX I, produce extra ROS, activate NLRP3, ASC and Caspase 1, and cause apoptosis. (3) A large amount of ROS can destroy the single strand / double strand of DNA and is expected to result in apoptosis. (4) F-activates Ca^{2+} dependent enzyme captain and apoptosis factor Bcl-2 through ER stress, which further triggers caspase cascade reaction, releases CAD and RARP, DNA single strand / double strand destruction, and further causes cell apoptosis. It eventually causes symptoms such as dementia, skeletal fluorosis, hepatomegaly toxicity.

into mitochondria, manipulating cell energy metabolism. ROS production and programmed cell death, all of which are essential for fluorosis (53). Studies have shown that fluoride may induce osteoblast apoptosis and mitochondrial dysfunction by increasing endoparasitic reticulum stress, and then activate the endoparasitic reticulum pathway induced by calcium. Fluoride induces endoparasitic reticulum stress; however, long-term endoparasitic reticulum stress induces apoptosis (121). Ca^{2+} is involved in almost all physiological activities and is the main messenger of the endoplasmic reticulum. Endoplasmic reticulum calcium pool is the main calcium pool in osteoblasts, and endoplasmic reticulum stress can induce increased intracellular Ca^{2+} level. Ca^{2+} activates Ca^{2+} dependent enzymes, such as Calpain, and divides and activates Caspase 12. Once activated, Caspase 12 acts at promoters (Caspase 9) and effectors (Caspase 7 and Caspase 3) to induce apoptosis (54). In particular, recent studies have demonstrated the relationship between ER, Mitochondria and calcium-apoptotic connection. In mitochondrial-mediated Caspase activation, the increase in intracellular Ca^{2+} level is effectively transmitted to mitochondria by pro-apoptotic BCL-2 family proteins (Bax and Bak), and indirectly acts as an important upstream signal of apoptosis. The increase of mitochondrial calcium level stimulated the release of pro-apoptotic molecules such as CtyC. In addition, CtyC and APAF-1 formed apoptosis bodies and treated pro-Caspase 9, which led to the division of downstream Caspase 3 and Caspase 7 in the cytoplasm and endoplasmic lumen (as shown in **Figure 1**).

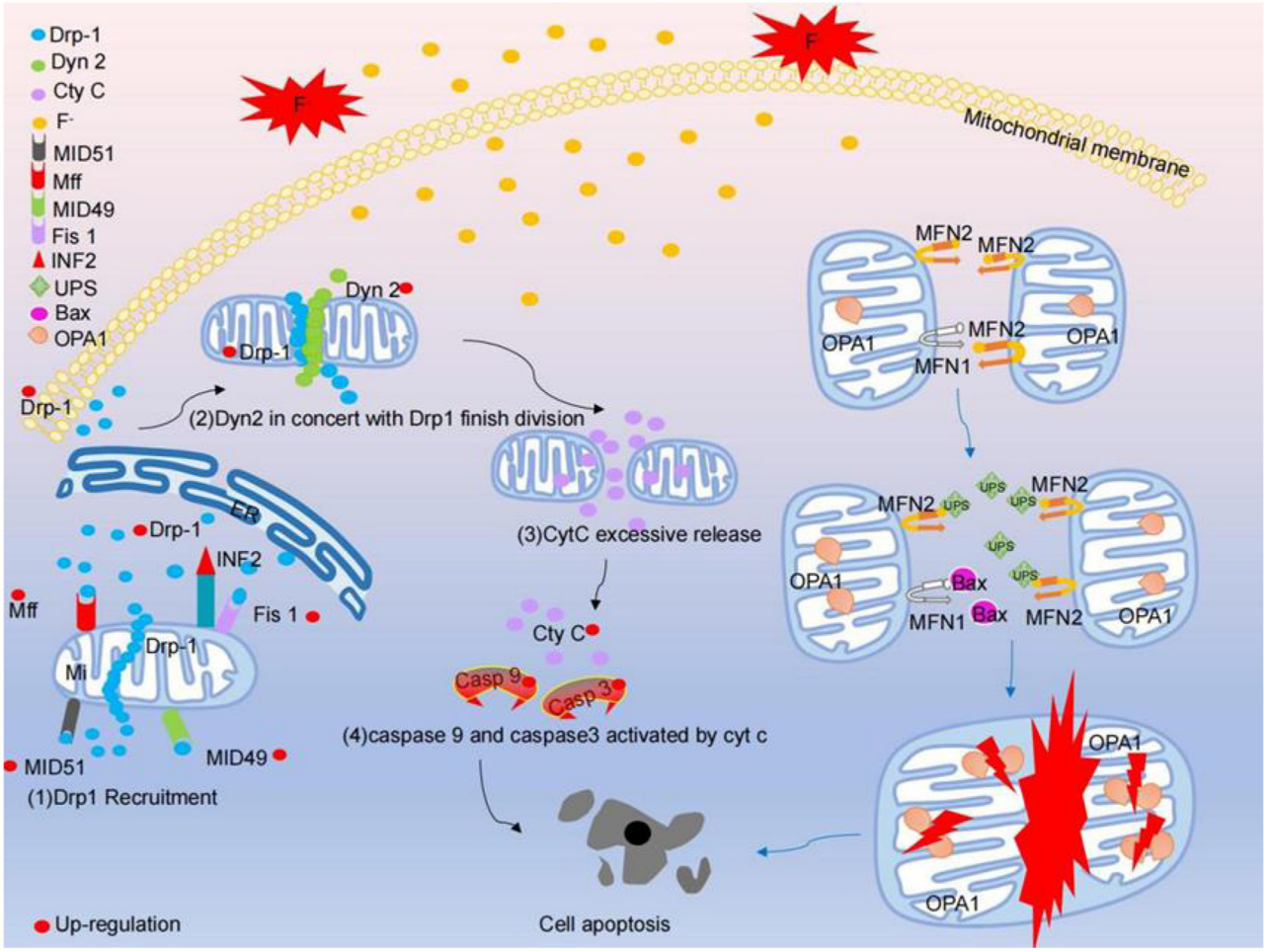

FIGURE 2 | Fluoride stimulates mitochondria, causing excessive mitosis and fusion disorders that result in apoptosis. Fluoride stimulates the fission pathway of mitochondria: (1) The expression of Mff, Fis1, MiD49 and MiD51 on the surface of mitochondria increased, and Drp1 was recruited from cytoplasm and endoplasmic reticulum. A large number of Drp1 form a circular structure in the middle of the mitochondria and compress the mitochondria. (2) Dyn2 and Drp1 are up-regulated together to finalize the division of mitochondria. (3) Excessive mitosis of mitochondria lead to structural damage of mitochondria, resulting in excessive release of Cyt c from the interior of mitochondria in the cytoplasm. (4) Caspase 9 and Caspase 3 are activated and eventually lead to apoptosis (5) (50). The mitochondrial fusion pathway stimulated by fluoride: after fluoride stimulation, the binding of mitochondrial surface fusion protein MFN1 to Bax increased, the UPS (ubiquitin-proteasome) in mitochondrial surface fusion protein MFN2 degraded, and the activity of mitochondrial membrane fusion protein OPA1 decreased, which comprehensively destroyed the process of mitochondrial fusion and finally led to apoptosis.

Fluoride-Induced Mitochondrial Fission and Fusion Are Involved in the Potential Molecular Mechanism of Cell Damage Induced by Fluorosis

Mitochondria play an important role in apoptosis, cell signal transduction and iron metabolism, which are related to mitochondrial dynamics, which are the process in which mitochondria form a network through the dynamic balance of fission and fusion. Fluorosis can cause mitochondrial dysfunction, which is partly due to the disruption of the balance between mitochondrial fission and fusion, which leads to changes in the morphology of mitochondria, which in turn leads to mitochondrial dysfunction (122). The neurotoxicity of fluoride is related to the destruction of mitochondria (123). Mitochondrial fission / fusion kinetics is very important for maintaining functional mitochondria (124). MID49, MID51, Mff, Fis-1, Drp1 and Dyn2 are necessary fission molecules to maintain mitochondrial division. However, the fusion between the outer membrane of mitochondria is mediated by dynamic protein family members called Mfn1 and Mfn2. The fusion between the inner membrane of mitochondria is mediated by a single dynamic protein family protein called fusion protein, optic nerve dystrophy 1 (OPA1). Under specific physiological conditions or under the pressure of harmful external factors, Drp1 aggregates on the surface of the outer membrane of mitochondria, forming a spiral structure to squeeze mitochondria (48). Then, Dyn2 and Drp1 interact cooperatively to regulate the final mitochondrial division step (47). Knockout of Drp1 can inhibit mitochondrial division and enhance mitochondrial networking

to form giant mitochondria, which supports the key role of Drp1 in mitochondrial fission (125). Overexpression of Drp1 can accelerate mitochondrial fission and lead to extensive mitochondrial breakage. Division in cells exhausted by Dyn2 can be concluded because the contraction of the mitochondrial membrane fails, resulting in non-division (47). In the brain of rats with chronic fluorosis, the level of mitotic protein increased and the mitochondria of cortical neurons split and redistributed. It has been reported that NaF increased the mRNA and protein levels of Mfn1 and Mfn2 and decreased the mRNA and protein levels of Fis1. At the same time, the level of Drp1 mRNA increased and the protein level of Drp1 reduced. The abnormal mitochondrial division induced by excessive fluoride is characterized by the increase in the number of mitochondria and the structural damage of this organelle. Mitochondrial damage induces the opening of mPTP, and mPTP releases Cyt C from the mitochondria into the cytoplasm (126). The Pro-Caspase 9 is then activated through the intermediate recruitment domain. Once activated, Caspase-9 cleaves and activates the executioner Caspase-3 to induce apoptosis degradation events (127). Fluoride stimulation lead to the increased mRNA expression levels of Cyt C, Caspase-9 and Caspase-3 in a dose-dependent manner, especially in 100 mg/L. Moreover, NaF significantly decreased the level of fission protein and increased the level of fusion protein in the hippocampus of offspring rats, suggesting that fluoride can induce mitochondrial fission / fusion imbalance (49, 50). Once the division / fusion balance is disturbed, the mitochondria will undergo morphological and functional changes. Studies have shown that mitochondrial fission inhibition plays a central role in NaF-induced mitochondrial abnormalities, autophagy defects, increased apoptosis and neuronal damage in human neuroblastoma cells treated with NaF. Mechanically, despite the partial recovery of autophagy, the pharmacological inhibition of mitochondrial fission aggravates NaF-induced mitochondrial defects and cell death by promoting apoptosis. It is suggested that exposure to environment-related levels of fluoride can lead to learning and memory impairment, accompanied by morphological changes of hippocampus mitochondria, such as fission inhibition and accelerated fusion, as well as autophagy deficiency, excessive apoptosis and neuronal loss. The disturbance of the cycle level of identified mitochondrial fission / fusion molecules are closely related to the mental loss of children exposed to fluoride in drinking water for a long time. In general, mitochondrial fission inhibition induces mitochondrial abnormalities, leading to abnormal autophagy and apoptosis, resulting in neuronal death (as shown in **Figure 2**).

Fluoride-Induced Mitochondrial Apoptosis Pathway Is Involved in the Potential Molecular Mechanism of Cell Injury Induced by Fluorosis

Fluorosis is primarily due to apoptosis caused by damage to mitochondria. It has been proved that fluoride or fluoride can increase the amount of apoptosis. A large number of literature have reported that mitochondrial-mediated pathway is involved in fluoride-induced apoptosis. As an important subcellular organelle, mitochondria are considered to be the center of the apoptosis pathway. There are three main types of proteins involved in this pathway: Bcl-2 family proteins, caspase and mitochondrial pro-apoptotic proteins. Mitochondrial damage results in the release of Cyt C from mitochondria to cytoplasmic sol, which can activate Caspase-3 and Caspase-9, leading to the formation of apoptosis bodies (46). Cyt C is the key factor that triggers the rapid activation of cysteine and key cellular proteases, which eventually leads to cell death. The release of Cyt C from mitochondria promotes the binding of APAF-1 to Caspase-9, which activates Caspase-9 and initiates the cascade of caspases. In addition, the downstream effector Caspase-3 in the cascade of cysteine aspartate enzymes can be triggered by the activation of Caspase-9, resulting in DNA fragmentation and apoptosis. Apoptosis factors Bcl-2 and Bax play an important role in initiating the permeability of the mitochondrial outer membrane and releasing pro-apoptotic proteins from mitochondria. Bax and Bcl-2 antagonist Bak can help apoptosis through the formation of pure compounds, while Bcl-2 and Bcl-Extra (BclxL) have been reported as endogenous permeability conversion inhibitors (128). In addition, the increase in intracellular reactive oxygen species (ROS), as a signal of oxidative stress, can also activate the apoptosis signal pathway. Once the apoptosis stimulation signal occurs, excessive ROS production contributes to macromolecular oxidation, causing free radicals to attack membrane phospholipids, resulting in membrane damage (129) by inducing lipid peroxidation, mitochondrial membrane depolarization and apoptosis. Sodium fluoride can increase the amount of cAMP and promote apoptosis. Through transcription analysis, mitochondria may play an important role in cAMP-induced apoptosis (130).

Fluorine-Induced Mitochondrial Autophagy Is Involved in the Potential Molecular Mechanism of Cell Damage Induced by Fluorosis

Autophagy is induced by many cytotoxic stimuli. The relationship between apoptosis and autophagy is complex and difficult to clarify. The process of apoptosis is often accompanied by autophagy (40). Most evidence show that autophagy is the protective mechanism of cell initiation. When autophagy is up-regulated, autophagy can inhibit apoptosis; similarly, apoptosis can also reduce autophagy (131). Under certain conditions, autophagy can not only promote survival, but also promote apoptosis. This process recovers damaged/outdated macromolecules and organelles (132). Autophagy mainly plays a survival role in adapting to unfavorable growth conditions or subsequent cell stress (133). It is mainly involved in differentiation, development, pathogen defense, aging, apoptosis and cell death (134, 135). Autophagy plays a significant role in cell protection under physiological conditions (136). The cytoarchitecture function of autophagy is realized through the negative regulation of apoptosis (137); After fluoride invasion, autophagy and apoptosis are activated at the same time, and can be regulated by the same factors, such as BCL-2 family

protein, caspase, ATG protein and p53 (42). On the other hand, autophagy and apoptosis are mutually antagonistic, and autophagy of damaged mitochondrial cells can reduce the transmission of apoptosis signals and protect normal cells. Studies have shown that fluorine can not only induce apoptosis of MC3T3-E1 cells, but also induce autophagy (138). Mammalian mitochondria autophagy is mainly mediated by the following pathways, such as PINK1/Parkin pathway (43), Nix/BNIP3L (42), BNIP3 (44) and FUNDC1 (41). PINK1/Parkin pathway is recognized as one of the important ways of mitochondrial autophagy, which is mainly involved in the elimination of damaged mitochondria (139). PHB2 is an inner mitochondrial membrane protein, which mainly plays a role in regulating the assembly and function of mitochondria. It is the receptor of PINK1/Parkin pathway and a marker of mitochondrial autophagy (140). It is observed that fluorine induced autophagy damage in testis is due to; by inhibiting autophagy degradation and causing autophagy bodies to accumulate in testis. Studies on liver injury caused by dioxapropium poisoning have shown that mitochondria can regulate apoptosis and autophagy, and the damaged mitochondria activate autophagy mechanism to inhibit the release of cytochrome C (Cyt C) and induce apoptosis. Damaged mitochondria can also reduce the accumulation of ROS, thus inhibiting mitochondrial division and preventing its degradation by autophagy (141). Liver damage caused by acute duck poisoning demonstrated that hepatotoxicity on the one hand activated apoptosis and anti-apoptotic system, on the other hand, autophagy protective system was activated, and found that autophagy and apoptotic system inhibited each other, further confirming the mutual inhibitory relationship between autophagy and apoptotic system.

CONCLUSION

In this review, we focused on the potential molecular mechanisms of mitochondrial dynamics, energy metabolism, oxidative stress, apoptosis and cell damage induced by steady-state mediated fluorosis. It was found that fluorosis can destroy the ultrastructure of cell mitochondria, break the dynamic balance between fission and fusion, thus causing the transmission of mitochondrial respiratory chain to be blocked, a small amount of electrons escaping from the respiratory chain, and the change of mitochondrial membrane potential, resulting in the increase of ATP, ROS and Ca^{2+} contents, triggering the cascade reaction of capacity, and finally causing cell apoptosis. Mitochondrial dynamics, energy metabolism, oxidative stress, apoptosis and other pathways can be used as molecular targets to explore the probable molecular mechanism of cell damage induced by fluorosis. However, when exploring the cytotoxic mechanism of fluoride from the perspective of mitochondrial dysfunction, it is still found that the specific mechanism of the common regulatory pathway of mitochondrial autophagy and apoptosis after fluorosis cannot be confirmed. In addition, the molecular targets for diagnosis, treatment and intervention measures of fluorosis are still unclear. In mitochondrial dynamics, energy metabolism, oxidative stress, cell apoptosis and mitochondrial homeostasis mediated by calcium ion homeostasis, the interaction between various trade-off mechanisms is not clear, and the precise mechanisms needed to explore further.

AUTHOR CONTRIBUTIONS

MW and YY conceived and designed the review. MW and PS analyzed the data. MA, YC, and PS provided manuscript editing. All authors statistically analyzed, discussed, critically revised the contents, and approved the final manuscript.

FUNDING

This work was supported by the major science and technology projects of Tibet autonomous region (XZ202101ZD0005N), the key R&D plan of Bayi District, Nyingchi City (2021-GX-SY-01), and the basic research funds of China Agricultural University (2021TC002).

REFERENCES

1. Tang Z, Lai CC, Luo J, Ding YT, Chen Q, Guan ZZ. Mangiferin prevents the impairment of mitochondrial dynamics and an increase in oxidative stress caused by excessive fluoride in SH-SY5Y cells. *J Biochem Mol Toxicol.* (2021) 35:e22705. doi: 10.1002/jbt.22705
2. Herath S, Kawakami T, Tafu M. Repeated heat regeneration of bone char for sustainable use in fluoride removal from drinking water. *Healthcare.* (2018) 6:143–55. doi: 10.3390/healthcare6040143
3. Cook J, Seagrove M, Mumm S, Veis J, McAlister H, Bijanki N, et al. Non-endemic skeletal fluorosis: causes and associated secondary hyperparathyroidism (case report and literature review). *Bone.* (2021) 145:115839. doi: 10.1016/j.bone.2021.115839
4. Ma Q, Huang H, Sun L, Zhou T, Zhu J, Cheng X, et al. Gene-environment interaction: does fluoride influence the reproductive hormones in male farmers modified by ERα gene polymorphisms? *Chemosphere.* (2017) 188:525–31. doi: 10.1016/j.chemosphere.2017.08.166
5. Ando M, Tadano M, Yamamoto S, Tamura K, Asanuma S, Watanabe T, et al. Health effects of fluoride pollution caused by coal burning. *Sci Total Environ.* (2001) 271:107–16. doi: 10.1016/S0048-9697(00)00836-6
6. He L, Tu C, He S, Long J, Sun Y, Sun Y, et al. Fluorine enrichment of vegetables and soil around an abandoned aluminium plant and its risk to human health. *Environ Geochem Health.* (2021) 43:1137–54. doi: 10.1007/s10653-020-00568-5
7. Stangvaltaite L, Puriene A, Stankeviciene I, Aleksejuniene J. Fluoride in the drinking water and dental caries experience by tooth surface susceptibility among adults. *BMC Oral Health.* (2021) 21:234. doi: 10.1186/s12903-021-01598-w
8. Davoudi M, Barjasteh F, Sarmadi M, Ghorbani M, Yaseri M, Bazrafshan E, et al. Relationship of fluoride in drinking water with blood pressure and essential hypertension prevalence: a systematic review and meta-analysis. *Int Arch Occup Environ Health.* (2021) 94:1137–46. doi: 10.1007/s00420-021-01714-x

9. Srivastava S, Flora S. Fluoride in drinking water and skeletal fluorosis: a review of the global impact. *Curr Environ Health Rep*. (2020) 7:140–6. doi: 10.1007/s40572-020-00270-9
10. Liang C, Gao Y, He Y, Han Y, Manthari RK, Tikka C, et al. Fluoride induced mitochondrial impairment and PINK1 mediated mitophagy in Leydig cells of mice: *in vivo* and *in vitro* studies. *Environ Pollut.* (2020) 256:113438. doi: 10.1016/j.envpol.2019.113438
11. Ge Q, Xie C, Zhang H, Tan Y, Wan C, Wang W, et al. Differential expression of miRNAs in the hippocampi of offspring rats exposed to fluorine combined with aluminum during the embryonic stage and into adulthood. *Biol Trace Elem Res.* (2019) 189:463–77. doi: 10.1007/s12011-018-1445-4
12. Vuong AM, Yolton K, Xie C, Dietrich KN, Braun JM, Webster GM, et al. Childhood exposure to per- and polyfluoroalkyl substances (PFAS) and neurobehavioral domains in children at age 8 years. *Neurotoxicol Teratol.* (2021) 88:107022. doi: 10.1016/j.ntt.2021.107022
13. Niu R, Chen H, Manthari RK, Sun Z, Wang J, Zhang J, et al. Effects of fluoride on synapse morphology and myelin damage in mouse hippocampus. *Chemosphere.* (2018) 194:628–33. doi: 10.1016/j.chemosphere.2017.12.027
14. Wang C, Liang C, Ma J, Manthari RK, Niu R, Wang J, et al. Co-exposure to fluoride and sulfur dioxide on histological alteration and DNA damage in rat brain. *J Biochem Mol Toxicol.* (2018) 32:e22023. doi: 10.1002/jbt.22023
15. Liang C, Gao Y, Zhao Y, Manthari RK, Ma J, Niu R, et al. Effects of fluoride and/or sulfur dioxide on morphology and DNA integrity in rats' hepatic tissue. *Biol Trace Elem Res.* (2018) 183:335–41. doi: 10.1007/s12011-017-1152-6
16. Zhao WP, Wang HW, Liu J, Tan PP, Luo XL, Zhu SQ, et al. Positive PCNA and Ki-67 expression in the testis correlates with spermatogenesis dysfunction in fluoride-treated rats. *Biol Trace Elem Res.* (2018) 186:489–97. doi: 10.1007/s12011-018-1338-6
17. Gao Y, Liang C, Zhang J, Ma J, Wang J, Niu R, et al. Combination of fluoride and SO[[sb]]2 [[/s]] induce DNA damage and morphological alterations in male rat kidney. *Cell Physiol Biochem.* (2018) 50:734–44. doi: 10.1159/000494239
18. Mittal M, Chatterjee S, Flora S. Combination therapy with vitamin C and DMSA for arsenic-fluoride co-exposure in rats. *Metallomics.* (2018) 10:1291–306. doi: 10.1039/C8MT00192H
19. Thanusha P, Shirani R, Neil A, Roshitha W. Experimental rat model for acute tubular injury induced by high water hardness and high water fluoride: efficacy of primary preventive intervention by distilled water administration. *BMC Nephrol.* (2020) 21:103. doi: 10.1186/s12882-020-01763-3
20. Dec K, Łukomska A, Baranowska I, Pilutin A, Maciejewska D, Skonieczna K, et al. Pre- and postnatal exposition to fluorides induce changes in rats liver morphology by impairment of antioxidant defense mechanisms and COX induction. *Chemosphere.* (2018) 211:112–9. doi: 10.1016/j.chemosphere.2018.07.145
21. Li HJ, Fan J, Zhao Y, Yang J, Xu H, Manthari RK, et al. Calcium alleviates fluoride-induced kidney damage via FAS/FASL, TNFR/TNF, DR5/TRAIL pathways in rats. *Ecotoxicol Environ Saf.* (2021) 226:112851. doi: 10.1016/j.ecoenv.2021.112851
22. Philippe G. Developmental fluoride neurotoxicity: An updated review. *Environ Health*. (2019) 18:110. doi: 10.1186/s12940-019-0551-x
23. Sun X, Reuthe JF, Phillips ST, Anslyn EV. Coupling activity based detection, target amplification, colorimetric and fluorometric signal amplification, for quantitative chemosensing of fluoride generated from nerve agents. *Chemistry.* (2017) 23:3903–9. doi: 10.1002/chem.201604474
24. Toms J, Reshetnikov V, Maschauer S, Mokhir A, Prante O. Radiosynthesis of an F-fluoroglycosylated aminoferrocene for in-vivo imaging of reactive oxygen species activity by PET. *J Labelled Comp Radiopharm.* (2018) 61:1081–8. doi: 10.1002/jlcr.3687
25. Bortolozzi R, Carta D, Prà D, Antoniazzi G, Mattiuzzo E, Sturlese M, et al. Evaluating the effects of fluorine on biological properties and metabolic stability of some antitubulin 3-substituted 7-phenyl-pyrroloquinolinones. *Eur J Med Chem.* (2019) 178:297–314. doi: 10.1016/j.ejmech.2019.05.092
26. Wang Y, Cui Y, Zhang D, Chen C, Hou C. Cao L. Moderating Role of TSHR and PTPN22 Gene Polymorphisms in Effects of Excessive Fluoride on Thyroid: a School-Based Cross-Sectional Study. *Biol Trace Elem Res.* (2021) 200:1–13. doi: 10.1007/s12011-021-02753-8
27. De I, Pavon D, Paz M, Oropesa M, de M, Alcocer-Gomez E, et al. The connections among autophagy, inflammasome and mitochondria. *Curr Drug Targets.* (2017) 18:1030–8. doi: 10.2174/1389450117666160527143143
28. Wei W, Pang S, Fu XY, Tan SW, Wang Q, Wang S, et al. The role of PERK and IRE1 signaling pathways in excessive fluoride mediated impairment of lymphocytes in rats' spleen in vivo and in vitro. *Chemosphere.* (2019) 223:1–11. doi: 10.1016/j.chemosphere.2019.02.031
29. Natalie W, Kerstin D, Petr O. Electrophysiology of respiratory chain complexes and the ADP-ATP exchanger in native mitochondrial membranes. *Biochem*. (2010) 49:10308–18. doi: 10.1021/bi1011755
30. Filipe MS, Filipa VS, Ana PB, Diogo A, José AB, Margarida A, et al. The key role of glutamate 172 in the mechanism of type II NADH:quinone oxidoreductase of Staphylococcus aureus. *Biochim Biophys Acta Bioener*. (2017) 1858:823–32. doi: 10.1016/j.bbabio.2017.08.002
31. Beutner G, Alavian N, Jonas A, Porter A. Erratum to: the mitochondrial permeability transition pore and ATP synthase. *Handb Exp Pharmacol.* (2017) 240:21–46. doi: 10.1007/164_2016_5
32. Blum B, Hahn A, Meier T, Davies M, Kühlbrandt W. Dimers of mitochondrial ATP synthase induce membrane curvature and self-assemble into rows. *Proc Natl Acad Sci USA.* (2019) 116:4250–5. doi: 10.1073/pnas.1816556116
33. Campbell I, Campbell H. A pyruvate dehydrogenase complex disorder hypothesis for bipolar disorder. *Med Hypotheses.* (2019) 130:109263. doi: 10.1016/j.mehy.2019.109263
34. Fels A, Manfredi G. Sex differences in ischemia/reperfusion injury: the role of mitochondrial permeability transition. *Neurochem Res.* (2019) 44:2336–45. doi: 10.1007/s11064-019-02769-6
35. Buckalew R, Wang J, Murr S, Deisenroth C, Stewart M, Stoker E, et al. Evaluation of potential sodium-iodide symporter (NIS) inhibitors using a secondary Fischer rat thyroid follicular cell (FRTL-5) radioactive iodide uptake (RAIU) assay. *Arch Toxicol.* (2020) 94:873–85. doi: 10.1007/s00204-020-02664-y
36. Mohiuddin M, Kasahara K. Cisplatin activates the growth inhibitory signaling pathways by enhancing the production of reactive oxygen species in non-small cell lung cancer carrying an EGFR Exon 19 deletion. *Cancer Genomics Proteomics.* (2021) 18:471–86. doi: 10.21873/cgp.20273
37. Mitra S, Nguyen LN, Akter M, Park G, Choi EH, Kaushik NK. Impact of ROS generated by chemical, physical, and plasma techniques on cancer attenuation. *Cancers*. (2019) 11:1030. doi: 10.3390/cancers11071030
38. Sarwar S, Quadri JA, Kumar M, Singh S, Das P, Nag TC, et al. Apoptotic and degenerative changes in the enteric nervous system following exposure to fluoride during pre- and post-natal periods. *Biol Trace Elem Res.* (2021) 199:1456–68. doi: 10.1007/s12011-020-02249-x
39. Slade L, Chalker J, Kuksal N, Young A, Gardiner D, Mailloux RJ. Examination of the superoxide/hydrogen peroxide forming and quenching potential of mouse liver mitochondria. *Biochim Biophys Acta Gen Subj.* (2017) 1861:1960–9. doi: 10.1016/j.bbagen.2017.05.010
40. Kumar S, Ashraf R, Aparna K. Mitochondrial dynamics regulators: implications for therapeutic intervention in cancer. *Cell Biol Toxicol.* (2021) 61960–79. doi: 10.1007/s10565-021-09662-5
41. Chai P, Cheng Y, Hou C, Yin L, Zhang D, Hu Y, et al. USP19 promotes hypoxia-induced mitochondrial division via FUNDC1 at ER-mitochondria contact sites. *J Cell Biol.* (2021) 220:e202010006. doi: 10.1083/jcb.202010006
42. Chen M, Peng L, Gong P, Zheng X, Sun T, Zhang, et al. Baicalein mediates mitochondrial autophagy *via* miR-30b and the NIX/BNIP3 signaling pathway in parkinson's disease. *Biochem Res Int.* (2021) 412–22. doi: 10.1155/2021/2319412
43. Sulkshane P, Ram J, Thakur A, Reis N, Kleifeld O, Glickman MH. Ubiquitination and receptor-mediated mitophagy converge to eliminate oxidation-damaged mitochondria during hypoxia. *Redox Biol.* (2021) 45:102047. doi: 10.1016/j.redox.2021.102047
44. Zeng C, Zou T, Qu J, Chen X, Zhang S, Lin Z. Cyclovirobuxine D induced-mitophagy through the p65/BNIP3/LC3 axis potentiates its apoptosis-inducing effects in lung cancer cells. *Int J Mol Sci.* (2021) 22:5820. doi: 10.3390/ijms22115820

45. Chen L, Li S, Zhu J, You A, Huang X, Yi X, et al. Mangiferin prevents myocardial infarction-induced apoptosis and heart failure in mice by activating the Sirt1/FoxO3a pathway. *J Cell Mol Med.* (2021) 25:2944–55. doi: 10.1111/jcmm.16329
46. Lee YJ, Lee C. Porcine deltacoronavirus induces caspase-dependent apoptosis through activation of the cytochrome c-mediated intrinsic mitochondrial pathway. *Virus Res.* (2018) 253:112–23. doi: 10.1016/j.virusres.2018.06.008
47. Lee JE, Westrate LM, Wu H, Page C, Voeltz GK. Multiple dynamin family members collaborate to drive mitochondrial division. *Nature.* (2016) 540:139–43. doi: 10.1038/nature20555
48. Oshima Y, Cartier E, Boyman L, Verhoeven N, Polster BM, Huang W, et al. Parkin-independent mitophagy via Drp1-mediated outer membrane severing and inner membrane ubiquitination. *J Cell Biol.* (2021) 220:6043. doi: 10.1083/jcb.202006043
49. Chen Y, Guo S, Tang Y, Mou C, Hu X, Shao F, et al. Mitochondrial fusion and fission in neuronal death induced by cerebral ischemia-reperfusion and its clinical application: A mini-review. *Med Sci Monit.* (2020) 26:e928651. doi: 10.12659/MSM.928651
50. Zhou BH, Wei SS, Jia LS, Zhang Y, Miao CY, Wang HW. Drp1/Mff signaling pathway is involved in fluoride-induced abnormal fission of hepatocyte mitochondria in mice. *Sci Total Environ.* (2020) 725:138192. doi: 10.1016/j.scitotenv.2020.138192
51. AlRefeai M, AlHamdan E, Al-Saleh S, Farooq I, Abrar E, Vohra F, et al. Assessment of bond integrity, durability, and degree of conversion of a calcium fluoride reinforced dentin adhesive. *Polymers.* (2021) 13:1–12. doi: 10.3390/polym13152418
52. Song B, Fu M, He F, Zhao H, Wang y, Nie Q, et al. Methionine deficiency affects liver and kidney health, oxidative stress, and ileum mucosal immunity in broilers. *Front Vet Sci.* (2021) 8:722567. doi: 10.3389/fvets.2021.722567
53. Aulestia J, Groeling J, Bomfim H, Costiniti V, Manikandan V, Chaloemtoem A, et al. Fluoride exposure alters Ca signaling and mitochondrial function in enamel cells. *Sci Signal.* (2020) 13:1937–45. doi: 10.1126/scisignal.aay0086
54. Lezmy J, Arancibia-Cárcamo IL, Quintela-López T, Sherman DL, Brophy PJ, Attwell D. Astrocyte Ca-evoked ATP release regulates myelinated axon excitability and conduction speed. *Science.* (2021) 374:eabh2858. doi: 10.1126/science.abh2858
55. Johnston NR, Strobel SA. Principles of fluoride toxicity and the cellular response: a review. *Arch Toxicol.* (2020) 94:1051–69. doi: 10.1007/s00204-020-02687-5
56. National Research Council. *Fluoride in drinking water: A scientific review of EPA's standards*. Washington D.C. (2006).
57. Zhao Q, Niu Q, Chen J, Xia T, Zhou G, Li P, et al. Roles of mitochondrial fission inhibition in developmental fluoride neurotoxicity: mechanisms of action in vitro and associations with cognition in rats and children. *Arch Toxicol.* (2019) 93:709–26. doi: 10.1007/s00204-019-02390-0
58. Adamek E, Pawłowska-Góral K, Bober K. *In vitro* and *in vivo* effects of fluoride ions on enzyme activity. *Ann Acad Med Stetin.* (2005) 51:69–85.
59. Barbier O, Arreola M, Del R. Molecular mechanisms of fluoride toxicity. *Chem Biol Interact.* (2010) 188:319–33. doi: 10.1016/j.cbi.2010.07.011
60. Podder S, Ghoshal N, Banerjee A, Ganguly B, Upadhyay R, Chatterjee A. Interaction of DNA-lesions induced by sodium fluoride and radiation and its influence in apoptotic induction in cancer cell lines. *Toxicol Rep.* (2015) 2:461–71. doi: 10.1016/j.toxrep.2015.02.001
61. Jyoti B, Jitender G. Purple acid phosphatases: roles in phosphate utilization and new emerging functions. *Plant Cell Rep.* (2022) 41:33–51. doi: 10.1007/s00299-021-02773-7
62. Fina L, Lombarte M, Rigalli P, Rigalli A. Fluoride increases superoxide production and impairs the respiratory chain in ROS 17/28 osteoblastic cells. *PLOS ONE.* (2014) 9:e100768. doi: 10.1371/journal.pone.0100768
63. Li QS, Lin XM, Qiao RY, Zheng XQ, Lu JL, Ye JH, et al. Effect of fluoride treatment on gene expression in tea plant (Camellia sinensis). *Sci Rep.* (2017) 7:9847. doi: 10.1038/s41598-017-08587-6
64. Kim JW, Byun MS Yi D, Lee JH, Jeon SY, Ko K, et al. Blood hemoglobin, *in-vivo* alzheimer pathologies, and cognitive impairment: a cross-sectional study. *Front Aging Neurosci.* (2021) 13:625511. doi: 10.3389/fnagi.2021.625511
65. Gassowska M, Gutowska I, Baranowska I, Chlubek D. Effect of fluoride on sodium-proton exchanger activity, intracellular pH and calcium concentration in human non-stimulated platelets. *Ann Acad Med Stetin.* (2013) 59:54–61.
66. Cai J, Jung J, Lee M, Choi H. Jeon J. Sucrose challenges to Streptococcus mutans biofilms and the curve fitting for the biofilm changes. *FEMS Microbiol Ecol.* (2018) 94:fiy091. doi: 10.1093/femsec/fiy091
67. Han Y. Effects of brief sodium fluoride treatments on the growth of early and mature cariogenic biofilms. *Sci Rep.* (2021) 11:18290. doi: 10.1038/s41598-021-97905-0
68. Agalakova NI, Gusev GP. Molecular mechanisms of cytotoxicity and apoptosis induced by inorganic fluoride. *Int Sch Res Not.* (2011) 2012:1–16. doi: 10.5402/2012/403835
69. Matsuo S, Nakagawa H, Kiyomiya K, Kurebe M. Fluoride-induced ultrastructural changes in exocrine pancreas cells of rats: fluoride disrupts the export of zymogens from the rough endoplasmic reticulum (rER). *Arch Toxicol.* (2000) 73:611–7. doi: 10.1007/s002040050015
70. Kubota K, Lee DH, Tsuchiya M, Young S, Everett ET, Martinez-Mier A, et al. Fluoride induces endoplasmic reticulum stress in ameloblasts responsible for dental enamel formation. *J Biol Chem.* (2005) 280:23194–202. doi: 10.1074/jbc.M503288200
71. Wang Y, Duan X, Zhao Z, Zhang X, Wang H, Liu D, et al. Fluoride affects calcium homeostasis by regulating parathyroid hormone, PTH-Related peptide, and calcium-sensing receptor expression. *Biol Trace Elem Res.* (2015) 165:159–66. doi: 10.1007/s12011-015-0245-3
72. Choi S, Quan X, Bang S, Yoo H, Kim J, Park J, et al. Drosophila Mitochondrial calcium uniporter in transfers calcium between the endoplasmic reticulum and mitochondria in oxidative stress-induced cell death. *J Biol Chem.* (2017) 292:14473–85. doi: 10.1074/jbc.M116.765578
73. Zhang Y, Zhang KQ, Ma L, Gu HF, Li J, et al. Fluoride induced endoplasmic reticulum stress and calcium overload in ameloblasts. *Arch Oral Biol.* (2016) 69:95–101. doi: 10.1016/j.archoralbio.2016.05.015
74. Van AM. G protein activation at the Golgi. *Science Signaling.* (2015) 8:ec109. doi: 10.1126/scisignal.aab4170
75. Yan XY, Yang X, Hao XH, Ren Q, Gao J, Wang Y, et al. Sodium fluoride induces apoptosis in H9c2 cardiomyocytes by altering mitochondrial membrane potential and intracellular ROS Level. *Biol Trace Elem Res.* (2015) 166:210–5. doi: 10.1007/s12011-015-0273-z
76. Kanezashi M, Murata M, Nagasawa H, Tsuru T. Fluorine doping of microporous organosilica membranes for pore size control and enhanced hydrophobic properties. *ACS Omega.* (2018) 3:8612–20. doi: 10.1021/acsomega.8b01370
77. Wang M, Liu L, Li H, Li Y, Liu H, Hou C, et al. Thyroid function, intelligence, and low-moderate fluoride exposure among Chinese school-age children. *Environ Int.* (2020) 134:105229. doi: 10.1016/j.envint.2019.105229
78. Nunnari J, Suomalainen A. Mitochondria: in sickness and in health. *Cell.* (2012) 148:1145–59. doi: 10.1016/j.cell.2012.02.035
79. Harbauer A, Zahedi P, Sickmann A, Pfanner N, Meisinger C. The protein import machinery of mitochondria-a regulatory hub in metabolism, stress, and disease. *Cell Metabol.* (2014) 19:357–72. doi: 10.1016/j.cmet.2014.01.010
80. Lillo-Moya J, Rojas-Solé C, Muñoz-Salamanca D, Panieri E, Saso L. Rodrigo R targeting ferroptosis against ischemia/reperfusion cardiac injury. *Antioxidants.* (2021) 10:667. doi: 10.3390/antiox10050667
81. Zhao HX, Pan X. Mitochondrial Ca and cell cycle regulation. *Int Rev Cell Mol Biol.* (2021) 362:171–207. doi: 10.1016/bs.ircmb.2021.02.015
82. Wang HW, Zhu SQ, Liu J, Miao CY, Zhang Y, Zhou BH. Fluoride-induced renal dysfunction via respiratory chain complex abnormal expression and fusion elevation in mice. *Chemosphere.* (2020) 238:124607. doi: 10.1016/j.chemosphere.2019.124607
83. Zhao MX, Zhou GY, Zhu JY, Gong B, Hou JX, Zhou T, et al. Fluoride exposure, follicle stimulating hormone receptor gene polymorphism and hypothalamus-pituitary-ovarian axis hormones in chinese women. *Biomed Environ Sci.* (2015) 28:696–700. doi: 10.3967/bes2015.099
84. Lu Y, Luo Q, Cui H, Deng H, Kuang P, Liu H, et al. Sodium fluoride causes oxidative stress and apoptosis in the mouse liver. *Aging.* (2017) 9:1623–39. doi: 10.18632/aging.101257
85. Wang JJ, Wei ZK, Han Z, Liu ZY, Zhang Y, Zhu XY, et al. Sodium fluoride exposure triggered the formation of neutrophil extracellular

traps. *Environ Pollut.* (2020) 257:113583. doi: 10.1016/j.envpol.2019.113583
86. Moore JK, Chen J, Pan H, Gaut JP, Jain S, Wickline SA. Quantification of vascular damage in acute kidney injury with fluorine magnetic resonance imaging and spectroscopy. *Magn Reson Med.* (2018) 79:3144–53. doi: 10.1002/mrm.26985
87. Liu X, Nie ZW, Gao YY, Chen L, Yin SY, Zhang X, et al. Sodium fluoride disturbs DNA methylation of NNAT and declines oocyte quality by impairing glucose transport in porcine oocytes. *Environ Mol Mutagen.* (2018) 59:223–33. doi: 10.1002/em.22165
88. Ke HJ, Dass S, Morrisey M, Mather W, Vaidya B. The mitochondrial ribosomal protein L13 is critical for the structural and functional integrity of the mitochondrion in *Plasmodium falciparum*. *J Biol Chem.* (2018) 293:8128–37. doi: 10.1074/jbc.RA118.002552
89. Sarah KY, Roderick AC. The F(1)F(0) ATP synthase and mitochondrial respiratory chain complexes are present on the plasma membrane of an osteosarcoma cell line: An immunocytochemical study. *Mitochondrion.* (2006) 6:305–14. doi: 10.1016/j.mito.2006.10.001
90. Mama N, Lorena M-B, Roger S, Prakash SA, Martin O. Biogenesis of the bc Complex of the mitochondrial respiratory chain. *J Mol Biol.* (2018) 430:3892–905. doi: 10.1016/j.jmb.2018.04.036
91. Subir RC, Jelena D, Ella T, Darrell RS, Benedict CA, Fernyhough P. Depressed mitochondrial function and electron transport Complex II-mediated HO production in the cortex of type 1 diabetic rodents. *Mol Cell Neurosci.* (2018) 90:49–59. doi: 10.1016/j.mcn.2018.05.006
92. Jang S, Javadov S. Association between ROS production, swelling and the respirasome integrity in cardiac mitochondria. *Arch Biochem Biophys.* (2017) 630:1–8. doi: 10.1016/j.abb.2017.07.009
93. Zhou BH, Tan PP, Jia LS, Zhao WP, Wang JC, Wang, et al. PI3K/AKT signaling pathway involvement in fluoride-induced apoptosis in C2C12 cells. *Chemosphere.* (2018) 199:297–302. doi: 10.1016/j.chemosphere.2018.02.057
94. Huang Q, Liu L, Wu Y, Wang X, Luo LZ, Nan B, et al. Seminal plasma metabolites mediate the associations of multiple environmental pollutants with semen quality in Chinese men. *Environ Int.* (2019) 132:105066. doi: 10.1016/j.envint.2019.105066
95. Sánchez M, Martínez E, Madrigal EO, Betanzos G, Hernández A, Mojica MA, et al. Exposure of fluoride with streptozotocin-induced diabetes aggravates testicular damage and spermatozoa parameters in mice. *J Toxicol.* (2019) 2019:5269380. doi: 10.1155/2019/5269380
96. Chaithra B, Shivabasavaiah SH. Dose and time-dependent effects of sodium fluoride on sperm motility: an *in vitro* study. *Toxicol Ind Health.* (2018) 34:813–8. doi: 10.1177/0748233718795926
97. Chaithra B, Shivabasavaiah SH. Time-dependent effect of ground water fluoride on motility, abnormality and antioxidant status of spermatozoa: an *in vitro* study. *Toxicol Ind Health.* (2019) 35:368–77. doi: 10.1177/0748233719842499
98. Chaithra B, Shivabasavaiah SH. A comparative analysis of fluoride contaminated groundwater and sodium fluoride induced reproductive toxicity and its reversibility in male rats. *Biol Trace Elem Res.* (2020) 197:507–21. doi: 10.1007/s12011-019-01994-y
99. Jitschin R, Böttcher M, Saul D, Lukassen S, Bruns H, Loschinski R, et al. Inflammation-induced glycolytic switch controls suppressivity of mesenchymal stem cells via STAT1 glycosylation. *Leukemia.* (2019) 33:1783–96. doi: 10.1038/s41375-018-0376-6
100. Tourmente M, Hirose M, Ibrahim S, Dowling DK, Tompkins DM, Roldan S, et al. mtDNA polymorphism and metabolic inhibition affect sperm performance in conplastic mice. *Reproduction.* (2017) 154:341–54. doi: 10.1530/REP-17-0206
101. Raad G, Mansour J, Ibrahim R, Azoury J, Azoury J, Mourad Y, et al. What are the effects of vitamin C on sperm functional properties during direct swim-up procedure? *Zygote.* (2019) 27:69–77. doi: 10.1017/S0967199419000030
102. Song C, Heping H, Shen Y, Jin S, Li D, Zhang A, et al. AMPK/p38/Nrf2 activation as a protective feedback to restrain oxidative stress and inflammation in microglia stimulated with sodium fluoride. *Chemosphere.* (2020) 244:125495. doi: 10.1016/j.chemosphere.2019.125495
103. Deutsch A, Craig G. Unexpected sequel to silver fluoride followed by stannous fluoride treatment of root stumps supporting an overlay denture in an aged-care patient. *Spec Care Dentist.* (2018) 38:405–8. doi: 10.1111/scd.12329
104. Green L, DeSisto J, Flannery P, Lemma R, Knox A, Lemieux M, et al. BPTF regulates growth of adult and pediatric high-grade glioma through the MYC pathway. *Oncogene.* (2020) 39:2305–27. doi: 10.1038/s41388-019-1125-7
105. Ghassemi K, Farhangi S. Biochar alleviates fluoride toxicity and oxidative stress in safflower (*Carthamus tinctorius* L.) seedlings. *Chemosphere.* (2019) 23:406–15. doi: 10.1016/j.chemosphere.2019.02.087
106. Liu GY, Zhai Q, Chen JZ, Zhang ZQ. Yang J. 2, 2'-Fluorine mono-carbonyl curcumin induce reactive oxygen species-mediated apoptosis in human lung cancer NCI-H460 cells. *Eur J Pharmacol.* (2016) 786:161–8. doi: 10.1016/j.ejphar.2016.06.009
107. Qi H, Xu G, Peng XL, Li X, Shuai J, Xu R. Roles of four feedback loops in mitochondrial permeability transition pore opening induced by Ca^{2+} and reactive oxygen species. *Phys Rev E.* (2020) 102:062422. doi: 10.1103/PhysRevE.102.062422
108. Imamura H, Sakamoto S, Matsui Y, Yoshida T, Penuela S, Laird DW, et al. Single-cell dynamics of pannexin-1-facilitated programmed ATP loss during apoptosis. *Elife.* (2020) 9:e61960. doi: 10.7554/eLife.61960
109. Prinz C, Starke L, Millward JM, Fillmer A, Delgado PR, Waiczies H, et al. *In vivo* detection of teriflunomide-derived fluorine signal during neuroinflammation using fluorine MR spectroscopy. *Theranostics.* (2021) 11:2490–504. doi: 10.7150/thno.47130
110. Yang JH, Wu Q, Lv JG, Nie HY. 4-Phenyl butyric acid prevents glucocorticoid-induced osteoblast apoptosis by attenuating endoplasmic reticulum stress. *J Bone Miner Metab.* (2017) 35:366–74. doi: 10.1007/s00774-016-0778-3
111. Nagendra AH, Bose B. Shenoy PS. Recent advances in cellular effects of fluoride: an update on its signalling pathway and targeted therapeutic approaches. *Mol Biol Rep.* (2021) 48:5661–73. doi: 10.1007/s11033-021-06523-6
112. Tang XN, Yao W, Yao HX, Zhang Y, Yue J. Influence of isoflurane exposure for 15 consecutive days on ovarian function in adult female mice. *Curr Med Sci.* (2020) 40:1177–81. doi: 10.1007/s11596-020-2300-3
113. Ying J, Xu J, Shen L, Mao Z, Liang J, Lin S, et al. The effect of sodium fluoride on cell apoptosis and the mechanism of human lung BEAS-2B cells *in vitro*. *Biol Trace Elem Res.* (2017) 179:59–69. doi: 10.1007/s12011-017-0937-y
114. Liu J, Wang H, Wei, Zhao WP, Li XT, Lin L, et al. Induction of pathological changes and impaired expression of cytokines in developing female rat spleen after chronic excess fluoride exposure. *Toxicol Ind Health.* (2019) 35:43–52. doi: 10.1177/0748233718809773
115. Yuan D, Huang S, Berger E, Liu L, Gross N, Heinzmann F, et al. Kupffer cell-derived tnf triggers cholangiocellular tumorigenesis through JNK due to chronic mitochondrial dysfunction and ROS. *Cancer Cell.* (2017) 31:771–89. doi: 10.1016/j.ccell.2017.05.006
116. Li R, Yang W, Yin Y, Zhang P, Wang Y, Tao K. Protective role of 4-octyl itaconate in murine LPS/D-GalN-induced acute liver failure via inhibiting inflammation, oxidative stress, and apoptosis. *Oxid Med Cell Longev.* (2021) 9932099. doi: 10.1155/2021/9932099
117. Green R, Galluzzi L, Kroemer G. Mitochondria and the autophagy inflammation cell death axis in organismal aging. *Science.* (2021) 333:1109–12. doi: 10.1126/science.1201940
118. Ooi K, Hu L, Feng Y, Han C, Ren X, Qian X, et al. Sigma-1 receptor activation suppresses microglia M1 polarization *via* regulating endoplasmic reticulum-mitochondria contact and mitochondrial functions in stress-induced hypertension rats. *Mol Neurobiol.* (2021) 58:6625–46. doi: 10.1007/s12035-021-02488-6
119. Araujo T, Barbosa S, Dionizio A, Sanchez CDC, de Souza Carvalho T, da Silva Fernandes M, et al. Changes in energy metabolism induced by fluoride: insights from inside the mitochondria. *Chemosphere.* (2019) 236:124357. doi: 10.1016/j.chemosphere.2019.124357
120. Mohamed NE. The role of calcium in ameliorating the oxidative stress of fluoride in rats. *Biol Trace Elem Res.* (2016) 170:128–44. doi: 10.1007/s12011-015-0421-5
121. Ameeramja J, Perumal E. Pulmonary fluorosis: a review. *Environ Sci Pollut Res Int.* (2017) 24:119–32. doi: 10.1007/s11356-017-9951-z

122. Adebayo M, Singh S, Singh AP, Dasgupta S. Mitochondrial fusion and fission: the fine-tune balance for cellular homeostasis. *FASEB J.* (2021) 35:e21620. doi: 10.1096/fj.202100067R
123. Puty B, Bittencourt LO, Nogueira IC, Buzalaf R, Oliveira EH, Lima R. Human cultured IMR-32 neuronal-like and U87 glial-like cells have different patterns of toxicity under fluoride exposure. *PLoS ONE.* (2021) 16:e0251200. doi: 10.1371/journal.pone.0251200
124. Di Pietro V, Lazzarino G, Amorini AM, Signoretti S, Hill LJ, Porto E, et al. Fusion or fission: the destiny of mitochondria in traumatic brain injury of different severities. *Sci Rep.* (2017) 7:9189. doi: 10.1038/s41598-017-09587-2
125. Valera-Alberni M, Joffraud M, Miro-Blanch J, Capellades J, Junza A, Dayon L, et al. Crosstalk between Drp1 phosphorylation sites during mitochondrial remodeling and their impact on metabolic adaptation. *Cell Rep.* (2021) 36:109565. doi: 10.1016/j.celrep.2021.109565
126. Feng Z, Liang C, Manthari K, Wang C, Zhang J. Effects of fluoride on autophagy in mouse sertoli cells. *Biol Trace Elem Res.* (2019) 187:499–505. doi: 10.1007/s12011-018-1405-z
127. Ommati M, Tanideh N, Rezakhaniha B, Wang J, Sabouri S, Vahedi M, et al. Is immunosuppression, induced by neonatal thymectomy, compatible with poor reproductive performance in adult male rats? *Andrology.* (2018) 6:199–213. doi: 10.1111/andr.12448
128. Nakatogawa H. Mechanisms governing autophagosome biogenesis. *Nat Rev Mol Cell Biol.* (2020) 21:439–58. doi: 10.1038/s41580-020-0241-0
129. Wei Y, Zeng B, Zhang H, Chen C, Wu Y, Wang N, et al. Comparative proteomic analysis of fluoride treated rat bone provides new insights into the molecular mechanisms of fluoride toxicity. *Toxicol Lett.* (2018) 291:39–50. doi: 10.1016/j.toxlet.2018.04.006
130. You BJ, Tien N, Lee MH, Bao BY, Wu YS, Hu TC, et al. Induction of apoptosis and ganoderic acid biosynthesis by cAMP signaling in Ganoderma lucidum. *Sci Rep.* (2017) 7:318. doi: 10.1038/s41598-017-00281-x
131. Yuan Z, ShanshanZ, Moxin Z, Yian W, Yuhang L, Zhang MI, et al. Potential applications of N-methyladenosine modification in the prognosis and treatment of cancers via modulating apoptosis, autophagy, and ferroptosis. *Wiley Interdiscip Rev RNA*. (2022) e1719. doi: 10.1002/wrna.1719
132. Finkbeiner S. The autophagy lysosomal pathway and neurodegeneration. *Cold Spring Harb Perspect Biol.* (2020) 12:a033993. doi: 10.1101/cshperspect.a033993
133. Montalvo RN, Doerr V, Kwon OS, Talbert E, Yoo JK, Hwang MH, et al. Protection against doxorubicin-induced cardiac dysfunction is not maintained following prolonged autophagy inhibition. *Int J Mol Sci.* (2020) 21:8105. doi: 10.3390/ijms21218105
134. Sun RJ, Yin DM, Yuan D, Liu SY, Zhu J, Shan N. Quantitative LC-MS/MS uncovers the regulatory role of autophagy in immune thrombocytopenia. *Cancer Cell Int.* (2021) 21:548. doi: 10.1186/s12935-021-02249-4
135. Zhou GZ, Li J, Sun YH, Zhang Q, Zhang L, Pei C. Autophagy delays apoptotic cell death induced by *Siniperca chuatsi* rhabdovirus in epithelioma papulosum cyprinid cells. *Viruses.* (2021) 13:1554. doi: 10.3390/v13081554
136. Ma C, Wen B, Zhang Q, Shao PP, Gu W, Qu K, et al. Emodin induces apoptosis and autophagy of fibroblasts obtained from patient with ankylosing spondylitis. *Drug Des Devel Ther.* (2019) 13:601–9. doi: 10.2147/DDDT.S182087
137. Zhang SY, Zhang Y, Zhang XY, Luo CH, Cao Y, Ji DY, et al. Nitrative stress-related autophagic insufficiency participates in hyperhomocysteinemia-induced renal aging. *Oxid Med Cell Longev.* (2020) 2020:4252047. doi: 10.1155/2020/4252047
138. Yang X, Zhang J, Ji Q, Wang F, Song M, Li Y. Autophagy protects MC3T3-E1 cells upon aluminum-induced apoptosis. *Biol Trace Elem Res.* (2018) 185:433–9. doi: 10.1007/s12011-018-1264-7
139. Leites EP, Morais VA. The PINK1-mediated crosstalk between neural cells and the underlying link to parkinson's disease.*Cells.* (2021) 10:1395. doi: 10.3390/cells10061395
140. Xiao Y, Zhou Y, Lu Y, Zhou K, Cai W. PHB2 interacts with LC3 and SQSTM1 is required for bile acids-induced mitophagy in cholestatic liver. *Cell Death Dis.* (2018) 9:160. doi: 10.1038/s41419-017-0228-8
141. Huang L, Zeng X, Li B, Wang C, Zhou M, Lang H, et al. Dihydromyricetin attenuates palmitic acid-induced oxidative stress by promoting autophagy via SIRT3-ATG4B signaling in hepatocytes. *Nutr Metab.* (2021) 18:83–94. doi: 10.1186/s12986-021-00612-w

Conflict of Interest: The authors declare that the research was conducted in the absence of any commercial or financial relationships that could be construed as a potential conflict of interest.

frontiers | Frontiers in Veterinary Science

ORIGINAL RESEARCH
published: 22 April 2022
doi: 10.3389/fvets.2022.855447

A Novel Intranasal Vaccine With PmpGs + MOMP Induces Robust Protections Both in Respiratory Tract and Genital System Post *Chlamydia psittaci* Infection

Qiang Li[1,2], *Siyu Chen*[2], *Zhuanqiang Yan*[3], *Huanxin Fang*[3], *Zhanxin Wang*[3]* and *Cheng He*[1,2]*

[1] College of Life Science and Engineering, Foshan University, Foshan, China, [2] Key Lab of Animal Epidemiology and Zoonoses of Ministry of Agriculture and Rural Affairs, College of Veterinary Medicine, China Agricultural University, Beijing, China, [3] Wen's Group Academy, Wen's Foodstuffs Group Co., Ltd., Yunfu, China

OPEN ACCESS

Edited by:
Fazul Nabi,
Lasbela University of Agriculture, Water and Marine Sciences, Pakistan

Reviewed by:
Sukumar Pal,
University of California, Irvine, United States
Shanli Zhu,
Wenzhou Medical University, China

***Correspondence:**
Zhanxin Wang
wangzhanxin1985@163.com
Cheng He
hecheng@cau.edu.cn

Specialty section:
This article was submitted to Comparative and Clinical Medicine, a section of the journal Frontiers in Veterinary Science

Received: 15 January 2022
Accepted: 14 February 2022
Published: 22 April 2022

Citation:
Li Q, Chen SY, Yan ZQ, Fang HX, Wang ZX and He C (2022) A Novel Intranasal Vaccine With PmpGs + MOMP Induces Robust Protections Both in Respiratory Tract and Genital System Post Chlamydia psittaci Infection. Front. Vet. Sci. 9:855447. doi: 10.3389/fvets.2022.855447

Chlamydia psittaci (*C. psittaci*) is a crucial zoonotic pathogen that causes severe respiratory and reproductive system disease in humans and animals. In our pioneer study, polymorphic membrane protein G (PmpG) mediated attachment to host cells as the adhesions and induced immunity against *C. psittaci* infection. We hypothesize that multiple PmpG antigens adjuvanted with *Vibrio cholerae* ghost (VCG) and chitosan gel might trigger full protection *via* the intranasal route (i.n). In the present study, 40 SPF chickens were randomly divided into four groups, including the PmpGs + MOMP group (i.n), major outer membrane protein (MOMP) group (i.n), PmpGs (Pmp17G + Pmp20G + Pmp21G) group (i.n), and control groups (VCG + chitosan gel) (i.n). Post twice immunizations, the PmpGs + MOMP group yielded highly level-specific IgG, IgA antibodies, and lymphocyte proliferation. As for cytokines, IFN-γ expression was upregulated significantly, while IL-10 concentration was downregulated in the PmpGs + MOMP group compared with other groups. Post challenge, exudate inflammations in air sacs, bacterial loads in lungs, and bacterial shedding in throat swabs were reduced significantly in the PmpGs + MOMP group. In the second experiment, 100 breeder ducks were divided into the PmpGs + MOMP group (i.n), the commercial MOMP group (*via* intramuscular injection, i.m), the inactivated EBs group (i.n), and the control group (i.n), 25 ducks per group. Post challenge, the reduced egg production recovered soon in the inactivated EBs group and the PmpGs + MOMP group. Moreover, the aforementioned two groups induced higher robust IgG antibodies, lymphocyte proliferation, and IFN-γ secretions than the commercial MOMP vaccine did. Postmortem, lower bacterial loads of spleens were determined in the PmpGs + MOMP group and the inactivated EBs group. However, bacterial clearance of follicular membranes and shedding from the vaginal tract were not significant differences among the three tested groups. Furthermore, the PmpGs + MOMP group induced lower inflammations

in the follicles and oviducts. Based on the above evidence, the combination of PmpGs and MOMP adjuvanted with chitosan gel and VCG *via* intranasal route could induce full protection both in the respiratory system and genital tract post *C. psittaci* infection. More importantly, the combination antigens are superior to the inactivated EBs antigen due to no contamination to the environment and less genital inflammation. The combination of PmpGs + MOMP adjuvanted with VCG and chitosan gel might be a promising novel vaccine by blocking *C. psittaci* infection from animals to human beings.

Keywords: *Chlamydia psittaci*, polymorphic membrane proteins G, major outer membrane proteins, respiratory tract, genital tract, intranasal immunity

INTRODUCTION

Chlamydia psittaci (*C. psittaci)* is a typical intracellular pathogen that obligately parasitizes in eukaryotic cells. It infects birds, poultry, livestock, and wild animals, causing severe respiratory, reproductive disease, and economic loss as well (1). More important, human psittacosis and mortality cases are reported frequently due to the increasing application of next-generation sequencing, especially the employees or pet hosts closely contacted with pet birds and poultry (2). The latest statistics indicated that 1% of community-acquired pneumonia was triggered by *C. psittaci* infection (3). Clinical signs are comparable to influenza infection as flu-like fever and human psittacosis are underestimated and ignored due to lack of rapid diagnosis and good treatment (4). Therefore, how to cut Chlamydial transmission from animals to humans is urgently needed in light of public health implications. Both scientists from veterinary fields and hospital researchers are seeking joint efforts to combat *C. psittaci* infection.

In the past decades, Chlamydia vaccines for animal use have been developed from killed vaccines, live attenuated vaccines, subunit vaccines, live vector vaccines, DNA vaccines to mRNA vaccines (5). As for the vaccines against *C. psittaci* infection, the first recombinant MOMP vaccine was registered successfully in 2006 and commercialized for broilers in China. After that, the recombinant MOMP vaccine was available for sheep and goats in 2014. Subsequently, the recombinant MOMP vaccines are not recognized due to partial protection for poultry and livestock. Recently, inactivated whole elemental body (EB) adjuvanted with VCG and chitosan induced better protection against *C. psittaci* infection in SPF chickens (6). Compared with intramuscular injection, intranasal immunity was identified to induce better protection post challenge with the virulent strain. Chlamydia PmpG family has high diversity within one species and among genus, suggesting potentially associated with host tropism (7). The numbers of PmpGs ranged from 5 to 15 in *C. psittaci*, while only one PmpG was found in *Chlamydia trachomatis* (*C. trachomatis*). Pmp20G-N ELISA has the potential to be a diagnostic antigen for detection of *C. psittaci* antibody (8). Recent studies indicate that PmpG is a promising vaccine candidate against Chlamydial infection. Intranasal inoculation of the combination of MOMP, PmpG, inclusion protein TC0500, and TC0873 with adjuvant ISCOMATRIX-IMX can induce mice against *C. muridarum* infection, manifested by lesion reduction in the reproductive tract and bacterial clearance (9). In another test, mice were protected in the reproductive tracts and conjunctiva after immunization with a combination of CpG-1826 and Montanide ISA720 as the adjuvants, and Pmps (PmpC, PmpG, and PmpH) as antigens, and a cross-protection was found post challenge with *C. trachomatis* (10). As for PmpG-elicited protection against *C. psittaci*, it remains unknown except for inducting Pmp17G antibodies against *C. psittaci* 02DC15 strain in calves (11).

In this study, we hypothesized that multiple antigens (PmpGs + MOMP) adjuvanted with VCG and chitosan gel could provide a full protection in the respiratory tract and genital system post inoculation *via* the intranasal route. Assessment of vaccine efficacy will provide a new approach for the prevention and control of *C. psittaci* infection, and blocks the transmission from animals to humans, contributing to one health concept.

MATERIALS AND METHODS

Recombinant Proteins, Inactivated Elementary Bodies, and Major Outer Membrane Protein Vaccines

Recombinant Pmp20G and MOMP were expressed by *E. coli* and purified as previously described (8). In this study, we further cloned and expressed Pmp17G and Pmp21G. Briefly, full-length genes of *pmp17G* and *pmp21G* were amplified from DNA genomics of *C. psittaci* 6BC (a gift from Professor Wu Yimo, University of South China, Hunan, China). The amplified fragments were inserted into the shuttle vector pET-28a (Novagen, Darmstadt, Germany) and then transformed into *E. coli* DH5a (New England Biolabs, Ipswich, UK). Positive clones were validated by PCR, and plasmids were extracted with Plasmid DNA Kit (OMEGA, Norcross, USA) following the protocols of the manufacturer. Plasmids were transformed into *E. coli* Rossetta (DE3) (New England Biolabs, Ipswich, UK), and the recombinant proteins were purified using Ni Sepharose (GE, MA, USA) and identified by SDS-PAGE and Western blot.

Regarding whole EBs preparation, roughly 1×10^6 IFU EBs of *C. psittaci* 6BC strain were inactivated by UV. *C. psittaci* suspensions were placed under a 15-W UV light at a distance of 20 cm for 30 min. Afterward, the inactivation was confirmed by inoculating onto fresh Buffalo green monkey kidney (BGMK) cells for 24 h (12).

Adjuvants and Vaccine Formulation

Vibrio cholerae ghost (VCG) was manufactured, and the endotoxin was removed (Binzhou Animal Science and Veterinary Medicine Academy, Shandong Province, China) following previous reports (6). Chitosan gels were provided by Professor Wu Jie, Institute of Process Engineering, Chinese Academy of Sciences, Beijing, China.

As for vaccine formulation, the hydrogels and W/O droplet uniforms were prepared using Shirasu porous glass membrane emulsification. Afterward, 100 μg of recombinant antigens (50 μg of PmpGs + 50 μg of MOMP, or 100 μg of MOMP, or 100 μg of PmpGs), or inactivated EBs, 50 μg of VCG adjuvant and comparable volume of chitosan gels were mixed and blended completely as previously described (6). Finally, vaccines were stored at 4°C until use. Meanwhile, the commercial MOMP vaccine (100 μg/dose) was purchased from Huaxin Nongwei Biotech Co. Ltd., Beijing, China.

Pathogens

Chlamydia psittaci SZ18-1 strains (GenBank MK751470.1) were isolated from breeder ducks with egg drop and severe salpingitis (13). The strain was propagated onto BGMK cells at 37°C in a flow of 5% CO_2 for 72 h. Live elementary bodies (EBs) were harvested and purified by density gradient centrifugation, and inclusion-forming units (IFUs) were determined by Chlamydia immunofluorescence assay (IMAGEN™; Oxoid, Cambridge, UK). Finally, live EBs were stored in sucrose phosphate glutamate buffer at −70°C (14).

Experimental Procedures

In experiment I, 40 SPF chickens aged 7 days old, were purchased from a commercial company (Boehringer Ingelheim Vertron Biotechnology Co., Ltd., Beijing, China). In Experiment II, 100 breeder ducks, aged 80 days old, were purchased from Wen's Food Group, Co., Ltd. (Yun Fu, Guangdong, China). All animals were kept in an isolated room to reduce cross-infection during the test. The protocols used in this study were approved by the Laboratory Animal Ethical Committee of China Agricultural University (Beijing, China). All animals were handled in strict accordance with the Regulations for the Administration of Affairs Concerning Experimental Animals of the State Council of the People's Republic of China. Humane protocols that minimize pain to the birds have been followed. Briefly, both SPF chickens and breeder ducks were euthanized at the end of the study in a CO_2 chamber at a flow rate of 40% of the chamber volume per minute. After the loss of respiratory signs, CO_2 flow lasted for an additional 1 min to make sure they were complete euthanasia. Death was confirmed by the absence of breathing and lack of heartbeat. After confirmation of death, an additional secondary physical euthanasia (cervical dislocation) was performed before tissue collection and disposal of the carcass.

Experiment I was used to determine vaccine efficacy among the PmpGs + MOMP group, the PmpGs group alone, and the MOMP vaccine post immunization *via* the intranasal route (i.n). In the present study, 40 SPF chickens were randomly divided into four groups, including the PmpGs + MOMP group, the PmpGs (Pmp17 + Pmp20 + Pmp21G) group, the commercial MOMP group, and the control (VCG + chitosan gel) group. All the birds received the aforementioned vaccines *via* i.n. Post twice immunities specific IgG, IgA antibody, splenic lymphocyte proliferation index, and cytokines were determined. Subsequently, the birds were inoculated with 10^8 IFUs live EBs by intralaryngeal infection. The experimental flow was designed in **Table 1**.

Experiment II was conducted to determine whether the combination of PmpGs and MOMP vaccines might trigger genital protection compared with intramuscular injection (i.m) of the commercial MOMP vaccine. Briefly, 100 aged 80-day-old breeder ducks were randomly assigned to four groups (25 birds/per group) and reared in different isolated rooms. Vaccines were blended completely with antigens (100 μg), VCG (50 μg), and the same volume of chitosan gel. MOMP commercial vaccine was recommended to inject 100 μg per duck *via* i.m. Meanwhile, birds received 1×10^6 IFUs UV-inactivated EBs adjuvanted with chitosan gel and VCG as the EBs group, while birds were inoculated with the same amount of chitosan gel and VCG as the control group. At post-booster immunization 14 days, breeder ducks were challenged *via* intra-vagina with 1×10^8 IFUs of live *C. psittaci* EBs. During the experimental period, egg production and living conditions were monitored daily. Specific IgG antibodies, splenic lymphocyte proliferation, and cytokines were determined as mentioned above. Post challenge, bacterial clearance, and genital lesions were checked as previously described. The experimental flow was designed in **Table 2**.

Clinical Scoring of the Respiratory and Genital System

Respiratory System

Air sac and lung lesions were determined as the previous description (15). Briefly, unilateral air sac lesions were divided into five grades: grade 0—normal, clean, thin, and transparent; grade 1—slightly thickened and slightly turbid, or individual local white exudate; grade 2—grayish-white exudate in a few areas of the air sac, moderate sac thickness; grade 3—the majority of the

TABLE 1 | Inoculations and challenge of SPF chickens.

Group	Birds	Antigens and adjuvants	Route	Challenge
PmpGs + MOMP	10	Pmp17G, Pmp20G, Pmp21G, MOMP, VCG, Chitosan	i.n	10^8IFU live EBs
MOMP	10	MOMP, VCG, Chitosan	i.n	10^8IFU live EBs
PmpGs	10	Pmp17G, Pmp20G, Pmp21G, VCG, Chitosan	i.n	10^8IFU live EBs
Control	10	VCG, Chitosan	i.n	10^8IFU live EBs

TABLE 2 | Inoculations and challenge of breeder ducks.

Group	Birds	Antigens and adjuvants	Route	Challenge
PmpGs + MOMP	25	Pmp17G, Pmp20G, Pmp21G, MOMP, VCG, Chitosan	i.n	10^8IFU live EBs
MOMP	25	MOMP, White oil adjuvant	i.m	10^8IFU live EBs
EBs	25	Inactivated EBs, VCG, Chitosan	i.n	10^8IFU live EBs
Control	25	VCG, Chitosan	i.n	10^8IFU live EBs

air sacs are fully covered with yellow-white caseous exudate, and thickening of air sacs is obvious; grade 4—serious air sac lesions with white thick exudate on the thoracic cavity and abdominal cavity. Three degrees of edema were graded in unilateral lung sections: grade 0—none; grade 1—slight edema of the alveolar walls; grade 2—moderate edematous thickening of alveolar walls with occasional alveoli containing coagulated edema fluid; grade 3—extensive occurrence of alveolar and interstitial edema.

Genital System

Follicle and oviduct lesions were determined as the previous description (13). Briefly, follicle lesions were divided into five grades: grade 0—normal, yellow; grade 1—slight hemorrhage; grade 2—atrophy; grade 3—break, collapse; grade 4—degeneration, necrosis; grade 5—yolk peritonitis. Oviduct lesions were divided into five grades: grade 0—normal, clean; grade 1—slight inflammation; grade 2—edema; grade 3—hemorrhage; grade 4—white granular exudate; grade 5—degeneration, necrosis.

Humoral Response

Blood samples were collected post prime-boost regime from all groups, 10 birds per group. Serums were centrifuged at 3,500 rpm/min for 10 min and stored at −20°C until use. *C. psittaci*-specific antibody levels were determined with customized inactivated EBs ELIAS kit as previously described (8). Regarding IgA antibody test, six throat swabs were collected from each group before the challenge test, and then samples were vortexed for 5 min with sterilized PBS, and *C. psittaci*-specific IgA antibody levels were analyzed using ELIAS assay as previously described (6).

Lymphocyte Proliferation and Cytokine Secretions

Before challenge, spleens were collected from six birds per group on day 36. Splenic lymphocytes were isolated by separating reagent (Solarbio Science and Technology Co. Ltd., Beijing, China), and 1×10^5 cells in 100 μl/well were seeded in a 96-well plate for 48 h cultivation. Afterward, 1×10^5 IFUs-inactivated EBs were inoculated in each well, while Concanavalin A (Sigma–Aldrich, Germany) was added at 5 μg/well as a positive control, and medium was used as background control. The 96-well plates were incubated at 37°C in 5% CO_2 for 24 h stimulation. All experiments were performed in triplicate. Proliferation was determined using BrdU kits (Abcam, Cambridge, UK), and the proliferation index was calculated according to the protocol of the manufacturer.

Supernatants from splenic lymphocytes were collected from the above groups, with six samples per group. The cytokine secretions of IFN-γ, IL-2, IL-10, and IL-12 were measured by commercial ELISA kits (Kingfisher Biotech Inc., USA) according to the instructions provided by the manufacturer.

Bacterial Clearance and Chlamydial Shedding

Six throat swabs were collected from SPF birds in Experiment I on day 36, while six vaginal swabs were sampled from breeder ducks in Experiment II on day 36.

To quantitate live chlamydia, each swab was soaked in 0.5 ml of SPG buffer and vortexed. The supernatants were titrated on HeLa cell monolayers in duplicate. Live Chlamydia were evaluated using a direct immunofluorescence kit (IMAGEN^{TM}; Oxoid, Cambridge, UK). Inclusions were counted in five random fields per coverslip under a fluorescence microscope. The mean number of IFUs/swab was derived from the serially diluted and duplicate samples. The total number of IFUs/swab was converted into $\log_{10}$, which was used to calculate the mean value and standard deviation (16).

DNA was extracted by a commercial kit (QIAGEN, Hilden, Germany). The concentration of extracted DNA was determined with a Nano300 instrument. The quantity of *C. psittaci* was detected by quantitative real-time PCR using SYBR Green PCR kit (TransGen Biotech, Beijing, China) and Step One Plus Real-time PCR system (ABI, NY, USA). Based on the Chlamydia *omcA* gene, forward primer (5′-AGCCATGCAATCCTTGTGGT-3′) and reverse primer (5′-GCATGGCTTGGAGCAAGAAG-3′) were used to amplify the target fragment of 80 bp. The performance was following conditions: denaturing (one cycle at 95°C for 5 min), PCR (40 cycles at 95°C for 30 s each; 60°C annealing for 30 s; 72°C for 30 s), melting (one cycle at 95°C for 5 s; 60°C for 20 s; 95°C for 5 s) (14).

Statistical Analysis

Statistical significance was analyzed by one-way ANOVA with the LSD *post-hoc* test. Data were expressed as the mean ± standard deviation. All data were calculated and analyzed using the SPSS 22.0 software (IBM Corp., Armonk, NY, USA), and graphs were generated using the GraphPad Prism 7 software (GraphPad Software, San Diego, CA, USA). $p < 0.05$ or < 0.01 denoted statistically significant differences in the figures ($^*p < 0.05$; $^{**}p < 0.01$).

RESULTS

Expression and Identification of Recombinant Pmp17G and Pmp21G

C. psittaci-specific Pmp20G was expressed and identified in the previous report. To further investigate function of Pmp17G and Pmp21G, *pmp17G* and *pmp21G* genes were ligated into the pET-28a vector, positive transformants were picked out, and target proteins were expressed in *E. coli* Rossetta (DE3) strain. Recombinant Pmp17G and Pmp21G produced 50 and 68 kDa bands, respectively. Moreover, two proteins were identified by SDS-PAGE and Western blot using anti-His label and positive *C. psittaci* antibody. No cross-reaction to *E. coli* Rossetta (DE3) cells was observed (**Figure 1**).

Polymorphic Membrane Protein Gs + Major Outer Membrane Protein Vaccine Highly Induces Protections in Respiratory Tract Post *Chlamydia psittaci* Infection *via* Intranasal Immunity in SPF Chickens

Compared with the other three groups in Experiment I, the PmpGs + MOMP group induced higher levels of specific IgG antibodies from day 21 to day 28 ($p < 0.05$). Unfortunately, no statistical difference was found between the PmpGs group and the MOMP group (**Figure 2A**). Regarding IgA antibody levels on day 28, the PmpGs + MOMP group yielded a robust immune response compared with the PmpGs group and the MOMP group ($p < 0.05$), indicating that the combination of PmpGs and MOMP might trigger a good mucosal immunity (**Figure 2B**). As for lymphocyte proliferation, the PmpGs + MOMP group mediated significantly increasing stimulation index compared with the PmpGs group and the MOMP group on day 36 (**Figure 3A**). Later, IFN-γ expressions were upregulated significantly, while IL-10 concentrations were downregulated in the PmpGs + MOMP group in comparison with other groups ($p < 0.05$). On the other hand, IL-12 expressions were increased significantly both in the PmpGs + MOMP group and the MOMP group compared with the PmpGs alone. However, no significant difference of IL-4 secretions was observed among all the tested groups (**Figure 3B**).

Post challenge, lesion scores of air sacs were dramatically reduced in the PmpGs + MOMP group compared with the PmpGs group and the MOMP group ($p < 0.05$) (**Figure 4A**). However, no statistical difference of lung lesion was found among the three tested groups (**Figure 4B**). As for Chlamydial shedding throat swabs, lower shedding was determined in the PmpGs + MOMP group than the other two groups did ($p < 0.05$) (**Figure 5A**). More interestingly, bacterial clearances in the lungs were reduced significantly in the PmpGs + MOMP group compared with those of the PmpGs group and the MOMP group ($p < 0.05$) (**Figure 5B**).

Polymorphic Membrane Protein Gs + Major Outer Membrane Protein Vaccine Highly Induces Protections in Genital Tract Post *Chlamydia psittaci* Infection *via* Intranasal Immunity in Breeder Ducks

In Experiment II, egg performance was dramatically reduced in the commercial MOMP group and the control group in comparison with the PmpGs + MOMP group and the inactivated EBs group postchallenge from day 1 to day 4 ($p < 0.05$). More interestingly, the PmpGs + MOMP group recovered egg productions quickly compared with those of the inactivated EBs vaccine from day 4 to day 13. On day 16, increasing egg numbers were observed both in the PmpGs + MOMP group and the inactivated EBs group, while the MOMP group produced limited eggs (**Figure 6A**). Regarding IgG antibody levels, both the inactivated EBs group and the PmpGs + MOMP group induced

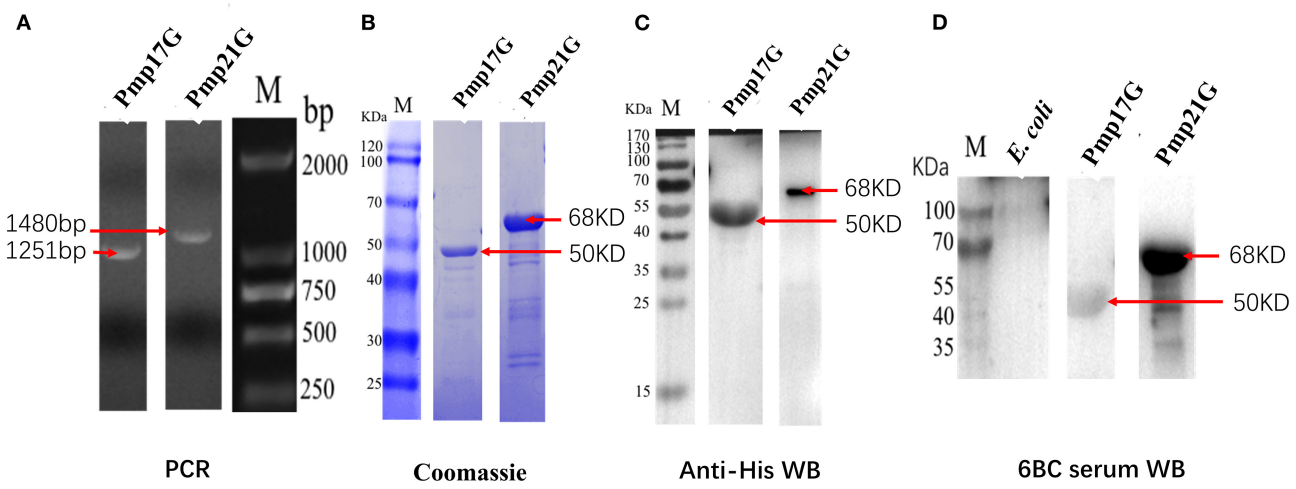

FIGURE 1 | Expression and identification of Pmp17G and Pmp21G. **(A)** The *pmp17G* and *pmp21G* genes fragments were amplified to be 1,251 and 1,480 bp, respectively, by PCR. **(B)** Recombinant Pmp17G and Pmp21G were 50 and 68 kDa, respectively, using Coomassie blue staining. **(C)** Two recombinant proteins were reacted to anti-His antibody and positive *Chlamydia psittaci* by Western blot. **(D)** No cross reaction to *Escherichia coli* Rossetta (DE3) cells was observed.

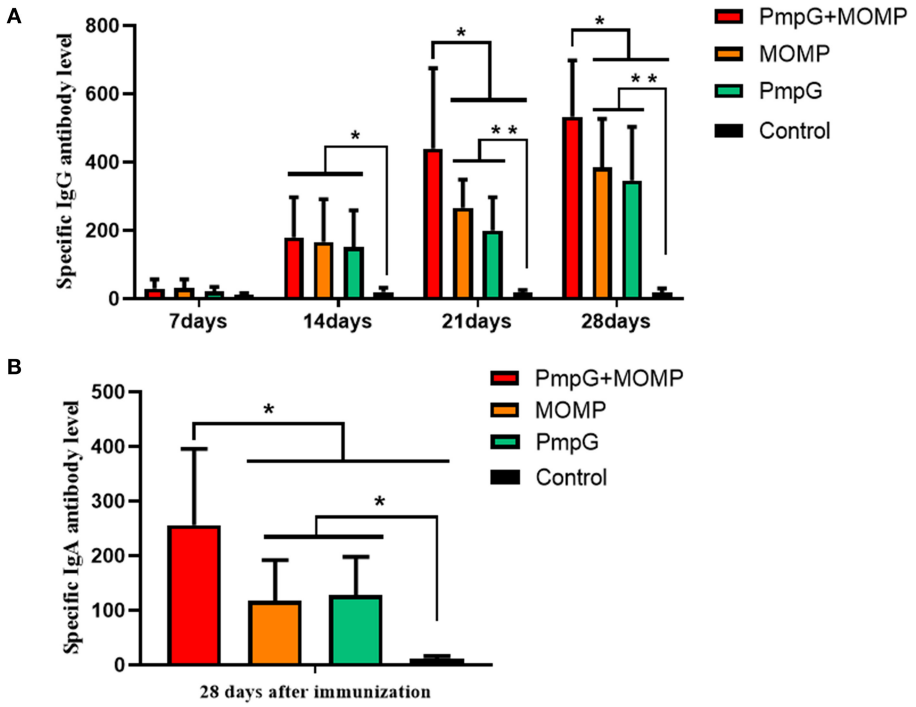

FIGURE 2 | Specific IgG and IgA antibody levels post inoculation into SPF chickens. **(A)** The PmpGs + MOMP group induced higher IgG antibody levels than the other three groups did from day 21 to day 28 ($p < 0.05$). No statistical difference was found between the PmpGs group alone and MOMP group. **(B)** On day 28, the PmpGs + MOMP group yielded robust IgA antibody levels compared with the PmpGs group alone and the MOMP group ($p < 0.05$). The differences were analyzed by ANOVA (*$p < 0.05$, **$p < 0.01$).

higher robust antibodies *via* i.n than the MOMP vaccine *via* i.m on day 28 ($p < 0.05$). No statistical difference was found between the inactivated EBs group and the PmpGs + MOMP group (**Figure 6B**). On day 28, the spleens were collected to determine lymphocyte proliferation using a commercial kit. Compared with the MOMP group, a significant increase of stimulation index was observed both in the PmpGs + MOMP group and the EBs group ($p < 0.05$). However, no statistical difference was found between the inactivated EBs group and the PmpGs + MOMP group (**Figure 7A**). As for cytokines, the PmpGs + MOMP group and the inactivated EBs group induced higher IFN-γ expressions than the MOMP group did on day 28 ($p < 0.05$). Compared with the above SPF chickens, breeder ducks inoculated with the PmpGs + MOMP vaccine yielded significantly increasing IL-12 in comparison with the control group. Although highly IL-2 and IL-10 expressions were found among the PmpGs + MOMP group, the inactivated EBs group, and the MOMP group, no significant difference was found (**Figure 7B**).

Postmortem, follicle lesions were significantly decreased in the PmpGs + MOMP group and the inactivated EBs group compared with the MOMP group and the control group ($p < 0.05$) (**Figure 8A**). As for oviduct lesions, fewer exudate inflammations were observed in the PmpGs + MOMP group and the inactivated EBs vaccine compared with those of the MOMP group ($p < 0.05$). Obviously, the PmpGs + MOMP vaccine induced lower inflammations than the inactivated EBs vaccine did, but no significant difference was determined (**Figure 8B**). Additionally, vaginal swabs were used to assess bacterial excretions post challenge at day 7. Compared with the control group, the PmpGs + MOMP vaccine, the inactivated EBs vaccine, and the commercial MOMP vaccine reduced Chlamydial shedding from the vaginal tract (**Figure 9A**). Moreover, lower bacterial loads of spleens and follicular membranes were determined in the PmpGs + MOMP group and the inactivated EBs group compared with the commercial MOMP vaccine and the control group ($p < 0.05$) (**Figures 9B,C**).

DISCUSSION

In the present study, we evaluated vaccine efficacy using multiple PmpGs and MOMP as the antigen candidates *via* different inoculation routes. More important, immunity against *C. psittaci* infection in the respiratory system was assessed in SPF chickens, while breeder ducks were used to determine the protection in the genital tract. As for the humoral immune response, the PmpGs + MOMP group significantly induced highly level specific IgG and IgA antibody levels in comparison with the PmpGs group alone and the commercial MOMP vaccine post booster immunization. Particularly, the PmpGs + MOMP group yielded comparable IgG responses as the inactivated EBs group did in breeder ducks. Moreover, the PmpGs + MOMP group and the inactivated EBs group induced a significant increase in lymphocyte proliferation. On the other hand, the PmpGs + MOMP group and inactivated EBs group generated higher

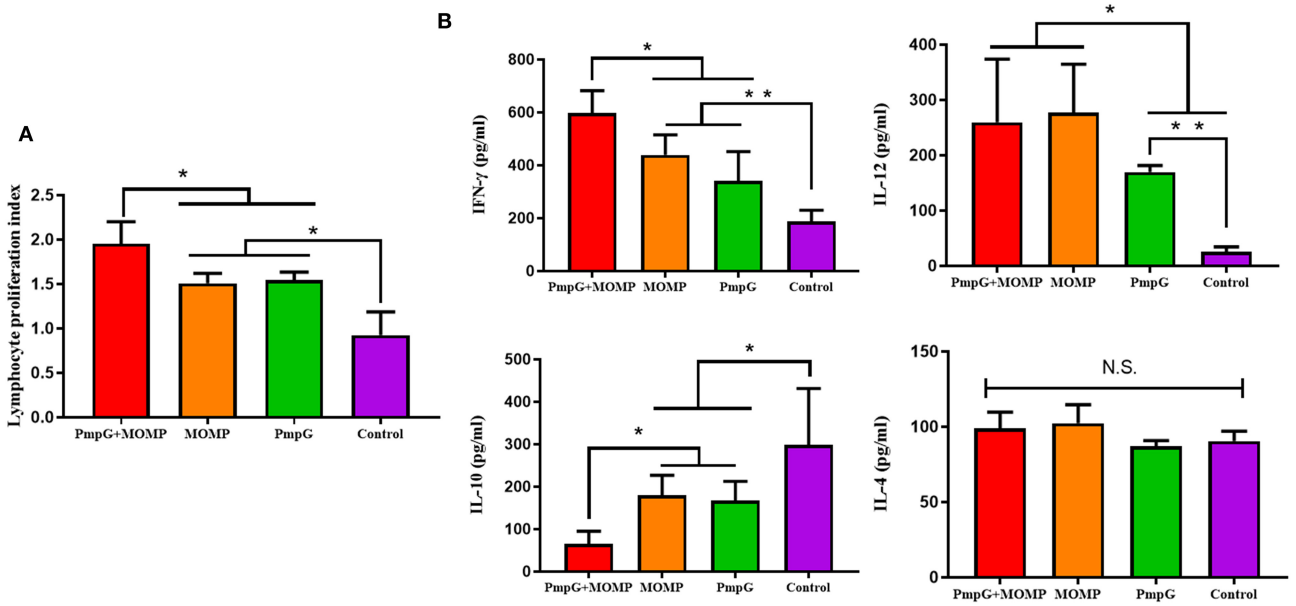

FIGURE 3 | Lymphocyte proliferation and cytokines post inoculation into SPF chickens. **(A)** Post twice immunizations, the PmpGs + MOMP group induced significant increase of lymphocyte proliferation index compared with the PmpGs group alone and the MOMP group on day 36 ($p < 0.05$). **(B)** IFN-γ expressions were upregulated significantly while IL-10 concentrations were downregulated in the PmpGs + MOMP group in comparison with other groups ($p < 0.05$). IL-12 expressions were increased significantly both in the PmpGs + MOMP group and the MOMP group compared with the PmpGs group alone. No significant difference of IL-4 secretion was observed among all the tested groups. The differences were analyzed by ANOVA (*$p < 0.05$, **$p < 0.01$, n.s., no statistical significance).

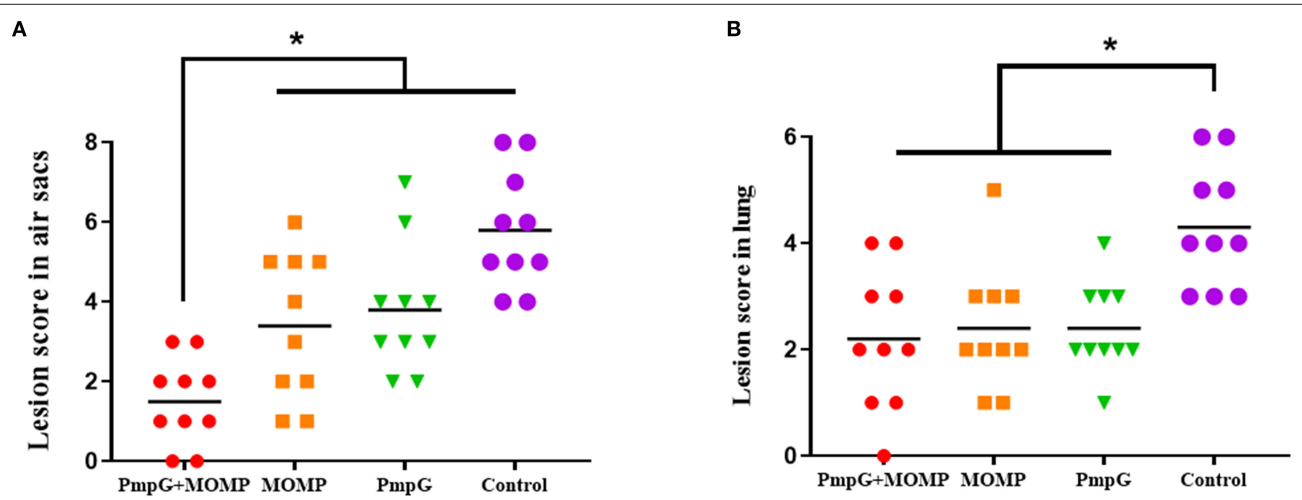

FIGURE 4 | Lesions of air sacs and lungs post Chlamydia challenge in SPF chickens. **(A)** Lesions of air sacs were dramatically reduced in the PmpGs + MOMP group compared with the PmpGs group alone and the MOMP group ($p < 0.05$). **(B)** No statistical difference in lung lesions was determined among the three tested groups. The differences were analyzed by ANOVA (*$p < 0.05$).

IFN-γ expressions compared with the MOMP group. Post challenge, egg performance was recovered in breeder ducks inoculated with the PmpGs + MOMP group. Chlamydial loads and shedding in the throat and vaginal swabs were completely reduced in the PmpGs + MOMP group and the inactivated EBs group. Therefore, the combination of multi-PmpGs and MOMP adjuvanted with chitosan gel and VCG *via* i.n is able to generate robust immune protection against *C. psittaci* infection in the respiratory system and genital tract. This is a novel approach to replace the whole inactivated EBs as the vaccine candidate, contributing to the eradication of Chlamydial transmission from animals to human beings.

C. psittaci PmpG function is unclear due to diverse genomics across different genotypes. Compared with 1 *pmpG* gene in

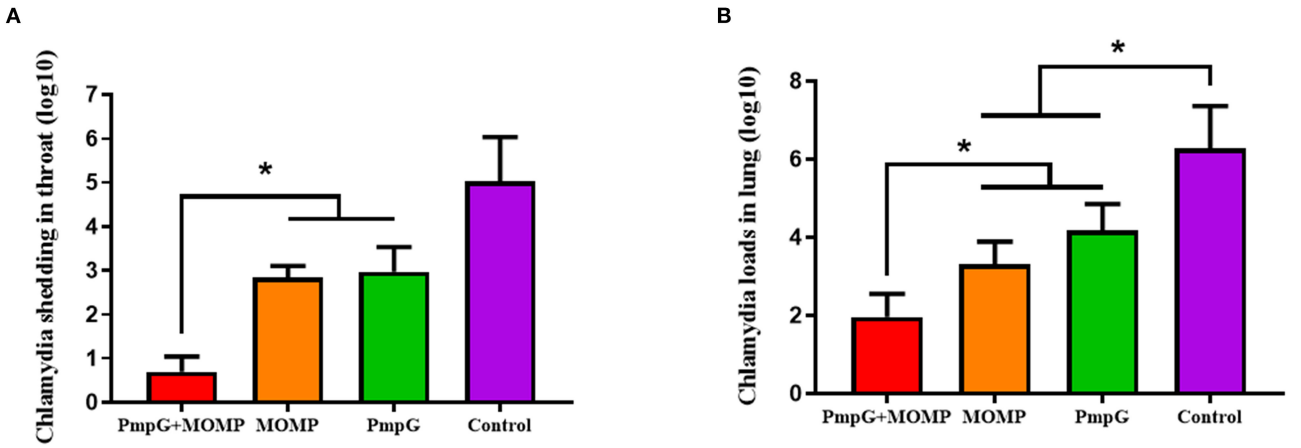

FIGURE 5 | Chlamydial loads and shedding of SPF chickens post Chlamydial challenge. **(A)** Lower shedding was determined in the PmpGs + MOMP group than the other three groups did ($p < 0.05$). **(B)** Bacterial clearances in the lungs were reduced significantly in the PmpGs + MOMP group compared with those of the PmpGs group alone and the MOMP group ($p < 0.05$). The differences were analyzed by ANOVA (*$p < 0.05$).

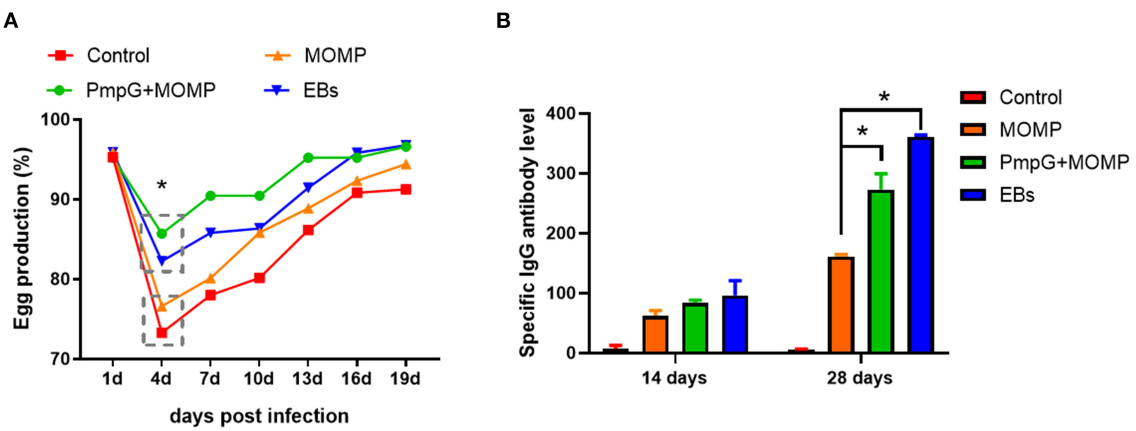

FIGURE 6 | Egg productions and specific IgG antibody level of breeder ducks. **(A)** Egg performance was dramatically reduced in the commercial MOMP group and the control group in comparison with the PmpGs + MOMP group and the inactivated EBs group post challenge ($p < 0.05$). **(B)** Both the inactivated EBs group and the PmpGs + MOMP group induced higher robust IgG antibodies *via* intranasal route than the MOMP vaccine did *via* intramuscular injection on day 28 ($p < 0.05$). The differences were analyzed by ANOVA (*$p < 0.05$).

C. trachomatis, *pmpG* genes enriched in *C. psittaci* might be associated with host tropism and host diversity. In our previous study, we evaluated the immune efficacy among Pmp7G, Pmp17G, Pmp19G, Pmp20G, and Pmp21G in the chicken model and the above five PmpGs were determined to be good vaccine candidates (data unpublished). Moreover, both Pmp17G and Pmp20G were used as coating antigens for detecting *C. psittaci* antibody (8). In a recent report, Pmp17G was associated with host adaptions as an adhesin (17). Furthermore, *C. psittaci*-specific Pmp17G activated Chlamydial invasion in a dependent way by recognizing EGFR, activating Tyr1068 phosphorylation of EGFR, and forming the EGFR–Grb2 complex, contributing to intracellular attachment and internalization during *C. psittaci* infection (18). In the present study, multiple PmpGs as antigens, Pmp17G, Pmp20G, and Pmp21G were based on our pioneer study. Whether Pmp20G and Pmp21G are potential adhesins to host cells, future work is required to be done. Compared with the whole inactivated EBs as vaccine antigens, the combination of multiple PmpGs and MOMP showed several advantages. First, the preparation of PmpGs and MOMP creates an environmental-friendly manufacturing process and no risk for employees. Whole EBs are purified from the embryonated eggs and external pathogens could be released from the remaining egg yolks and albumens, resulting in employee infection and flu-like fever. Second, PmpGs and MOMP located in the outer membrane complex could induce full immune responses as the whole EBs antigens did. By post inoculation into SPF chickens and breeder ducks, PmpGs + MOMP vaccine induced full protection both in the respiratory tract and genital tract, which is superior to the MOMP vaccine and PmpGs alone. More interestingly,

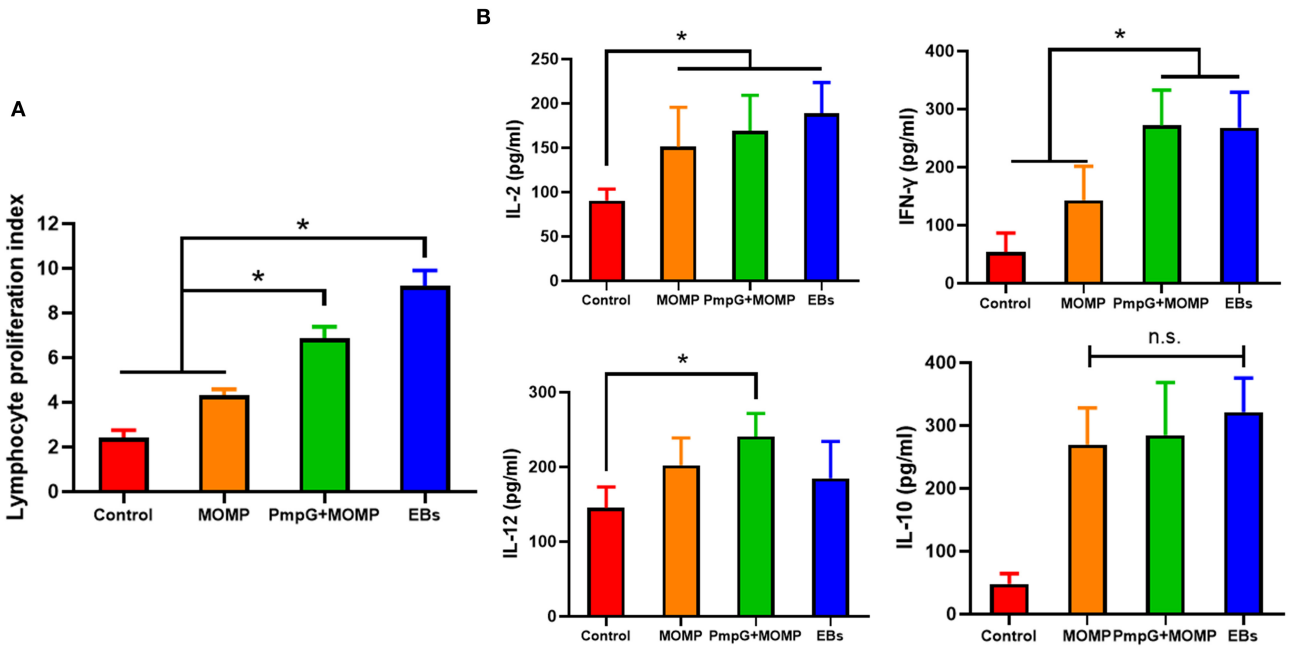

FIGURE 7 | Lymphocyte proliferation and cytokines secretions post inoculation into breeder ducks. **(A)** After booster immunization, the PmpGs + MOMP group and the inactivated EBs group upregulated significantly lymphocyte proliferations index compared with the commercial MOMP vaccine ($p < 0.05$). **(B)** IFN-γ expressions were increased significantly in the PmpGs + MOMP group compared with the commercial MOMP group ($p < 0.05$), IL-2 production was upregulated among the PmpGs + MOMP group, the inactivated EBs group, and the commercial MOMP group in comparison with the control group ($p < 0.05$). IL-10 secretions showed no significant difference among all groups. The differences were analyzed by ANOVA (*$p < 0.05$, n.s., no statistical significance).

its protection was better than the inactivated EBs vaccine regarding egg performance and inflammations of the genital tract. High immunity might be associated with humoral IgG, IgA antibody responses, and cellular immunity characterized as high stimulation index and IFN-γ secretions. Our investigation was correlated to the previous study that PmpG-combined DDA/TDB adjuvant significantly enhanced IFN-γ expression in CD4+ T cells and reduced Chlamydial shedding against vaginal infection by *C. muridarum* (19). In the previous report, PmpG stimulated a more robust immune response and protection in the mice's vagina compared with PmpE, PmpF, Aasf, RpIF, TC0420, or TC0825 as antigen (20). *C. abortus*-specific PmpG induced good protection for sheep during *C. abortion* A/22 infection due to PmpG enriched with T cell and B cell epitopes (21). Multiple antigens of MOMP, PmpG, inclusion protein TC0500, and TC0873 with adjuvant ISCOMATRIX-IMX could protect mice against *C. muridarum* infection in the reproductive tract, indicating that multiple antigens and mucosal adjuvant *via* intranasal route might be a promising approach combating Chlamydia infection (9).

C. psittaci infection triggers transmission *via* entering the ocular, respiratory system, gastrointestinal tract, and genital tract, leading to multiple clinical symptoms and economic loss for the animal industry. Commercial MOMP vaccine is recommended to be injected intramuscularly, but it does not provide full protection due to partial immune response and no barrier to the respiratory tract, and ocular as well. In our recent document, birds that received the inactivated EBs vaccine *via* i.n generated better immune protection compared with live EBs as the vaccine candidate, and intranasal inoculation was confirmed to be a better option than the intramuscular route (6). Regarding the large-scale poultry industry, the intramuscular injection was blamed for heavy labor for employees and strong stress for heavy body-weight birds, like breeder ducks, geese, and turkey. Clinically, breeder ducks and geese will stop egg production for a couple of weeks and develop secondary bacterial or viral infection, leading to the prevalence of salpingitis and culling from breeder flock. Notably, the intranasal route can be achieved by aerosol spray for the large-scale animal industry. In the present study, we utilized chitosan gels as a delivery system to immunize birds *via* the intranasal route. Chitosan is a natural cationic polysaccharide with good biocompatibility, biodegradability, and mucosal adhesion. Chitosan gel will attach Chlamydial antigens by electrostatic adsorption that ensures the slow release of antigens into the mucosa, leading to continuous immune stimulation. To compare traditional intramuscular routes, mucosal immunity could provide better protection in the respiratory tract and genital system. Especially, lower Chlamydial loads were detected in the follicle membrane, and bacterial shedding was significantly decreased in the genital tract. It indicated that the intranasal immunization route could protect the genital system against Chlamydial infection, which was superior to the intramuscular route. The previous report confirmed that FMS-like tyrosine kinase 3 ligand with VCG as adjuvant *via* mucosal routes induced good humoral and cellular responses compared with the injection

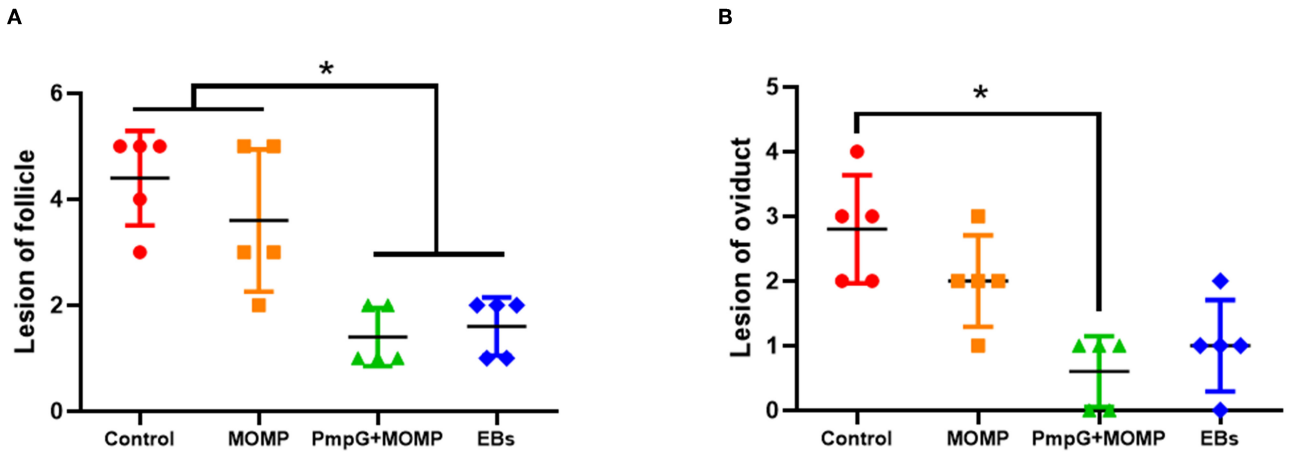

FIGURE 8 | Lesions of follicles and oviducts post-Chlamydial challenge in breeder ducks. **(A)** Follicular lesions were significantly decreased in the PmpGs + MOMP group and the inactivated EBs group compared with the commercial MOMP group or the control group ($p < 0.05$). **(B)** Oviduct lesions were obviously reduced in the PmpGs + MOMP group compared with the control group. The differences were analyzed by ANOVA (*$p < 0.05$).

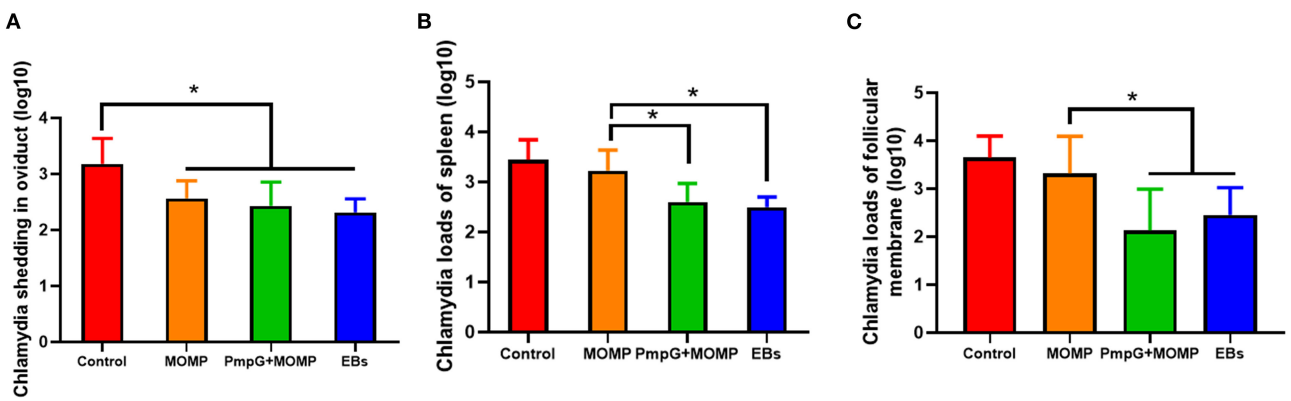

FIGURE 9 | Chlamydial loads and shedding in genital tract of breeder ducks. **(A)** No significant difference of Chlamydial shedding in the oviduct of breeder ducks was detected among the three tested groups. **(B)** Less Chlamydial loads of spleens were determined in the PmpGs + MOMP group and the inactivated EBs group compared with the commercial MOMP vaccine or the control group ($p < 0.05$). **(C)** Chlamydial loads of follicular membranes were significantly decreased in the PmpGs + MOMP group and the inactivated EBs group in comparison with the commercial MOMP vaccine and the control group ($p < 0.05$). The differences were analyzed by ANOVA (*$p < 0.05$).

route (22). Furthermore, intranasal immunity is responsible for the eradication of *C. psittaci* infection *via* the respiratory tract and genital tract, contributing to blocking Chlamydial transmission risk.

In summary, the combination of multi-PmpGs and MOMP adjuvanted with chitosan gels and VCG induced a robust humoral, cellular immune response, and better bacterial clearance against *C. psittaci* infection. Not only did it provide good immune efficacy in the respiratory system, but also highly generated protection in the genital tract in poultry. Although cross-protection against different serotypes is not determined in the study, future work is urgently needed to illustrate the mechanism and potential protection against other Chlamydial infections. Finally, the combination of PmpGs and MOMP vaccine containing chitosan gels and VCG as adjuvants is a promising approach for large-scale animal industry *via* aerosol immunization, leading to blockage of the Chlamydial transmission from animals to human beings.

DATA AVAILABILITY STATEMENT

The original contributions presented in the study are included in the article/**Supplementary Material**, further inquiries can be directed to the corresponding authors.

ETHICS STATEMENT

The animal study was reviewed and approved by Laboratory Animal Ethical Committee of China Agricultural University.

AUTHOR CONTRIBUTIONS

CH (animal model, adjuvant, and immunization strategy) and ZW (Chlamydial strain): conceptualization. QL, HF, and ZY: methodology. SC: statistical analysis. HF and ZW: investigation. QL: writing—original draft preparation. CH: writing—review and editing and funding acquisition. All authors have read and agreed to the published version of the manuscript.

FUNDING

This work was supported by Wen's Research Foundation (Grant No. 202005410510320) and partially funded by the Taishan Scholar Foundation of Shandong Province (Grant No. ts201511084).

SUPPLEMENTARY MATERIAL

The Supplementary Material for this article can be found online at: https://www.frontiersin.org/articles/10.3389/fvets.2022.855447/full#supplementary-material

Supplementary Figure 1 | Pathological section of SPF chicken's lung post Chlamydial challenge. **(A)** PmpGs + MOMP group: Less alveolar damage and hemorrhagic inflammation were observed in the alveolar cavity (arrow). **(B)** MOMP group: The focal intra-alveolar hemorrhagic lesions were observed and whole alveolar structures were well protected post infection (arrow). **(C)** PmpGs group: Scattered hemorrhage was observed in the alveolar septa and mild interstitial lesions were observed in the lungs (arrow). **(D)** Control group: Typical hyaline membrane formation in alveolar space and exudative fluid containing fibrin and epithelial cells in alveolar walls were observed. Also, severe interstitial lesions were observed in the lungs due to inflammatory infiltrates (arrow). Hematoxylin & Eosin staining (Magnification X20).

REFERENCES

1. Beeckman DS, Vanrompay DC. Zoonotic Chlamydophila psittaci infections from a clinical perspective. *Clin Microbiol Infect.* (2009) 15:11–7. doi: 10.1111/j.1469-0691.2008.02669.x
2. Chen X, Cao K, Wei Y, Qian Y, Liang J, Dong D, et al. Metagenomic next-generation sequencing in the diagnosis of severe pneumonias caused by Chlamydia psittaci. *Infection.* (2020) 48:535–42. doi: 10.1007/s15010-020-01429-0
3. Hogerwerf L, DE Gier B, Baan B, VAN DER Hoek W. Chlamydia psittaci (psittacosis) as a cause of community-acquired pneumonia: a systematic review and meta-analysis. *Epidemiol Infect.* (2017) 145:3096–105. doi: 10.1017/S0950268817002060
4. Knittler MR, Sachse K. Chlamydia psittaci: update on an underestimated zoonotic agent. *Pathog Dis.* (2015) 73:1–158. doi: 10.1093/femspd/ftu007
5. Howard S, Richardson S, Benyeogor I, Omosun Y, Dye K, Medhavi F, et al. Differential miRNA profiles correlate with disparate immunity outcomes associated with vaccine immunization and chlamydial infection. *Front Immunol.* (2021) 12:625318. doi: 10.3389/fimmu.2021.625318
6. Zuo Z, Zou Y, Li Q, Guo Y, Zhang T, Wu J, et al. Intranasal immunization with inactivated chlamydial elementary bodies formulated in VCG-chitosan nanoparticles induces robust immunity against intranasal Chlamydia psittaci challenge. *Sci Rep.* (2021) 11:10389. doi: 10.1038/s41598-021-89940-8
7. Holzer M, Barf LM, Lamkiewicz K, Vorimore F, Lataretu M, Favaroni A, et al. Comparative Genome Analysis of 33 Chlamydia Strains Reveals Characteristic Features of Chlamydia Psittaci and Closely Related Species. *Pathogens.* (2020) 9:899. doi: 10.3390/pathogens9110899
8. Cui L, Qu G, Chen Y, Wu Y, Wang C, Cheng H, et al. Polymorphic membrane protein 20G: a promising diagnostic biomarker for specific detection of Chlamydia psittaci infection. *Microb Pathog.* (2021) 155:104882. doi: 10.1016/j.micpath.2021.104882
9. O'Meara CP, Armitage CW, Andrew DW, Kollipara A, Lycke NY, Potter AA, et al. Multistage vaccines containing outer membrane, type III secretion system and inclusion membrane proteins protects against a Chlamydia genital tract infection and pathology. *Vaccine.* (2017) 35:3883–8. doi: 10.1016/j.vaccine.2017.05.063
10. Pal S, Favaroni A, Tifrea DF, Hanisch PT, Luczak SET, Hegemann JH, et al. Comparison of the nine polymorphic membrane proteins of Chlamydia trachomatis for their ability to induce protective immune responses in mice against a C. muridarum challenge. *Vaccine.* (2017) 35:2543–9. doi: 10.1016/j.vaccine.2017.03.070
11. Kastner J, Saluz HP, Hanel F. Identification of *in vivo*-induced bacterial protein antigens during calf infection with Chlamydia psittaci. *Int J Med Microbiol.* (2015) 305:310–21. doi: 10.1016/j.ijmm.2014.12.022
12. Stary G, Olive A, Radovic-Moreno AF, Gondek D, Alvarez D, Basto PA, et al. A mucosal vaccine against Chlamydia trachomatis generates two waves of protective memory T cells. *Science.* (2015) 348:aaa8205. doi: 10.1126/science.aaa8205
13. Fang H, Quan H, Zhang Y, Li Q, Wang Y, Yuan S, et al. Co-Infection of *Escherichia coli*, Enterococcus faecalis and chlamydia psittaci contributes to salpingitis of laying layers and breeder ducks. *Pathogens.* (2021) 10:755. doi: 10.3390/pathogens10060755
14. Campbell LA, Kuo CC. Cultivation and laboratory maintenance of Chlamydia pneumoniae. *Curr Protoc Microbiol.* (2009) Chapter 11: Unit11B 1. doi: 10.1002/9780471729259.mc11b01s12
15. Zhang Q, Zuo Z, Guo Y, Zhang T, Han Z, Huang S, et al. Contaminated feed-borne Bacillus cereus aggravates respiratory distress post avian influenza virus H9N2 infection by inducing pneumonia. *Sci Rep.* (2019) 9:7231. doi: 10.1038/s41598-019-43660-2
16. Zhang T, Huo Z, Ma J, He C, Zhong G. The plasmid-encoded pGP3 promotes chlamydia evasion of acidic barriers in both stomach and vagina. *Infect Immun.* (2019) 87:e00844–18. doi: 10.1128/IAI.00844-18
17. Favaroni A, Trinks A, Weber M, Hegemann JH, Schnee C. Pmp repertoires influence the different infectious potential of avian and mammalian chlamydia psittaci strains. *Front Microbiol.* (2021) 12:656209. doi: 10.3389/fmicb.2021.656209
18. Li XH, Zuo ZH, Wang YH, Hegemann JH, He C. Polymorphic membrane protein 17G of Chlamydia psittaci mediated the invasion of bacteria to host cells by binding EGFR. *Front Immunol.* (2022) 12:818487. doi: 10.3389/fimmu.2021.818487
19. Yu H, Jiang X, Shen C, Karunakaran KP, Jiang J, Rosin NL, et al. Chlamydia muridarum T-cell antigens formulated with the adjuvant DDA/TDB induce immunity against infection that correlates with a high frequency of gamma interferon (IFN-gamma)/tumor necrosis factor alpha and IFN-gamma/interleukin-17 double-positive CD4+ T cells. *Infect Immun.* (2010) 78:2272–82. doi: 10.1128/IAI.01374-09
20. Yu H, Karunakaran KP, Jiang X, Shen C, Andersen P, Brunham RC. Chlamydia muridarum T cell antigens and adjuvants that induce protective immunity in mice. *Infect Immun.* (2012) 80:1510–8. doi: 10.1128/IAI.06338-11
21. Cevenini R, Donati M, Brocchi E, De Simone F, La Placa M. Partial characterization of an 89-kDa highly immunoreactive protein from Chlamydia psittaci A/22 causing ovine abortion. *FEMS Microbiol Lett.* (1991) 65:111–5. doi: 10.1111/j.1574-6968.1991.tb04722.x
22. Pais R, Omosun Y, Igietseme JU, Fujihashi K, Eko FO. Route of vaccine administration influences the impact of Fms-like tyrosine kinase 3 ligand (Flt3L) on chlamydial-specific protective immune responses. *Front Immunol.* (2019) 10:1577. doi: 10.3389/fimmu.2019.01577

Conflict of Interest: ZY, HF, and ZW were employed by Wen's Foodstuffs Group Co., Ltd.

The remaining authors declare that the research was conducted in the absence of any commercial or financial relationships that could be construed as a potential conflict ofinterest.

Publisher's Note: All claims expressed in this article are solely those of the authors and do not necessarily represent those of their affiliated organizations, or those of the publisher, the editors and the reviewers. Any product that may be evaluated in this article, or claim that may be made by its manufacturer, is not guaranteed or endorsed by the publisher.

frontiers | Frontiers in Veterinary Science

ORIGINAL RESEARCH
published: 25 April 2022
doi: 10.3389/fvets.2022.891286

Dermal Microvascular Units in Domestic Pigs (*Sus scrofa domestica*): Role as Transdermal Passive Immune Channels

Xiangfei Meng[1], Zhaoxuan Zhu[1], Nisar Ahmed[2], Qianhui Ma[1], Qi Wang[1], Bihua Deng[3], Qiusheng Chen[1], Yu Lu[3] and Ping Yang[1]**

[1] MOE Joint International Research Laboratory of Animal Health and Food Safety, College of Veterinary Medicine, Nanjing Agricultural University, Nanjing, China, [2] Department of Veterinary Anatomy and Histology, Faculty of Veterinary and Animal Sciences, Lasbela University of Agriculture, Water & Marine Sciences (LUAWMS), Uthal, Pakistan, [3] National Research Center of Engineering and Technology for Veterinary Biologicals, Institute of Veterinary Immunology and Engineering, Jiangsu Academy of Agricultural Sciences, Nanjing, China

OPEN ACCESS

Edited by:
Fazul Nabi,
Lasbela University of Agriculture, Water and Marine Sciences, Pakistan

Reviewed by:
Qianqian Hu,
Anhui Science and Technology University, China
Zhantao Yu,
The University of Tennessee, Knoxville, United States

***Correspondence:**
Ping Yang
yangping@njau.edu.cn
Yu Lu
luyu@jaas.ac.cn

Specialty section:
This article was submitted to Comparative and Clinical Medicine, a section of the journal Frontiers in Veterinary Science

Received: *07 March 2022*
Accepted: *30 March 2022*
Published: *25 April 2022*

Citation:
Meng X, Zhu Z, Ahmed N, Ma Q, Wang Q, Deng B, Chen Q, Lu Y and Yang P (2022) Dermal Microvascular Units in Domestic Pigs (Sus scrofa domestica): Role as Transdermal Passive Immune Channels. Front. Vet. Sci. 9:891286. doi: 10.3389/fvets.2022.891286

The dermal microvascular unit (DMU) is a perivascular functional unit in the dermis. It is composed of microvascular and capillary lymphatics surrounded by immune cells. In this study, jet needle-free injection system was used to injected biocompatible carbon nanoparticles into the cervical skin of domestic pigs (*Sus scrofa domestica*) and assessed the morphological distribution of DMUs by hematoxylin erythrosine staining, immunohistochemistry (IHC), and transmission electron microscopy (TEM), and TEM was also used to observe the ultrastructural changes of DMUs after jet needle-free injection. Following our study, we identified DMUs in the dermis stratum papillare and similar structures in the dermis stratum reticulare, but the aggregation of $CD68^+$ and $CD1a^+$ cells in the dermis stratum papillare of DMUs by IHC confirmed that DMUs act as reservoirs of dermal immune cells, while similar structures in the dermis stratum reticulare should not be considered as DMUs. Ultrastructure of DMUs was revealed by TEM. Marvelous changes were found following xenobiotics attack, including the rearrangement of endothelial cells and pericytes, and the reactivity of immune cells. Novel interstitial cell telocyte (TC) was also identified around the microvasculature, which may have been previously known as the veil cell. Our results successfully identified the distribution of DMUs in the skin of domestic pigs, which might act as reservoirs of immune cells in the skin and play a role in immune surveillance and immune defense.

Keywords: dermal microvascular unit, domestic pigs (*Sus scrofa domestica*), macrophages, jet needle-free injection, skin immunity, veil cells, telocyte

INTRODUCTION

The skin is the first line of defense against the outside world in higher vertebrates. Not until Streilein introduced the concept of skin-associated lymphoid tissue (SALT) did people regard the skin as having dual roles as physical barrier and immune function. It is found that the dermis is the major site where immune function occurs and contains twice as many immune cells in the circulatory system. These immune cells are not randomly distributed in the dermal structures, but share a close

anatomical relationship with the microvessels of the dermal superficial vascular plexuses (DSVPs) (1, 2). The dermal microvascular unit (DMU) is the basic model for this constellation of dermal cells centered on the vasculature. In the original study, DMUs were considered to contain dermal microvascular endothelial cells (DMECs), dermal perivascular dendrocytes (DPDCs, including dendritic-like macrophages and dendritic cells), dermal perivascular T cells (DPTCs), dermal perivascular mast cells (DPMCs) and other cells unrelated to immunity (e.g., fibroblasts, and pericytes), which could not completely reveal the mechanism of its involvement in cutaneous immunity as a functional unit. Therefore, recent studies have complemented the original theory by including capillary lymphatics, which share an intimate anatomical relationship with these structures, in DMUs (3, 4).

Since capillary lymphatics and capillaries are not easily identifiable in routine histological evaluation, electron microscopy remains the best method for identifying DMUs (5). Ultrastructural evidences suggest that the center of DMUs is composed of DMECs that originate from the horizontal papillary plexuses (6). These structures are responsible for the blood supply to the dermis stratum papillare and are responsive to injury (7), hypoxia (8), and stress (9, 10), which manifests in the ultrastructure by gap formation and altered deposition in the basement membrane material of the vascular wall (11–13). Pericytes are located adjacent to or above endothelial cell junctions, which can control the contraction of DMECs by upregulating endothelin-1 (ET-1) and downregulating of iNOS expressed by DMECs (14, 15). During inflammation, pericytes can cover the endothelial cell gap through rearrangements, which is important in the study of skin pathology (16, 17). The existence of DPDCs, DPTCs and DPMCs located on the periphery of pericytes allows the DMU to act as a functional unit of cutaneous immunity, these cells accumulate near DMECs and serve as a possible reservoir for lymphocyte recirculation in the skin (18, 19). The capillary lymphatics that comprise belonging to DMUs are superficial dermal lymphatic plexuses and not mentioned in the manuscript originally introducing the concept of DMUs, but their unique immunological role in the dermis has encouraged the possibility of exploring them as part of DMUs (3, 4). It has been found that during the inflammatory or immune response phase, lymphendothelial cells (LECs) guide the directional migration of dermal dendritic cells (d DCs, 10–15%) and T cells (80–90%) *via* CCL21 and sphingosine-1 phosphate (S1P) signaling, and LYVE-1 has also been identified to guide the migration of d DCs (20–23).

Domestic pigs (*Sus scrofa domestica*) are economically important animals and a major source of meat in many countries. Vaccination of domestic pigs is usually performed by injection, but this may cause lesions in pork carcasses and losses to the pig industry (24). In recent years, transdermal immunization methods including transdermal delivery system (TDS), transdermal needle-free injection (NFI) and solid microstructured transdermal system (sMTS) have endeavored to solve the problems caused by traditional injections, which have been used on a small scale with good effects (25–27). However, there are no reports confirming the presence of DMUs in domestic pigs, and even a few studies have dug deep into the ultrastructural changes of DMUs during xenobiotics (i.e., antigenic or non-antigenic substance) attack on the skin of domestic pigs. In this study, the presence of DMUs in domestic pig skin was confirmed for the first time by histological analysis and immunohistochemistry (IHC), and DMUs were identified as reservoirs of immune cells for the first time. In addition, transmission electron microscopy (TEM) was employed to analyze the ultrastructural changes of DMUs after attack of the skin by xenobiotics, which have elucidated the ultrastructure of DMUs and validated the potential role of DMUs involved in passive skin immunity. Our results will contribute to a profound understanding of the mechanisms of passive skin immunity under foreign substance attack and provide new ideas for the development of transdermal immunization methods in domestic pigs.

MATERIALS AND METHODS

Animals and Ethics Statement

Three-month-old male domestic pigs, 45 to 49 kg, were purchased from Jiangsu Zhongcheng Company (Yancheng, China). Pigs were randomly divided into two groups: Control and 5% biocompatible carbon nanoparticles, five pigs in each group. Under pentobarbital sodium (30 mg/kg, Sinopharm Chemical Reagent Co., Shanghai, China) anesthesia, biocompatible carbon nanoparticles was injected into the cervical skin by group through the POK-MBX jet needle-free injection system (DERM-G1-2, German Derm Co., Hong Kong, China), and the control group was left untreated. One hour later, animals were sacrificed and the cervical skin was collected.

The study protocol was approved by the Animal Ethics Committee of Nanjing Agricultural University. The animals were housed in the experimental animal center of Nanjing Agricultural University and leave libitum access to filtered water and food, adaptive feeding was given for 5 days before the experiment.

Histological Evaluation

Cervical skin was fixed in 4% paraformaldehyde for 48 h, embedded in paraffin, sectioned at a thickness of 7 μm. After deparaffinization, the sections were stained with hematoxylin eosin staining solution (Leagene biotechnology, Beijing, China) for light microscopic analysis using Olympus microscope (DP73, Tokyo, Japan).

Immunohistochemistry

Paraffin sections (7 μm) were deparaffinized on positively charge slides, blocked endogenous peroxidase with 3% hydrogen peroxide for 10 min at 37 °C, and used sodium citrate buffer (0.01 M, pH 6.0, 95°C) to expose antigenic epitopes. Treated samples were blocked with 5% bovine serum albumin for 40 min (BSA, Boster Biological Technology, Wuhan, China) and incubated with rabbit anti-CD68 antibody (1:100, Boster Biological Technology, Wuhan, China), rabbit anti-CD1c antibody (1:100, Bioss Biological Technology, Beijing, China), and rabbit anti-CD1a antibody (1:100, Boster Biological

Technology, Wuhan, China) overnight at 4°C, negative controls were set up with phosphate buffered saline (PBS, 0.1 M, pH 7.4) instead of primary antibody. The next day, samples washed with PBS (0.1 M, pH 7.4) were incubated with anti-rabbit IgG antibody (1:100, Servicebio Technology, Wuhan, China) at 37°C for 1 h, washed again and analyzed for peroxidase activity with diaminobenzidine (DAB, Boster Biological Technology, Wuhan, China), and nuclei were stained with hematoxylin.

Transmission Electron Microscopy

Skin tissue sectioned to 1 mm^3 in size was fixed overnight in 2.5% glutaraldehyde at 4°C. After PBS (0.1 M, pH 7.4) rinsing, 1% osmium tetroxide (Polysciences Inc. Warrington, Pennsylvania, USA) was used to fix the tissue at room temperature. Following the dehydration treatment, the tissue was embedded in Epon812 (Merck & Co Inc., New Jersey, USA) for 3 days at 60°C. The treated tissue samples were fine-sliced into 50 nm ultrathin sections and anchored on copper grids. Sections were stained with uranyl acetate and lead citrate, observed under the Hitachi TEM system (H-7650, Tokyo, Japan).

Statistical Analysis

Ten randomly selected DMUs and similar structure consisting of deep dermal vascular plexuses (DDVPs) in the dermis stratum reticulare from the same immunohistochemical section were photographed under the same field of view, and gray-scale analysis of the integral optical density (IOD) was done by using Imagepro Plus 6.0. Statistical differences between the two groups were analyzed by student's *t*-test (R version 4.1.1 and Rstudio version 1.4). The ggplot 2 visualization package (version 3.3.5) for the R (version 4.1.1) programming language was used to generate box plots, $P < 0.05$ was considered statistically significant.

RESULTS

Distribution and Identification of DMUs

HE results of pig neck skin showed that the DMU was composed of capillary lymphatic, microvessel and peritubular cells (**Figure 1A**). However, the morphology of capillary lymphatics in HE results is often "collapsed" and difficult to identify. Nevertheless, we can observe that DMUs were observed to be widely distributed in the dermis, mainly in the papillary dermis near the epidermis (**Figure 1A**) rather than in the dermis stratum reticulare. Although blood vessels and lymphatics are also distributed in the dermis stratum reticulare, they tend to be separate and do not function in concert (**Figure 1A**). Based on previous knowledge and this study, we drew a model diagram to describe the spatial position of the DMUs in the microcirculation: Blood vessels and lymphatic vessels are widely distributed in the dermis, with the DMUs found mainly in the papillary dermis, consisting of a network of microvessels belonging to DSVPs and lymphatic vessels belonging to the superficial dermal lymphatic plexuses. The reticular dermis is blood supplied by DDVPs and few immune cells existed, although it also has a similar structure of intertwined vascular lymphatic vessels. Immune cells in the skin can enter the draining lymph nodes through DMUs from lymphatic vessels or high endothelial microvessels (**Figure 1B**).

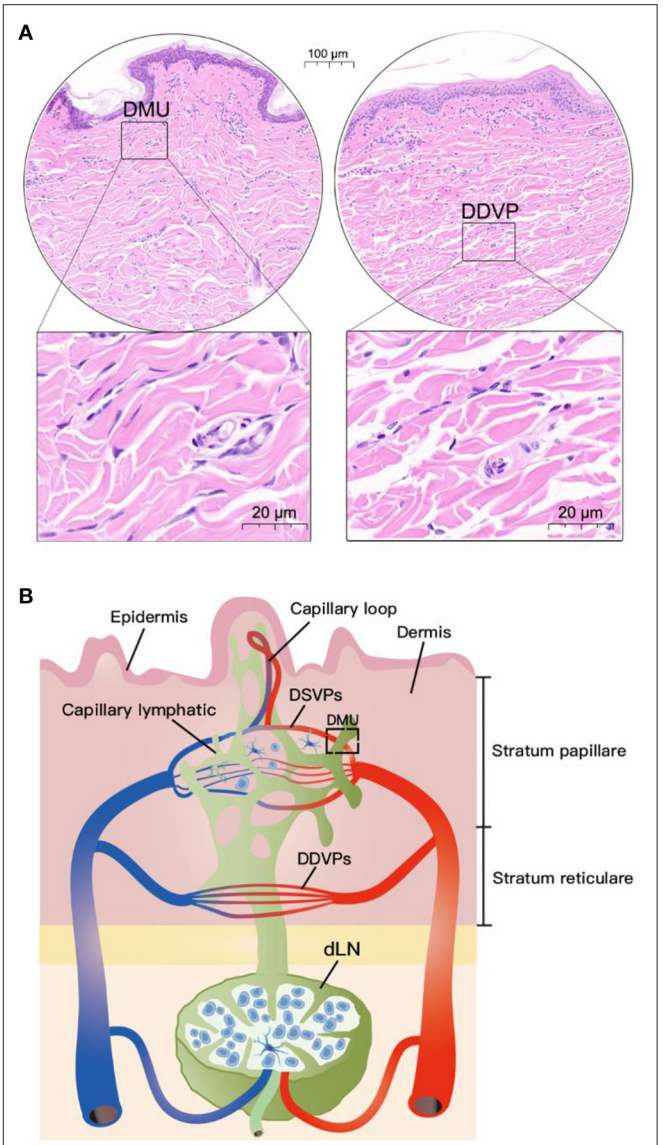

FIGURE 1 | Location of DMUs in the skin with HE staining. **(A)** Localization of DMUs as well as DDVPs in the skin; **(B)** Describe the distribution and structure of DMUs in the skin. DMU, dermal microvascular unit; DSVPs, dermal superficial vascular pleauxes; DDVPs, deep dermal vascular plexuses; dLN, draining lymph node; Scale bar in circular region denotes 100 μm and scale bar in square area denotes 20 μm.

Immunological Structural Characteristics of DMUs

IHC was used to identify the relationship between immune cells and DMUs in the dermis. We labeled immune-associated cells in DMUs with CD68, CD1a, and CD1c. $CD68^+$, $CD1a^+$ and $CD1c^+$ cells were observed in the interwoven lymphatic

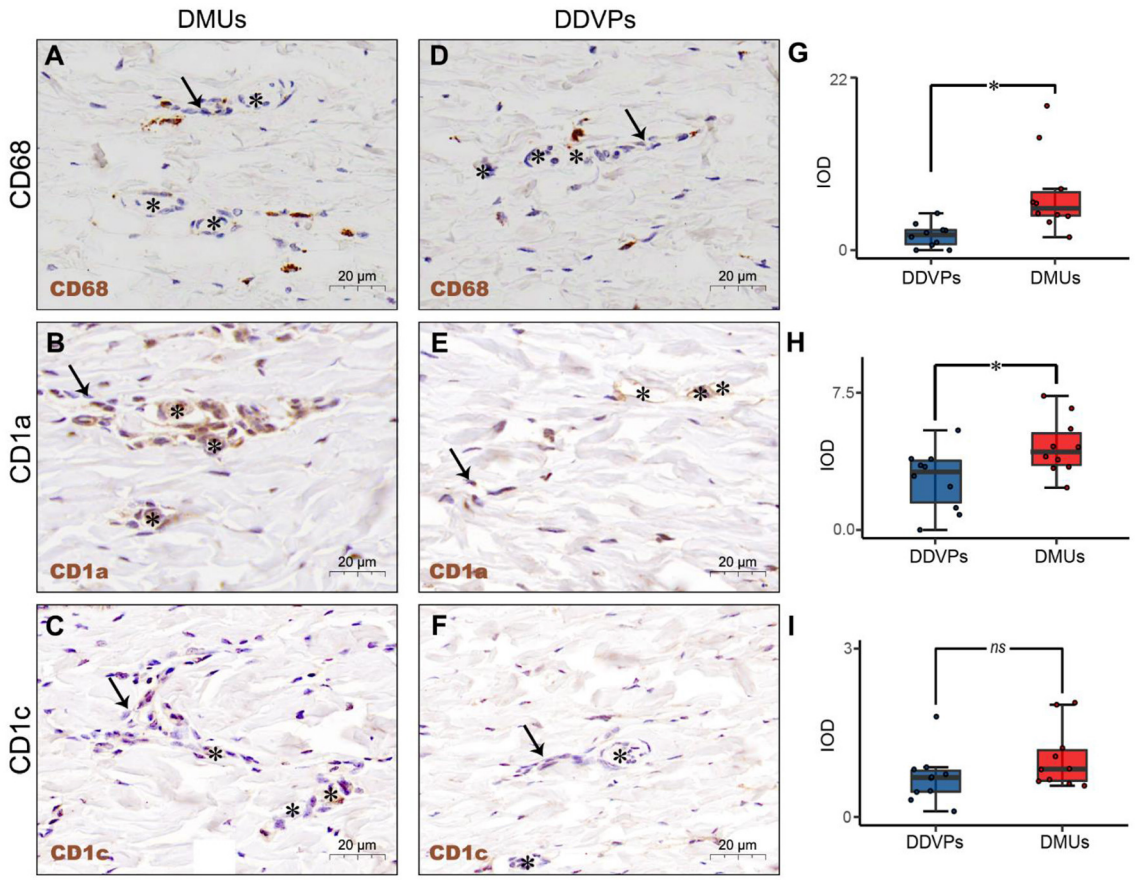

FIGURE 2 | The immunological structure of DMUs identified by IHC. **(A)** DMUs in pig cervical skin marked by CD68; **(B)** DMUs in pig cervical skin marked by CD1a; **(C)** DMUs in pig cervical skin marked by CD1c; **(D)** DDVPs in pig cervical skin marked by CD68; **(E)** DDVPs in pig cervical skin marked by CD1a; **(F)** DDVPs in pig cervical skin marked by CD1c; **(G)** $CD68^+$ expression quantified by IOD in DMUs and DDVPs; **(H)** $CD1a^+$ expression quantified by IOD in DMUs and DDVPs; **(I)** $CD1c^+$ expression quantified by IOD in DMUs and DDVPs. **(J)** The anatomical location of DMUs in the skin and the structure of DMUs are presented in a schematic diagram. *ns* indicates no significant difference; $^*P < 0.05$ indicates significant difference. Asterisks (*) point to microvasculature and arrows (→) point to capillary lymphatics; DMU, dermal microvascular unit; DDVPs, deep dermal vascular plexus; IOD, integrity optical density; scale bar **(A–E)** = 20 μm.

and microvascular areas (**Figures 2A–C**). Although a small number of $CD68^+$, $CD1a^+$ and $CD1c^+$ cells accumulated near vessels in DDVPs, they were not common and some of these immune-positive cells were not even found near DDVPs (**Figures 2D–F**). We performed student's *t*-test on mean IOD of the positive results presented by the IHC to show that there were significantly more $CD68^+$ cells ($P < 0.05$, **Figure 2G**) and $CD1a^+$ cells ($P < 0.05$, **Figure 2H**) clustered near lymphatic vessels and blood vessels of DMUs than DDVPs. $CD1c^+$ cells located in DMUs were slightly more than those near DDVPs, but the statistical significance was not recognized (*ns*, **Figure 2I**).

Ultrastructural Analysis of DMUs

TEM evaluation observed that the capillary wall was mainly composed of a layer of endothelial cells and basal membrane (**Figures 3A,B**). The thin cross section of capillaries was surrounded by a single endothelial cell (**Figure 3c**), and the thicker capillaries were surrounded by multiple endothelial cells (**Figure 3a**). A little connective tissue was found outside the basal membrane of endothelial cells. Kinds of flat and protuberant pericytes, which forms a tight connection with the endothelial cells through the rupture of the basal membrane were found between the endothelial cells and the basal membrane (**Figure 3a**). DPMCs, macrophages (**Figure 3A**), and d DCs (**Figure 3B**) were seen around the microvasculars. Among them, mast cells are oval with irregular membrane and a large number of basophilic particles can be seen in cytoplasm (**Figure 3b**). Capillary lymphatics were thin-walled lumens made up of monolayer lymphatic endothelial cells (**Figure 4A**), which have very thin cytoplasm except for the perinuclear region. The connections between LECs were loose, lacking tight connections and adhesion connections, and intercellular stacked tile-like structures at the junctions existed at adjacent endothelial cell connections (**Figure 4a**). The lymphatic vessels also contain a variety of cells: T cells (**Figure 4b**), dendritic cells (**Figure 4c**), and macrophages (**Figure 4d**). This led us to draw a pattern of DMUs: microvascular and capillary lymphatic in the region share an intimate anatomical relationship, and DPMCs, macrophages, d

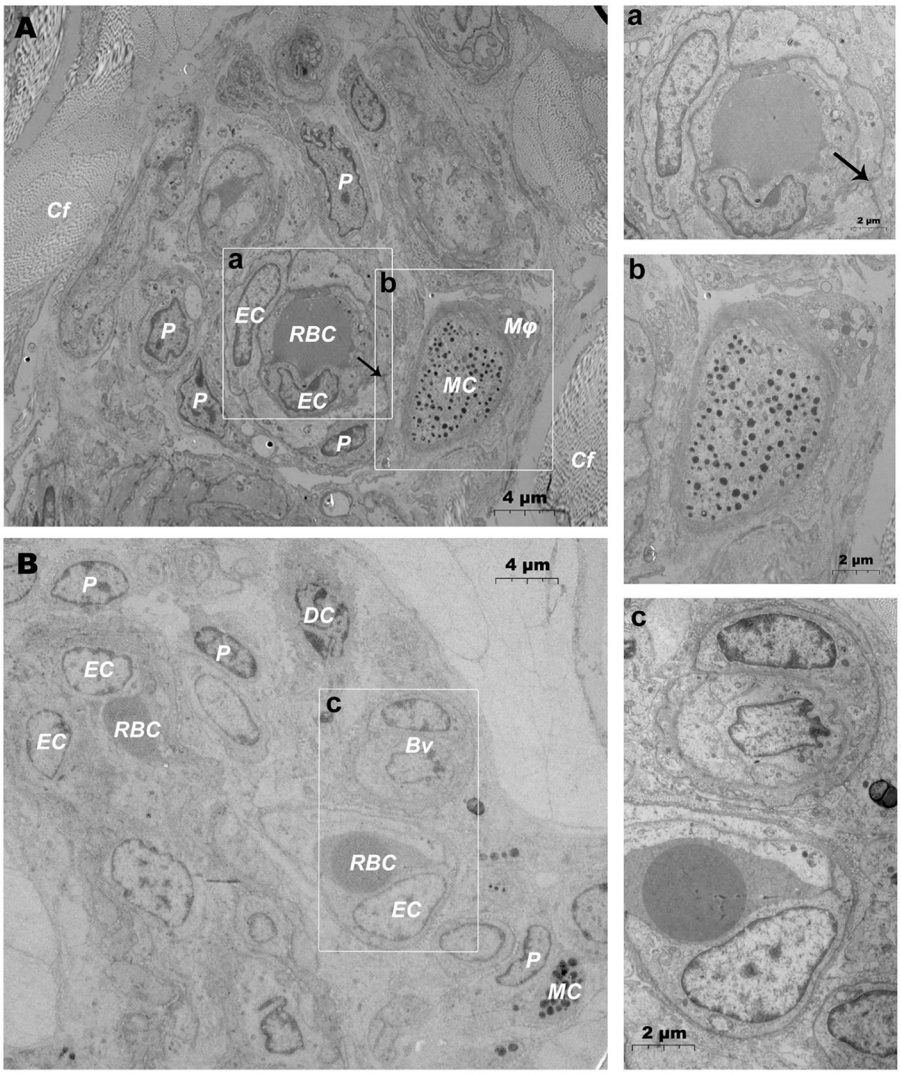

FIGURE 3 | Ultrastructural analysis of microvessels at the steady state *via* TEM. **(A,B)** Ultrastructure of microvessels and surrounding cells in steady state; (a) is the magnification of the microvessel in **(A)**; (b) is the magnification of the mast cells in **(A)**; (c) is the magnification of microvessels in **(B)**. RBC, red blood cell; EC, endothelial cell; P, pericyte; MC, mast cell; Mϕ, macrophage; Cf, collagen fiber; Bv, blood vessel; DC, dendritic cell; →, Tight junctions between the pericyte and the endothelial cell. Scale bar **(A,B)** = 4 μm; (a–c) = 2 μm.

DCs, and T cells were present around or in the lumen of the vessels (**Figure 4B**).

Ultrastructural Changes in DMUs After Jet Needle-Free Injection

After needlefree injection of biocompatible carbon nanoparticles, we observed *via* TEM that the DMECs showed varying degrees of swelling, with increased cytoplasm in the area surrounding the nucleus (**Figures 5A**,a). d DCs (**Figures 5b,c**), T cells (**Figure 5c**) and macrophages (**Figure 5B**) surrounded the microvessels, and the number of cells gathered was larger than before. Carbon nanoparticles also appears in the phagocytes of surrounding macrophages (**Figure 5B**). We also observed thickening of the basement membrane of blood vessels was observed (**Figure 6b**), and the connection junction between DMECs and pericytes was tighter (**Figure 6B**). In addition, the number of perivascular neutrophils increased (**Figure 6a**), and magnification viewing revealed the presence of obvious nanocarbon particles around the neutrophils (**Figure 6a**). In addition, some of DMECs already showed degranulation (**Figure 6C**). Similarly, the LECs appeared significantly swollen. There were fewer cells in the lumen of the lymphatic vessels than before, but dendritic cells appeared outside the lumen (**Figure 6D**).

Association Between TCs and DMUs

In addition, when observing DMUs, we found that interstitial cell telocyte (TC) newly discovered in recent years was inextricately related to DMUs (**Figures 7**, **8**). The morphology

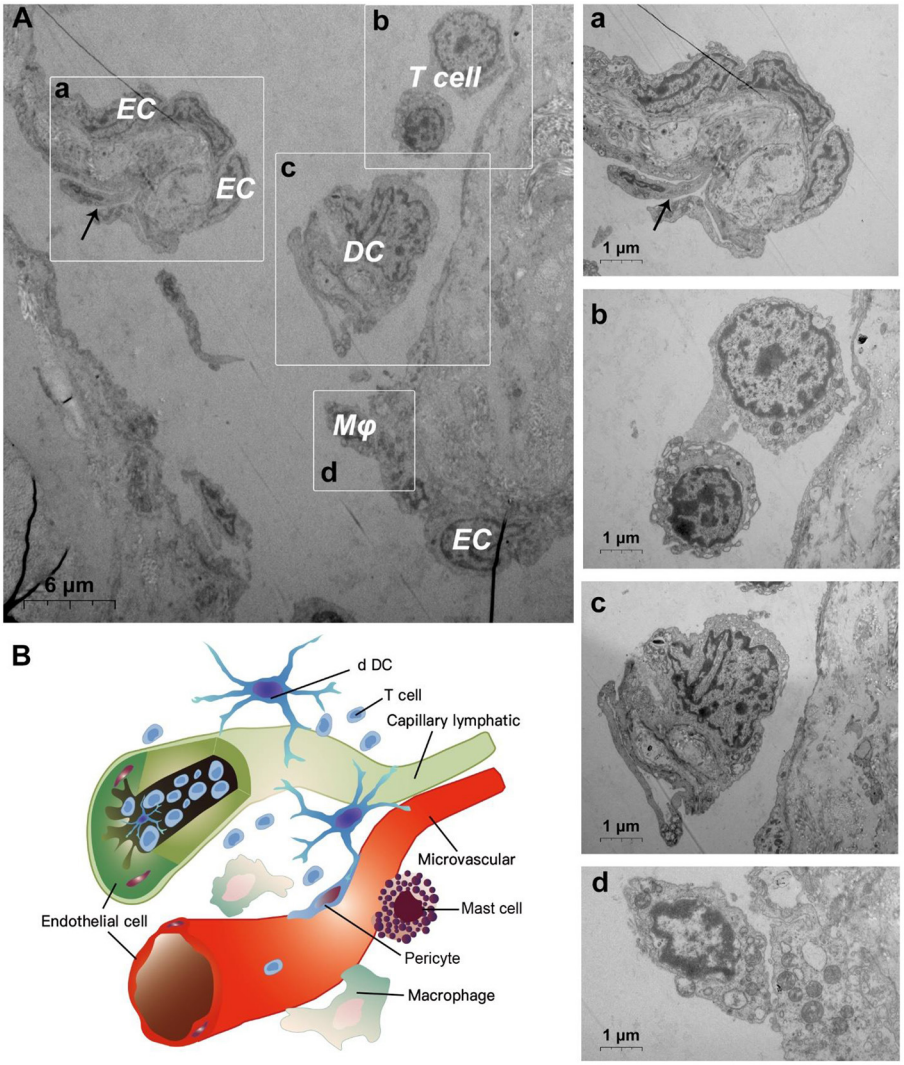

FIGURE 4 | Ultrastructural analysis of lymphatic vessels at the steady state *via* TEM. **(A)** The ultrastructure of lymphatic vessel and surrounding cells in the steady state; (a) is the enlargement of lymphatic endothelium in **(A)**; (b) is the enlargement of T cells in **(A)**; (c) is the enlargement of the dendritic cell in **(A)**; (d) is the enlargement of the macrophage in **(A)**; **(B)** Pattern diagram of DMUs in the steady state. EC, endothelial cell; Mϕ, macrophage; DC, dendritic cell; →, Imbricate overlap of endothelial cells. The scale bar **(A)** = 6 μm; (a–d) = 1 μm.

and distribution of TCs are very similar to the characteristics of veil cells described in the previous article. The cell bodys of TCs are small and fusiform, with a spindle or oval nucleus whose processes extend tens or even hundreds of microns in length (**Figures 7A,B**). The elongated protuberations of TCs allow it to contact other components such as microvessels (**Figure 7B**), DPMCs (**Figure 7a**), T cells (**Figure 7b**), and d DCs (**Figure 7c**) in the DMUs, forming homomorphic or heteromorphic connections and complex three dimensions (3D) networks. In addition, a portion of TCs were located between DMUs and collagen fiber (**Figure 7C**), which may be the barrier between DMUs and the dermis. A large number of unreleased vesicles were observed in the telopodes (Tps, cytoplasmic protrusion of TCs), (**Figures 7B,C**). However, after jet needle-free injection of carbon nanoparticles, it was observed that the TCs around the DMUs released many vesicles of different sizes (**Figures 8A–D**).

DISCUSSION

The immune mechanism of the skin remains poorly understood despite SALT has been proposed for a long time. The dermal microvascular unit, or the DMU, a unique immune structure in the skin, is considered to be significant for the immune function of the skin (3, 4). With the innovation of modern veterinary medicine, there is a recognized need for non-invasive and efficient injection methods that can be used to reduce injection costs and prevent animal stress, and DMUs naturally became a widely acknowledged research point. An initial aim of this project was to identify the

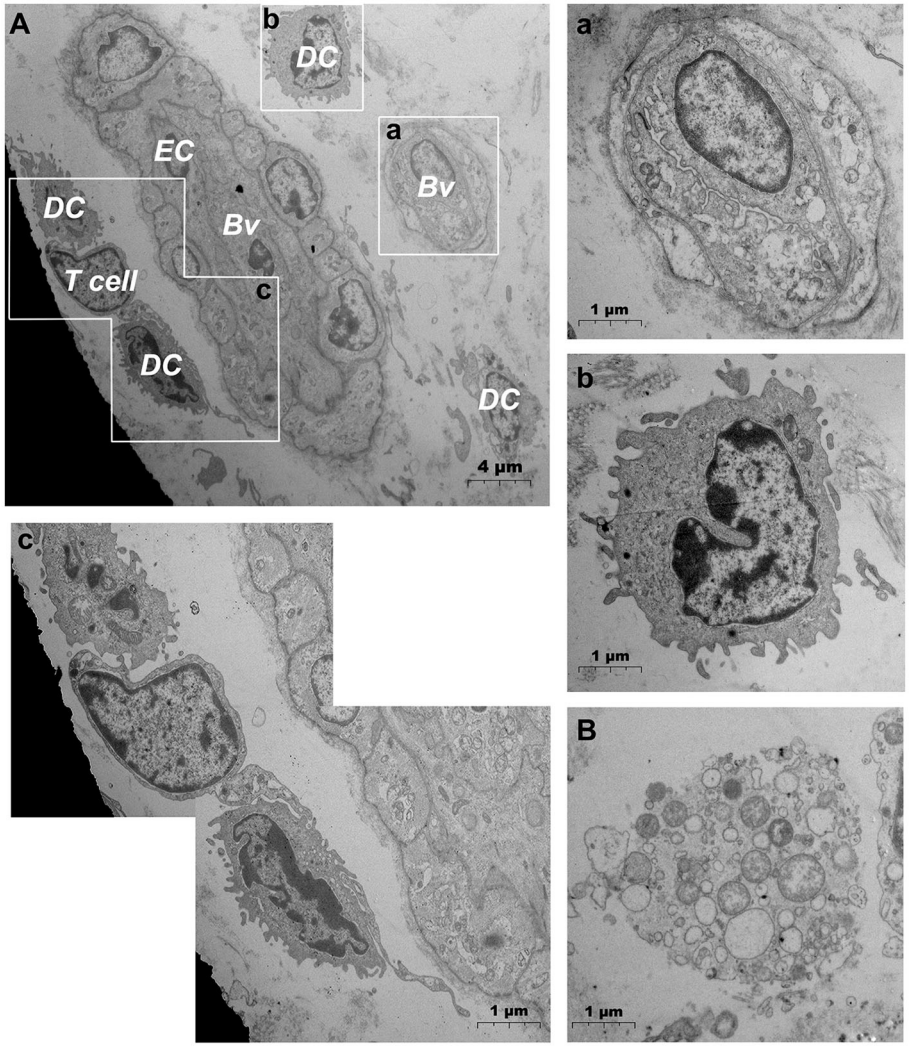

FIGURE 5 | Ultrastructural analysis of microvascular groups via TEM after jet needle-free injection. **(A)** Ultrastructure of microvessels and surrounding cells after jet needle-free injection; (a) is the enlargement of the capillarie in **(A)**; (b) is the enlargement of the dendritic cell in **(A)**; (c) is the enlargement of dendritic cells and the T cell in **(A)**; **(B)** Macrophages that engulf carbon nanoparticles. Bv, blood vessel; EC, endothelial cell; DC, dendritic cell. The scale bar **(A)** = 4 μm; **(B)** (a–c) = 1 μm.

predictive ability of DMUs in domestic pigs, which is an important consideration, especially when manipulating them for immunoprophylaxis.

This is the first study that confirms that DMUs is significantly associated with intradermal immune responses based on jet needle-free injection technology in domestic pigs. These findings correlate with previous description of the ultrastructure of DMUs and further support a role of DMUs in Transdermal passive immunity. DMUs are composed of microvessels, capillary lymphatics and peritubular cells, which jointly constitute the immune units within the dermis and acts as reservoirs for skin immune cells. We also found that DMUs undergo ultrastructural changes, including endothelial cell changes and migration of immune cells, in response to xenobiotics attack. Surprisingly, a type of novel interstitial cell TC has been found to participate in the composition of DMUs, perhaps what used to be known as veil cells.

In histological analysis, DSVPs and DDVPs were identified as responsible for the blood supply to the papillary and dermis stratum reticulare, respectively, and DSVPs also have an intimate anatomical relationship with the superficial dermal lymphatic plexuses (28). CD1a, CD1c and CD68 are all faithful markers of immune cells within the skin. Interestingly, there are significantly more $CD1a^+$, $CD1c^+$, and $CD68^+$ cells around DSVPs intertwined with superficial dermal lymphatic plexuses (i.e., DMUs) than in similar structures composed of DDVPs (28, 29). This perivascular immune structure is often mediated by vascular endothelial growthfactor receptors (VEGFR) family, monocyte chemoattractant protein-1 (MCP-1) and endogenous nitric oxide (NO) and is important

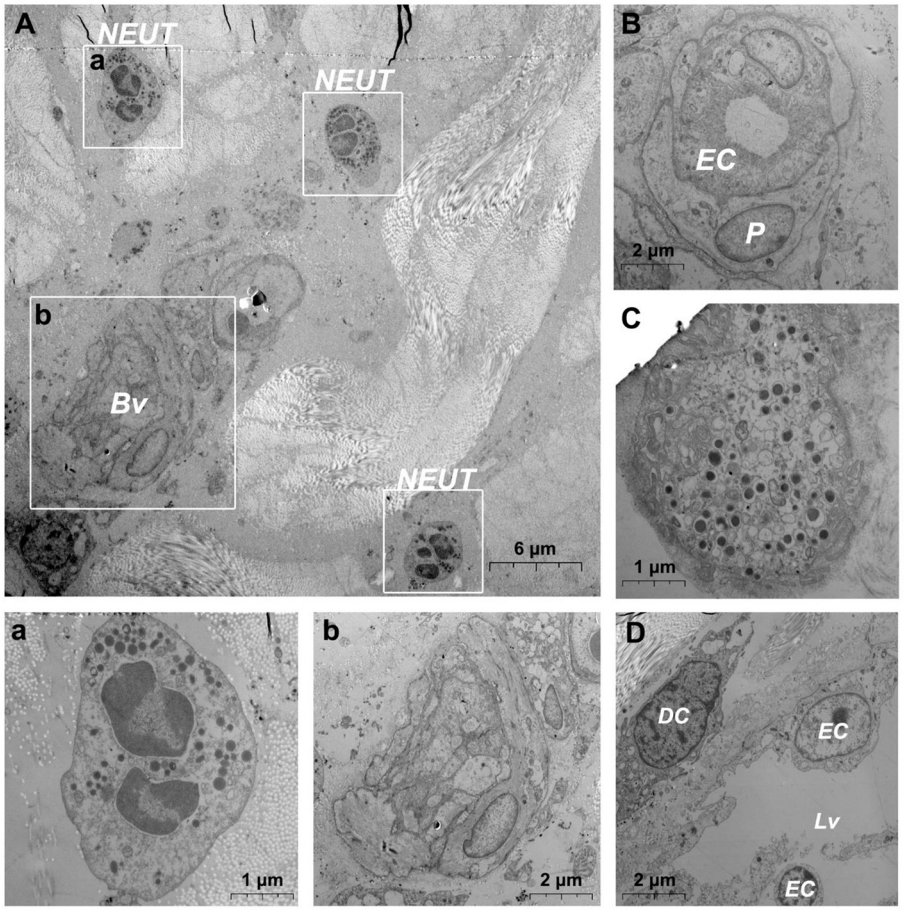

FIGURE 6 | Ultrastructural analysis of the microvessel *via* TEM after jet needle-free injection. **(A)** Ultrastructure of the microvessel and surrounding cells after jet needle-free injection; (a) is the enlargement of neutrophils in **(A)**; (b) is the enlargement of blood vessels in **(A)**; **(B)** Swollen microvessels after jet needle-free injection; **(C)** Mast cell that is degranulating after jet needle-free injection. **(D)** Swollen lymphatic vessel and surrounding dendritic cell after jet needle-free injection**.** Bv, blood vessel; NEUT, neutrophil; DC, dendritic cell; Lv, lymphatic vessel. The scale bar **(A)** = 6 μm; **(B,D)** (b) = 2 μm; **(C)** (a) = 1 μm.

evidence that DMUs play an immune surveillance role at steady state (30–33).

At steady state, immune cells in the skin of domestic pigs were found to be clustered around capillaries and in capillary lymphatics *via* TEM. Macrophages, DPMCs, d DCs and T cells were regularly distributed around the microvasculature. DPMCs were often found at the peripheral edge of the pericytes, and intercellular gap junctions were observed. In contrast, other immune cells were often located at the periphery of mast cells, within collagen fibers. We also noted immune cells within the stacked LECs, which lack the regularity of the vascular microenvironment but bridging the skin to the draining lymph nodes. Recent studies have indicated that DPMCs and macrophages can stimulate angiogenesis through potent pro-angiogenic factors, and secretory DPMCs, macrophages and T cells have also been noted to affect adjacent non-endothelial cells or to recruit each other *via* chemotactic signals, and these potential factors jointly maintain the stability of the skin microenvironment (34, 35).Marvelous ultrastructural changes appeared during xenobiotics attack. Pericytes underwent tighter junctions with DMECs but did not generate the pathological changes of gap formation (9, 10, 36–40). We tend to identify it as a physiological change caused by altered local permeability pressure after needle-free injection, since pericytes play an important role in regulating microvascular permeability, which would permit more hemolymph exchange to proceed (41). Postcapillary microvenules and lymphatic vessels have been considered to be important channels for the entry and exit of immune cells into draining lymph nodes, as well as constituting an important component of DMUs. TEM evaluation revealed a large number of macrophages, d DCs and T cells clustered around postcapillary microvenules, concomitant hypertrophy and linkage rearrangement of lymphatic endothelial cells (29), which providing direct cytological evidence for the synergistic involvement of the components of DMUs in the immune response. We therefore concluded with caution that the large number of immune cells in the dermis and surrounding blood vessels during the immune response may be partly derived

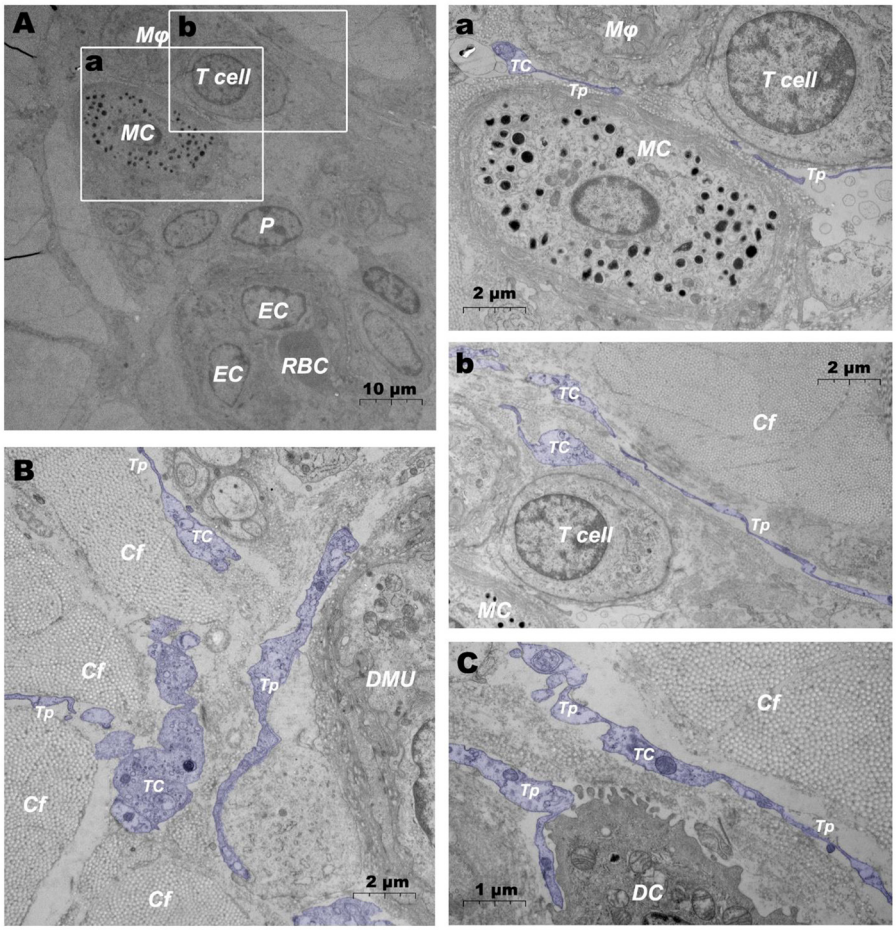

FIGURE 7 | Ultrastructural analysis of TCs in the steady state *via* TEM. **(A)** Location of TC in the DMUs in the steady state; (a) is the enlargement of the mast cell and surrounding TCs in **(A)**; (b) is the enlargement of T cells and surrounding TCs in **(A)**; **(B)** TCs surrounds the DMUs; **(C)** TC between collagen fibers and dendritic cells. RBC, red blood cell; EC, endothelial cell; P, Pericyte; MC, mast cell; Mϕ, macrophage; TC, telocyte; Tp, telopode; Cf, collagen fiber; DMU, dermal microvascular unit; DC, dendritic cell; Blue mark, telocytes. The scale bar **(A)** = 10 μm; **(B)** (a,b) = 2 μm; **(C)** = 1 μm.

from blood-lymphatic exchange within the skin, as these cells are abundant in normal cutaneous lymphatic vessels and rare around microvessels.

DPMCs, as immune sentinel cells within the skin, have been found to degranulate and migrate following xenobiotic attack. Neutrophils were observed after needle-free injection. Recent studies have suggested that neutrophil recruitment may be related to the synthesis of MIP-2 and tumor necrosis factor (TNF) by mast cell degranulation (42–44). Similarly, histamine released by DPMCs degranulation contributes to increased endothelial permeability and promotes hemolymph exchange. Histamine also enhances the modulatory effects of macrophages and interleukin-8 (IL-8) by increasing granulocyte-macrophage colony-stimulating factor (GM-CSF) production, which facilitates an efficient immune response (45, 46). These factors, although increased immune efficiency, may trigger unnecessary inflammation. Therefore, how transdermal immunity controls the stability of mast cell membranes to mitigate possible inflammatory responses remains to be investigated thoroughly.

TC is a novel type of interstitial cell, similar in morphological characteristics with the interstitial cells of Cajal (ICCs), and was named interstitial Cajal-Like cells (ICLCs) at a time until Popescu identified it as a completely new interstitial cell (47). According to the identification criteria proposed by Popescu, we identified TCs in DMUs (48). TCs were mainly distributed in the periphery of microvessels, separating DMUs from the dermis, and we also found TCs in the periphery of dendritic cells, T cells, mast cells, and macrophages, suggesting that TCs may be involved in the regulation of skin immunity (49). Following attack by xenobiotics, TCs were observed to produce vesicles of varying sizes, which were believed to contain proteins, lipids, microRNA (miRNA), long non-coding RNA (lncRNA) and mRNA, indicating that TCs play a crucial role in signaling skin immunity and potentially control the transcriptional activity of the cells involved (50–52).

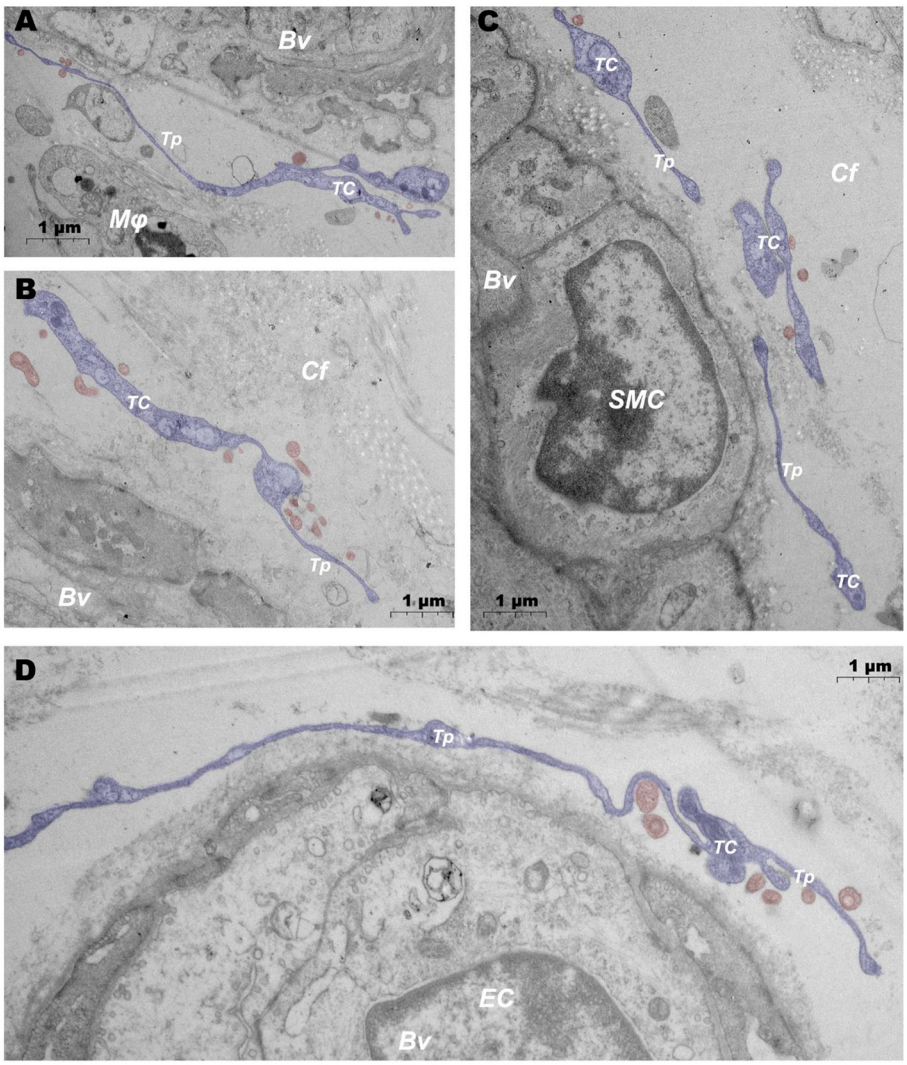

FIGURE 8 | Ultrastructural analysis of TCs after jet needle-free injection via TEM. **(A–D)** After jet needle-free injection, TCs at different locations in the DMUs releases a large number of vesicles. BV, blood vessels; Mϕ, macrophage; TC, telocyte; Tp, telopode; Cf, collagen fiber; SMC, smooth muscle cell; EC, endothelial cell; Blue mark, telocytes; Red mark, vesicles. Scale bar **(A–D)** = 1 μm.

It is worth mentioning that a mysterious cell called veil cell was proposed in early studies and it was thought to form part of the DMU (53). Veil cells were described as separating the DMU from the dermis, 3D computer reconstruction showed their cell bodies with multiple wing-like projections, and were factor XIIIa^{+} (54). TEM evaluation revealed veil cells with vesicles and candy-like protrusions, and showed non-specific morphological changes in response to microenvironmental alterations (55, 56). Since TCs had not been discovered at that time and the characteristics of veil cells were similar to TCs, we cautiously inferred that veil cells might be the same type of cells as TCs, a speculation that needs further proof by immunological means.

In a nutshell, our results firstly identified DMUs consisting of DSVPs and capillary lymphatics in domestic pig skin, which occur in the dermis stratum papillare and confirmed as reservoirs of immune cells *via* IHC. TEM evaluation was used to understand the ultrastructure of DMUs in the dermis stratum papillare, which underwent ultrastructural changes and migration of immune cells after attack with xenobiotics. These changes supported the involvement of lymphatic vessels and microvessels as a whole unit in the cutaneous immune response. The role of lymphatic vessels during jet needle-free injection may be substantial because of their uncharacteristic endothelial ultrastructural changes. Evidence to date is lacking to confirm the role arising from endothelial changes in lymphatic vessels, which is potentially fertile ground for cutaneous immune studies. TCs was found to produces heterogeneous junctions with DPMCs, T cells, d DCs and DMECs in DMUs and separates microvessels from dermal collagen fibers. The ultramorphology of TCs resembles that of veil cells around microvessels in the early

literature, unfortunately, we did not further demonstrate whether they are the same type of cells. This study provides morphological evidence for DMUs as reservoirs of immune cells and channels of passive immunity in the skin, and morphological evidence for the possible role of TCs in regulating the function of DMUs is also revealed.

DATA AVAILABILITY STATEMENT

The original contributions presented in the study are included in the article/supplementary material, further inquiries can be directed to the corresponding authors.

ETHICS STATEMENT

The animal study was reviewed and approved by the Animal Ethics Committee of Nanjing Agricultural University.

AUTHOR CONTRIBUTIONS

XM, ZZ, and PY: conceptualization, data curation, and writing—review and editing. BD, QC, PY, and YL: formal analysis. XM, ZZ, NA, QM, QW, and PY: methodology. XM and ZZ: writing—original draft. All authors have read and agreed to the published version of the manuscript.

FUNDING

The authors disclosed receipt of the following financial support for the research, authorship, and/or publication of this article: this work was supported by the Key Research and Development Program of Jiangsu Province (Grant Number: BE2020336), the Nanjing Agricultural University Student Research Training Project Fund (Grant Number: 202110307114Y), and the Priority Academic Program Development of Jiangsu Higher Education Institutions, China.

REFERENCES

1. Kissenpfennig A, Malissen B. Langerhans cells–revisiting the paradigm using genetically engineered mice. *Trends Immunol.* (2006) 27:132–9. doi: 10.1016/j.it.2006.01.003
2. Clark RA. Skin-Resident T cells: the ups and downs of on site immunity. *J Invest Dermatol.* (2010) 130:362–70. doi: 10.1038/jid.2009.247
3. Sontheimer RD. Perivascular dendritic macrophages as immunobiological constituents of the human dermal microvascular unit. *J Invest Dermatol.* (1989) 93:S96–S101. doi: 10.1038/jid.1989.17
4. Nicolas J-F, Guy B. Intradermal, epidermal and transcutaneous vaccination: from immunology to clinical practice. *Expert Rev Vaccines.* (2008) 7:1201–14. doi: 10.1586/14760584.7.8.1201
5. Criado PR, Criado RF, Valente NY, Queiroz LB, Martins JE, Vasconcellos C. The inflammatory response in drug-induced acute urticaria: ultrastructural study of the dermal microvascular unit. *J Eur Acad Dermatol Venereol.* (2006) 20:1095–9. doi: 10.1111/j.1468-3083.2006.01744.x
6. Braverman IM. The cutaneous microcirculation: ultrastructure and microanatomical organization. *Microcirculation.* (1997) 4:329–40. doi: 10.3109/10739689709146797
7. O'Brien TD. Impaired dermal microvascular reactivity and implications for diabetic wound formation and healing: an evidence review. *J Wound Care.* (2020) 29:S21–S8. doi: 10.12968/jowc.2020.29.Sup9.S21
8. Sun Y, Xiong X, Wang X. Hif1alpha/Mir-199a/Adm feedback loop modulates the proliferation of human dermal microvascular endothelial cells (HDMECS) under hypoxic condition. *Cell Cycle.* (2019) 18:2998–3009. doi: 10.1080/15384101.2019.1666611
9. Cao N, Chen T, Guo Z-p, Qin S, Li M-m. Monoammonium glycyrrhizate suppresses tumor necrosis factor-A induced chemokine production in HMEC-1 cells, possibly by blocking the translocation of nuclear factor-Kb into the nucleus. *Can J Physiol Pharm.* (2014) 92:859–65. doi: 10.1139/cjpp-2014-0022
10. Sanchez B, Li L, Dulong J, Aimond G, Lamartine J, Liu G, et al. Impact of human dermal microvascular endothelial cells on primary dermal fibroblasts in response to inflammatory. *Stress*. (2019) 7:44. doi: 10.3389/fcell.2019.00044
11. Roy S, Sato T. Role of vascular basement membrane components in diabetic microangiopathy. *Drug News Perspect.* (2000) 13:91–8. doi: 10.1358/dnp.2000.13.2.858468
12. Tan W, Wang J, Zhou F, Gao L, Yin R, Liu H, et al. Coexistence of Eph Receptor B1 and Ephrin B2 in port-wine stain endothelial progenitor cells contributes to clinicopathological vasculature dilatation. *Br J Dermatol.* (2017) 177:1601–11. doi: 10.1111/bjd.15716
13. Frech TM, Revelo MP, Drakos SG, Murtaugh MA, Markewitz BA, Sawitzke AD, et al. Vascular leak is a central feature in the pathogenesis of systemic sclerosis. *J Rheumatol.* (2012) 39:1385–91. doi: 10.3899/jrheum.111380
14. Martin AR, Bailie JR, Robson T, McKeown SR, Al-Assar O, McFarland A, et al. Retinal pericytes control expression of nitric oxide synthase and endothelin-1 in microvascular endothelial cells. *Microvasc Res.* (2000) 59:131–9. doi: 10.1006/mvre.1999.2208
15. Imayama S, Urabe H. Pericytes on the dermal microvasculature of the rat skin. *Anat Embryol.* (1984) 169:271–4. doi: 10.1007/BF00315632
16. Mirancea N, Hausser I, Beck R, Metze D, Fusenig NE, Breitkreutz D. Vascular anomalies in lipoid proteinosis: basement membrane components and ultrastructure. *J Dermato Sci.* (2006) 42:231–9. doi: 10.1016/j.jdermsci.2006.01.004
17. Ansell DM, Izeta A. Pericytes in wound healing: friend or foe? *Exp Dermatol.* (2015) 24:833–4. doi: 10.1111/exd.12782
18. Sueki H, Telegan B, Murphy GF. Computer-assisted 3-dimensional reconstruction of human dermal dendrocytes. *J Invest Dermatol.* (1995) 105:704–8. doi: 10.1111/1523-1747.ep12324502
19. Cassisa A. Cutaneous and systemic vasculitis: cellular players and pathogenetic aspects. *Giorn Ital Dermatv.* (2015) 150:29–40.
20. Randolph GJ, Ivanov S, Zinselmeyer BH, Scallan JP. The lymphatic system: integral roles in immunity. *Annu Rev Immunol.* (2017) 35:31–52. doi: 10.1146/annurev-immunol-041015-055354
21. Teijeira A, Hunter MC, Russo E, Proulx ST, Frei T, Debes GF, et al. T cell migration from inflamed skin to draining lymph nodes requires intralymphatic crawling supported by Icam-1/Lfa-1 interactions. *Cell Rep.* (2017) 18:857–65. doi: 10.1016/j.celrep.2016.12.078
22. Baeyens A, Fang V, Chen C, Schwab SR. Exit strategies: S1p signaling and T cell migration. *Trends Immunol.* (2015) 36:778–87. doi: 10.1016/j.it.2015.10.005
23. Hunter MC, Teijeira A, Halin C. T cell trafficking through lymphatic vessels. *Front Immunol.* (2016) 7:613. doi: 10.3389/fimmu.2016.00613
24. Ferreira LCL, Cooke RF, Marques RS, Fernandes HJ, Fernandes CE, Stelato R, et al. Effects of vaccination against foot-and-mouth disease virus on reproductive performance of bos indicus beef cows. *J Anim Sci.* (2016) 94:401–5. doi: 10.2527/jas.2015-9537
25. Ko EY, Cho J, Cho JH, Jo K, Lee SH, Chung YJ, et al. Reduction in lesion incidence in pork carcass using transdermal needle-free injection of foot-and-mouth disease vaccine. *Korean J Food Sci Anim Resour.* (2018) 38:1155–9. doi: 10.5851/kosfa.2018.e46
26. McCrudden MT, Torrisi BM, Al-Zahrani S, McCrudden CM, Zaric M, Scott CJ, et al. Laser-engineered dissolving microneedle arrays for protein delivery: potential for enhanced intradermal vaccination. *J Pharm Pharmacol.* (2015) 67:409–25. doi: 10.1111/jphp.12248

27. Kohli AK, Alpar HO. Potential use of nanoparticles for transcutaneous vaccine delivery: effect of particle size and charge. *Int J Pharm.* (2004) 275:13–7. doi: 10.1016/j.ijpharm.2003.10.038
28. Petrova TV, Koh GY. Organ-specific lymphatic vasculature: from development to pathophysiology. *J Exp Med.* (2018) 215:35–49. doi: 10.1084/jem.20171868
29. Huxley VH, Scallan J. Lymphatic fluid: exchange mechanisms and regulation. *J Physiol.* (2011) 589:2935–43. doi: 10.1113/jphysiol.2011.208298
30. Murray PJ, Wynn TA. Protective and pathogenic functions of macrophage subsets. *Nat Rev Immunol.* (2011) 11:723–37. doi: 10.1038/nri3073
31. Deshmane SL, Kremlev S, Amini S, Sawaya BE. Monocyte chemoattractant protein-1 (Mcp-1): an overview. *J Interf Cytok Res.* (2009) 29:313–26. doi: 10.1089/jir.2008.0027
32. Olsson AK, Dimberg A, Kreuger J, Claesson-Welsh L. VEGF receptor signalling-in control of vascular function. *Nat Rev Mol Cell Bio.* (2006) 7:359–71. doi: 10.1038/nrm1911
33. Kubes P, Suzuki M, Granger DN. Nitric-oxide-an endogenous modulator of leukocyte adhesion. *P Natl Acad Sci USA.* (1991) 88:4651–5. doi: 10.1073/pnas.88.11.4651
34. Norrby K. Mast cells and angiogenesis. *APMIS.* (2002) 110:355–71. doi: 10.1034/j.1600-0463.2002.100501.x
35. DeNardo DG, Ruffell B. Macrophages as regulators of tumour immunity and immunotherapy. *Nat Rev Immunol.* (2019) 19:369–82. doi: 10.1038/s41577-019-0127-6
36. Sluimer JC, Kolodgie FD, Bijnens AP, Maxfield K, Pacheco E, Kutys B, et al. Thin-walled microvessels in human coronary atherosclerotic plaques show incomplete endothelial junctions relevance of compromised structural integrity for intraplaque microvascular leakage. *J Am Coll Cardiol.* (2009) 53:1517–27. doi: 10.1016/j.jacc.2008.12.056
37. Yun JH. Interleukin-1beta induces pericyte apoptosis *via* the Nf-Kappab pathway in diabetic retinopathy. *Biochem Biophys Res Commun.* (2021) 546:46–53. doi: 10.1016/j.bbrc.2021.01.108
38. Hosaka K, Yang Y, Nakamura M, Andersson P, Yang X, Zhang Y, et al. Dual roles of endothelial Fgf-2-Fgfr1-Pdgf-Bb and perivascular Fgf-2-Fgfr2-Pdgfrbeta signaling pathways in tumor vascular remodeling. *Cell Discov.* (2018) 4:3. doi: 10.1038/s41421-017-0002-1
39. Ogura S, Kurata K, Hattori Y, Takase H, Ishiguro-Oonuma T, Hwang Y, et al. Sustained inflammation after pericyte depletion induces irreversible blood-retina barrier breakdown. *JCI Insight.* (2017) 2:e90905. doi: 10.1172/jci.insight.90905
40. Gautam J, Cao Y, Yao Y. Pericytic laminin maintains blood-brain barrier integrity in an age-dependent manner. *Transl Stroke Res.* (2020) 11:228–42. doi: 10.1007/s12975-019-00709-8
41. Adair TH, Moffatt DS, Paulsen AW, Guyton AC. Quantitation of changes in lymph protein concentration during lymph node transit. *Am J Physiol.* (1982) 243:H351–9. doi: 10.1152/ajpheart.1982.243.3.H351
42. Schultz GS, Davidson JM, Kirsner RS, Bornstein P, Herman IM. Dynamic reciprocity in the wound microenvironment. *Wound Repair Regen.* (2011) 19:134–48. doi: 10.1111/j.1524-475X.2011.00673.x
43. Ngo Nyekel F, Pacreau E, Benadda S, Msallam R, Åbrink M, Pejler G, et al. Mast cell degranulation exacerbates skin rejection by enhancing neutrophil recruitment. *Front Immunol.* (2018) 9:2690. doi: 10.3389/fimmu.2018.02690
44. Marzano AV, Lipsker D, Cugno M. Editorial: neutrophil-mediated skin diseases: immunology and genetics. *Front Immunol.* (2019) 10:2377. doi: 10.3389/fimmu.2019.02377
45. Ishikawa T, Kanda N, Hau CS, Tada Y, Watanabe S. Histamine induces human β-defensin-3 production in human keratinocytes. *J Dermatol Sci.* (2009) 56:121–7. doi: 10.1016/j.jdermsci.2009.07.012
46. Nakamura T, Murata T. Regulation of vascular permeability in anaphylaxis. *Br J Pharmacol.* (2018) 175:2538–42. doi: 10.1111/bph.14332
47. Popescu LM, Faussone-Pellegrini MS. Telocytes - a case of serendipity: the winding way from interstitial cells of cajal (ICC), via interstitial cajal-like cells (ICLC) to telocytes. *J Cell Mol Med.* (2010) 14:729–40. doi: 10.1111/j.1582-4934.2010.01059.x
48. Gherghiceanu M, Manole CG, Popescu LM. Telocytes in endocardium: electron microscope evidence. *J Cell Mol Med.* (2010) 14:2330–4. doi: 10.1111/j.1582-4934.2010.01133.x
49. Gherghiceanu M, Popescu LM. Cardiac telocytes-their junctions and functional implications. *Cell Tissue Res.* (2012) 348:265–79. doi: 10.1007/s00441-012-1333-8
50. Fertig ET, Gherghiceanu M, Popescu LM. Extracellular vesicles release by cardiac telocytes: electron microscopy and electron tomography. *J Cell Mol Med.* (2014) 18:1938–43. doi: 10.1111/jcmm.12436
51. Zheng Y, Cretoiu D, Yan G, Cretoiu SM, Popescu LM, Fang H, et al. Protein profiling of human lung telocytes and microvascular endothelial cells using itraq quantitative proteomics. *J Cell Mol Med.* (2014) 18:1035–59. doi: 10.1111/jcmm.12350
52. Xu MY, Ye ZS, Song XT, Huang RC. Differences in the cargos and functions of exosomes derived from six cardiac cell types: a systematic review. *Stem Cell Res Ther.* (2019) 10:194. doi: 10.1186/s13287-019-1297-7
53. Goldsmith LA. The veil cell: a shy cell. *Arch Dermatol.* (1986) 122:828–9. doi: 10.1001/archderm.122.7.828
54. Braverman IM, Sibley J, Keh-Yen A. A study of the veil cells around normal, diabetic, and aged cutaneous microvessels. *J Invest Dermato.* (1986) 86:57–62. doi: 10.1111/1523-1747.ep12283816
55. Nuttall RP, Wessells NK. Veils, mounds, and vesicle aggregates in neurons elongating *in vitro*. *Exp Cell Res.* (1979) 119:163–74. doi: 10.1016/0014-4827(79)90345-8
56. Braverman IM, Fonferko E. Studies in Cutaneous Aging: Ii. The microvasculature. *J Invest Dermato.* (1982) 78:444–8. doi: 10.1111/1523-1747.ep12508027

Conflict of Interest: The authors declare that the research was conducted in the absence of any commercial or financial relationships that could be construed as a potential conflict of interest.

frontiers | Frontiers in Veterinary Science

ORIGINAL RESEARCH
published: 02 May 2022
doi: 10.3389/fvets.2022.882423

Comparative Analysis of Gut Microbiota Between Healthy and Diarrheic Horses

Yaonan Li, Yanfang Lan, Shuang Zhang and Xiaoli Wang*

Wuhan Business University, Wuhan, China

Increasing evidence reveals the importance of gut microbiota in animals for regulating intestinal homeostasis, metabolism, and host health. The gut microbial community has been reported to be closely related to many diseases, but information regarding diarrheic influence on gut microbiota in horses remains scarce. This study investigated and compared gut microbial changes in horses during diarrhea. The results showed that the alpha diversity of gut microbiota in diarrheic horses decreased observably, accompanied by obvious shifts in taxonomic compositions. The dominant bacterial phyla (*Firmicutes*, *Bacteroidetes*, *Spirochaetes*, and *Kiritimatiellaeota*) and genera (*uncultured_bacterium_f_Lachnospiraceae*, *uncultured_bacterium_f_p-251-o5*, *Lachnospiraceae_AC2044_group*, and *Treponema_2*) in the healthy and diarrheic horses were same regardless of health status but different in abundances. Compared with the healthy horses, the relative abundances of *Planctomycetes*, *Tenericutes*, *Firmicutes*, *Patescibacteria*, and *Proteobacteria* in the diarrheic horses were observably decreased, whereas *Bacteroidetes*, *Verrucomicrobia,* and *Fibrobacteres* were dramatically increased. Moreover, diarrhea also resulted in a significant reduction in the proportions of 31 genera and a significant increase in the proportions of 14 genera. Taken together, this study demonstrated that the gut bacterial diversity and abundance of horses changed significantly during diarrhea. Additionally, these findings also demonstrated that the dysbiosis of gut microbiota may be an important driving factor of diarrhea in horses.

Keywords: diarrhea, horse, dysbiosis, gut microbiota, healthy

OPEN ACCESS

Edited by:
Fazul Nabi,
Lasbela University of Agriculture, Water and Marine Sciences, Pakistan

Reviewed by:
Waseem Ali,
Sindh Agriculture University, Pakistan
Aftab Shaukat,
Huazhong Agricultural University, China

****Correspondence:***
Yanfang Lan
lanyanf0926@sina.com

Specialty section:
This article was submitted to Comparative and Clinical Medicine, a section of the journal Frontiers in Veterinary Science

Received: *23 February 2022*
Accepted: *30 March 2022*
Published: *02 May 2022*

Citation:
Li Y, Lan Y, Zhang S and Wang X (2022) Comparative Analysis of Gut Microbiota Between Healthy and Diarrheic Horses. Front. Vet. Sci. 9:882423. doi: 10.3389/fvets.2022.882423

INTRODUCTION

Mammal intestines contain more than 10^{14} microorganisms including bacteria, fungi, viruses, and protozoa, which are approximately 10 times the total quantity of host cells and play crucial roles in intestinal physiological function, metabolism, and host health (1–3). Furthermore, increasing evidence indicated that gut microbiota also functions in epithelial differentiation, intestinal homeostasis, and immunity (4, 5). Early investigations demonstrated that the consistency of the gut microbial community is the precondition for conducting digestive absorption and complicated metabolic functions, whereas gut microbial dysbiosis is closely related to many diseases (6–8). Currently, gut microbial dysbiosis has been shown to be an important driving factor of non-alcoholic fatty liver disease, high blood pressure, and diabetes (9, 10). Recent research on gut

microbiota has also provided evidence that obesity, colonitis, and colorectal cancer may be the result of gut microbial dysbiosis (11, 12).

Diarrhea is one of the main reasons for decreased production performance and death in farmed animals and has been regarded as a key factor affecting the development of the livestock industry in many countries. Previous studies indicated that diarrhea was present in nearly all mammals, especially in newborn pigs, chickens, and sheep with susceptible gut microbiota (13–15). Considering the negative impact of diarrhea on animal husbandry, it is important to investigate its etiology and treatment. Numerous studies indicated that gut microbiota played key roles in the prevention, control, and diagnosis of diarrhea (16, 17). Wang et al. revealed that the gut microbial community of diarrheic goats changed dramatically accompanied by high mortality (13). Similarly, Li et al. also reported that the gut microbiota of giraffes changed significantly during diarrhea (18).

Metagenomics is a key tool for investigating shifts in gut microbiota during diseases (19, 20). By systematically exploring and comparing acquired information, the relationship between gut microbiota and diseases could be further understood, and prevention and control measures can be developed to minimize economic losses (21–23). Presently, the complicated composition and structure of gut microbiota in diarrheic pigs, yaks, and giraffes have been successfully analyzed based on the high-throughput sequencing technology (24–26). However, there are few reports on the gut microbiota of horses, and even fewer studies on the composition and structure of gut microbiota in horses in different health statuses. Therefore, the objective of this study was to compare and investigate the composition and discrepancy of gut microbial populations between healthy and diarrheic horses.

MATERIALS AND METHODS

Animals and Sample Collection

A total of 16 horses (8 healthy horses and 8 diarrheic horses) from Wuhan Business University (Wuhan, China) were used for this experiment. The horses we screened possessed the same immune background. Moreover, the health statuses of the horses were diagnosed and evaluated by a professional veterinarian before sample collection. The rectum was swabbed by a trained technician using sterile swabs in a rotating fashion. The obtained samples including healthy and diarrheic feces were immediately placed into sterile plastic containers and transported to the laboratory and later stored at −80°C for further study.

16S rDNA Gene Amplicon Sequencing

Prior to the DNA extraction, 16 fecal samples from control and diarrheic horses were unfrozen and homogenized at room temperature. Afterward, the treated fecal samples were subjected to bacterial DNA extraction based on the manufacturer's protocol. Quantification and electrophoresis of the extracted DNA were performed to ensure that the concentration and integrity of extracts meet analysis demands. To dissect the changes in the gut bacterial community, we amplified the V3/V4 regions utilizing bacterial primers (338F: ACTCCTACGGGAGGCAGCA and 806R: GGACTACHVGGGTWTCTAAT). The PCR amplification procedure was set based on previous studies. PCR products were conducted target fragment recovery and gel electrophoresis detection to acquire purified products. The PCR products were recovered by fluorescence quantification and proportionally mixed following sequencing requirements. The qualified products were used to prepare sequencing libraries by using the PacBio platform (Biomarker Technologies, China). To acquire qualified libraries, the original libraries were required to suitably embellish such as sequence repair, quality evaluation, purification, and fluorescent quantitation. Libraries that passed quality screening were subjected to 2 × 300 bp paired-end sequencing using a MiSeq sequencing machine.

Bioinformatics and Data Analysis

The initial data from Illumina MiSeq sequencing was performed a quality assessment to obtain effective data. Briefly, raw data containing problematical sequences including short, unqualified, and mismatched sequences were subjected to screening and removal of primer sequences to achieve clean reads utilizing the Trimmomatic (v0.33) and Cutadapt software (1.9.1). The Usearch software (v10) was used for splicing clean reads and then the spliced sequences were secondary screened based on sequence length range. Subsequently, identification and elimination of chimera sequences were performed to obtain final effective reads utilizing the UCHIME software (v4.2). Effective reads that passed quality inspection were clustered, and OTUs were partitioned based on 97% similarity. Additionally, Venn maps were also generated to characterize the distribution and richness of bacterial OTUs in each sample. To further investigate the shifts in gut microbial diversity and abundance during diarrhea, we computed multiple alpha diversity indexes based on OTU distribution. Principal component analysis was also conducted to dissect gut bacterial beta diversities between both groups. The sequencing depth and evenness of each sample were evaluated through rank abundance and rarefaction curves. Differential bacterial taxa associated with diarrhea exposure were recognized by Metastats and LEfSe analysis. An SPSS statistical program (v20.0) was used for conducting data analysis, and P-values (means ± SD) <0.05 were determined statistically significant.

RESULTS

Sequences Analyses

In this research, 8 healthy and 8 diarrheic fecal samples were subjected to high-throughput sequencing analysis. After optimizing the original data, a total of 127,8741 high-quality sequences were obtained from the 16 samples (**Table 1**). In addition, the number of valid sequences in the healthy horses ranged from 794.84 to 803.09, while the number of valid sequences in the diarrheic populations varied from 794.85 to 801.39. The Chao1, Shannon, and Rank abundance curves showed a tendency to saturate, implying eligible depth and evenness (**Figures 1A–C**). High-quality sequences with 97%

TABLE 1 | Bacterial sequence information of each sample.

Sample	Raw reads	Clean reads	Effective reads	AvgLen (bp)	GC (%)	Q20 (%)	Q30 (%)	Effective (%)
CH1	79824	79497	78225	413	52.74	99.07	96.12	98.00
CH2	79487	79172	77656	415	52.69	99.06	96.09	97.70
CH3	79834	79480	77935	414	52.68	99.06	96.09	97.62
CH4	79951	79625	78834	413	52.88	99.09	96.18	98.60
CH5	79990	79678	78425	413	52.71	99.06	96.10	98.04
CH6	80309	79962	77878	415	52.68	99.08	96.14	96.97
CH7	79670	79355	77824	414	52.81	99.07	96.12	97.68
CH8	79921	79622	78072	414	52.91	99.09	96.17	97.69
DH1	79485	79167	77895	414	53.10	99.06	96.09	98.00
DH2	80084	79777	78397	414	52.88	99.06	96.10	97.89
DH3	79807	79505	78279	414	53.00	99.05	96.08	98.09
DH4	80152	79833	78676	414	52.97	99.08	96.16	98.16
DH5	79940	79603	78517	414	52.69	99.03	96.02	98.22
DH6	80139	79838	78773	416	52.90	99.05	96.06	98.30
DH7	80081	79776	78666	415	52.94	99.04	96.04	98.23
DH8	80067	79774	78525	413	53.02	99.08	96.15	98.07

nucleotide sequence similarity were identified as one OTU. A total of 1,175 OTUs have been recognized in gut bacterial communities, varying from 1,035 to 1,124 in each sample (**Figure 1E**). Moreover, there were 1,156 and 1,144 OTUs in the healthy and diarrheic horses, respectively, and 1,125 OTUs in common, accounting for approximately 95.74% of the total OTUs (**Figure 1D**).

Analysis of Microbial Diversity in the Healthy and Diarrheic Horses

The indicates of Chao1, ACE, Shannon, and Good's coverage were calculated to evaluate the alpha diversity of the microbial community. Good's coverage estimates varied from 99.88 to 99.96% for all of the samples, showing excellent coverage. The average Chao1 and ACE indices in the healthy horses were 1,130.99 and 1,123.46, while those in the diarrheic populations were 1,098.34 and 1,089.36 (**Figures 2A,B**). Furthermore, the average Shannon index was 5.861 and 6.41 in the healthy and diarrheic horses, respectively (**Figure 2C**). Statistical analysis showed that the diversity indices including Chao1, ACE, and Shannon of the healthy horses were significantly higher than those of the diarrheic populations. The results of Chao1, ACE, and Shannon indices showed that there were significant differences in the richness and diversity of gut microbial population between the healthy and diarrheic horses. The PCoA scatterplot of gut microbiota showed a separation of samples in the healthy and diarrheic horses, which was in line with the UPGMA results, indicating a significant shift in gut microbial principal compositions (**Figures 2D–F**).

Composition Analysis of the Gut Microbial Community in the Healthy and Diarrheic Horses

Gut microbial community composition in the healthy and diarrheic horses was assessed at different taxonomical levels. At the phylum level, *Firmicutes* (61.07, 68.87%), *Bacteroidetes* (25.77, 16.29%), *Spirochaetes* (4.48, 4.72%), and *Kiritimatiellaeota* (4.01, 3.88%) were dominant in the healthy and diarrheic horses regardless of health statuses (**Figure 3A**). Moreover, other phyla such as *Actinobacteria* (1.23, 1.1%), *Fibrobacteres* (1.25, 0.47%), *Tenericutes* (0.33, 1.05%), and *Patescibacteria* (0.4, 0.75%) in both groups were represented with a lower abundance. At the level of genus, *uncultured_bacterium_f_Lachnospiraceae* (13.67, 12.36%), *uncultured_bacterium_f_p-251-o5* (10.79, 4.94%), *Lachnospiraceae_AC2044_group* (6.61, 5.88%), and *Treponema_2* (4.47, 4.7%) were the predominant bacteria in both groups (**Figure 3B**). The heatmap also displayed the distribution and variability of the bacterial genera in the diarrheic horses (**Figure 4**).

A comparison of gut microbiota at the levels of phylum and genus was also conducted between the healthy and diarrheic horses. At the level of phylum, the relative abundances of *Bacteroidetes*, *Fibrobacteres*, and *Verrucomicrobia* in the diarrheic horses were significantly higher than in the healthy populations, while the *Planctomycetes*, *Tenericutes*, *Firmicutes*, *Patescibacteria*, and *Proteobacteria* contents were lower (**Table 2**). Moreover, a comparison of the diarrheic and healthy horses showed a significant increase in the abundance of 14 genera (*Breznakia*, *Enterorhabdus*, *Mailhella*, *Oscillospira*, *Proteus*, *Anaerorhabdus_furcosa_group*, *Erysipelotrichaceae_UCG-009*, *Prevotellaceae_UCG-004*, *Fibrobacter*, *Parvibacter*, *Acetitomaculum*, *Pygmaiobacter*, *Succinivibrionaceae_UCG-002*, and*Candidatus_Soleaferrea*) as well as an obvious reduction in the abundance of 31 genera (*Anaerofustis*, *Christensenellaceae_R-7_group*, *Defluviitaleaceae_UCG-011*, *Glutamicibacter*, *Lysinibacillus*, *Phoenicibacter*, *Pseudobutyrivibrio*, *Quinella*, *Ruminiclostridium_1*, *Ruminiclostridium_6*, *Ruminococcus_2*, *Selenomonas_1*, *Shuttleworthia*, *Solibacillus*, *Weissella*, *Eubacterium_coprostanoligenes_group*, *Marvinbryantia*, *Rikenellaceae_RC9_gut_group*, *Erysipelotrichaceae_UCG-004*, *Blautia*, *Candidatus_Saccharimonas*, *Coprococcus_1*, *Ruminococcaceae_UCG-014*, *Agathobacter*, *Ruminococcaceae_UCG-004*, *Vagococcus*, *Kurthia*,

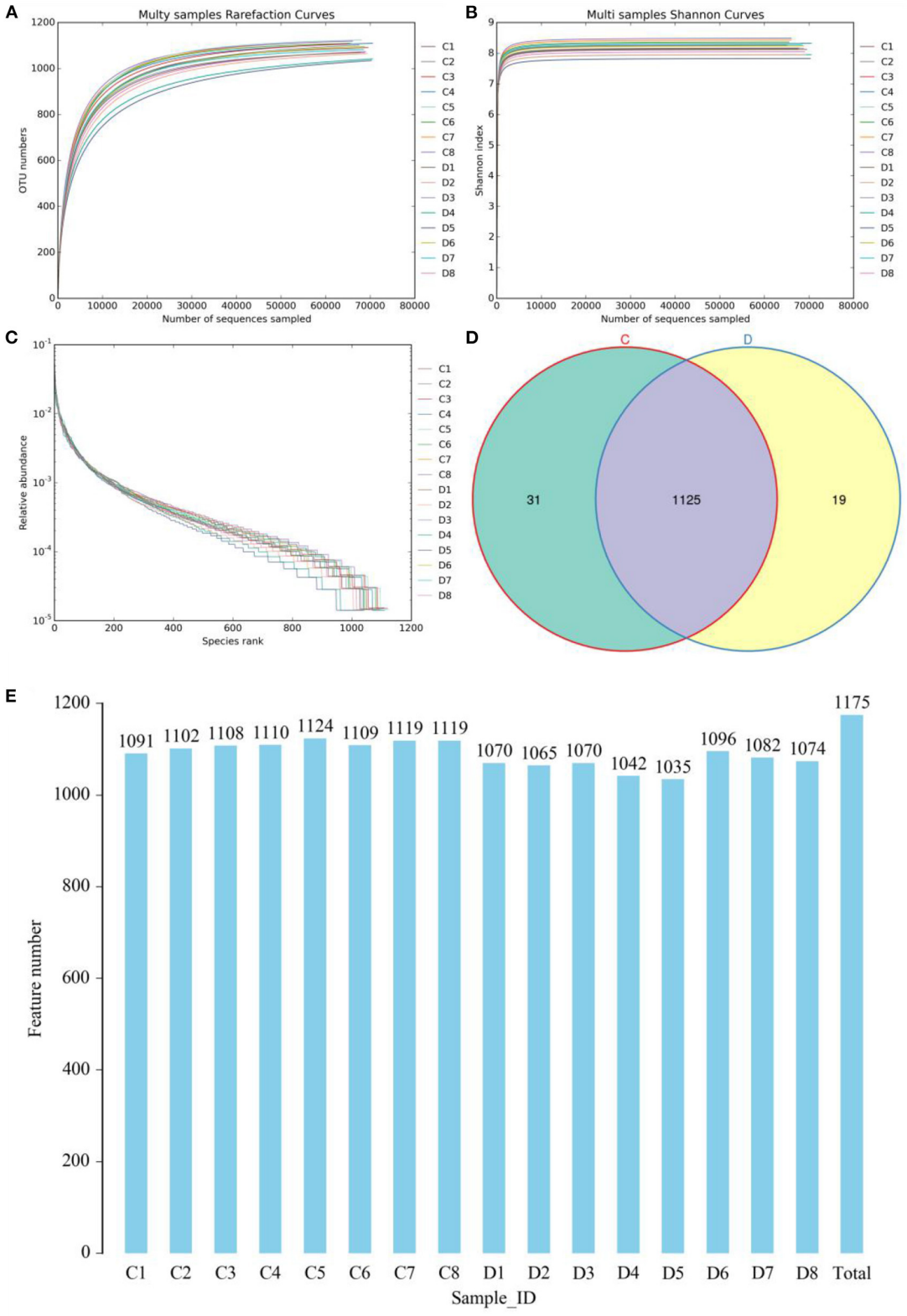

FIGURE 1 | Feasibility analysis of sequencing data. Sequencing depth and evenness of gut microbiota could be assessed with **(A,B)** rarefaction and **(C)** rank abundance curves. **(D)** Venn diagrams for shared and unique operational taxonomic unit (OTU) distribution. **(E)** Quantity of OTUs in each sample.

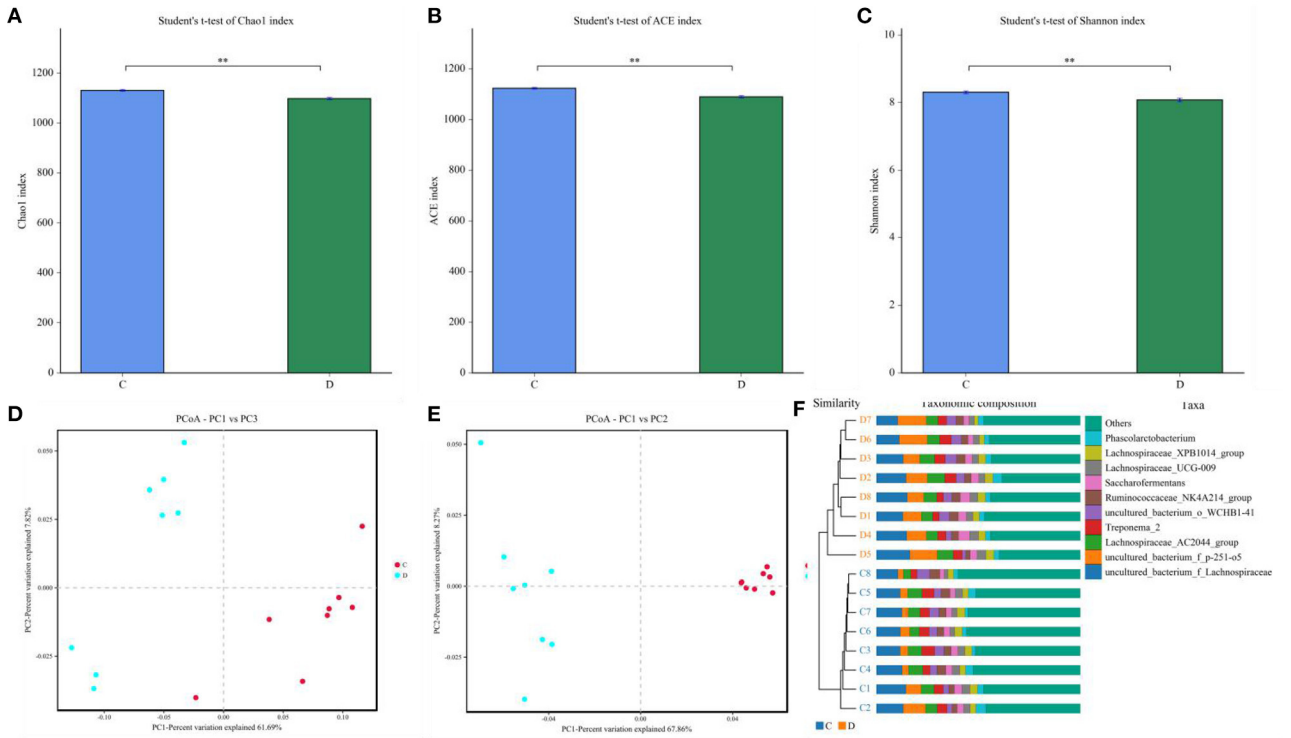

FIGURE 2 | Comparative analysis of alpha and beta diversity of gut microbiota between the healthy and diarrheic horses. **(A–C)** represent Chao, ACE, and Shannon indices, respectively. **(D,F)** indicate PCoA map based on **(E)** weighted and **(F)** unweighted UniFrac distance. **(F)** Clustering analysis map.

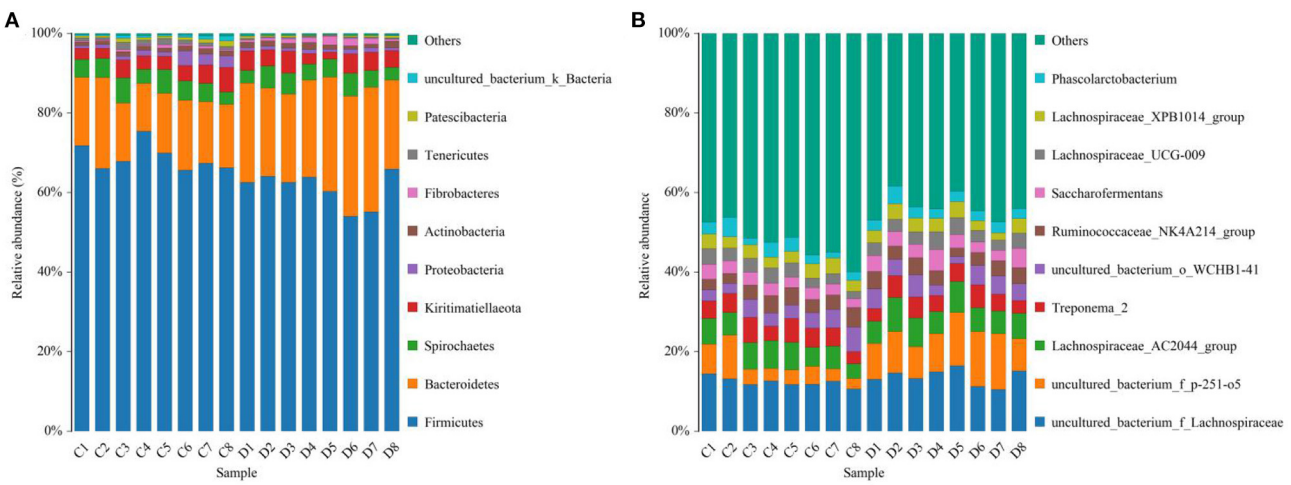

FIGURE 3 | Proportion of preponderant bacterial **(A)** phyla and **(B)** genera in the healthy and diarrheic horses.

Lachnospiraceae_UCG-002, *Eubacterium_ruminantium_group*, *Brevibacterium*, and *Ruminococcaceae_UCG-002*). LEfSe combined with LDA scores was conducted to further dissect the shifts in gut microbiota. Besides the above-mentioned differential taxa, the diarrheic horses also showed significantly higher abundances of *Acinetobacter*, *Ruminococcaceae_UCG_010*, and *Streptococcus*, and low abundances of *Fibrobacter* (**Figures 5A,B**).

Correlation Network Analysis

The results indicated that *Christensenellaceae_R-7_group* was positively associated with *Weissella* (0.8206), *Phoenicibacter*

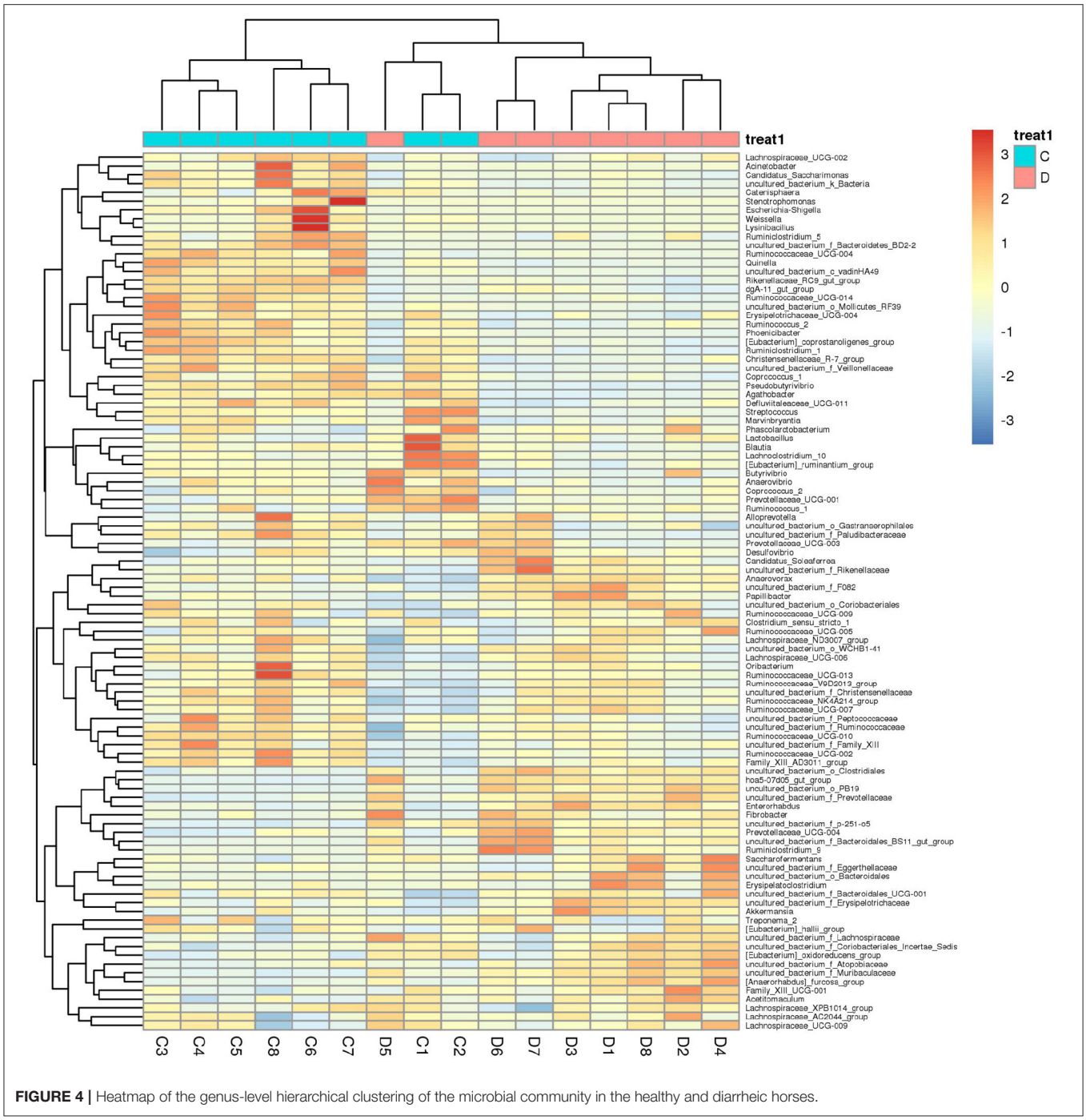

FIGURE 4 | Heatmap of the genus-level hierarchical clustering of the microbial community in the healthy and diarrheic horses.

(0.8206), *Quinella* 0.8412), *Defluviitaleaceae_UCG-011* (0.8088), and *Ruminococcus_2* (0.8382) (**Figure 6**). *Defluviitaleaceae_UCG-011* was positively correlated with *Weissella* (0.8059). *Rikenellaceae_RC9_gut_group* was positively related to *Lysinibacillus* (0.8344) and *Stenotrophomonas* (0.803). *Ruminococcaceae_UCG-002* was positively correlated with *Ruminococcaceae_UCG-014* (0.8647), *Ruminococcaceae_UCG-010* (0.9324), and *Mogibacterium* (0.8471). *Ruminococcaceae_UCG-014* was positively associated with *Phoenicibacter* (0.8618), *Ruminococcaceae_UCG-004* (0.8206), and *Ruminiclostridium_1* (0.8176). *Weissella* was positively correlated with *Coprococcus_1* (0.8647) and *Stenotrophomonas* (0.8608).

DISCUSSION

Gut microbiota are a complicated and interactive ecosystem involving trillions of microbes (27, 28). Gut microbial interaction

TABLE 2 | Statistical comparison of differential taxa between the healthy and diarrheic horses. All the data are represented as mean ± SD.

Taxa	C (%)	D (%)	P
Bacteroidetes	16.3	25.8	0.000999
Planctomycetes	0.0851	0.00525	0.000999
Tenericutes	1.05	0.337	0.000999
Firmicutes	68.8	61.1	0.002
Fibrobacteres	0.476	1.24	0.004
Patescibacteria	0.755	0.397	0.005
Verrucomicrobia	0.089	0.174	0.014
Proteobacteria	1.81	0.917	0.039
Anaerofustis	0.0355	0.000181	0.000999
Breznakia	0.000905	0.0116	0.000999
Christensenellaceae_R-7_group	2.82	1.74	0.000999
Defluviitaleaceae_UCG-011	0.521	0.316	0.000999
Enterorhabdus	0.0592	0.126	0.000999
Glutamicibacter	0.0205	0.00451	0.000999
Lysinibacillus	0.34	0.00761	0.000999
Mailhella	0.00569	0.0435	0.000999
Oscillospira	0.000185	0.0134	0.000999
Phoenicibacter	0.0939	0.0219	0.000999
Proteus	0.00351	0.0166	0.000999
Pseudobutyrivibrio	1.06	0.606	0.000999
Quinella	1.72	0.425	0.000999
Ruminiclostridium_1	0.071	0.0154	0.000999
Ruminiclostridium_6	0.0226	0.00235	0.000999
Ruminococcus_2	0.0909	0.0406	0.000999
Selenomonas_1	0.0262	0.00451	0.000999
Shuttleworthia	0.012	0.000903	0.000999
Solibacillus	0.0429	0.00688	0.000999
Weissella	0.577	0.0101	0.000999
[Anaerorhabdus]_furcosa_group	0.0541	0.18	0.000999
[Eubacterium]_coprostanoligenes_group	2.76	1.35	0.000999
Erysipelotrichaceae_UCG-009	0.00628	0.0152	0.002
Marvinbryantia	0.118	0.0725	0.002
Prevotellaceae_UCG-004	0.824	1.3	0.002
Rikenellaceae_RC9_gut_group	2.92	1.25	0.002
Erysipelotrichaceae_UCG-004	0.205	0.112	0.003
Blautia	0.282	0.206	0.004
Candidatus_Saccharimonas	0.755	0.371	0.004
Coprococcus_1	0.0538	0.0311	0.004
Fibrobacter	0.476	1.24	0.004
Ruminococcaceae_UCG-014	1.62	0.704	0.004
Agathobacter	0.882	0.531	0.00599
Parvibacter	0.0132	0.0252	0.00899
Ruminococcaceae_UCG-004	0.216	0.0861	0.00899
Vagococcus	0.0176	0.000718	0.011
Acetitomaculum	0.0342	0.0524	0.012
Kurthia	0.0151	0.000544	0.014
Pygmaiobacter	0.0105	0.0349	0.015
Lachnospiraceae_UCG-002	0.142	0.0852	0.016
Succinivibrionaceae_UCG-002	0.00186	0.00952	0.016
[Eubacterium]_ruminantium_group	0.164	0.117	0.017
Brevibacterium	0.0156	0.00233	0.018
Ruminococcaceae_UCG-002	3.01	1.85	0.02
Solobacterium	0.00732	0.0161	0.028
Candidatus_Soleaferrea	0.185	0.356	0.04

plays a key role in host health (29, 30). Gut microbiota could decrease the invasion and colonization of pathogens by regulating the intestinal barrier and environment, indicating its vital role in gastrointestinal diseases (31, 32). Consequently, the investigation of gut microbiota has attracted widespread attention. However, only a few studies have been conducted to investigate the gut microbiota in horses with different health statuses. In this study, we compared and analyzed gut microbial differences between healthy and diarrheic horses.

Gut microbial diversity and abundance change dynamically within certain limits and affect by age, diet, and environment, but these normal changes cannot damage intestinal functions (33, 34). However, some intense stimuli and diseases such as heavy metals, antibiotics, and gastrointestinal diseases may destroy

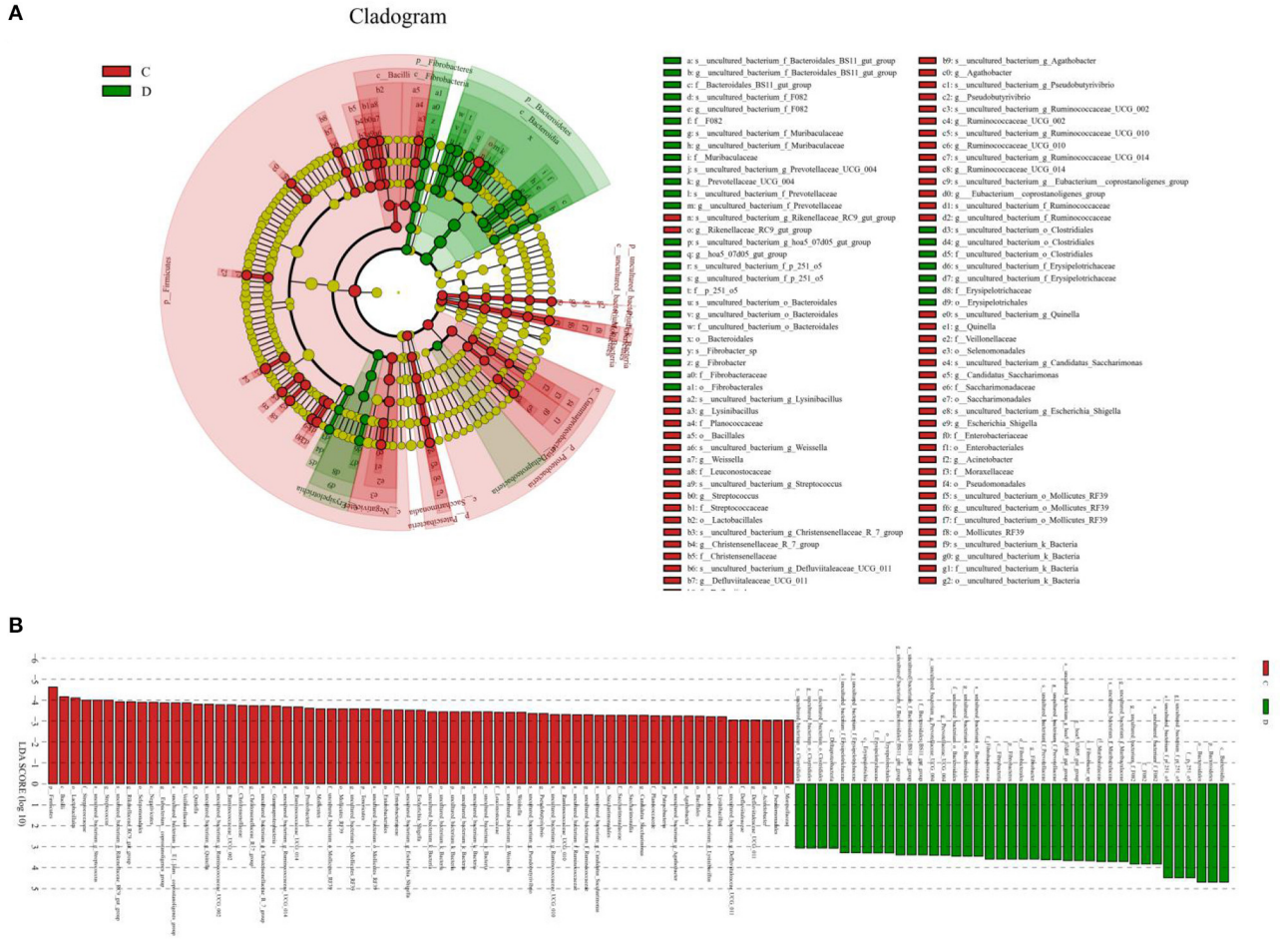

FIGURE 5 | Differential biomarkers in gut microbiota of the horses associated with diarrhea. **(A)** Phylogenetic distribution of taxa with significant differences are visualized through the cladogram. **(B)** The criterion of significance was determined at LDA scores > 3.

ecological balance and induce gut microbial dysbiosis (35–37). Li et al. revealed reduced alpha diversity of gut microbiota in giraffes during diarrhea (18). Furthermore, He et al. reported that the gut microbial diversity of piglets with diarrhea was significantly decreased (38). In this study, we observed that diarrhea results in a significant reduction in gut microbial diversity of horses, indicating gut microbial dysbiosis. Research showed that higher gut microbial abundance and diversity were conducive to maintaining intestinal homeostasis and functions (39). Conversely, gut microbial dysbiosis may impair intestinal barrier functions and mucosal immunity, which, in turn, increases morbidity caused by pathogenic bacteria and opportunistic pathogens (40, 41). Consequently, diarrheic horses suffering from gut microbial dysbiosis are at increased risk of bowel dysfunction and other diseases. A PCoA was conducted to dissect the effect of diarrhea on gut microbial main components of horses. The results demonstrated that the samples of healthy horses were clustered together and separated from the diarrheic samples, suggesting that the main components of gut microbiota changed significantly under the influence of diarrhea. Although all the selected horses possessed the same diet and environment, the gut microbiota changed during diarrhea. Consequently, we suspected that diarrhea was the main driving force of gut microbial dysbiosis in horses.

This research indicated that *Firmicutes* and *Bacteroidetes* were the most preponderant bacterial phyla in horses regardless of health status, which was consistent with previous findings on other mammals such as pigs, cattle, and goats, implying their key roles in intestinal ecology and function (42, 43). However, although the species of the dominant phyla were not altered, their abundances changed dramatically. In this study, we observed that the proportions of *Bacteroidetes*, *Fibrobacteres,* and *Verrucomicrobia* in the gut microbial community of the horses were significantly increased during diarrhea. Interestingly, Li et al. also reported that these bacterial phyla in the gut microbiota of diarrheic giraffes were significantly increased (18). For herbivores, *Firmicutes* participated in the degradation of cellulose, which is essential for nutrition and energy intake (44). Moreover, most members of *Firmicutes* are regarded as

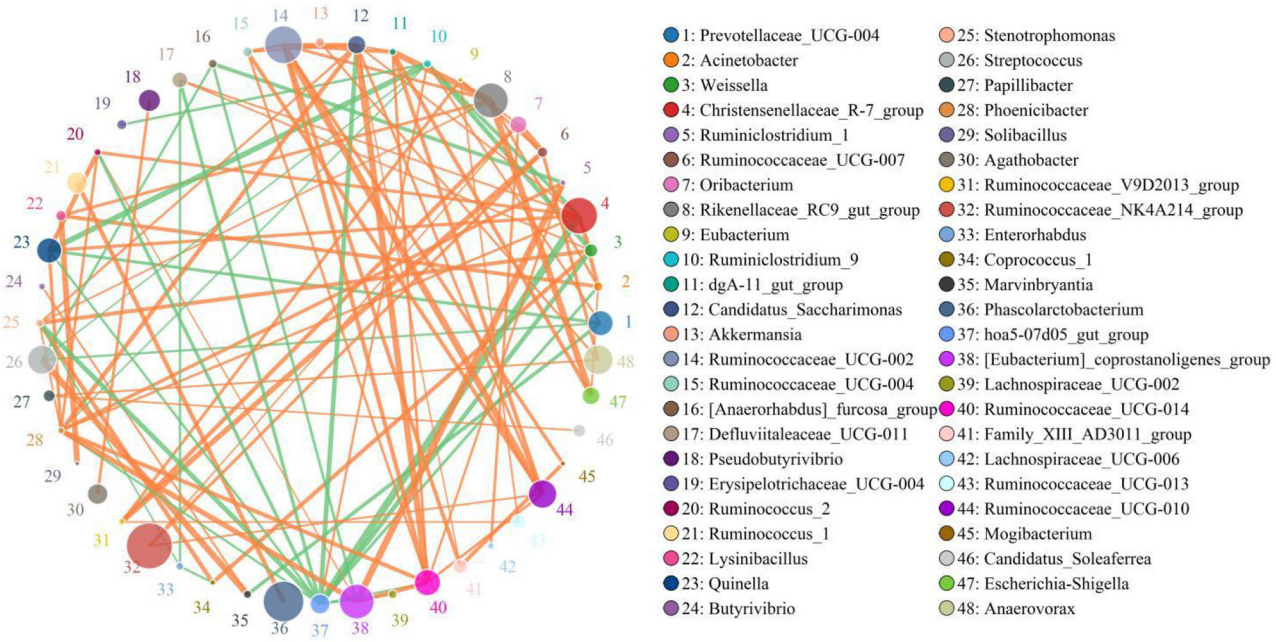

FIGURE 6 | Network analysis indicates a connection among different bacteria. The orange lines indicate positive correlation and the green lines indicate negative correlation.

intestinal beneficial bacteria, showing positive regulation of intestinal homeostasis, disease resistance, and growth performance (45, 46). *Proteobacteria* exhibits multiple metabolic functions that contribute to meeting host nutrient and energy requirements (44).

We also found significant changes in some bacterial genera during diarrhea, which may play key roles in gut microbial balance and the development of diarrhea. Moreover, some dramatically decreased bacterial genera in the diarrheic horses including *Ruminiclostridium*, *Ruminococcus*, *Rikenellaceae*, *Christensenellaceae*, *Pseudobutyrivibrio*, *Weissella*, *Eubacterium_coprostanoligenes*, *Ruminococcaceae*, *Lachnospiraceae*, *Blautia*, *Lachnospiraceae*, and *Coprococcus*and *Blautia* are considered as intestinal beneficial bacteria and are critical for intestinal functions and host health. *Ruminiclostridium,* which mostly resides in the gastrointestinal tract, displayed the characteristics of decreasing gastrointestinal diseases and improving the growth performance of animals (47). Previous studies have reported that *Ruminococcus* participated in the degradation of starch and cellulose (48). *Rikenellaceae* has been previously demonstrated to degrade plant-derived polysaccharides as well as control colitis by stimulating the differentiation of T-regulatory cells (49). As a recognized beneficial bacterium, *Christensenellaceae* not only is associated with immunoregulation and host health but also contributes to the regulation of intestinal homeostasis and the environment (50). Moreover, *Christensenellaceae* can also produce several hydrolases including β-glucosidase, β-galactosidase, and α-arabinosidase (24). *Pseudobutyrivibrio* can produce butyrate, which is conducive to reducing angiocardiopathy and diabetes by activating brown adipose tissues (51). Moreover, recent investigations on butyrate-producing bacteria have provided evidence that they were potentially intestinal beneficial bacteria because of their important roles in alleviating inflammatory bowel disease and regulating immunologic functions (52, 53). *Weissella* exhibits the characteristics of antioxidation and anti-inflammatory, which contributes to maintaining intestinal homeostasis and improving disease resistance of the host (54). Additionally, *Weissella* has been reported to reduce fat accumulation and protect the liver in mice induced by a high-fat diet (55). Earlier research indicated that the relative abundance of *Eubacterium_coprostanoligenes* in the intestine was negatively correlated to the severity of anxiety (56). *Eubacterium_coprostanoligenes* also displayed the characteristics of reducing cholesterol (57). Numerous bodies of evidence demonstrated that *Ruminococcaceae* was primarily responsible for digesting starch and cellulose and showed positive regulation of intestinal homeostasis and environment (58). Notably, the higher abundance of *Ruminococcaceae* contributes to reducing intestinal permeability, non-alcoholic fatty liver, and liver cirrhosis (59, 60). *Lachnospiraceae* plays an important role in intestinal homeostasis by ameliorating intestinal inflammation (61). Remarkably, some of the above-mentioned bacteria such as *Blautia*, *Lachnospiraceae*, *Coprococcus*, *Ruminococcaceae*, *Ruminococcus,* and *Ruminiclostridium* were considered producers of short-chain fatty acids (SCFAs) (47). Consistent with this study, several previous research studies on other animals have also indicated a significant

reduction in SCFA-producing bacteria during diarrhea (18, 62). Previous studies have indicated that SCFAs not only participated in the positive regulation of intestinal homeostasis, immunization, and barrier function but also play key roles in reducing inflammation and regulating energy intake (63, 64). Importantly, SCFAs can also inhibit the proliferation of pathogenic bacteria, showing significant effects of improving the intestinal environment to prevent diseases (65). These decreased beneficial bacteria in diarrheic horses play key roles in maintaining host health and intestinal homeostasis. Consequently, we speculated that these decreased bacteria may be important drivers of diarrhea in horses. Notably, we also observed that some decreased intestinal beneficial bacteria showed a significant correlation with other bacteria. It suggested that diarrhea can also indirectly impair other bacteria by interaction, which may further enhance the influence of diarrhea on the gut microbial community and induce gut microbial dysbiosis.

In summary, this study first explored changes in the gut microbiota in diarrheic horses. The results showed that diarrhea dramatically decreased the gut microbial diversity and altered the taxonomic composition, characterized by a reduced percentage of intestinal beneficial bacteria. This study fills in the gaps in the characteristics of gut microbiota in healthy and diarrheic horses and conveys a vital message that gut microbial dysbiosis may be one of the causes of diarrhea in horses. Importantly, this study contributes to the prevention and treatment of diarrheic horses from the gut microbial perspective.

DATA AVAILABILITY STATEMENT

The datasets presented in this study can be found in online repositories. The names of the repository/repositories and accession number(s) can be found below: https://www.ncbi.nlm.nih.gov/, PRJNA808959.

ETHICS STATEMENT

The animal study was reviewed and approved by the Ethics Committee of the Wuhan Business University.

AUTHOR CONTRIBUTIONS

YanL and YaoL conceived and designed the experiments. YaoL contributed to sample collection and preparation. YaoL analyzed the data. YaoL wrote the manuscript. SZ and XW revised the manuscript. All authors reviewed the manuscript. All authors contributed to the article and approved the submitted version.

FUNDING

The study was supported by the Wuhan Business University project (No. 2019KY003).

ACKNOWLEDGMENTS

We would like to thank Aoyun Li for uploading the data and the first phases of the animal experiment.

REFERENCES

1. Liu J, Wang HW, Lin L, Miao CY, Zhang Y, Zhou BH. Intestinal barrier damage involved in intestinal microflora changes in fluoride-induced mice. *Chemosphere.* (2019) 234:409–18. doi: 10.1016/j.chemosphere.2019.06.080
2. Li A, Wang Y, He Y, Liu B, Iqbal M, Mehmood K, et al. Environmental fluoride exposure disrupts the intestinal structure and gut microbial composition in ducks. *Chemosphere.* (2021) 277:130222. doi: 10.1016/j.chemosphere.2021.130222
3. Cao Q, Li R, Fu R, Zhang X, Yue B, Wang J, et al. Intestinal fungal dysbiosis in mice induced by fluoride. *Chemosphere.* (2020) 245:125617. doi: 10.1016/j.chemosphere.2019.125617
4. Hu L, Geng S, Li Y, Cheng S, Fu X, Yue X, et al. Exogenous fecal microbiota transplantation from local adult pigs to crossbred newborn piglets. *Front Microbiol.* (2017) 8:2663. doi: 10.3389/fmicb.2017.02663
5. Wickramasuriya SS, Park I, Lee K, Lee Y, Kim WH, Nam H, Lillehoj HS. Role of physiology, immunity, microbiota, and infectious diseases in the gut health of poultry. *Vaccines (Basel).* (2022) 10. doi: 10.3390/vaccines10020172
6. Wang J, Zhu G, Sun C, Xiong K, Yao T, Su Y, et al. TAK-242 ameliorates DSS-induced colitis by regulating the gut microbiota and the JAK2/STAT3 signaling pathway. *Microb Cell Fact.* (2020) 19:158. doi: 10.1186/s12934-020-01417-x
7. Li A, Ding J, Shen T, Han Z, Zhang J, Abadeen ZU, et al. Environmental hexavalent chromium exposure induces gut microbial dysbiosis in chickens. *Ecotoxicol Environ Saf.* (2021) 227:112871. doi: 10.1016/j.ecoenv.2021.112871
8. Kong A, Zhang C, Cao Y, Cao Q, Liu F, Yang Y, et al. The fungicide thiram perturbs gut microbiota community and causes lipid metabolism disorder in chickens. *Ecotoxicol Environ Saf.* (2020) 206:111400. doi: 10.1016/j.ecoenv.2020.111400
9. Tanase DM, Gosav EM, Neculae E, Costea CF, Ciocoiu M, Hurjui LL, et al. Role of gut microbiota on onset and progression of microvascular complications of type 2 diabetes (T2DM). *Nutrients.* (2020) 12. doi: 10.3390/nu12123719
10. Wan H, Wang Y, Zhang H, Zhang K, Chen Y, Chen C, et al. Chronic lead exposure induces fatty liver disease associated with the variations of gut microbiota. *Ecotoxicol Environ Saf.* (2022) 232:113257. doi: 10.1016/j.ecoenv.2022.113257
11. Yan H, Qin Q, Chen J, Yan S, Li T, Gao X, et al. Gut microbiome alterations in patients with visceral obesity based on quantitative computed tomography. *Front Cell Infect Microbiol.* (2021) 11:823262. doi: 10.3389/fcimb.2021.823262
12. Dreisbach C, Morgan H, Cochran C, Gyamfi A, Henderson WA, Prescott S. Metabolic and microbial changes associated with diet and obesity during pregnancy: what can we learn from animal studies? *Front Cell Infect Microbiol.* (2021) 11:795924. doi: 10.3389/fcimb.2021.795924
13. Wang Y, Zhang H, Zhu L, Xu Y, Liu N, Sun X, et al. Dynamic distribution of gut microbiota in goats at different ages and health states. *Front Microbiol.* (2018) 9:2509. doi: 10.3389/fmicb.2018.02509
14. Gryaznova MV, Dvoretskaya YD, Syromyatnikov MY, Shabunin SV, Parshin PA, Mikhaylov EV, et al. Changes in the microbiome profile in different parts of the intestine in piglets with diarrhea. *Animals (Basel).* (2022) 12. doi: 10.3390/ani12030320
15. Han Z, Li K, Shahzad M, Zhang H, Luo H, Qiu G, et al. Analysis of the intestinal microbial community in healthy and diarrheal perinatal yaks by high-throughput sequencing. *Microb Pathog.* (2017) 111:60–70. doi: 10.1016/j.micpath.2017.08.025
16. Wang Y, Li A, Zhang L, Waqas M, Mehmood K, Iqbal M, et al. Probiotic potential of Lactobacillus on the intestinal microflora against Escherichia coli induced mice model through high-throughput sequencing. *Microb Pathog.* (2019) 137:103760. doi: 10.1016/j.micpath.2019.103760

17. Wang Y, Li A, Liu J, Mehmood K, Wangdui B, Shi H, et al. L. pseudomesenteroides and L johnsonii isolated from yaks in Tibet modulate gut microbiota in mice to ameliorate enteroinvasive Escherichia coli-induced diarrhea. *Microb Pathog.* (2019) 132:1–9. doi: 10.1016/j.micpath.2019.04.020
18. Li A, Liu B, Li F, He Y, Wang L, Fakhar-E-Alam KM, et al. Integrated Bacterial and Fungal Diversity Analysis Reveals the Gut Microbial Alterations in Diarrheic Giraffes. *Front Microbiol.* (2021) 12:712092. doi: 10.3389/fmicb.2021.712092
19. Han Z, Li A, Pei L, Li K, Jin T, Li F, et al. Milk replacer supplementation ameliorates growth performance and rumen microbiota of early-weaning yimeng black goats. *Front Vet Sci.* (2020) 7:572064. doi: 10.3389/fvets.2020.572064
20. Guo X, Liu S, Wang Z, Zhang XX Li M, Wu B. Metagenomic profiles and antibiotic resistance genes in gut microbiota of mice exposed to arsenic and iron. *Chemosphere.* (2014) 112:1–8. doi: 10.1016/j.chemosphere.2014.03.068
21. Cao QQ, Lin LX, Xu TT, Lu Y, Zhang CD, Yue K, et al. Aflatoxin B1 alters meat quality associated with oxidative stress, inflammation, and gut-microbiota in sheep. *Ecotoxicol Environ Saf.* (2021) 225:112754. doi: 10.1016/j.ecoenv.2021.112754
22. Li Y, Zuo Z, Zhang B, Luo H, Song B, Zhou Z, et al. Impacts of early-life paraquat exposure on gut microbiota and body weight in adult mice. *Chemosphere.* (2022) 291:133135. doi: 10.1016/j.chemosphere.2021.133135
23. Zhou J, Shu R, Yu C, Xiong Z, Xiao Q, Li Z, et al. Exposure to low concentration of trifluoromethanesulfonic acid induces the disorders of liver lipid metabolism and gut microbiota in mice. *Chemosphere.* (2020) 258:127255. doi: 10.1016/j.chemosphere.2020.127255
24. Xin J, Chai Z, Zhang C, Zhang Q, Zhu Y, Cao H, et al. Comparing the microbial community in four stomach of dairy cattle, yellow cattle and three yak herds in qinghai-tibetan plateau. *Front Microbiol.* (2019) 10:1547. doi: 10.3389/fmicb.2019.01547
25. Xi L, Song Y, Qin X, Han J, Chang YF. Microbiome analysis reveals the dynamic alternations in gut microbiota of diarrheal giraffa camelopardalis. *Front Vet Sci.* (2021) 8:649372. doi: 10.3389/fvets.2021.649372
26. Li A, Yang Y, Qin S, Lv S, Jin T, Li K, et al. Microbiome analysis reveals gut microbiota alteration of early-weaned Yimeng black goats with the effect of milk replacer and age. *Microb Cell Fact.* (2021) 20:78. doi: 10.1186/s12934-021-01568-5
27. Liu Z, Li A, Wang Y, Iqbal M, Zheng A, Zhao M, et al. Comparative analysis of microbial community structure between healthy and Aeromonas veronii-infected Yangtze finless porpoise. *Microb Cell Fact.* (2020) 19:123. doi: 10.1186/s12934-020-01383-4
28. Li A, Yang Y, Zhang Y, Lv S, Jin T, Li K, et al. Microbiome analysis reveals the alterations in gut microbiota in different intestinal segments of Yimeng black goats. *Microb Pathog.* (2021) 155:104900. doi: 10.1016/j.micpath.2021.104900
29. Eberl C, Ring D, Munch PC, Beutler M, Basic M, Slack EC, et al. Reproducible colonization of germ-free mice with the oligo-mouse-microbiota in different animal facilities. *Front Microbiol.* (2019) 10:2999. doi: 10.3389/fmicb.2019.02999
30. Pilla R, Suchodolski JS. The role of the canine gut microbiome and metabolome in health and gastrointestinal disease. *Front Vet Sci.* (2019) 6:498. doi: 10.3389/fvets.2019.00498
31. Zhou A, Yuan Y, Yang M, Huang Y, Li X, Li S, et al. Crosstalk between the gut microbiota and epithelial cells under physiological and infectious conditions. *Front Cell Infect Microbiol.* (2022) 12:832672. doi: 10.3389/fcimb.2022.832672
32. Wu Y, Nie C, Luo R, Qi F, Bai X, Chen H, et al. Effects of multispecies probiotic on intestinal microbiota and mucosal barrier function of neonatal calves infected with E. coli K99. *Front Microbiol.* (2021) 12:813245. doi: 10.3389/fmicb.2021.813245
33. Dias J, Marcondes MI, Motta DSS, Cardoso DMES, Fontes NM, Tassinari RR, et al. Bacterial community dynamics across the gastrointestinal tracts of dairy calves during preweaning development. *Appl Environ Microbiol.* (2018) 84. doi: 10.1128/AEM.02675-17
34. Li B, Zhang K, Li C, Wang X, Chen Y, Yang Y. Characterization and comparison of microbiota in the gastrointestinal tracts of the goat (Capra hircus) during preweaning development. *Front Microbiol.* (2019) 10:2125. doi: 10.3389/fmicb.2019.02125
35. Jin C, Zeng Z, Fu Z, Jin Y. Oral imazalil exposure induces gut microbiota dysbiosis and colonic inflammation in mice. *Chemosphere.* (2016) 160:349–58. doi: 10.1016/j.chemosphere.2016.06.105
36. Mayneris-Perxachs J, Cardellini M, Hoyles L, Latorre J, Davato F, Moreno-Navarrete JM, et al. Iron status influences non-alcoholic fatty liver disease in obesity through the gut microbiome. *Microbiome.* (2021) 9:104. doi: 10.1186/s40168-021-01052-7
37. Chang X, Kang M, Shen Y, Yun L, Yang G, Zhu L, et al. Bacillus coagulans SCC-19 maintains intestinal health in cadmium-exposed common carp (Cyprinus carpio L) by strengthening the gut barriers, relieving oxidative stress and modulating the intestinal microflora. *Ecotoxicol Environ Saf.* (2021) 228:112977. doi: 10.1016/j.ecoenv.2021.112977
38. He K, Yan W, Sun C, Liu J, Bai R, Wang T, et al. Alterations in the diversity and composition of gut microbiota in weaned piglets infected with Balantioides coli. *Vet Parasitol.* (2020) 288:109298. doi: 10.1016/j.vetpar.2020.109298
39. Bui AT, Williams BA, Hoedt EC, Morrison M, Mikkelsen D, Gidley MJ. High amylose wheat starch structures display unique fermentability characteristics, microbial community shifts and enzyme degradation profiles. *Food Funct.* (2020) 11:5635–46. doi: 10.1039/D0FO00198H
40. Kosiewicz MM, Zirnheld AL, Alard P. Gut microbiota, immunity, and disease: a complex relationship. *Front Microbiol.* (2011) 2:180. doi: 10.3389/fmicb.2011.00180
41. Wang B, Deng B, Yong F, Zhou H, Qu C, Zhou Z. Comparison of the fecal microbiomes of healthy and diarrheic captive wild boar. *Microb Pathog.* (2020) 147:104377. doi: 10.1016/j.micpath.2020.104377
42. Zhang L, Jiang X, Li A, Waqas M, Gao X, Li K, et al. Characterization of the microbial community structure in intestinal segments of yak (Bos grunniens). *Anaerobe.* (2020) 61:102115. doi: 10.1016/j.anaerobe.2019.102115
43. Li K, Mehmood K, Zhang H, Jiang X, Shahzad M, Dong X, et al. Characterization of fungus microbial diversity in healthy and diarrheal yaks in Gannan region of Tibet Autonomous Prefecture. *Acta Trop.* (2018) 182:14–26. doi: 10.1016/j.actatropica.2018.02.017
44. Sun B, Wang X, Bernstein S, Huffman MA, Xia DP, Gu Z, et al. Marked variation between winter and spring gut microbiota in free-ranging Tibetan Macaques (Macaca thibetana). *Sci Rep.* (2016) 6:26035. doi: 10.1038/srep26035
45. Li A, Wang Y, Li Z, Qamar H, Mehmood K, Zhang L, et al. Probiotics isolated from yaks improves the growth performance, antioxidant activity, and cytokines related to immunity and inflammation in mice. *Microb Cell Fact.* (2019) 18:112. doi: 10.1186/s12934-019-1161-6
46. Garneau JE, Tremblay DM, Moineau S. Characterization of 1706, a virulent phage from Lactococcus lactis with similarities to prophages from other Firmicutes. *Virology.* (2008) 373:298–309. doi: 10.1016/j.virol.2007.12.002
47. Tan J, McKenzie C, Potamitis M, Thorburn AN, Mackay CR, Macia L. The role of short-chain fatty acids in health and disease. *Adv Immunol.* (2014) 121:91–119. doi: 10.1016/B978-0-12-800100-4.00003-9
48. Miller TL, Currenti E, Wolin MJ. Anaerobic bioconversion of cellulose by Ruminococcus albus, Methanobrevibacter smithii, and Methanosarcina barkeri. *Appl Microbiol Biotechnol.* (2000) 54:494–8. doi: 10.1007/s002530000430
49. Seshadri R, Leahy SC, Attwood GT, Teh KH, Lambie SC, Cookson AL, et al. Cultivation and sequencing of rumen microbiome members from the Hungate1000 Collection. *Nat Biotechnol.* (2018) 36:359–67. doi: 10.1038/nbt.4110
50. Kong F, Hua Y, Zeng B, Ning R, Li Y, Zhao J. Gut microbiota signatures of longevity. *Curr Biol.* (2016) 26:R832–3. doi: 10.1016/j.cub.2016.08.015
51. Cai W, Xu J, Li G, Liu T, Guo X, Wang H, et al. Ethanol extract of propolis prevents high-fat diet-induced insulin resistance and obesity in association with modulation of gut microbiota in mice. *Food Res Int.* (2020) 130:108939. doi: 10.1016/j.foodres.2019.108939
52. Karlsson FH, Tremaroli V, Nookaew I, Bergstrom G, Behre CJ, Fagerberg B, et al. Gut metagenome in European women with normal, impaired and diabetic glucose control. *Nature.* (2013) 498:99–103. doi: 10.1038/nature12198
53. Bui TP, Ritari J, Boeren S, de Waard P, Plugge CM, de Vos WM. Production of butyrate from lysine and the Amadori product fructoselysine by a human gut commensal. *Nat Commun.* (2015) 6:10062. doi: 10.1038/ncomms10062

54. Yu HS, Lee NK, Choi AJ, Choe JS, Bae CH, Paik HD. Antagonistic and antioxidant effect of probiotic Weissella cibaria JW15. *Food Sci Biotechnol.* (2019) 28:851–5. doi: 10.1007/s10068-018-0519-6
55. Choi SI, You S, Kim S, Won G, Kang CH, Kim GH. Weissella cibaria MG5285 and Lactobacillus reuteri MG5149 attenuated fat accumulation in adipose and hepatic steatosis in high-fat diet-induced C57BL/6J obese mice. *Food Nutr Res.* (2021) 65. doi: 10.29219/fnr.v65.8087
56. Chen YH, Bai J, Wu D, Yu SF, Qiang XL, Bai H, et al. Association between fecal microbiota and generalized anxiety disorder: Severity and early treatment response. *J Affect Disord.* (2019) 259:56–66. doi: 10.1016/j.jad.2019.08.014
57. Liu Z, Yin B. Alterations in the gut microbial composition and diversity of tibetan sheep infected with echinococcus granulosus. *Front Vet Sci.* (2021) 8:778789. doi: 10.3389/fvets.2021.778789
58. Zhao J, Yao Y, Li D, Xu H, Wu J, Wen A, et al. Characterization of the gut microbiota in six geographical populations of Chinese rhesus macaques (Macaca mulatta), implying an adaptation to high-altitude environment. *Microb Ecol.* (2018) 76:565–77. doi: 10.1007/s00248-018-1146-8
59. Rai R, Saraswat VA, Dhiman RK. Gut microbiota: its role in hepatic encephalopathy. *J Clin Exp Hepatol.* (2015) 5:S29–36. doi: 10.1016/j.jceh.2014.12.003
60. Huang C, Song P, Fan P, Hou C, Thacker P, Ma X. Dietary sodium butyrate decreases postweaning diarrhea by modulating intestinal permeability and changing the bacterial communities in weaned piglets. *J NUTR.* (2015) 145:2774–80. doi: 10.3945/jn.115.217406
61. Zhao L, Zhang Q, Ma W, Tian F, Shen H, Zhou M, et al. Combination of quercetin and resveratrol reduces obesity in high-fat diet-fed rats by modulation of gut microbiota. *Food Funct.* (2017) 8:4644–56. doi: 10.1039/C7FO01383C
62. Xi L, Song Y, Han J, Qin X. Microbiome analysis reveals the significant changes in gut microbiota of diarrheic Baer's Pochards (Aythya baeri). *Microb Pathog.* (2021) 157:105015. doi: 10.1016/j.micpath.2021.105015
63. Melbye P, Olsson A, Hansen TH, Sondergaard HB, Bang OA. Short-chain fatty acids and gut microbiota in multiple sclerosis. *Acta Neurol Scand.* (2019) 139:208–19. doi: 10.1111/ane.13045
64. Goverse G, Molenaar R, Macia L, Tan J, Erkelens MN, Konijn T, et al. Diet-derived short chain fatty acids stimulate intestinal epithelial cells to induce mucosal tolerogenic dendritic cells. *J Immunol.* (2017) 198:2172–81. doi: 10.4049/jimmunol.1600165
65. Puddu A, Sanguineti R, Montecucco F, Viviani GL. Evidence for the gut microbiota short-chain fatty acids as key pathophysiological molecules improving diabetes. *Mediators Inflamm.* (2014) 2014:162021. doi: 10.1155/2014/162021

Conflict of Interest: The authors declare that the research was conducted in the absence of any commercial or financial relationships that could be construed as a potential conflict of interest.

Publisher's Note: All claims expressed in this article are solely those of the authors and do not necessarily represent those of their affiliated organizations, or those of the publisher, the editors and the reviewers. Any product that may be evaluated in this article, or claim that may be made by its manufacturer, is not guaranteed or endorsed by the publisher.

frontiers | Frontiers in Veterinary Science

ORIGINAL RESEARCH
published: 12 May 2022
doi: 10.3389/fvets.2022.891429

Effects of Glycyrrhiza Polysaccharides on Chickens' Intestinal Health and Homeostasis

*Yu Wu[1†], Chenyang Wu[2†], Yanyun Che[3†], Tao Zhang[4], Chen Dai[5], Audrey D. Nguyễn[6], Kun Duan[7], Yanyu Huang[6], Nannan Li[1], Hui Zhou[1], Xin Wan[1], Yuedi Wang[1], Hongjun Lei[1], Ping Hao[1], Caiyue Li[1] and Yi Wu[1]**

[1] Institute of Traditional Chinese Veterinary Medicine, College of Veterinary Medicine, Nanjing Agricultural University, Nanjing, China, [2] Beijing Key Laboratory of Traditional Chinese Veterinary Medicine, Beijing University of Agriculture, Beijing, China, [3] Engineering Laboratory for National Healthcare Theories and Products of Yunnan Province, College of Pharmaceutical Science, Yunnan University of Chinese Medicine, Kunming, China, [4] College of Animal Science and Technology, Nanjing Agricultural University, Nanjing, China, [5] College of Life Sciences, Experimental Teaching Center of Life Science, Nanjing Agricultural University, Nanjing, China, [6] Department of Biochemistry and Molecular Medicine, School of Medicine, University of California, Davis, Sacramento, CA, United States, [7] China Tobacco Henan Industrial Co., Ltd., Zhengzhou, China

OPEN ACCESS

Edited by:
Fazul Nabi,
Water and Marine Sciences, Pakistan

Reviewed by:
Khalid Mehmood,
Islamia University of Bahawalpur, Pakistan
Kenneth James Genovese,
United States Department of Agriculture (USDA), United States

***Correspondence:**
Yi Wu
wuyi2001cn@163.com;
wuyi2001cn@njau.edu.cn

[†]These authors have contributed equally to this work

Specialty section:
This article was submitted to Comparative and Clinical Medicine, a section of the journal Frontiers in Veterinary Science

Received: *07 March 2022*
Accepted: *05 April 2022*
Published: *12 May 2022*

Citation:
Wu Y, Wu C, Che Y, Zhang T, Dai C, Nguyễn AD, Duan K, Huang Y, Li N, Zhou H, Wan X, Wang Y, Lei H, Hao P, Li C and Wu Y (2022) Effects of Glycyrrhiza Polysaccharides on Chickens' Intestinal Health and Homeostasis. Front. Vet. Sci. 9:891429. doi: 10.3389/fvets.2022.891429

The overuse of antibiotics in poultry farming causes the accumulation of drug residue in animals' bodies and the occurrence of antibiotic-resistant bacteria, which not only compromise animals' health but ultimately endanger human health. Thus, there is an urgent need for a novel poultry feed additive to substitute for excessive antibiotics. Glycyrrhiza polysaccharides (GPS) derived from Chinese licorice have shown promising immunomodulatory effects in previous studies. The present study investigated the pharmacological effects of GPS on poultry intestines to assess whether it can be used as a feed additive. The results show that GPS can increase production of sIgA, promote the secretion activity of goblet cells, alter the gut microbial composition and lead to changes in short-chain fatty acids. GPS also elevated both Th1 and Th2 immune responses by facilitating the expression of IL-2, IL-4, IL-1β, and IFN-γ while increasing the proportion of both CD4+ and CD8+ cells in the intestine. Moreover, the results of 16S rRNA gene sequencing showed that GPS could significantly change intestinal microbiota composition in the intestine, evidenced by the increased proportion of Bacteroides, Butyricicoccus and Eisenbergiella, as well as a decreased portion of Erysipelatoclostridium, leading to a healthier intestinal microbiota composition for the host. Taken together, it can be concluded that GPS is safe to use as a novel feed additive that can be used as an alternative to prophylactic antibiotics in poultry feeding.

Keywords: glycyrrhiza polysaccharides, gut immunity, intestinal barrier, gut microbes, feed additives

INTRODUCTION

In recent decades, the global poultry farming industry developed rapidly in response to accelerating consumer demand. There are numerous feed additives used in industrial livestock and poultry husbandry to improve productivity, maintain intestinal health, and prevent pathogenic microorganisms (1, 2). Low-cost antibiotics are widely used in industrial farming to prevent bacterial infection and promote animal survival. However, abuse of antibiotics causes a number

of unintended consequences, including drug residue in animal products and antibiotic-resistant microbes, both of which can damage human health (3). New research indicates the global death toll from such antimicrobial resistance in 2019 was upward of four million people 47. Therefore, there is an urgent need to find a novel feed additive to substitute for the overuse of antibiotics in industrial poultry farming.

The gastrointestinal tract is the first line of defense against the many considerable challenges posed by harmful pathogens ingested daily. If the health and balance of the intestine is disrupted, the entire body can become infected with pathogens. Therefore, supporting intestinal health is key to maintaining overall animal health. It is well-documented that the intestine has an expansive surface area in which microbiota thrive and interact with the immune system to achieve intestinal homeostasis and maintain host health (4, 5). SIgA, the dominant antibody found in intestinal mucosa, protects the intestine from pathogens and regulates the intestinal microbiota during its development from birth to adulthood (6, 7). In animals, sIgA deficiency can lead to immunodeficiency and incomplete intestinal barrier function, resulting in reduced poultry productivity and even death (7). Based on this, improving the level of sIgA in animals' intestinal mucosa is a useful strategy to maintain the intestine's homeostasis and host health (8).

Licorice, a traditional medicinal and food plant (9), has a long history of application in both diet and pharmacology (10). The edible and medicinal parts of licorice are the root and rhizome. Because of its sweet taste, its soaking liquid is often used as a drinking additive in China, and as a food sweetener in Europe (11). In recent years, more and more active ingredients in licorice such as polysaccharides, flavones, and saponins have been obtained, showing some potential effects in drug development and food industry (12). Glycyrrhiza polysaccharides (GPS) in particular show great potential for use in medical and food industries. GPS consist of a series of biological polysaccharides, mainly glucose, galactose, and mannose (13). Many studies have confirmed that GPS possess various pharmaceutical properties, acting as an antitumor (14), antibacterial (15), antioxidant (16), and immunomodulation (14) agent. It has also been reported that GPS could be used as an immunopotentiator, as it can directly facilitate a robust immune response to inoculation by promoting the proliferation of lymphocytes, especially T lymphocytes (13). Additionally, GPS can activate innate cells, such as macrophages and dendritic cells (DCs), which prime an immune response that can efficiently eliminate pathogens and senescent cells (17, 18). However, the effectiveness of GPS in maintaining intestinal health and regulating intestinal microbiota is still unknown.

Previous studies did not examine the question of GPS as a promoter of intestinal health, nor its potential ability as an immunopotentiator specifically for an intestinal immune response. The present study investigated whether feeding poultry GPS could benefit their overall intestinal health and beneficially regulate their intestinal microbiota. GPS was extracted and purified from Chinese licorice, then fed to male Hy-Line Brown chickens. Next, the effect of GPS on the intestine was explored and its mechanisms investigated.

MATERIALS AND METHODS

Animals

Male 1-day-old Hy-Line Brown roosters were bought from Hai'an Shuangli Hatchery (Jiangsu, China). All animals were housed in wire cages under 12-h light/dark cycles at 30°C. All animal experiments were conducted in accordance with the guidelines of the Nanjing Agricultural University Institutional Animal Care and Use Committee (IACUC), detailed in the IACUC-approved protocol (No.:2021BAD34B04).

After one week of acclimatization, the roosters were randomly divided into four groups ($n = 5$) and treated either with isotonic saline (control group), GPS at a high dose (GPS-H, 600 mg/kg), GPS at a medium dose (GPS-M, 450 mg/kg), or GPS at a low dose (GPS-L, 300 mg/kg). The roosters in all groups were given these formulations intragastrically for 14 days. Meanwhile, the body weight of all roosters was measured every day to determine the safety of GPS. On the 15th day, all roosters were sacrificed and their contents, small intestine, bursa of Fabricius, spleen, and thymus were collected for further examination. The contents were directly transferred to −80°C for cryopreservation. The small intestine, bursa of Fabricius, bursa, and spleen were fixed with tissue fixative and stored under normal temperature conditions.

Measurement of SIgA in the Intestine

On day 15, 8 cm of the duodenum from each rooster ($n = 5$ per group) was collected and washed eight times with PBS (phosphate buffer solution, pH = 7.4) containing phenylmethylsulfonyl fluoride (PMSF) protease inhibitor. Next, these solutions were centrifuged at 10,000 rpm for 15 min at 4°C. Afterward, the supernatant was collected and used to determine the level of sIgA in the intestines using an enzyme-linked immunosorbent assay (ELISA).

Determination of Cytokines in Jejunum

The jejunums of 5 roosters from each group were collected, homogenized, then centrifuged at 12,000 rpm for 10 min at 4°C. Afterward, the supernatant was collected to analyze IL-2, IL-4, IL-1β, and IFN-γ levels in the intestine using ELISA kits.

Immunofluorescence of Jejunum

On day 15, all jejunums were collected to detect proportions of CD4+ and CD8+ T cells. Jejunums were briefly incubated in primary antibodies CD4+ and CD8+. Then, secondary antibodies CY3 (red) and FITC (green) were incubated with the mixture for 1 h to stain CD4+ and CD8+, respectively. After rinsing, the expression of these markers in the specimen images was observed and captured using confocal microscopy.

Histopathological Analysis

The paraffin-embedded bursa of Fabricius, spleen, thymus, liver, kidney, duodenum, jejunum, and ileum were sectioned using a pathology slicer (Leica RM2016), and a hematoxylin and eosin (HE) stain was applied to the sectioned tissue. Then, the stained intestinal segments were observed by using a Nikon Eclipse 80i microscope.

Determination of Short-Chain Fatty Acids (SCFAs) in the Intestine

The contents samples from the intestine were collected to measure the level of short-chain fatty acids (SCFAs) using gas chromatography (GC) and then calculate standard curves. The contents of the cecum were vortexed with ultrapure water at a 1:5 ratio. Then, the mixture was centrifuged at 10,000 rpm for 10 min at 4°C and the supernatant was collected. Afterward, each supernatant was mixed 1:1 with 2-methyl butyric acid. The treatment of each sample and the GC analysis were conducted based on the product instructions (19).

ABPAS Stain Assay

The jejunums were embedded in paraffin and sectioned using a Leica RM2016 pathology slicer. Then, the sections were sequentially treated with Periodic Acid Solution, Schiff reagent, and hematoxylin. After rinsing, the stained sections of the jejunums were observed by using a Nikon Eclipse 80i microscope.

Investigation of Intestinal Microbiota by 16S RRNA Gene Sequencing

Roosters' feces were snap-frozen using liquid nitrogen, followed by storage at −80°C. DNA was extracted using the FastDNA™ Spin Kit for Feces (MP Biomedicals, Santa Ana, CA) following their manual. The purity and quality of the genomic DNA were checked in 0.8% agarose gels. The V3-V4 hypervariable regions of the 16S rRNA gene were amplified with the primers 338F (ACTCCTACGGGAGGCAGCAG) and 806R (GGACTACHVGGGTWTCTAAT) then sequenced using an Illumina NovaSeq 6000 System. The raw data were screened and sequences shorter than 200 bp, those with a low-quality score (≤20), those containing ambiguous bases, or those that did not exactly match to primer sequences and barcode tags were removed from consideration. Qualified sequences were separated using the sample-specific barcode sequences and trimmed with the Illumina Sequencing Analysis Pipeline Version 2.6. Afterward, the dataset was analyzed using QIIME. The sequences were clustered into operational taxonomic units (OTUs) at a similarity level of 97%. Taxonomic assignments of operational taxonomic units (OTUs) representative sequences were performed with a confidence threshold of 0.8 by a Naïve Bayes classifier trained on the GreenGenes database (version 13.8).

Statistical Analysis

All statistical analyses were conducted using R (version 3.5.1) and GraphPad Prism (version 8.0), with all results reported as mean ± standard deviation (SD) or box-and-whisker plots. A one-way ANOVA test of multiple comparisons followed by Dunnett's *post-hoc* test was used to evaluate statistical significance between groups. Differences in the relative abundances of OTUs were assessed using Tukey's honest significant difference (HSD) test in R version 3.4.0. The level of statistical significance for our analyses is $p < 0.05$.

RESULTS

GPS Improves SIgA Production in the Intestine

To assess the effects of GPS on roosters' intestinal lining, the intestinal juice of roosters was collected to determine if GPS could increase local sIgA concentration. As shown in **Figure 1A**, sIgA was significantly increased in both the GPS-M and GPS-H treatment groups, relative to the control group. This suggests that GPS were able to boost production of sIgA in roosters' intestine in a dose-dependent manner.

GPS Promotes an Increased Number of Small Intestinal Villi

The physical barrier of the intestine is composed of the lamina propria, the intestinal villi, the intestinal epithelium, and various tightly attached proteins in the intestinal cells. As shown in **Figure 1B**, the intestinal lamina propria was structurally intact and the small intestinal epithelium was healthy across all GPS treatment groups. There was also a significant and dose-dependent increase in the number of villi in the duodenum, jejunum, and ileum of the small intestine in the GPS groups.

GPS Boosts Goblet Cell Secretion in the Intestine

The secretion activity of goblet cells in the intestine significantly affects the intestinal barrier and immunity (20). Thus, we further examined whether GPS could regulate goblet cell secretion in the intestine. As shown in **Figure 1C**, the secretion activity of goblet cells was significantly improved after treatment with GPS, compared to the saline group. This finding suggests that GPS are able to facilitate increased secretion from intestinal goblet cells, which promotes over-all intestinal health and a robust barrier against ingested pathogens.

GPS Facilitates Production of Short-Chain Fatty Acids (SCFAs) in Intestines

Short-chain fatty acids (SCFAs) including acetic acid, propionic acid, isobutyric acid, butyric acid, isovaleric acid, and valeric acid help regulate intestinal homeostasis and metabolism, which are key to intestinal health (21). Therefore, the content of these SCFAs in roosters' intestines was also examined. As shown in **Figures 2A–F**, the quantity of these SCFAs in the intestines of chickens from GPS-L, GPS-M, and GPS-H groups was significantly elevated compared with the control group, which suggests that GPS could promote the secretion of SCFAs. The high dose of GPS (GPS-H) elicited the strongest promotion effect compared to two lower GPS doses. Among them, the content of acetic acid, isobutyric acid, and butyric acid in the high-dose GPS group was significantly different from that in the low-dose group, indicating that this effect is dose- dependent.

GPS Promotes Expression of Cytokines in the Intestine

Maintaining intestinal health and homeostasis is inseparable from the regulation of cytokines (22), which influence

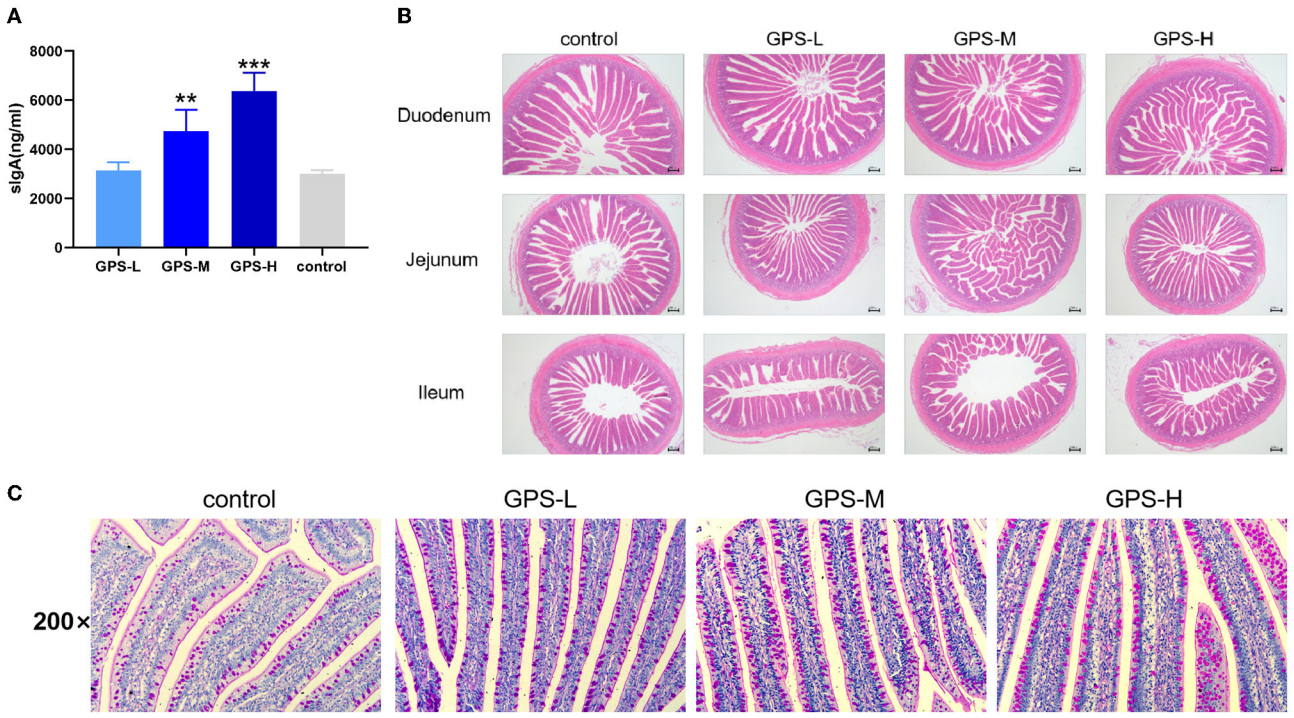

FIGURE 1 | (A) Effects of 14-day oral administration of GPS on intestinal secretion of sIgA in laying hens. **(B)** Hematoxylin-Eosin (HE) staining was used to observe the effect of GPS on the histology of the small intestine of laying hens after 14 days of oral administration. **(C)** Glycogen was labeled using PAS staining to show goblet cells (darker granules) in the gut, and the effect of 14-day GPS oral administration on the number of intestinal goblet cells in laying hens. $^{*}P < 0.05$, $^{**}P < 0.01$, and $^{***}P < 0.001$, all relative to the saline (control) group.

immune cells, tissue repair, and infection responses (23). As shown in **Figures 3A,B**, after treatment with GPS, levels of IL-2 and IL-4 were significantly elevated in the intestine compared to control group chickens treated with isotonic saline. After treatment with GPS, the production of IL-1β and IFN-γ was promoted in the intestine (see **Figures 3C,D**). These results suggest that GPS could enhance intestinal health through facilitation of IL-2, IL-4, IL-1β, and IFN-γ secretion.

GPS Improves Expression of CD4+ and CD8+ T Cells in the Intestine

Having confirmed the promotion effect of GPS on intestinal cytokine expression, we further explored whether GPS would affect activation of CD4+ and CD8+ T cells, which indirectly or directly prevent pathogen invasion and maintain homeostasis in the intestinal immune response (24). The immunofluorescence results in **Figure 4** show that different doses of GPS could improve expressions of CD4+ and CD8+ to different extents, compared with saline treatments. Noticeably, the levels of both CD4+ and CD8+ were highest in the GPS-H group, suggesting both that GPS are able to promote the expression of CD4+ and CD8+ in the intestine, and that the effect is dose-dependent.

GPS Enhances Beneficial Intestinal Microbiota Composition

The influence of GPS on the intestinal barrier and local immune response may be attributed to changes in intestinal microbiota. Therefore, the experiment further investigated intestinal microbiota for changes in evenness (uniformity) and richness (the number of species observed in each sample). As shown in **Figures 5A,B**, Shannon and Chao1 indices, which represent the evenness and total richness of intestinal microbiota, respectively, were both significantly increased in the GPS-H group relative to the control, suggesting that GPS-H could improve the evenness and richness of intestinal microbiota. Additionally, a principal component analysis (PCA) revealed that after treatment with GPS, the intestinal microbiota composition is fundamentally altered from that of the control group, indicating that GPS could dramatically change the intestinal microbial composition (**Figures 5C,D**). These changes in alpha diversity (**Figures 5A,B**) and beta diversity (**Figures 5C,D**) can be attributed to GPS treatment rather a chance variation in this specific sample collection.

The experiment further analyzed which specific intestinal microbes had changed to induce these alterations in alpha and beta diversity. From the phylum analysis shown in **Figures 6A,B**, it was observed that the proportion of Firmicutes were significantly decreased in the GPS-H group compared

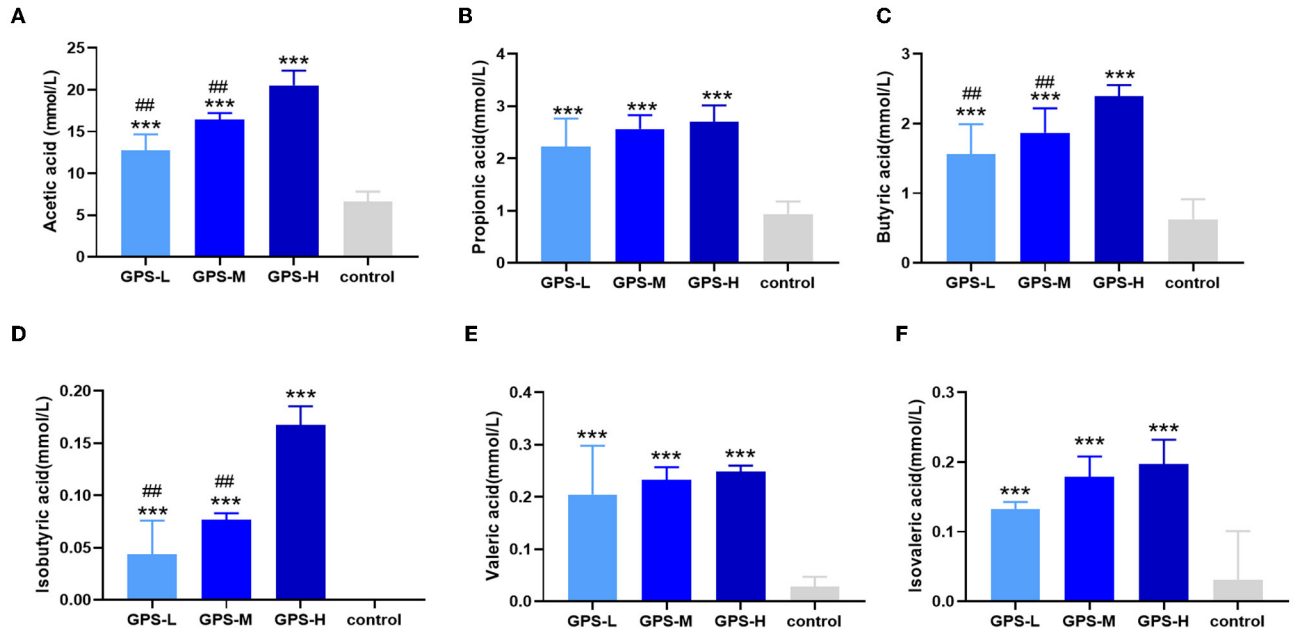

FIGURE 2 | Effects of 14-day oral administration of GPS on SCFAs production in chicken intestines. The use of gas chromatography (GC) determined that after GPS treatment, significantly increased intestinal levels of **(A)** acetic acid, **(B)** propionic acid, **(C)** butyric acid, **(D)** isobutyric acid, **(E)** valeric acid, and **(F)** isovaleric acid content. $^{*}P < 0.05$, $^{**}P < 0.01$, and $^{***}P < 0.001$, all relative to the saline (control) group.

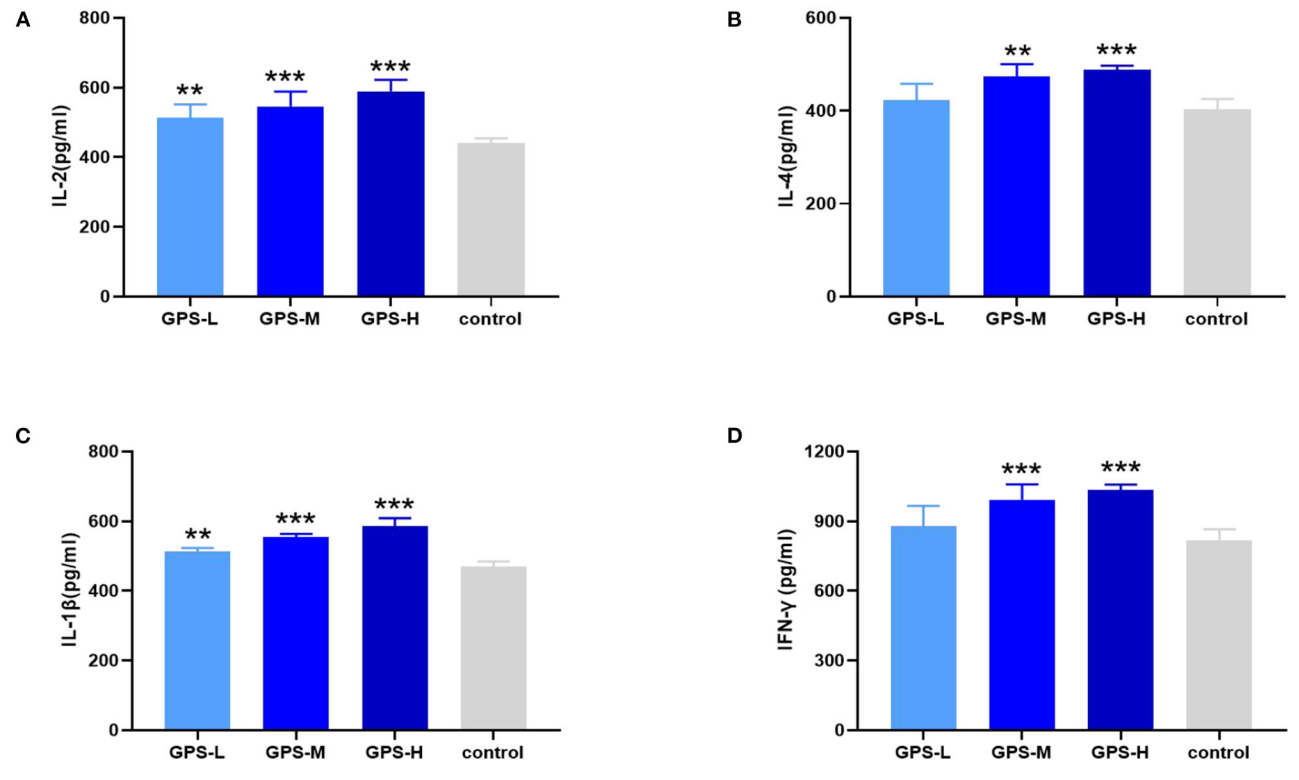

FIGURE 3 | After the laying hens were orally administered GPS for 14 days, the changes of cytokines in the serum of laying hens were determined by ELISA.GPS enhances the expression of **(A)** IL-2, **(B)** IL-4, **(C)** IL-1β, and **(D)** IFN-γ. $^{*}P < 0.05$, $^{**}P < 0.01$, and $^{***}P < 0.001$, all relative to the saline (control) group.

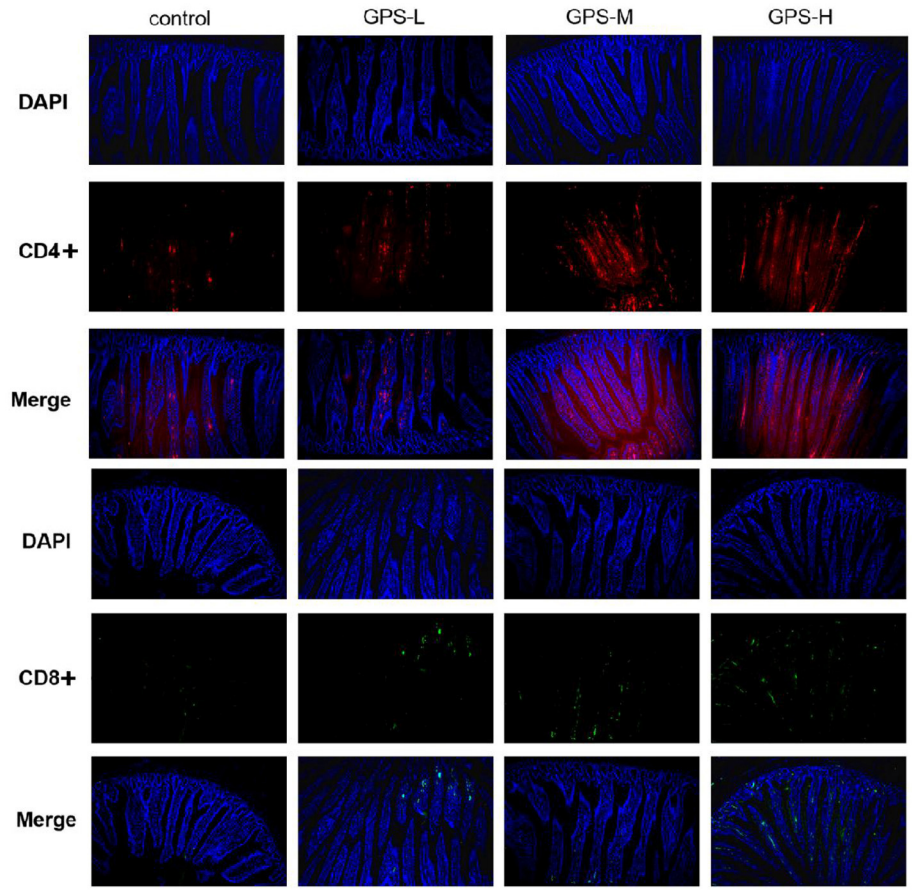

FIGURE 4 | The proportion of CD4+ and CD8+ T cells in the gut of laying hens after 14 days of oral GPS was analyzed using immunofluorescence. The nuclei were stained with DAPI (blue), the cell surface differentiation antigen CD4+ was stained with CY3 (red), and the cell surface differentiation antigen CD8+ was stained with FITC (green), which is convenient for visual inspection of the fluorescence intensity.

to the control. Meanwhile, relative to the control group, the proportion of Bacteroidetes was substantially increased in the GPS-H group; thus, the ratio of Firmicutes to Bacteroidetes was significantly reduced in the GPS-H group compared to the control. Notably, compared with roosters treated with saline alone, the proportion of Actinobacteria was increased in the intestines of roosters treated with GPS-H (**Figure 6B**), which suggests that GPS-H could not only reduce the ratio of Firmicutes to Bacteroidetes, but also regulate the proportion of specific microbes such as Actinobacteria. Further intestinal microbiota composition on a genus level is displayed in **Figure 7**. Bacteroides are the dominant flora in the intestines of roosters in the GPS-H group, and many microbes believed to be beneficial to the host were significantly increased in the GPS-H group compared to the control group (**Figure 7A**). These include Bacteroides, Butyricicoccus, Eisenbergiella, Enterococcus, Ruminococcaceae, and Lactobacillus. In addition, some pathogenic bacteria like Erysipelatoclostridium, Lachnoclostridium, and Escherichia–Shigella were significantly decreased in the GPS-H group compared to the control group (**Figure 7B**), suggesting that GPS are able to regulate the proportions of some harmful bacteria, which may contribute to the positive effect of GPS on roosters' intestinal health. Furthermore, this study defined which bacteria are primarily influenced by GPS using the method of linear discriminant analysis effect size (LEfSe.) As shown in **Figure 8**, the quantities of Bacteroidales, Bacteroidia, Lactobacillales, bacilli, Enterococcus, Butyricicoccus, and Eisenbergiella in the GPS-H group were significantly elevated relative to the control group, and the amounts of Clostridiales, Lachnospiraceae, Ruminococcaceae, Anaerotruncus, and Caproiciproducens were significantly decreased within the GPS-H group vs. the control, which accounts for the differences observed in **Figure 5**. These results taken together suggest that GPS-H could alter specific intestinal microbiota composition, and this change could help shape a better gut barrier and immune system.

Administration of GPS Shows No Evidence of Toxicity

Commercial feed additives are rightly scrutinized for safety as well as efficacy, thus, this study also examined the toxicity of GPS on roosters. For this purpose, body weight was monitored

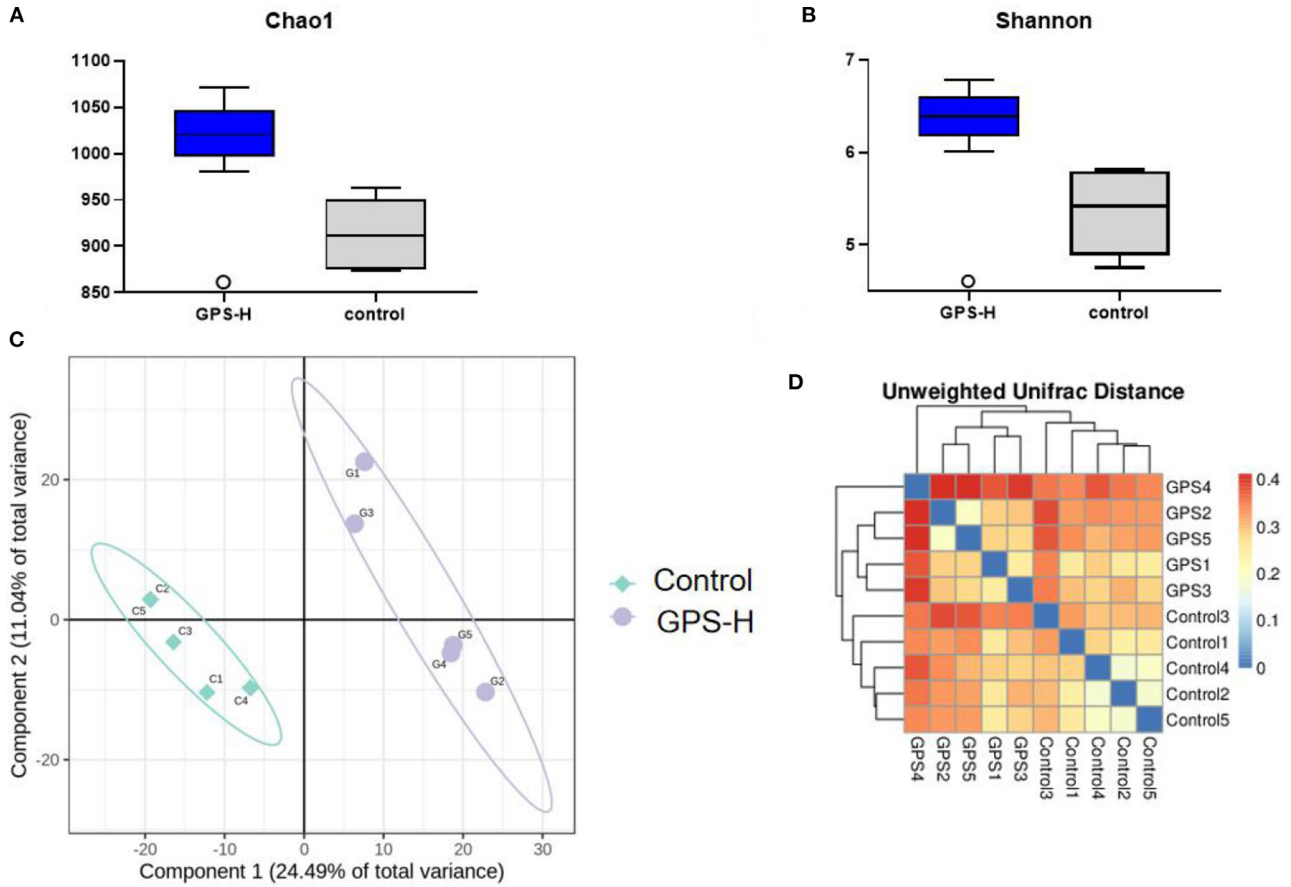

FIGURE 5 | Changes in gut microbes in GPS-H-treated and untreated layers. **(A)** Chao1 and **(B)** Shannon indices represent microbial richness and evenness, respectively, represents the change in the alpha diversity of gut microbes between the two groups of samples. And **(C)** principal component analysis (PCA) and **(D)** heat map relationship (the horizontal and vertical axes are the names of the samples, and the color depth represents the similarity between samples.) The analysis represents the beta diversity between each sample variety.

and the bursa of Fabricius, spleen, thymus, liver, and kidneys were examined to determine the potential toxicity of GPS. As shown in **Figure 9B**, there are no obvious pathological changes in the bursa of Fabricius, spleen, thymus, liver, or kidneys between the control and GPS-L, GPS-M, or GPS-H groups. Body weights all increased similarly; differences between the control and the three GPS groups (GPS-L, GPS-M, and GPS-H) are negligible, as illustrated in **Figure 9A**. These results indicate that GPS poses no toxicity as a feed additive for roosters.

DISCUSSION

Maintaining intestinal health and homeostasis is a complex balancing act influenced by many physiological factors in the interaction between the immune system, intestinal barrier, and intestinal microbiota (25). There are enormous quantities of bacteria living in animals' intestines, and differences in the composition of intestinal microbiota may dramatically alter the host's physiological and biochemical reactions, potentially destabilizing host homeostasis and general health (26). An animal's immune system recognizes and responds to the intestinal microbiota, which results in a moderate promotion of innate and adaptive immune pathways that reinforce the intestinal barrier and respond to invasive pathogens while maintaining tolerance to beneficial microbiota and antigens in food (27–29). These immune responses in the intestine help shape the intestinal microbiota composition by changing the nutrient substrates through mucus production or epithelial fucosylation (30). Thus, promoting the immune system, reinforcing the intestinal barrier, and improving intestinal microbiota are keys to enhancing animals' intestinal health. For the poultry farming industry, finding a potent feed additive to enhance animals' intestinal health is a useful strategy which can increase profits while lessening the risk of antibiotic resistant microbes threatening human health.

SIgA possesses many protective functions in the intestine, including as a defender to neutralize bacterial toxins in the gut lumen and disable viruses during transcytosis through the epithelial barrier (31). SIgA also inhibits abnormal epithelial cell

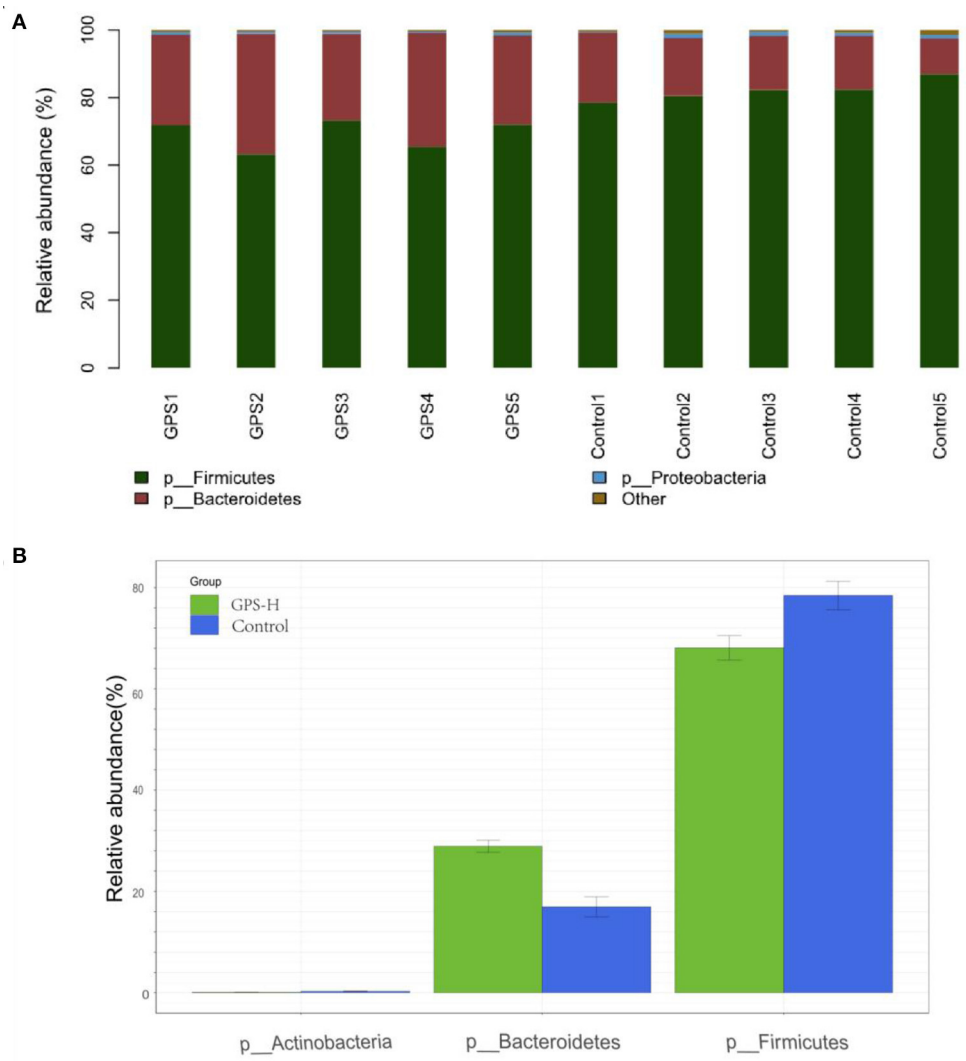

FIGURE 6 | Analysis of significant differences between two groups was analyzed using Metastats analysis, which compares multiple samples under two conditions to find the types of microorganisms that are significantly different in the two groups. Analysis of intestinal microbiota composition by phylum. **(A)** The specific intestinal microbiota composition in individuals in GPS-H and control groups. **(B)** The relative abundance of intestinal microbes between GPS-H and control groups.

translocation and excessive inflammatory responses induced by Shigella lipopolysaccharide (LPS) (32). In addition, sIgA can bind luminal bacteria into Peyer's patches (PPs) (33), which trains the immune system to tolerate beneficial bacteria and eliminate harmful bacteria (34). The present study verifies that GPS possess the ability to increase the sIgA content in the intestine, suggesting that GPS could promote roosters' intestinal health and beneficially alter intestinal microbiota. Goblet cells secrete mucus to protect the intestine and promote the expression of antimicrobial peptides that maintain intestinal homeostasis (20, 35). After treatment with GPS, secretion activity of goblet cells was significantly enhanced. This collective evidence leads to the conclusion that GPS are able to reinforce intestinal barrier health by increasing the content of sIgA and promoting the secretion activity of goblet cells.

Cytokines participate in the activation and derivation of immune cells, and thus are regarded as central to the immune system (36). Different cytokines exhibit diverse functions. They regulate the secretion of physiologically active substances and help maintain homeostasis. IL-2 and IL-4 are cytokines involved in appropriate immune responses and help avoid uncontrolled inflammation while promoting tissue repair (37). IL-1β and IFN-γ cytokines are able to protect the intestine from infection by triggering an immune response and preventing the spread of pathogens, respectively (38, 39). IL-2, a cytokine that can activate Tregs (T) cells and reinforce the inhibitory effect of Tregs on Teff, is also able to prevent the occurrence of spontaneous inflammation, and therefore plays a significant role in intestinal health (40). Our results show that GPS can promote the expression of IL-2, suggesting that GPS

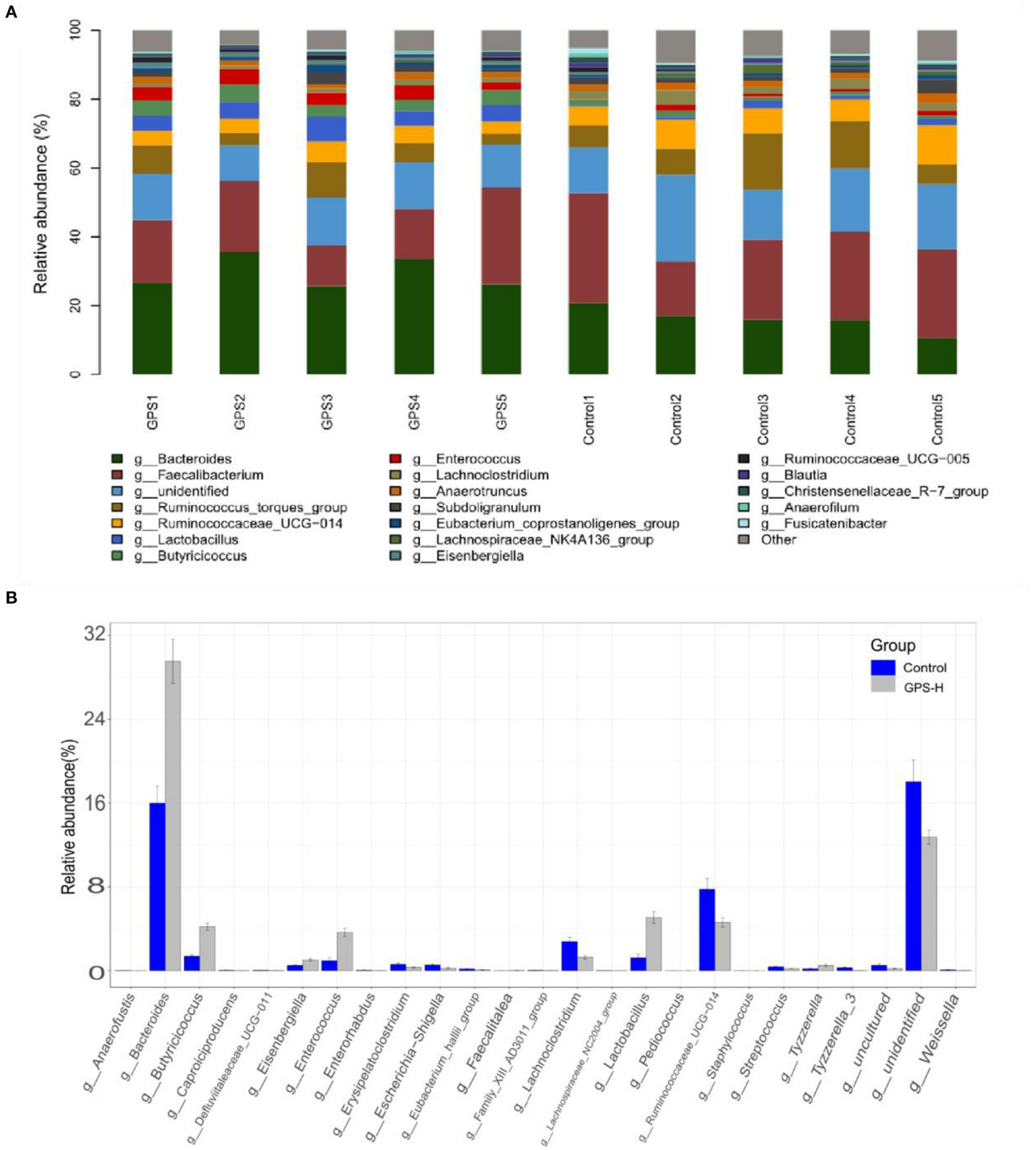

FIGURE 7 | Analysis of significant differences between two groups was analyzed using Metastats analysis, which compares multiple samples under two conditions to find the types of microorganisms that are significantly different in the two groups.The specific composition of intestinal microbiota by genus. **(A)** The intestinal microbiota structure of each individual in GPS-H and control groups and **(B)** the average relative abundances of those intestinal microbes.

may regulate intestinal inflammation. IL-4, a typical Th2-type cytokine, has a potent anti-inflammatory effect (41). IFN-γ, a Th1-type cytokine, also exerts a protective effect on the intestine (42). The ratio of IL-4 to IFN-γ reflects the balance between Th2 and Th1 immune responses. The results show that GPS can increase the production of both IL-4 and IFN-γ,

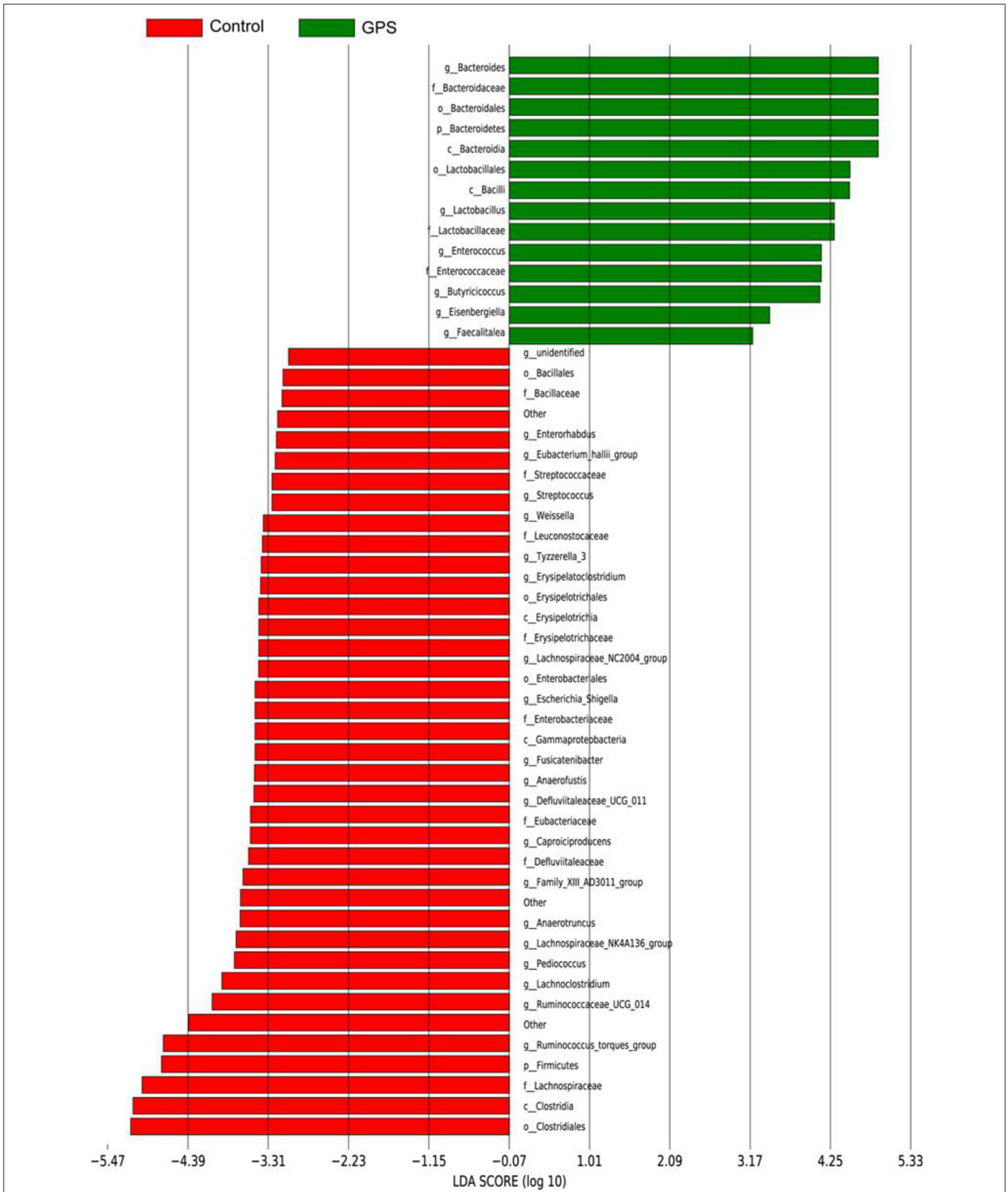

FIGURE 8 | The LDA Effect Size was used to analyze the comparison between the GPS-H group and the control group, and an intra-subgroup comparison analysis between the two groups was also performed to find substances with significant differences in abundance between the groups.

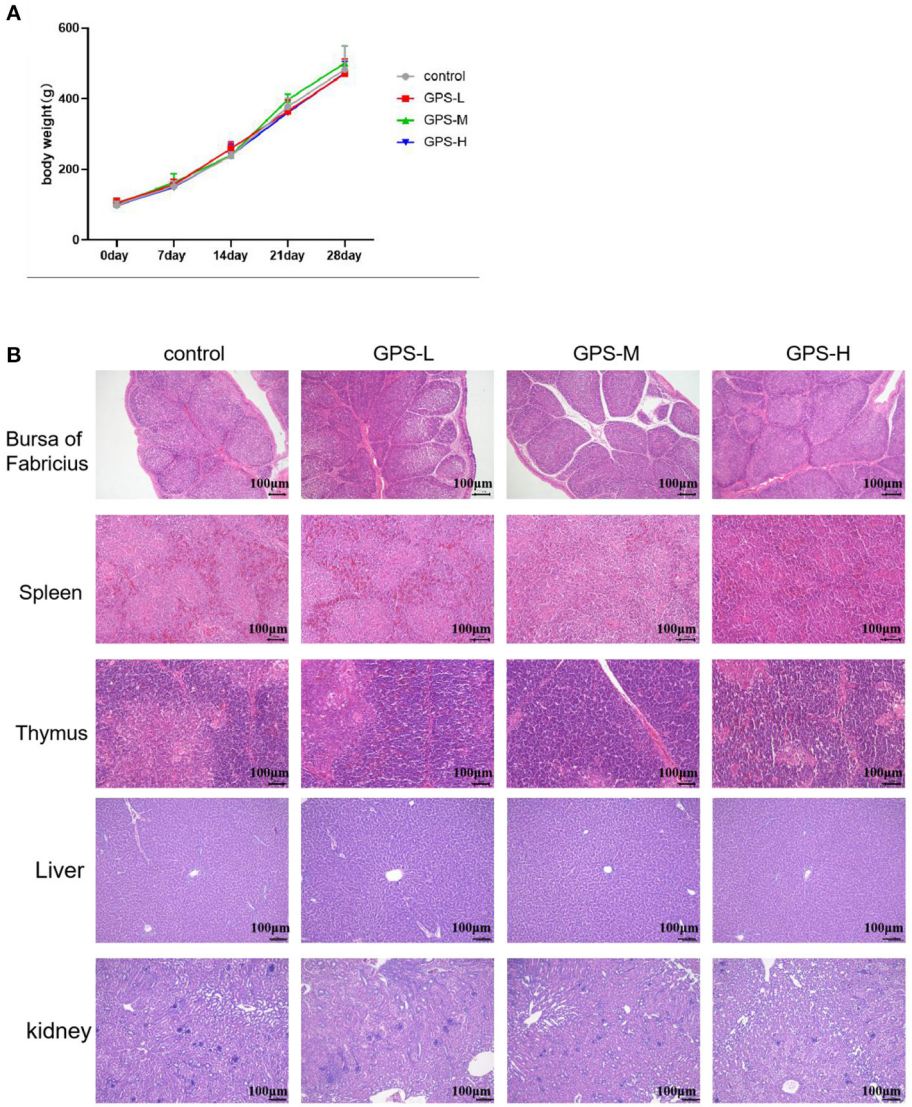

FIGURE 9 | Examination of potential toxicity of GPS on roosters. **(A)** The influence of GPS on body weight. **(B)** The influence of GPS on immune organs (bursa of Fabricius, spleen, thymus, liver, and kidneys) after 14 days (100 × magnification, 100 μm scale bar).

maintaining homeostasis in the intestine while boosting the overall immune response and promoting intestinal health. Having confirmed the effect of GPS on cytokine expression, we further explored whether immune cells in the intestine would be changed, and the proportion of CD4+ and CD8+ T cells were selected for this purpose. CD4+ and CD8+ T cells represent the Th1-type and Th2-type immune responses, respectively (43). The results showed that the numbers of both CD4+ and CD8+ T cells were increased after treatment with GPS, which is in agreement with the promotion effect on cytokine expression. Taken together, these results indicate that GPS can promote intestinal health by regulating the expression of cytokines and activation of CD4+ and CD8+ T cells while maintaining the homeostasis of Th1-type and Th2-type immune responses.

Given the interactions between sIgA, the immune system, and intestinal microbiota, our experiment further examined the effect of GPS on intestinal microbiota. It has been reported that sIgA can coat specific bacteria in the intestine, selectively enriching some members of the microbiota, as microbes vary in their propensity to acquire an sIgA coat when needed (44). Based on the increase of sIgA observed in our roosters treated with high-dose GPS (GPS-H), we further investigated the changes in these rooster's intestinal microbiotas. Many studies have concluded that the evenness and richness of intestinal microbiota are closely related to intestinal homeostasis, and the greater these measures, the more robust the immune response to pathogens (45). The results showed that GPS-H could increase both evenness and richness in the intestinal microbiota, suggesting that GPS-H could improve the host's

ability to maintain intestinal homeostasis and improve immune responses. Also of note, the results show that GPS-H altered the composition of the intestinal microbiota, significantly improving the proportion of Bacteroidetes in the intestine, which could be attributed to the increase in sIgA allowing more Bacteroidetes to outcompete other microbes (46). Bacteroidetes break down complex polysaccharides like GPS into components like SCFAs and ferulic acid that they can metabolize, which would explain the jump in SCFAs in the intestine after GPS treatment (47) (**Figures 2A–F**). From the genus analysis, we found six bacteria significantly increased in the GPS-H group: Bacteroides, Butyricicoccus, Eisenbergiella, Enterococcus, Ruminococcaceae, and Lactobacillus. Butyricicoccus has been reported to promote the accumulation of butyric acid in the intestine (48). Meanwhile, there is evidence that chickens with a higher proportion of Eisenbergiella in their intestines possess a better metabolism and more efficiently use amino acids, nucleotides, and short-chain fatty acids (49). Enterococcus is a beneficial bacterium which plays a role in decomposing food and promoting the absorption of nutrients (50). Ruminococcaceae is the main microorganism that converts primary bile acids into secondary bile acids, which are severely lacking in patients with ulcerative colitis. Supplementation of Ruminococcaceae reduced inflammation and symptoms of colitis in mice (51). Lactobacillus is beneficial in treating irritable bowel syndrome (IBS) and reduces inflammation (51). Conversely, Erysipelatoclostridium, Lachnoclostridium, and Escherichia–Shigella are typical pathogenic bacteria in the intestine, and were seen in lower proportions after GPS-H treatment, compared to the control group. This suggests that GPS-H can effectively reduce the proportion of harmful bacteria in the intestine. Over-all, GPS-H treatment is able to regulate roosters' intestinal microbial composition in a manner beneficial for the host. Furthermore, roosters treated with GPS-H exhibited no signs of drug toxicity, which makes it possible for GPS to be used as a novel feed additive.

CONCLUSIONS

GPS can improve intestinal health in three ways: improving the function of the intestinal barrier by increasing levels of sIgA and promoting goblet cell secretion, boosting the activation of the immune system by increasing the expression of cytokines and elevating levels of CD4+ and CD8+ T cells in the intestine while maintaining the homeostasis of Th1 to Th2 responses, and beneficially regulating the intestinal microbiota composition. These findings, combined with no evidence of toxicity, lead us to conclude that GPS shows promise as a novel feed additive and warrants further investigation as a substitute to prophylactic antibiotics in commercial poultry.

DATA AVAILABILITY STATEMENT

The original contributions presented in the study are included in the article/Supplementary Material, further inquiries can be directed to the corresponding author.

ETHICS STATEMENT

The animal study was reviewed and approved by Nanjing Agricultural University No. PZ2020101.

AUTHOR CONTRIBUTIONS

YiW: conceptualization, funding acquisition, project administration, and supervision. YuW: data curation, writing—original draft preparation, and visualization. CW and YueW: data curation. YC: writing—original draft preparation and methodology. TZ: methodology and editing. CD: methodology. NL: data curation and visualization. KD: reviewing and editing. AN and YH: writing—reviewing and editing. HZ, XW, and HL: data validation. PH: editing. CL: writing—reviewing. All authors contributed to the article and approved the submitted version.

FUNDING

This research was financially supported by the National Natural Science Foundation of China (NSFC, Grant No. 31872514 and 32172900), the Open Project Program of Bei-jing Key Laboratory of Traditional Chinese Veterinary Medicine at Beijing University of Agriculture (No. kf-tcvm202101), Yunnan Provincial Science and Technology Department-Applied Basic Research Joint Special Funds of Yunnan University of Chinese Medicine [2018FF001 (-020), 2019FF002(-012)], and a project funded by the Priority Academic Program Development of Jiangsu Higher Education Institutions (PAPD). We appreciate the assistances from our distinguished colleagues in the Institute of Traditional Chinese Veterinary Medicine of Nanjing Agricultural University.

ACKNOWLEDGMENTS

The author would like to express our sincere gratitude to Nanjing Agricultural University for providing reasonable experimental conditions and equipment. At the same time, thanks for the support of the above funding.

REFERENCES

1. Clavijo V, Florez MJV. The gastrointestinal microbiome and its association with the control of pathogens in broiler chicken production: a review. *Poult Sci.* (2018) 97:1006–21. doi: 10.3382/ps/pex359
2. Patra AK, Amasheh S, Aschenbach JR. Modulation of gastrointestinal barrier and nutrient transport function in farm animals by natural plant bioactive compounds - A comprehensive review. *Crit Rev Food Sci Nutr.* (2019) 59:3237–66. doi: 10.1080/10408398.2018.1486284
3. Conradie F, Diacon AH, Ngubane N, Howell P, Everitt D, Crook AM, et al. Treatment of highly drug-resistant pulmonary tuberculosis. *N Engl J Med.* (2020) 382:893–902. doi: 10.1056/NEJMoa1901814

4. Hooper LV, Macpherson AJ. Immune adaptations that maintain homeostasis with the intestinal microbiota. *Nat Rev Immunol.* (2010) 10:159–69. doi: 10.1038/nri2710
5. Aureli P, Capurso L, Castellazzi AM, Clerici M, Giovannini M, Morelli L, et al. Probiotics and health: an evidence-based review. *Pharmacol Res.* (2011) 63:366–76. doi: 10.1016/j.phrs.2011.02.006
6. Hendrickx AP, Top J, Bayjanov JR, Kemperman H, Rogers MR, Paganelli FL, et al. Antibiotic-driven dysbiosis mediates intraluminal agglutination and alternative segregation of Enterococcus faecium from the intestinal epithelium. *mBio.* (2015) 6:e01346–e01315. doi: 10.1128/mBio.01346-15
7. Bemark M, Boysen P, Lycke NY. Induction of gut IgA production through T cell-dependent and T cell-independent pathways. *Ann N Y Acad Sci.* (2012) 1247:97–116. doi: 10.1111/j.1749-6632.2011.06378.x
8. Cheng SL, Li X, Lehmler HJ, Phillips B, Shen D, Cui JY. Gut microbiota modulates interactions between polychlorinated biphenyls and bile acid homeostasis. *Toxicol Sci.* (2018) 166:269–87. doi: 10.1093/toxsci/kfy208
9. Aydin BD. Investigation of antibacterial effects of some medicinal plants and spices on food pathogens. *Kafkas Universitesi Veteriner Fakultesi Dergisi.* (2008) 14:83–7. doi: 10.9775/kvfd.2008.11-A
10. Chen M, Zhu J, Kang J, Lai X, Gao Y, Gan H, et al. Exploration in the mechanism of action of licorice by network pharmacology. *Molecules.* (2019) 24:2959. doi: 10.3390/molecules24162959
11. Li Y, Gong Y, Zhang X, Wang J, Cheng Y, Liu F, et al. Exploring the synergistic mechanism of Gegen Qinlian Decoction on the Wnt signaling pathway using an integrated strategy of network pharmacology and RNA-seq. *J Ethnopharmacol.* (2021) 278:114283. doi: 10.1016/j.jep.2021.114283
12. Hayama K, Takahashi M, Suzuki M, Ezawa K, Yamazaki M, Matsukawa T, et al. [Anti-Candida activity of aroma candy and its protective activity against murine oral candidiasis]. *Med Mycol J.* (2015) 56:J23–29. doi: 10.3314/mmj.56.J23
13. Wu Y, Yi L, Li E, Li Y, Lu Y, Wang P, et al. Optimization of Glycyrrhiza polysaccharide liposome by response surface methodology and its immune activities. *Int J Biol Macromol.* (2017) 102:68–75. doi: 10.1016/j.ijbiomac.2017.04.006
14. Ayeka PA, Bian Y, Githaiga PM, Zhao Y. The immunomodulatory activities of licorice polysaccharides (Glycyrrhiza uralensis Fisch.) in CT 26 tumor-bearing mice. *BMC Complement Altern Med.* (2017) 17:536. doi: 10.1186/s12906-017-2030-7
15. Wittschier N, Faller G, Hensel A. Aqueous extracts and polysaccharides from liquorice roots (Glycyrrhiza glabra L.) inhibit adhesion of Helicobacter pylori to human gastric mucosa. *J Ethnopharmacol.* (2009) 125:218–23. doi: 10.1016/j.jep.2009.07.009
16. Rozi P, Abuduwaili A, Ma S, Bao X, Xu H, Zhu J, et al. Isolations, characterizations and bioactivities of polysaccharides from the seeds of three species *Glycyrrhiza*. *Int J Biol Macromol.* (2020) 145:364–71. doi: 10.1016/j.ijbiomac.2019.12.107
17. Cheng A, Wan F, Wang J, Jin Z, Xu X. Macrophage immunomodulatory activity of polysaccharides isolated from *Glycyrrhiza uralensis* Fish. *Int Immunopharmacol.* (2008) 8:43–50. doi: 10.1016/j.intimp.2007.10.006
18. Aipire A, Yuan P, Aimaier A, Cai S, Mahabati M, Lu J, et al. Preparation, characterization, and immuno-enhancing activity of polysaccharides from *Glycyrrhiza uralensis*. *Biomolecules.* (2020) 10:159. doi: 10.3390/biom10010159
19. Rohe I, Vahjen W, Metzger F, Zentek J. Effect of a "diluted" diet containing 10% lignocellulose on the gastrointestinal tract, intestinal microbiota, and excreta characteristics of dual purpose laying hens. *Poult Sci.* (2020) 99:310–9. doi: 10.3382/ps/pez492
20. Knoop KA, Newberry RD. Goblet cells: multifaceted players in immunity at mucosal surfaces. *Mucosal Immunol.* (2018) 11:1551–7. doi: 10.1038/s41385-018-0039-y
21. Rauf A, Khalil AA, Rahman UU, Khalid A, Naz S, Shariati MA, et al. Recent advances in the therapeutic application of short-chain fatty acids (SCFAs): an updated review. *Crit Rev Food Sci Nutr.* (2021) 1—21. doi: 10.1080/10408398.2021.1895064
22. Lassenius MI, Fogarty CL, Blaut M, Haimila K, Riittinen L, Paju A, et al. Intestinal alkaline phosphatase at the crossroad of intestinal health and disease - a putative role in type 1 diabetes. *J Intern Med.* (2017) 281:586–600. doi: 10.1111/joim.12607
23. Abt MC, Artis D. The intestinal microbiota in health and disease: the influence of microbial products on immune cell homeostasis. *Curr Opin Gastroenterol.* (2009) 25:496–502. doi: 10.1097/MOG.0b013e328331b6b4
24. Wu C, Sartor RB, Huang K, Tonkonogy SL. Transient activation of mucosal effector immune responses by resident intestinal bacteria in normal hosts is regulated by interleukin-10 signalling. *Immunology.* (2016) 148:304–14. doi: 10.1111/imm.12612
25. Chen GY, Shaw MH, Redondo G, Nunez G. The innate immune receptor Nod1 protects the intestine from inflammation-induced tumorigenesis. *Cancer Res.* (2008) 68:10060–7. doi: 10.1158/0008-5472.CAN-08-2061
26. Mach N, Fuster-Botella D. Endurance exercise and gut microbiota: a review. *J Sport Health Sci.* (2017) 6:179–97. doi: 10.1016/j.jshs.2016.05.001
27. Schnupf P, Gaboriau-Routhiau V, Cerf-Bensussan N. Host interactions with Segmented Filamentous Bacteria: an unusual trade-off that drives the post-natal maturation of the gut immune system. *Semin Immunol.* (2013) 25:342–51. doi: 10.1016/j.smim.2013.09.001
28. Iweala OI, Nagler CR. The microbiome and food allergy. *Annu Rev Immunol.* (2019) 37:377–403. doi: 10.1146/annurev-immunol-042718-041621
29. Man AL, Gicheva N, Nicoletti C. The impact of ageing on the intestinal epithelial barrier and immune system. *Cell Immunol.* (2014) 289:112–8. doi: 10.1016/j.cellimm.2014.04.001
30. Pickard JM, Maurice CF, Kinnebrew MA, Abt MC, Schenten D, Golovkina TV, et al. Rapid fucosylation of intestinal epithelium sustains host-commensal symbiosis in sickness. *Nature.* (2014) 514:638–41. doi: 10.1038/nature13823
31. Keren DF, Brown JE, McDonald RA, Wassef JS. Secretory immunoglobulin A response to Shiga toxin in rabbits: kinetics of the initial mucosal immune response and inhibition of toxicity *in vitro* and *in vivo*. *Infect Immun.* (1989) 57:1885–9. doi: 10.1128/iai.57.7.1885-1889.1989
32. Boullier S, Tanguy M, Kadaoui KA, Caubet C, Sansonetti P, Corthesy B, et al. Secretory IgA-mediated neutralization of Shigella flexneri prevents intestinal tissue destruction by down-regulating inflammatory circuits. *J Immunol.* (2009) 183:5879–85. doi: 10.4049/jimmunol.0901838
33. Wang P, Li Y, Xiao H, Shi Y, Le GW, Sun J. Isolation of lactobacillus reuteri from Peyer's patches and their effects on sIgA production and gut microbiota diversity. *Mol Nutr Food Res.* (2016) 60:2020–30. doi: 10.1002/mnfr.201501065
34. Wu M, Xiao H, Liu G, Chen S, Tan B, Ren W, et al. Glutamine promotes intestinal SIgA secretion through intestinal microbiota and IL-13. *Mol Nutr Food Res.* (2016) 60:1637–48. doi: 10.1002/mnfr.201600026
35. Yang S, Yu M. Role of goblet cells in intestinal barrier and mucosal immunity. *J Inflamm Res.* (2021) 14:3171–83. doi: 10.2147/JIR.S318327
36. Ma X, Nakayamada S. Multi-source pathways of T Follicular helper cell differentiation. *Front Immunol.* (2021) 12:621105. doi: 10.3389/fimmu.2021.621105
37. Bartemes KR, Kephart GM, Fox SJ, Kita H. Enhanced innate type 2 immune response in peripheral blood from patients with asthma. *J Allergy Clin Immunol.* (2014) 134:671–8. doi: 10.1016/j.jaci.2014.06.024
38. Andoh A, Bamba S, Brittan M, Fujiyama Y, Wright NA. Role of intestinal subepithelial myofibroblasts in inflammation and regenerative response in the gut. *Pharmacol Ther.* (2007) 114:94–106. doi: 10.1016/j.pharmthera.2006.12.004
39. Monteleone G, Pender SL, Alstead E, Hauer AC, Lionetti P, McKenzie C, et al. Role of interferon alpha in promoting T helper cell type 1 responses in the small intestine in coeliac disease. *Gut.* (2001) 48:425–9. doi: 10.1136/gut.48.3.425
40. Shin MH, Kim J, Lim SA, Kim J, Kim SJ, Lee KM. NK Cell-based immunotherapies in cancer. *Immune Netw.* (2020) 20:e14. doi: 10.4110/in.2020.20.e14
41. Kucharzik T, Lugering N, Pauels HG, Domschke W, Stoll R. IL-4, IL-10 and IL-13 down-regulate monocyte-chemoattracting protein-1 (MCP-1) production in activated intestinal epithelial cells. *Clin Exp Immunol.* (1998) 111:152–7. doi: 10.1046/j.1365-2249.1998.00481.x
42. Jakobi V, Petry F. Humoral immune response in IL-12 and IFN-gamma deficient mice after infection with Cryptosporidium parvum. *Parasite Immunol.* (2008) 30:151–61. doi: 10.1111/j.1365-3024.2007.01013.x
43. Lee SK, Choi BK, Kim YH, Kang WJ, Kim KH, Sakaguchi S, et al. Glucocorticoid-induced tumour necrosis factor receptor family-related

receptor signalling exacerbates hapten-induced colitis by CD4+ T cells. *Immunology.* (2006) 119:479–87. doi: 10.1111/j.1365-2567.2006.02459.x
44. Nagatake T, Hirata SI, Koga T, Kuroda E, Kobari S, Suzuki H, et al. BLT1 mediates commensal bacteria-dependent innate immune signals to enhance antigen-specific intestinal IgA responses. *Mucosal Immunol.* (2019) 12:1082–91. doi: 10.1038/s41385-019-0175-z
45. Carbone EA, D'Amato P, Vicchio G, De Fazio P, Segura-Garcia C. A systematic review on the role of microbiota in the pathogenesis and treatment of eating disorders. *Eur Psychiatry.* (2020) 64:e2. doi: 10.1192/j.eurpsy.2020.109
46. Zhu W, Zhou S, Liu J, McLean RJC, Chu W. Prebiotic, immuno-stimulating and gut microbiota-modulating effects of Lycium barbarum polysaccharide. *Biomed Pharmacother.* (2020) 121:109591. doi: 10.1016/j.biopha.2019.109591
47. Sack EL, van der Wielen PW, van der Kooij D. Polysaccharides and proteins added to flowing drinking water at microgram-per-liter levels promote the formation of biofilms predominated by bacteroidetes and proteobacteria. *Appl Environ Microbiol.* (2014) 80:2360–71. doi: 10.1128/AEM.04105-13
48. Geirnaert A, Wang J, Tinck M, Steyaert A, Van den Abbeele P, Eeckhaut V, et al. Interindividual differences in response to treatment with butyrate-producing Butyricicoccus pullicaecorum 25-3T studied in an *in vitro* gut model. *FEMS Microbiol Ecol.* (2015) 91:fiv054. doi: 10.1093/femsec/fiv054
49. Zhang Y, Liu Y, Li J, Xing T, Jiang Y, Zhang L, et al. Dietary resistant starch modifies the composition and function of caecal microbiota of broilers. *J Sci Food Agric.* (2020) 100:1274–84. doi: 10.1002/jsfa.10139
50. Yehia HM, Hassanein WA, Ibraheim SM. Purification and characterisation of the extracellular cholesterol oxidase enzyme from Enterococcus hirae. *BMC Microbiol.* (2015) 15:178. doi: 10.1186/s12866-015-0517-2
51. Singh V, Yeoh BS, Abokor AA, Golonka RM, Tian Y, Patterson AD, et al. Vancomycin prevents fermentable fiber-induced liver cancer in mice with dysbiotic gut microbiota. *Gut Microbes.* (2020) 11:1077–91. doi: 10.1080/19490976.2020.1743492

Conflict of Interest: KD was employed by China Tobacco Henan Industrial Co. Ltd.

The remaining authors declare that the research was conducted in the absence of any commercial or financial relationships that could be construed as a potential conflict of interest.

Publisher's Note: All claims expressed in this article are solely those of the authors and do not necessarily represent those of their affiliated organizations, or those of the publisher, the editors and the reviewers. Any product that may be evaluated in this article, or claim that may be made by its manufacturer, is not guaranteed or endorsed by the publisher.

frontiers | Frontiers in Veterinary Science

ORIGINAL RESEARCH
published: 23 May 2022
doi: 10.3389/fvets.2022.875629

Enhanced Healing Activity of Manuka Honey and Nitrofurazone Composite in Full-Thickness Burn Wounds in the Rabbit Model

Muhammad Fakhar-e-Alam Kulyar[1,2,3], Khurram Ashfaq[3], Amjad Islam Aqib[4], Kun Duan[5], Muhammad Asif[6], Zeeshan Ahmad Bhutta[7], Muhammad Shoaib[8], Samina Shabbir[9,10], Shah Nawaz[11], Muhammad Aamir Naseer[3], Iqra Sarwar[3], Muhammad Akhtar[2], Ayesha Safdar Chaudhry[6], Riaz Hussain[12], Hafiz Iftikhar Hussain[13], Yi Wu[1] and Kun Li[1]**

[1] Institute of Traditional Chinese Veterinary Medicine, College of Veterinary Medicine, Nanjing Agricultural University, Nanjing, China, [2] College of Veterinary Medicine, Huazhong Agricultural University, Wuhan, China, [3] Department of Clinical Medicine and Surgery, University of Agriculture, Faisalabad, Pakistan, [4] Department of Medicine, Cholistan University of Veterinary and Animal Sciences, Bahawalpur, Pakistan, [5] China Tobacco Henan Industrial Co. Ltd., Zhengzhou, China, [6] Department of Surgery, University of Veterinary and Animal Sciences, Lahore, Pakistan, [7] Laboratory of Biochemistry and Immunology, College of Veterinary Medicine, Chungbuk National University, Cheongju, South Korea, [8] Key Laboratory of New Animal Drug Project, Gansu Province, Key Laboratory of Veterinary Pharmaceutical Development, Ministry of Agriculture, Lanzhou Institute of Husbandry and Pharmaceutical Sciences of Chinese Academy of Agricultural Sciences, Lanzhou, China, [9] Key Laboratory of Development and Application of Rural Renewable Energy, Ministry of Agriculture and Rural Affairs, Biogas Institute of Ministry of Agriculture and Rural Affairs, Chengdu, China, [10] Graduate School of Chinese Academy of Agricultural Sciences, Beijing, China, [11] Department of Pathology, University of Agriculture, Faisalabad, Pakistan, [12] Department of Pathology, Faculty of Veterinary Sciences, The Islamia University of Bahawalpur, Bahawalpur, Pakistan, [13] Department of Pathology, Cholistan University of Veterinary and Animal Sciences, Bahawalpur, Pakistan

OPEN ACCESS

Edited by:
Fazul Nabi,
Lasbela University of Agriculture, Water and Marine Sciences, Pakistan

Reviewed by:
Prerona Boruah,
Chinese Academy of Agricultural Sciences (CAAS), China
Montaser Elsayed Ali,
Al-Azhar University, Egypt
Awais Ihsan,
COMSATS University Islamabad, Pakistan

***Correspondence:**
Kun Li
lik2014@sina.com
Yi Wu
wuyi2001cn@163.com

Specialty section:
This article was submitted to Comparative and Clinical Medicine, a section of the journal Frontiers in Veterinary Science

Received: 14 February 2022
Accepted: 16 March 2022
Published: 23 May 2022

Citation:
Kulyar MF-e-A, Ashfaq K, Aqib AI, Duan K, Asif M, Bhutta ZA, Shoaib M, Shabbir S, Nawaz S, Naseer MA, Sarwar I, Akhtar M, Chaudhry AS, Hussain R, Hussain HI, Wu Y and Li K (2022) Enhanced Healing Activity of Manuka Honey and Nitrofurazone Composite in Full-Thickness Burn Wounds in the Rabbit Model. Front. Vet. Sci. 9:875629. doi: 10.3389/fvets.2022.875629

Burns cause many significant changes in metabolism and inflammatory reactions, leading to poor regeneration in animals and humans. A list of medicines to treat burns is available in the market. But due to the high cost of these medicines, these are unaffordable, especially for farmers of middle-class families of Africa and Asia. Therefore, a low-cost complementary treatment has always been a topic of many researchers, and there is a dire need of time for the welfare of animals to save them. The current study was planned to scrutinize the therapeutic effects of Manuka honey and Nitrofurazone ointments on full-thickness burn wounds in the rabbit model. The healing efficacy was performed through wound contraction rate, hematological analysis, the thickness of dermis and epidermis, and collagen content percentage. Histopathology was performed after taking biopsy samples at the end of the research. Based on statistical analysis using wound healing time (days, D), the combination (MO + NT) resulted in a shorter period (27 D ± 1) than the average healing time of controlled (36 ± 2), Manuka ointment (31.33 D ± 1.52), and Nitrofurazone ointment (32 ± 1). A significant decrease in the count of red blood cell (RBC), mean corpuscular volume (MCV), and mean corpuscular hemoglobin (MCH) in all treatments was noticed mainly in MO + NT. Furthermore, burns induced a significant difference ($p < 0.05$) in the white blood cells (WBCs) count levels in the MO-treated group. While the level of platelets (PLTs) was not significantly different from the healthy control group. Histopathological assessment (epithelialization, fibrosis, and angiogenesis) of skin showed burn healing to be better in MO and MO + NT groups. In conclusion, the composite of Manuka honey with Nitrofurazone led to the faster recovery than other treatments.

Keywords: Manuka, honey, Nitrofurazone, burns, natural remedies

INTRODUCTION

Skin is a coated barrier that protects internal organs from harsh environments. This barrier is essential for maintaining the homeostasis of body fluids, controlling temperature, and protecting the body from infection. The skin also has immunological, nervous, and metabolic functions (1, 2), devastating issues that affect such a barring ability (3). According to a study, wounds account for 30% of the total emergency caseload in veterinary healthcare centers (4). Animals (especially pets) with severe burns need immediate access to professional facilities. Such modern resuscitation and emergency burn therapies are designed to mitigate systemic changes caused by the sudden destruction of skin barriers, but unfortunately, these facilities are not available in the developing countries of Asia and Africa. The majority of burns is unintentional that occurred at veterinary clinics, relating to the use of adjunct heat to reduce the risk of developing hypothermia. Veterinarians often encounter burns that are <20% of the animal's body surface. Thus, severe metabolic disturbances, such as electrolyte levels imbalances, red blood cells destruction, and high susceptibility toward systemic infection, might not be seen (5). But the use of such animals as a model is still a viable option in overall healthcare in translational medical studies (6). A list of medicines to treat burns, i.e., Nitrofurazone and silver sulfadiazine, is available in the markets. But due to the high cost of these medicines, most people cannot afford them. Hence, more traditional herbal products have been used in African and Asian middle-class families (7). According to the WHO statistics, 265,000 deaths annually occur due to burning, most of which happen in these regions (8). The herbal products used by these people seem moderately effective, less toxic, and less expensive than other market products. Honey has been used in folk medicine for a long time, but it has only recently been discovered by medical researchers that it can be used to treat both acute and long-term wounds.

Traditionally, honey has been used to treat burns (9) due to its antimicrobial properties, especially to cover up burn wounds. It has been shown to inhibit a wide spectrum of bacteria and is as efficient against antibacterial drugs resistant bacteria (10–12). Interestingly, one of the earliest experiments of honey's efficiency against antibiotic-resistant was conducted, using Manuka honey to treat a hydroxyurea-induced leg ulcer colonized by methicillin-resistant Staphylococcus aureus (MRSA). This research established that honey has antibacterial capabilities against resistant bacteria and may also aid in the healing process of wounds (13). Such antibacterial action of honey is due to its acidity, hydrogen peroxide contents, osmotic effects, nutritional and antioxidant contents, stimulation of immunity, and unidentified compounds (14). Generally, honey has glucose, maltose, sucrose, fructose, water, and a few other things, such as amino acids, organic acids, proteins, vitamins, acetylcholine, and flavonoids (15). Many scientific studies have been urged on its medicinal properties in Ayurvedic, Chinese and Roman traditions (14). Manuka honey is the purest form of unifloral honey that is derived from Manuka trees and Leptospermum scoparium, belongs to the family Myrtaceae in New Zealand and the Eastern region of Australia (16). It is dark honey as compared to other honey types. It contains the highest concentration of phenolic and flavonoid compounds (pinobanksin, pinocembrin, and chrysin) that have been identified as having potent reactive oxygen species (ROS) scavenging activity (17). Flavonoids polyphenolic compound is a group of secondary metabolites that naturally occur in the plant kingdom that possesses numerous pharmacological activities (18).

Nitrofurazone (C6H6N4O4) is a commercially available product used as an antimicrobial agent on different wounds, especially burn wounds (19). It has been reported to show bactericidal activity against many gram-positive and gram-negative bacteria, inhibiting bacterial enzymes involved in carbohydrate metabolism. It exhibits bactericidal activity against most pathogens that commonly cause surface skin infections (20). But Nitrofurazone (NT) therapy has a limit on its low aqueous solubility. The poor solubility of NT urges a slow-release rate, causing less penetration of an effective drug concentration into the skin. Moreover, due to its high permeability through the skin, NT remains for a limited time at the applied area (21). Others include sensitivity, itching, contact dermatitis, and longer time period (8).

The current experimental study explored the effects of topical application of Manuka honey ointment on full-thickness burns, in comparison with commercially available Nitrofurazone at the thoracoabdominal regions of rabbits. The evaluation parameters, such as healing time, contraction rate, hematological, and histopathological assessment, were compared with untreated thermally injured rabbits.

MATERIALS AND METHODS

Treatment Preparations

The Manuka honey (batch no. GMH4765; lot no. KMH15816) was purchased from an online store, while Nitrofurazone was purchased from a local market. According to our one pilot project, all treatments were prepared according to their minimum effective levels. 1% Manuka honey ointment (MO), 1% Nitrofurazone ointment (NT), and 1% of their combination (MO + NT) were prepared by mixing them with 99 g of petroleum jelly. The quantity of both treatments was calculated on the base of their total percentage and purity. The final form of concerning ointments was then stored in the plastic bottles.

Induction of Burn Wound

The ethics committee of the University of Agriculture Faisalabad, Pakistan approved this work (DGS/39257-60), in accordance with institutional and national guidelines. The nine rabbits from three different groups (MO, NT, MO + NT) were anesthetized by injectable anesthesia with xylazine (4 mg/kg) and ketamine hydrochloride at a dose rate of 35 mg/kg intramuscular (22). The thoracoabdominal side of the skin was shaved, and burn wounds were created using a metal plate (with a 10-mm diameter) heated at 100°C on an

Abbreviations: PC, positive control; NS, normal saline; MO, Manuka; NT, Nitrofurazone; MO + NT, Manuka + Nitrofurazone.

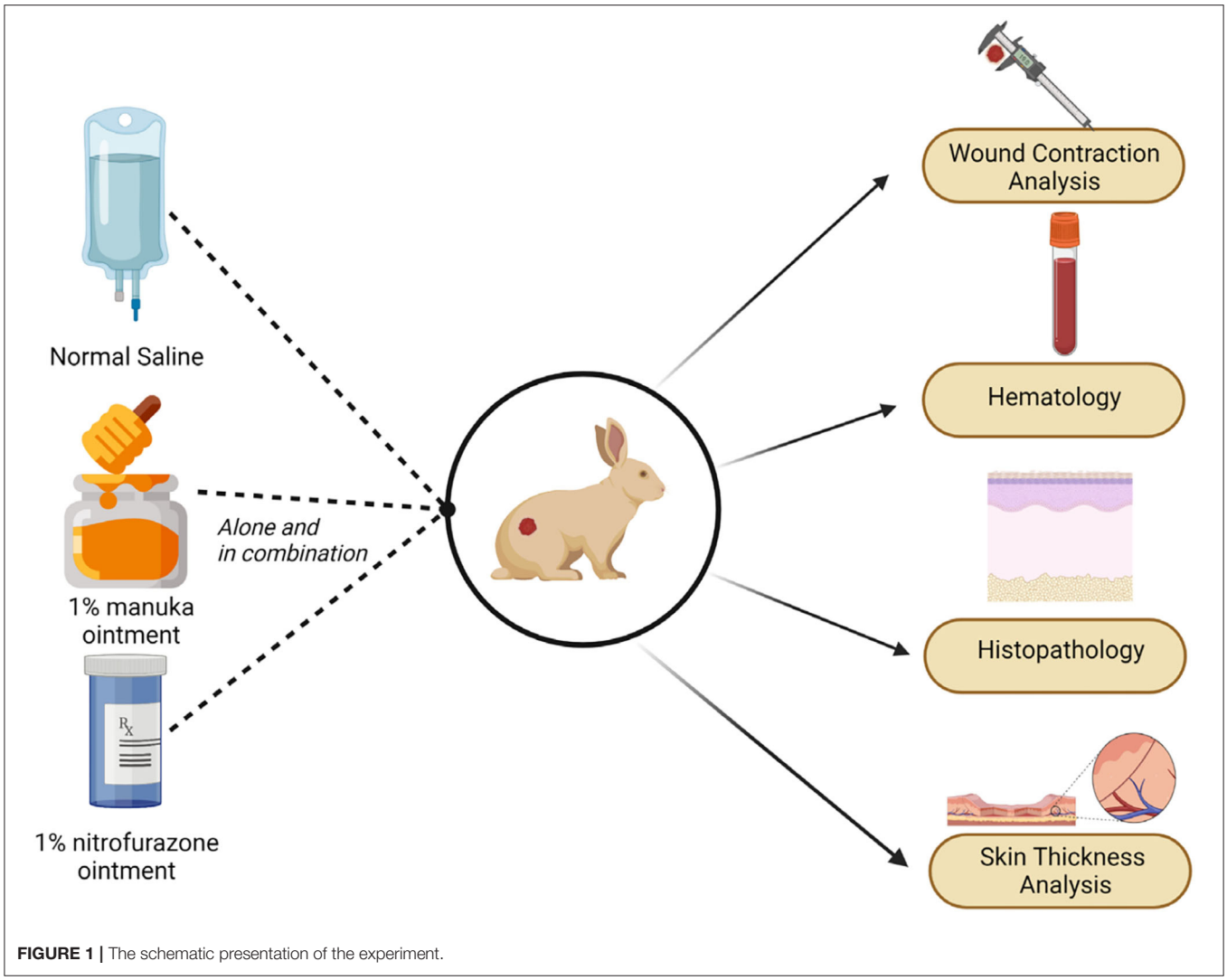

FIGURE 1 | The schematic presentation of the experiment.

open flame of a Bunsen burner with equal pressure over the shaved area (23). After creating wounds, Ketoprofen (1 mg/kg) was injected as an analgesic to the rabbits (24). The administration of analgesic was performed for the next 3 days in order to attain an equal immune response for each individual.

Experimental Design

Fifteen male healthy rabbits (8–10 weeks old) weighing 1,500 g ± 20 g were randomly allocated to five treatment groups. Each treatment group was comprised of three rabbits. The acclimatization period of 3 days was provided to rabbits with the same conditions of environment and feeding in order to attain equal immune response for each individual. Rabbits were divided as follows: NS (negative control) received no treatment, PS (positive control) was allocated to normal saline, whereas MO (Manuka honey ointment), NT (Nitrofurazone ointment), and MO + NT were treated topically twice a day (**Figure 1**). The healing efficacy was performed through healing time, wound contraction rate, and hematological analysis on days 0, 7, 14, 21, and 28. Histopathology was performed after taking biopsy samples at the end of the research. All rabbits were fed pelleted food with *ad libitum* water throughout the experiment and were housed in the animal experimentation unit.

In the preliminary test, the wound stopped increasing on the fourth day. Therefore, the observation period was set from days 0 to 4 after the injury (**Figure 2A**). After topical application of treatments, the wound was carefully covered with a bandage (**Figure 2B**).

Measurement of Parameters

Healing Time

Healing time was considered from the time of wound induction to re-epithelialization. All the observations were estimated randomly (7, 14, 21, and 28) until the scar fell off (25).

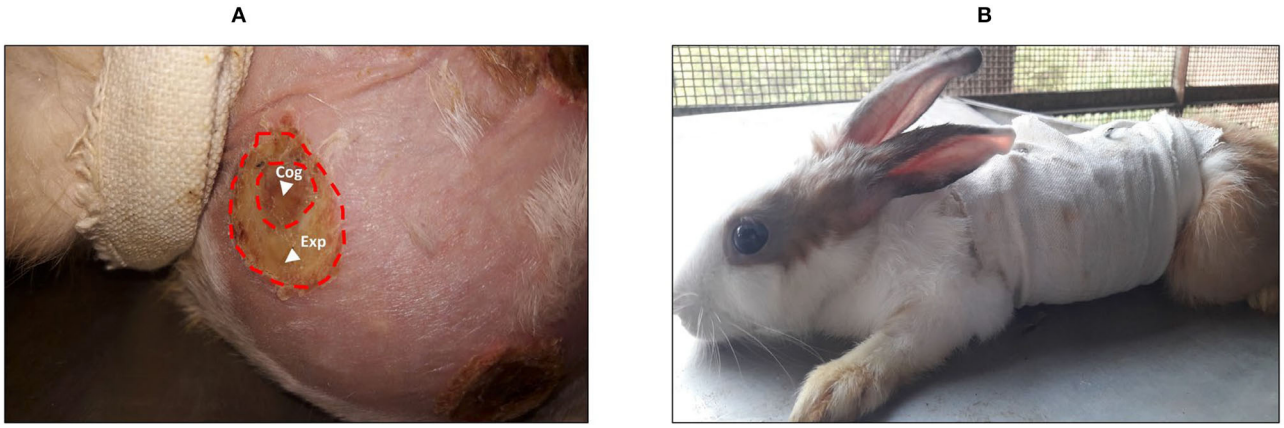

FIGURE 2 | (A) Burn wound with the area of expansion that reveals a white color when compared with the coagulation zone. **(B)** A rabbit in a bandage after treatment protocol. Cog, coagulation zone; Exp, expansion zone.

Wound Contraction Rate

The wound healing was examined by digital photography every seventh day under general anesthesia (26). While the contraction rate percentage was determined by the following formula (27).

$$Contraction\ \% = \frac{\left[Area\ on\ day\ zero\ \ (mm) - Area\ on\ day\ measurement\ \ (mm)\right]}{Area\ on\ day\ zero\ \ (mm)} \times 100$$

Hematological Analysis

Hematological analyses were accessed (0, 7, 14, 21, and 28) to compare the relative success rate of treatment groups (28).

Histopathological Analysis

Histopathological analyses were performed to compare the relative healing rate for different treatments. The parameters (thickness of the epidermis and collagen content) were evaluated during the histopathological examination, in which a tissue sample was collected at the wound site (at the end of the research). The different percentages were measured to indicate the degree of compression and orientation of the collagen fibers. Cells that are part of the immune system were also examined in the tissue that had been treated.

Statistical Analysis of Data

All statistical data analyses were carried out using ANOVA through SPSS statistical computer software (version 25.00). The recovery rates observed for various groups were compared using the independent sample *t*-test. The statistical significance level was set < 0.05.

RESULTS

Healing Time

According to the *t*-test analysis, it is inappropriate to compare the values of two or more groups. Therefore, we performed ANOVA and *post-hoc* tests among four groups. The range of healing of full burns in the combination group was significantly different, and the frequency of treatment was also significantly improved. Rabbits were better in the first 2 weeks after that healing was gradually becoming better among different groups e.g., Manuka honey, Nitrofurazone, and the control group. The MO + NT resulted in a shorter period (27 D ± 1) than the average healing time of controlled (36 ± 2), MO (31.33 D ± 1.52), and NT (32 ± 1) (**Figure 4A**). Rabbits treated with the combination had significantly more prophylactic effects than untreated rabbits. Significant healing ornamentation ($p < 0.05$) within 14 days was noticed in two treatment groups (MO + NT and MO). There was also a significant reduction ($p < 0.05$) of wound size on day 7 in treated animals as compared to control group.

Wound Contraction Rate

The frequency of wound closure was higher in the groups that were treated with combination in rabbits. On day 14, rabbits of "MO + NT" group showed better granulation tissue formation. After 21 days, "MO + NT" showed remarkable healing and scarring (**Figure 3A**). The significance levels of "MO + NT" among other treatments, such as Manuka honey and Nitrofurazone, were 0.026 and 0.012, respectively. While the significant level with the control group was 0.00. Similarly, in the individual comparison of Manuka honey ointment with "MO + NT" and Nitrofurazone, the significance levels were 0.026 and 0.94, respectively (**Figures 3B,C**).

In the initial days, the wound area of all groups was increased. The enlarged area showed a bright white color as compared to the burned area. This area was white and became necrotic, corresponding to a stasis area. On the second day, the wound area of all groups continued to increase, and the new expansion area appeared white as compared to the coagulated site. On day 3, all groups formed a full red ring around the edges of the wound. This area corresponds to the hyperemic area, indicating increased blood flow. On the fourth day, all the wounds stopped expanding. All groups showed almost identical properties, but the MO + NT group showed intense redness at the wound's edges. The MO and the NT formed a scar at the edge of the wound.

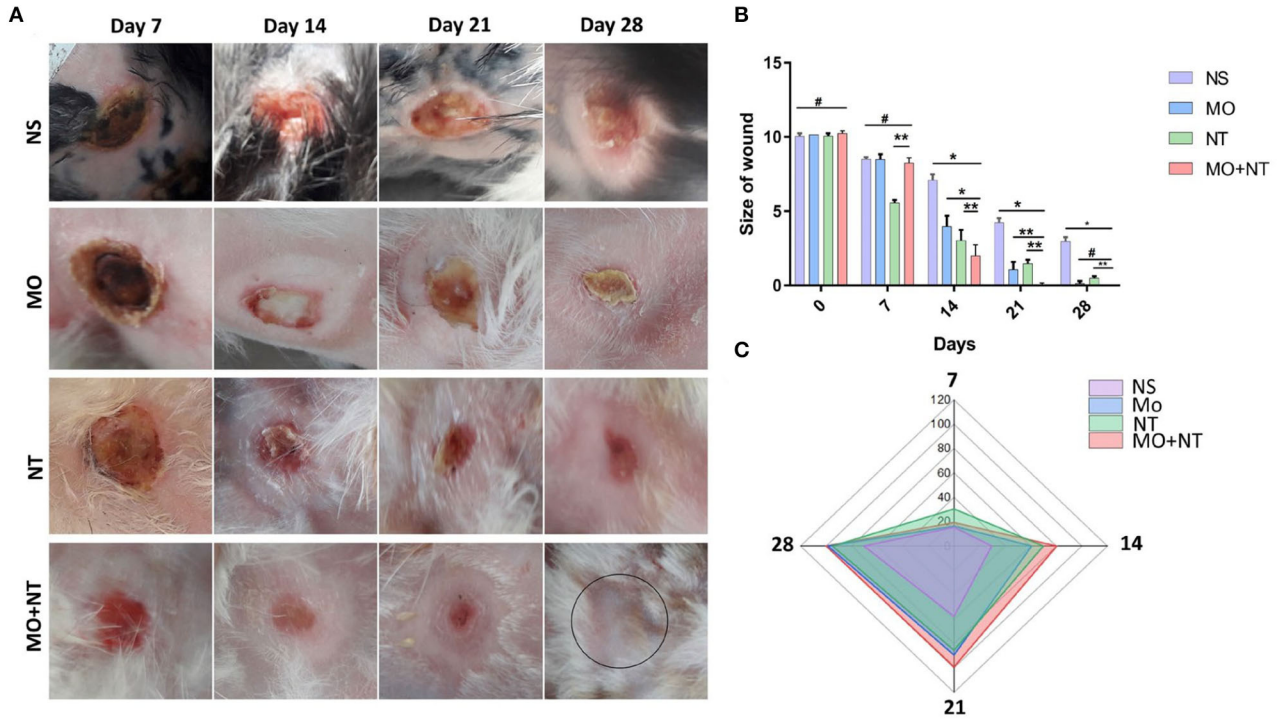

FIGURE 3 | (A) Digital photographs of wounds taken on different days (7, 14, 21, and 28). NS, normal saline; NS, normal saline; MO, Manuka honey ointment; NT, Nitrofurazone ointment; MO + NT, Manuka honey + Nitrofurazone. **(B)** Size of wounds, **(C)** contraction rate percentage (*p < 0.05, **p < 0.01, #p > 0.05).

Hematological Analysis

A significant decrease in RBC count, mean corpuscular volume (MCV), and mean corpuscular hemoglobin (MCH) on days 7, 14, 21, and 28 was noticed, except for MO + NT in all treatments. Furthermore, burns induced a significant difference ($p < 0.05$) in the WBCs count levels in the MO + NT treated group. The level of platelets (PLT) was not significantly different from the healthy control group (**Figure 4**). As it depends on heat damage and an increased level of lymphocytes. So, the number of neutrophils and eosinophils did not change as compared to the control group.

Histopathological Analysis

A histopathological examination of different treatments was analyzed. For this purpose, the epidermis, dermis, upper dermis, lower dermis, sweat glands, sebaceous glands, newly formed blood vessels, granular tissues or granulation, hair follicles, fibrous tissue or collagen fibers, and keratin layer were investigated. Our findings in the positive control showed that the keratin layer was absent, the epidermal closure was not firm, and dermal differentiation between the upper and lower layers was not evident. There were no glandular structures in the epidermis, only a few blood vessels and collagen fibers could be seen in the lower epidermis, which indicated a much slower repair process. In the "MO" group, the glandular structures of the skin were recovered but comparatively had fewer collagen fibers and angiogenesis than those of the group "MO + NT." Moreover, keratinocytes and epidermal thickness were not fully restored. In the "NT" group, an incomplete keratin layer with ongoing re-epithelization was noticed. The glandular portion of the epidermis was not fully developed, but sweat and sebaceous were evident. Finally, we checked the "MO" and "NT" groups. Here, we found that all the structures were fully recovered with more collagen, angiogenesis, and keratin layer. The thickness of the epidermis was equal to the negative control group while tissue granulation was also optimum, indicating excellent treatment results (**Figure 5**).

The Thickness of Epidermis

Wounds treated with "MO + NT" were found to have a higher epidermis thickness than other treatments. Concerning the epidermal thickness, all three treatment results were analyzed. It was concluded that the wounds treated with "MO + NT" had a better epidermal thickness of 151.92 μm. The result was much better in contrast to those who were treated with Manuka honey and Nitrofurazone alone. Therefore, the combination was proved to be more significant ($p < 0.05$). The honey ointment results were also better than control in epidermal thickness (**Figure 6**).

Collagen Content Percentage

Tissue samples were analyzed in the laboratory on the 28th day. "MO + NT" wounds were found to have higher collagen ($p < 0.05$) content as compared to the other wounds treated with Manuka honey and Nitrofurazone ointments. While the

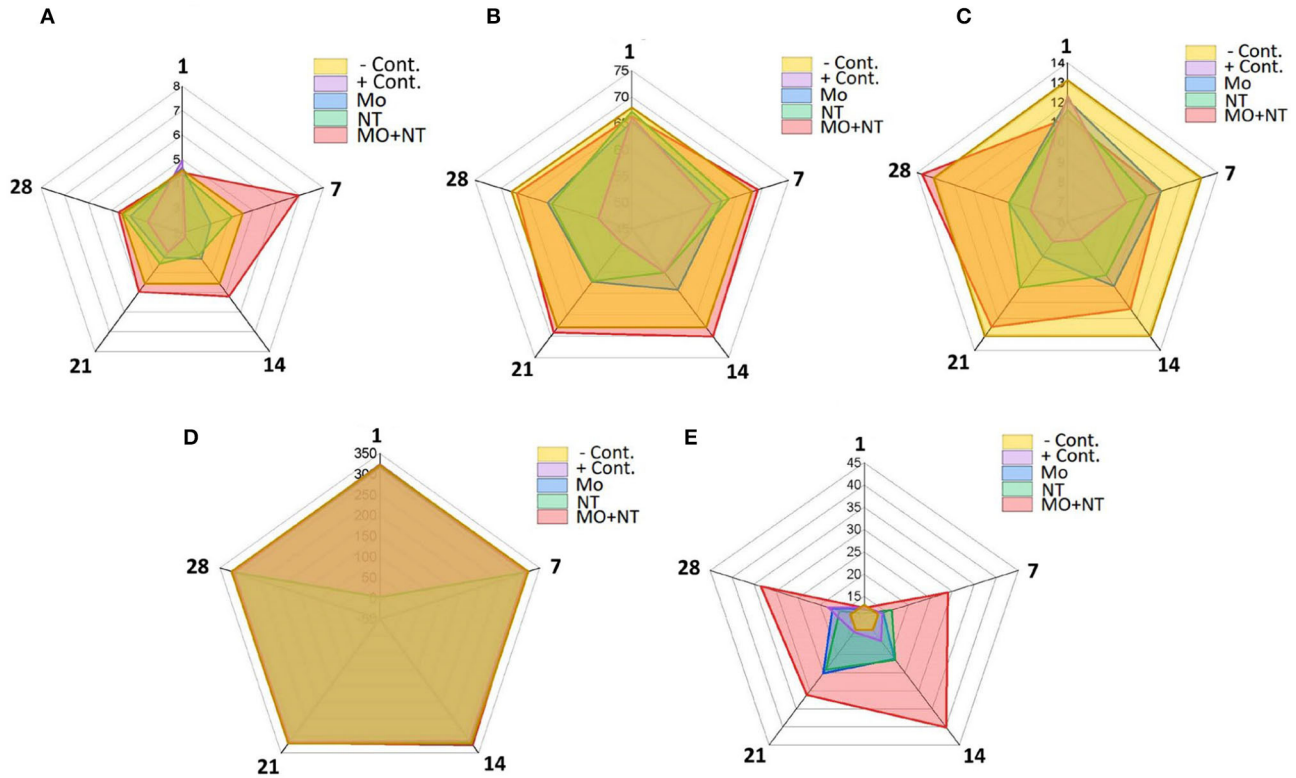

FIGURE 4 | Hematological changes at different days (1, 7, 14, 21, and 28). **(A)** Ref blood cell (RBC) (10^{12}/l), **(B)** MCV (Fl), **(C)** MCH (pg), **(D)** PLT (10^{9}/l), and **(E)** white blood cell (WBC) (10^{9}/l).

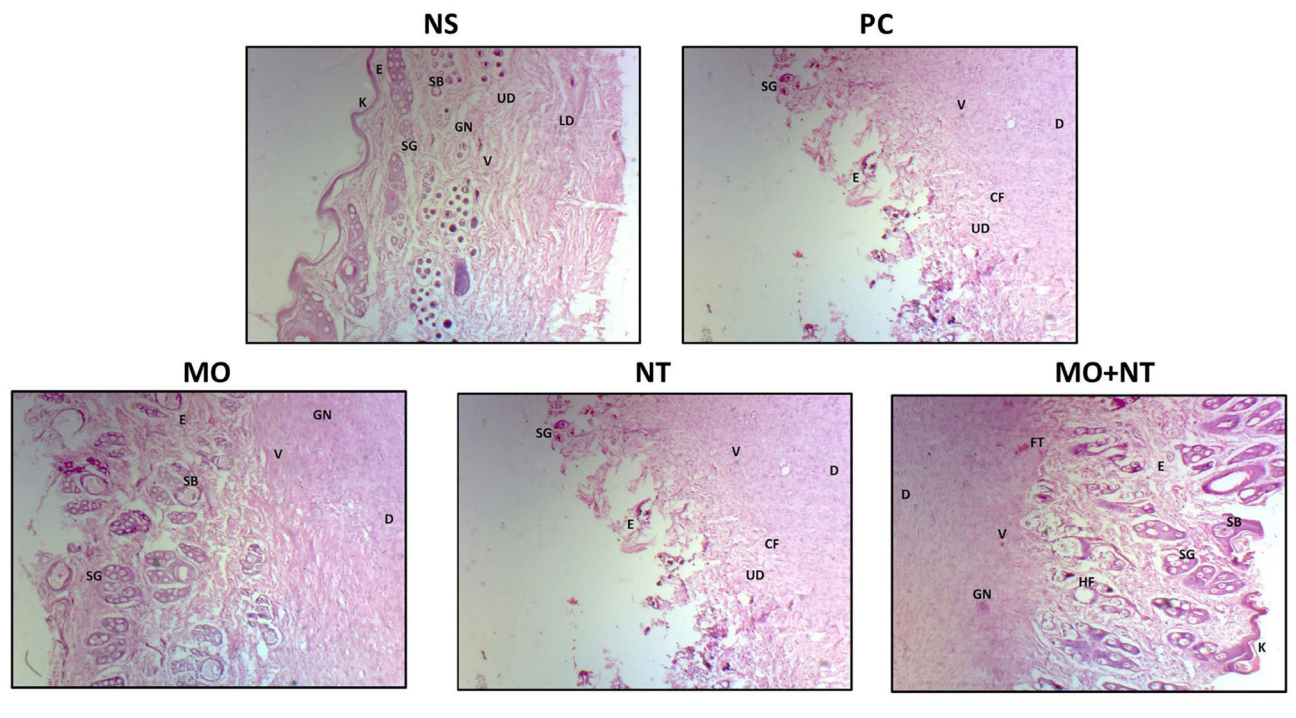

FIGURE 5 | Histopathology of different treatments. E, epidermis; D, dermis; UD, upper dermis; LD, lower dermis; SG, sweat glands; SB, sebaceous glands; V, newly farmed blood vessels; GN, granular tissues or granulation; HF, hair follicle; FT, fibrous tissue or collagen fibers (Cf); K, keratin layer.

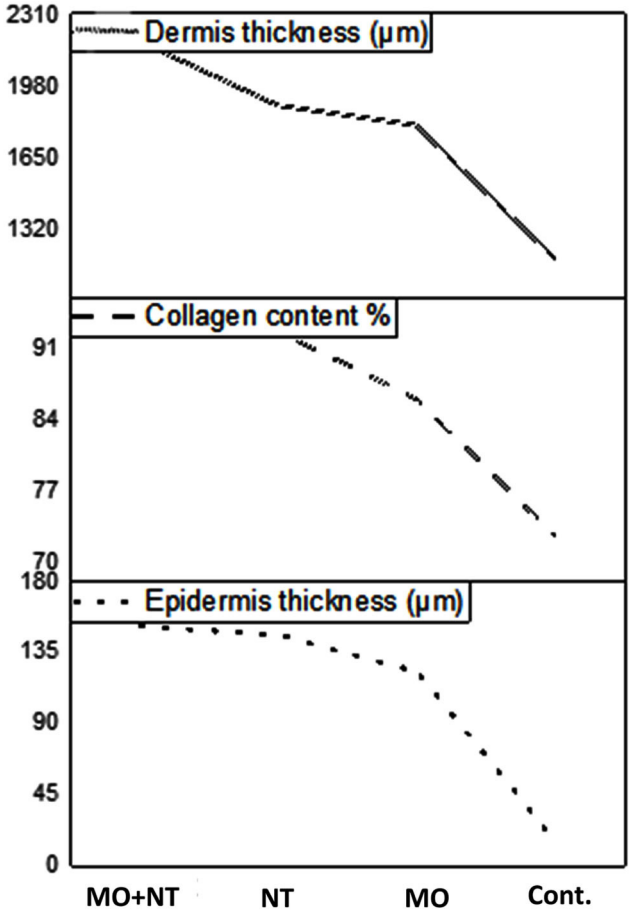

FIGURE 6 | Dermis, epidermis, and collagen analyses of different treatments.

wounds with no treatment had loose arrangements of collagen and minimal vascularization.

The Thickness of Dermis

After careful examination, it was noticed that "MO + NT" has a better dermis thickness than other treatments. Statistically, G_3 showed a significant ($p < 0.05$) improvement in the dermis as compared to the other three treatments.

DISCUSSION

The skin is the largest organ in the body that performs many important functions, e.g., homeostasis, body temperature, immunity, nervous sensations, and metabolism. The skin also acts as a physical barrier against infections (29). If this barrier is damaged, pathogens can penetrate directly into the body. Several studies have shown that burns are the leading cause of death with severe burns. Therefore, many researchers have sought to develop appropriate treatments to reduce the risk of wound infection and reduce the duration of treatment for burn injuries. These treatments include topical antimicrobials that effectively reduce mortality (30, 31), with low toxicity and sensitivity (32, 33). However, the occurrence of reactions related to allergies, toxicity, and irritation reduces skin regeneration ability, which can minimize their efficacy (29, 34). For example, the Nitrofurazone is one of the commonly used antimicrobial agents against gram-positive and gram-negative bacteria. As a consequence of its action, Nitrofurazone breaks down ribosomal proteins and some other macromolecules, which slow down the production of proteins, DNA, and RNA and stop the cellular proliferation. Additionally, it may impair bacterial cells' aerobic metabolism and carbohydrate metabolism activities (35). Meanwhile, oxidative processes produce reactive superoxide and hydroxyl radicals (36). Despite the fact that these actions take place in milliseconds or less, they have the potential to be harmful if left uncontrolled (34). As a result, the second choice is to employ natural products, which have been used since ancient times. These products are less toxic and cheaper than synthetic drugs. It has been shown that many plants and plant products effectively heal wounds. Nowadays, most drugs are a mixture of several plants or herbs, but these traditional ointments are not scientific. Using medicinal herbs has been noticed in the therapy of wounds from the very beginning due to its reduced financial load and its medical effects. Our study results are in line with the results of Bischofberger et al. (37). Where Manuka honey provided a protective barrier over the wound in preventing microbial infection. Its immunological activity accelerates wound repair and anti-inflammatory effects (38). Some other factors and bioactive components have also been involved that trigger the direct and indirect actions against the bacteria in wound repair (14). A 5.8 kDa bioactive component of Manuka honey has been identified as responsible for stimulating monocyte activity by activating the toll-like receptor 4 (TLR4). Activation of TLR4 and subsequently the intracellular signaling pathway nuclear factor kappaB (NF-κB) enhance the production of interleukin-1β (IL-1β), interleukin-6 (IL-6), and tumor necrosis factor-α (TNF-α), which are important in regulating the inflammatory response (39) (**Figure 7**).

Besides being able to reduce Cyclooxygenases 1 (COX-2) expression, Manuka honey can also have an antioxidant effect by changing the production of ROS and phenolic compounds (17). This is because of the production of ROS and other compounds.

Methylglyoxal is another active antibacterial ingredient of Manuka honey, which has been reported to react with lysine, arginine, and cysteine residues of structural proteins, such as collagen. Further it gives genesis to advanced glycation end products (AGEs). It promotes fibrosis in chronic tissue infections, impairs immune response microcirculation, promotes atherosclerosis and neovascularization, induces endothelial cell dysfunction, and impairs wound closure (40). Our study results are in line with the results of Bischofberger et al. (37), in which Manuka honey was found effective in experimental equine wounds in minimizing the wound area by decreasing retraction and overall healing time. The mechanism p38 is evolved during wound repair through Manuka honey. This mechanism

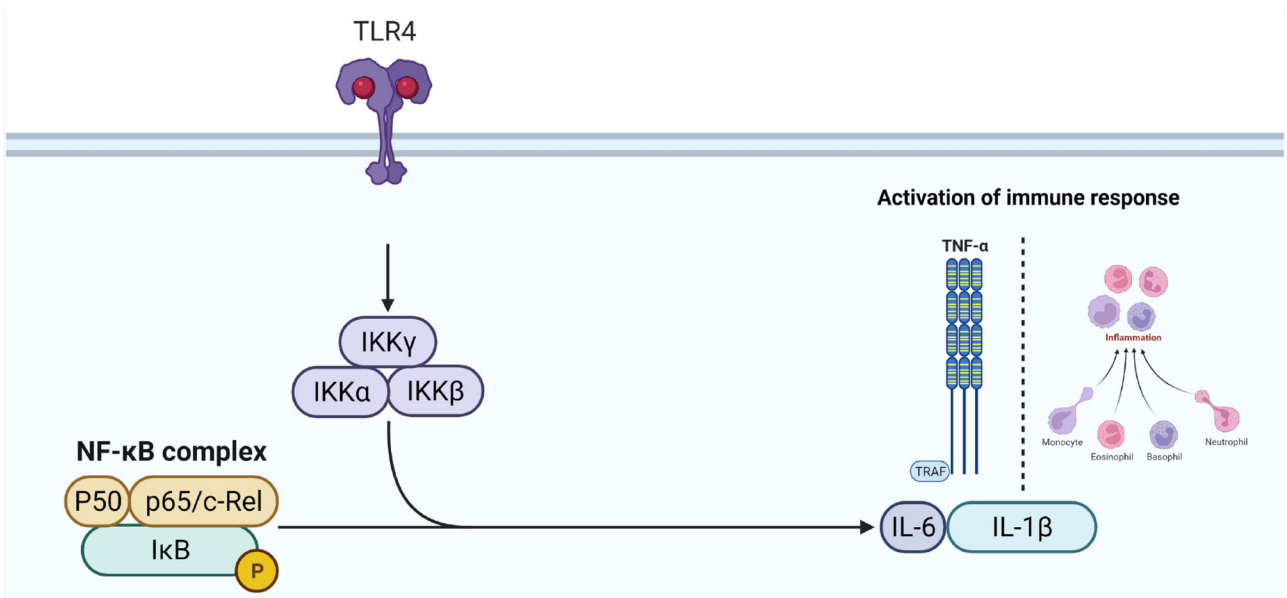

FIGURE 7 | Mechanism insight of Manuka honey in the activation of inflammatory response.

mediates the stimulation of locomotion and proliferation by plate derivative growth factor (PDGF), the main growth factor in the early phases of wound healing (41). Our study is also in line with study of Moore et al. (42), who reviewed previous randomized controlled trials comparing honey with different treatments. Moore et al. concluded that honey is a useful treatment for burns.

The results of this study give a free hand to the companies to start the formation of medicines in the form of ointments or creams. We hope that a new burn ointment or cream can be used with herbal medicines, which will help to decrease the healing period and hypertrophic scar rate.

CONCLUSION

Manuka honey ointment may provide an alternative medication for managing extensive burns. However, there are some regulatory barriers to introducing a new product containing just honey. Therefore, changing attitudes toward clinical practice might take longer due to these barriers. Such prominent factors may decrease the acceptability of such treatment option. Hence, to address such acceptability concerns, the therapeutic options must be in combination with allopathic medications. It would place more emphasis on promoting the acceptability and would be helpful in providing a better option throughout the globe. Moreover, further research with randomized prospective is also needed to fully elucidate MO's effect on burns.

DATA AVAILABILITY STATEMENT

The original contributions presented in the study are included in the article/supplementary material, further inquiries can be directed to the corresponding author/s.

ETHICS STATEMENT

The animal study was reviewed and approved by Departmental Ethical Committee.

AUTHOR CONTRIBUTIONS

MK: methodology and writing original draft. KA and AA: supervision. MS, MN, and IS: reagents, materials, and analysis tools. ZB, SS, HH, and MK: writing review and editing. AC, MA, and RH: visualization. KD, YW, and KL: conceptualization, funding, and resources. All authors listed have made a substantial, direct, and intellectual contribution to the work and approved it for publication.

FUNDING

This study was supported by the Start-up fund of Nanjing Agricultural University (804131) and the Start-up Fund for Distinguished Scholars of Nanjing Agricultural University (80900219).

REFERENCES

1. DeBoer S, O'Connor A. Prehospital and emergency department burn care. *Crit Care Nurs Clin.* (2004) 16:61–73. doi: 10.1016/j.ccell.2003.10.004
2. Wysocki AB. Evaluating and managing open skin wounds: colonization versus infection. *Adv Crit Care.* (2002) 13:382–97. doi: 10.1097/00044067-200208000-00005
3. World Health Organization. *International Statistical Classification of Diseases and Related Health Problems: 10th Revision, Version for 2007-ICD-10*. World Health Organization (2009).
4. Saito E, Rhoads C. Emergency visits to primary care veterinary hospitals. *Vet Focus.* (2003) 25:18–9. doi: 10.1055/s-0035-1570539
5. Pavletic MM, Trout NJ. Bullet, bite, and burn wounds in dogs and cats. *Vet Clin Small Anim Pract.* (2006) 36:873–93. doi: 10.1016/j.cvsm.2006.02.005
6. Volk SW, Bohling MW. Comparative wound healing—are the small animal veterinarian's clinical patients an improved translational model for human wound healing research? *Wound Repair Regen.* (2013) 21:372–81. doi: 10.1111/wrr.12049
7. Manafi A, Kohanteb J, Mehrabani D, Japoni A, Amini M, Naghmachi M, et al. Active immunization using exotoxin A confers protection against *Pseudomonas aeruginosa* infection in a mouse burn model. *BMC Microbiol.* (2009) 9:23. doi: 10.1186/1471-2180-9-23
8. Bagheri T, Fatemi MJ, Hosseini SA, Saberi M, Niazi M, Momeni M, et al. Comparing the effects of topical application of honey and nitrofurazone ointment on the treatment of second-degree burns with limited area: a randomized clinical trial. *Matrix.* (2017) 2:4.
9. Yaghoobi R, Kazerouni A. Evidence for clinical use of honey in wound healing as an anti-bacterial, anti-inflammatory anti-oxidant and anti-viral agent: a review. *Jundishapur J Nat Pharm Prod.* (2013) 8:100. doi: 10.17795/jjnpp-9487
10. Maddocks SE, Jenkins RE. Honey: a sweet solution to the growing problem of antimicrobial resistance? *Fut Microbiol.* (2013) 8:1419–29. doi: 10.2217/fmb.13.105
11. Combarros-Fuertes P, Estevinho LM, Dias LG, Castro JM, Tomás-Barberán FA, Tornadijo ME, et al. Bioactive components and antioxidant and antibacterial activities of different varieties of honey: a screening prior to clinical application. *J Agric Food Chem.* (2018) 67:688–98. doi: 10.1021/acs.jafc.8b05436
12. Cooper R, Jenkins R. Are there feasible prospects for manuka honey as an alternative to conventional antimicrobials? *Exp Rev Anti Infect Ther.* (2012) 10:623–5. doi: 10.1586/eri.12.46
13. Natarajan S, Williamson D, Grey J, Harding K, Cooper R. Healing of an MRSA-colonized, hydroxyurea-induced leg ulcer with honey. *J Dermatol Treat.* (2001) 12:33–6. doi: 10.1080/095466301750163563
14. Al-Waili NS, Salom K, Butler G, Al Ghamdi AA. Honey and microbial infections: a review supporting the use of honey for microbial control. *J Med Food.* (2011) 14:1079–96. doi: 10.1089/jmf.2010.0161
15. Tewari J, Irudayaraj J. Quantification of saccharides in multiple floral honeys using fourier transform infrared microattenuated total reflectance spectroscopy. *J Agric Food Chem.* (2004) 52:3237–43. doi: 10.1021/jf035176+
16. Kato Y, Umeda N, Maeda A, Matsumoto D, Kitamoto N, Kikuzaki H. Identification of a novel glycoside, leptosin, as a chemical marker of manuka honey. *J Agric Food Chem.* (2012) 60:3418–23. doi: 10.1021/jf300068w
17. Almasaudi SB, El-Shitany NA, Abbas AT, Abdel-dayem UA, Ali SS, Al Jaouni SK, et al. Antioxidant, anti-inflammatory, and antiulcer potential of manuka honey against gastric ulcer in rats. *Oxid Med Cell Long.* (2016) 3643824. doi: 10.1155/2016/3643824
18. de Lira Mota KS, Dias GEN, Pinto MEF, Luiz-Ferreira Â, Monteiro Souza-Brito AR, Hiruma-Lima CA, et al. Flavonoids with gastroprotective activity. *Molecules.* (2009) 14:979–1012. doi: 10.3390/molecules14030979
19. Ahmed SW, Anwar H, Siddiqui A, Shah MR, Ahmed A, Ali SA. Synthesis and chemosensing of nitrofurazone using olive oil based silver nanoparticles (O-AgNPs). *Sens Actuators B Chem.* (2018) 256:429–39. doi: 10.1016/j.snb.2017.10.111
20. Shen C, Shen B, Liu X, Yuan H. Nanosuspensions based gel as delivery system of nitrofurazone for enhanced dermal bioavailability. *J Drug Deliv Sci Technol.* (2018) 43:1–11. doi: 10.1016/j.jddst.2017.09.012
21. Kouchak M, Ameri A, Naseri B, Boldaji SK. Chitosan and polyvinyl alcohol composite films containing nitrofurazone: preparation and evaluation. *Iran J Basic Med Sci.* (2014) 17:14. doi: 10.1016/j.phrp.2014.12.001
22. Henke J, Astner S, Brill T, Eissner B, Busch R, Erhardt W. Comparative study of three intramuscular anaesthetic combinations (medetomidine/ketamine, medetomidine/fentanyl/midazolam and xylazine/ketamine) in rabbits. *Vet Anaesth Analg.* (2005) 32:261–70. doi: 10.1111/j.1467-2995.2005.00242.x
23. Ashkani-Esfahani S, Imanieh MH, Meshksar A, Khoshneviszadeh M, Noorafshan A, Geramizadeh B, et al. Enhancement of fibroblast proliferation, vascularization and collagen synthesis in the healing process of third-degree burn wounds by topical arnebia euchroma, a herbal medicine. *Galen Med J.* (2013) 1:53–9. doi: 10.31661/gmj.v1i2.19
24. Liao H, Guo Y, Na MJ, Lane KB, Light RW. The short-term administration of Ketoprofen does not decrease the effect of Pleurodesis induced by talc or Doxycycline in rabbits. *Respir Med.* (2007) 101:963–8. doi: 10.1016/j.rmed.2006.09.007
25. Mirnezami M, Rahimi H, Fakhar HE, Rezaei K. The role of topical estrogen, phenytoin, and silver sulfadiazine in time to wound healing in rats. *Ostomy Wound Manage.* (2018) 64:30–4. doi: 10.25270/owm.2018.8.3034
26. Akhoondinasab MR, Akhoondinasab M, Saberi M. Comparison of healing effect of aloe vera extract and silver sulfadiazine in burn injuries in experimental rat model. *World J Plast Surg.* (2014) 3:29.
27. Khiati B, Ahmed M. Comparison of efficacy of unheated and heat-treated Sahara honey on wound healing in rabbits. *J Coast Life Med.* (2015) 3:162–5. doi: 10.12980/JCLM.3.201514J91
28. Udefa AL, Archibong AN, Akwari AA, Leilei SA. Effect of Aloe vera gel on some haematological parameters and serum electrolytes in high salt loaded Wistar rats. *MicroMedicine.* (2018) 6:69–77. doi: 10.5281/zenodo.1318287
29. Upadhyay NK, Kumar R, Siddiqui M, Gupta A. Mechanism of wound-healing activity of *Hippophae rhamnoides* L. leaf extract in experimental burns. *Evid Based Comp Altern Med.* (2011) 659705. doi: 10.1093/ecam/nep189
30. Hazrati M, Mehrabani D, Japoni A, Montasery H, Azarpira N, Hamidian-Shirazi A, et al. Effect of honey on healing of *Pseudomonas aeruginosa* infected burn wounds in rat. *J Appl Anim Res.* (2010) 37:161–5. doi: 10.1080/09712119.2010.9707117
31. Hosseini SV, Tanideh N, Kohanteb J, Ghodrati Z, Mehrabani D, Yarmohammadi H. Comparison between Alpha and silver sulfadiazine ointments in treatment of Pseudomonas infections in 3rd degree burns. *Int J Surg.* (2007) 5:23–6. doi: 10.1016/j.ijsu.2006.03.007
32. Kimura Y, Sumiyoshi M, Kawahira K, Sakanaka M. Effects of ginseng saponins isolated from Red Ginseng roots on burn wound healing in mice. *Br J Pharmacol.* (2006) 148:860–70. doi: 10.1038/sj.bjp.0706794
33. Mohajeri G, Masoudpour H, Heidarpour M, Khademi EF, Ghafghazi S, Adibi S, et al. The effect of dressing with fresh kiwifruit on burn wound healing. *Surgery.* (2010) 148:963–8. doi: 10.1016/j.surg.2010.02.013
34. Filomeni G, De Zio D, Cecconi F. Oxidative stress and autophagy: the clash between damage and metabolic needs. *Cell Death Differ.* (2015) 22:377–88. doi: 10.1038/cdd.2014.150
35. Karapolat S, Karapolat B, Buran A, Okatan BK, Turkyilmaz A, Set T, et al. The effects of nitrofurazone on wound healing in thoracoabdominal full-thickness skin defects. *Wounds.* (2020) 32:134–41.
36. Senel O, Cetinkale O, Ozbay G, Ahçioglu F, Bulan R. Oxygen free radicals impair wound healing in ischemic rat skin. *Ann Plast Surg.* (1997) 39:516–23. doi: 10.1097/00000637-199711000-00012
37. Bischofberger AS, Dart CM, Perkins NR, Kelly A, Jeffcott L, Dart AJ. The effect of short-and long-term treatment with manuka honey on second intention healing of contaminated and noncontaminated wounds on the distal aspect of the forelimbs in horses. *Vet Surg.* (2013) 42:154–60. doi: 10.1111/j.1532-950X.2012.01083.x
38. Mandal MD, Mandal S. Honey: its medicinal property and antibacterial activity. *Asian Pac J Trop Biomed.* (2011) 1:154. doi: 10.1016/S2221-1691(11)60016-6
39. Tsang AS, Dart AJ, Dart CM, Jeffcott LB. Mechanisms of action of manuka honey in an equine model of second intention wound healing: current thoughts and future directions. *Med Res Arch.* (2018) 6.
40. Kamaratos AV, Tzirogiannis KN, Iraklianou SA, Panoutsopoulos GI, Kanellos IE, Melidonis AI. Manuka honey-impregnated dressings in the treatment

of neuropathic diabetic foot ulcers. *Int Wound J.* (2014) 11:259–63. doi: 10.1111/j.1742-481X.2012.01082.x
41. Ranzato E, Martinotti S, Burlando B. Honey exposure stimulates wound repair of human dermal fibroblasts. *Burns Trauma.* (2013) 1:32–8. doi: 10.4103/2321-3868.113333
42. Moore OA, Smith LA, Campbell F, Seers K, McQuay HJ, Moore RA. Systematic review of the use of honey as a wound dressing. *BMC Comp Altern Med.* (2001) 1:2. doi: 10.1186/1472-6882-1-2

Conflict of Interest: KD is employed by China Tobacco Henan Industrial Co., Ltd., China.

The remaining authors declare that the research was conducted without any commercial or financial relationships that could be construed as a potential conflict of interest.

Publisher's Note: All claims expressed in this article are solely those of the authors and do not necessarily represent those of their affiliated organizations, or those of the publisher, the editors and the reviewers. Any product that may be evaluated in this article, or claim that may be made by its manufacturer, is not guaranteed or endorsed by the publisher.

frontiers | Frontiers in Veterinary Science

ORIGINAL RESEARCH
published: 02 June 2022
doi: 10.3389/fvets.2022.900480

Tracking Infection and Genetic Divergence of Methicillin-Resistant *Staphylococcus aureus* at Pets, Pet Owners, and Environment Interface

Muhammad Shoaib[1,2], Amjad Islam Aqib[3], Muhammad Muddassir Ali[4], Muhammad Ijaz[5], Huma Sattar[6], Awais Ghaffar[7], Muhammad Sajid Hasni[8], Zeeshan Ahmad Bhutta[9], Khurram Ashfaq[10], Muhammad Fakhar-e-Alam Kulyar[11] and Wanxia Pu[1]**

[1] Key Laboratory of New Animal Drug Project, Gansu Province, Key Laboratory of Veterinary Pharmaceutical Development, Ministry of Agriculture and Rural Affairs, Lanzhou Institute of Husbandry and Pharmaceutical Sciences of CAAS, Lanzhou, China, [2] Institute of Microbiology, Faculty of Veterinary Science, University of Agriculture Faisalabad, Faisalabad, Pakistan, [3] Department of Medicine, Cholistan University of Veterinary and Animal Sciences, Bahawalpur, Pakistan, [4] Institute of Biochemistry and Biotechnology, University of Veterinary and Animal Sciences, Lahore, Pakistan, [5] Department of Veterinary Medicine, University of Veterinary and Animal Sciences, Lahore, Pakistan, [6] Institute of Molecular Biology and Biotechnology, The University of Lahore, Lahore, Pakistan, [7] Department of Clinical Sciences, KBCMA, College of Veterinary and Animal Sciences, Narowal, University of Veterinary and Animal Sciences, Lahore, Pakistan, [8] Directorate General Farms and Feed Resources, Livestock and Dairy Development Department, Quetta, Pakistan, [9] Laboratory of Biochemistry and Immunology, College of Veterinary Medicine, Chungbuk National University, Cheongju, South Korea, [10] Department of Clinical Medicine and Surgery, University of Agriculture, Faisalabad, Pakistan, [11] College of Veterinary Medicine, Huazhong Agricultural University, Wuhan, China

OPEN ACCESS

Edited by:
Fazul Nabi,
Lasbela University of Agriculture, Water and Marine Sciences, Pakistan

Reviewed by:
Ahsan Naveed,
University of Kentucky, United States
Immane Lamraoui,
Ecole Nationale Supérieure de Biotechnologie, Algeria

***Correspondence:**
Wanxia Pu
puwanxia@caas.cn
Amjad Islam Aqib
amjadislamaqib@cuvas.edu.pk

Specialty section:
This article was submitted to Comparative and Clinical Medicine, a section of the journal Frontiers in Veterinary Science

Received: 20 March 2022
Accepted: 12 April 2022
Published: 02 June 2022

Citation:
Shoaib M, Aqib AI, Ali MM, Ijaz M, Sattar H, Ghaffar A, Sajid Hasni M, Bhutta ZA, Ashfaq K, Kulyar MF-e-A and Pu W (2022) Tracking Infection and Genetic Divergence of Methicillin-Resistant Staphylococcus aureus at Pets, Pet Owners, and Environment Interface. Front. Vet. Sci. 9:900480. doi: 10.3389/fvets.2022.900480

Staphylococcus aureus (*S. aureus*) has become a leading animal and public health pathogen that keeps on transferring from one host to other, giving rise to newer strains by genetic shifts. The current study was designed to investigate the epidemiology and genetic relatedness of *mecA* gene in *S. aureus* isolated from pets, immediate individuals in contact with pets, and veterinary clinic environments. A total of $n = 300$ samples were collected from different veterinary hospitals in Pakistan using convenience sampling. The collected samples were subjected to microbiological and biochemical examination for the isolation of *S. aureus*. Methicillin resistance was investigated by both phenotypically using oxacillin disk diffusion assay and by genotypically targeting *mecA* gene by PCR. PCR amplicons were subjected for sequencing by Sanger method of sequencing, which were subsequently submitted to NCBI GenBank under the accession numbers MT874770, MT874771, and MT874772. Sequence evolutionary analysis and *mecA* gene characterization was done using various bioinformatics tools. Overall, 33.66% *mecA* genes harboring *S. aureus* strains were isolated from all sources (33.33% from pets, 46.0% from surrounding, and 28.0% from immediate contact individuals). The bioinformatics analysis noted that one SNP was identified at position c.253C>A (Transvertion). The phylogenetic tree (two clades) of *S. aureus mecA revealed a possibility of inter-transmission of disease* between the environment and pets. Frequency of adenine and thymine nucleotide in motifs were found to be the same (0.334). Cytosine and guanine frequency were also the same (0.166). Threonine was replaced by asparagine (p.T84D) in each sample of cat, environment, and human. On the other hand, protein

structures of cat-1 and cat-2 proteins were found identical while cat-3, environmental, and human proteins shared identical structures. The study thus concludes rising circulation of methicillin-resistant *S. aureus* (MRSA) strains in animal-human-environment interfaces, forecasting the development of novel strains with modified range of resistance.

Keywords: *S. aureus*, mecA gene, pets, MRSA, phylogenetic analysis, pet owners

INTRODUCTION

Over the last decade, with growing trends in pet or companion adoption, pedigree animals are imported for various purposes (shows, sports, pets, and breeding), and public awareness of animal welfare have raised concerns among veterinary researchers of Pakistan for treatment of animal diseases and/or common human and veterinary pathogens in Pakistan. *Staphylococcus aureus* (*S. aureus*) is a key pathogen that causes illnesses ranging from mild skin infections to life-threatening diseases in humans and animals, such as sepsis, pneumonia, endocarditis, deep rooted abscesses, and toxic shock syndrome. *Staphylococcus aureus* is an opportunistic pathogen that is capable of colonizing the skin, mucosal surface, gastrointestinal tract (GIT), urogenital tract, and respiratory tract (1). Within a couple of years, *S. aureus* has emerged to be a well-known pathogen due to its ability to develop resistance to commonly

Abbreviations: *S. aureus*, *Staphylococcus aureus*; MRSA, Methicillin-resistant *Staphylococcus aureus*; HGT, horizontal gene transfer; ARG, antibiotic resistance genes; VFG, virulence factors-encoding genes; LA-MRSA, livestock-associated MRSA; HA-MRSA, healthcare-associated MRSA; CA-MRSA, community-associated MRSA; SCCmec, Staphylococcal Chromosomal Cassette mec; MIC, minimum inhibitory concentration; NCBI, National Center for Biotechnology Information; ST, sequence type.

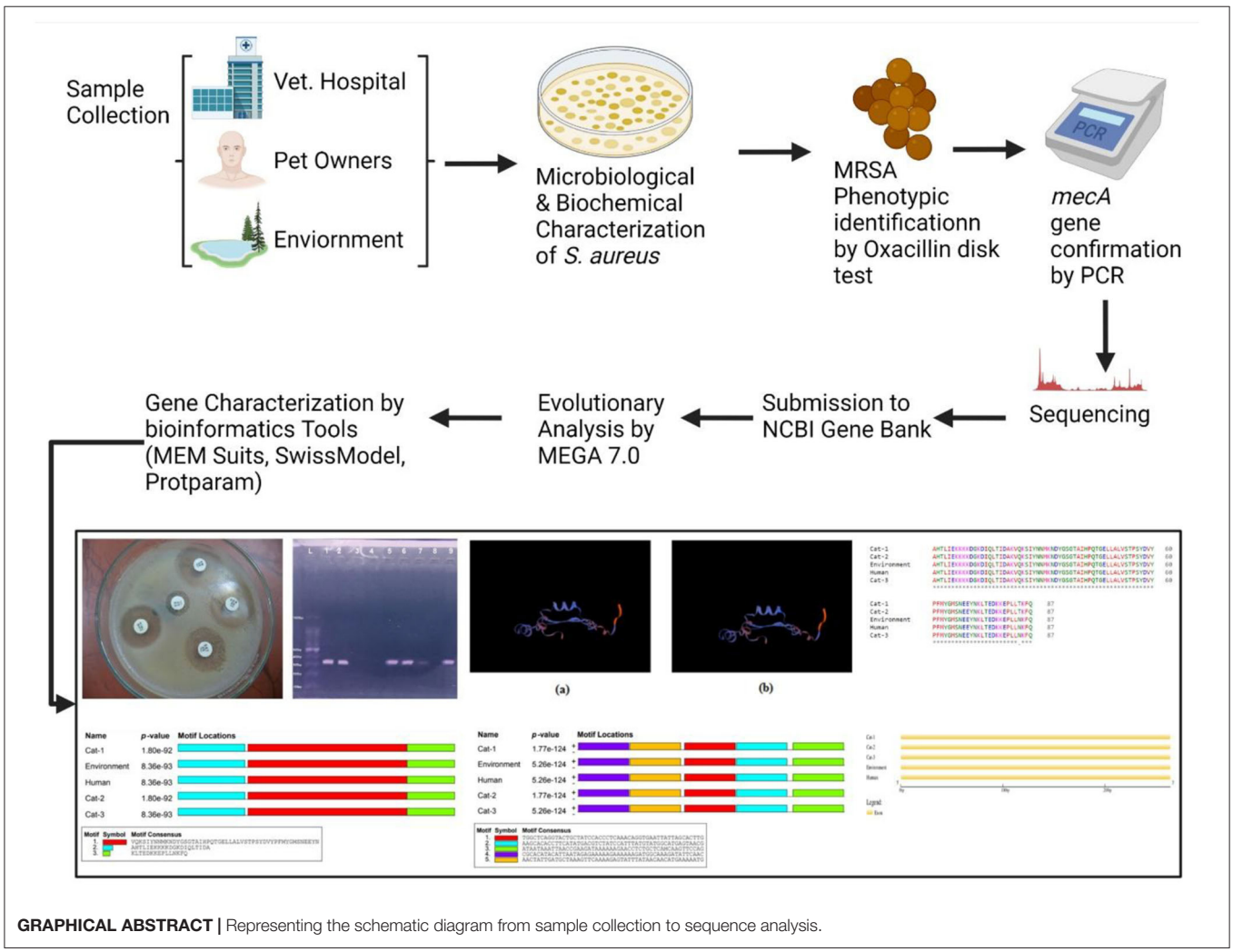

GRAPHICAL ABSTRACT | Representing the schematic diagram from sample collection to sequence analysis.

used antimicrobials and infect a significantly wider range of hosts (2–4). After horizontal gene transfer (HGT) and recombination, it becomes the storehouse of antibiotic resistance genes (ARG) and other virulence factor-encoding genes. The genomic divergence of *S. aureus* has led to the development of highly resistant strains that may cause serious problems with antibiotic treatment (5). Methicillin-resistant *S. aureus* (MRSA) that harbors the *mec A* gene has emerged to be a serious problem worldwide and is becoming more common in humans and animals. These strains are now recognized worldwide as livestock-associated (LA-MRSA), healthcare-associated (HA-MRSA), and community-associated (CA-MRSA) infections (6).

The transmission of *S. aureus* occurs either through direct human-to-human and/or human-to-animals contact with asymptomatic carriers (7). Until 2003, most of the identified MRSA clones belong to multi-locus sequence clones associated with human transmission and infection. The outbreak of the CC398 clone, considered as LA-MRSA clone, was found in farm animals and farm workers, indicating that certain MRSA strains are not strictly restricted to host species (8). A study conducted in the Netherlands found a high prevalence of MRSA in slaughtering pigs despite of reduction in antibiotic usage among pigs. Among the detected MRSA, 39% belonged to the ST398 complex (9). MRSA ST398 can cause infections in humans, suggesting that close contact with animals is an important risk factor for transfer of MRSA clones between human and animals (10).

Methicillin-resistant *S. aureus* harboring *mecA* gene is present within Staphylococcal Chromosomal Cassette mec (*SCCmec*) (11), and exhibits a decreased affinity to β-lactam and penicillin classes of antibiotics (12). *SCCmec* is a mobile element involved in the development of resistance to major antibiotics (e.g., β-lactams, macrolides, aminoglycosides, etc.). The phylogenetic patterns of the resistance genes encoded by *staphylococcus* SCCmec significantly differ from the phylogenetic patterns of the main genes, indicating that these genes are frequently switched between staphylococcal species. Due to the large population and the short replication time of bacteria, resistance develops within 2–4 years after the introduction of new antibiotics (13). Majority of isolated *S. aureus* strains have been identified using disk diffusion test. Further, *mec A* gene confirmation can done through PCR after preliminary identification by disk diffusion test (14).

Many reports of MRSA infections from animals to humans have been documented, but in Pakistan, there is lack of knowledge on MRSA transmission at the pet-human and environment cadre. The present study was planned to study the evolutionary phylogenetic analysis of *mecA* gene in *S. aureus* to analyze the distribution of *S. aureus*-causing infections within the same geographical environment within a certain period. We also discuss the phylogenetic placement of sequenced strains from Pakistan and worldwide by investigating the evolutionary histories of methicillin resistance in a phylogenetic framework.

MATERIALS AND METHODS

Ethical Concern

A consent form was filled before taking samples by nasal swabs from nostrils of humans and animals in accordance with the standard ethical guidelines. The study was approved by departmental and faculty research committee and completion of study was notified *via* no.: CE/1701/2019.

Collection of Samples

A total of 300 samples were collected including cats ($n = 150$), cat owners ($n = 100$), and environment ($n = 50$) from public and private veterinary hospitals located in Faisalabad, Punjab, Pakistan. During sampling, sterilized swabs were inserted into the nostril at a depth of approximately 1 cm before being rotated five times, while environmental samples were taken from the surface of instruments, tables, and animal keepings. Samples were transported in Amie's medium to the laboratory of Institute of Microbiology, University of Agriculture Faisalabad and maintained in a cold chain (4°C) for further investigation.

Phenotypic Identification of MRSA

Each sample (10 μl) was disseminated on blood agar and incubated at 37°C for 24 h. These were then subsequently placed on Mannitol Salt Agar (MSA) for identification of *S. aureus* which was confirmed through culture characteristics, biochemical tests, and microscopic examination as recommended in the Bergey's Handbook of Determinative Bacteriology (15). Phenotypic identification of MRSA was carried out by oxacillin disk diffusion test in accordance with the recommendations of Clinical Laboratory Standard Institute (16).

Molecular Detection and Sequencing of *MecA* Gene

The DNA of *S. aureus* isolates were extracted through WizPrep™ gDNA Mini Kit (Cell/Tissue; Wizbiosolutions Inc. South Korea) following the manufacturer's guidelines. For PCR amplification, a total of 20 μl reaction mixture containing 10 μl of master mix (GeneDireX, Inc. USA), 3 μl extracted DNA (50 ng/μl) that was used as template, 3 μl of DNA free water, and 2 μl (20 pmoL) of each forward and reverse primer of *mecA* gene (**Table 1**) was prepared. The thermocycler conditions were as follows: initial denaturation at 95°C for 5 min, followed by 35 cycles of final denaturation 95°C for 30 s, annealing at 58°C for 30 s, initial extension at 72°C for 30 s, and a final extension at 72°C for 10 min. The presence of amplicons was determined by gel electrophoresis of 10 μl of products in 1.5% agarose gel containing 10 μl ethidium bromide for staining of DNA at 200 amperes and 120 volts for 30 min. The stained gel was visualized under UV light. The amplicons were subjected for sequencing to a 1st BASE DNA sequencing company (Singapore) that uses Applied Biosystems™ BigDye™ Terminator v3.1 Cycle Sequencing Kit (Thermo Fisher Scientific, USA) using Sanger method of sequencing.

Sequence Analysis

The *mecA* gene sequences from each source (cat, cat owner, and environment) was subjected to evolutionary analysis by MEGA 7.0 software. For this, the sequence was first analyzed through BLAST to get highly similar nucleotide sequences ($n = 36$) from NCBI nucleotide GenBank, and alignment was done through Clastal W software. The evolutionary history was accomplished by employing the Minimum Evolution (ME) methodology and replicating tree percentage, in which the associated taxa was clustered together in the bootstrap test (1,000 replicates). The distance of evolution was calculated in relation to the number of base substitutions at each site using the 2-parameter Kimura method. The initial phylogenetic tree was developed with *mecA* gene sequences from all sources by using neighbor-joining with a bootstrap value of 1,500, minimum evolution algorithm at 1.91 optimal tree branch length, and 0.1 evolutionary distance. The final phylogeny tree was constructed using a MEGA 7.0 software to investigate the evolution of *mecA* homologs.

Single nucleotide polymorphisms were identified in sequencing chromatograms using chromas software. Multiple Expectation maximizations for Motif Elicitation (MEME) Suit was used for the construction of nucleic acid and protein motifs. Gene structure display server software was used to construct the gene structure. Protein structures (3D) were predicted by Swiss model. Protparam was used to predict the proteins physical and chemical parameters.

Submission of Sequence to NCBI GenBank

The *mecA* gene sequences analyzed by Sanger method of sequencing from all sources were subjected to submission under NCBI GenBank. After complete submission and evaluation, sequences were accepted for publication in their repository. Accession numbers were issued as identifiers for each submitted sequence, namely, MT874770 (Environment), MT874771 (pet-owner), and MT874772 (Cat).

Analysis of Data

The data were analyzed using SPSS statistical computer software version 26, and sequence analyses was done using various online and offline bioinformatics tools.

TABLE 1 | Nucleotide sequence of the primers used for detection of *mecA* gene.

Primer gene	Oligonucleotide sequence (5′-3′)	Amplicon size (bp)	Reference
mec A gene	**F:** 5′-TGGCATTCGTGTCACAATCG-3′	310	(17)
	R: 5′-CTGGAACTTGTTGAGCAGAG-3′	310	

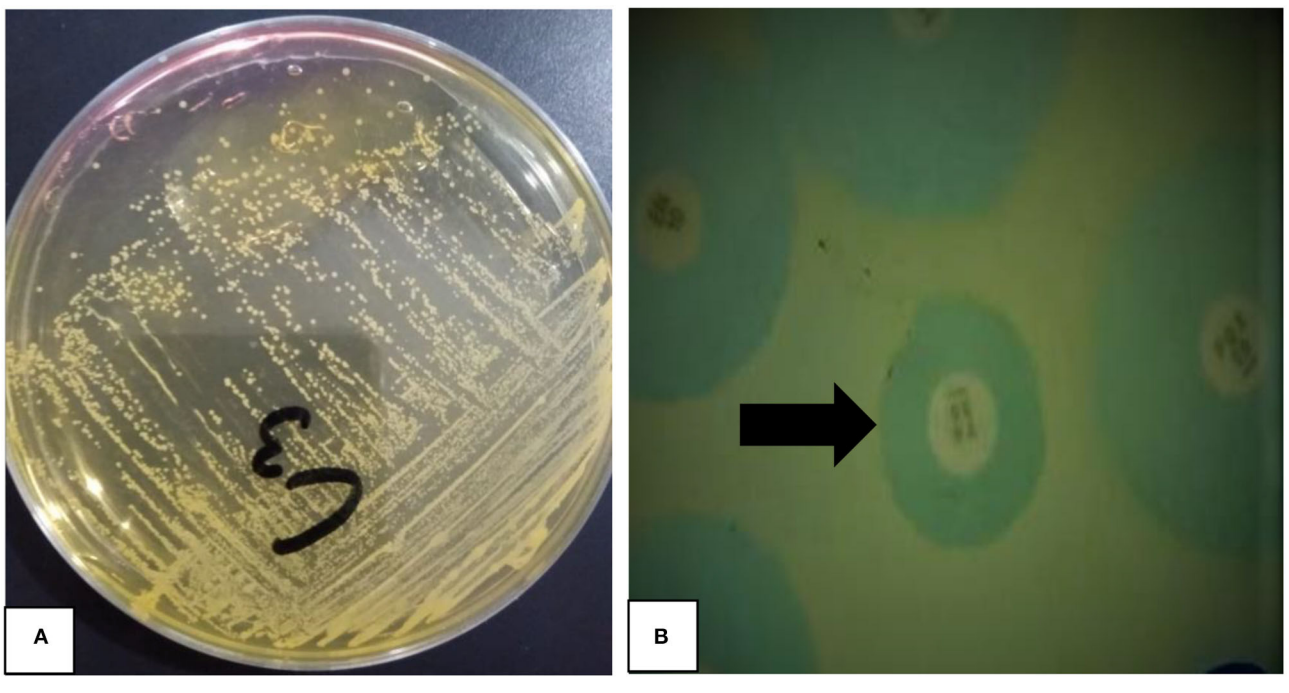

FIGURE 1 | Phenotypic identification of *Staphylococcus aureus* and methicillin-resistant *S. aureus* (MRSA). **(A)** A Yellow color growth of *S. aureus* (pinpoint colonies) on mannitol salt agar, NB: C3 mentioned on plate is sample number tested **(B)** methicillin resistant *S. aureus* (MRSA) identified by oxacillin disc (black arrow) diffusion assay.

RESULTS

The present study found 101 (33.66%) *mecA* gene positive (MRSA) isolates from 300 pets (cats), individuals having direct contact with pet, and pet environment. The phenotypic identification of *S. aureus* and MRSA was done by MSA culture and oxacillin disk diffusion test, respectively (**Figure 1**). The *mecA* gene was identified by amplification through PCR, and *mecA* positive isolates from different sources were presented (**Figure 2**). Thirty-three-point-thirty-three percent (50/150) of *mecA* gene harboring *S. aureus* isolates were found in cats, 46.0% (23/50) from environment, which were twice to the isolates from pet owners [28.0% (28/100)]. In this study, there were no significant differences between *S. aureus* in animal, animal, and human interactions ($P > 0.05$), but a significant difference was noted in *mecA* gene prevalence among members ($P < 0.05$; **Table 2**).

In present study, bacteriological and biochemical analysis of samples from cats, cat owners, and environments depicted the harboring of the *mecA* positive *S. aureus*. The conventional PCR results show the significant bands of *mecA* gene isolated from cats, cat owners, and environments (310 bp), as shown in **Figure 2**. The retrieved nucleotide sequences of targeted *mecA* genes were submitted to the NCBI GenBank with accession numbers MT874770 (Environment origin), MT874771 (pet-owner origin), and MT874772 (Cat origin).

Nucleic acid sequence alignment are given in **Figure 3**, and protein sequences alignment are given in **Figure 4**. One SNP was identified at position c.253C>A (Transvertion; **Table 3**). Cat-1 and Cat-2 sequences were 100% identical, while Cat-3, environmental and human sequences, were 100% identical. The phylogenetic tree (two clades) of *S. aureus mecA* gene was observed. *Staphylococcus aureus mecA* genes of cat, environment, and human samples were compared with NCBI database sequences. Local isolates of *S. aureus mecA* (Cat-1 and Cat-2) gene sequences were closely related to the *S. aureus mecA* gene isolated from *Homo sapiens* (nasal swab) from Japan. Environmental and human *mecA* gene sequences were closely related to *Staphylococcus epidermidis*. All samples (Cat-1, Cat-2, Cat-3, Environmental, and Human) cluster together with *S. aureus* from *H. sapiens* (pus, secretions, skin and nasal swab), *Staphylococcus argenteus* from *H. sapiens*, *Staphylococcus pseudintermedius* (dog), and *Staphylococcus epidermidis* (*H. sapiens*; **Figure 5**).

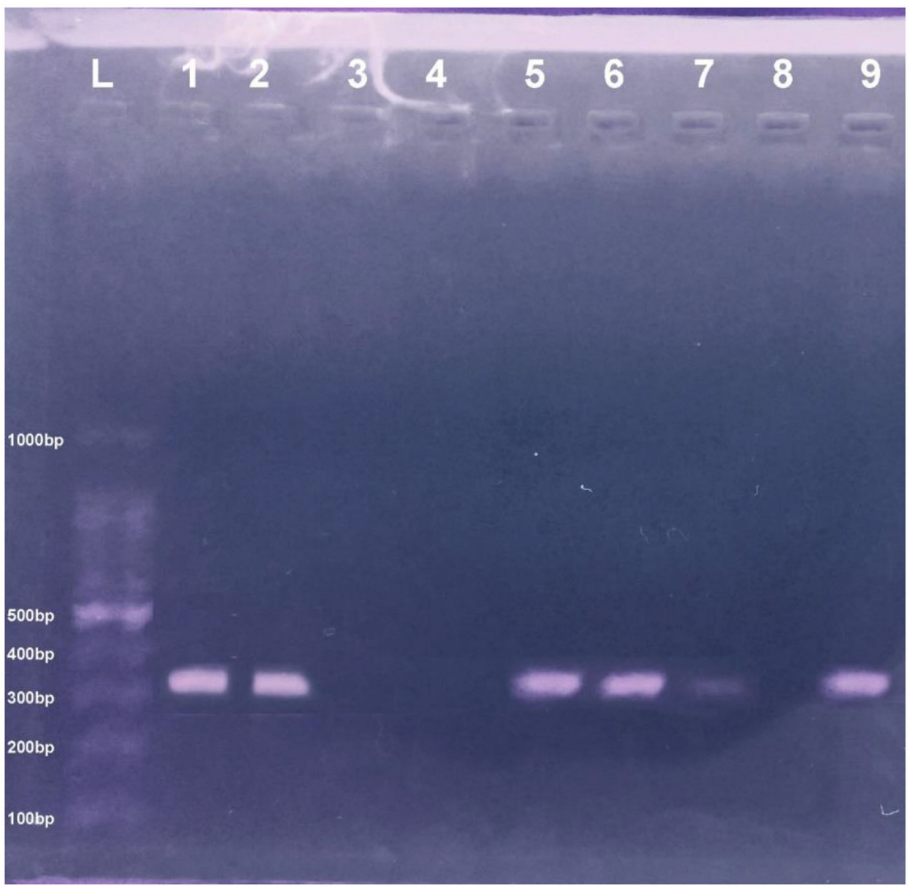

FIGURE 2 | PCR pic of *mecA* gene at 310 bp. Lane L showing the ladder DNA, where Lane 8 and 9 are negative and positive control, respectively, and Lane 1–2 and 5–7 show *mecA* positive samples while Lane 3–4 express negative *mecA* isolates.

TABLE 2 | Infection status of methicillin resistance *Staphylococcus aureus* (*mecA* gene) isolates.

Sample sources	Location/hospital name	Total sample	Positive *S. aureus* (%)*	*mecA* gene positive (%)**
Cats	UAF Teaching Hospital Faisalabad, Pakistan	70	62 (88.57)	27 (38.57)
	Al-Huda Pet Clinic and Boarding Center Faisalabad, Pakistan	30	21 (70.0)	13 (43.33)
	Pet-Aid Clinic Faisalabad, Pakistan	50	37 (74.0)	10 (20.0)
	Total	150	120 (80.0)	50 (33.33)
Pet-Owner	UAF Teaching Hospital Faisalabad, Pakistan	40	28 (70.0)	12 (30.0)
	Al-Huda Pet Clinic and Boarding Center Faisalabad, Pakistan	30	17 (56.66)	9 (30.0)
	Pet-Aid Clinic Faisalabad, Pakistan	30	20 (66.66)	7 (23.33)
	Total	100	65 (65.0)	28 (28.0)
Environment	UAF Teaching Hospital Faisalabad, Pakistan	20	15 (75.0)	10 (50.0)
	Al-Huda Pet Clinic and Boarding Center Faisalabad, Pakistan	15	10 (66.66)	8 (53.33)
	Pet-Aid Clinic Faisalabad, Pakistan	15	10 (66.66)	5 (33.33)
	Total	50	35 (70.0)	23 (46.0)
Overall total		300	220 (73.33)	101 (33.66)

**No significant difference (P > 0.05) was noted at Staphylococcus aureus cadre.*

***Significant difference (P < 0.05) was noted at MRSA cadre among different sources.*

```
Cat-1           TCGCACATACATTAATAGAGAAAAAGAAAAAAGATGGCAAAGATATTCAACTAACTATTG      60
Cat-2           TCGCACATACATTAATAGAGAAAAAGAAAAAAGATGGCAAAGATATTCAACTAACTATTG      60
Environment     TCGCACATACATTAATAGAGAAAAAGAAAAAAGATGGCAAAGATATTCAACTAACTATTG      60
Human           TCGCACATACATTAATAGAGAAAAAGAAAAAAGATGGCAAAGATATTCAACTAACTATTG      60
Cat-3           TCGCACATACATTAATAGAGAAAAAGAAAAAAGATGGCAAAGATATTCAACTAACTATTG      60
                ************************************************************

Cat-1           ATGCTAAAGTTCAAAAGAGTATTTATAACAACATGAAAAATGATTATGGCTCAGGTACTG      120
Cat-2           ATGCTAAAGTTCAAAAGAGTATTTATAACAACATGAAAAATGATTATGGCTCAGGTACTG      120
Environment     ATGCTAAAGTTCAAAAGAGTATTTATAACAACATGAAAAATGATTATGGCTCAGGTACTG      120
Human           ATGCTAAAGTTCAAAAGAGTATTTATAACAACATGAAAAATGATTATGGCTCAGGTACTG      120
Cat-3           ATGCTAAAGTTCAAAAGAGTATTTATAACAACATGAAAAATGATTATGGCTCAGGTACTG      120
                ************************************************************

Cat-1           CTATCCACCCTCAAACAGGTGAATTATTAGCACTTGTAAGCACACCTTCATATGACGTCT      180
Cat-2           CTATCCACCCTCAAACAGGTGAATTATTAGCACTTGTAAGCACACCTTCATATGACGTCT      180
Environment     CTATCCACCCTCAAACAGGTGAATTATTAGCACTTGTAAGCACACCTTCATATGACGTCT      180
Human           CTATCCACCCTCAAACAGGTGAATTATTAGCACTTGTAAGCACACCTTCATATGACGTCT      180
Cat-3           CTATCCACCCTCAAACAGGTGAATTATTAGCACTTGTAAGCACACCTTCATATGACGTCT      180
                ************************************************************

Cat-1           ATCCATTTATGTATGGCATGAGTAACGAAGAATATAATAAATTAACCGAAGATAAAAAAG      240
Cat-2           ATCCATTTATGTATGGCATGAGTAACGAAGAATATAATAAATTAACCGAAGATAAAAAAG      240
Environment     ATCCATTTATGTATGGCATGAGTAACGAAGAATATAATAAATTAACCGAAGATAAAAAAG      240
Human           ATCCATTTATGTATGGCATGAGTAACGAAGAATATAATAAATTAACCGAAGATAAAAAAG      240
Cat-3           ATCCATTTATGTATGGCATGAGTAACGAAGAATATAATAAATTAACCGAAGATAAAAAAG      240
                ************************************************************

Cat-1           AACCTCTGCTCACCAAGTTCCAGA       264
Cat-2           AACCTCTGCTCACCAAGTTCCAGA       264
Environment     AACCTCTGCTCAACAAGTTCCAGA       264
Human           AACCTCTGCTCAACAAGTTCCAGA       264
Cat-3           AACCTCTGCTCAACAAGTTCCAGA       264
                ************ ************
```

FIGURE 3 | Alignment of *Staphylococcus aureus mecA* gene (Cat-1, Cat-2, Cat-3, Environmental, and Human sequence).

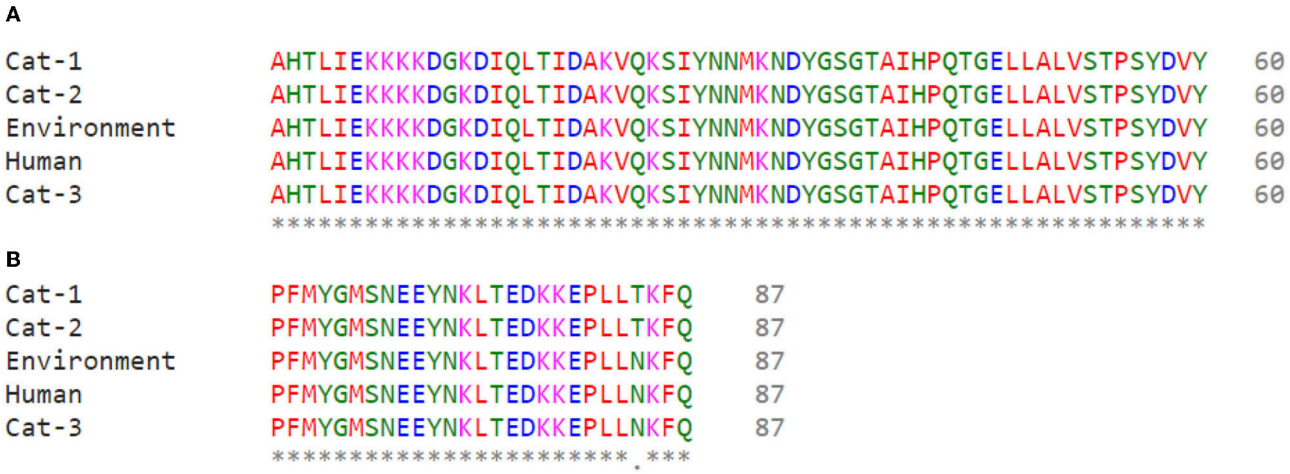

FIGURE 4 | Alignment of Staphylococcus aureus mecA protein sequences **(A)** Cat-1 and Cat-2 **(B)** Environment, Human, and Cat-3.

TABLE 3 | Polymorphic sites in the *Staphylococcus aureus mecA* gene.

Nucleotide position	Position 253
Cat-1	C
Cat-2	C
Cat-3	A
Environmental	A
Human	A

Nucleic acid motifs (1,320 bp sequence) of Cat-1 and Cat-2 sequences *P*-value were found to be the same (1.77e-124), while Cat-3, environmental, and human sequences share same *P*-value (5.26e-124; **Figure 6**). The *P*-values of protein motifs (435 bp sequence) of Cat-1 and Cat-2 sequences were also found to be the same (1.80e-92). Similarly, Cat-3, environmental, and human sequences share same *P*-value (8.36e-93; **Figure 7**). Frequency of adenine and thymine nucleotide in motifs (0.334) and that of cytosine and guanine were the same (0.166). The coding region in yellow color was involved in the nucleotide structure (**Figure 8**). Threonine was replaced by asparagine (p.T84D) in Cat-3, environmental, and human samples (**Table 4**).

The protein structure of Cat-1 and Cat-2 proteins is found to be identical while Cat-3, environmental, and human proteins share identical structures (**Figure 9**). Physical and chemical properties of proteins Cat-1 and Cat-2 were found to be identical, while Cat-3, environmental, and human proteins have same physical and chemical properties (**Table 5**).

DISCUSSION

The human–animal bond has changed over the time. For example, the job of pets has shifted from working animals, e.g., catching mice and protecting houses, to animals that play roles as social pets, providing companionship. Pets may be important for their owners because they provide physical and mental health support but can also transmit number of zoonotic diseases (18). *Staphylococcus aureus* is one of the zoonotic pathogens that colonizes in the nasal cavity of pets and humans. *Staphylococcus aureus* is an infectious pathogen that acquires the ability to horizontally transfer genes between humans and animals (19). *Staphylococcus aureus* is recognized as major pathogen that causes major health problems in a community and is characterized by high rate of treatment failure worldwide (20). The One Health program is a global initiative plan for enhancing collaborations in every aspect of health care that involves humans, animals, and the environment. However, the role of dogs and cats in One Health communication is often underestimated. Therefore, the present study was conducted to investigate epidemiology and genetic relatedness of *S. aureus* by targeting the *mecA* gene at pet, pet owner, and environment interface. Nowadays, pets have become the major source of transmission of this pathogen to other animals and humans (21). In the last few years, much consideration has been paid on pets due to them serving as reservoir of antibiotic resistant bacteria and potential source of transfer of resistant genes from pets to humans (22). A study was conducted in Spain which reported co-carriage of ST398 strain of *S. aureus* in dogs and dog owners (23). Meanwhile, another study reported indistinguishable MRSA strains in humans and pets, suggesting the interspecies transmission of MRSA and *S. aureus* strains (24). Habibullah et al. (25) reported *S. aureus* that the prevalence in dogs (42.62%) and cats (37.50%) is twice higher than the current study. The prevalence of reported *S. aureus* contamination and/or infection in pet care workers is about six times less compared to current study findings (10% vs. 65.0%) (26). The high prevalence may be associated with unhygienic management practices in the study area, geographical differences, and unprotected interactions with pets (27). *Staphylococcus aureus* nasal colonization is associated with a number of factors, such as population type, geographical location, environmental factors, genetic factors, hormonal status, cell-wall composition, nasal secretions, antibiotic use, other infections, and immune level, which have been reported to be correlated with colonization

FIGURE 5 | Phylogenetic tree of *Staphylococcus aureus mecA* gene.

(28). MRSA, increasingly being identified in both healthy and ill dogs and cats. It has been reported that *mecA* gene is the major evidence for the detection of MRSA isolates in Sudan (29). Consistent with current research, the results from two previous studies reported 46% and 49% MRSA in companion animals, respectively (30, 31). The relatively high prevalence in current studies and the high infection rate in hospitals and clinics are justified. High population density at clinics can cause the spread of pathogenic microorganisms into the environment.

Potential risks of carrying MRSA may include veterinary hospital staff, exposure to suppressant drugs, repeated utilization of the same antibiotics, use of non-specific antibiotics, and exposure to sources of infection carrying MRSA. MRSA can persist due to its antibiotic resistance ability, evolutionary adoption of biofilm covering, and its ability to bypass the immune system of hosts by utilizing specific molecular structures. Moreover, typical CA-MRSA, HA-MRSA, and LA-MRSA infecting non-specific hosts with MRSA strains is an additional indication for prolonged and persistent spread of MRSA strains (17). The high incidence of antibiotic resistance may be associated with the acquisition of resistance determinants (e.g., integrin's, plasmids, transposons, etc.) by vertical or horizontal gene transfer and, to a certain extent, with the misuse of antibiotics (5).

To curb the global spread of penicillin-resistant *S. aureus*, methicillin β-lactam antibiotics and subsequently oxacillin were manufactured. However, shortly after the use of methicillin, a MRSA emerged, making it one of the most life-threatening antibiotic-resistant pathogen (32). Methicillin resistance results from two distinct mechanisms. One is production of β-lactamases, which leads to a decrease in the antibiotic activity of β-lactams, and production of penicillin-binding protein 2a (PBP2a). PBP2a is an enzyme that is actively involved in the synthesis of peptidoglycan and promotes bacterial cell wall resistance. However, it does not have access to its active site, which binds to β-lactams, thereby interfering with its action and disrupting the normal process of bacterial cell wall synthesis (33). It is encoded by the mec gene, while the β-lactamase is encoded by the blaZ gene. The origin of the *mecA* gene is unknown. However, in some studies, the homologs of the *mecA* gene are found in *S. sciuri*, *S. lentus*, and *S. vitulinus* species. Since then, it has been hypothesized that these resistance determinants are derived from certain coagulase-negative staphylococci (CoNs). The species vitulinus suggests

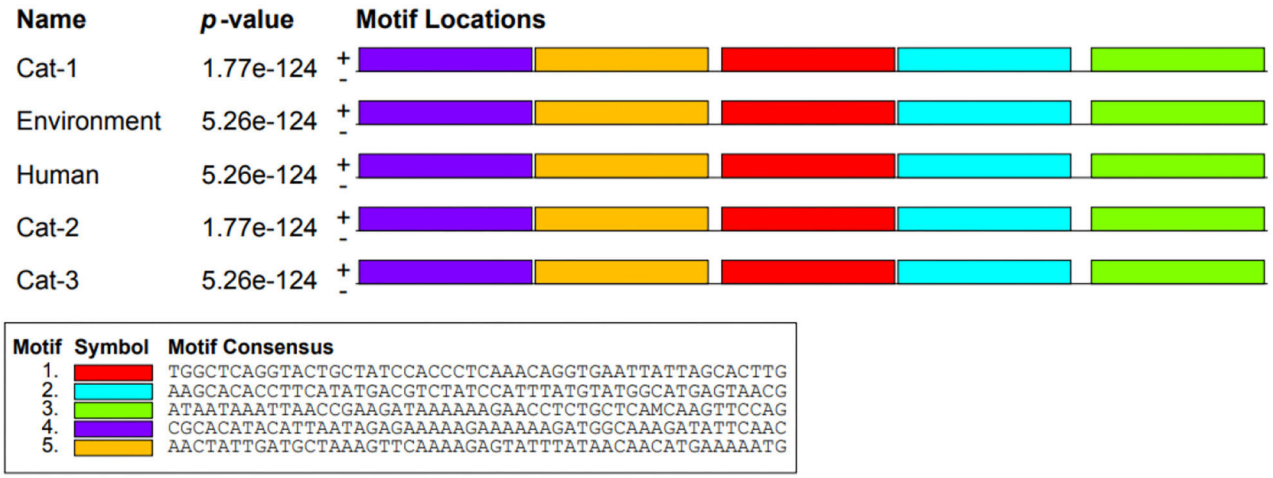

FIGURE 6 | Nucleotide motifs of *Staphylococcus aureus mecA* gene.

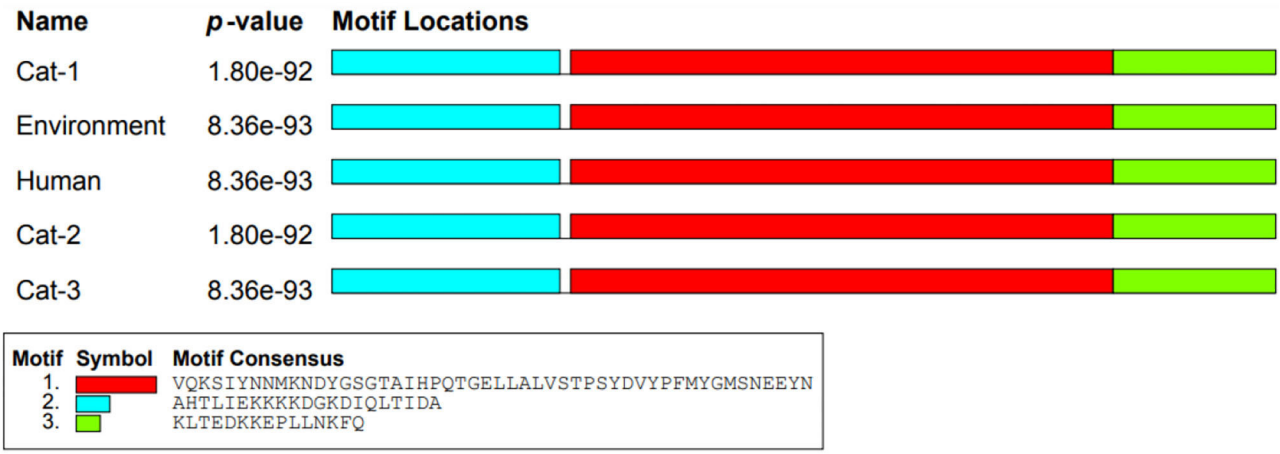

FIGURE 7 | *mecA* protein motifs of *Staphylococcus aureus*.

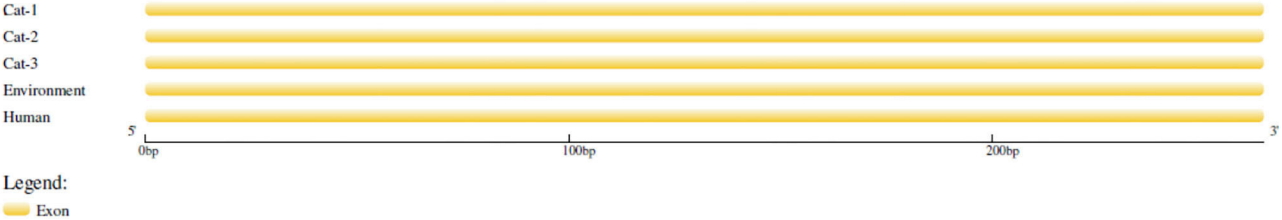

FIGURE 8 | Gene structure of *Staphylococcus aureus mecA* gene amplified fragment.

TABLE 4 | Amino acid change in *Staphylococcus aureus mecA* protein.

Amino acid position	Cat-1	Cat-2	Cat-3	Environmental	Human
84	Threonine	Threonine	Asparagine	Asparagine	Asparagine

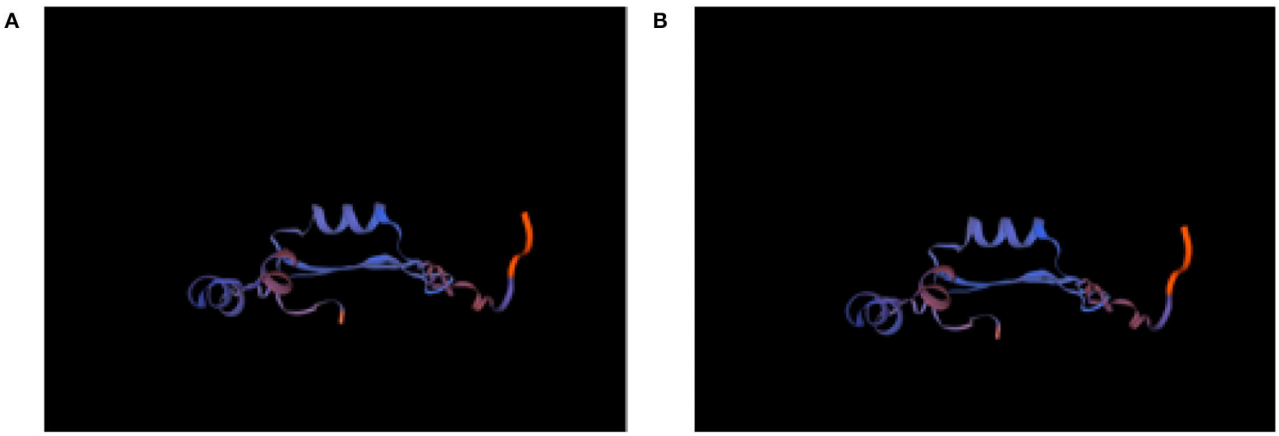

FIGURE 9 | Protein structure of *Staphylococcus aureus mecA* gene **(A)** Cat-1 and Cat-2, and **(B)** Environment, Human, and Cat-3.

TABLE 5 | *Staphylococcus aureus mecA* protein physical and chemical properties of proteins (Cat-1. Cat-2, Cat-3, Environmental, and Human).

Sample ID	Cat-1 protein	Cat-2 protein	Cat-3 protein	Environmental protein	Human protein
Number of amino acids	87	87	87	87	87
MW	9,915.28	9,915.28	9,928.28	9,928.28	9,928.28
pI	6.97	6.97	6.97	6.97	6.97
Number of negatively charged residues	12	12	12	12	12
Number of positively charged residues	12	12	12	12	12
Total number of atoms	1,397	1,397	1,397	1,397	1,397
II	36.30	36.30	39.03	39.03	39.03
Aliphatic index	72.87	72.87	72.87	72.87	72.87
GRAVY	−0.779	−0.779	−0.811	−0.811	−0.811

that this group may be the evolutionary ancestor of mecA. The mec genes are contained in the staphylococcal chromosome cassette mec (SCCmec), which is a mobile genetic component of staphylococci (34).

Another study conducted by Neamah et al. (1) found that *mecA* sequences from two clinically isolated cattle and human strains belong to the same group. Furthermore, another study conducted by Rolo et al. (35) studied the distribution pattern of the *mecA* gene, and showed that the earliest *Staphylococcus* species, including *S. sciuri, S. vitulinus,* and *S. fleurettii,* had an inclusive role in the stepwise aggregation of *SCCmec* elements and subsequently transferred to *S. aureus*. John et al. (36) conducted research to study 4,562 protein families and 1,764 unique genes of *S. aureus* and found 47 protein families that belonged to genes encoded by *SCCmec*, which include *mecA* gene, regulation genes (*mecR* and *mecI*), recombinase gene (ccrABC), transposons, insertion elements, heavy metals, and drug-resistant genes. Of the 152 *S. aureus* isolates, 73% were drug resistant and positive for *mecA* gene, while the remaining isolates were categorized as sensitive ones. Unsurprisingly, *mecA* was noted to be absent in most of the exposed strains, but, surprisingly, in scientist's dataset, 10% of sensitive *S. aureus* strains were composed of *SCCmec* elements that do not contain the *mecA* gene. The findings suggest that the presence of *SCCmec* element is not limited to only resistant strains of *S. aureus*.

The genomic composition of the core *SCCmec* gene, *mecA-mecR-mecI* was found in resistant strains of *S. aureus* and some species of *Staphylococcaceae,* such as *S. pseudointermedius, S. epidermidis, S. sciuri, S. argenteus, S. schleiferi, S. haemolyticus,* and *M. caseolyticus,* with mec-box genes found at 51 kb genes. The phylogenetic analysis based on the 16S rRNA gene sequence is widely used to study the evolutionary relationship of microorganisms (37). Interestingly, our study highlights the importance of those isolates as potential zoonotic agents. Hence, there is need to control and prevent this transmission by adopting clean living habits of pets and humans. Furthermore, the results of current study recommend more studies on whole genome sequence analysis along with multi locus sequence type (ST) approach in the future analyses to rule out the ST of each strain and the probability of raising a novel ST from the strains under study.

CONCLUSION

The study witnessed rise in MRSA from pets, pet owners, and the environment as threat for public and animal health. Phylogenetic tree of submitted sequences revealed significant relatedness of MRSAs of animals, humans, and environment to each other. Replacement of amino acids and variation in structural proteins of MRSAs of different sources are indicative of genetic shifts. In such scenarios, novel strains of MRSAs are expected to emerge with modified resistance to antibiotics if stern precautions are not adopted.

DATA AVAILABILITY STATEMENT

The original contributions presented in the study are included in the article/supplementary material, further inquiries can be directed to the corresponding authors.

ETHICS STATEMENT

The studies involving human and animal participants were reviewed and approved by the faculty and advanced studies board before the start of work, while approval of the completed research notified CE/1701/M.Phil., 2019 dated 11/10/2019. Post study ethical permission certificate was also obtained vide FVS/379/26.02.2020. The patients/participants provided their written informed consent to participate in this study. Written informed consent was obtained from the owners for the participation of their animals in this study.

AUTHOR CONTRIBUTIONS

MS did research and wrote the original manuscript draft. AA, MI, and WP contributed in project design and check the validity of the research. MA and HS executed the bioinformatics analysis. AG and MSH helped in laboratory work. ZB and MK did review and editing of manuscript. KA helped in clinical data collection. All authors contributed to the article and approved the submitted version.

FUNDING

This work was supported by the Agricultural Science and Technology Innovation Program of the Chinese Academy of Agricultural Sciences (25-LZIHPS-03).

REFERENCES

1. Neamah AJ, Ayyez HN, Klaif SF, Khudhair YI, Hussain MH. Molecular and phylogenetic study of *Staphylococcus aureus* isolated from human and cattle of Al-Qadisiyah Governorate, Iraq. *Vet World.* (2019) 12:1378. doi: 10.14202/vetworld.2019.1378-1382
2. Javed MU, Ijaz M, Fatima Z, Anjum AA, Aqib AI, Ali MM, et al. Frequency and antimicrobial susceptibility of methicillin and vancomycin-resistant *Staphylococcus aureus* from bovine milk. *Pak Vet J.* (2021) 41:463–8. doi: 10.29261/pakvetj/2021.060
3. Altaf M, Ijaz M, Iqbal MK, Rehman A, Avais M, Ghaffar A, et al. Molecular characterization of methicillin resistant *Staphylococcus aureus* (MRSA) and associated risk factors with the occurrence of goat mastitis. *Pak Vet J.* (2020) 40:1–6. doi: 10.29261/pakvetj/2019.079
4. Sarwar I, Ashar A, Mahfooz A, Aqib AI, Saleem MI, Butt AA, et al. Evaluation of antibacterial potential of raw turmeric, nano-turmeric, and NSAIDs against multiple drug resistant *Staphylococcus aureus* and *E. coli* isolated from animal wounds. *Pak Vet J.* (2021) 41:209–14. Available online at: http://pvj.com.pk/pdf-files/41_2/209-214.pdf
5. Naorem RS, Urban P, Goswami G, Fekete C. Characterization of methicillin-resistant *Staphylococcus aureus* through genomics approach. *3 Biotech.* (2020) 10:1–19. doi: 10.1007/s13205-020-02387-y
6. Lee AS, de Lencastre H, Garau J, Kluytmans J, Malhotra-Kumar S, Peschel A, et al. Methicillin-resistant *Staphylococcus aureus*. *Nat Rev Dis Primers.* (2018) 4:1–23. doi: 10.1038/nrdp.2018.33
7. Matuszewska M, Murray GG, Harrison EM, Holmes MA, Weinert LA. The evolutionary genomics of host specificity in *Staphylococcus aureus*. *Trends Microbiol.* (2020) 28:465–77. doi: 10.1016/j.tim.2019.12.007
8. Ballhausen B, Kriegeskorte A, van Alen S, Jung P, Köck R, Peters G, et al. The pathogenicity and host adaptation of livestock-associated MRSA CC398. *Vet Microbiol.* (2017) 200:39–45. doi: 10.1016/j.vetmic.2016.05.006
9. Dierikx CM, Hengeveld PD, Veldman KT, de Haan A, van der Voorde S, Dop PY, et al. Ten years later: still a high prevalence of MRSA in slaughter pigs despite a significant reduction in antimicrobial usage in pigs the Netherlands. *J Antimicrob Chemother.* (2016) 71:2414–8. doi: 10.1093/jac/dkw190
10. Haag AF, Fitzgerald JR, Penadés JR. *Staphylococcus aureus* in animals. *Microbiol Spectr.* (2019) 7:1–10. doi: 10.1128/microbiolspec.GPP3-0060-2019
11. Singh G, Broor S, Agarwal P. Staphylococcus cassette chromosome mec types among methicillin-resistant *Staphylococcus aureus* isolates from Haryana, India. *Indian J Health Sci Care.* (2017) 4:47–56. doi: 10.5958/2394-2800.2017.00010.4
12. Mistry H, Sharma P, Mahato S, Saravanan R, Kumar PA, Bhandari V. Correction: prevalence and characterization of oxacillin susceptible mecA-positive clinical isolates *of Staphylococcus aureus* causing bovine mastitis in India. *PLoS ONE.* (2020) 15:e0232348. doi: 10.1371/journal.pone.0232348
13. Harkins CP, Pichon B, Doumith M, Parkhill J, Westh H, Tomasz A, et al. Methicillin-resistant *Staphylococcus aureus* emerged long before the introduction of methicillin into clinical practice. *Genome Biol.* (2017) 18:1–11. doi: 10.1186/s13059-017-1252-9
14. Rahman M, Amin K, Rahman S, Khair A, Rahman M, Hossain A, et al. Investigation of methicillin-resistant *Staphylococcus aureus* among clinical isolates from humans and animals by culture methods and multiplex PCR. *BMC Vet Res.* (2018) 14:1–6. doi: 10.1186/s12917-018-1611-0
15. Bergey DH. *Bergey's Manual of Determinative Bacteriology*. Philadelphia, PA: Lippincott Williams & Wilkins (1994). ISBN: 0683006037.
16. Schwarz S, Silley P, Simjee S, Woodford N, van Duijkeren E, Johnson AP, et al. Assessing the antimicrobial susceptibility of bacteria obtained from animals. *J Antimicrob Chemother.* (2010) 65:601–4. doi: 10.1093/jac/dkq037
17. Shoaib M, Rahman SU, Aqib AI, Ashfaq K, Naveed A, Kulyar MF-e-A, et al. Diversified epidemiological pattern and antibiogram of mecA gene in *Staphylococcus aureus* isolates of pets, pet owners and environment. *Pak Vet J.* (2020) 40:331–6. doi: 10.29261/pakvetj/2020.039
18. Overgaauw PA, Vinke CM, van Hagen MA, Lipman LJ. A one health perspective on the human–companion animal relationship with emphasis on zoonotic aspects. *Int J Environ Res Public Health.* (2020) 17:3789. doi: 10.3390/ijerph17113789
19. Crespo-Piazuelo D, Lawlor PG. Livestock-associated methicillin-resistant *Staphylococcus aureus* (LA-MRSA) prevalence in humans in close contact with animals and measures to reduce on-farm colonisation. *Ir Vet J.* (2021) 74:1–12. doi: 10.1186/s13620-021-00200-7
20. Islam MA, Parveen S, Rahman M, Huq M, Nabi A, Khan ZUM, et al. Occurrence and characterization of methicillin resistant *Staphylococcus aureus* in processed raw foods and ready-to-eat foods in an urban

setting of a developing country. *Front Microbiol.* (2019) 10:503. doi: 10.3389/fmicb.2019.00503
21. Bierowiec K, Płoneczka-Janeczko K, Rypuła K. Is the colonisation of *Staphylococcus aureus* in pets associated with their close contact with owners? *PLoS ONE.* (2016) 11:e0156052. doi: 10.1371/journal.pone.0156052
22. Ye X, Wang X, Fan Y, Peng Y, Li L, Li S, et al. Genotypic and phenotypic markers of livestock-associated methicillin-resistant *Staphylococcus aureus* CC9 in humans. *Appl Environ Microbiol.* (2016) 82:3892–9. doi: 10.1128/AEM.00091-16
23. Gomez-Sanz E, Torres C, Ceballos S, Lozano C, Zarazaga M. Clonal dynamics of nasal *Staphylococcus aureus* and *Staphylococcus pseudintermedius* in dog-owning household members. Detection of MSSA ST398. *PLoS ONE.* (2013) 8:e69337. doi: 10.1371/journal.pone.0069337
24. Faires MC, Tater KC, Weese JS. An investigation of methicillin-resistant *Staphylococcus aureus* colonization in people and pets in the same household with an infected person or infected pet. *J Am Vet Med Assoc*. (2009) 235:540–3. doi: 10.2460/javma.235.5.540
25. Habibullah A, Rahman A, Haydar M, Nazir K, Rahman M. Prevalence and molecular detection of methicillin-resistant *Staphylococcus aureus* from dogs and cats in Dhaka City. *Bangl J Vet Med.* (2017) 15:51–7. doi: 10.3329/bjvm.v15i1.34055
26. Tarazi YH, Almajali AM, Ababneh MMK, Ahmed HS, Jaran AS. Molecular study on methicillin-resistant *Staphylococcus aureus* strains isolated from dogs and associated personnel in Jordan. *Asian Pac J Trop Biomed.* (2015) 5:902–8. doi: 10.1016/j.apjtb.2015.06.015
27. El-Deeb W, Fayez M, Elmoslemany A, Kandeel M, Zidan K. Methicillin resistant *Staphylococcus aureus* among goat farms in Eastern province, Saudi Arabia: Prevalence and risk factors. *Prev Vet Med.* (2018) 156:84–90. doi: 10.1016/j.prevetmed.2018.05.005
28. Sakr A, Brégeon F, Mège J-L, Rolain J-M, Blin O. *Staphylococcus aureus* nasal colonization: an update on mechanisms, epidemiology, risk factors, and subsequent infections. *Front Microbiol.* (2018) 9:2419. doi: 10.3389/fmicb.2018.02419
29. Elhassan MM, Ozbak HA, Hemeg HA, Elmekki MA, Ahmed LM. Absence of the mecA gene in methicillin resistant *Staphylococcus aureus* isolated from different clinical specimens in Shendi City, Sudan. *Biomed Res Int*. (2015) 2015. doi: 10.1155/2015/895860
30. Hogan PG, Mork RL, Boyle MG, Muenks CE, Morelli JJ, Thompson RM, et al. Interplay of personal, pet, and environmental colonization in households affected by community-associated methicillin-resistant *Staphylococcus aureus*. *J Infect.* (2019) 78:200–7. doi: 10.1016/j.jinf.2018.11.006
31. Ng W, Faheem A, McGeer A, Simor AE, Gelosia A, Willey BM, et al. Community-and healthcare-associated methicillin-resistant *Staphylococcus aureus* strains: an investigation into household transmission, risk factors, and environmental contamination. *Infect Control Hosp Epidemiol.* (2017) 38:61–7. doi: 10.1017/ice.2016.245
32. Zarazaga M, Gómez P, Ceballos S, Torres C. Molecular epidemiology of *Staphylococcus aureus* lineages in the animal–human interface. In: Fetsch A, editor. *Staphylococcus aureus*. Cambridge, MA: Academic Press (2018), p. 189–214. doi: 10.1016/B978-0-12-809671-0.00010-3
33. Fishovitz J, Hermoso JA, Chang M, Mobashery S. Penicillin-binding protein 2a of methicillin-resistant *Staphylococcus aureus*. *IUBMB Life.* (2014) 66:572–7. doi: 10.1002/iub.1289
34. Silva V, Capelo JL, Igrejas G, Poeta P. Molecular epidemiology of *Staphylococcus aureus* lineages in wild animals in Europe: a review. *Antibiotics.* (2020) 9:122. doi: 10.3390/antibiotics9030122
35. Rolo J, Worning P, Nielsen JB, Bowden R, Bouchami O, Damborg P, et al. Evolutionary origin of the staphylococcal cassette chromosome mec (SCCmec). *Antimicrob Agents Chemother*. (2017) 61:302–16. doi: 10.1128/AAC.02302-16
36. John J, George S, Nori SRC, Nelson-Sathi S. Phylogenomic analysis reveals the evolutionary route of resistant genes in *Staphylococcus aureus*. *Genome Biol Evol.* (2019) 11:2917–26. doi: 10.1093/gbe/evz213
37. Goswami G, Deka P, Das P, Bora SS, Samanta R, Boro RC, et al. Diversity and functional properties of acid-tolerant bacteria isolated from tea plantation soil of Assam. *3 Biotech.* (2017) 7:1–16. doi: 10.1007/s13205-017-0864-9

Conflict of Interest: The authors declare that the research was conducted in the absence of any commercial or financial relationships that could be construed as a potential conflict of interest.

Publisher's Note: All claims expressed in this article are solely those of the authors and do not necessarily represent those of their affiliated organizations, or those of the publisher, the editors and the reviewers. Any product that may be evaluated in this article, or claim that may be made by its manufacturer, is not guaranteed or endorsed by the publisher.

frontiers | Frontiers in Veterinary Science

ORIGINAL RESEARCH
published: 09 June 2022
doi: 10.3389/fvets.2022.919904

Transcriptomics-Based Study of Differentially Expressed Genes Related to Fat Deposition in Tibetan and Yorkshire Pigs

Xinglong Gong[1,2†], *Min Zheng*[1,2†], *Jian Zhang*[1,2], *Yourong Ye*[1,2], *Mengqi Duan*[1,2], *Yangzom Chamba*[1,2], *Zhongbin Wang*[1,2*] and *Peng Shang*[1,2*]

[1] Tibet Agriculture and Animal Husbandry College, Tibet, China, [2] The Provincial and Ministerial Co-founded Collaborative Innovation Center for R&D in Tibet Characteristic Agricultural and Animal Husbandry Resources, Tibet, China

OPEN ACCESS

Edited by:
Fazul Nabi,
Lasbela University of Agriculture, Water and Marine Sciences, Pakistan

Reviewed by:
Tariq Jamil,
Friedrich Loeffler Institut, Germany
Hao Zhang,
China Agricultural University, China

***Correspondence:**
Peng Shang
nemoshpmh@126.com
Zhongbin Wang
0823yuan1020@163.com

[†] These authors have contributed equally to this work

Specialty section:
This article was submitted to Comparative and Clinical Medicine, a section of the journal Frontiers in Veterinary Science

Received: 14 April 2022
Accepted: 09 May 2022
Published: 09 June 2022

Citation:
Gong X, Zheng M, Zhang J, Ye Y, Duan M, Chamba Y, Wang Z and Shang P (2022) Transcriptomics-Based Study of Differentially Expressed Genes Related to Fat Deposition in Tibetan and Yorkshire Pigs. Front. Vet. Sci. 9:919904. doi: 10.3389/fvets.2022.919904

Fat deposition traits are one of the key factors in pig production and breeding. The fat deposition capacity of pigs mainly affects the quality of pork and pig productivity. The aim of this study was to analyze the differential expression of mRNA levels in dorsal adipose tissue of Tibetan and York pigs at different growth stages using transcriptomic data to estimate key genes that regulate fat deposition in pigs. The results showed that a total of 32,747 positively expressed genes were present in the dorsal adipose tissue of the two breeds. Differentially expressed gene (DEG) screening of multiple combinations between the two breeds yielded 324 DEGS. Gene ontology (GO) biofunctional enrichment and Kyoto Encyclopedia of Genes and Genomes (KEGG) analyses showed that these DEGS were mainly involved in lipid metabolic pathways, steroid biosynthetic pathways and lipid biosynthetic processes, sterol biosynthetic processes, brown adipocyte differentiation, and other pathways related to lipid deposition and metabolism. The results showed that ACACA, SLC2A4 and THRSP genes positively regulated the lipid deposition ability and CHPT1 gene negatively regulated the lipid deposition ability in pigs. The results of this experiment suggest a theoretical basis for further studies on the regulatory mechanisms of fat deposition in pigs.

Keywords: Tibetan pig, large white pig, fat deposition, transcriptomic, backfat

INTRODUCTION

In China, pigs are commonly used for meat production and hundreds millions people need meat products from pigs (1, 2). Fat is a metabolic tissue that plays an important role in fatty acid synthesis, and mediates adipocyte differentiation and metabolism (3, 4). At the time of selection of pig for breeding, meat quality traits are considered important indicators while the intramuscular fat (IMF) contents directly affect the sensory quality of pork (5–7). The process of fat deposition is regulated by a cascade of multiple transcription factors including lipid secretion factors, and porcine fat deposition is a complex multiple micro-effective gene control quantitative trait (8, 9). York pigs breed with high leanness is largely introduced in China which is very much in line with modern people's requirements for pork diet and is one of the main sources of pork food in China (10). Tibetan pigs are smaller and a rough-feeding tolerant pig breed with high fat deposition which is a preferred test animal for studying fat deposition traits (11, 12). Therefore, these two breeds can

be used as comparative models to study the genetic differences and molecular mechanisms of the phenotypic differences.

At present, there are many studies on fat deposition-related genes, and new genes are gradually discovered, but there is still a need to explore the involvement of potential candidate genes in deposition of fat. RNA-seq technology is a transcriptome analysis tool that provides great advantages for exploring new genes and their related functional properties (13–15). In order to investigate the relationship between different genes in fat deposition in different growth stages of different breeds of pigs, this experiment took Tibetan pigs, a fatty breed, and Yorkshire pigs, a lean breed, as the subjects of the study, and explored three key time points, namely the weaning period of 30-day-old piglets, the fattening period of 90-day-old pigs and the breeding period of 180-day-old pigs. The involvement of each gene in the regulation of lipid deposition and lipid metabolism in dorsal fat tissue was determined by transcriptome sequencing analysis in order to provide a scientific basis for quality selection and breeding of Tibetan and Yorkshire pigs.

MATERIALS AND METHODS

Sample Preparation

The test animals like Tibetan pigs (TP) and York pigs (LW) were reared in the teaching practice pasture of Tibet Agricultural and Animal Husbandry College, Linzhi, Tibet. The dorsal fat tissue was used as the study material. The test animals were reared according to the national feed standard until 30, 90, and 180 days of age, and 8 animals with similar growth conditions and age were randomly selected for slaughtering. A total of 24 Tibetan pigs and 24 York pigs were slaughtered. Dorsal lipid tissues were collected and immediately placed in liquid nitrogen. After collection, all the samples were stored at −80°C for extraction of total RNA. Finally, total RNA of 8 pigs at the same age stage was randomly mixed into 4 biological replicates for transcriptome sequencing. All the research work was carried out in strict accordance with the guidelines approved by the Animal Welfare Committee of Tibet Agriculture and Animal Husbandry University.

RNA Isolation and Library Construction

Total RNA was extracted from back adipose tissue using TRIZOL reagent (Invitrogen, San Diego, CA, USA) according to the manufacturer's instructions. Degradation and contamination of RNA were monitored on a 1% agarose gel. RNA purity was checked using a NanoPhotometer® spectrophotometer (IMPLEN, CA, USA). RNA integrity was assessed using the Bioanalyzer 2100 system (Agilent Technologies, CA, USA) using RNA Nano 6000 Assay Kit. A total of 1 μg of RNA per sample was used as input material for RNA sample preparation. Sequencing libraries were generated using the NEBNext® UltraTM RNA Library Prep Kit for Illumina® (NEB, USA) following the manufacturer's recommendations, and index codes were added to group sequences into each sample. After library construction, initial quantification was performed using a Qubit2.0 Fluorometer, diluting the library to 1.5 ng/ul, followed by detection of the insert size of the library using an Agilent 2100 bioanalyzer, and after the insert size met expectations, qRT-PCR was performed to accurately quantify the effective concentration of the library. After the insert size met the expectation, qRT-PCR was performed to accurately quantify the effective concentration of the library (effective library concentration above 2nM) to ensure the quality of the library.

Data Analysis of RNA-Seq

Data analysis included quality control of raw reads, filtering, alignment, assembly, expression count, and annotation. Raw data (raw reads) of fastq format were firstly processed through in-house perl scripts. In this step, clean data (clean reads) were obtained by removing reads containing adapter, reads containing ploy-N and low quality reads from raw data. At the same time, Q20, Q30 and GC content the clean data were calculated. All the downstream analyses were based on the clean data with high quality. Clean reads were mapped to the reference genome (Sus scrofa genome v11.1, downloaded from ENSEMBL web server) using HISAT2 v2.1.0. Reads for each gene in each sample were counted by HTSeq v0.6.0 (https://github.com/simonanders/htseq). Fragments per kilobase per million mapped reads were then calculated to estimate the expression level of each gene. The differentially expressed genes (DEGs) were identified using the statistical significance of the absolute value of $|\log2FoldChange| > 0$ and $padj < 0.01$.

Functional Enrichment Analysis

Matescape (http://metascape.org/) was used to analyze differential genes. Go and KEGG analysis was performed using the OmicShare tools, a free online platform for data analysis (https://www.omicshare.com/tools.From). Cellular Component (CC), Molecular Function (MF) and Biological Process (BP) functions are described. This experiment uses Go and KEGG are both commonly used bioinformatics analysis methods.

Verification of RNA-Seq Data

To validate the results of sequencing analysis, 7 mRNAs were selected for RT-qPCR analysis (**Supplementary Table S1**). Total RNA from each sample was extracted using TRIzol reagent (Invitrogen, Carlsbad, CA, U.S.A.), and All-in-one TM First-Strand cDNA Synthesis Kit was used for reverse transcription PCR in accordance with the manufacturer's instructions (GeneCopocie, Inc, Rockville, MD, U.S.A.). qPCR was performed using 2 × All-in-oneTMqPCR mix with 2 μl of cDNA template and a final concentration of 0.2 μl All-in-oneTMqPCR primer. The reactions were carried out as follows: 10 min at 95°C (1 cycle), 20 sec at 95°C, 10 sec at 60°C and 10 sec at 72°C (38 cycles).

Correlation Analysis of RT-qPCR and Pig Backfat Thickness

The results of RT-qPCR tests of the seven key candidate genes screened in this experiment were used as material for correlation analysis with backfat thickness of Tibetan and York pigs at 180 days of age to further demonstrate the regulatory functions of these genes on fat deposition traits in pigs.

RESULTS

RNA Sequencing Data Mapping and Annotation

The quality of sequencing data for all samples in this experiment is summarized in **Supplementary Table S2**. After filtering the raw data, the amount of data for each sample ranged between 44.49 to 5.43 million clean reads, and the average Clean bases per sample was not <6.6 Gb, and the comparison rate was above 93 %, among which the number of reads compared to multiple positions of the reference genome did not exceed 2.5 %. Q20 was above 97.23% and Q30 was above 92.38%. This indicates that the

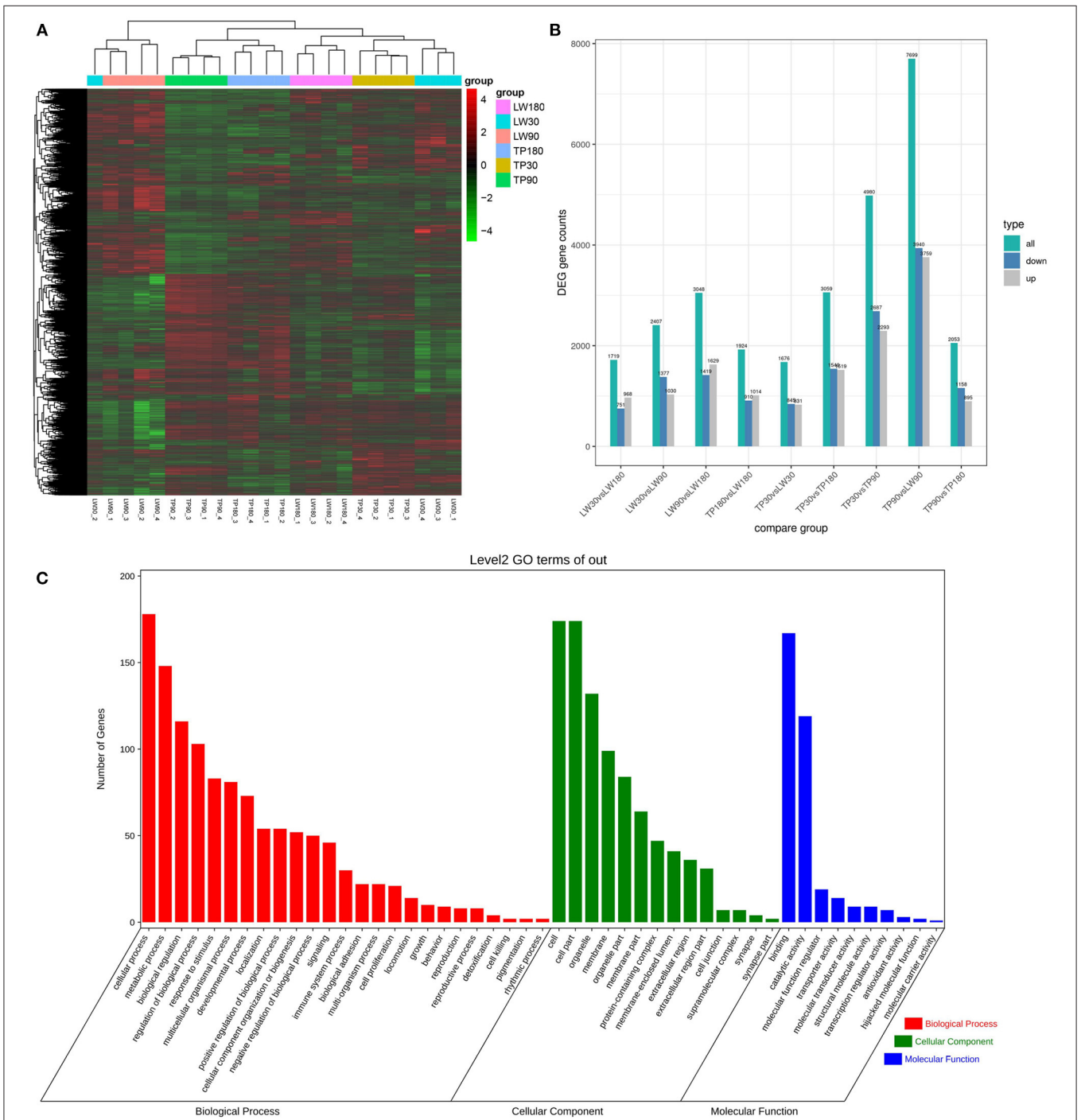

FIGURE 1 | Analysis of differentially expressed genes (DEGs). **(A)** Plot of correlation coefficient among samples. **(B)** Histogram of the number of DEGS statistics for difference comparison combinations. **(C)** The column diagrams for gene ontology (GO) analysis of DEGs, the X-axis represents the functions of GO analysis and the Y-axis represents the numbers of DEGs.

sequencing quality is high and the valid sequences can be used for subsequent analysis.

Cluster Analysis of Differential Genes

The FPKM values of 24 RNA library samples were clustered using the mainstream hierarchical clustering method, and their rows were mean-scored (Z-score). Heat maps of gene correlations between the samples were analyzed and plotted. The results showed (**Figure 1A**) that the overall differences in expression of all genes were not prominent, and the correlation of gene expression between samples was good, reflecting the reliability of the experiments and sample selection, which can be applied to the subsequent differential gene screening and analysis.

Analysis of Differentially Expressed Genes (DEGs)

The conditions of Padj <0.01 and |log2FoldChange|>0 were used as screening criteria for differentially expressed genes, and the number of differential genes (including up-regulation and down-regulation) for each comparison combination was displayed in a histogram (**Figure 1B**), and a Venn diagram was used to show the overlap of differential genes between different comparison combinations to screen the differential genes of each comparison combination, and a total of 324 differential genes were screened in this experiment (**Figure 2**).

Functional Analysis of DEGs

To further determine the functions of DEGS, all DEGS were functionally classified using GO annotations. The annotation results were divided into three parts: biological processes, cellular components, and molecular functions (**Figure 1C**). The top 5 of each section are shown as (1) Biological processes: (I) Cellular processes; (II) Metabolic processes; (III) Biological regulation; (IV) Regulation of biological processes; (V) Response to stimuli. (2) Cellular components: (I) cell; (II) cell part; (III) organelle; (IV) membrane; (V) organelle part. (3) Molecular functions: (I) binding; (II) catalytic activity; (III) molecular function regulator; (IV) transporter activity; (V) molecular transducer activity. KEGG analysis of DEG was also performed. As shown in **Figure 3** and **Supplementary Figure S1**, KEGG was mainly enriched to metabolic pathways, carbon metabolism, TCA cycle, pyruvate metabolism, glucagon signaling pathway, and steroid biosynthesis and fatty acid metabolism pathways.

RT-qPCR Validation of Transcriptome Data Results

Results on further screening of 324 differential genes in the intersection of the TP30 vs. LW30 group, TP90 vs. LW90 and TP180 vs. LW180 groups, joint statistical analysis of FPKM values of differentially expressed genes related to lipid metabolism and fatty acid synthesis and comprehensive studies of their related functions, IDI1, PLAC8, ELOVL5, ACACA, SLC2A4, THRSP and CHPT1 were screened out. The RNA-seq data were consistent with those obtained by RT-qPCR (**Figure 4**). In addition, RT-qPCR analysis confirmed the DEG expression patterns observed in two pig breeds at different growth stages.

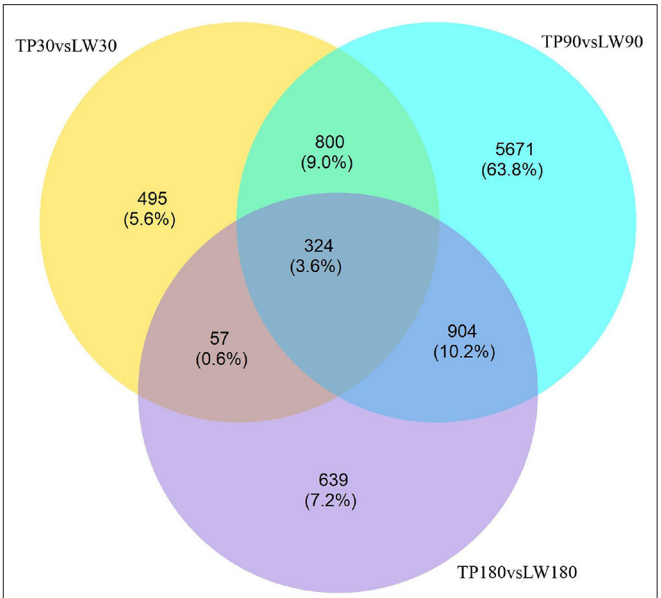

FIGURE 2 | Differential genetic Venn diagram.

Correlation Analysis of RT-qPCR Results With Backfat Thickness of Pigs

The results on backfat thickness measurement of Tibetan and York pigs (**Table 1**) showed that the backfat thickness of 180-day-old Tibetan carcasses was significantly higher than that of York pigs ($P < 0.05$).

The correlation analysis between the backfat thickness data and the key candidate genes screened by transcriptome sequencing (**Table 2**) showed that the backfat thickness of York pigs was significantly positively correlated with IDI1, ACACA, ELOVL5, PLAC8, SLC2A4 and THRSP genes ($P < 0.01$), the correlation coefficients were 0.921, 0.935, 0.916, 0.934, 0.908, and 0.884, respectively. A highly significant negative correlation ($P < 0.01$) was found with CHPT1 gene, and the correlation coefficient was −0.928; the correlation analysis of each gene showed that CHPT1 gene showed a highly significant negative correlation with all genes, while all other genes showed a strong positive correlation with each other.

Correlation analysis of Tibetan pig backfat thickness data with key candidate genes screened by transcriptome sequencing (**Table 3**) showed that the Tibetan pig backfat thickness was highly significant positive correlation with ACACA, SLC2A4 and THRSP genes ($P < 0.01$) with correlation coefficients of 0.868, 0.890 and 0.894, respectively, and negative correlation with CHPT1 gene, positive correlation with IDI1, ELOVL5, and PLAC8 genes, and the differences were not significant; CHPT1 gene was negatively correlated with all other genes, and all other genes showed positive correlations with each other.

DISCUSSION

With the rapid development of high-throughput sequencing technology, transcriptome sequencing has been widely used

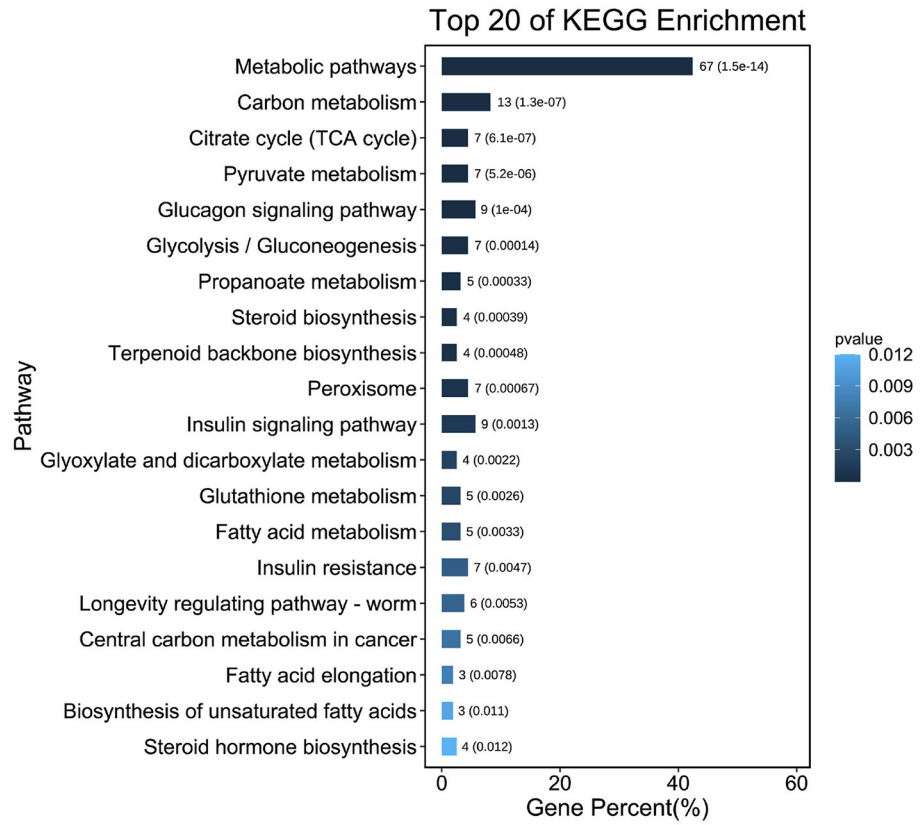

FIGURE 3 | The column diagrams of top 20 Kyoto encyclopedia of genes and genomes (KEGG) analysis.

in animal studies. Pooling and biological replicate are two conventional methods used in RNA-seq experiments. Pooling RNA-seq refers to mixing individuals in the same treatment group into one pool for sequencing, which is more efficient, less time-consuming, and incurs lower cost when there are many samples (16).

Various reports have shown that RNA-seq is also capable of detecting differentially expressed genes (DEGs) in mammals of different age and breeds (17, 18). Transcriptome comparison of adipose and muscle tissues from different pig breeds is a novel approach to study functional genes during adipogenesis (19). The adipose tissue is a complex and metabolically active tissue, and the adipocytes of which it is composed are a dynamic and highly regulated population of cells (20). Fat deposition is an important biological process in pig growth. Fatty traits are critical in pig production and are closely related to pork quality as well as the production efficiency and reproductive traits of pigs (21, 22).

Back fat thickness of pigs is an important indicator to determine the fat deposition in commercial pigs. Back fat thickness of pigs can directly reflect their body fat content (23). Investigation on measures to reduce back fat deposition is an important way to effectively promote genetic improvement of pigs. Therefore, it is important to explore the regulatory mechanisms and molecular mechanisms of pig back fat deposition.

At present, many studies have focused to identify mechanisms of fat deposition traits in local pig breeds at the molecular and genetic level but to date few studies have determined fat metabolism patterns in pigs at different growth stages. Therefore our study describes the scientific significance of studying of mechanisms involve in fat metabolism in pigs (24). In this study, we compared the dorsal fat tissues of Tibetan pigs (fatty breed) and York pigs (lean breed) at 30, 90 and 180 days of age by RNA-seq sequencing, and used Padj$<$0.01 and |log2FoldChange|$>$0 as the screening criteria for differentially expressed genes (DEGs), and obtained 800 DEGs by analysis in the 30 and 90 days of age groups. DEGs 904 were obtained in the 90-day-old group compared with the 180-day-old group; 57 DEGs were obtained in the 30-day-old group compared with the 180-day-old group; and 324 DEGs were obtained in the intersection of the three groups. In the process of fat deposition and metabolism, the specific expression of a large number of genes forms a complex regulatory network and signaling pathways. The functional annotation of differentially expressed genes revealed that the results of the remaining groups were basically consistent, except for the results of the 30-day-old and 180-day-old groups, which were mainly involved in monocarboxylic acid transport, lipid catabolism process, neutral lipid catabolism process, steroid metabolic process, carnitine shuttle and brown fat cell differentiation. The functional annotation of 57 DEGs obtained from the comparison

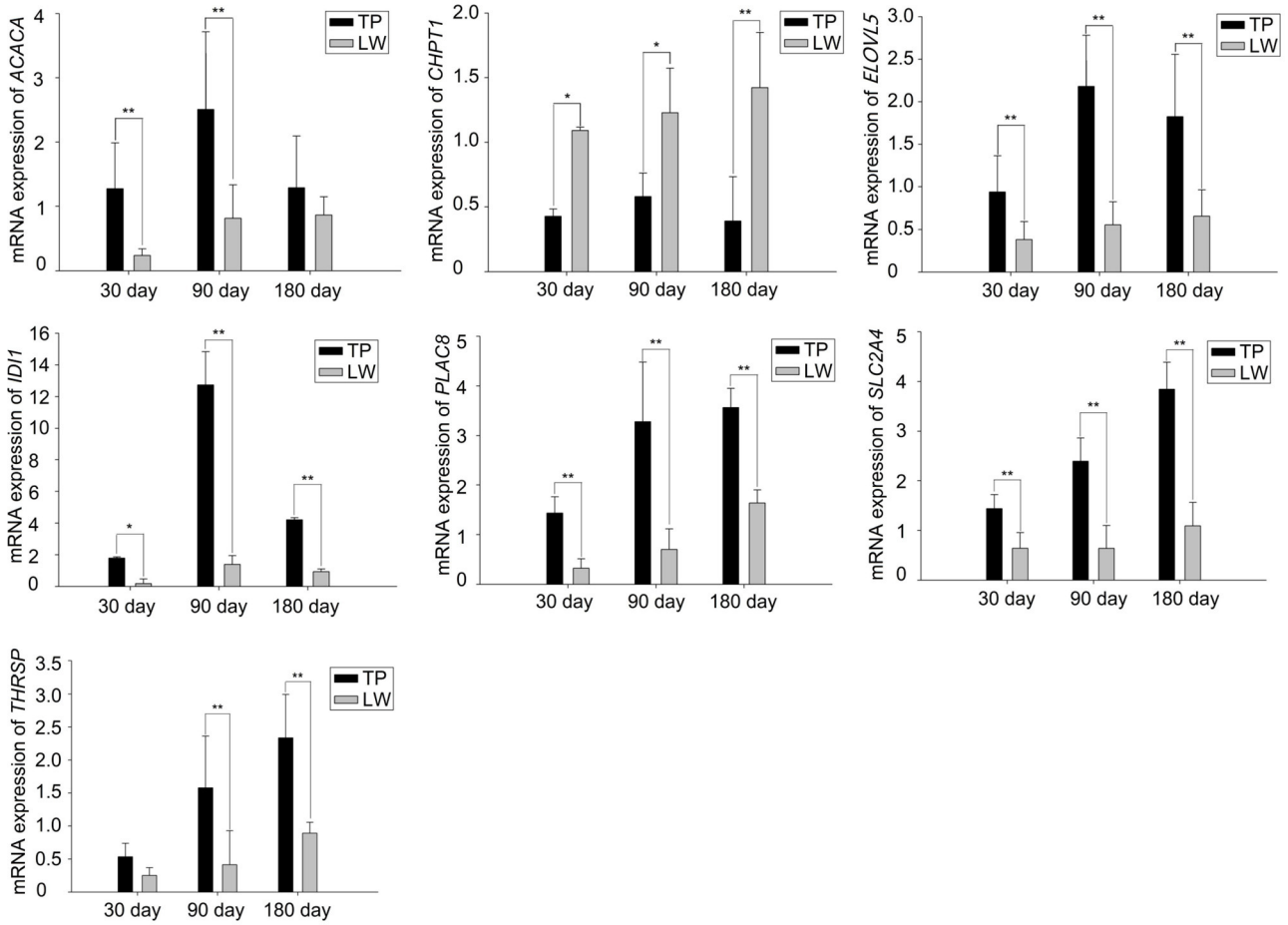

FIGURE 4 | Real-time PCR validation of the DEGs analyzed by RNA-seq. The *symbol indicates the significant difference ($P < 0.05$). The **symbol indicates extremely significant difference ($P < 0.01$).

TABLE 1 | Comparison of backfat thickness determination.

Species	Backfat thickness/mm
Tibetan pig	21.27 ± 1.08a
York pigs	16.41 ± 1.16b

of 30-day-old and 180-day-old groups was enriched to two GO entries of lipid transport and muscle organ development. Although the amount of data was small, the results fully indicated that lipid transport and muscle growth and development existed in the whole growth stage of pigs, reflecting the authenticity and accuracy of the data. The number of DEGs obtained by comparing the 30-day-old group with the 90-day-old group and the number of DEGs obtained by comparing the 90-day-old group with the 180-day-old group, i.e,57<800<904, because the process of lipid deposition in pigs is mainly reflected in the middle and late stages of growth, and this increment in number is fully consistent with the trend of growth and development of pigs, which further indicates the reliability of the data.

Seven key candidate genes were finally screened out based on the FPKM values of the differential genes integrated with their functional studies, among which acetyl-CoA carboxylase alpha (ACACA), an important key gene in the pathways of propionate metabolism, fatty acid biosynthesis, AMPK signaling pathway, insulin signaling pathway and glucagon signaling, plays an important role in the ab initio synthesis of fatty acids. The insulin signaling pathway not only plays an important role in muscle development and growth. It also plays an important role in the metabolism of carbohydrates and fats (25). It has been shown that in animal organisms, the ACACA gene is highly expressed in tissues with strong fatty acid metabolic activity, and the acetyl coenzyme A carboxylase (ACACA) gene plays an important role in lipid metabolism by promoting fatty acid biosynthesis (26). The results of our study also showed extremely high expression in porcine dorsal lipid tissues, which is consistent with the findings of previous studies (27, 28). Solute carrier family 2 member 4 (SLC2A4), also known as glucose transporter protein 4 (GLUT4), is an important transporter protein for cellular uptake of glucose, mainly expressed in muscle and adipose tissues, involved in active cellular uptake of glucose

TABLE 2 | Correlation analysis between backfat thickness and various genes in York pigs.

Projects	Backfat thickness	IDI1	ACACA	ELOVL5	PLAC8	SLC2A4	THRSP	CHPT1
Backfat thickness	1							
IDI1	0.921**	1						
ACACA	0.935**	0.959**	1					
ELOVL5	0.916**	0.991**	0.952**	1				
PLAC8	0.934**	0.959**	0.948**	0.967**	1			
SLC2A4	0.908**	0.928**	0.965**	0.910**	0.873*	1		
THRSP	0.884**	0.915**	0.967**	0.918**	0.915**	0.970**	1	
CHPT1	−0.928**	−0.889**	−0.885**	−0.890**	−0.955**	−0.855*	−0.898**	1

*The *symbol indicates the significant difference ($P < 0.05$). The **symbol indicates extremely significant difference ($P < 0.01$).*

TABLE 3 | Correlation analysis between backfat thickness and various genes in Tibetan pigs.

Projects	Backfat thickness	IDI1	ACACA	ELOVL5	PLAC8	SLC2A4	THRSP	CHPT1
Backfat thickness	1							
IDI1	0.741	1						
ACACA	0.868**	0.953	1					
ELOVL5	0.823	0.700	0.930*	1				
PLAC8	0.766	0.999*	0.964	0.727	1			
SLC2A4	0.890**	0.706	0.991**	0.830	0.732	1		
THRSP	0.894**	0.934	0.991**	0.947*	0.947	0.976**	1	
CHPT1	−0.134	−0.743	−0.958*	−0.652	−0.768	−0.958*	−0.909*	1

*The *symbol indicates the significant difference ($P < 0.05$). The **symbol indicates extremely significant difference ($P < 0.01$).*

across membranes, and plays an important role in glucose metabolism, and was enriched in the present assay in AMPK signaling pathway, insulin signaling pathway and adipocyte factor signaling pathways. KEGG results showed the meaningful signaling pathways were mainly focused on glucose metabolism. Some of these pathways, such as 'glycolysis/gluconeogenesis', although they are not directly related to lipid synthesis and metabolism, glucose and lipids can be interconverted and jointly participate in the tricarboxylic acid cycle. Therefore, glucose metabolic processes may have an indirect effect on lipid metabolism. The KEGG results showed the pathways were mostly concentrated on glucose metabolism. some of these pathways, such as 'Glycolysis/Gluconeogenesis', although they are not directly related to lipid synthesis and metabolism, glucose and lipids can change Therefore, the process of glucose metabolism can have an indirect effect on lipid metabolism (23). Thyroid hormone response protein (THRSP), alias LPGP1, SPOT14, THRP, is induced by thyroid hormone expression and is closely related to lipid deposition in animals. The changes in THRSP gene mRNA content in tissues directly affect the ability of tissues to synthesize lipids. In previous studies, THRSP was considered as a candidate gene for growth traits and played an important role in adipogenesis, and was significantly expressed in subcutaneous adipose tissue of yaks. The sequencing results in this paper showed that THRSP was also highly expressed in pig dorsal lipid tissue, and the conclusion was consistent with it, which is of scientific significance for further study as a key candidate gene for fat deposition.

The choline phosphotransferase 1 gene (CHPT1), alias CPT and CPT1, was first successfully cloned in humans in 2000, but its cloning in pigs has not yet been reported. The CHPT1 gene is involved in lipid metabolism, transferring part of the phosphorylcholine from CDP-Choline to lipid The CHPT1 gene is involved in the process of lipid metabolism and can transfer part of the phosphorylcholine from CDP-Choline to the raw material of lipid production (diglycerides) to produce phosphatidylcholine, which has the biological functions of regulating the normal synthesis and metabolism of lipids and reducing the concentration of cholesterol and triglyceride levels (29); the CHPT1 gene expression differs more than 20-fold in the dorsal fat of Rongchang pigs at 240 days of age and 30 days of age (30). In the present study, the CHPT1 gene was differentially expressed in dorsal fat tissues at different age stages and was negatively correlated with pig backfat thickness. It is speculated that this gene may be a potential gene for fat deposition traits in pigs.

The mRNA expressions of IDI1, PLAC8 and ELOVL5 genes in this study, although is not significantly different in the correlation analysis with backfat thickness in Tibetan pigs, was still positively correlated, suggesting that these three genes are potential candidates for regulating fat deposition traits in pigs. Isopentenyl-diphosphate isomerase 1 (isopentenyl-diphosphate delta-isomerase 1, IDI1), was screened in GO entries regulating the terpene skeleton biosynthesis pathway and cholesterol biosynthesis process. It is a cytoplasmic enzyme involved in the biosynthesis of isoprenoids, including cholesterol, and is

associated with fatty acid metabolism, lipoprotein signaling and cholesterol metabolism (31). The expression of placenta-specific protein 8 (PLAC8) has not been shown in pigs, but in this experiment the expression of PLAC8 gene on dorsal lipid tissues showed an increasing trend with increasing age.PLAC8 affects the differentiation and formation of brown adipocytes and is an important regulator in the process of adipogenesis (32). The elongase of very long-chain fatty acids 5 (ELOVL5), as the initiator and rate-limiting enzyme of fatty acid synthesis, plays an important role in the synthesis of fatty acids in animals and is involved in the extension of fatty acid chains and regulation of fatty acid synthesis, respectively, affecting the body's blood glucose and lipid concentrations, and is extremely relevant to fat deposition traits. It is extremely relevant to fat deposition traits and is important to be further validated as a key gene for fat deposition traits.

CONCLUSIONS

In this study, Tibetan and York pigs at different growth stages were used as test subjects, and their dorsal fat tissues were collected for transcriptome sequencing, and a total of 32,747 differentially expressed genes were screened. The range was narrowed down to 324 differentially expressed genes by screening the differentially expressed genes between breeds and days of age. The functional enrichment analysis revealed significant enrichment to the entries of metabolic pathways, steroid biology, unsaturated fatty acid synthesis pathway and lipid metabolism. And finally, seven differential genes were screened for joint validation of the regulatory role of pig backfat thickness on fat deposition, and it was hypothesized that Tibetan pig backfat thickness was highly significantly and positively associated with ACACA, SLC2A4 and THRSP genes, and York pigs were highly and positively associated with IDI1, ACACA, ELOVL5, PLAC8, SLC2A4 and THRSP genes, and Tibetan pigs Both Tibetan pigs and York pigs showed highly significant negative correlations with CHPT1 gene. This study initially revealed the differentially expressed genes and signaling pathways affecting fat deposition and metabolism in Tibetan and York pigs, and laid a theoretical foundation for the improvement of fat deposition ability in pigs.

DATA AVAILABILITY STATEMENT

The datasets presented in this study can be found in online repositories. The names of the repository and accession number can be found below: SRA database, accession number SRP372504.

ETHICS STATEMENT

The animal study was reviewed and approved by the Animal Welfare Committee of Tibet Agriculture and Animal Husbandry University.

AUTHOR CONTRIBUTIONS

PS and ZW conceived the experiments. PS and YC performed the experiments and analyzed the data. XG and MZ wrote and revised the paper. JZ and YY revised the paper. MD reviewed the paper. All authors have read and agreed to the published version of the manuscript.

FUNDING

This study was supported by the National Natural Science Foundation of China (32160773), Major Science and Technology Projects of the Tibet Autonomous Region (XZ202101ZD0005N), the Graduate Innovation Program of Tibet Institute of Agriculture and Animal Husbandry (YJS2022-21), and Key R&D Plan of Bayi District, Nyingchi City (2021-GX-SY-01).

SUPPLEMENTARY MATERIAL

The Supplementary Material for this article can be found online at: https://www.frontiersin.org/articles/10.3389/fvets.2022.919904/full#supplementary-material

REFERENCES

1. Vergne T, Chen-Fu C, Li S, Cappelle J, Edwards J, Martin V, et al. Pig empire under infectious threat: risk of African swine fever introduction into the People's Republic of China. *Veterinary Rec.* (2017) 181:117–117. doi: 10.1136/vr.103950
2. Wang B, Li P, Zhou W, Gao C, Liu H, Li H, et al. Association of twelve candidate gene polymorphisms with the intramuscular fat content and average backfat thickness of Chinese Suhuai pigs. *Animals.* (2019) 9:858. doi: 10.3390/ani9110858
3. Wang G, Kim WK, Cline MA, Gilbert ER. Factors affecting adipose tissue development in chickens: a review. *Poult Sci.* (2017) 96:3687–99. doi: 10.3382/ps/pex184
4. Wang W, Li X, Ding N, Teng J, Zhang S, Zhang Q, et al. miR-34a regulates adipogenesis in porcine intramuscular adipocytes by targeting ACSL4. *BMC Genetics.* (2020) 21:7. doi: 10.1186/s12863-020-0836-7
5. Xu K, Ji M, Huang X, Peng Y, Wu W, Zhang J. Differential regulatory roles of micrornas in porcine intramuscular and subcutaneous adipocytes. *J Agric Food Chem.* (2020) 68:3954–62. doi: 10.1021/acs.jafc.9b08191
6. Laghouaouta H, Sosa-Madrid BS, Zubiri-Gaitán A, Hernández P, Blasco A. Novel genomic regions associated with intramuscular fatty acid composition in rabbits. *Animals.* (2020) 10:2090. doi: 10.3390/ani10112090
7. Zhang Q, Cai R, Tang G, Zhang W, Pang W. MiR-146a-5p targeting SMAD4 and TRAF6 inhibits adipogenensis through TGF-β and AKT/mTORC1 signal pathways in porcine intramuscular preadipocytes. *J Anim Sci Biotechnol.* (2021) 12:1. doi: 10.1186/s40104-020-00525-3
8. Shen S, Liao Q, Zhang T, Pan R, Lin L. Myricanol modulates skeletal muscle-adipose tissue crosstalk to alleviate high-fat diet-induced obesity and insulin resistance. *Br J Pharmacol.* (2019) 176:3983–4001. doi: 10.1111/bph.14802
9. Chen G, Cheng X, Shi G, Zou C, Chen L, Li J, et al. Transcriptome analysis reveals the effect of long intergenic noncoding rnas on pig muscle growth and fat deposition. *Biomed Res Int.* (2019) 2019:1–15. doi: 10.1155/2019/2951427

10. Song SQ, Ma WW, Zeng SX, Zhang CL, Yan J, Sun CC, et al. Transcriptome analysis of differential gene expression in the longissimus dorsi muscle from Debao and landrace pigs based on RNA-sequencing. *Biosci Rep.* (2019) 39:12. doi: 10.1042/BSR20192144
11. Ma YF, Han XM, Huang CP, Zhong L, Adeola AC, Irwin DM, et al. Population genomics analysis revealed origin and high-altitude adaptation of tibetan pigs. *Scientific Rep.* (2019) 9:6. doi: 10.1038/s41598-019-47711-6
12. Huang Z, Li Q, Li M, Li C. Transcriptome analysis reveals the long intergenic noncoding RNAs contributed to skeletal muscle differences between Yorkshire and Tibetan pig. *Scientific Rep.* (2021) 11:2. doi: 10.1038/s41598-021-82126-2
13. Zhao X, Mo D, Li A, Gong W, Xiao S, Zhang Y, et al. Comparative analyses by sequencing of transcriptomes during skeletal muscle development between pig breeds differing in muscle growth rate and fatness. *PLoS One.* (2011) 6:e19774. doi: 10.1371/journal.pone.0019774
14. Dang P, Fisher SA, Stefanik DJ, Kim J, Raper JA. Coordination of olfactory receptor choice with guidance receptor expression and function in olfactory sensory neurons. *PLoS Genet.* (2018) 14:e1007164. doi: 10.1371/journal.pgen.1007164
15. Yang J, Chen X, Zhu C, Peng X, He X, Fu J, et al. Using RNA-seq to profile gene expression of spikelet development in response to temperature and nitrogen during Meiosis in rice (*Oryza sativa L.*) *PLoS One.* (2015) 10:e0145532. doi: 10.1371/journal.pone.0145532
16. Hill JT, Demarest BL, Bisgrove BW, Gorsi B, Su Y-C, Yost HJ. MMAPPR: mutation mapping analysis pipeline for pooled RNA-seq. *Genome Res.* (2013) 23:687–97. doi: 10.1101/gr.146936.112
17. Talbott H, Hou X, Qiu F, Zhang P, Guda C, Yu F, et al. Transcriptomic and bioinformatics analysis of the early time-course of the response to prostaglandin F2 alpha in the bovine corpus luteum. *Data Brief.* (2017) 14:695–706. doi: 10.1016/j.dib.2017.08.026
18. Tao X, Liang Y, Yang X, Pang J, Zhong Z, Chen X, et al. Transcriptomic profiling in muscle and adipose tissue identifies genes related to growth and lipid deposition. *PLoS One.* (2017) 12:e0184120. doi: 10.1371/journal.pone.0184120
19. Ramayo-Caldas Y, Mercadé A, Castelló A, Yang B, Rodríguez C, Alves E, et al. Genome-wide association study for intramuscular fatty acid composition in an Iberian × Landrace cross1. *J Anim Sci.* (2012) 90:2883–93. doi: 10.2527/jas.2011-4900
20. Xing K, Wang K, Ao H, Chen S, Tan Z, Wang Y, et al. (2019). Comparative adipose transcriptome analysis digs out genes related to fat deposition in two pig breeds. *Scientific Rep.* 9:5. doi: 10.1038/s41598-019-49548-5
21. Liu L, Wang Y, Liang X, Wu X, Liu J, Yang S, et al. Stearoyl-CoA desaturase is essential for porcine adipocyte differentiation. *Int J Mol Sci.* (2020) 21:2446. doi: 10.3390/ijms21072446
22. Tummaruk P, Lundeheim N, Einarsson S, Dalin AM. Effect of birth litter size, birth parity number, growth rate, backfat thickness and age at first mating of gilts on their reproductive performance as sows. *Anim Reprod Sci.* (2001) 66:225–37. doi: 10.1016/S0378-4320(01)00095-1
23. Liu Y, Yu Y, Ao H, Zhang F, Zhao X, Liu H, et al. Identification of long non-coding RNAs involved in porcine fat deposition using two high-throughput sequencing methods. *Genes.* (2021) 12:9. doi: 10.3390/genes12091374
24. Yin H, Wang X, Zhang X, Wang Y, Zeng Y, Xiong Y, et al. Integrated analysis of lncRNA associated-competing endogenous RNAs as prognostic biomarkers in clear cell renal carcinoma. *Cancer Sci.* (2018) 28:138. doi: 10.1111/cas.13778
25. Liu Y, Yang X, Jing X, He X, Wang L, Liu Y, et al. Transcriptomics analysis on excellent meat quality traits of skeletal muscles of the chinese indigenous min pig compared with the large white breed. *Int J Mol Sci.* (2017) 19:21. doi: 10.3390/ijms19010021
26. Barber MC, Price NT, Travers MT. Structure and regulation of acetyl-CoA carboxylase genes of metazoa. *Biochimica et Biophysica Acta.* (2005) 1733:1–28. doi: 10.1016/j.bbalip.2004.12.001
27. Wang L, Zhang Y, Zhang B, Zhong H, Lu Y, Zhang H. Candidate gene screening for lipid deposition using combined transcriptomic and proteomic data from Nanyang black pigs. *BMC Genomics.* (2021) 22:2. doi: 10.1186/s12864-021-07764-2
28. Michael C, Maureen T. Elucidation of a promoter activity that directs the expression of acetyl-CoA carboxylase α with an alternative N-terminus in a tissue-restricted fashion. *Biochem J.* (1998) 333:17–25. doi: 10.1042/bj3330017
29. Boumann A, de Kruijff B, Heck AR, de Kroon Anton I. The selective utilization of substrates in vivo by the phosphatidylethanolamine and phosphatidylcholine biosynthetic enzymes Ept1p and Cpt1p in yeast. *FEBS Lett.* (2004) 569:173–7. doi: 10.1016/j.febslet.2004.05.043
30. Wilhelm JA. *Next-generation DNA Sequencing Techniques.* New Biotechnology (2009).
31. Nakamura K, Mori F, Tanji K, Miki Y, Yamada M, Kakita A, et al. Isopentenyl diphosphate isomerase, a cholesterol synthesizing enzyme, is localized in Lewy bodies. *Neuropathology.* (2015) 35:432–40. doi: 10.1111/neup.12204
32. Li M, Liu D, Wang L, Wang W, Wang A, Yao Y. Expression of placenta-specific 8 in human oocytes, embryos, and models of in vitro implantation. *Fertil Steril.* (2016) 106:781–89. doi: 10.1016/j.fertnstert.2016.05.018

Conflict of Interest: The authors declare that the research was conducted in the absence of any commercial or financial relationships that could be construed as a potential conflict of interest.

frontiers | Frontiers in Veterinary Science

ORIGINAL RESEARCH
published: 27 June 2022
doi: 10.3389/fvets.2022.918541

Integrated Bacteria-Fungi Diversity Analysis Reveals the Gut Microbial Changes in Buffalo With Mastitis

Xiushuang Chen[1,2†], Miao An[3†], Wenqian Zhang[3†], Kun Li[1,2], Muhammad Fakhar-e-Alam Kulyar[3], Kun Duan[4], Hui Zhou[1], Yu Wu[1], Xin Wan[1], Jianlong Li[5], Lingtong Quan[6], Zhanhai Mai[5], Wenxia Bai[7] and Yi Wu[1,2]*

[1] College of Veterinary Medicine, Nanjing Agricultural University, Nanjing, China, [2] MOE Joint International Research Laboratory of Animal Health and Food Safety, College of Veterinary Medicine, Nanjing Agricultural University, Nanjing, China, [3] College of Veterinary Medicine, Huazhong Agricultural University, Wuhan, China, [4] China Tobacco Henan Industrial Co. Ltd., Zhengzhou, China, [5] College of Veterinary Medicine, Xinjiang Agricultural University, Urumqi, China, [6] College of Life Sciences, Nanjing Agricultural University, Nanjing, China, [7] Nanjing Superbiotech Co. Ltd., Nanjing, China

The gut microbial community is closely related to mastitis, but studies regarding the influences of mastitis on gut microbiota in buffalo remain scarce. Herein, we characterized the differences in gut bacterial and fungal communities between mastitis-affected and healthy buffalos. Interestingly, although mastitis had no effect on gut bacterial and fungal diversities in the buffalos, some bacterial and fungal taxa were significantly altered. Bacterial and fungal taxonomic analysis showed that the preponderant bacterial phyla (Firmicutes and Bacteroidetes) and fungal phyla (Ascomycota and Basidiomycota) in buffalo were the same regardless of health status. At the level of genus, the changes in some gut bacterial and fungal abundances between both groups were gradually observed. Compared with healthy buffalos, the proportions of 3 bacterial genera (*uncultured_bacterium_f_Muribaculaceae*, *Eubacterium_nodatum_group,* and *Lachnoclostridium_10*) and 1 fungal genus (*Pichia*) in the mastitis-affected buffalo were significantly increased, whereas 4 bacterial genera (*Ruminococcus_2*, *Candidatus_Stoquefichus*, *Turicibacter,* and *Cellulosilyticum*) and 4 fungal genera (*Cladosporium*, *Thermothelomyces*, *Ganoderma* and *Aspergillus*) were significantly decreased. Taken together, this research revealed that there was significant difference in the compositions of the gut microbial community between the healthy and mastitis-affected buffalos. To our knowledge, this is the first insight into the characteristics of the gut microbiota in buffalos with mastitis, which is beneficial to understand the gut microbial information of buffalo in different health states and elucidate the pathogenesis of mastitis from the gut microbial perspective.

Keywords: gut microbiota, bacterial, fungal, buffalo, mastitis

OPEN ACCESS

Edited by:
Fazul Nabi,
Lasbela University of Agriculture, Water and Marine Sciences, Pakistan

Reviewed by:
Tariq Jamil,
Friedrich Loeffler Institut, Germany
Prerona Boruah,
DY Patil Deemed to be University, India

****Correspondence:***
Yi Wu
wuyi2001cn@163.com

† These authors have contributed equally to this work

Specialty section:
This article was submitted to Comparative and Clinical Medicine, a section of the journal Frontiers in Veterinary Science

Received: *12 April 2022*
Accepted: *24 May 2022*
Published: *27 June 2022*

Citation:
Chen X, An M, Zhang W, Li K, Kulyar MF-e-A, Duan K, Zhou H, Wu Y, Wan X, Li J, Quan L, Mai Z, Bai W and Wu Y (2022) Integrated Bacteria-Fungi Diversity Analysis Reveals the Gut Microbial Changes in Buffalo With Mastitis. Front. Vet. Sci. 9:918541. doi: 10.3389/fvets.2022.918541

INTRODUCTION

Mastitis, an inflammatory response of the mammary parenchyma, affects almost all lactating mammals especially high-yield cows (1). It can lead to decreased milk production, severely restraining dairy industry development (2). Early investigation revealed that fecal microbiota transplantation from cows with mastitis to germ-free mice caused inflammations in

multiple tissues, such as colon, spleen, and serum, as well as mastitis symptoms in the mammary gland (3). Moreover, probiotic administration has been demonstrated to effectively alleviate mastitis symptoms in some exploratory human clinical trials, indicating that the mechanism of mastitis protection may be mediated through the gut microbiota (4).

Growing evidence indicated that gut microbiota participated in multiple physiological and metabolic functions of the host, including nutrient acquisition, intestinal epithelium differentiation, and intestinal metabolism (5–8). Moreover, the gut microbiota has also been demonstrated to play role in intestinal mucosal barrier and immune system maturation, implying its contribution in disease prevention and immunologic functions (9, 10). However, multiple environmental-related factors, such as diet, nutritional deficiencies, antibiotic treatment, and exposure to contaminants, may affect gut microbial homeostasis or even induce gut microbial dysbiosis (11, 12). Stable gut microbiota enabled the intestines to function properly, whereas gut microbial dysbiosis may cause etiopathologic consequences (13, 14). Currently, gut microbial dysbiosis has been shown to be the core and critical factor of many gastrointestinal diseases, such as colonitis and diarrhea (15, 16). Additionally, disturbed gut microbiota and its metabolites could pass through the intestinal mucosal barrier and affect peripheral organ systems by blood circulation, causing physiological dysfunction and even disease, such as lipid disorders, diabetes, and non-alcoholic fatty liver (17, 18).

Recently, culture-independent techniques, mainly including metagenomic and 16S rDNA amplicon sequencing, have been successfully developed and widely applied to dissect the complicated gut microbial ecosystem, as well as investigate gut microbial alterations after suffering certain diseases (19, 20). By systematically investigating and analyzing the microbial information acquired, we can further understand the gut microbiota-host interaction and mechanisms contributing to ill-health, thereby formulating effective measures to minimize the collateral damage. Presently, high-throughput sequencing technologies have successfully dissected the gut microbiota of giraffes, yaks, goats, and dairy cattle, making considerable contributions to the etiological analysis, diagnosis, and treatment of multiple gastrointestinal and systemic diseases (5, 21, 22). As an important source of protein acquisition for humans, buffalo milk has increasingly attracted widespread attention due to its high fat, protein, mineral, and vitamin contents. However, mastitis dramatically decreases buffalo milk production and quality, causing significant health and economic burden in buffalo farming. Although the gut microbial importance in host health is widely acknowledged, scarce knowledge is known about the interaction between mastitis and gut microbiota in buffalo. Herein, we investigated the gut bacterial and fungal shifts of buffalo with mastitis.

MATERIALS AND METHODS

Animals and Sample Collection

In this investigation, 10 buffalos (5 healthy and 5 with mastitis) in Jingzhou, China were used for sample acquisition, and all selected buffalos had similar characteristics, including age, weight, diet, immune background, and dwelling environment. Buffalo mastitis was diagnosed by the California mastitis test (CMT) using a commercial kit. Moreover, the confirmed cases did not receive any treatment prior to the sample collection. On the day of sample collection, all the selected buffalos were placed in separate areas to maximally decrease potential contamination among different samples of subjects. The sterilized fecal samplers were used for collecting the rectal feces of each buffalo. The collected samples were immediately placed intosterile plastic containers and transported to the laboratory and later stored at −80°C for further study.

16S rDNA and ITS Genes Amplicon Sequencing

Five fecal samples (∼200 mg) from healthy and mastitis-affected buffaloes were unfrozen and homogenized before DNA extraction. Subsequently, the bacterial and fungal DNA of the processed fecal samples were extracted using QIAamp DNA Mini Kit (QIAGEN, Hilden, Germany) based on the manufacturer's recommendations. The quality and quantity of the gDNA were evaluated *via* 0.8% (w/v) agarose gel electrophoresis and UV-Vis spectrophotometer (NanoDrop 2000, United States), respectively. To characterize the gut bacterial and fungal shifts, we amplified the V3/V4 and ITS2 regions utilizing bacterial (338F: ACTCCTACGGGAGGCAGCA and 806R: GGACTACHVGGGTWTCTAAT) and fungal (ITS5F: GGAAG TAAAAGTCGTAACAAGG and ITS2R: GCTGCGT TCTTCATCGA TGC) primers, respectively. PCR amplification was conducted as per the procedure previously described (5, 6). PCR products were subjected to target fragment recovery and quality evaluation and gel electrophoresis to obtain purified products. The recovered products were quantified by fluorescence using Quant-iT PicoGreen dsDNA Assay Kit on the Promega QuantiFluor fluorescent quantitative system and the libraries with a concentration above 2 nM and only one peak were considered qualified. The final purified products were applied for preparing the sequencing library using MiSeq Reagent Kit V3 (600 cycles) on the MiSeq sequencing machine.

Bioinformatics and Statistical Analysis

The raw data was requested to be preprocessed. Specifically, quality detection and primer removal were applied to initial data with some problematic sequences, including unqualified, short, or mismatched sequences, to acquire clean reads through the Trimmomatic (v0.33) and Cutadapt software (1.9.1). The collected clean reads were subjected to splice and secondary filter as per the length range of different regions using Usearch software (v10). Afterward, recognition and removal of chimera sequences were conducted to achieve effective reads. The effective reads with 97 similarities were clustered into the same operational taxonomic unit (OTU). Moreover, Venn graphs were also generated to visualize the OTUs abundance and distribution in each group. To further dissect the influence of mastitis on gut microbial diversity and abundance, we computed multiple alpha diversity indexes according to the OTUs' distribution. On the other hand, beta diversity analysis was used for characterizing

TABLE 1 | Bacterial sequence information from amplicon sequencing.

Sample	Raw reads	Clean reads	Effective reads	AvgLen (bp)	GC (%)	Q20 (%)	Q30 (%)	Effective (%)
CB1	48,793	35,977	33,927	413	52.44	99.90	99.32	69.53
CB2	48,184	35,934	33,823	415	52.01	99.89	99.24	70.20
CB3	45,977	35,014	30,642	409	53.04	99.89	99.30	66.65
CB4	56,419	41,677	39,317	414	52.23	99.90	99.30	69.69
CB5	64,898	48,378	45,206	410	53.00	99.90	99.35	69.66
MB1	52,600	38,853	36,284	413	52.50	99.90	99.33	68.98
MB2	58,347	44,008	41,694	413	52.29	99.91	99.34	71.46
MB3	46,523	34,649	32,959	412	52.75	99.90	99.28	70.84
MB4	54,475	39,900	38,014	411	53.01	99.89	99.32	69.78
MB5	59,573	42,703	40,291	410	53.25	99.91	99.34	67.63

TABLE 2 | Fungal sequence information from amplicon sequencing.

Sample	Raw reads	Clean reads	Effective reads	AvgLen (bp)	GC (%)	Q20 (%)	Q30 (%)	Effective (%)
CB1	63,677	46,541	46,229	211	46.99	99.98	99.92	72.60
CB2	74,384	52,096	51,858	191	41.95	99.98	99.94	69.72
CB3	71,417	57,065	56,948	172	37.96	99.99	99.95	79.74
CB4	70,972	56,774	56,609	179	38.77	99.99	99.95	79.76
CB5	72,719	56,777	56,667	166	34.39	99.99	99.97	77.93
MB1	69,180	50,752	50,668	168	36.58	99.98	99.95	73.24
MB2	71,736	48,949	48,859	163	34.15	99.97	99.93	68.11
MB3	70,243	50,350	50,268	179	36.95	99.98	99.95	71.56
MB4	72,266	60,497	60,382	180	36.45	99.99	99.96	83.56
MB5	71,335	56,069	55,943	166	35.48	99.99	99.95	78.42

the differences between gut bacterial and fungal principal components. The assessment of sequencing depth for each sample was based on rank abundance and rarefaction curves. Differential bacterial and fungal taxa were determined by the LEfSe and Metastats analysis. Data analysis was performed by SPSS statistical program (v20.0) and *P*-values (means ± SD) <0.05 were recognized as statistically significant.

RESULTS

Sequence Analysis

In this study, we collected a total of 10 fecal samples for amplicon sequencing and 535,789 (CB = 264,271, MB = 271,518), and 707,929 (CB = 353,169, MB = 354,760) original sequences were achieved from the gut bacterial and fungal communities, respectively (**Table 1**). After quality assessment, 906,588 (CB = 372,157, MB = 534,431) eligible sequences were identified, with a median read count of 372,15 (ranging from 306,42 to 452,06) and 534,43 (ranging from 462,29 to 603,82) reads from bacterial V3/4 and fungal ITS2 regions from each sample, respectively (**Table 2**). The qualified sequences were clustered into 671 bacterial OTUs and 142 fungal OTUs as per 97% sequence similarity (**Figures 1A–C,G–I**). Additionally, the amounts of unique bacterial OTUs in CB and MB were 16 and 2 and 653 OTUs were shared in both groups, accounting for approximately 97.31% of the total bacterial OTUs. Meanwhile, we also observed 142 common OTUs in CB and MB, which consisted of more than 100% of the overall fungal OTUs. The results of accumulation and rarefaction curves demonstrated that almost all species can be detected (**Figures 1D–F,J–L**).

Microbial Diversities Analysis Associated With Mastitis

To further explore the influence of mastitis on the gut microbiota of a buffalo, we calculated the alpha and beta diversity indices that could reflect gut microbial diversity. Bacterial and fungal Good's coverage estimates in each sample of CB and MB were almost 100%, implying excellent coverage. Furthermore, there were no significant differences in the bacterial and fungal Chao1 (496.79 ± 144.06 vs. 534.90 ± 79.22, $P = 0.62$; 134.77 ± 3.85 vs. 133.91 ± 7.35, $P = 0.82$), ACE (495.99 ± 143.39 vs. 529.78 ± 77.53, $P = 0.65$; 134.01 ± 2.01 vs. 134.20 ± 5.87, $P = 0.94$), Simpson (0.96 ± 0.011 vs. 0.96 ± 0.010, $P = 0.69$; 0.83 ± 0.025 vs. 0.82 ± 0.030, $P = 0.44$) and Shannon (6.47 ± 0.72 vs. 6.62 ± 0.37, $P = 0.70$; 3.62 ± 0.17 vs. 3.53 ± 0.26, $P = 0.53$) indices between CB and MB (**Figures 2A–H**). Alpha-diversity analysis indicated that mastitis had no distinct effect on the gut bacterial and fungal diversity and abundance in buffalos. Principal coordinate analysis (PCoA) plots that reflect the similarities and differences among different samples were used to assess the gut bacterial and fungal beta-diversity. Results of the beta-diversity analysis showed that the

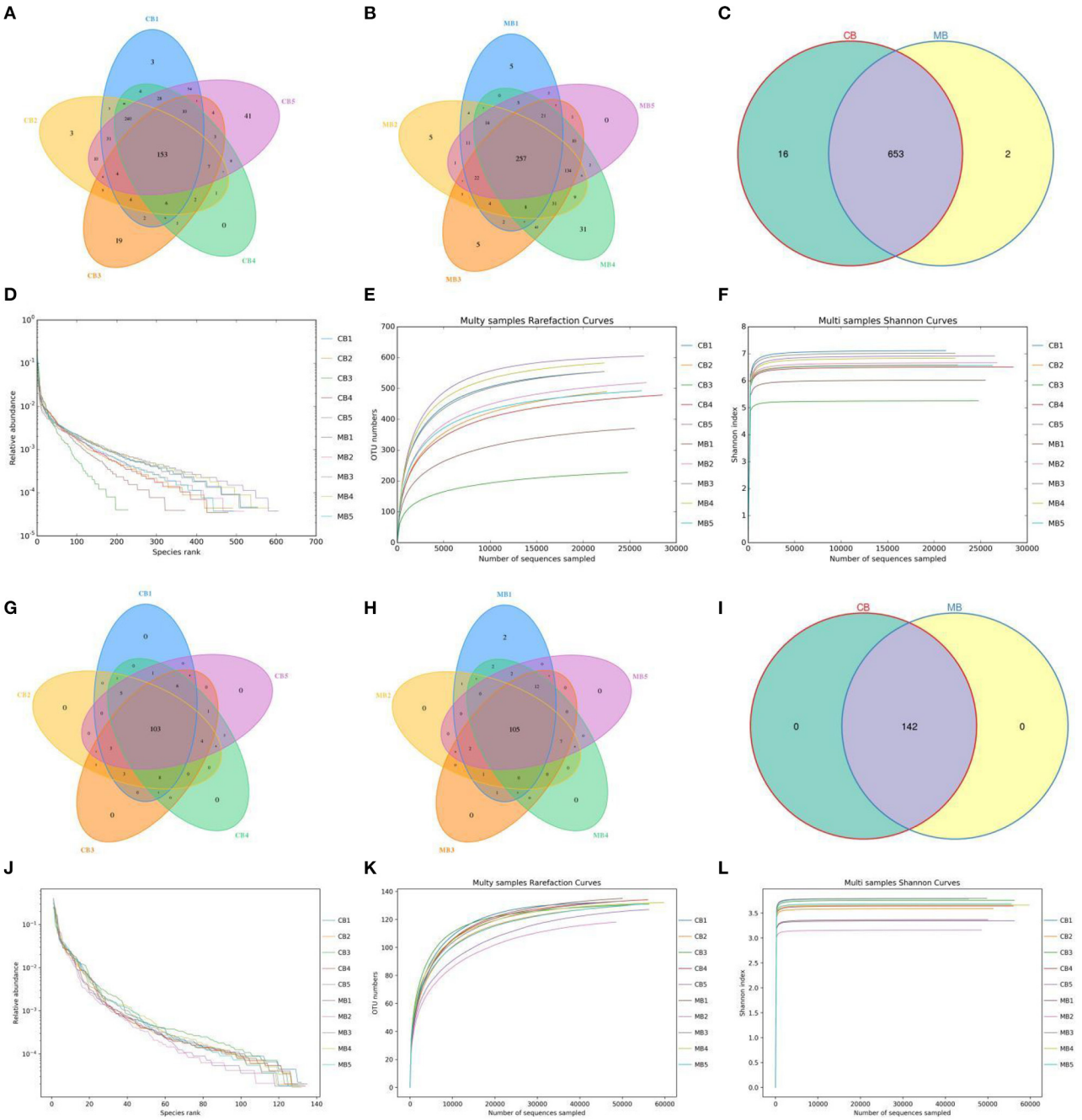

FIGURE 1 | Operational taxonomic units (OTUs) distribution and sequencing data analysis. Venn diagrams for gut bacterial **(A–C)** and fungal **(G–I)** OTUs distribution. Gut bacterial **(D–F)** and fungal **(J–L)** sequencing depth and evenness were assessed by rank abundance and rarefaction curves.

samples in CB and MB were clustered together, implying similar gut microbial principal components (**Figures 2I–L**).

Comparative Analysis of Bacterial Taxonomic Composition

In this microbiome investigation, a total of 9 bacterial phyla and 155 genera were recognized in CB and MB, ranging from 7 to 9 phyla and 103 to 134 genera per sample, respectively. The phyla *Firmicutes* (70.31, 68.19%), *Bacteroidetes* (27.88, 27.50%), *Spirochaetes* (0.53, 1.84%), and *Proteobacteria* (0.56, 1.46%) were the four most preponderant bacterial phyla in samples of CB and MB regardless of health condition, which accounted for approximately 99.00% of the total composition (**Figure 3A**). Other phyla, such as *Patescibacteria* (0.32, 0.45%), *Tenericutes*

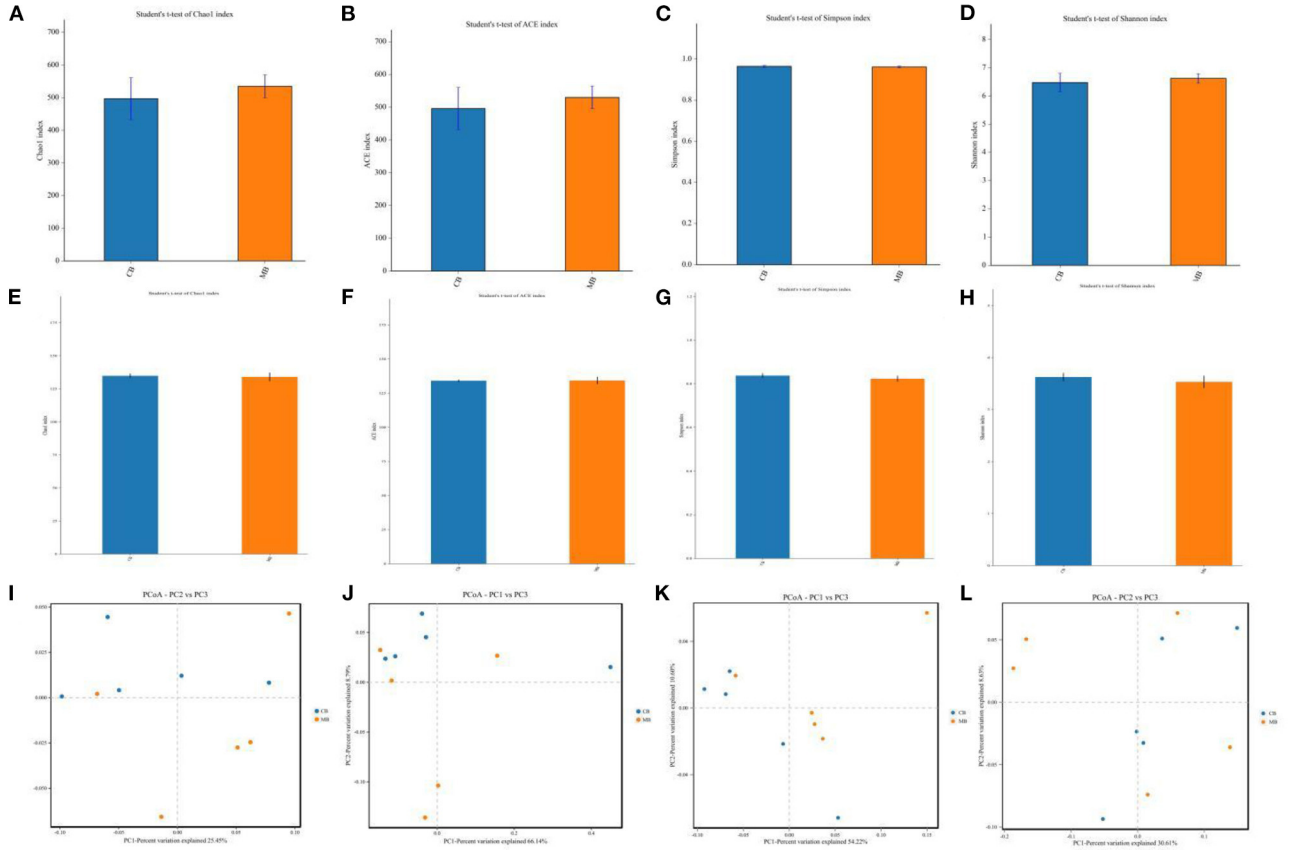

FIGURE 2 | Changes of gut bacterial and fungal diversities associated with mastitis in buffalos. **(A–D)** Represent gut bacterial Chao, ACE, Simpson, and Shannon indices, respectively. **(E–H)** Represent gut fungal Chao, ACE, Simpson, and Shannon indices, respectively. **(I,J)** Represent gut bacterial PCoA maps, whereas **(K,L)** Represent gut fungal PCoA maps.

(0.25, 0.33%), *Actinobacteria* (0.091, 0.10%), *Verrucomicrobia* (0.028, 0.10%), and *Cyanobacteria* (0.024, 0.020%), in CB and MB were identified in lower abundances. At the genus level, the most dominant bacterial genera in the CB were *Ruminococcaceae_UCG-005* (13.79%) followed by the *Bacteroides* (6.88%) and *Rikenellaceae_RC9_gut_group* (6.42%). However, *Ruminococcaceae_UCG-005* (19.25%), *Rikenellaceae_RC9_gut_group* (7.06%) and *uncultured_bacterium_f_Lachnospiraceae* (6.70%) were abundantly present in the MB (**Figure 3B**). Bacterial distribution, as well as correlation of both groups during mastitis could also be observed by the clustering heatmap and network diagram, respectively (**Figures 3E**, **4**).

To further assess the influences of mastitis on the gut microbiota in buffalos, we performed Metastats analysis on different classification levels. At the genus level, *uncultured_bacterium_f_Muribaculaceae*, *Eubacterium_nodatum_group,* and *Lachnoclostridium_10* were significantly more dominant in the MB group than in the CB group, whereas the *Ruminococcus_2* was lower (**Figure 5A**). Besides the above-mentioned differential taxa, the MB group also showed dramatically lower richness of *Candidatus_Stoquefichus*, *Turicibacter,* and *Cellulosilyticum* (**Figures 6A,B**).

Comparative Analysis of Fungal Taxonomic Composition

There were 3 phyla and 66 genera recognized in the gut fungal community of CB and MB and the dominant phyla and genera were presented in **Figures 3C,D**. The *Ascomycota* (77.11, 80.05%) and *Basidiomycota* (22.83, 19.91%) were the most prevalent fungal phyla in both groups, making up approximately 99.00% of the overall fungal composition. The *Ascomycota* (77.11, 80.05%) and *Basidiomycota* (22.83, 19.91%) were the most prevalent fungal phyla in both groups, making up approximately 99.00% of the overall fungal composition. At the genus level, the *Galactomyces* (33.66, 32.91%), *Trichosporon* (21.62, 18.51%), and *unclassified_Dipodascaceae* (11.13, 10.24%) were the most prevalent fungal genera in both groups, which accounted for over 60.00% of the total taxonomical group identified. The clustering heatmap also showed the distribution and changes of gut fungal community in buffalo with mastitis (**Figure 3F**).

Metastats analysis was used to compare the differences in the gut fungal community of both groups (**Figure 5B**). At the genus level, *Cladosporium*, *Thermothelomyces*,

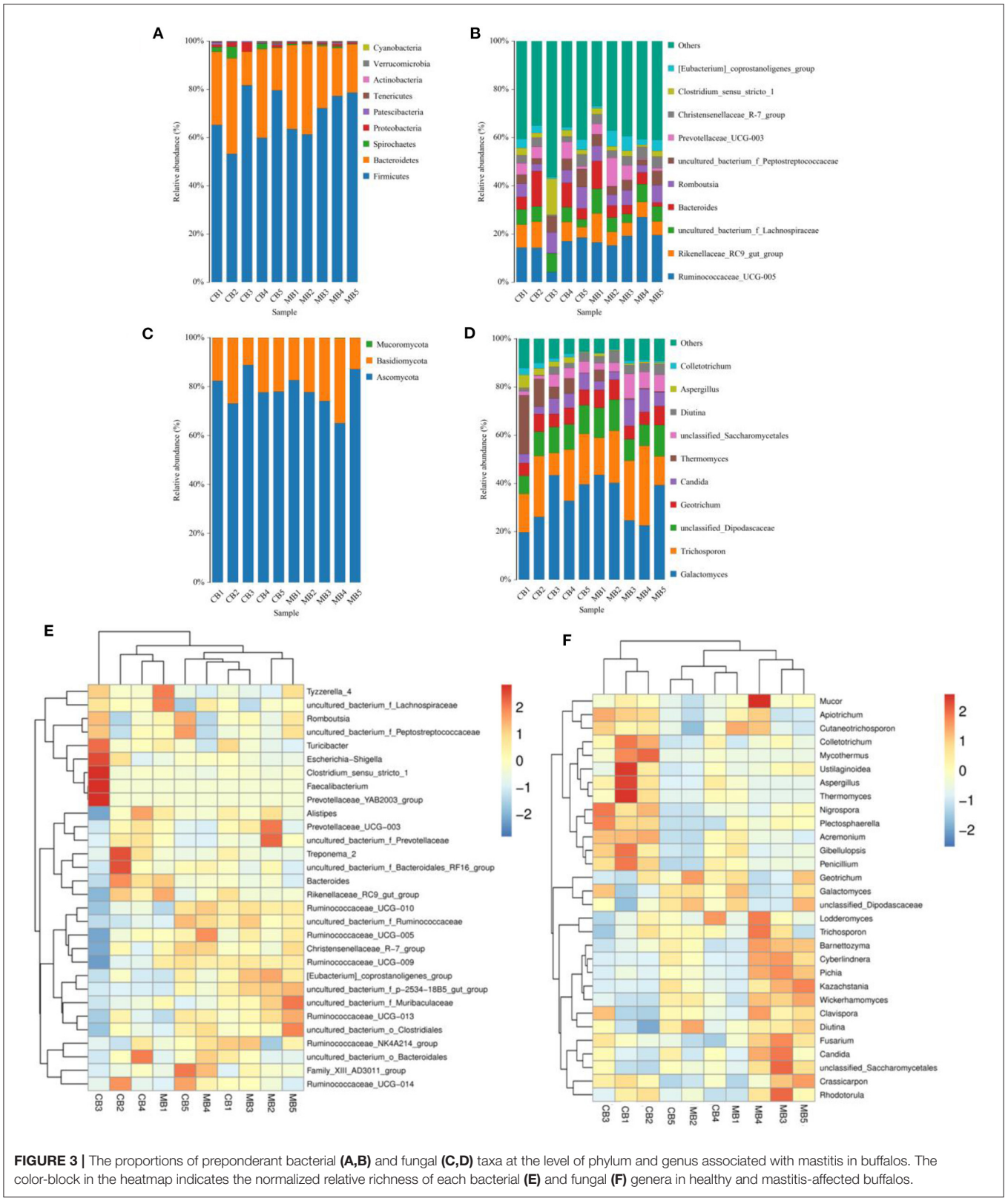

FIGURE 3 | The proportions of preponderant bacterial **(A,B)** and fungal **(C,D)** taxa at the level of phylum and genus associated with mastitis in buffalos. The color-block in the heatmap indicates the normalized relative richness of each bacterial **(E)** and fungal **(F)** genera in healthy and mastitis-affected buffalos.

Ganoderma, and *Aspergillus* were all significantly overrepresented in the CB group, whereas *Pichia* was the most abundant fungus in MB. Similar results were also observed in **Figures 6C,D**.

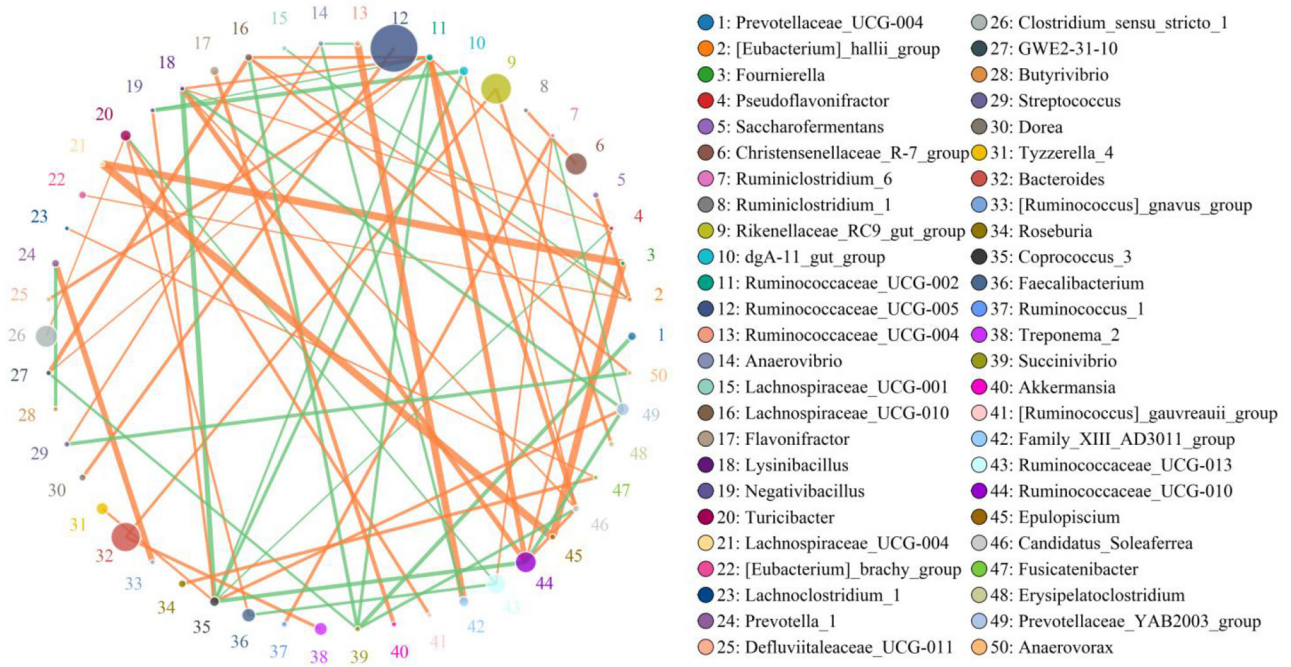

FIGURE 4 | The network diagram visualizes correlations between different bacterial genera. The orange lines indicate a positive correlation and the green lines indicate a negative correlation.

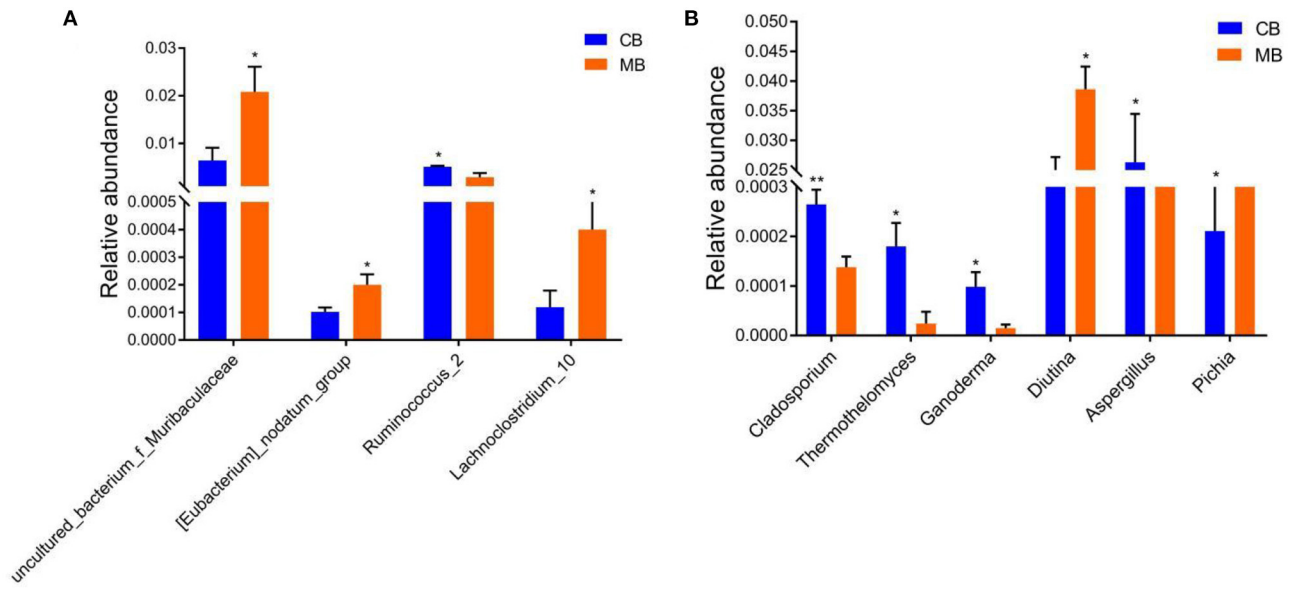

FIGURE 5 | Significant changes in the intestinal bacteria **(A)** and fungi **(B)** associated with mastitis in buffalos. Data was indicated as mean ± SD. $^{*}p < 0.05$, $^{**}p < 0.01$.

DISCUSSION

Mastitis is a common disease in buffalos that seriously affects milk production and animal health, causing enormous economic loss (23). However, multiple factors, including pathogen infection, unclean environment, nutritional deficiency, and stress reaction, cause mastitis to be difficult to control (23–25). A gut microbial community containing trillions of microorganisms has been demonstrated to be a complex and interactive ecosystem that participates in the positive regulation of host metabolism

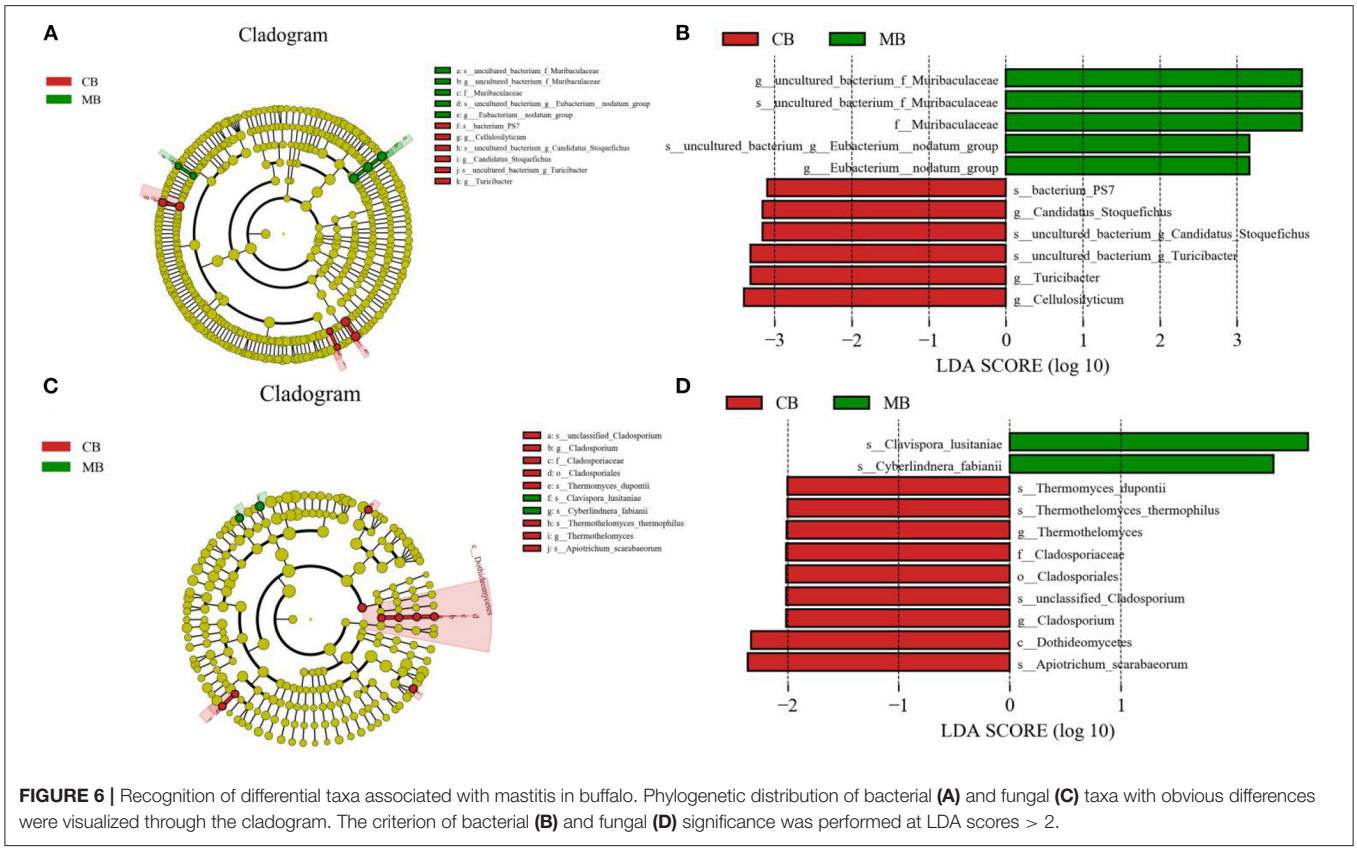

FIGURE 6 | Recognition of differential taxa associated with mastitis in buffalo. Phylogenetic distribution of bacterial **(A)** and fungal **(C)** taxa with obvious differences were visualized through the cladogram. The criterion of bacterial **(B)** and fungal **(D)** significance was performed at LDA scores > 2.

and health (22, 26). Although, these microorganisms, including bacteria and fungi, colonize the intestine, they can expand their negative impact beyond the gastrointestinal tract and thus cause the development of other diseases (27–29). Recent investigations about gut microbiota have also indicated its key role in the development of mastitis in dairy cows (30, 31). Presently, the study of the relationship between gut microbiota and mastitis has covered many species, but research regarding the gut bacterial and fungal communities in buffalo with mastitis remains scarce. Here, we systematically dissected the gut bacterial and fungal changes in buffalo associated with mastitis and indicated distinct changes in gut bacterial and fungal taxa in buffalo during mastitis.

Growing evidence indicated that the gut microbiota was a dynamic system that was inevitably influenced by multiple intrinsic and extrinsic factors, including diet, age, and sex environment (32–34). Generally, the physiological fluctuations of gut microbiota caused by the above-mentioned factors cannot affect intestinal normal function and homeostasis. However, intestinal-related diseases, such as diarrhea, colitis, and colorectal cancer, have been demonstrated to perturb intestinal homeostasis, resulting in dysbiosis (35, 36). Moreover, recent studies have also shown that diabetes, high blood pressure, and obesity could also cause significant changes in the gut microbiota (37–39). In this study, we selected feces to explore the gut microbial changes in buffalos with mastitis in consideration of the samples' availability and subjects' particularity. Results indicated that there were no significant differences in the gut microbial alpha-diversity between healthy and mastitis-affected buffalo, suggesting that mastitis had no effect on the gut microbial diversity and abundance of the buffalos. Consistent with this study, Ma et al. (3) also demonstrated that there were no obvious differences in the gut microbiota alpha-diversity between healthy and mastitis-affected cows. Notably, although the differences in gut bacterial and fungal diversities between controls and mastitis-affected subjects were not significant, the percentages of some bacteria and fungi altered markedly, implying that these intestinal bacteria and fungi are constantly self-adjusting to the current intestinal environment.

In this microbiome investigation, we observed that Firmicutes and Bacteroidetes were the most preponderant bacteria, whereas Basidiomycota and Ascomycota were the most dominant fungi in buffalos, regardless of health status (40–42). Notably, these microbial phyla have also been demonstrated to be widespread in other ruminants, such as goats, cows, giraffes, and yaks, indicating their key roles in intestinal ecology and function (43, 44). Earlier studies indicated that most members of Firmicutes were intestinal beneficial bacteria involved in the regulation of the immune system, gut microbial homeostasis, and intestinal barrier function (45). Moreover, its members contribute to the degradation of cellulose in ruminants (40). As the dominant bacteria in the gut, Bacteroidetes was responsible for degrading carbohydrates and proteins, showing the great potential for promoting the maturation of the gastrointestinal immune system (43). At the genus level, *Bacteroides* were abundantly present in the healthy buffalo, which was inconsistent with the findings of mastitis-affected

buffalo. As intestinal anaerobion, *Bacteroides* can decompose polysaccharides and play a key role in the intestinal ecosystem (46). As intestinal beneficial bacteria, *Rikenellaceae* has been demonstrated to possess multiple probiotic properties and control the development of colitis by regulating T-regulatory cell differentiation (47). *Ruminococcaceae* can degrade cellulose and starch, displaying positive regulation in growing development and feed efficiency (48). Moreover, *Ruminococcaceae*, a potential probiotic candidate, plays active roles in the secretion of short-chain fatty acids (SCFAs), intestinal homeostasis, and host health (49).

The shifts of some specific bacteria and fungi could dissect the potential relationship between gut microbial community and mastitis, thus we further investigated the gut bacterial and fungal changes associated with mastitis. Results showed a significant decrease in 4 bacterial genera (*Ruminococcus_2*, *Candidatus_Stoquefichus*, *Turicibacter,* and *Cellulosilyticum)* and 4 fungal genera *(Cladosporium, Thermothelomyces*, *Ganoderma,* and *Aspergillus*), as well as an increase in 3 bacterial genera (*uncultured_bacterium_f_Muribaculaceae*, *Eubacterium_nodatum_group* and *Lachnoclostridium_10*) and 1 fungal genus (*Pichia*) in mastitis-affected buffalo. These bacteria and fungi may play an important role in intestinal homeostasis and functions, as well as the development of buffalo with mastitis. *Ruminococcus* and *Cellulosilyticum* have been shown to possess the characteristics of decomposing cellulose and starch (50–52). Notably, *Ruminococcus* is also a potential producer of SCFAs (53). Numerous pieces of evidence indicated that SCFAs play a fundamental role in gut microbial homeostasis and host metabolism (54, 55). Furthermore, SCFAs were also involved in the regulation of intestinal permeability, immunologic function, and cell proliferation (56, 57). Therefore, the higher proportions of *Ruminococcus* and *Cellulosilyticum* in the ruminant are beneficial to maintain energy intake and intestinal function.

Taken together, this study first compared and analyzed the differences in gut microbiota between healthy and mastitis-affected buffalos. Results showed that mastitis did not alter the gut bacterial and fungal diversity, but the proportions of some bacterial and fungal taxa altered significantly. This study also contributes to understanding the gut microbial information of buffalos and shows that the changes in gut bacterial and fungal communities may be an important factor of mastitis. Notably, this research is also beneficial to prevent and treat mastitis in buffalos from the gut microbial perspective.

DATA AVAILABILITY STATEMENT

The original contributions presented in the study are included in the article/supplementary material, further inquiries can be directed to the corresponding author/s.

ETHICS STATEMENT

The animal study was reviewed and approved by Ethics Committee of the Nanjing Agricultural University. Written informed consent was obtained from the owners for the participation of their animals in this study.

AUTHOR CONTRIBUTIONS

XC, MA, and WZ conceived and designed the experiments. MA and WZ contributed sample collection and reagents preparation. HZ, YiW, and XW analyzed the data. XC wrote the manuscript. YuW, MFK, KD, JL, LQ, ZM, and WB revised the manuscript. All authors reviewed the manuscript. All authors contributed to the article and approved the submitted version.

FUNDING

This research was financially supported by the National Natural Science Foundation of China (NSFC, Grant Nos. 31872514 and 32172900).

REFERENCES

1. Omaleki L, Browning GF, Allen JL, Markham PF, Barber SR. Molecular epidemiology of an outbreak of clinical mastitis in sheep caused by Mannheimia haemolytica. *Vet Microbiol.* (2016) 191:82–7. doi: 10.1016/j.vetmic.2016.06.005
2. Swinkels JM, Hilkens A, Zoche-Golob V, Kromker V, Buddiger M, Jansen J, et al. Social influences on the duration of antibiotic treatment of clinical mastitis in dairy cows. *J Dairy Sci.* (2015) 98:2369–80. doi: 10.3168/jds.2014-8488
3. Ma C, Sun Z, Zeng B, Huang S, Zhao J, Zhang Y, et al. Cow-to-mouse fecal transplantations suggest intestinal microbiome as one cause of mastitis. *Microbiome.* (2018) 6:200. doi: 10.1186/s40168-018-0578-1
4. Hu X, Guo J, Zhao C, Jiang P, Maimai T, Yanyi L, et al. The gut microbiota contributes to the development of Staphylococcus aureus-induced mastitis in mice. *ISME J.* (2020) 14:1897–910. doi: 10.1038/s41396-020-0651-1
5. Li A, Liu B, Li F, He Y, Wang L, Fakhar-E-Alam KM, et al. Integrated bacterial and fungal diversity analysis reveals the gut microbial alterations in diarrheic giraffes. *Front Microbiol.* (2021) 12:712092. doi: 10.3389/fmicb.2021.712092
6. Hu J, Nie Y, Chen J, Zhang Y, Wang Z, Fan Q, et al. Gradual changes of gut microbiota in weaned miniature piglets. *Front Microbiol.* (2016) 7:1727. doi: 10.3389/fmicb.2016.01727
7. Liu X, Nagy P, Bonfini A, Houtz P, Bing XL, Yang X, et al. Microbes affect gut epithelial cell composition through immune-dependent regulation of intestinal stem cell differentiation. *Cell Rep.* (2022) 38:110572. doi: 10.1016/j.celrep.2022.110572
8. Guo X, Sha Y, Lv W, Pu X, Liu X, Luo Y, et al. Sex differences in rumen fermentation and microbiota of Tibetan goat. *Microb Cell Fact.* (2022) 21:55. doi: 10.1186/s12934-022-01783-8
9. Xiong Y, Ji L, Zhao Y, Liu A, Wu D, Qian J. Sodium butyrate attenuates taurocholate-induced acute pancreatitis by maintaining colonic barrier and regulating gut microorganisms in mice. *Front Physiol.* (2022) 13:813735. doi: 10.3389/fphys.2022.813735
10. Li MX, Li MY, Lei JX, Wu YZ, Li ZH, Chen LM, et al. Huangqin decoction ameliorates DSS-induced ulcerative colitis: role of gut microbiota and amino acid metabolism, mTOR pathway and intestinal epithelial barrier. *Phytomedicine.* (2022) 100:154052. doi: 10.1016/j.phymed.2022.154052
11. Li A, Wang Y, He Y, Liu B, Iqbal M, Mehmood K, et al. Environmental fluoride exposure disrupts the intestinal structure

and gut microbial composition in ducks. *Chemosphere.* (2021) 277:130222. doi: 10.1016/j.chemosphere.2021.130222
12. Liao J, Liu Y, Yi J, Li Y, Li Q, Li Y, et al. Gut microbiota disturbance exaggerates battery wastewater-induced hepatotoxicity through a gut-liver axis. *Sci Total Environ.* (2022) 809:152188. doi: 10.1016/j.scitotenv.2021.152188
13. Li A, Ding J, Shen T, Han Z, Zhang J, Abadeen ZU, et al. Environmental hexavalent chromium exposure induces gut microbial dysbiosis in chickens. *Ecotoxicol Environ Saf.* (2021) 227:112871. doi: 10.1016/j.ecoenv.2021.112871
14. Zhu L, Xu F, Wan W, Yu B, Tang L, Yang Y, et al. Correction to: gut microbial characteristics of adult patients with allergy rhinitis. *Microb Cell Fact.* (2020) 19:192. doi: 10.1186/s12934-020-01441-x
15. Wang Y, Zhang H, Zhu L, Xu Y, Liu N, Sun X, et al. Dynamic distribution of gut microbiota in goats at different ages and health states. *Front Microbiol.* (2018) 9:2509. doi: 10.3389/fmicb.2018.02509
16. Xi L, Qin X, Song Y, Han J, Li Z, Zhang J. Gut microbial alterations in diarrheal baer's pochards (Aythya baeri). *Front Vet Sci.* (2021) 8:756486. doi: 10.3389/fvets.2021.756486
17. Sun CY, Zheng ZL, Chen CW, Lu BW, Liu D. Targeting gut microbiota with natural polysaccharides: effective interventions against high-fat diet-induced metabolic diseases. *Front microbiol.* (2022) 13:859206. doi: 10.3389/fmicb.2022.859206
18. Bauer KC, Littlejohn PT, Ayala V, Creus-Cuadros A, Finlay BB. Nonalcoholic fatty liver disease and the gut-liver axis: exploring an undernutrition perspective. *Gastroenterology.* (2022) 162:1858-75. doi: 10.1053/j.gastro.2022.01.058
19. Ning Y, Qi J, Dobbins MT, Liang X, Wang J, Chen S, et al. Comparative analysis of microbial community structure and function in the gut of wild and captive amur tiger. *Front microbiol.* (2020) 11:1665. doi: 10.3389/fmicb.2020.01665
20. Hu L, Geng S, Li Y, Cheng S, Fu X, Yue X, et al. Exogenous fecal microbiota transplantation from local adult pigs to crossbred newborn piglets. *Front Microbiol.* (2017) 8:2663. doi: 10.3389/fmicb.2017.02663
21. Xin J, Chai Z, Zhang C, Zhang Q, Zhu Y, Cao H, et al. Comparing the microbial community in four stomach of dairy cattle, yellow cattle and three yak herds in qinghai-tibetan plateau. *Front Microbiol.* (2019) 10:1547. doi: 10.3389/fmicb.2019.01547
22. Li A, Yang Y, Qin S, Lv S, Jin T, Li K, et al. Microbiome analysis reveals gut microbiota alteration of early-weaned Yimeng black goats with the effect of milk replacer and age. *Microb Cell Fact.* (2021) 20:78. doi: 10.1186/s12934-021-01568-5
23. Singha S, Ericsson CD, Chowdhury S, Nath SC, Paul OB, Hoque MA, et al. Occurrence and aetiology of subclinical mastitis in water buffalo in Bangladesh. *J Dairy Res.* (2021) 88:314–20. doi: 10.1017/S0022029921000698
24. Krishnamoorthy P, Suresh KP, Jayamma KS, Shome BR, Patil SS, Amachawadi RG. An Understanding of the global status of major bacterial pathogens of milk concerning bovine mastitis: a systematic review and meta-analysis (Scientometrics). *Pathogens.* (2021) 10:545. doi: 10.3390/pathogens10050545
25. Zaatout N. An overview on mastitis-associated Escherichia coli: Pathogenicity, host immunity and the use of alternative therapies. *Microbiol Res.* (2022) 256:126960. doi: 10.1016/j.micres.2021.126960
26. Podar PT, Yang Z, Bjornsdottir SH, Podar M. Comparative analysis of microbial diversity across temperature gradients in hot springs from yellowstone and iceland. *Front Microbiol.* (2020) 11:1625. doi: 10.3389/fmicb.2020.01625
27. Gao Y, Liu Y, Ma F, Sun M, Song Y, Xu D, et al. Lactobacillus plantarum Y44 alleviates oxidative stress by regulating gut microbiota and colonic barrier function in Balb/C mice with subcutaneous d-galactose injection. *Food Funct.* (2021) 12:373–86. doi: 10.1039/D0FO02794D
28. Zhong G, Wan F, Lan J, Jiang X, Wu S, Pan J, et al. Arsenic exposure induces intestinal barrier damage and consequent activation of gut-liver axis leading to inflammation and pyroptosis of liver in ducks. *Sci Total Environ.* (2021) 788:147780. doi: 10.1016/j.scitotenv.2021.147780
29. Xu R, Aruhan, Xiu L, Sheng S, Liang Y, Zhang H, et al. Exopolysaccharides from lactobacillus buchneri TCP016 attenuate LPS- and d-GalN-Induced liver injury by modulating the gut microbiota. *J Agric Food Chem.* (2019) 67:11627–37. doi: 10.1021/acs.jafc.9b04323
30. Pang M, Xie X, Bao H, Sun L, He T, Zhao H, et al. Insights into the bovine milk microbiota in dairy farms with different incidence rates of subclinical mastitis. *Front Microbiol.* (2018) 9:2379. doi: 10.3389/fmicb.2018.02379
31. Hu X, Li S, Fu Y, Zhang N. Targeting gut microbiota as a possible therapy for mastitis. *Eur J Clin Microbiol Infect Dis.* (2019) 38:1409–23. doi: 10.1007/s10096-019-03549-4
32. Yuan X, Chen R, Zhang Y, Lin X, Yang X. Sexual dimorphism of gut microbiota at different pubertal status. *Microb Cell Fact.* (2020) 19:152. doi: 10.1186/s12934-020-01412-2
33. Chen L, Li S, Xiao Q, Lin Y, Li X, Qu Y, et al. Composition and diversity of gut microbiota in Pomacea canaliculata in sexes and between developmental stages. *BMC Microbiol.* (2021) 21:200. doi: 10.1186/s12866-021-02259-2
34. Chang J, Yao X, Zuo C, Qi Y, Chen D, Ma W. The gut bacterial diversity of sheep associated with different breeds in Qinghai province. *BMC VET RES.* (2020) 16:254. doi: 10.1186/s12917-020-02477-2
35. Chen F, Dai X, Zhou CC, Li KX, Zhang YJ, Lou XY, et al. Integrated analysis of the faecal metagenome and serum metabolome reveals the role of gut microbiome-associated metabolites in the detection of colorectal cancer and adenoma. *Gut.* (2021) 71:1315–25. doi: 10.1136/gutjnl-2020-323476
36. Yang Y, Misra BB, Liang L, Bi D, Weng W, Wu W, et al. Integrated microbiome and metabolome analysis reveals a novel interplay between commensal bacteria and metabolites in colorectal cancer. *Theranostics.* (2019) 9:4101–14. doi: 10.7150/thno.35186
37. Calabrese CM, Valentini A, Calabrese G. Gut microbiota and type 1 diabetes mellitus: the effect of mediterranean diet. *Front Nutr.* (2020) 7:612773. doi: 10.3389/fnut.2020.612773
38. Li X, Wei T, Li J, Yuan Y, Wu M, Chen F, et al. Tyrosol ameliorates the symptoms of obesity, promotes adipose thermogenesis, and modulates the composition of gut microbiota in HFD fed mice. *Mol Nutr Food Res.* (2022) e2101015. doi: 10.1002/mnfr.202101015
39. Ye Y, Xu H, Xie Z, Wang L, Sun Y, Yang H, et al. Time-restricted feeding reduces the detrimental effects of a high-fat diet, possibly by modulating the circadian rhythm of hepatic lipid metabolism and gut microbiota. *Front Nutr.* (2020) 7:596285. doi: 10.3389/fnut.2020.596285
40. Zhang L, Jiang X, Li A, Waqas M, Gao X, Li K, et al. Characterization of the microbial community structure in intestinal segments of yak (Bos grunniens). *Anaerobe.* (2020) 61:102115. doi: 10.1016/j.anaerobe.2019.102115
41. Zhuang Y, Chai J, Cui K, Bi Y, Diao Q, Huang W, et al. Longitudinal Investigation of the Gut Microbiota in Goat Kids from Birth to Postweaning. *Microorganisms.* (2020) 8:1111. doi: 10.3390/microorganisms8081111
42. Li K, Mehmood K, Zhang H, Jiang X, Shahzad M, Dong X, et al. Characterization of fungus microbial diversity in healthy and diarrheal yaks in Gannan region of Tibet Autonomous Prefecture. *Acta Trop.* (2018) 182:14–26. doi: 10.1016/j.actatropica.2018.02.017
43. Sun B, Wang X, Bernstein S, Huffman MA, Xia DP, Gu Z, et al. Marked variation between winter and spring gut microbiota in free-ranging Tibetan Macaques (Macaca thibetana). *Sci Rep.* (2016) 6:26035. doi: 10.1038/srep26035
44. Garneau JE, Tremblay DM, Moineau S. Characterization of 1706, a virulent phage from Lactococcus lactis with similarities to prophages from other Firmicutes. *Virology.* (2008) 373:298–309. doi: 10.1016/j.virol.2007.12.002
45. Wang Y, Li A, Liu J, Mehmood K, Wangdui B, Shi H, et al. L pseudomesenteroides and L johnsonii isolated from yaks in Tibet modulate gut microbiota in mice to ameliorate enteroinvasive Escherichia coli-induced diarrhea. *Microb Pathog.* (2019) 132:1–9. doi: 10.1016/j.micpath.2019.04.020
46. Spence C, Wells WG, Smith CJ. Characterization of the primary starch utilization operon in the obligate anaerobe bacteroides fragilis: regulation by carbon source and oxygen. *J Bacteriol.* (2006) 188:4663–72. doi: 10.1128/JB.00125-06
47. Seshadri R, Leahy SC, Attwood GT, Teh KH, Lambie SC, Cookson AL, et al. Cultivation and sequencing of rumen microbiome members from the Hungate1000 Collection. *Nat Biotechnol.* (2018) 36:359–67. doi: 10.1038/nbt.4110
48. Kong F, Hua Y, Zeng B, Ning R, Li Y, Zhao J. Gut microbiota signatures of longevity. *Curr Biol.* (2016) 26:R832–3. doi: 10.1016/j.cub.2016.08.015
49. Reddivari L, Veeramachaneni D, Walters WA, Lozupone C, Palmer J, Hewage M, et al. Perinatal Bisphenol A Exposure Induces Chronic Inflammation in Rabbit Offspring via Modulation of Gut Bacteria and Their Metabolites. *mSystems.* (2017) 2:e00093–17. doi: 10.1128/mSystems.00093-17
50. Miller TL, Currenti E, Wolin MJ. Anaerobic bioconversion of cellulose by Ruminococcus albus, Methanobrevibacter smithii,

and Methanosarcina barkeri. *Appl Microbiol Biotechnol.* (2000) 54:494–8. doi: 10.1007/s002530000430
51. Cai S, Li J, Hu FZ, Zhang K, Luo Y, Janto B, et al. Cellulosilyticum ruminicola, a newly described rumen bacterium that possesses redundant fibrolytic-protein-encoding genes and degrades lignocellulose with multiple carbohydrate- borne fibrolytic enzymes. *Appl Environ Microbiol.* (2010) 76:3818–24. doi: 10.1128/AEM.03124-09
52. De Filippo C, Cavalieri D, Di Paola M, Ramazzotti M, Poullet JB, Massart S, et al. Impact of diet in shaping gut microbiota revealed by a comparative study in children from Europe and rural Africa. *Proc Natl Acad Sci U S A.* (2010) 107:14691–6. doi: 10.1073/pnas.1005963107
53. Juste CGM, Stampini DMH, Tako E. Effects of iron and zinc biofortified foods on gut microbiota in vivo (Gallus gallus): a systematic review. *Nutrients.* (2021) 13:189. doi: 10.3390/nu13010189
54. Cherta-Murillo A, Pugh JE, Alaraj-Alshehhi S, Hajjar D, Chambers ES, Frost GS. The effect of short-chain fatty acids on glycemic control in humans: a systematic review and Meta-analysis. *Am J Clin Nutr.* (2022). doi: 10.1093/ajcn/nqac085. [Epub ahead of print].
55. Zhen Y, Ge L, Xu Q, Hu L, Wei W, Huang J, et al. Normal light-dark and short-light cycles regulate intestinal inflammation, circulating short-chain fatty acids and gut microbiota in period2 gene knockout mice. *Front Immunol.* (2022) 13:848248. doi: 10.3389/fimmu.2022.848248
56. Feng Y, Wang Y, Wang P, Huang Y, Wang F. Short-chain fatty acids manifest stimulative and protective effects on intestinal barrier function through the inhibition of nlrp3 inflammasome and autophagy. *Cell physiol biochem.* (2018) 49:190–205. doi: 10.1159/000492853
57. Blottiere HM, Buecher B, Galmiche JP, Cherbut C. Molecular analysis of the effect of short-chain fatty acids on intestinal cell proliferation. *Proc Nutr Soc.* (2003) 62:101–6. doi: 10.1079/PNS2002215

Conflict of Interest: KD was employed by China Tobacco Henan Industrial Co. Ltd. WB was employed by Nanjing Superbiotech Co. Ltd.

The remaining authors declare that the research was conducted in the absence of any commercial or financial relationships that could be construed as a potential conflict of interest.

frontiers | Frontiers in Veterinary Science

ORIGINAL RESEARCH
published: 28 June 2022
doi: 10.3389/fvets.2022.926906

Evaluating the Effect of Forage Rape (*Brassica napus*) Ensiling Kinetics on Degradability and Milk Performance as Non-conventional Forage for Dairy Buffalo

Mohamed Abdelrahman[1,2], Wei Wang[1], HaiMiao Lv[1], Zhou Di[1], Zhigao An[1], Wang Lijun[1], Aftab Shaukat[1], Wang Bo[3], Zhou Guangsheng[3], Yang Liguo[1,4,5] and Hua Guohua[1,4,5]**

[1] Key Lab of Agricultural Animal Genetics, Breeding and Reproduction of Ministry of Education, Huazhong Agricultural University, Wuhan, China, [2] Animal Production Department, Faculty of Agriculture, Assuit University, Asyut, Egypt, [3] College of Plant Science and Technology, Huazhong Agricultural University, Wuhan, China, [4] National Center for International Research on Animal Genetics, Breeding and Reproduction (NCIRAGBR), Key Laboratory of Smart Farming for Agricultural Animals, Huazhong Agricultural University, Wuhan, China, [5] Hubei Province's Engineering Research Center in Buffalo Breeding and Products, Wuhan, China

OPEN ACCESS

Edited by:
Fazul Nabi,
Lasbela University of Agriculture, Water and Marine Sciences, Pakistan

Reviewed by:
Montaser Elsayed Ali,
Al-Azhar University, Egypt
Zeeshan Ahmad Bhutta,
Chungbuk National University, South Korea

***Correspondence:**
Yang Liguo
ylg@mail.hzau.edu.cn
Hua Guohua
huaguohua@mail.hzau.edu.cn

Specialty section:
This article was submitted to Comparative and Clinical Medicine, a section of the journal Frontiers in Veterinary Science

Received: 23 April 2022
Accepted: 23 May 2022
Published: 28 June 2022

Citation:
Abdelrahman M, Wang W, Lv H, Di Z, An Z, Lijun W, Shaukat A, Bo W, Guangsheng Z, Liguo Y and Guohua H (2022) Evaluating the Effect of Forage Rape (Brassica napus) Ensiling Kinetics on Degradability and Milk Performance as Non-conventional Forage for Dairy Buffalo. Front. Vet. Sci. 9:926906. doi: 10.3389/fvets.2022.926906

The recent increase in demand for animal protein sources has led to the urgency to introduce non-conventional feed sources and opened the space to study feed management and its effects on animal productivity. Forage rape (*Brassica napus* L.) is a high-quality forage crop with a remarkable nutritional value and productive and fast growth capacity; however, studies on processing methods are limited. This study evaluates the effect of an ensiling process on rape silage quality kinetics, *in situ* degradability, and milk responses in dairy buffaloes. Firstly, the whole-plant forage rape was ensiled, and silage samples were collected 30, 60, and 90 days after ensiling to determine pH, evaluation of sensory characteristics, and chemical composition. Then, samples were taken for further chemical analysis at days 30, 60, and 90. After that, the degradability of the dry matter (DM) and crude protein (CP) of the silage was evaluated by an *in situ* degradability experiment using three fistulated buffalos (550 ± 20 kg body weight, 4.7 ± 0.76 years). Finally, whole-plant rape silage (after 60 days) was included in a 10, 20, and 30% of DM dairy buffalo diet in the lactating buffalo ration. The results showed that silage pH did not change significantly during the ensiling process ($p > 0.05$); however, the silage achieved the optimal comprehensive sensory characteristic score from days 30 to 60. There was also a significant change in neutral detergent fiber (NDF) content and acid detergent fiber content, which decreased significantly ($p = 0.001$ and $p < 0.001$, respectively). Ensiling of the whole-plant rape significantly reduced effective DM degradability ($p < 0.05$) without altering CP degradability ($p > 0.05$). Furthermore, the inclusion of forage rape silage linearly ($p = 0.03$) increased milk fat and protein contents and did not affect milk yield, lactose, and urea nitrogen contents in raw buffalo milk.

In conclusion, whole-plant rape silage could significantly maintain the optimal ether extract (EE) protein content without affecting CP degradability, in addition to improving milk fat and milk protein. Therefore, ensiling may be an efficient method of forage rape utilization, and forage rape silage can be recommended as a good forage source for dairy buffaloes.

Keywords: silage, ruminal degradability, buffalo (*Bubalus bubalis*), milk performance, *Brassica napus*

INTRODUCTION

Feed resource limitations are becoming the main obstacle for the livestock production sector, which threatens future expansion opportunities due to increasing global demand for meat and milk. Therefore, the introduction of new forage resources can play an essential role in feed safety and support food production sustainability. For example, forage rape (*Brassica napus*) is a high-quality green forage capable of providing fast-growing and plentiful feed (1, 2). According to the European Economic Community (EEC), the global rapeseed yield reached 68 million tons in 2021/2022, where Canada ranked first globally in terms of total rapeseed yield (28.04%), followed by the EEC (25.10%), China (19.34%), India (11.37%), and Ukraine (4.87%) (3). Also, forage rape is known as "double-low" rape (4, 5) because, compared to traditional rape, forage rape has a lower content of erucic acid (<3%) and glucosinolate (<30 μmol/g) (6). These two compounds are the main anti-nutritive factors found in rape, which reduce feed acceptability and cause goiter, metabolic disorders, and even death. Moreover, forage rape can be intercropped in a pasture-based system due to its higher feed quality during a decline in the yield of other pasture crops such as ryegrass, in addition to high nutritional characteristics, i.e., higher metabolizable energy (ME), crude protein (CP), lower neutral detergent fiber (NDF) content, and reduced CH_4 production (7). In addition, the relatively low cost of producing forage rape promoted this crop as an economical choice for fast-growing feed in resource-limited regions.

There are two significant ways to use rape as feed, the first is to use rapeseed as a meal. Rapeseed meal or canola meal (CM) is now widely used in North American dairy rations as a cost-effective alternative to soybean meal (SBM) (8). Compared to SBM and other protein sources, the inclusion of CM has been shown to increase nitrogen (N) utilization and production performance when fed to lactating dairy cows (9). The second form of rapeseed used as feed is rape straw as a roughage source. As CP content is an essential criterion for evaluating feed quality; rape straw contains (5.24%) CP, which is relatively higher than corn stalks (5%) and wheat straw (3.6%), and also higher than the average of roughage feeds used for ruminants (2.57%) (10).

Nevertheless, the proportion of rape stalks used as fodder feed is relatively low (<10%). Also, rape stalks are burned or wasted in the field, which causes many environmental pollutions, such as smoke. With the exception of rape straw, no previous reports have discussed the processing of whole-plant rape and its effect on improving silage quality and avoiding misuse of by-products.

Although previous works studied the effect of including forage rape silage in buffalo diets as a replacement for other silage sources (11) and did not discuss the dynamics during the ensiling process. Such changes during the ensiling process will alter the chemical analysis and, in turn, the feed properties, which will reflect animal performance.

Therefore, this study evaluates the whole-plant rape (*B. napus* L.) silage on its quality kinetics, dry matter (DM), and CP degradability, and milk production performance in dairy buffaloes to investigate the changes in forage rape silage during the ensiling process, which can provide a reference for developing and utilizing forage rape silage as a new forage form.

MATERIALS AND METHODS

Forage Rape Culture, Silage Preparation, and Quality Scoring

Harvesting and Chopping

Forage rape (*B. napus* L. "Huayouza 62") from Shahu farm (Xiantao, Hubei, China) sown at a 0.35 kg/mu seed rate and harvested after 196-day growth period was chopped to a length of 50 mm with a chopper machine. The chopped rape was mixed with 7% dry rice straw to adjust the moisture content to 75%, and the chemical analysis is shown in **Table 1**.

Filling and Sealing

The silage mixture was preserved in the bunker silo, spreading each 20 cm layer to the end of all the filling. After compaction and filling, a layer of polyethylene film is packed on the whole silage bunker, the four corners of the film are inserted between the raw material and the silage pit, and finally, waste tires are used to cover the center, the edges, and the four corners of the canvas to prevent wind blowing.

Sampling

Silage samples were taken after 30, 60, and 90 days, samples followed five-point sampling and mixed after each sampling.

TABLE 1 | Fresh forage rape chemical composition [% dry matter (DM)].

DM	16.7
CP	12.05
EE	1.68
CF	28.43
ADF	42.97
NDF	56.19

TABLE 2 | Silage quality evaluation standards.

Parameter	Total score	Excellent	Good	Generally	Poor
pH	25	3.4 (25)	3.9 (17)	4.2 (8)	4.8 and above (0)
		3.5 (23)	4.0 (14)	4.3 (7)	
		3.6 (21)	4.1 (10)	4.4 (5)	
		3.7 (20)		4.5 (4)	
		3.8 (18)		4.6 (3)	
				4.7 (1)	
Moisture (%)	20	70 (20)	76 (13)	81 (7)	Above 86 (0)
		71 (19)	77 (12)	82 (6)	
		72 (18)	78 (11)	83 (5)	
		73 (17)	79 (10)	84 (3)	
		74 (16)	80 (8)	85 (1)	
Color	20	Turquoise (14–20)	Yellow-green (8–13)	Brownish-yellow (1–7)	Dark brown (0)
Odor	25	Sour scent, acceptable (25)	Light sour (9–17)	Pungent wine Sour (1–8)	Moldy (0)
Texture	10	Loose and soft Soft and non-sticky (8–10)	Middle (4–7)	Slightly viscosity (1–3)	Sticky (0)
Total	100	100–76	75–51	50–26	25 or less
Grading					
Grade		Excellent	Good	Generally	Poor quality
Score		100–76	75–51	50–26	25 or less

TABLE 3 | Feed composition and chemical analysis of fistulated buffalo %.

Feeding composition	
Ingredients	**Content (% of DM)**
Cornstalk silage	30
Peanut vine	10
Rice straw	45
Corn	7
Rice bran	2.5
Soybean meal	3
Wheat bran	2.5
Chemical composition	
DM	57.58
OM	89.5
CP	8.95
Ether extract	1.8
CF	26.9
NDF	48.2
ADF	29.9

As opening the silo would cause secondary fermentation, the samples were collected as quickly as possible during sampling and then thoroughly compacted and quickly sealed. After sample collection, the samples were dried and stored at 65°C for standby.

Silage Evaluation

The pH of silage samples at different intervals was measured with the pH meter (HI 8424 Shandong Yuesheng Instruments Co., Ltd.), whereas the odor, color, and texture evaluated silage quality. Silage quality parameters were based on the "standard for silage quality evaluation" (**Table 2**) issued by the Ministry of Agriculture of the People's Republic of China in 1996.

Chemical Analysis

As described previously (12), all samples were dried at 65°C for 48 h to determine the initial moisture content. Then, the samples were ground using a multifunctional pulverizer (Old Bank Boou Hardware Factory, Zhejiang, China) and passed through a 40-mesh sieve (manufactured by Tianxing Wusi Yarn Sieve Factory in Shangyu City, Zhejiang, China) to be stored at 20°C for further analysis. DM, crude ash (CA), CP, ether extract (EE), NDF, and acid detergent fiber (ADF) of the feed were determined according to the Association of Official Analytical Chemists (13), and by the methods described (14, 15) the concentrations of NDF and ADF were determined by the ANKOM Filter Bag Method. In addition, both heat-stable amylase and sodium sulfite were added during NDF extraction (16, 17), and the anthrone sulfate method determined the concentration of water-soluble carbohydrates (WSC) (18).

Sample Preparation and Incubation

Three fistulated buffaloes (550 ± 20 kg body weight, 4.7 ± 0.76 years) at Shayang buffalo farm, Jingmen, China, were fed two times daily with a total mixed ration (TMR), as shown in **Table 3**. As described previously (19), the nylon bags were made from nylon fabric (15 cm × 10 cm; 48 μm pore size), sewn with double

TABLE 4 | Experimental diet content and composition (DM basis).

Ingredient	Groups			
	Control	**10%**	**20%**	**30%**
Corn	5.5	5.5	5.5	5.5
Soybean meal	10	10	10	10
Wheat bran	3.2	3.2	3.2	3.2
Rice straw	65	55	45	35
Brick lick[a]	0.3	0.3	0.3	0.3
Flammulina velutipes	15	15	15	15
Whole-plant rape Silage	0	10	20	30
Chemical composition (%DM)				
DM%	74.4	67.2	60.8	54.4
OM	83.2	88.3	88.4	88.6
CP	9.4	11.7	12.5	13.3
EE	1.6	1.7	2.1	2.4
WSC	6.6	16.6	16.2	15.9
CF	25.3	22.0	21.4	20.9
ADF	25.1	22.0	22.2	22.5
NDF	41.6	36.4	36.0	35.6

[a]*A lick brick weighs 5 kg and consists of 98% salt, 25 mg of calcium, 250 mg of phosphorus, 1,000 mg of magnesium, 20 mg of selenium, 150 mg of copper, 50 mg of cobalt, 500 mg of iron, and 200 mg of manganese in each group of four lick bricks.*

fine polyester thread to make the bottom of the bag blunt and rounded to prevent the feed samples from being trapped and close the pinhole with the non-dissolvable glue. Next, the bags were heat pressed through an alcohol lamp to guarantee the stability and uniformity of the bag. Next, the nylon rope was inserted into a plastic hose and knotted at both ends to prevent rope breakage. After being labeled by a permanent rumen-stable marker, the nylon bags were filled with 6 g of dry samples, and the weighing of the nylon bags and samples was accurate to 0.0001 g.

Next, each silage sample was incubated in three replicates in the rumen, and the incubation time was set for the tested time points. Each sample from the different ensiling times (0, 30, 60, and 90 days) was incubated in the rumen in triplicate for 0, 6, 12, 24, 36, 48, and 72 h; in addition, at each time, the blanks were secured with nylon thread to a piece of string (30 cm long, weight 150 g). After removal, the nylon bags were removed from the mesh bag and placed in a washing machine. The bags were washed repeatedly until the rinse water became clear. Then, the samples were dried in an oven at 65°C until constant weight was reached.

A blank sample is prepared like the previous operations; each sample was packed in three nylon bags but not put into the rumen and treated directly according to the above washing and drying operations.

Calculations

The nutrient degradation was calculated as described by the exponential equation (20), which was as follows:

$$D = a + b \times (1 - e^{-c \times t})$$

where D is the degradation after t hours of rumen incubation; a is the water-soluble and rapidly degradable fraction; b is the insoluble but degradable fraction; and c is the degradation rate of the fraction b.

The effective degradability (ED) of nutrients was calculated:

$$ED = a + (b \times c) / (c + k) \quad (5)$$

where a is the rapidly degradable fraction (%); b is the insoluble but degradable fraction (%); c is the degradation rate of the b part (%); ED is the effective degradability calculated at a flow rate in the rumen (K) 0.06 h^{-1}.

The Dairy Buffalo Feeding Experiment

In this study, 28 crossbred (Mediterranea X Nili-Ravi hybrid) lactating buffaloes (*Bubalus bubalis*; 588 ± 89 kg BW, 6.5 ± 1.3 years) were used to investigate the effects of rape silage inclusion on feed intake, daily milk yield, and milk composition. Animals were randomly assigned to four groups ($n = 7$); each group was randomly divided into four treatment groups (groups C, T1, T2, and T3). Group C was the control group, and rape silage (after 60 days) replaced straw by 10, 20, and 30% (based on DM), respectively, in the diet of TMR groups T1, T2, and T3. The experiment lasted 60 days. The diet concentrate-to-forage ratio was 2:8, supplemented with lick bricks to cover Ca, salt, vitamins, and mineral requirements. The experimental diet content is shown in **Table 4**. Animals were housed in individual tie stalls and were offered TMR two times daily at 9 a.m. and 3 p.m., for *ad libitum* intake. Animals were fed individually, and feed was weighed and recorded two times a day for each group, and the amount of feed intake was calculated for each

FIGURE 1 | The color of silage rape [**(left)**: silage 60 days; **(right)**: silage 90 days].

group of animals. In addition, milk samples were collected every 20 days from each animal group and stored at 4°C for further determination. Milk samples were mixed 1:1 and conserved with a preservative (0.2 g of bronopol solution/40 ml of milk), kept refrigerated at 4°C, and afterward analyzed for fat, total protein, lactose, and urea at an official milk control laboratory (Hubei Provincial Animal husbandry Bureau, Wuhan, China), using Fourier transform infrared (IR) spectroscopy (MilkoScan 7RM, FOSS Analytical, Hillerød, Denmark) (21).

Statistical Analysis

All statistical analyses were analyzed with SAS 9.4 (SAS Institute, Cary, NC, USA, 2017) (22). Data were normally distributed and homoscedastic. Degradation parameters were subjected to the analysis of variance (ANOVA) least significant difference (LSD) procedure. Differences between means were considered significant when $p < 0.05$ for the milk performance study. The following statistical mixed model (repeated measure) was used :

$$Y_{ijk} = \mu + \tau_i + \delta_{ij} + t_k + (\tau^* t)_{ik} + \varepsilon_{ijk}$$

whereas Y_{ijk} is the dependent variable, μ is the overall mean, τ_i is the fixed effect of dietary treatment i, t_k is the random effect of time, $(\tau^* t)_{ik}$ is the interaction effect of group and time, δ_{ij} is the random effect of covariance between repeated measures within an individual, and ε_{ijk} is the random error of the variance between the measures within the individual. All reported values are least significant means (LSM), and significance was declared at $p < 0.05$.

RESULT

Effect of Ensiling Duration on Silage Quality

Effect of Ensiling Duration on pH

Silage pH at 30, 60, and 90 days were 4.09, 4.08, and 4.39, respectively, and there were no significant differences between ensiling periods. According to the standard of silage quality evaluation, the quality of rape silage ranged from good to average. Silage between 30 and 60 days could keep good quality; however, the quality score dropped after 60 days.

The Effects of Ensiling Time on Silage Quality

Silage quality was comprehensively evaluated by pH, moisture content, and sensory characteristics, including color (**Figure 1**), odor, and texture. According to the standard of silage quality criteria, we evaluated the effect of ensiling time on silage quality through comprehensive scoring (**Table 4**). The moisture score increased gradually before 60 days and showed a rapid decrease after day 60. Sensory characteristics scoring results showed that the silage color score was all over 14 before day 60; however, silage odor scores dropped intensely at day 90. Also, the silage was noticed to be sticky at day 90. Finally, the total silage score at days 30 and 60 was 55 and 61, respectively, which achieved a good level (higher than 50). However, silage quality showed a downward trend after day 60 (**Table 5**), and the score of 31 after 90 days was not a good level, which recommended that the silage needed to be consumed before day 60, which was the optimum quality.

The Influence of Ensiling Time on Nutrient Composition

Silage samples were collected from different ensiling timepoints for proximate chemical analysis (**Table 6**). The CP content of

TABLE 5 | Effect of ensiling duration on the comprehensive sensory investigation score.

Ensiling time	pH	Moisture	Color		Smell		Texture		Comprehensive score	
	Score (Mean)	Score (Mean %)	Color	Score	Smell	Score	Texture	Score	Level	Total score
30 days	10 (4.1)	7 (81.2)	Green	14	Weak aromatic	16	Loose & soft	8	Good	55
60 days	10 (4.1)	13 (76.91)	Green	15	Weak aromatic	16	Medium	7	Good	61
90 days	5 (4.4)	6 (82.21)	Yellow green	9	Pungent	7	sticky	4	low	31
SEM	0.55	1.15	Different letters indicated a significant difference was indicated by ($p < 0.05$), while the remaining indicated no significant difference ($p > 0.05$)							
p-Value	>0.05	>0.05								

silage showed an upward trend from 0 to 30 days and a downward trend from 60 to 90 days. On the other hand, the EE content is relatively low from 0 to 30 days but increases from 60 to 90 days; it was the highest after 60 days (4.33%). Although the average EE content increased 1.7 times ($p < 0.05$) compared with fresh rape (day 0), there was a decline in NDF among treatments after ensiling ($p < 0.05$), and it reached its lowest value between 30 and 60 days (46.75 and 47.82%, respectively). Also, ADF decreased significantly ($p < 0.05$) during ensiling; it reached its lowest value between 30 and 60 days (30.70 and 34.14%, respectively). Thus, NDF and ADF reached their lowest level at the early ensiling period (30–60 days) and gradually increased as fermentation time was prolonged.

Effect of Ensiling Duration on the DM and CP *in situ* Degradability

These data from the *in situ* degradability results for DM and CP from different ensiling time points can reflect nutrient intake in animals.

With the prolongation of silage time, compared with 0 (no change), the instantaneous DM degradation rate decreased significantly at 0, 6, 12, 24, 36, 48, 60, and 72 h. The instantaneous degradation of the rumen degradation rate of DM for 0–24 h was 0 > 30 > 90 > 60 days, and that for 36–72 h was 0 > 30 > 60 > 90 days (**Tables 7**,**8**). However, the instantaneous degradation of the rumen degradation rate of CP showed no significant differences.

As, at day 90 of ensiling, DM ED was significantly dropped ($p < 0.05$), the degradation rate of silage DM at both 90 and 60 days was significantly lower than ($p < 0.05$) after 30 days of silage. The DM effective degradation rate showed a decreasing trend from 0 to 90 days after ensiling; and a significant decrease after 90 days. However, the CP effective degradation rate showed no significant differences from different ensiling time samples ($p > 0.05$) (**Tables 9**,**10**).

Effect of Silage Inclusion on the DM Intake, Milk Yield, and Composition

Rape silage was included in the TMR at 10%, 20%, and 30% of the total DM. Although DM intake (DMI) and concentrations of milk lactose and urea nitrogen were not affected by treatment ($p > 0.05$), fat and protein content increased linearly ($p < 0.05$) (**Table 11**).

DISCUSSION

Effects of Ensiling Time on Silage Sensory Characteristics

There are many microbes on the silage surface; some are beneficial to silage, e.g., lactic acid bacteria, but others are more harmful, e.g., spoilage bacteria, yeasts, and molds. To obtain optimum silage quality, the amount of lactic acid bacteria in the silage material needs to reach 5 log to 6 log colony forming units/g (CFU/g) of fresh weight (23, 24). In addition, bacterial lactic acid maintains the silage system in a stable pH range, which is closely related to silage fermentation activity, thus reducing the pH value and increasing silage quality. Furthermore, the

TABLE 6 | Effect of ensiling duration on the rape silage nutrient content.

Nutrient component	Control (Day 0)	Fermentation time			SE*M*	*p*-Value		
		30 days	60 days	90 days		Diet	*L*	*Q*
DM	19.45	17.89	21.32	17.48	0.14	0.45	0.71	0.32
CP	12.05	12.32	12.28	12.00	0.11	0.71	0.86	0.27
EE	2.18^{c}	2.77^{b}	4.33^{a}	4.15^{a}	0.27	<0.001	<0.001	<0.001
NDF	56.19^{a}	46.57^{c}	47.82^{c}	52.62^{b}	1.25	0.001	0.08	<0.001
ADF	42.97^{a}	30.70^{c}	34.14^{bc}	37.14^{b}	1.44	<0.001	0.02	<0.001

CP, crude protein; EE, ether extract; CF, crude fiber; ADF, acid detergent fiber; NDF, neutral detergent fiber.
Differences between treatment and period were considered significant at $p < 0.05$.

TABLE 7 | Effect of the ensiling duration on average DM degradability of forage rape silage after 0, 6, 12, 24, 36, 48, 60, and 72 h incubation *in situ* technique.

	Incubation time (h)							
Ensiling days	**0**	**6**	**12**	**24**	**36**	**48**	**60**	**72**
0	27.082^{a}	44.726^{a}	39.6^{a}	60.12^{a}	72.6^{a}	80.4^{a}	85.074^{a}	82.12^{a}
30	24.62^{a}	40.66^{b}	36^{ab}	54.66^{b}	66.41^{b}	70.34^{ab}	77.34^{b}	74.66^{b}
60	13.413^{b}	23.8^{c}	30.6^{b}	42.5^{c}	52.7^{c}	60.63^{b}	65.739^{bc}	70.26^{b}
90	13.96^{b}	28.38^{c}	38.93^{a}	46.66^{c}	48.8^{c}	53.06^{c}	60.26^{c}	65.06^{c}
S.E.M	5.66	7.25	7.59	6.85	8.46	8.65	9.95	5.6
p-Value				<0.05				

Means within the same column with different superscripts differ ($p < 0.05$).

TABLE 8 | Effect of ensiling duration on average crude protein (CP) degradability of forage rape silage after 0-, 6-, 12-, 24-, 36-, 48-, 60-, and 72-h incubation *in situ* technique.

	Incubation time (h)							
Ensiling days	**0**	**6**	**12**	**24**	**36**	**48**	**60**	**72**
0	25.41	31.67	39.00	46.00	48.33	50.33	56.67	58.33
30	26.57	37.00	46.67	48.67	49.67	48.67	56.00	55.33
60	20.32	28.33	36.33	40.00	47.33	48.33	49.67	44.67
90	22.13	38.67	40.00	44.33	52.33	51.33	52.67	59.00
S.E.M	1.45	2.39	2.20	1.82	1.08	0.71	1.62	1.45
p-Value				>0.05				

Different letters indicated a significant difference ($p < 0.05$), while the remaining indicated no significant difference ($p > 0.05$).

optimum pH for the protease activity in silage is around 6, and the enzyme activity decreases when pH is 4–6, the protease activity at pH 4 is 15%−35% at pH 6 (25). Therefore, the pH value and its rate of decline during silage will determine the final silage quality. In corn silage, the silage quality grade is excellent, good, average, and low when the pH is between 3.8 and 4.2, between 4.1 and 4.3, between 4.4 and 5.0, and higher than 5.0, respectively (26).

During ensiling, the silage pH ranged between 4 and 4.3, and the pH value of whole-plant rape silage in 30–60 days is lower in the whole silage period. This indicates that direct silage in that period, whole-plant rape, can maintain a moderate amount of beneficial bacterial colonies and achieve a good acidity balance. Moreover, we scored the five indicators of moisture, pH, color, odor, and texture of silage, referring to the "silage quality assessment standard." During the 30–60 days ensiling, the silage color is green, similar to the color of raw materials; the odor is sour, the texture is loose, smooth, and non-sticky; the total score reached the maximum in 60 days. However, the total score drops rapidly after 60 days and has a sticky texture and pungent odor at 90 days. Therefore, rape silage could maintain good quality between 30 and 60 days of ensiling, and it is recommended to open the cellar at 60 days; silage quality should be optimized.

Effect of Ensiling on Silage Kinetics and Ruminal Degradability

During the ensiling process, the fermentation activity of lactic acid bacteria prevented CP loss, and could effectively maintain the CP content of rape. Also, the EE content was significantly

higher at 60–90 days than at 0–30 days, and in the control group, the silage EE content at 60 and 90 days increased by 2.65 and 2.47, respectively, which was 1.5 times higher than the control after ensiling 60 days. Moreover, the ensiling process increased protoplasm osmosis with the death of plant cells; therefore, the nutrient concentration effect of soluble nutrients with water loss might increase EE concentration. On the other hand, it was noticed that both NDF and ADF of silage decreased significantly after ensiling 30–60 days. While NDF is an essential indicator for fiber quality and for determining the appropriate diet ratio, ADF is the crucial indicator of forage energy; its low content can facilitate feed digestion. Also, NDF digestibility is slow, which is generally considered a significant factor affecting DMI (27, 28). Although NDF content is negatively correlated with non-fiber carbohydrates (NFC) (29), plant carbohydrates are either oligosaccharides or their polymers, such as cellulose and starch, are the primary substrates for fermentation by rumen microbial activity (30). Therefore, the higher concentration of WSC might also contribute to a higher degradability of DM and organic matter (OM) in silage (31). The latter factors may explain the rapid decline in NDF and ADF due to some microbial cellulase activity (26); lactobacillus activity in silage fermentation consumed a certain amount of WSC, making the ratio of NDF and ADF to increase relatively slowly afterward.

Although nutrient changes do not necessarily reflect the nutritional value of silage, they can give an idea about the extent of intake and utilization; therefore, a rumen nylon bag is the most effective method to evaluate the degradation rate in the *in vivo* environment (20, 32). The concentration of cell wall components in forages is highly variable according to the variety and stage of plant maturity; lignin concentration increases with plant maturation and reduces cell wall degradability (33). NDF degradability is limited primarily by the cross-linking of lignin with other fibrous components (33). In theory, cellulose and hemicellulose can be completely digested by ruminants, but the ester bond formed by lignin and hemicellulose encapsulates cellulose (34). Thus, lignin cannot be entirely degraded by rumen microorganisms, which affects the digestion and utilization of cellulose and hemicellulose. Presumably, the ensiling process increased the cross-linking of lignin in rape silage with other fiber compounds (35), resulting in reduced microbial access and, therefore, less crude fiber degradability and, in turn, DM degradability.

TABLE 9 | Effect of ensiling duration on the rapidly degradable nutrient (a, %), slowly degradable nutrient (b, %), effective degradation rate (c), and the effective degradability (ED, %) of forage rape silage.

Ensiling days	a	b	c	ED
0	15.53^{c}	36.45^{c}	0.0493^{a}	39.72^{b}
30	23.37^{b}	47.62^{b}	0.0427^{b}	35.83^{b}
60	27.8^{a}	58.44^{a}	0.0363^{c}	43.33^{a}
90	15.41^{c}	54.89^{b}	0.035^{c}	24.30^{c}
SEM	1.38	1.85	0.003	1.30
p-Value	0.04	0.02	0.0234	0.009

The different letters means significant difference ($P < 0.05$).

TABLE 10 | Effect of ensiling duration on the rapidly degradable nutrient (a, %), slowly degradable nutrient (b, %), effective degradation rate (c), and the ED (%).

Ensiling days	a	b	c	ED
0	56.70	41.47	0.055	41.56
30	60.47	37.34	0.0290	42.86
60	62.13	36.69	0.0363	44.33
90	54.64	42.45	0.0297	41.56
SEM	1.52	1.03	0.008	1.13
p-Value	0.359	0.050	0.393921	0.384

Different letters indicated a significant difference ($p < 0.05$), while the remaining indicated no significant difference ($p > 0.05$).

TABLE 11 | Effects of rape silage inclusion on dry matter intake (DMI) and milk composition of lactating buffaloes.

Items	Treatment				SEM	*p*-Value		
	Control	10%	20%	30%		Diet	*L*	*Q*
Dry matter intake, DMI (kg)	21.12	19.93	19.45	19.92	3.38	0.81	0.47	0.52
Milk yield (kg/day)	3.39	3.82	3.20	3.38	0.48	0.98	0.89	0.91
Milk fat, %	7.39^{b}	7.83^{b}	8.21^{a}	8.22^{a}	0.14	0.14	0.03	0.43
Milk protein, %	4.60^{c}	5.15^{b}	5.16^{b}	5.35^{a}	0.11	0.11	0.03	0.40
Milk lactose, %	5.49	5.46	5.47	5.32	0.06	0.79	0.40	0.65
Urea nitrogen, mg/dl	11.15	12.20	13.35	12.60	0.37	0.27	0.16	0.22

The different letters means significant difference ($P < 0.05$).

Effect of Silage Inclusion on the Milk Production Response

One of the most valuable advantages of buffaloes is their increased ability to utilize unpalatable agricultural by-products, which can be further incorporated into rations because their coarser texture, odors, and flavors are ameliorated by ensiling (11, 36, 37). In this study, we included rape silage in the dairy buffalo diet; the difference in DMI was not significant in each group, which showed that the whole-plant rape silage did not reduce the diet's palatability. NDF is an essential factor limiting DMI; when NDF is more than 35%, it may inhibit DMI by physical rumen filling; when it is lower than 25%, energy intake becomes the main factor limiting DMI (38, 39).

On the other hand, milk fat and protein rates increased linearly with whole-plant rape silage ($p < 0.05$), reflecting the feeding value of rape silage for dairy buffaloes. There is a positive correlation between a linear increase in EE content, degradability of rape silage, and a significant increase in milk fat percentage. Also, the milk protein rate increased linearly ($p < 0.05$) as the proportion of addition increased; these results could be supported by non-significant changes in degradation rate and palatability after ensiling.

Moreover, the difference in milk lactose and milk urea nitrogen (MUN) is not significant; it may be linked to a decrease in DM degradability. However, the MUN content of each treatment group was higher than that of the control group. It has been reported that 87% of the (MUN) variation is caused by nutritional factors and 13% by non-nutritive factors (40); MUN is essential for assessing dietary protein and energy levels (41, 42). MUN concentration is correlated with CP, rumen degradable protein (RDP), undegradable protein (UDP), non-fiber carbohydrates (NFC), and energy protein ratios in the diet (43–45). The normal range of MUN concentration in milk is 10–15 mg/dl (46, 47); the urea nitrogen level of the whole-plant rape silage treatment group in this study was within this range. Although the difference in MUN in each group was not significant, the replacement of whole-plant rape silage had no effect on buffalo's rumen N energy balance. However, the sample needs to be expanded further to confirm this trend.

CONCLUSIONS

Whole-plant rape ensiling can effectively maintain CP, increase EE content, and reduce NDF and ADF content. Silage reaches optimum silage quality between 30 and 60 days of ensiling; thus, the right time to open the cellar can be set in this period. Whole-plant rape silage significantly reduces DM degradability, but does not change CP degradability. In addition, whole-plant rape silage linearly increased milk fat content, protein level, lactose level, and MUN did not change significantly after ensiling rape. Therefore, whole-plant rape silage can be used as a good forage source; however, improvements of its species and ruminal microbial interactions with fatty acid changes need to be further examined.

DATA AVAILABILITY STATEMENT

The original contributions presented in the study are included in the article/supplementary material, further inquiries can be directed to the corresponding authors.

ETHICS STATEMENT

The animal study was reviewed and approved by the Ethical Committee of the Hubei Research Center of Experimental Animals [Approval ID: SCXK (Hubei) 20080005].

AUTHOR CONTRIBUTIONS

Conceptualization, project administration, funding acquisition, and supervision: YL and HG. Methodology, writing-review, and editing: MA, ZD, YL, and HG. Formal analysis: WW, ZD, and MA. Investigation: WW, AS, ZD, MA, HL, WL, ZA, ZG, and WB. Writing-original draft preparation: ZD and MA. All authors have read and agreed to the published version of the manuscript.

FUNDING

This study was supported by National Natural Science Foundation of China (No. 32172731), Fundamental Research Funds for the Central Universities (No. 2662022DKYJ002) the earmarked fund for CARS36, and Hubei Key Research and Development Program (No. 2020BC001).

REFERENCES

1. Xuehai Y, Wanzheng G, Shaowen H, Jintao W, Tingdong F, Guangsheng Z, et al. Study on rape forage nutritive value evaluation in different growth stages. *Feed Industry.* (2017) 38:19–22.
2. Dong-Hui FU, Jiang LY, Mason AS, Xiao ML, Zhu LR, Li-Zhi LI, et al. Research progress and strategies for multifunctional rapeseed: a China case study. *J Integr Agric.* (2016) 15:1673–84. doi: 10.1016/S2095-3119(16)61384-9
3. Index Mundi. *Rapeseed Oilseed Production*. (2019). Available online at: https://www.indexmundi.com/agriculture/?commodity=rapeseed-oilseedandgraph=production (accessed April 30, 2020).
4. Shahidi F. *Canola and Rapeseed: Production, Chemistry, Nutrition, and Processing Technology*. Berlin, Heidelberg: Springer Science and Business Media (1990).
5. Spragg J, Mailer R. *Canola meal value chain quality improvement: stage 2*. Canola Meal Value Chain Quality Improvement Stage (2008). Available online at: https://www.cabdirect.org/cabdirect/abstract/20103063923
6. Maison T, Stein H. Digestibility by growing pigs of amino acids in canola meal from North America and 00-rapeseed meal and 00-rapeseed expellers from Europe. *J Anim Sci.* (2014) 92:3502–14. doi: 10.2527/jas.2014-7748
7. Brask M, Lund P, Weisbjerg MR, Hellwing ALF, Poulsen M, Larsen MK, et al. Methane production and digestion of different physical forms of rapeseed as fat supplements in dairy cows. *J Dairy Sci.* (2013) 96:2356–65. doi: 10.3168/jds.2011-5239
8. Maxin G, Ouellet DR, Lapierre H. Effect of substitution of soybean meal by canola meal or distillers grains in dairy rations on amino acid and glucose availability. *J Dairy Sci.* (2013) 96:7806. doi: 10.3168/jds.2013-6976

9. Broderick GA, Faciola AP, Armentano LE. Replacing dietary soybean meal with canola meal improves production and efficiency of lactating dairy cows. *J Dairy Sci.* (2015) 98:5672–87. doi: 10.3168/jds.2015-9563
10. Cui X, Yang Z, Yang W, Zhang G, Jiang S, Liu L, et al. Correlations of shearing force and feed nutritional characteristics of crop straws. *Sci Agric Sin.* (2012) 45:3137–46.
11. Zhou D, Abdelrahman M, Zhang X, Yang S, Yuan J, An Z, et al. Milk Production responses and digestibility of dairy buffaloes (*Bubalus bubalis*) partially supplemented with forage rape (*Brassica napus*) silage replacing corn silage. *Animals.* (2021) 11:2931. doi: 10.3390/ani11102931
12. Jia T, Wang B, Yu Z, Wu Z. The effects of stage of maturity and lactic acid bacteria inoculants on the ensiling characteristics, aerobic stability and *in vitro* digestibility of whole-crop oat silages. *Grassl Sci.* (2021) 67:55–62. doi: 10.1111/grs.12285
13. AOAC International. *Official Methods of Analysis of Aoac International*. Arlington, VA: AOAC International (1995).
14. McCarthy JF, Aherne FX, Okai DB. Use of HCl insoluble ash as an index material for determining apparent digestibility with pigs. *Can J Anim Sci.* (1974) 54:107–9. doi: 10.4141/cjas74-016
15. Van Keulen J, Young BA. Evaluation of acid-insoluble ash as a natural marker in ruminant digestibility studies. *J Anim Sci.* (1977) 44:282–7. doi: 10.2527/jas1977.442282x
16. Van Soest PJ, Wine RH. Use of detergents in the analysis of fibrous feeds. IV. Determination of plant cell-wall constituents. *J Assoc Off Anal Chem.* (1967) 50:50–5. doi: 10.1093/jaoac/50.1.50
17. Van Soest PJ, Robertson JB, Lewis BA. Methods for dietary fiber, neutral detergent fiber, and nonstarch polysaccharides in relation to animal nutrition. *J Dairy Sci.* (1991) 74:3583–97. doi: 10.3168/jds.S0022-0302(91)78551-2
18. McDonald P, Henderson AR. Determination of water-soluble carbohydrates in grass. *J Sci Food Agric.* (1964) 15:395–8. doi: 10.1002/jsfa.2740150609
19. Li X, Kellaway RC, Ison RL, Annison G. Chemical composition and nutritive value of mature annual legumes for sheep. *Anim Feed Sci Technol.* (1992) 37:221–231. doi: 10.1016/0377-8401(92)90006-R
20. Ørskov ER, McDonald I. The estimation of protein degradability in the rumen from incubation measurements weighted according to rate of passage. *J Agric Sci.* (1979) 92:499–503. doi: 10.1017/S0021859600063048
21. Laporte MF, Paquin P. Near-infrared analysis of fat, protein, and casein in cow's milk. *J Agric Food Chem.* (1999) 47:2600–2605. doi: 10.1021/jf980929r
22. SAS Institute. *Base SAS 9.4 Procedures Guide*: *Statistical Procedures*. Rockville, MD: SAS Institute (2017).
23. Li J, Shen Y, Cai Y. Improvement of fermentation quality of rice straw silage by application of a bacterial inoculant and glucose. *Asian-Australas J Anim Sci.* (2010) 23:901–6. doi: 10.5713/ajas.2010.90403
24. Sifeeldein A, Wang S, Li J, Dong Z, Chen L, Kaka NA, et al. Phylogenetic identification of lactic acid bacteria isolates and their effects on the fermentation quality of sweet sorghum (*Sorghum bicolor*) silage. *J Appl Microbiol.* (2019) 126:718–29. doi: 10.1111/jam.14123
25. Mckersie BD. Effect of pH on proteolysis in ensiled legume forage 1. *Agron J.* (1985) 77:81–6. doi: 10.2134/agronj1985.00021962007700010019x
26. Yang YG, Zhang YL, Xin DU, Liu GY, Cao SH. Study on the major microorganism changes during the silage processing of two kinds of corn silage. *Chin J Anim Vet Sci.* (2012) 43:397–403. Available online at: http://www.xmsyxb.com/EN/abstract/abstract12595.shtml
27. Mertens DR. Creating a system for meeting the fiber requirements of dairy cows. *J Dairy Sci.* (1997) 80:1463. doi: 10.3168/jds.S0022-0302(97)76075-2
28. Robinson PH, Fadel JG, Tamminga S. Evaluation of mathematical models to describe neutral detergent residue in terms of its susceptibility to degradation in the rumen. *Anim Feed Sci Technol.* (1986) 15:249–71. doi: 10.1016/0377-8401(86)90079-9
29. Armentano L, Pereira M. Measuring the effectiveness of fiber by animal response trials. *J Dairy Sci.* (1997) 80:1416–25. doi: 10.3168/jds.S0022-0302(97)76071-5
30. Ntaikou I, Gavala HN, Kornaros M, Lyberatos G. Hydrogen production from sugars and sweet sorghum biomass using *Ruminococcus albus*. *Int J Hydrogen Energy.* (2008) 33:1153–63. doi: 10.1016/j.ijhydene.2007.10.053
31. Zhang SJ, Chaudhry AS, Ramdani D, Osman A, Guo XF, Edwards GR, et al. Chemical composition and *in vitro* fermentation characteristics of high sugar forage sorghum as an alternative to forage maize for silage making in Tarim Basin, China. *J Integr Agric.* (2016) 15:175–82. doi: 10.1016/S2095-3119(14)60939-4
32. McDonald IM. A revised model for the estimation of protein degradability in the rumen. *J Agric Sci.* (1981) 96:251–2. doi: 10.1017/S0021859600032081
33. Jung HG, Deetz DA. Cell wall lignification and degrada. 1993.
34. Jung HJ, Samac DA, Sarath G. Modifying crops to increase cell wall digestibility. *Plant Sci.* (2012) 185–186:65–77. doi: 10.1016/j.plantsci.2011.10.014
35. Zhong H, Zhou J, Abdelrahman M, Xu H, Wu Z, Cui L, et al. The effect of lignin composition on ruminal fiber fractions degradation from different roughage sources in water buffalo (*Bubalus bubalis*). *Agriculture.* (2021) 11:1015. doi: 10.3390/agriculture11101015
36. Nishino N, Hattori H. Resistance to aerobic deterioration of total mixed ration silage inoculated with and without homofermentative or heterofermentative lactic acid bacteria. *J Sci Food Agric.* (2007) 87:2420–6. doi: 10.1002/jsfa.2911
37. Cao Y, Cai Y, Takahashi T, Yoshida N, Tohno M, Uegaki R, et al. Effect of lactic acid bacteria inoculant and beet pulp addition on fermentation characteristics and *in vitro* ruminal digestion of vegetable residue silage. *J Dairy Sci.* (2011) 94:3902–12. doi: 10.3168/jds.2010-3623
38. Dado RG, Allen MS. Enhanced intake and production of cows offered ensiled alfalfa with higher neutral detergent fiber digestibility. *J Dairy Sci.* (1996) 79:418. doi: 10.3168/jds.S0022-0302(96)76381-6
39. Allen MS. Physical constraints on voluntary intake of forages by ruminants. *J Anim Sci.* (1996) 74:3063. doi: 10.2527/1996.74123063x
40. Arunvipas P, Dohoo IR, Vanleeuwen JA, Keefe GP. The effect of non-nutritional factors on milk urea nitrogen levels in dairy cows in Prince Edward Island, Canada. *Prev Vet Med.* (2003) 59:83–93. doi: 10.1016/S0167-5877(03)00061-8
41. Jonker JS, Kohn RA, High J. Use of milk urea nitrogen to improve dairy cow diets. *J Dairy Sci.* (2002) 85:939–46. doi: 10.3168/jds.S0022-0302(02)74152-0
42. Wattiaux MA, Nordheim EV, Crump P. Statistical evaluation of factors and interactions affecting dairy herd improvement milk urea nitrogen in commercial midwest dairy herds. *J Dairy Sci.* (2005) 88:3020–35. doi: 10.3168/jds.S0022-0302(05)72982-9
43. Oltner R, Wiktorsson H. Urea concentrations in milk and blood as influenced by feeding varying amounts of protein and energy to dairy cows. *Livest Prod Sci.* (1983) 10:457–67. doi: 10.1016/0301-6226(83)90073-8
44. Roseler DK, Ferguson JD, Sniffen CJ, Herrema J. Dietary protein degradability effects on plasma and milk urea nitrogen and milk nonprotein nitrogen in holstein cows. *J Dairy Sci.* (1993) 76:525–34. doi: 10.3168/jds.S0022-0302(93)77372-5
45. Baker LD, Ferguson JD, Chalupa W. Responses in urea and true protein of milk to different protein feeding schemes for dairy cows. *J Dairy Sci.* (1995) 78:2424–34. doi: 10.3168/jds.S0022-0302(95)76871-0
46. Carlsson J, Bergström J. The diurnal variation of urea in cow's milk and how milk fat content, storage and preservation affects analysis by a flow injection technique. *Acta Vet Scand.* (1994) 35:67. doi: 10.1186/BF03548356
47. Butler WR, Calaman JJ, Beam SW. Plasma and milk urea nitrogen in relation to pregnancy rate in lactating dairy cattle. *J Anim Sci.* (1996) 74:858–65. doi: 10.2527/1996.744858x

Conflict of Interest: The authors declare that the research was conducted in the absence of any commercial or financial relationships that could be construed as a potential conflict of interest.

frontiers | Frontiers in Veterinary Science

ORIGINAL RESEARCH
published: 15 July 2022
doi: 10.3389/fvets.2022.925847

Protective Effect on Pancreatic Acinar Cell by Maintaining Cardiac Output in Canine Heart Failure Model With Decreased Pancreatic Blood Flow

*Aritada Yoshimura[1], Takahiro Ohmori[1], Daiki Hirao[1], Miori Kishimoto[2], Tomoko Iwanaga[3], Naoki Miura[3], Kazuhiko Suzuki[2] and Ryuji Fukushima[1]**

[1] Animal Medical Center, Faculty of Agriculture, Tokyo University of Agriculture and Technology, Fuchu, Japan, [2] Cooperative Department of Veterinary Medicine, Tokyo University of Agriculture and Technology, Fuchu, Japan, [3] Veterinary Teaching Hospital, Joint Faculty of Veterinary Medicine, Kagoshima University, Kagoshima, Japan

Heart failure cause hypoperfusion-induced damage to abdominal organs due to decreased cardiac output (CO). Using a model dog with heart failure caused by rapid ventricular pacing (RVP), we have previously demonstrated that a decrease in CO reduces pancreatic blood flow (PBF). Furthermore, we have revealed that pancreatic acinar cell atrophy, which is a change in the pre-stage of pancreatitis was caused. However, the mechanism by which pancreatic acinar cell atrophy was caused in RVP dogs remains unknown. This study aimed to clarify the association between cardiac function, PBF, and histopathological changes in pancreatic acinar cells by administrating pimobendan, which increase CO, to RVP dogs. RVP dogs were divided into the control group (no medication, $n = 5$) and the pimobendan group (pimobendan at 0.25 mg/kg BID, $n = 5$). Non-invasive blood pressure measurement, echocardiography, and contrast-enhanced ultrasonography for PBF measurement were performed before initiating RVP and at 4 weeks after initiating RVP (4 weeks). At 4 weeks, the decreases in CO, mean blood pressure and PBF due to RVP were suppressed in pimobendan group. Furthermore, histopathological examination showed no changes in pancreatic acinar cells in the pimobendan group. Overall, it was clarified that the decrease in PBF due to cardiac dysfunction was a direct cause of pancreatic acinar cell atrophy. This suggests that maintaining PBF is clinically important for treating dogs with heart failure. In addition, these findings offer a reliable basis for developing new therapeutic strategies for heart failure in dogs, that is, pancreatic protection.

Keywords: cardiac output, dog, heart failure, hypoperfusion, ischemia, pancreas, pancreatic acinar cell, pimobendan

OPEN ACCESS

Edited by:
Fazul Nabi,
Lasbela University of Agriculture, Water and Marine Sciences, Pakistan

Reviewed by:
Alessandro Carrer,
Veneto Institute of Molecular Medicine (VIMM), Italy
Shin Hamada,
Tohoku University, Japan

***Correspondence:**
Ryuji Fukushima
ryu-ji@cc.tuat.ac.jp

Specialty section:
This article was submitted to Comparative and Clinical Medicine, a section of the journal Frontiers in Veterinary Science

Received: *22 April 2022*
Accepted: *23 June 2022*
Published: *15 July 2022*

Citation:
Yoshimura A, Ohmori T, Hirao D, Kishimoto M, Iwanaga T, Miura N, Suzuki K and Fukushima R (2022) Protective Effect on Pancreatic Acinar Cell by Maintaining Cardiac Output in Canine Heart Failure Model With Decreased Pancreatic Blood Flow. Front. Vet. Sci. 9:925847. doi: 10.3389/fvets.2022.925847

INTRODUCTION

Heart diseases, such as cardiomyopathy and valvular disease, reduce cardiac function and make it challenging to pump sufficient arterial blood, eventually leading to heart failure. Heart failure is defined as a condition in which various clinical signs appear due to decreased cardiac output (CO) (1). In particular, severely decreased CO can cause various ischemic/hypoperfusion injuries

or disorders in the abdominal organs (2–4). Among the abdominal organs, the pancreas is known to be vulnerable to hypoperfusion (5). Previously, we developed a heart failure model in a dog by performing rapid ventricular pacing (RVP) and demonstrated the association between cardiac function and pancreatic perfusion by evaluating the change in pancreatic blood flow (PBF) in these animals (6). The findings of the study clarified that a decrease in CO lowers blood pressure and reduces PBF (6). Furthermore, examination of the pancreatic tissue revealed that pancreatic acinar cell atrophy, which is a change in the pre-stage of pancreatitis, was caused (7). However, the mechanism by which RVP causes pancreatic acinar cell atrophy in dogs remains unknown. Furthermore, the causal association between the decrease in PBF and this histopathological change has not been clarified. We hypothesized that if we could mitigate the decrease in PBF following the RVP-induced decrease in CO, then the association between the decrease in PBF and pancreatic acinar cell atrophy could be clarified by histopathological examination of the pancreas of the test animal.

One way to increase CO is to increase cardiac contractility (8). Conventional cardiotonic agents such as cardiac glycosides and catecholamines exert pharmacological effects by increasing the Ca^{2+} concentration in cardiomyocytes (8–10). However, these drugs both have arrhythmogenic effects due to intracellular Ca^{2+} overload and risk damaging the cardiomyocytes (8). Therefore, the emergence of new alternative drugs to treat heart failure is expected.

Recently, pimobendan, a calcium sensitizer, was widely used as a cardiotonic drug to treat heart failure in dogs (11–15). Pimobendan exerts a positive inotropic effect by enhancing the sensitivity of myocardial troponin C to Ca^{2+} (8, 16). This makes it possible to increase CO without increasing the heart rate (HR) (17, 18). Additionally, pimobendan relaxes vascular smooth muscles by inhibiting phosphodiesterase III; the blood pressure is thus maintained by increasing CO (18). Previously, pimobendan also improved renal blood flow in dogs with experimentally induced myxomatous mitral valve degeneration (19). Therefore, we suspected that administering pimobendan could mitigate the decrease in PBF in RVP dogs.

Pimobendan was administered to RVP dogs in this study with the expectation that CO would be increased, despite the actions of RVP. Subsequently, we examined whether the decrease in PBF is mitigated and examined the changes observed in the morphology of pancreatic acinar cells at that time. This study aimed to clarify the association between cardiac function, PBF, and histopathological changes in pancreatic acinar cells.

Abbreviations: AUC, area under the curve; CEUS, contrast-enhanced ultrasonography; CI, cardiac index; CO, cardiac output; CVP, central venous pressure; DBP, diastolic blood pressure; FS, fractional shortening; HR, heart rate; LA/Ao, left atrial to aortic ratio; LVIDd, left ventricular end-diastolic dimension; LVIDs, left ventricular end-systolic dimension; MBP, mean blood pressure; PBF, pancreatic blood flow; PEP/ET, ratio of pre-ejection period to ejection time; RVP, rapid ventricular pacing; SBP, systolic blood pressure; SV, stroke volume; SVR, systemic vascular resistance; TIC, time-intensity increase rate curve; TP, time to peak; TTU, time to initial up-slope; TTW, time to washout.

MATERIALS AND METHODS

Healthy beagle dogs (five male and five female) were randomly divided into two groups. Under general anesthesia, epicardial pacemaker leads were placed in each animal. These dogs were 2–3 years old and weighed between 9.3 and 11.2 kg (median: 9.7 kg). Pimobendan (Pimobeheart®, Kyoritsu Seiyaku Corporation, Tokyo, Japan) was administered to one group at a dose of 0.25 mg/kg BID. This dose is generally used to improve clinical signs associated with chronic heart failure due to mitral valve degeneration. The drug was orally administered at 8 a.m. and 4 p.m. The group without medication was defined as the control group, and the group that received pimobendan was defined as the pimobendan group. RVP was implemented in both groups for a period of 4 weeks.

The procedure of pacemaker implantation and pancreatic tissue sampling, in addition to evaluation of cardiac function, PBF, and pancreatic tissue, were the same as described in our previous reports (6, 7). Therefore, the methods for evaluating the cardiac function, PBF, and pancreatic tissue will only be briefly described here. These evaluations were conducted before initiating RVP (baseline) and at 4 weeks after initiating RVP (4 weeks). Cardiac function was evaluated using echocardiography and non-invasive blood pressure measurements using the same device (Vivid E 95 and 7s probe, GE Healthcare Japan Co., Tokyo, Japan, and BP-100D, Fukuda M-E Kogyo Co., Ltd., Tokyo, Japan.). Moreover, PBF was evaluated using contrast-enhanced ultrasonography (CEUS). The items measured by echocardiography and non-invasive blood pressure measurements were as follows. Left atrial to aortic ratio (LA/Ao) was determined from B mode measurements. Left ventricular end-diastolic dimension (LVIDd), left ventricular end-systolic dimension (LVIDs), and fractional shortening (FS) was measured using the M mode. Additionally, ratio of pre-ejection period to ejection time (PEP/ET), stroke volume (SV), CO, and cardiac index (CI) were measured using the Doppler mode. Systolic blood pressure (SBP), mean blood pressure (MBP), and diastolic blood pressure (DBP) were measured by oscillometric methods. Systemic vascular resistance (SVR) was calculated using CO, MBP, and assumed central venous pressure (CVP). CVP was hypothesized to be 5 mmHg at baseline, and 5, 10, or 15 mmHg at 4 weeks, based on previous reports in the same heart failure model (20).

Contrast-enhanced ultrasonography was performed using the same device (Logiq7 and 9L probe, GE Healthcare Japan, Tokyo) and the same contrast agents (perflubutane microbubbles; Sonazoid®, Daiichi-Sankyo Co., Ltd., Tokyo, Japan) as in the previous study. Blood flow delivers the contrast media and the rate of inflow of the bubbles increases the intensity of the CEUS signal. We measured the signal intensity at 5-s intervals from 0 to 180 s and at 10-s intervals from 180 to 300 s after administration of the contrast agents. Similar to our previous report, we defined the intensity before contrast administration as 100% and created a time-intensity increase rate curve (TIC) from 0 to 300 s. Moreover, time to peak (TP), time to initial up-slope (TTU), time to washout (TTW), peak intensity (PI), and area under the curve (AUC) were calculated as blood flow index

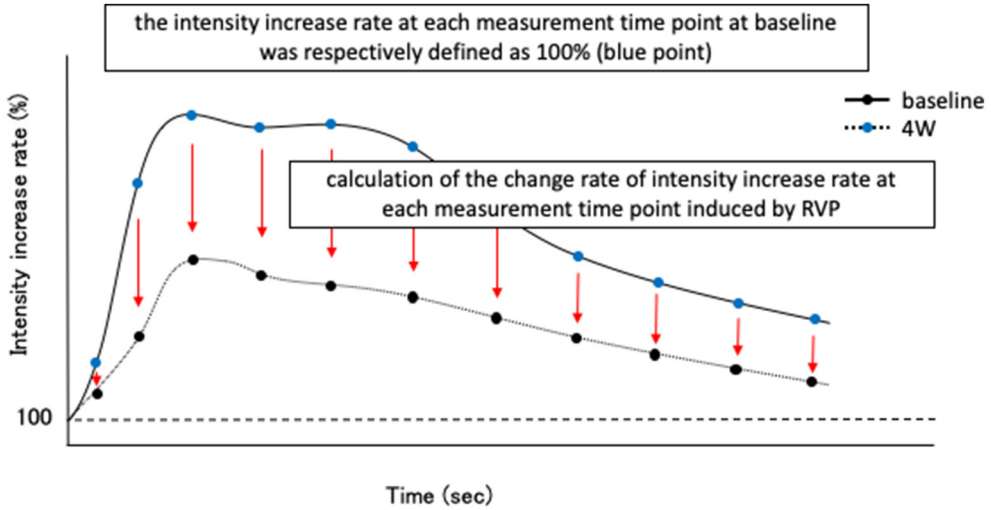

FIGURE 1 | Schematic diagram of evaluation method of intensity reduction level due to rapid ventricular pacing (RVP) in contrast-enhanced ultrasonography (CEUS). First, before initiating RVP (baseline) in both control group and pimobendan group, the intensity increase rate at each measurement time point after Sonazoid® administration (in this study, from 0 to 300 s) was respectively defined as 100% (blue point). Then, the change rate of intensity increase rate at each time point at 4 weeks after initiating RVP (4 weeks) was calculated.

parameters. Then, the degree of decrease in the intensity due to RVP was examined. Specifically, at baseline in both groups, the intensity increase rate at each measurement time point from 0 to 300 s was respectively defined as 100% (**Figure 1**). Moreover, we calculated the change rate of intensity increase rate at each measurement time point induced by RVP for 4 weeks (**Figure 1**).

Pancreatic tissue was evaluated by histopathological examination using hematoxylin and eosin staining. A semiquantitative evaluation was performed based on the extent of zymogen granules in pancreatic acinar cells of 20 consecutive microscopic fields (×400). The following scoring was applied: "0" for <5% pancreatic acinar cells containing zymogen granules, "1" for 5–25%, "2" for 26–50%, and "3" for 51% or more. Moreover, immunohistochemical staining was performed targeting trypsinogen in pancreatic acinar cells using the same anti-trypsin antibodies (×50, rabbit monoclonal, Abcam Plc, Cambridge, UK) as in previous report.

The RVP for inducing heart failure was set at 4 V and 260 beats/min for 4 weeks. This prospective study was performed with approval from Tokyo University of Agriculture and Technology Animal Experiment Committee (Approval number: 31-2).

Statistical Analysis

Statistical analysis was conducted using BellCurve for Excel (Social Survey Research Information Co., Ltd., Tokyo, Japan). The normality of data was tested with the Shapiro–Wilk test. The change rate of intensity increase rate at each time point for CEUS and histopathological scoring data are shown as the mean ± standard error. Other data are shown as mean ± standard deviation. Intra-group comparisons in echocardiographic measurements, blood pressure value, CEUS measurements other than the change in the signal intensity, and histopathological scores were performed using paired *t*-test or Wilcoxon's signed-rank test. Moreover, inter-group comparisons in these data were performed using the unpaired *t*-test or Mann–Whitney *U*-test. Regarding the change rate of intensity increase rate at each time point, intra-group comparisons were conducted using the Friedman test with *post-hoc* Mann–Whitney *U*-test. For all tests, a P value <0.05 was considered statistically significant.

RESULTS

Echocardiography

The results of echocardiographic measurements are shown in **Table 1**. FS decreased significantly at 4 weeks compared to baseline readings in both groups ($P < 0.01$ in both groups). However, at 4 weeks, FS in the pimobendan group was significantly greater than in the control group ($P < 0.01$). In the pimobendan group, compared to baseline, no significant difference was shown in SV, CO, and CI at 4 weeks. In contrast, in the control group, SV, CO, and CI were significantly smaller at 4 weeks than at baseline (SV; $P < 0.01$, CO and CI; $P < 0.05$). Moreover, at 4 weeks, CO and CI in the pimobendan group were significantly greater compared to the control group ($P < 0.05$).

Left atrial to aortic ratio, LVIDd, LVIDs, and PEP/ET were significantly greater at 4 weeks than at baseline in both groups ($P < 0.01$ in both groups). However, PEP/ET at 4 weeks in the pimobendan group was significantly smaller compared to the control group ($P < 0.05$). In the pimobendan group, no significant difference was shown in HR between baseline and 4 weeks. In contrast, HR was significantly greater at 4 weeks than at baseline in the control group ($P < 0.05$).

TABLE 1 | Values of echocardiography and blood pressure measurement.

	Group	Baseline	4 weeks
HR (bpm)	Control	101 ± 10	150 ± 8*
	Pimobendan	108 ± 15	137 ± 25
LA/Ao	Control	1.4 ± 0.1	1.9 ± 0.2**
	Pimobendan	1.3 ± 0.1	1.7 ± 0.1**
LVIDd (mm)	Control	30.2 ± 2.4	39.9 ± 3.6**
	Pimobendan	32.4 ± 1.5	40.4 ± 2.4**
LVIDs (mm)	Control	17.8 ± 1.9	35.7 ± 2.9**
	Pimobendan	20.2 ± 2.2	32.8 ± 2.1**
FS (%)	Control	40.9 ± 4.6	10.6 ± 2.5**
	Pimobendan	37.6 ± 5.8	18.8 ± 3.7**,##
PEP/ET	Control	0.3 ± 0.0	0.5 ± 0.0**
	Pimobendan	0.3 ± 0.0	0.4 ± 0.1**,#
SV (ml)	Control	18.3 ± 3.3	10.3 ± 1.5**
	Pimobendan	19.4 ± 3.0	16.4 ± 5.9
CO (L/min)	Control	2.1 ± 0.2	1.5 ± 0.4*
	Pimobendan	2.1 ± 0.3	2.1 ± 0.5#
CI (L/min/m^2)	Control	4.3 ± 0.6	3.0 ± 0.9*
	Pimobendan	4.4 ± 0.7	4.5 ± 1.0#
SBP (mmHg)	Control	142.7 ± 12.7	102.6 ± 7.8**
	Pimobendan	147.7 ± 17.2	124.0 ± 10.2##
MBP (mmHg)	Control	97.9 ± 4.1	72.9 ± 12.0*
	Pimobendan	110.0 ± 12.3	88.1 ± 7.9#
DBP (mmHg)	Control	77.2 ± 6.5	57.9 ± 13.5
	Pimobendan	84.7 ± 10.0	71.6 ± 9.4

*HR, heart rate; LA/Ao, left atrial to aortic ratio; LVIDd, left ventricular end-diastolic dimension; LVIDs, left ventricular end-systolic dimension; FS, fractional shortening; PEP/ET, ratio of pre-ejection period to ejection time; SV, stroke volume; CO, cardiac output; CI, cardiac index; SBP, systolic blood pressure; MBP, mean blood pressure; DBP, diastolic blood pressure; baseline, before initiating rapid ventricular pacing; 4 weeks, 4 weeks after initiating rapid ventricular pacing. *, $P < 0.05$ vs. baseline; **, $P < 0.01$ vs. baseline; #, $P < 0.05$ vs. control; ##, $P < 0.01$ vs. control. All values are expressed as a mean ± standard deviation.*

Blood Pressure Measurement

In the pimobendan group, no significant difference was shown in SBP and MBP between baseline and 4 weeks. On the other hand, these pressures were significantly lower at 4 weeks than at baseline in the control group (SBP, $P < 0.01$; MBP, $P < 0.05$). Furthermore, SBP and MBP at 4 weeks in the pimobendan group were significantly greater compared to the control group (SBP, $P < 0.01$; MBP, $P < 0.05$). There was no significant difference in DBP between the groups or within each group (**Table 1**). Assuming that CVP at baseline is 5 mmHg, and at 4 weeks is 5, 10, or 15 mmHg, no significant difference was shown in SVR between baseline and 4 weeks in the pimobendan group. However, when CVP at 4 weeks was assumed to be 10 or 15 mmHg, the value tended to decrease (10 mmHg; $P = 0.097$, 15 mmHg; $P = 0.058$). Moreover, no significant difference was shown in SVR between baseline and 4 weeks in the control group, at any combination of CVP values (**Table 2**).

Contrast-Enhanced Ultrasonography

Subjectively, in the pimobendan group, an increase in pancreatic intensity was observed at 4 weeks and at the baseline (**Figure 2**). Furthermore, no significant difference was shown in PI and AUC between baseline and 4 weeks. In contrast, in the control group, PI and AUC were significantly smaller at 4 weeks compared with baseline (both $P < 0.05$) (**Table 3**). As a result, at 4 weeks, AUC and PI in the pimobendan group were significantly greater than in the control group (both $P < 0.05$). In the pimobendan group, no significant difference was shown in TP between baseline and 4 weeks. In contrast, TP was significantly greater at 4 weeks than at baseline in the control group ($P < 0.05$). No significant difference was shown in TTU and TTW in terms of the intra-group and inter-group comparisons. Furthermore, the change rate of intensity increase rate in the pimobendan group was significantly greater than in the control group at almost all time points after Sonazoid® administration (145–160 s and 280 s; $P < 0.05$, other times; $P < 0.01$) (**Figure 3**).

Histopathological Examination

No unusual histopathological findings were observed at baseline in either group. In the pimobendan group, no unusual histopathological findings were observed in any animal at 4 weeks (**Figure 4**). In contrast, pancreatic acinar cell atrophy characterized by degranulation, that is, loss of zymogen granules, was observed in all five dogs at 4 weeks in the control group. Furthermore, this histopathological change was observed in the whole pancreas ($P < 0.01$), and no site-specific difference was shown in the level of the lesion. As a result, the histopathological score at 4 weeks in the pimobendan group was significantly greater compared with that of the control group ($P < 0.05$) (**Table 4**).

Immunohistological Examination

A trypsinogen-positive reaction of the zymogen granules was observed in pancreatic acinar cells at baseline in both groups. There was no change in the extent of the trypsinogen-positive reaction at 4 weeks in the pimobendan group (**Figure 5**). In contrast, at 4 weeks the trypsinogen-positive reaction was attenuated in all animals in the control group.

DISCUSSION

In this study, similar to our previous reports, we found that a decrease in CO caused a decrease in PBF in unmedicated RVP dogs. Moreover, pancreatic tissue in these dogs showed pancreatic acinar cell atrophy with a decrease in zymogen granules, meaning that the hypoperfusion was significant enough to induce cellular damage. In contrast, in RVP dogs treated with pimobendan, PBF was maintained by maintaining CO. As a result, no histopathological changes were observed in the pancreatic tissue.

Similar to our previous reports, in the unmedicated RVP dogs there was a decrease in FS and an increase in PEP/ET, which indicates a decrease in left ventricular contractility. Moreover, a decrease in CI was observed because of the reduction in left ventricular contractile force. The extent of change in these values

TABLE 2 | Systemic vascular resistance when central venous pressure is postulated to be 5–15 mmHg.

	mmHg	Group	Period	
			Baseline	4 weeks
SVR (dynes × s × cm^{-5})	5	Control	3,501 ± 401	3,554 ± 887
		Pimobendan	4,149 ± 917	3,232 ± 778
	10	Control		3,293 ± 849
		Pimobendan		3,037 ± 732
	15	Control		3,032 ± 811
		Pimobendan		2,841 ± 688

SVR, systemic vascular resistance; baseline, before initiating rapid ventricular pacing; 4 weeks, 4 weeks after initiating rapid ventricular pacing. All values are expressed as a mean ± standard deviation.

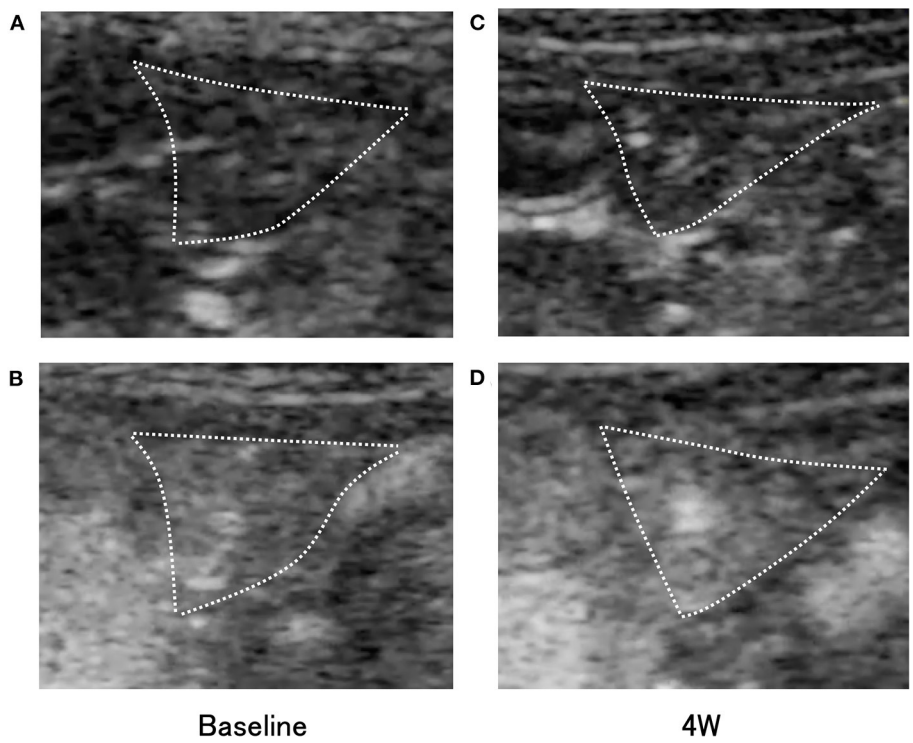

FIGURE 2 | Transverse contrast-enhanced ultrasonography (CEUS) images of the right pancreatic lobe (outlined by dotted lines) in the pimobendan group. **(A,B)** show the intensity increase in the pancreas with contrast agent before initiating rapid ventricular pacing (baseline). **(A)** Just after initiation of contrast imaging. **(B)** Peak of intensity increase. **(C,D)** show the intensity increase in the pancreas with contrast agent at 4 weeks after initiating rapid ventricular pacing (4 weeks). **(C)** Just after initiation of contrast imaging. **(D)** Peak of intensity increase.

was similar to that reported previously (6). Therefore, the RVP dog model used in this study might have good reproducibility of the changed hemodynamics. This heart failure model was determined to be appropriate for investigating the association between cardiac function, PBF, and histopathological changes in the pancreatic acinar cells.

Pimobendan is known to increase CO. Pimobendan has been shown to improve hemodynamics during heart failure due to mitral valve degeneration and dilated cardiomyopathy in dogs, improving quality of life and prolonging the prognosis (11, 12, 14, 15). Moreover, this hemodynamic-improving effect of pimobendan is thought to be mainly due to its positive inotropic effect (18). In this study, the changes in FS and PEP/ET observed in unmedicated RVP dogs were significantly alleviated by pimobendan administration. The decreases in SV, CO, and CI were also suppressed. These results suggest that the positive inotropic effect of pimobendan was effectively exerted on the test animals in this study and could be responsible for the effect of increasing CO. Furthermore, with regard to HR, administration of pimobendan suppressed the increase observed in the control group. Pimobendan is known to increase CO by increasing SV, independent of the increase in HR (17, 18). The results are consistent with this observation and are also considered to have been obtained in this test animal.

Furthermore, maintaining CO cannot enhance the compensatory reaction of increasing HR.

Pimobendan relaxes vascular smooth muscle by inhibiting phosphodiesterase III (21). This action causes dilation of the peripheral blood vessels and reduces SVR (21). However, in this study, while the positive inotropic effect was evident the peripheral vasodilatory effect showed a tendency, but no clear effect was observed. Verdouw et al. administered various doses of pimobendan to healthy pigs under general anesthesia and evaluated the positive inotropic and peripheral vasodilatory effects at each dose. In their study, pimobendan first exerted a positive inotropic effect at low doses and a peripheral vasodilatory effect at higher doses (22). Based on these

TABLE 3 | Values of parameters of the time-intensity change rate curve in the contrast-enhanced ultrasonography of the pancreas.

	Group	Baseline	4 weeks
PI (%)	Control	111.2 ± 3.4	105.5 ± 1.7*
	Pimobendan	109.9 ± 3.9	114.6 ± 7.3#
AUC	Control	324.9 ± 126.9	130.3 ± 43.2*
	Pimobendan	228.7 ± 90.3	389.7 ± 210.7#
TP (s)	Control	55.0 ± 21.2	113.0 ± 34.7*
	Pimobendan	79.0 ± 15.9	71.0 ± 10.2#
TTU (s)	Control	21.0 ± 4.9	36.0 ± 17.7
	Pimobendan	24.0 ± 3.7	28.0 ± 6.0
TTW (s)	Control	254.0 ± 54.6	211.0 ± 54.1
	Pimobendan	193.0 ± 54.6	214.0 ± 49.6

*PI, peak intensity; AUC, area under the curve; TP, time to peak; TTU, time to initial up-slope; TTW, time to washout; baseline, before initiating rapid ventricular pacing; 4 weeks, 4 weeks after initiating rapid ventricular pacing. *, $P < 0.05$ vs. baseline; #, $P < 0.05$ vs. control. All values are expressed as a mean ± standard deviation.*

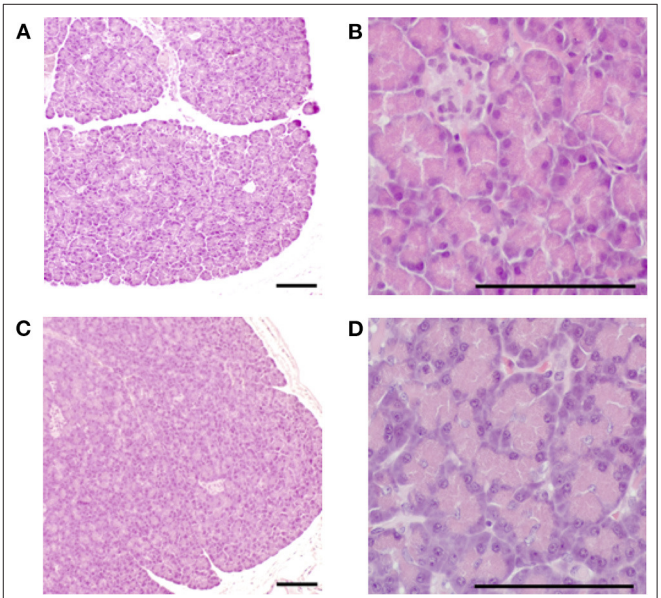

FIGURE 4 | Histopathological image of the pancreas in the pimobendan group. Eosinophilic zymogen granules were observed in the pancreatic acinar cell both before initiating rapid ventricular pacing (baseline) and at 4 weeks after initiating rapid ventricular pacing (4 weeks). **(A,B)** baseline. **(C,D)** 4 weeks. Bars = 100 μm.

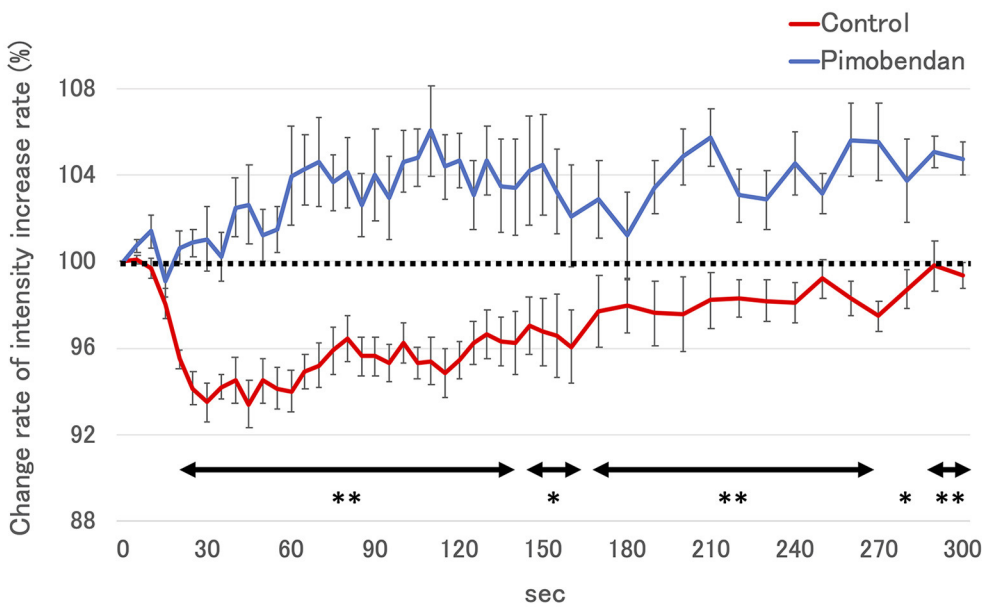

FIGURE 3 | The change rate of intensity increase rate in control group and the pimobendan group in contrast-enhanced ultrasonography (CEUS). The intensity increase rate at each measurement time point after Sonazoid® administration before initiating RVP (baseline) was defined as 100% (dotted line). These values are shown as the mean ± standard error. *; $P < 0.05$ vs. control, **; $P < 0.01$ vs. control.

TABLE 4 | Histological scoring data of pancreas.

	Group	Baseline	4 weeks
Score	Control	2.7 ± 0.0	1.3 ± 0.1**
	Pimobendan	2.7 ± 0.0	2.3 ± 0.0#

*Baseline, before initiating rapid ventricular pacing; 4 weeks, 4 weeks after initiating rapid ventricular pacing. **; $P < 0.01$ vs. baseline, #; $P < 0.05$ vs. control. All values are expressed as a mean ± standard error.*

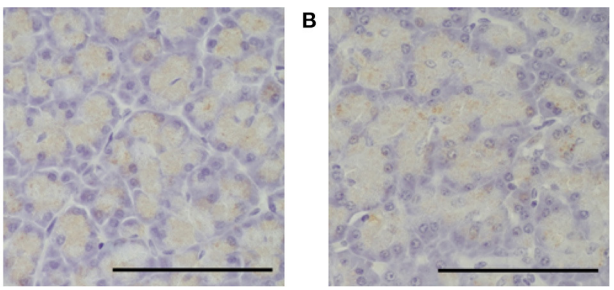

FIGURE 5 | Immunohistochemical image of the pancreas in the pimobendan group. A trypsinogen positive reaction of the zymogen granules was observed in the pancreatic acinar cells both before initiating rapid ventricular pacing (baseline) and at 4 weeks after initiating rapid ventricular pacing (4 weeks). **(A)** baseline. **(B)** 4 weeks. Bars = 100 μm.

observations, it appears the pimobendan dose used in this study led to a positive inotropic effect on the test animals, but did not reach the point where clear peripheral vasodilation could be observed.

In this study, CEUS was used to measure PBF. CEUS involved injecting microbubbles intravenously as a contrast medium, which acts as a reflection source for ultrasonic waves in capillaries to visualize blood flow and enhance echo intensity in organs (23). By calculating the blood flow index from the TIC, based on this increase in intensity over time, it is possible to quantify the blood flow in the target organ (24, 25). CEUS has proven useful as a non-invasive method to assess PBF (6, 25).

Similar to our previous reports, we observed a significant decrease in PI and AUC in the control group. PI indicates the maximum inflow of microbubbles in the region of interest, while AUC indicates the total inflow of microbubbles into the region within the observation period (24). Therefore, a decrease in these parameters indicates decreased blood flow in the pancreatic parenchyma. Compared to the control group, PI and AUC did not decrease, and PBF was maintained in the RVP dogs treated with pimobendan. This result was further clarified by the fact that a decrease in the intensity in the pimobendan group never occurred at almost all time points after administering Sonazoid®. Furthermore, regarding blood pressure measurements, administering pimobendan prevented the decrease in SBP and MBP. Arterial blood pressure, especially MBP, is thought to reflect the driving pressure that pumps blood to peripheral organs and is a key factor in regulating organ blood flow (26). In this study, we observed no clear change in SVR in the pimobendan group. Therefore, we considered that administering pimobendan maintained PBF because the maintenance of cardiac pump function suppressed the decrease in CO, and as a result alleviated the decrease in MBP.

Histopathological examination showed no changes in pancreatic tissue containing pancreatic acinar cells in the pimobendan group, in which CO and PBF were maintained. In contrast, in the control group, similar to previous reports, pancreatic acinar cell atrophy with a decrease in zymogen granules, and thus the trypsinogen contained therein, was observed over a wide area of the pancreas (7). Therefore, we concluded that a decrease in PBF was a direct cause of pancreatic acinar cell atrophy. Pancreatic acinar cell atrophy due to the decrease in PBF most likely corresponds to the pre-stage histopathological changes caused by chronic pancreatitis (7, 27). Moreover, the histopathological changes in pancreatic tissue may become more severe if the decrease in cardiac function and PBF is prolonged (7). This study showed that administering pimobendan to dogs experiencing decreased cardiac contractile force can prevent the development or aggravation of pancreatic acinar cell injury by helping maintain PBF.

This study has several limitations. First, we measured blood pressure non-invasively. In most cases, compared to invasive measures, this method is inferior in accuracy and immediacy. Therefore, it is possible that dynamic changes in blood pressure and SVR were not completely captured. Second, blood flow in organs other than the pancreas was not measured. In heart failure, biological defense reactions restrict blood flow to the peripheral organs and tissues to maintain blood flow to vital organs such as the brain and heart (28). Moreover, the extent of the decrease in blood flow in these peripheral organs and tissues is not uniform (28). Therefore, by measuring the blood flow of multiple organs simultaneously, it may be possible to better understand the association between changes in cardiac function and PBF. Third, we did not perform a histopathological examination of the heart. In this study, the mechanism by which CO was maintained seems to be due to the positive inotropic effect of pimobendan. However, it has been clarified that pimobendan also increases myocardial perfusion by dilating the coronary arteries (29). Myocardial ischemia due to extreme tachycardia is among the primary factors that cause RVP to decrease myocardial contractile force (30). Therefore, it is possible that the administration of pimobendan suppressed the decrease in cardiac function because the myocardium was protected by maintaining coronary blood flow. It may also be possible to clarify the mechanism of maintained CO by performing a histopathological assessment of the extent of myocardial injury. Finally, this study included only a small number of animals, which might have affected the results.

This study showed that the administration of pimobendan helps maintain PBF by suppressing the decrease in cardiac function in dogs with RVP. Furthermore, pimobendan also suppressed histopathological changes in pancreatic acinar cell atrophy. These results clarified that the decrease in PBF due to cardiac dysfunction was a direct cause of pancreatic acinar cell atrophy. This further suggests that maintaining PBF is clinically important for treating dogs with heart failure. In addition, these findings offer a reliable basis for developing new therapeutic strategies for heart failure in dogs, that is, pancreatic protection.

DATA AVAILABILITY STATEMENT

The original contributions presented in the study are included in the article/supplementary material, further inquiries can be directed to the corresponding author/s.

ETHICS STATEMENT

The animal study was reviewed and approved by Tokyo University of Agriculture and Technology Animal Experiment Committee (approval number 31-2).

AUTHOR CONTRIBUTIONS

AY and RF conceived and designed the experiments. AY, TO, DH, MK, and KS performed the experiments. AY analyzed the data and wrote the manuscript. TI, NM, and RF performed the critical revisions of the manuscript. All authors approved the final manuscript.

FUNDING

This work was partially supported by the 2017–2019 the JSPS KAKENHI Grant Number 17K08100 (representative researcher: RF).

ACKNOWLEDGMENTS

This work was conducted at the Animal Medical Center, Tokyo University of Agriculture and Technology in Tokyo, Japan. The authors thank Eita Sugano, Yoshito Momonoi, Ryo Ishii, and Kokoro Ito who are students for their technical assistance with this work.

REFERENCES

1. Ponikowski P, Voors AA, Anker SD, Bueno H, Cleland JGF, Coats AJS, et al. 2016 ESC guidelines for the diagnosis and treatment of acute and chronic heart failure: the task force for the diagnosis and treatment of acute and chronic heart failure of the European Society of Cardiology (ESC) developed with the special contribution of the heart failure association (HFA) of the ESC. *Eur Heart J.* (2016) 37:2129–200. doi: 10.1093/eurheartj/ehw128
2. Fouad YM, Yehia R. Hepato-cardiac disorders. *World J Hepatol.* (2014) 6:41–54. doi: 10.4254/wjh.v6.i1.41
3. Ronco C, Cicoira M, McCullough PA. Cardiorenal syndrome type 1: pathophysiological crosstalk leading to combined heart and kidney dysfunction in the setting of acutely decompensated heart failure. *J Am Coll Cardiol.* (2012) 60:1031–42. doi: 10.1016/j.jacc.2012.01.077
4. Sandek A, Swidsinski A, Schroedl W, Watson A, Valentova M, Herrmann R, et al. Intestinal blood flow in patients with chronic heart failure: a link with bacterial growth, gastrointestinal symptoms, and cachexia. *J Am Coll Cardiol.* (2014) 64:1092–102. doi: 10.1016/j.jacc.2014.06.1179
5. Warshaw AL, O'Hara PJ. Susceptibility of the pancreas to ischemic injury in shock. *Ann Surg.* (1978) 188:197–201. doi: 10.1097/00000658-197808000-00012
6. Yoshimura A, Ohmori T, Yamada S, Kawaguchi T, Kishimoto M, Iwanaga T, et al. Comparison of pancreatic and renal blood flow in a canine tachycardia-induced cardiomyopathy model. *J Vet Med Sci.* (2020) 82:836–45. doi: 10.1292/jvms.19-0694
7. Yoshimura A, Ohmori T, Itou K, Ishi R, Matsumura Y, Wada Y, et al. Histopathological changes in the pancreas due to decreased pancreatic blood flow in a canine tachycardia-induced cardiomyopathy model. *J Vet Med Sci.* (2021) 83:780–3. doi: 10.1292/jvms.20-0409
8. Endoh M. Cardiac Ca^{2+} signaling and Ca^{2+} sensitizers. *Circ J.* (2008) 72:1915–25. doi: 10.1253/circj.CJ-08-0838
9. Ding G, Wiegerinck RF, Shen M, Cojoc A, Zeidenweber CM, Wagner MB. Dopamine increases L-type calcium current more in newborn than adult rabbit cardiomyocytes *via* D1 and β2 receptors. *Am J Physiol Heart Circ Physiol.* (2008) 294:H2327–35. doi: 10.1152/ajpheart.00993.2007
10. Langer GA. Effects of digitalis on myocardial ionic exchange. *Circulation.* (1972) 46:180–7. doi: 10.1161/01.CIR.46.1.180
11. Boswood A, Häggström J, Gordon SG, Wess G, Stepien RL, Oyama MA, et al. Effect of pimobendan in dogs with pre-clinical myxomatous mitral valve disease and cardiomegaly: the EPIC study-a randomized clinical trial. *J Vet Intern Med.* (2016) 30:1765–79. doi: 10.1111/jvim.14586
12. Fuentes VL, Corcoran B, French A, Schober KE, Kleemann R, Justus C. A double-blind, randomized, placebo-controlled study of pimobendan in dogs with dilated cardiomyopathy. *J Vet Intern Med.* (2002) 16:255–61. doi: 10.1892/0891-6640(2002)016<0255:adrpso>2.3.co;2.2.3.CO;2
13. Keene BW, Atkins CE, Bonagura JD, Fox PR, Häggström J, Fuentes VL, et al. ACVIM consensus guidelines for the diagnosis and treatment of myxomatous mitral valve disease in dogs. *J Vet Intern Med.* (2019) 33:1127–40. doi: 10.1111/jvim.15488
14. O'Grady MR, Minors SL, O'Sullivan ML, Horne R. Effect of pimobendan on case fatality rate in doberman pinschers with congestive heart failure caused by dilated cardiomyopathy. *J Vet Intern Med.* (2008) 22:897–904. doi: 10.1111/j.1939-1676.2008.0116.x
15. Summerfield NJ, Boswood A, O'Grady MR, Gordon SG, Dukes-McEwan J, Oyama MA, et al. Efficacy of pimobendan in the prevention of congestive heart failure or sudden death in doberman pinschers with pre-clinical dilated cardiomyopathy (the PROTECT Study). *J Vet Intern Med.* (2012) 26:1337–49. doi: 10.1111/j.1939-1676.2012.01026.x
16. Solaro RJ, Fujino K, Sperelakis N. The positive inotropic effect of pimobendan involves stereospecific increases in the calcium sensitivity of cardiac myofilaments. *J Cardiovasc Pharmacol.* (1989) 14 Suppl 2:S7–12. doi: 10.1097/00005344-198906142-00003
17. Ohte N, Cheng CP, Suzuki M, Little WC. The cardiac effects of pimobendan (but not amrinone) are preserved at rest and during exercise in conscious dogs with pacing-induced heart failure. *J Pharmacol Exp Ther.* (1997) 282:23–31.
18. Suzuki S, Fukushima R, Ishikawa T, Hamabe L, Aytemiz D, Huai-Che H, et al. The effect of pimobendan on left atrial pressure in dogs with mitral valve regurgitation. *J Vet Intern Med.* (2011) 25:1328–33. doi: 10.1111/j.1939-1676.2011.00800.x
19. Kanno N, Kuse H, Kawasaki M, Hara A, Kano R, Sasaki Y. Effects of pimobendan for mitral valve regurgitation in dogs. *J Vet Med Sci.* (2007) 69:373–7. doi: 10.1292/jvms.69.373
20. Onogawa T, Sakamoto Y, Nakamura S, Nakayama S, Fujiki H, Yamamura Y. Effects of tolvaptan on systemic and renal hemodynamic function in dogs with congestive heart failure. *Cardiovasc Drugs Ther.* (2011) 25 Suppl 1:S67–76. doi: 10.1007/s10557-011-6350-4
21. Pagel PS, Hettrick DA, Warltier DC. Influence of levosimendan, pimobendan, and milrinone on the regional distribution of cardiac output in anesthetized dogs. *Br J Pharmacol.* (1996) 119:609–15. doi: 10.1111/j.1476-5381.1996.tb15716.x
22. Verdouw PD, Hartog JM, Duncker DJ, Roth W, Saxena PR. Cardiovascular profile of pimobendan, a benzimidazole-pyridazinone derivative with vasodilating and inotropic properties. *Eur J Pharmacol.* (1986) 126:21–30. doi: 10.1016/0014-2999(86)90733-8
23. Greis C. Ultrasound contrast agents as markers of vascularity and microcirculation. *Clin Hemorheol Microcirc.* (2009) 43:1–9. doi: 10.3233/CH-2009-1216

24. Haers H, Daminet S, Smets PMY, Duchateau L, Aresu L, Saunders JH. Use of quantitative contrast-enhanced ultrasonography to detect diffuse renal changes in beagles with iatrogenic hypercortisolism. *Am J Vet Res.* (2013) 74:70–7. doi: 10.2460/ajvr.74.1.70
25. Kersting S, Ludwig S, Ehehalt F, Volk A, Bunk A. Contrast-enhanced ultrasonography in pancreas transplantation. *Transplantation.* (2013) 95:209–14. doi: 10.1097/TP.0b013e31827864df
26. Bigatello LM, George E. Hemodynamic monitoring. *Minerva Anestesiol.* (2002) 68:219–25.
27. Tanaka T, Ichiba Y, Miura Y, Ito H, Dohi K. Canine model of chronic pancreatitis due to chronic ischemia. *Digestion.* (1994) 55:86–9. doi: 10.1159/000201130
28. Zelis R, Flaim SF, Liedtke AJ, Nellis SH. Cardiocirculatory dynamics in the normal and failing heart. *Annu Rev Physiol.* (1981) 43:455–76. doi: 10.1146/annurev.ph.43.030181.002323
29. Duncker DJ, van Dalen FJ, Hartog JM, Lamers JM, Rensen RJ, Saxena PR, et al. Usefulness of pimobendan in the treatment of heart failure. *Arzneimittelforschung.* (1986) 36:1740–4.
30. Shinbane JS, Wood MA, Jensen DN, Ellenbogen KA, Fitzpatrick AP, Scheinman MM. Tachycardia-induced cardiomyopathy: a review of animal models and clinical studies. *J Am Coll Cardiol.* (1997) 29:709–15. doi: 10.1016/S0735-1097(96)00592-X

Conflict of Interest: The authors declare that the research was conducted in the absence of any commercial or financial relationships that could be construed as a potential conflict of interest.

Publisher's Note: All claims expressed in this article are solely those of the authors and do not necessarily represent those of their affiliated organizations, or those of the publisher, the editors and the reviewers. Any product that may be evaluated in this article, or claim that may be made by its manufacturer, is not guaranteed or endorsed by the publisher.

frontiers | Frontiers in Veterinary Science

TYPE Original Research
PUBLISHED 22 July 2022
DOI 10.3389/fvets.2022.934907

OPEN ACCESS

EDITED BY
Fazul Nabi,
Lasbela University of Agriculture, Water and Marine Sciences, Pakistan

REVIEWED BY
Muhammad Fakhar-e-Alam Kulyar, Huazhong Agricultural University, China
Joycee Jogi, Nanaji Deshmukh Veterinary Science University, India

*CORRESPONDENCE
Yanfei Yu
yuyanfeihaha@163.com
Xiaomin Yuan
187027211@qq.com

SPECIALTY SECTION
This article was submitted to Comparative and Clinical Medicine, a section of the journal Frontiers in Veterinary Science

RECEIVED 03 May 2022
ACCEPTED 27 June 2022
PUBLISHED 22 July 2022

CITATION
Li S, Zhou Y, Yuan T, Feng Z, Zhang Z, Wu Y, Xie Q, Wang J, Li Q, Deng Z, Yu Y and Yuan X (2022) Selection of internal reference gene for normalization of reverse transcription-quantitative polymerase chain reaction analysis in *Mycoplasma hyopneumoniae*. *Front. Vet. Sci.* 9:934907. doi: 10.3389/fvets.2022.934907

Selection of internal reference gene for normalization of reverse transcription-quantitative polymerase chain reaction analysis in *Mycoplasma hyopneumoniae*

Shiyang Li[1,2], Yanqing Zhou[2,3,4], Ting Yuan[2], Zhixin Feng[2,3], Zhenzhen Zhang[2], Yuzi Wu[2], Qingyun Xie[2], Jia Wang[2], Quan Li[5], Zhibang Deng[1], Yanfei Yu[1,2,3,6]* and Xiaomin Yuan[1]*

[1]College of Veterinary Medicine, Hunan Agricultural University, Changsha, China, [2]Key Laboratory of Veterinary Biological Engineering and Technology, Institute of Veterinary Medicine, Jiangsu Academy of Agricultural Sciences, Ministry of Agriculture and Rural Affairs, Nanjing, China, [3]College of Veterinary Medicine, Nanjing Agricultural University, Nanjing, China, [4]Zhongshan Institute for Drug Discovery, Shanghai Institute of Materia Medica, Chinese Academy of Sciences, Zhongshan, China, [5]College of Veterinary Medicine, Yangzhou University, Yangzhou, China, [6]School of Food and Biological Engineering, Jiangsu University, Zhenjiang, China

Mycoplasma hyopneumoniae is the etiological agent of swine enzootic pneumonia (EP), which resulting in considerable economic losses in pig farming globally. Reverse transcription-quantitative polymerase chain reaction (RT-qPCR) is a major tool for gene expression studies. However, no internal reference genes for normalization of RT-qPCR data of *M. hyopneumoniae* have been reported. The aim of this study was to screen the most stable genes for RT-qPCR analysis in *M. hyopneumoniae* under different conditions. Therefore, a total of 13 candidate internal reference genes (*rpoC*, *Lipo*, *sgaB*, *oppB*, *hypo621*, *oppF*, *gyrB*, *uvrA*, *P146*, *prfA*, *proS*, *gatB*, and *hypo499*) of *M. hyopneumoniae* filtered according to the reported quantitative proteomic analysis and the *16S rRNA* internal reference gene frequently used in other bacteria were selected for RT-qPCR analysis. The mRNAs from different virulence strains (168, 168 L, J, NJ, and LH) at five different growth phases were extracted. The corresponding cycle threshold (Ct) values of the 25 reverse transcribed cDNAs using the 14 candidate genes were determined. Different internal reference genes or combinations were then screened for expression stability analysis using various statistical tools and algorithms, including geNorm, BestKeeper, and NormFinder software, to ensure the reliability of the analysis. Through further

comprehensive evaluation of the RefFinder software, it is concluded that the *gatB* gene was the most suitable internal reference gene for samples of the different virulence strains in different growth phases for *M. hyopneumoniae*, followed by *prfA*, *hypo499*, and *gyrB*.

KEYWORDS

***Mycoplasma hyopneumoniae*, RT-qPCR – real-time quantitative polymerase chain reaction, internal reference genes, gatB, virulence**

Introduction

Mycoplasma hyopneumoniae is the primary pathogen of enzootic pneumonia (EP), a chronic respiratory disease in pigs, and one of the primary agents involved in the porcine respiratory disease complex (PRDC) (1). Studies of virulence factors have mainly focused on adhesion proteins, such as P97 and P102 (2, 3). However, the pathogenic mechanism is still unclear and additional virulence factors need to be discovered. These discoveries will be aided by reverse transcription-quantitative polymerase chain reaction (RT-qPCR). RT-qPCR is frequently used to screen genes with different expression levels in different samples (4). The difference in expression level of genes under specific conditions can be linked to specific phenotypes. For instance, genes with significantly different expression levels in strains with different virulence strains can be used to correlate the gene products with the virulence of the strains. However, a credible RT-qPCR is not available for *M. hyopneumoniae*. The key to the establishment of a reliable RT-qPCR system is the identification of internal reference genes. The inclusion of reference genes enables the normalization of sample-to-sample variation and avoids misinterpretation of the RT-qPCR assays. An ideal internal reference gene should be expressed consistently under various conditions. However, despite many studies, no internal reference gene capable of stable expression under all test conditions has been identified. The expression of internal reference gene changes in different types of cells and during different stages of cell growth (5). Hence, it is vital to identify the stable internal reference gene under particular conditions used in a study to allow accurate interpretation of the results. Many reports have described the screening of internal reference genes under different conditions. Previous experimental analyses determined that *rec*A, *rho*, *pro*C, and *rpo*D are the most appropriate reference genes for the normalization of RT-qPCR data in *Klebsiella pneumoniae* (6). Analysis of the weighted average covariance and NormFinder stability index of the expression of 39 genes implicated *mdo*G as a stable internal reference gene in *Escherichia coli* K-12 (7). A study in *Streptococcus thermophilus* showed that, compared with traditional RG *16S rRNA*, genes encoding glycine-tRNA ligase subunit β GlyS and fatty acid-binding protein DegV were more stably expressed (8). However, no internal reference genes of *M. hyopneumoniae* have been reported. This has prevented data normalization from this bacterium, which has hindered scientific gene transcription analysis and the comparison of results from different laboratories.

In this study, mRNAs extracted from *M. hyopneumoniae* strains in different growth phases and with diverse virulence were reverse transcribed into cDNAs and subjected to gene expression stability analysis by various statistical tools and algorithms, including geNorm, NormFinder, BestKeeper, and RefFinder.

Materials and methods

Strains and cultivation

High virulence *M. hyopneumoniae* strains 168, LH, and NJ and low virulence strains 168 L and J were cultured in modified Friis broth, KM2 medium (pH 7.4), at 37°C until the red medium turned yellow (pH 6.8). Details of the strains were mentioned in Data Sheet 1. Bacteria were harvested by centrifugation at 12,000 × *g* for 20 min at 4°C after culture for 12, 24, 36, 48, and 60 h. The pellets were washed twice with phosphate-buffered saline (PBS) before preparation for RNA extraction.

Extraction of total RNA and reverse transcription

The extraction of RNA from a total of 25 samples of different strains at different growth stages was performed using the RNAprep Pure Cell/Bacteria Kit (TIANGEN BIOTECH CO., LTD., Beijing, China), followed by the manufacturer's instructions. First-strand cDNA synthesis was performed using a HiScriptIII Reverse Transcriptase Kit (Vazyme Biotech Co., Ltd., Nanjing, China), followed by the manufacturer's instructions. All cDNA samples were stored at −80°C until used. The details of the reverse transcription reaction system are summarized in Table 1.

Design and validation of specific primers

The candidate reference genes were chosen according to the proteomic analysis of *M. hyopneumoniae* (9). Genes displaying constant expression levels between the two strains with different virulence strains were used for further analysis of transcript levels. The threshold was defined with the abundance fold change between −1.1 and 1.1, because fold change > 1.2 (10), 1.5 (11), or 2.0 (12) was considered significant in most comparative proteomics analyses. According to the standards, a total of 13 candidates were chosen. These included DNA-directed RNA polymerase subunit beta (*rpoC*), lipoprotein (*Lipo*), pentitol phosphotransferase enzyme II, B component (*sgaB*), oligopeptide transport system permease protein (*oppB*), hypothetical protein (*hypo621*), oligopeptide transport system permease protein (*oppF*), DNA gyrase subunit B (*gyrB*), excinuclease ABC subunit A (*uvrA*), *P146* adhesin like-protein, p97 paralog (*P146*), peptide chain release factor 1 (*prfA*), prolyl-tRNA synthetase (*proS*), glutamyl-tRNA amidotransferase subunit B (*gatB*), and hypothetical protein (*hypo499*). In addition, another candidate commonly used in other bacteria, 16S ribosomal RNA (*16S*), was also evaluated in this study. *16S* is a housekeeping gene among different strains and its transcription level is reported to be relatively stable (13). Specific primers of the 14 candidates (Table 2) were synthesized by GenScript Biotech (Nanjing, China).

To evaluate the specificity of the candidate internal reference genes, both agarose gel electrophoresis and melting curves of primers analysis were performed. Using the strain cDNA as a template, the RT-qPCR amplification products of 14 internal reference genes were verified by 1% agarose gel electrophoresis to investigate the homogeneity and purity of the products, evident as a single band. The melting curves of the primer analyses determined using the QuantStudio 5 software were also analyzed to determine if the dissolution peaks were single and sharp. A sharp peak will appear in the curve if the reaction product is single. At least two or more peaks will appear if there is a dimer or non-specific amplification.

TABLE 1 Reverse transcription reaction system details.

Reagent	Volume
5 × HiScript II Buffer	4 μL
dNTP Mix (10 mM each)	1 μL
HiScript II Reverse Transcriptase (200 U/μl)	1 μL
RNase inhibitor (40 U/μl)	1 μL
Oligo (dT) 23VN (50 μM)	1 μL
Random hexamers (50 ng/μl)	1 μL
Total RNA	100 ng
RNase-free distilled deionized water	up to 20 μL

RT-qPCR analysis

Taq Pro Universal SYBR qPCR Master Mix was used for RT-qPCR analysis (Vazyme Biotech Co., Ltd.). All tests were carried out in biological triplicates and technical duplicates. The experimental reaction system conditions are presented in Table 3. RT-qPCR was performed for each candidate reference gene according to the procedures listed in Table 4. The cycle threshold (Ct) values of 25 samples were collected for statistical analyses.

Expression stability analysis

The stability of gene expression level was analyzed using the geNorm (14, 15), NormFinder (16, 17), and BestKeeper software (18, 19).

TABLE 2 RT-qPCR primers for candidate reference genes.

Gene	Forward primer (5'-3') Reverse primer (5-3')	Length of products, bp
16S	F: CGGCAGTATCTTTAGGGTTCTC R: GCTCGTGTCGTGAGATGTTAG	95
gyrB	F: AAACGCCCGGGAATGTATATC R: CTGCAAGAGCCTCATCAACT	97
gatB	F: AATGGATCACTTCGTGCTGATA R: TCAAGTTCGGCGGCTTT	125
hypo499	F: CATAGGAAGGCAAGCCTCAA R: CGATGAGGCAACTAGGGTAATAG	110
hypo621	F: CGCGAGTGCTGATCGTATTT R: AGATGGCGGTGATCTTTCTTG	135
Lipo	F: GCAAGTTGTTGGGAGGTAATTG R: AAGAAATCGCTGAGGGTAGTG	133
oppB	F: TCTATTCCCGGAGATCCAAGT R: AACGTTGTGCTTGTGGTAAATC	100
oppF	F: CTGTCTTTGACCACCGGAAA R: GAAGCACTTGAAAGCGTCAATC	78
P146	F: GAGGGTGAGGAAGATGAAGAAG R: GAAGTCAACTCCAAGACGAAGA	100
prfA	F: GAATTCGGCCCATTGTTTCAG R: CTTTAGCAGGCGGGTTTAGT	129
proS	F: CTCCCGAAAGAGAGCAAGAAA R: CCTGTCTGTGGTAAGGCAAA	94
rpoC	F: GGCCTTCTTTGGTTGTTACTTG R: CCGCTCATGCTCCTGTTATTA	117
sgaB	F: GCTGCTTGTGGAAATGGAATG R: CGCTTCAACTGTGGCATCTA	96
uvrA	F: GTAGGACATCCGGCTTGTATC R: CCAAGGAGACGGGCAAATTA	101

TABLE 3 RT-qPCR reaction system details.

Reagent	Volume
2× Taq PRO Universal SYBR qPCR Master Mix	10.0 μL
Primer F	0.4 μL
Primer R	0.4 μL
Template cDNA	2 μL
ddH2O	8 μL

TABLE 4 RT-qPCR reaction procedures.

Item	Reps	Temperature	Time
Predenaturation	1	95 °C	30 s
Cyclic response	40	95 °C	10 s
		60 °C	30 s
		95 °C	15 s
Dissolution curve	1	60 °C	60 s
		95 °C	15 s

GeNorm

The data analysis was first performed using geNorm (14). The Ct value of 25 samples was converted into a relative quantitative Q-value using the following formula: $Q = 2^{-\Delta Ct}$ (ΔCt=Ct sample–Ct min). "Ct sample" was the Ct value of the housekeeping gene in each of the samples of *M. hyopneumoniae* with different virulence strains and in different growth stages. "Ct min" indicated the lowest Ct value of the housekeeping genes among the 25 samples. Then, the expression stability measurement (M) value was calculated with Q-value by the geNorm program for each candidate reference gene. The optimal number of reference genes was determined by the paired coefficient of variation Vn/Vn+1. When Vn/V $(n + 1) < 0.15$, the optimal number of internal reference genes is n. When Vn/V $(n + 1) > 0.15$, the optimal number of internal reference genes is $n + 1$. GeNorm did not differentiate between groups of samples or treatments.

NormFinder

The principle of NormFinder was similar to that of the geNorm program. The stable value of gene expression was the same as the M-value of geNorm (16). However, NormFinder offered a method of reference gene selection that took into account intragroup and intergroup variability. The gene with the smallest stable value of expression was taken as the most stable. Another characteristic of the NormFinder software was that only one appropriate internal reference gene would be selected as the reference gene.

BestKeeper

BestKeeper is also a program designed for selection against internal reference genes (19). The raw data were filled into the table of the BestKeeper software. The expression stability was evaluated by calculating standard deviation (SD) and percentage covariance (CV). Both BestKeeper and geNorm were based on pairwise comparison, which carried the same vulnerabilities regarding co-regulated genes (20). Internal reference genes and target genes were analyzed separately in this program. The BestKeeper program produces paired correlation coefficients and BestKeeper indices (geometric mean of Ct values of each candidate gene) between genes, which are compared according to the magnitude of their values.

Integrated analysis by RefFinder

Finally, the results obtained from geNorm (M-values), NormFinder (stability values), and BestKeeper (CV and SD) were subjected to the RefFinder algorithm (http://150.216.56.64/referencegene.php?type=reference), which integrated the results of the aforementioned three standard analysis algorithms for the comprehensive ranking of candidate reference gene(s) (21).

Results

Validation of specificity of candidate internal reference genes

The expression stability of housekeeping genes is the determining factor for the screening of internal reference genes. According to this principle, the genes previously reported to be expressed constantly in two different virulence strains (9), as well as the frequently used internal reference target *16S*, were chosen for further evaluation. Prior to the RT-qPCR assay, the validity of the designed primers for a total of 14 candidates was subjected to reference genes specificity evaluation using cDNA transcribed from RNA as the template. RNA of 25 different samples from *M. hyopneumoniae* strains with different virulence strains and in different growth stages was obtained by RNA extraction. Equal amounts of RNA were further used as the template for the reverse transcription reaction to obtain cDNA. The obtained RT-qPCR amplification products of 14 internal reference genes using cDNA of 5 different strains as the template were verified by 1% agarose gel electrophoresis. As shown in Figure 1A, clear and specific target bands were obtained from all 14 tested internal reference genes using the genomes of five different strains as a template. In addition, the good specificity of the 14 primers was also validated by the melting curve analysis. As shown in Figure 1B, the melting curves of all the 14 primers exhibited a single and sharp peak in 5 different stains, which confirmed the specificity of every primer pair.

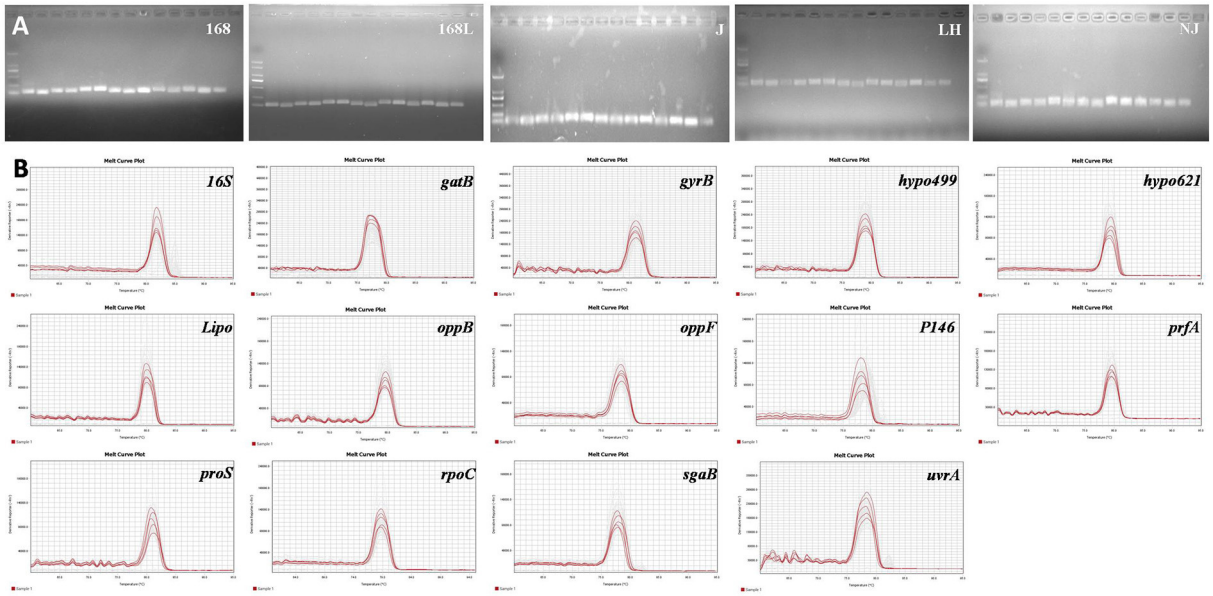

FIGURE 1
(A). Nucleic acid gel electrophoresis of candidate reference genes. M: DL2000;1: *16S*; 2: *gyrB*; 3: *gatB*; 4: *hypo499*; 5: *hypo621*; 6: *Lipo*; 7: *oppB*; 8: *oppF*; 9: *P146*; 10: *prfA*; 11: *proS*; 12: *rpoC*; 13: *sgaB*; 14: *uvrA*. **(B)**. Melting curves of the 14 candidate reference genes using genomes of different *M. hyopneumoniae* strains. Melting temperatures were visualized by plotting the negative first derivative of fluorescence relative to temperature (°C).

Abundance of transcripts of candidate internal reference genes

Analyzing the abundance of mRNA level was another important prerequisite for the selection of internal reference genes. A moderate level of gene expression was an optimal choice for reference genes, because it allows the evaluation of genes expressed at various levels, including very high and very low. The Ct value of reference genes was inversely proportional to the expression level of the genes in RT-qPCR analysis. The greater the Ct value of the reference gene, the lower the expression of the target gene in the sample and vice versa. Expression abundance of the 14 candidate reference genes in all 25 samples was analyzed using serial 10-fold dilutions of PCR products *via* RT-qPCR. The Ct values for each reference gene ranged from 8 to 29 (Figure 2). The large distribution of Ct values suggested that the expression abundance differed among the reference genes. The minimum Ct value of 8 was displayed by *16S*. Thus, the gene expression abundance of *16S* was the highest. The extremely high abundance of the reference genes will hinder the evaluation of the transcriptional level of those genes with low abundance. Thus, *16S* was excluded from the candidate reference genes pool in the following analysis. The Ct values of the other 13 genes were approximately 21, which was neither too high nor too low, and suitable to evaluate the transcription levels of other genes.

Stability of candidate internal reference genes

The transcription stability is vital for the internal reference of the 13 housekeeping genes with moderate abundance. This stability was determined for all 25 *M. hyopneumoniae* samples in different growth phases and with different virulence strains.

GeNorm analysi

All 25 *M. hyopneumoniae* samples were split into two sets according to the same strain at different growth stages and different virulence strains at the same growth stages, which were entered separately in the geNorm software package. Figures 3A,C shows the geNorm M analysis for all samples. Lower geNorm M values represented more stable reference genes. In addition, it is generally considered that when the value of Vn/V (n+1) calculated with Ct values of different primers and different samples by geNorm is < 0.15, it is unnecessary to introduce a new reference gene into the internal reference system. Otherwise, $(n+1)^{th}$ reference gene is needed. As shown in Figure 3B, the V2/3 values of reference genes in all samples, except for strain NJ, were less than the threshold value of 0.15. Gene expression analysis by geNorm recommended two reference genes to achieve the best performance for strains 168, 168 L, J, and LH, while 3 reference genes were suitable for strain

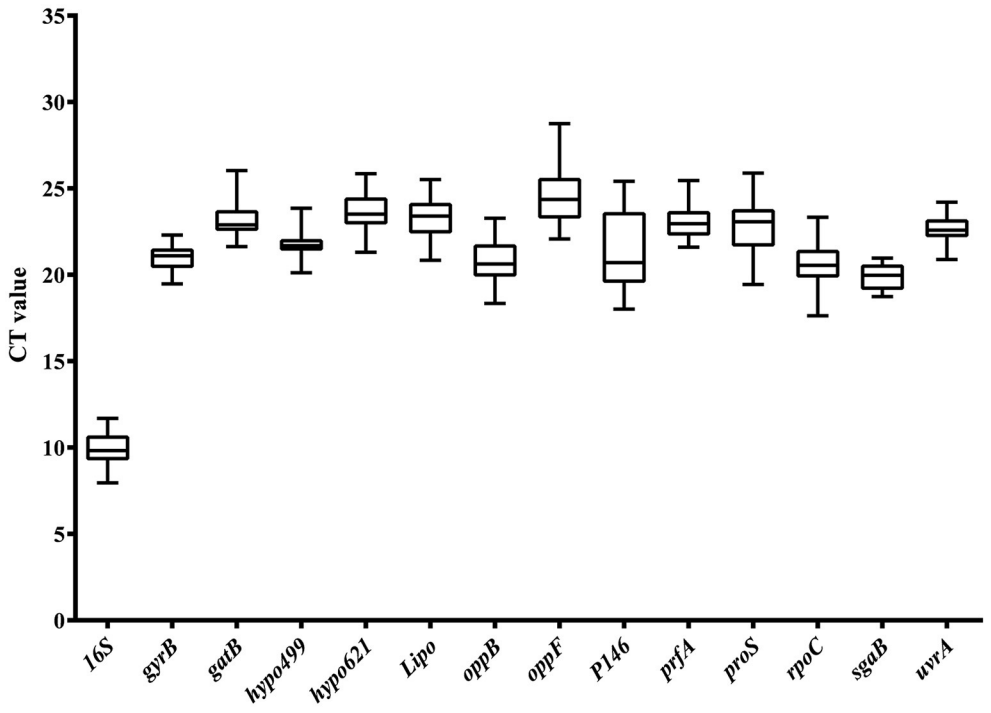

FIGURE 2
Ct value distribution of candidate reference genes in all samples by RT-qPCR. Boxes represent the mean Ct value and bars depict the mean ± standard deviation.

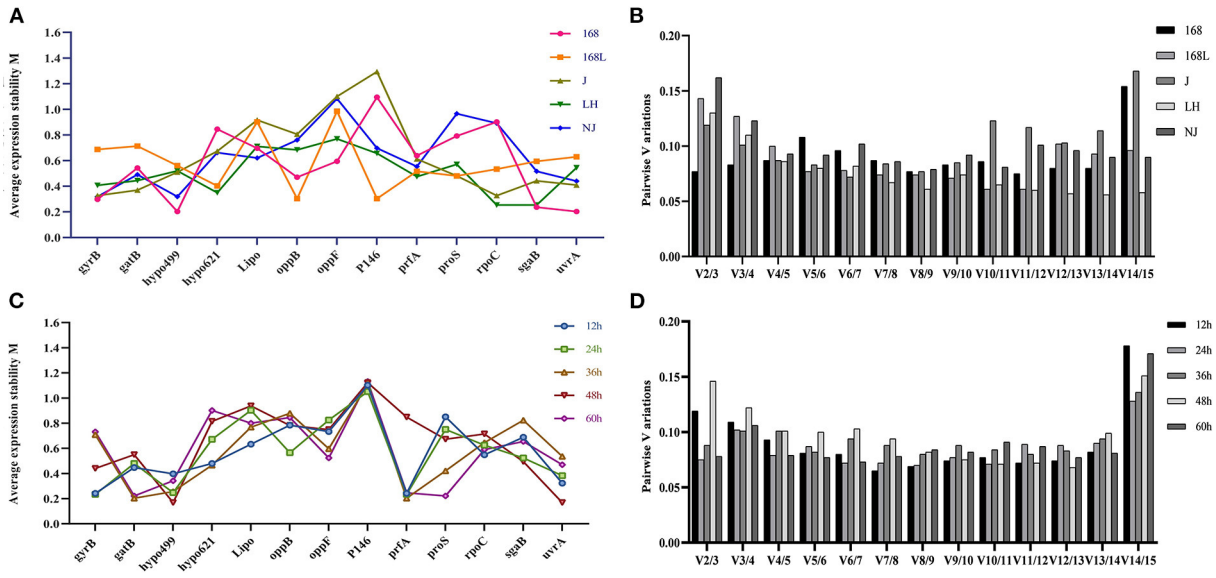

FIGURE 3
Average expression stability M-value and optimal number of reference genes according to geNorm analysis. The expression stability of 13 candidate genes in the same strain at different culture time **(A)** and different strains at the same culture time **(C)** was calculated. The x-axis represents various candidate reference genes. The y-axis represents stability value (M-value). Lower M-value suggests higher expression stability. **(B)** and **(D)** show the optimal number of reference genes in different subsets. The x-axis represents the number of genes selected for comprehensive analysis V (n/n+1), and the y-axis means the pairwise variation value (V-value). When the V-value is < 0.15, the corresponding combination is deemed stable; n is the best number of internal reference genes.

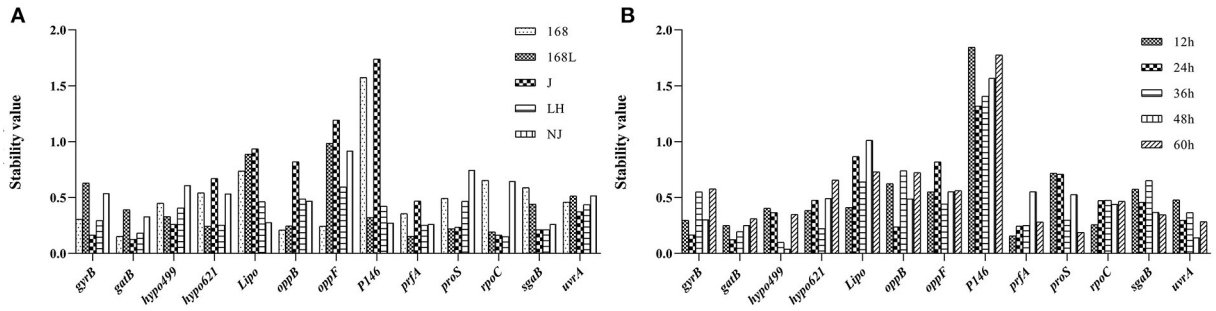

FIGURE 4
Stability analysis of internal reference genes using the NormFinder software. The x-axis represents various candidate reference genes. The y-axis represents stability value. **(A)**: stability value of reference gene of the same strain at different culture time. **(B)**: stability value of reference gene of different strains at the same culture time.

NJ. Results shown in Figure 3A demonstrated that for strain 168 at different growth stages, the candidate *hypo499* and *uvrA* genes had the lowest M-values and were ranked as the most stable candidates. Accordingly, the candidate *oppB* and *P146* genes ranked as the most stable genes in strain 168 L at different growth stages. In strain J, the stability of *gyrB* and *rpoC* was highest. For strain LH, the targets of highest transcriptional stability in different culture times were *rpoC* and *sgaB*. For strain NJ, *gyrB*, *hypo499*, and *uvrA* were the most stable.

The stability of internal reference genes for samples in the same growth phases of different strains was further evaluated. As shown in Figure 3D, two reference genes were suitable for RT-qPCR normalization in 12-h, 24-h, 36-h, 48-h, and 60-h cultures of different strains. The most stable candidates of 12-h cultures of the above five different strains were *gyrB* and *prfA*. Genes *gyrB* and *prfA* ranked as the two most stable candidates due to their minimum M-values. *P146* and *prfA* similarly ranked as the two most stable genes of 24-h cultures of the different strains. The most stable reference genes of 36-h cultures of the different strains were *gatB* and *prfA*. Genes *hypo499* and *uvrA* were the two most stable genes of 48-h cultures of the different strains. The candidate reference genes with maximum stability of 60-h cultures of the different strains were *gatB* and *proS*.

NormFinder analysis

NormFinder was a similar software to geNorm in the calculation method. The lower stability value calculated from NormFinder indicated the higher stability of the reference gene expression. The difference in NormFinder with geNorm was that NormFinder selected only one most suitable candidate internal reference gene. *GatB* was shown to be the most stable reference gene to evaluate the gene expression level in strains 168 and J at different growth phases (Figure 4A). *PrfA* ranked as the most stable reference gene at different growth stages of strains 168 L and NJ. *RpoC* ranked as the most stable reference gene for strain LH under different culture times.

In the samples of different strains with a fixed culture time of 12 h, *prfA* displayed the highest stability (Figure 4B). The gene with the highest stability in 24-h cultures of the five different strains was *gatB*. *Hypo499* displayed the highest stability in both 36-h and 48-h cultures among all five different strains. *ProS* was the most potential candidate for the evaluation of the gene expression changes in 60-h cultures of different strains.

For strain LH at different growth phases, the top two genes analyzed by geNorm analysis included the most stable gene *rpoC* obtained from the NormFinder algorithm. In the samples of different strains with fixed culture times of 12 h, 48 h, and 60 h, the respective most stable genes, *prfA*, *hypo499*, and *proS*, from NormFinder analysis ranked top two in geNorm.

BestKeeper analysis

BestKeeper was also used to determine the expression stability of the candidate reference genes by calculating the SD and CV of the Ct values obtained from samples of different stains in different growth phases. The lower the SD value, the higher the gene stability. Genes with SD value >1 were considered unsuitable as reference genes (22). As shown in Figure 5A, the *sgaB* gene was most stable in strain 168 in different growth stages. *Hypo499* was most stable in strain LH harvested at different times. *GyrB* was the most stable reference gene in strains 168 L, J, and NJ harvested at different times.

The *gatB* gene was the most stable reference gene in all strain samples cultured for 12 or 36 h (Figure 5B). For 24, 48, and 60 h cultures, *gyrB*, *hypo499*, and *sgaB* were the most stable genes, respectively. The most unstable internal reference gene among the 13 candidates at different culture times was *P146*, which was the same as the results obtained from both geNorm and NormFinder.

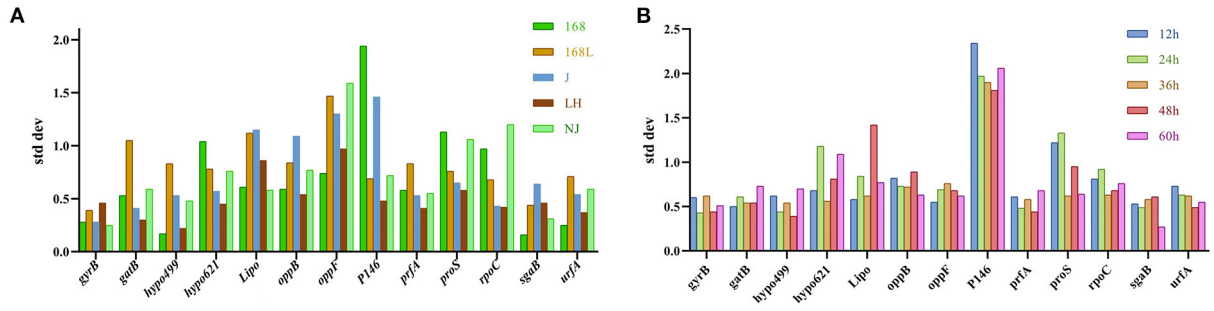

FIGURE 5
Analysis of internal reference gene standard deviation (SD) using the BestKeeper software. The x-axis represents various candidate reference genes. The y-axis represents stability value. **(A)**: SD value of reference gene of the same strain at different culture times. **(B)**: SD value of reference gene of different strains at the same culture time.

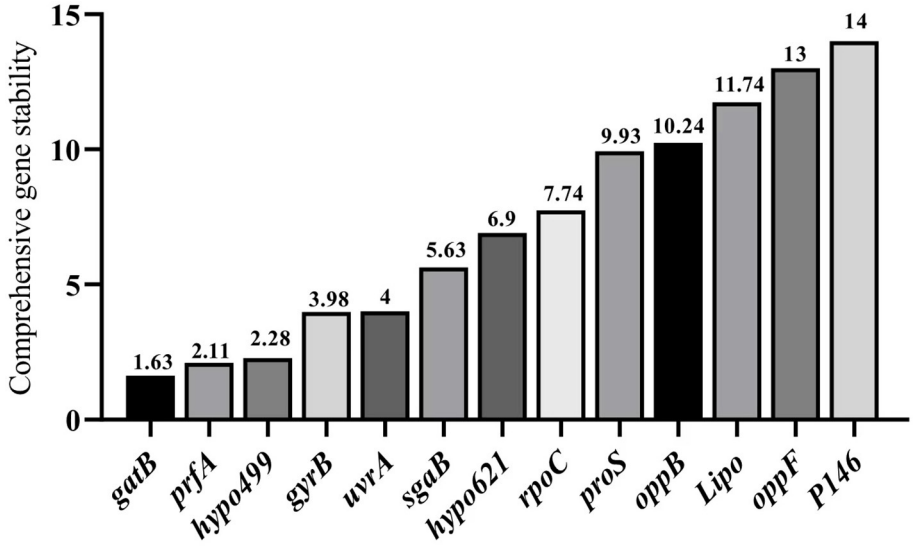

FIGURE 6
RefFinder analysis of expression stability of candidate internal reference genes. The x-axis represents various candidate reference genes. The y-axis represents stability value.

For strains J and NJ at different growth phases, the most stable gene *gyrB* analyzed by BestKeeper analysis was included in the top two genes obtained from the geNorm algorithm. In the samples of different strains with fixed culture times of 36 h and 48 h, the most stable gene *hypo499* from BestKeeper analysis ranked top one in NormFinder.

Integrated analysis by RefFinder

RefFinder integrates all the results of the three aforementioned methods to calculate the geometric mean for each reference gene and their comprehensive ranking index of stability. A lower index value indicates a higher stability of the reference gene. The RefFinder comprehensive analysis displayed in Figure 6 showed that the expression stability of 13 internal reference genes from high to low under different culture time conditions of different strains of *M. hyopneumoniae* was: *gatB*, *prfA*, *hypo499*, *gyrB*, *urfA*, *sgaB*, *hypo621*, *rpoC*, *16S*, *proS*, *oppB*, *Lipo*, *oppF*, and *P146*. In all samples, the top four most stable reference genes were *gatB*, *prfA*, *hypo499*, and *gyrB*, and the most unsuitable reference gene was *P146*, which was consistent with the results from geNorm and NormFinder (Figure 6). For simplicity of use, the most stable gene, *gatB*, can be used for gene expression analysis among different *M. hyopneumoniae* strains at different growth phases.

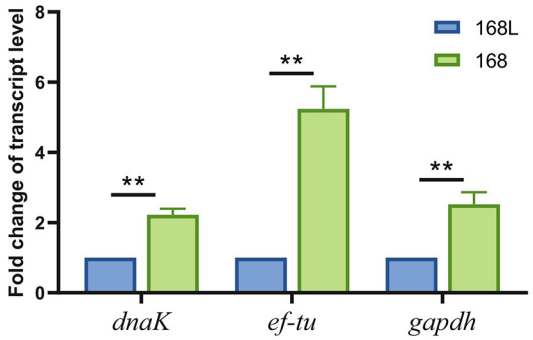

FIGURE 7
Transcription levels of *dnak*, *ef-tu*, and *gapdh* genes between high virulence *M. hyopneumoniae* strain 168 and low virulence strain 168 L.

Validation and application

To confirm the validity of using *gatB* as an internal reference gene for RT-qPCR analysis to screen the virulence-associated genes of *M. hyopneumoniae*, we evaluated the expression level of a reported virulence factor *ef-tu* in this study. We found that the abundance of *ef-tu* gene expression products in high virulence strain 168 was significantly higher than that in attenuated strain 168 L, which indicated the relevance of *ef-tu* with *M. hyopneumoniae* virulence (Figure 7). The results were consistent with the reported research, in which *ef-tu* encoding products were found to contribute to the adhesion process of *M. hyopneumoniae* (23). The consistency of the results using *gatB* as the internal reference gene in RT-qPCR and the reported data demonstrated the reliability of the established RT-qPCR method.

The established RT-qPCR method using *gatB* as the internal reference gene was then used to identify novel virulence-related genes. *Gapdh* and *dnaK* were found significantly different in transcript levels in high virulence strain 168 and low virulence strain 168 L. GAPDH of *Mycoplasma hyorhinis* was found to be an adhesin to epithelial cells as well as a plasminogen receptor mediating extracellular matrix (ECM) degradation (24). DnaK of *M. hyorhinis* functioned as a multi-binding protein on the surface of *M. hyorhinis* cells (25). GAPDH and DnaK of *M. hyopneumoniae* were also found to contribute to ECM degradation, which may help the pathogen break through the tissue barrier for further invasion (data unpublished). These findings demonstrated that the established RT-qPCR method can be used to discover novel phenotype (virulence/growth phases)-related genes.

Discussion

Discovering physiological and pathological functions of key genes is of great significance for studies of pathogenic mechanism of *M. hyopneumoniae*. The relative quantification of gene expression is mainly realized through RT-qPCR. Suitable reference genes are necessary for the quantification of key gene expression patterns. To date, although no study on identifying reference genes of *M. hyopneumoniae* had been conducted, many studies on identifying suitable reference genes of other bacteria had been reported (26). As found in these studies, genes with the most stable expression patterns were always different in different species, at different developmental stages, or with different virulence strains, indicating the complexity of suitable reference genes (6, 27, 28). Therefore, it was necessary to conduct careful verification to identify the most stable reference genes in different *M. hyopneumoniae* strains with various virulence strains at different growth phases.

In this study, to identify the most stable reference gene, we used four statistical approaches to estimate the expression stability of 14 candidate reference genes in 5 different *M. hyopneumoniae* strains with various virulence strains and at 5 different growth phases. Various combinations of internal reference genes for RT-qPCR analysis of *M. hyopneumoniae* in different conditions were proposed. Although the optimal internal reference genes calculated by geNorm, NormFinder, BestKeeper, and ReFinder for *M. hyopneumoniae* RT-qPCR analysis between different virulence strains and under diverse growth phases were not completely identical; the rank of the most stable reference genes did not show great differences. Of the 14 candidate reference genes, *gatB*, *prfA*, *hypo499*, and *gyrB* were consistently among the top few optimal internal reference genes in all three methods, geNorm, NormFinder, and BestKeeper, respectively. Other studies also reported different ranking orders using different statistical approaches when identifying suitable reference genes under different developmental stages and temperature stresses (29). To comprehensively utilize the data analyzed by the three methods to obtain one best reference gene for the sake of simplicity, integrated analysis by ReFinder was further performed. The online software selected *gatB* as the comprehensive optimum reference gene for the analysis of gene expression differences of both different virulence strains and strains at different growth phases.

The internal reference genes screened in this study were then subjected to reevaluation with the reported virulence-associated genes in *M. hyopneumoniae*. The known virulence factor *ef-tu* (30) and novel virulence-associated genes *gapdh* (24) and *dnaK* (25) were also highly transcribed in virulence strains when RT-qPCR analysis was performed using *gatB* as an internal reference gene. This further validated the credibility of our screened internal reference genes.

In addition to virulence and growth cycles, the *gatB* internal reference genes may be used to assess gene expression levels in dynamic conditions, such as cultures in different media. However, more validation needs to be done. Meanwhile, there are also some limitations in the application of this method. It

can certainly be used to evaluate changes in gene transcription levels. However, it cannot connect a specific gene to certain phenotypes, because in most cases proteins are the final functional form of the gene, and there are many ways of regulation from RNA to proteins.

Data availability statement

The original contributions presented in the study are included in the article/supplementary material, further inquiries can be directed to the corresponding authors.

Author contributions

SL performed most of the experiments. SL and YY prepared the manuscript. YZ and JW helped with the statistical analyses. TY and YW are responsible for the preparation of the experimental materials. ZZ, QX, and QL participated in the evaluation process. ZF, XY, and ZD supervised the work. All authors contributed to the article and approved the submitted version.

Acknowledgments

This study was supported by the Programs of Jiangsu Agricultural Science and Technology Innovation Fund [CX (20) 3090], the Programs of National Natural Science Foundation of China (32172860, 32102675, and 31900159), and the Natural Science Foundation of Jiangsu Province (BK20190269).

Conflict of interest

The authors declare that the research was conducted in the absence of any commercial or financial relationships that could be construed as a potential conflict of interest.

Publisher's note

All claims expressed in this article are solely those of the authors and do not necessarily represent those of their affiliated organizations, or those of the publisher, the editors and the reviewers. Any product that may be evaluated in this article, or claim that may be made by its manufacturer, is not guaranteed or endorsed by the publisher.

Supplementary material

The Supplementary Material for this article can be found online at: https://www.frontiersin.org/articles/10.3389/fvets.2022.934907/full#supplementary-material

References

1. Bandrick M, Pieters M, Pijoan C, Molitor TW. Passive transfer of maternal mycoplasma hyopneumoniae—specific cellular immunity to piglets. *Clin Vaccine Immunol.* (2008) 15:540–3. doi: 10.1128/CVI.00466-07

2. Minion FC, Adams C, Hsu T. R1 region of P97 mediates adherence of mycoplasma hyopneumoniae to swine cilia. *Infect Immun.* (2000) 68:3056–60. doi: 10.1128/IAI.68.5.3056-3060.2000

3. Seymour LM, Jenkins C, Deutscher AT, Raymond BBA, Padula MP, Tacchi JL, et al. Mhp182 (P102) binds fibronectin and contributes to the recruitment of plasmin(ogen) to the mycoplasma hyopneumoniae cell surface. *Cell Microbiol.* (2012) 14:81–94. doi: 10.1111/j.1462-5822.2011.01702.x

4. Huggett J, Dheda K, Bustin S, Zumla A. Real-time RT-PCR normalisation; strategies and considerations. *Genes Immun.* (2005) 6:279–84. doi: 10.1038/sj.gene.6364190

5. Giri A, Sundar IK. Evaluation of stable reference genes for qPCR normalization in circadian studies related to lung inflammation and injury in mouse model. *Sci Rep.* (2022) 12:1764. doi: 10.1038/s41598-022-05836-1

6. Gomes AEI, Stuchi LP, Siqueira NMG, Henrique JB, Vicentini R, Ribeiro ML, et al. Selection and validation of reference genes for gene expression studies in Klebsiella pneumoniae using reverse transcription quantitative real-time PCR. *Sci Rep.* (2018) 8:9001. doi: 10.1038/s41598-018-27420-2

7. Goswami M, Rao AVSSN. Transcriptome profiling reveals interplay of multifaceted stress response in escherichia coli on exposure to glutathione and ciprofloxacin. *mSystems*. (2018) 3:e00001-18. doi: 10.1128/mSystems.00001-18

8. Xiong ZQ, Fan YZ, Song X, Xia YJ, Zhang H, Ai LZ. Short communication: genome-wide identification of new reference genes for reverse-transcription quantitative PCR in *Streptococcus thermophilus* based on RNA-sequencing analysis. *J Dairy Sci.* (2020) 103:10001–5. doi: 10.3168/jds.2020-18672

9. Li S, Fang LR, Liu W, Song T, Zhao FW, Zhang RX, et al. Quantitative proteomic analyses of a pathogenic strain and its highly passaged attenuated strain of mycoplasma hyopneumoniae. *Biomed Res Int.* (2019) 2019:4165735. doi: 10.1155/2019/4165735

10. Wang H, Jiao PX, Zhang XX, Xing HJ. Quantitative proteomic analysis of trachea in fatting pig exposed to ammonia. *J Proteomics.* (2021) 247:104330. doi: 10.1016/j.jprot.2021.104330

11. Zhao M, Jia SJ, Gao XF, Qiu H, Wu RF, Wu HJ, et al. Comparative analysis of global proteome and lysine acetylome between naive CD4(+) T cells and CD4(+) T follicular helper cells. *Front Immunol.* (2021) 12:643441. doi: 10.3389/fimmu.2021.643441

12. Thiruvengadam SS, O'Malley M, LaGuardia L, Lopez R, Wang Z, Shadrach BL, et al. Gene expression changes accompanying the duodenal adenoma-carcinoma sequence in familial adenomatous polyposis. *Clin Transl Gastroen.* (2019) 10:e00053. doi: 10.14309/ctg.0000000000000053

13. Zhao WJ, Li Y, Gao PF, Sun ZH, Sun TS, Zhang HP. Validation of reference genes for real-time quantitative PCR studies in gene expression levels of Lactobacillus casei Zhang. *J Ind Microbiol Biot.* (2011) 38:1279–86. doi: 10.1007/s10295-010-0906-3

14. Albuquerque GMR, Fonseca FCA, Boiteux LS, Borges RCF, Miller RNG, Lopes CA, et al. Stability analysis of reference genes for RT-qPCR assays involving compatible and incompatible Ralstonia solanacearum-tomato 'Hawaii 7996' interactions. *Sci Rep.* (2021) 11:18719. doi: 10.1038/s41598-021-97854-8

15. Vandesompele J, De Preter K, Pattyn F, Poppe B, Van Roy N, De Paepe A, et al. Accurate normalization of real-time quantitative RT-PCR data by geometric averaging of multiple internal control genes. *Genome Biol.* (2002) 3:research0034.1. doi: 10.1186/gb-2002-3-7-research0034

16. Yang ZY, Zhang R, Zhou ZC. Identification and validation of reference genes for gene expression analysis in schima superba. *Genes.* (2021) 12:732. doi: 10.21203/rs.3.rs-361995/v1

17. Andersen CL, Jensen JL, Orntoft TF. Normalization of real-time quantitative reverse transcription-PCR data: a model-based variance estimation approach to identify genes suited for normalization, applied to bladder and colon cancer data sets. *Cancer Res.* (2004) 64:5245–50. doi: 10.1158/0008-5472.CAN-04-0496

18. Pfaffl MW, Tichopad A, Prgomet C. Neuvians TP. Determination of stable housekeeping genes, differentially regulated target genes and sample integrity: bestkeeper - excel-based tool using pair-wise correlations. *Biotechnol Lett.* (2004) 26:509–15. doi: 10.1023/B:BILE.0000019559.84305.47

19. Wang Y, Zhang Y, Liu Q, Tong H, Zhang T, Gu C, et al. Selection and validation of appropriate reference genes for RT-qPCR analysis of flowering stages and different genotypes of Iris germanica L. *Sci Rep.* (2021) 11:9901. doi: 10.1038/s41598-021-89100-y

20. Gao JQ, Liu J, Jiang C, Chen SL. Huang LQ. Identification of suitable reference genes for studies of Syringa pinnatifolia Hemsl, FEBS. *Open Bio.* (2021) 11:1041–53. doi: 10.1002/2211-5463.13097

21. de Lima CAD, de Lima SC, Barbosa AD, Sandrin-Garcia P, Pita WD, Silva JD, et al. Postmenopausal osteoporosis reference genes for qPCR expression assays. *Sci Rep.* (2019) 9:16533. doi: 10.1038/s41598-019-52612-9

22. Zhao N, Xu J, Jiao L, Qiu M, Zhang J, Wei X, et al. Transcriptome-based selection and validation of reference genes for gene expression analysis of alicyclobacillus acidoterrestris under acid stress. *Front Microbiol.* (2021) 12:731205. doi: 10.3389/fmicb.2021.731205

23. Yu YF, Wang HG, Wang J, Feng ZX, Wu M, Liu BB, et al. Elongation Factor Thermo Unstable (EF-Tu) moonlights as an adhesin on the surface of mycoplasma hyopneumoniae by binding to fibronectin. *Front Microbiol.* (2018) 9:974. doi: 10.3389/fmicb.2018.00974

24. Wang J, Li Y, Pan LJ, Li J, Yu YF, Liu BB, et al. Glyceraldehyde-3-phosphate dehydrogenase (GAPDH) moonlights as an adhesin in Mycoplasma hyorhinis adhesion to epithelial cells as well as a plasminogen receptor mediating extracellular matrix degradation. *Vet Res.* (2021) 52:80. doi: 10.1186/s13567-021-00952-8

25. Li Y, Wang J, Liu BB, Yu YF, Yuan T, Wei YN, et al. DnaK functions as a moonlighting protein on the surface of mycoplasma hyorhinis cells. *Front Microbiol.* (2022) 13:58. doi: 10.3389/fmicb.2022.842058

26. Rego ECS, Pinheiro TDM, Antonino JD, Alves GSC, Cotta MG, Fonseca FCD, et al. Stable reference genes for RT-qPCR analysis of gene expression in the musa acuminata-pseudocercospora musae interaction. *Sci Rep.* (2019) 9:14592. doi: 10.1038/s41598-019-51040-z

27. Takle GW, Toth IK, Brurberg MB. Evaluation of reference genes for real-time RT-PCR expression studies in the plant pathogen pectobacterium atrosepticum. *BMC Plant Biol.* (2007) 7:50. doi: 10.1186/1471-2229-7-50

28. Golpayegani A, Nodehi RN, Rezaei F, Alimohammadi M, Douraghi M. Real-time polymerase chain reaction assays for rapid detection and virulence evaluation of the environmental pseudomonas aeruginosa isolates. *Mol Biol Rep.* (2019) 46:4049–61. doi: 10.1007/s11033-019-04855-y

29. Wang G, Cheng H, Li M, Zhang C, Deng W, Li T. Selection and validation of reliable reference genes for Tolypocladium guangdongense gene expression analysis under differentially developmental stages and temperature stresses. *Gene.* (2020) 734:144380. doi: 10.1016/j.gene.2020.144380

30. Yu YF, Wang J, Han R, Wang L, Zhang L, Zhang AY, et al. Mycoplasma hyopneumoniaeevades complement activation by binding to factor H *via* elongation factor thermo unstable (EF-Tu). *Virulence.* (2020) 11:1059–74. doi: 10.1080/21505594.2020.1806664

frontiers | Frontiers in Veterinary Science

TYPE Original Research
PUBLISHED 28 July 2022
DOI 10.3389/fvets.2022.920080

OPEN ACCESS

EDITED BY
Fazul Nabi,
Lasbela University of Agriculture, Water and Marine Sciences, Pakistan

REVIEWED BY
Huan Li,
Lanzhou University, China
Mary Rooney,
Trinity College Dublin, Ireland

*CORRESPONDENCE
Li Xi
xili_0808@126.com
Caijuan Yang
94485170@qq.com

SPECIALTY SECTION
This article was submitted to Comparative and Clinical Medicine, a section of the journal Frontiers in Veterinary Science

RECEIVED 14 April 2022
ACCEPTED 04 July 2022
PUBLISHED 28 July 2022

CITATION
Wen X, Luo S, Lv D, Jia C, Zhou X, Zhai Q, Xi L and Yang C (2022) Variations in the fecal microbiota and their functions of Thoroughbred, Mongolian, and Hybrid horses. *Front. Vet. Sci.* 9:920080. doi: 10.3389/fvets.2022.920080

Variations in the fecal microbiota and their functions of Thoroughbred, Mongolian, and Hybrid horses

Xiaohui Wen[1], Shengjun Luo[1], Dianhong Lv[1], Chunling Jia[1], Xiurong Zhou[1], Qi Zhai[1], Li Xi[2]* and Caijuan Yang[3]*

[1]Institute of Animal Health, Scientific Observation and Experiment Station of Veterinary Drugs and Diagnostic Techniques of Guangdong Province, Ministry of Agriculture of Rural Affairs, Key Laboratory of Animal Disease Prevention of Guangdong Province, Guangdong Academy of Agricultural Sciences, Guangzhou, China, [2]Department of Animal Science, College of Biology and Food, Shangqiu Normal University, Shangqiu, China, [3]National S&T Innovation Center for Modern Agricultural Industry, Guangzhou, China

The horse gut is colonized by a rich and complex microbial community that has important roles in horse physiology, metabolism, nutrition, and immune functions. Fewer across-breed variations in horse gut microbial diversity have been illustrated. In this article, the gut microbiota of Thoroughbred, Mongolian, and Hybrid horses [first filial generation (F1) of Mongolian (maternal) and Thoroughbred (paternal)] were studied by second-generation high-throughput sequencing technology. Differences in gut microbiota composition and function between breeds were determined using diversity and functional prediction analysis. The alpha diversity analysis showed that Thoroughbred horses had a more abundant and diverse gut microbiota, while the diversity of gut microbiota in Hybrid horses was intermediate between Thoroughbred and Mongolian horses. Subsequent cluster analysis showed that Hybrid horses have a microbiota composition more similar to Mongolian horses. LEfSe analysis revealed that the bacterial biomarkers for Thoroughbred horses at the family level were Prevotellaceae, Rikenellaceae, Fibrobacteraceae, p_251_o5, Lactobacillaceae, and uncultured_bacterium_o_WCHB1_41; the bacterial biomarker for Mongolian horses was Planococcaceae; and the bacterial biomarkers for Hybrid horses were Moraxellaceae, Enterobacteriaceae, and Ruminococcaceae. The functional prediction results indicated that the metabolic pathways differ significantly between the breeds. Regarding metabolism, the Hybrid horses had the lowest proportion of the carbohydrate metabolic pathways, while the energy metabolic pathway had the highest proportion. The abundance ratios of the remaining eight metabolic pathways in Hybrid horses were between Thoroughbred and Mongolian horses. In conclusion, the results of this study showed an association between horse breeds and gut microbiota.

KEYWORDS

16S rRNA, breed, microbiota, diversity, fibrolytic bacteria

Introduction

The horse gut is well developed and colonizes a rich and complex microbiome composed of bacteria, fungi, protozoa, and archaea. The microbial communities interact with the host to maintain gut health. On the one hand, the host gut provides the necessary environmental conditions for microbial growth, such as nutrients, temperature, humidity, and pH (1). On the other hand, the gut microbiota convert complex carbohydrates into short-chain fatty acids (SCFAs) through fermentation, providing the host with essential nutrients and energy (2). Meanwhile, some beneficial microbes in the gut can also specifically bind to the mucosal epithelium to enhance the gut immune protection barrier, thus preventing the invasion of pathogenic microorganisms (3). In addition to nutritional and immune barrier roles, the composition of the gut microbiota and their stability also play an important role in the host behavior (4), metabolism (5), obesity (6), disease (7), and more.

Notably, many studies have found that host age (8), breed, gender, feeding pattern (9), forage type (10, 11), stress (12), and disease (13) in turn affect the composition and function of the gut microbiota. There were some interesting findings on the relationship between horse breeds and gut microbiota. The 16S rRNA analysis of fecal microbiota from Mongolian and Thoroughbred horses living in Inner Mongolia (China) revealed that the relative abundance of 31.25% (5/16) phyla and 40% (30/75) genera was significantly different between the two breeds (14). Another study showed that Thoroughbred horses had higher gut microbiota diversity than Jeju horses in Korea (15). Moreover, the abundance of beneficial commensal bacteria (Lachnospiraceae, *Oscillibacter*, Clostridium_XIVa, etc.) that produce SCFAs to supply the host with more energy sources was also higher in Thoroughbred horses than in Jeju horses (15). When comparing the differences in gut microbiota among six horse breeds in a study by Massacci et al., 27 genera were found significantly different among breeds (16). Approximately 33% of these 27 bacterial genera were reported to be heritable in humans or other animals (17, 18).

In addition to directly studying the effects of host breeds on gut microbiota abundance, some researchers have tried to find causal genes directly associated with gut-specific or core microbiota. Yang et al. (19) verified that the ABO gene is a causal gene affecting the gut abundance difference of Erysipelotrichaceae species and elucidated the mechanism that has important reference significance for cultivating new varieties of grain-saving and fast-growing pigs. Another study reported a strong impact of paternal inheritance on calf hindgut microbiota and growth performance in early life. Further investigation of the correlation between the SNP genotypes and the gut microbiota revealed that the SNP genotypes in the mucin-coding genes were significantly associated with the abundance of the mucin-degrading bacteria in the gut (20). Both studies speculated that host genotypes first affect the colonization of specific bacteria and then shape the gut microbial structure and composition through the interactions between bacteria.

As an important breed in northern China, Mongolian horses have rich genomic diversity (21) and have a variety of excellent traits, such as adaptability, cold resistance, roughage resistance, disease resistance, and good stamina (22, 23). Thoroughbred horses, a horse species bred in 17th-century Britain, were manually selected to meet the desired conditions of speed, temperament, and body size (24). In comparison with Mongolian horses who have substantial stamina (the speed race distance is generally 30–50 km), the suitable race distance of Thoroughbred horses is 1–4 km (25). In addition, due to severe inbreeding, the fecundity of Thoroughbred horses is relatively poor and not resistant to roughage (26, 27). The first filial generation of Mongolian horses (maternal) and Thoroughbred horses (paternal) emerged in the Horqin grassland (Inner Mongolia, China). The hybrid Mongolian-Thoroughbred horses not only inherit the stamina and toughness of Mongolian horses but also combine the size, speed, and good obedience of Thoroughbred horses (28). This study aimed to evaluate the similarities and differences in the composition of gut microbiota and their functions among breeds and to screen the breed-specific bacterial flora. Fecal samples from Thoroughbred, Mongolian, and their derived F1 hybrids under moderately controlled conditions were collected. Subsequently, high-throughput sequencing of the 16S rRNA V3-V4 region of the bacterial DNA was conducted. The differences in the diversity of gut microbiota and their functions across breeds were determined using QIIME 2 and PICRUSt2 software. The results of this study will provide data for the precision feeding of horses.

Materials and methods

Sample collection

Thoroughbred horses (4 years old, male, $n = 5$), Mongolian horses (4–6 years old, male, $n = 5$), and Hybrid horses [6 years old, male, F1 hybrid of Mongolian (maternal) and Thoroughbred (paternal) $n = 5$] were provided by Linyi Zoological and Botanical Garden (Linyi, China) for the experiment. The horses were kept under moderately controlled conditions for 4 months before collecting fecal samples and fed hay (oat and alfalfa) and concentrate feeds (Taifeng Animal Husbandry, Shijiazhuang, China), doing moderate exercise every day. The freshly excreted feces were collected in sterilized plastic sealing bags, stored in an icebox, and returned to the

laboratory. A portion of each sample (5 g) was placed in a sterilized tube and frozen at −80°C.

16S rRNA amplicon sequencing

Fecal microbial genomic DNA was extracted using FastDNA SPIN Soil Kit (MP Biomedicals, Santa Ana, CA). The DNA concentration and purity were determined by UV-vis spectrophotometer UV-1900i (Shimadzu Corporation, Tokyo, Japan), and its integrity was determined by 0.8% agarose gel electrophoresis. The DNA templates extracted above were amplified using universal primers in the V3-V4 region of the bacterial 16S rRNA gene (338F: 5′-ACTCCTAC GGGAGGCAGCA-3′ and 806R: 5′-GGACTACHVGGGTWTCTAAT-3′). The 20 μl reaction system was as follows: DNA 10 ng, 2.5 mmol/L dNTPs 2 μl, 5× FastPfu buffer 4 μl, BSA 0.2 μl, FastPfu polymerase 0.4 μl, 5 mol/L primers 0.8 μl, adding ddH_2O supplemented the reaction system. The PCR conditions were 95°C predenaturation for 3 min, 98°C denaturation for 20 s, 58°C annealing for 15 s, and 72°C was extended for 20 s, totaling 30 cycles. Finally, 72°C was maintained for 5 min. The PCR amplification products were detected using a 2% agarose gel electrophoresis and then recovered using a DNA gel extraction kit (Tiangen Biotech, Beijing, China). Sequencing libraries were constructed with the amplified fragments, and then, qualified sequencing libraries were sequenced using the Novaseq 6000 platform (Illumina, CA, USA).

16S rRNA gene-based microbiome analyses

The raw data obtained from sequencing were first filtered by Trimmomatic v0.33 software, and then, the primer sequences were removed using cutadapt 1.9.1 software. Subsequently, clean reads of each sample were stitched by overlap using Usearch v10 software, and then, post-splicing length data were filtered based on the length range of different regions. Finally, using the UCHIME v4.2 software, the chimera sequences were removed to obtain effective reads. The operational taxonomic unit (OTU) clustering was performed according to the 97% sequence similarity, using the Usearch v10 software. The number of shared and unique OTU between samples was calculated using the Venn diagram. Characteristic sequences were taxonomic annotated using a naive Bayesian classifier (confidence: 0.7) with SILVA (release 132) as a reference database. Species abundance figures were generated at different taxonomic levels using QIIME 2 software. The rarefaction curves and rank abundance curves were used to evaluate whether the sample sequencing volume met the requirements and the richness and evenness of the sample, respectively.

Statistical analysis

Alpha diversity was assessed using QIIME 2 software to calculate the Chao 1 index and Shannon index. The Chao 1 index estimates species richness, and the larger the value represents the more species were included in the sample. The Shannon index is used to measure species diversity, influenced by species richness and evenness in the sample microbial community. Differences in alpha diversity indices between groups were analyzed by one-way ANOVA with Tukey's *post-hoc* test, and $P < 0.05$ was considered significant. Beta diversity analysis was processed by QIIME 2 software to compare species diversity between different samples. The unweighted and weighted UniFrac algorithms were used to calculate the distance between samples. UniFrac measures the difference between samples considering phylogenetic linkage. The unweighted algorithm focuses on the existence of a species, while the weighted algorithm takes both existence and abundance into consideration. Linear discriminant analysis (LDA) effect size (LEfSe) was used to search for biomarkers with statistical differences between the groups. First, the OTUs with significant differences in abundance were detected using the nonparametric factorial Kruskal-Wallis sum rank test. Then, LDA was used to estimate the effect of each species on the differential effects. Differences in the microbial community at the genus level were compared using the one-way ANOVA with Tukey's *post-hoc* test, and $P < 0.05$ was considered significant. The correlation network was constructed by performing Spearman's rank correlation analysis and screening for data with a correlation $>$ 0.1 and a $P < 0.05$. PICRUSt2 software was applied to predict potential functional genes based on the Integrated Microbial Genomes database. The difference in functional genes and their effects on KEGG metabolic pathways between groups were analyzed by STAMP software.

Results

Sequencing quality assessment

A total of 1,199,516 pairs of reads were sequenced from 15 samples, and 736,739 effective reads were generated after low quality and length filtering (quality control data are detailed in Supplementary Table 1). In total, 1,107 OTUs were obtained by clustering effective reads at 97.0% similarity levels using the Usearch v10 software and were annotated to 20 phyla and 173 genera. The Venn diagram showed that three groups shared 875 OTUs (Figure 1A). The Thoroughbred horses contained 14 OTUs that were mainly annotated to the phyla Bacteroidetes and Firmicutes. The Mongolian horses contained 32 unique OTUs that were annotated to the phyla Bacteroidetes, Firmicutes, and Spirochaetes. There were six OTUs that belonged exclusively to Hybrid horses, and the mainly annotated phyla were

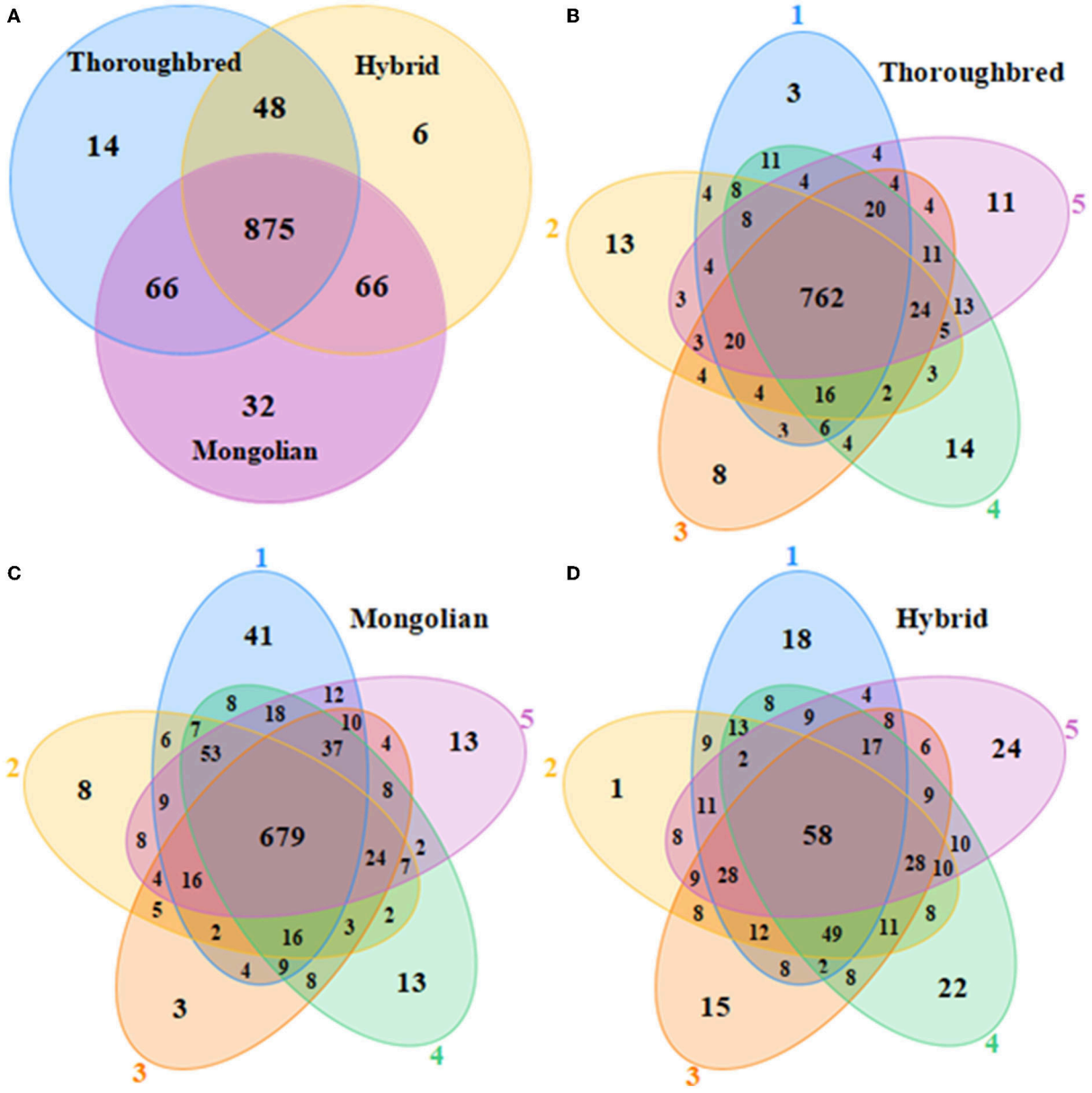

FIGURE 1
Venn diagrams. **(A)** Venn diagram of OTU distributions between Thoroughbred, Mongolian, and Hybrid horses. **(B–D)** Flower diagrams of OTU distribution between samples in Thoroughbred, Mongolian, and Hybrid horses, respectively.

Bacteroidetes and Firmicutes. The number of OTUs shared by each group of samples was 762 (75.97%), 586 (58.89%), and 995 (65.35%), respectively (Figures 1B–D). The rarefaction curve of the samples began to flatten when sampled at around 30 000, indicating sufficient sequencing depth to present most species in the samples (Supplementary Figure 1). The trends of the rank abundance curves were flat, indicating a good evenness of the species composition in the samples (Supplementary Figure 2).

Effect of breed on gut microbial diversity

The Good's coverage was 0.997 8 for Thoroughbred horses, 0.997 5 for Mongolian horses, and 0.996 9 for Hybrid horses, respectively, indicating that the sequencing data were sufficient to cover most species in the samples. The Chao 1 index of Hybrid horses was significantly lower than those in Thoroughbred and Mongolian horses (Figure 2A). The Shannon index of Thoroughbred horses was

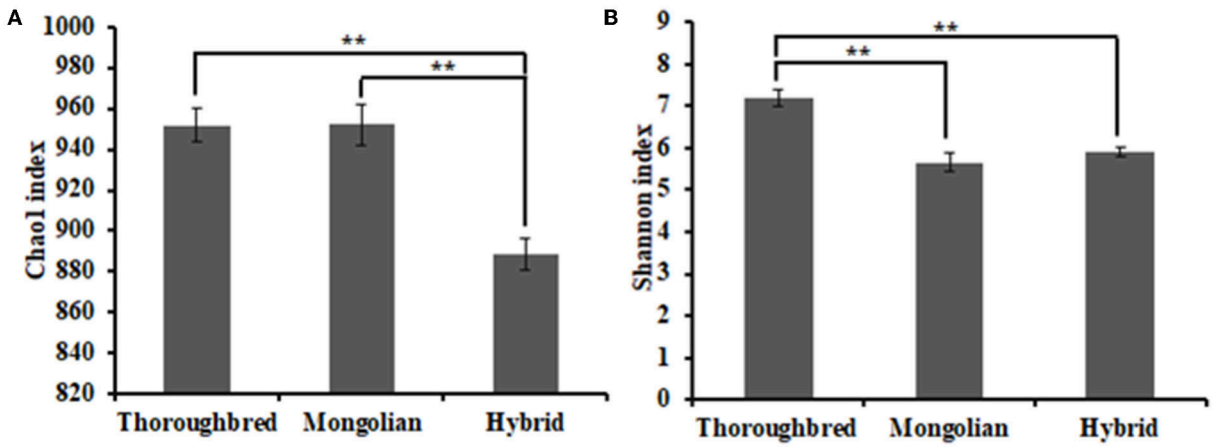

FIGURE 2
Differential analysis of the alpha diversity index. **(A)** Chao1 index. **(B)** Shannon index. Statistical method: one-way ANOVA with Tukey's *post-hoc* test. $^{**}P < 0.01$.

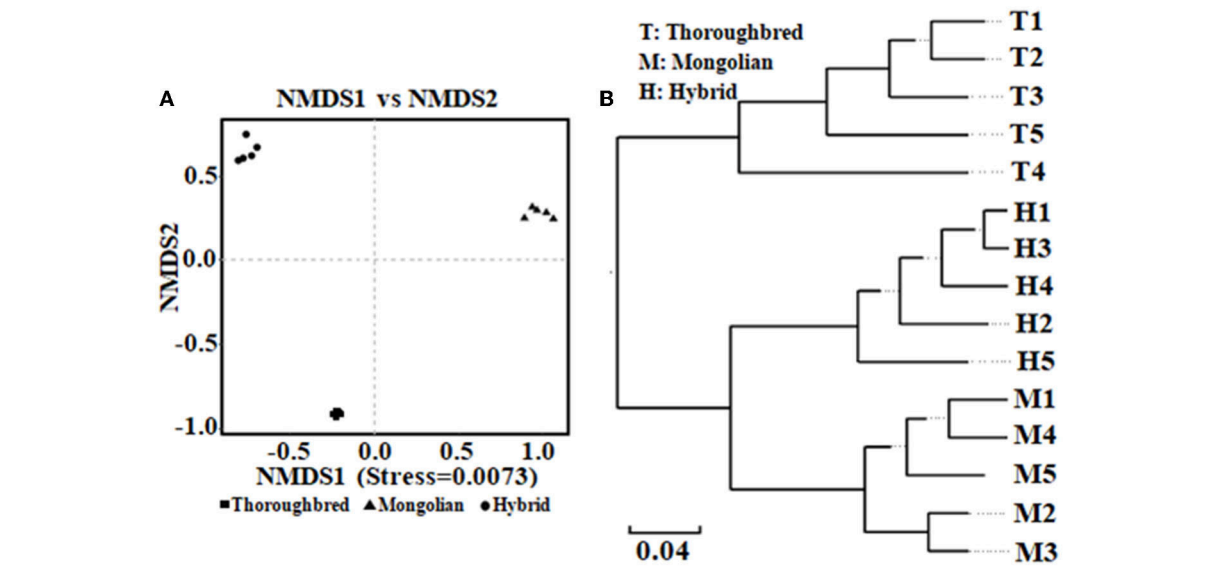

FIGURE 3
Analysis of beta diversity of microbial community between Thoroughbred, Mongolian, and Hybrid horses. **(A)** NMDS analysis (non-metric multidimensional scaling, using unweighted UniFrac algorithm). **(B)** UPGMA tree (unweighted pair group method with arithmetic mean, using weighted UniFrac algorithm). T, Thoroughbred horses; M, Mongolian horses; H, Hybrid horses.

7.21, which was significantly higher than that in Mongolian (5.66, $P < 0.01$) and Hybrid horses (5.91, $P < 0.01$) (Figure 2B). The statistical analysis showed that Thoroughbred horses had a more abundant and diverse gut microbiota, while the diversity of gut microbiota in Hybrid horses was intermediate between Thoroughbred and Mongolian horses. The beta diversity analysis was performed based on two distance matrices, namely, non-metric multidimensional scaling (NMDS) and unweighted pair group method with arithmetic mean (UPGMA). The result of NMDS indicated significant differences in gut microbiota among the three groups (Figure 3A). Sample hierarchical clustering trees (Figure 3B) showed that Mongolian and Hybrid horses shared higher similarities in microbial compositions.

Effect of breed on gut microbial composition

The species distribution histogram at the phylum level showed that Firmicutes is the most dominant phylum in the gut of Thoroughbred (53.44%), Mongolian (56.83%), and

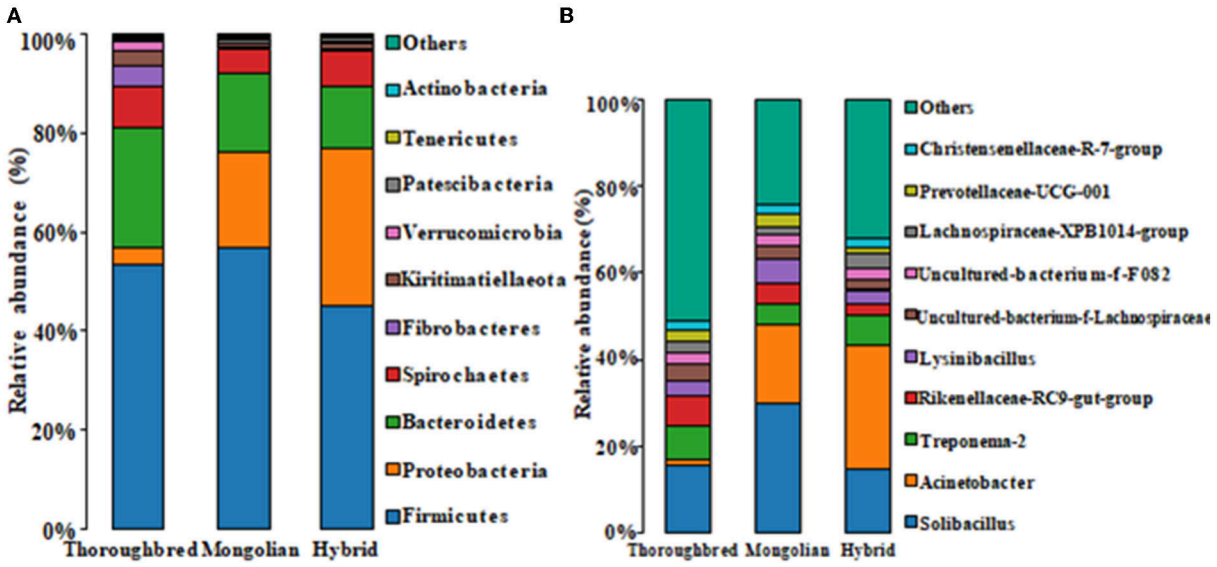

FIGURE 4
Species distribution histogram. **(A)** The top 10 phyla in abundance. **(B)** The top 10 genera in abundance.

Hybrid horses (45.02%) (Figure 4A). In addition, among the top 10 phyla in relative abundance, Bacteroidetes, Fibrobacteres, and Actinobacteria were significantly enriched in the gut of Thoroughbred horses. In contrast, the relative abundance of Proteobacteria in Thoroughbred horses was only 3.42%, which is significantly lower than in Mongolian (19.30%) and Hybrid horses (32.04%). Among the top 10 genera, the relative abundances of *Rikenellaceae_RC9_gut_group*, *uncultured_bacterium_f_Lachnospiraceae*, and *Acinetobacter* were significantly different between the three groups. The relative abundances of *Acinetobacter* and *Lachnospiraceae_XPB1014_group* in the gut of Hybrid horses were significantly higher compared with Thoroughbred and Mongolian horses, while the relative abundances of *Prevotellaceae_UCG-001* and *Rikenellaceae_RC9_gut_ group* were significantly lower (Figure 4B). The heatmap of species abundance cluster at the phylum level showed that the gut microbiota of Mongolian and Hybrid horses were first clustered together and then with Thoroughbred horses, indicating that Mongolian and Hybrid horses have a more similar microbial composition (Figure 5).

Differences in the abundance of the microbiota between the groups were studied using the one-way ANOVA with Tukey's *post-hoc* test. Among the top 10 phyla, Proteobacteria and Tenericutes varied significantly between the three groups ($P < 0.01$) (Table 1). Genus-level differential analysis revealed that a total of 112 bacterial genera varied significantly between at least two groups (Supplementary Table 2). Compared with the other two groups, the genera not detected in Thoroughbred horses included *Pusillimonas*, *Mailhella*, and five uncultured bacteria. Mongolian horses lacked *Bifidobacterium*, *Ruminococcus_2*, *Shuttleworthia*, and one uncultured bacterium. Meanwhile, Hybrid horses were missing with *dgA-11_gut_group* and one uncultured bacterium. LEfSe analysis showed that Bacteroidales, Clostridiales, Prevotellaceae, Rikenellaceae, *Fibrobacter*, *Rikenellaceae_RC9_gut_group*, p_251_o5, *Lactobacillus*, WCHB1_41, and Kiritimatiellae were significantly enriched in Thoroughbred horses. The relative abundances of Planococcaceae, Bacillales, *Solibacillus*, Firmicutes, and *Lysinibacillus* were significantly higher in Mongolian horses than in Thoroughbred and Hybrid horses. The relative abundances of Gammaproteobacteria, Pseudomonadales, Enterobacteriaceae, *Ruminococcaceae_UCG_005*, *Ruminococcaceae_UCG_002*, Moraxellaceae, and *Acinetobacter* were significantly higher in Hybrid horses than in the other two groups (Figure 6).

Correlation network analysis

Top 50 correlated genera are presented in Figure 7. There was a strong negative correlation between *Solibacillus* and *Candidatus_Saccharimonas* (0.9464). Acinetobacter showed a strong negative association with most genera, such as *Rikenellaceae_RC9_gut_group* (0.9429), *Saccharofermentans* (0.9393), *Lactobacillus* (0.9214), *[Anaerorhabdus]_furcosa_group* (0.9179), *Ruminiclostridium_1* (0.9107), and *Defluviitaleaceae_UCG-011* (0.8893). Rikenellaceae_RC9_gut_group was positively associated with some genera, including *[Anaerorhabdus]_furcosa_group*

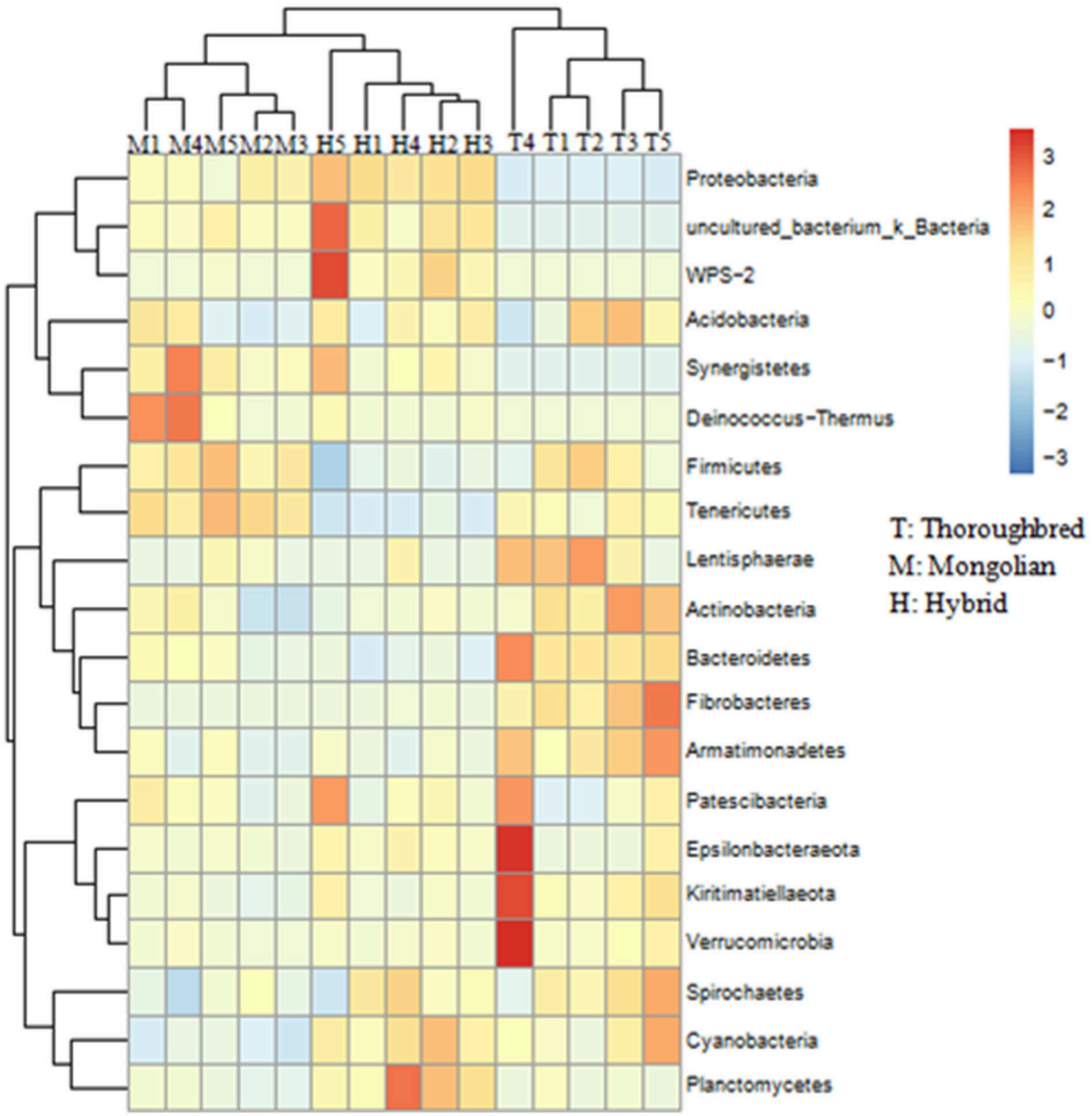

FIGURE 5
Heatmap of species abundance clustering at the phylum level. T, Thoroughbred horses; M, Mongolian horses; H, Hybrid horses.

(0.9214), *Oribacterium* (0.9036), *Ruminiclostridium_1* (0.8964), *Prevotellaceae_UCG-004* (0.8893), *Anaerofustis* (0.8821), *Defluviitaleaceae_UCG-011* (0.875), *Lactobacillus* (0.8536), and *Saccharofermentans* (0.8536), but negatively associated with *Streptococcus* (0.9036) and *Acinetobacter* (0.9429).

Prediction of 16S rRNA gene function

The PICRUSt2 prediction results showed that a total of 46 pathways (level 2) were obtained in the 15 fecal samples, mainly involving carbohydrate metabolism (8.55%), amino acid metabolism (7.54%), cofactors and vitamins (4.24%), energy metabolism (3.94%), membrane transport (3.57%), nucleotide metabolism (3.47%), and translation (3.22%). There were 13, 11, and 14 pathways with a relative abundance above 1% that significantly differ between Thoroughbred and Mongolian horses, Thoroughbred and Hybrid horses, and Mongolian and Hybrid horses, respectively. The level two pathways shown in Figure 8 belonged to metabolism, genetic information processing, cellular processes, and environmental information processing. The relative abundance of nucleotide

metabolism, translation, and replication and repair pathways was highest in Thoroughbred horses and lowest in Mongolian horses, while in Hybrid horses, it was intermediate. The relative abundance of amino acid metabolism, xenobiotics biodegradation and metabolism, other amino acids metabolism, terpenoids metabolism, and polyketides metabolism was highest in Mongolian horses and lowest in Thoroughbred horses, while in Hybrid horses, it was intermediate. However, the Hybrid horses had the lowest relative abundance of both carbohydrate and lipid metabolism pathways (Figure 8).

TABLE 1 Statistical analysis (*P*-value) of the top 10 phyla abundance between paired groups.

Phylum	Thoroughbred vs. Mongolian	Thoroughbred vs. Hybrid	Mongolian vs. Hybrid
Proteobacteria	< 0.001	< 0.001	< 0.001
Tenericutes	< 0.01	< 0.001	< 0.001
Bacteroidetes	< 0.01	< 0.001	≥ 0.1
Fibrobacteres	< 0.001	< 0.001	≥ 0.1
Actinobacteria	< 0.05	< 0.05	≥ 0.1
Firmicutes	≥ 0.1	< 0.05	< 0.01
Kiritimatiellaeota	< 0.05	< 0.1	≥ 0.1
Verrucomicrobia	≥ 0.1	≥ 0.1	≥ 0.1
Spirochaetes	≥ 0.1	≥ 0.1	≥ 0.1
Patescibacteria	≥ 0.1	≥ 0.1	≥ 0.1

Discussion

Changes in the stability and diversity of gut microbial communities can reflect the gastrointestinal health and growth performance of animals. In this assay, Firmicutes, Bacteroidetes, Spirochaetes, Proteobacteria, Verrucomicrobia, Fibrobacteres, and Kiritimatiellaeota were the predominant phyla, accounting for 95.39, 97.60, and 97.46% of the gut microbiota in Thoroughbred, Mongolian, and Hybrid horses, respectively. Although the predominant phyla identified in this study were the same as the dominant phyla detected by Zhao et al. in studying the gut microbiota difference between Thoroughbred and Mongolian horses, the proportion was different (98% for Thoroughbred horses and 99% for Mongolian horses), and the proportion of each phylum was also different. For instance, the proportion of Bacteroidetes in this study was 24% for Thoroughbred horses and 16% for Mongolian horses, while it was 32 and 33% in Zhao's study; the proportion of Proteobacteria is 3% for Thoroughbred horses and 19% for Mongolian horses in this study, while it was 4 and 1% in Zhao's study (14). There were many reasons for the difference between the two studies, including feeding manners (house feeding vs. grazing), age (4–6 vs. 2–12 years), and gender (male vs. male and female). Notably, the relative abundances of Proteobacteria differ significantly between the three groups in this study, while Kiritimatiellaeota differs significantly only between Thoroughbred and Mongolian horses. The competitive relationship between Firmicutes and Bacteroides has been reported to affect host nutrient uptake and can modulate host obesity genes (29, 30). The Firmicutes/Bacteroides ratio (F/B) of Mongolian and Hybrid horses was significantly higher than that of Thoroughbred horses (3.58, 3.65 vs. 2.20, $P < 0.01$), suggesting that Mongolian and Hybrid horses absorb heat from feed more efficiently than Thoroughbred horses and may be related to cold tolerance properties.

In this study, Prevotellaceae and Rikenellaceae (Bacteroidetes), Fibrobacteraceae (Fibrobacteres), Lactobacillaceae (Firmicutes), WCHB1_41 (Verrucomicrobia), and Kiritimatiellaeota were significantly enriched in the feces of Thoroughbred horses. Prevotellaceae has enzymes and gene clusters capable of fermenting and utilizing complex polysaccharides, and the abundance of the bacterial family in the gut is influenced by breed and gender (31). The RC9 gut group of Rikenellaceae increased the apparent digestibility of acid detergent fiber and neutral detergent fiber, thus improving the dry matter intake of animals (32). Fibrobacteraceae can reduce the inflammatory response and improve production performance by promoting fiber fermentation (33). Some studies have also found a correlation between beef cattle chromosome 27 and Prevotellaceae, Fibrobacteraceae, and RF16 (34). Lactobacillaceae belongs to lactic acid-producing bacteria, but when overgrown, it leads to the occurrence of animal intestinal disease by producing excessive lactate production and reducing the pH of horse hindgut (35). Guo et al. (36) found that Akkermansia and WCHB1_41 were significantly enriched in the gut of yaks during the cold season. Moreover, the functional analysis found that the arginine and fatty acid anabolic pathway encoded by Akkermansia, Kiritimatiellaeota, and WCHB1_41 can effectively improve the efficiency of energy and nitrogen utilization in yaks and facilitate yaks to survive the nutritional stress in the severe cold seasons (36). The above bacteria can produce SCFAs by fermenting the dietary fiber. It is well known that SCFAs can not only provide energy for the intestinal epithelial cells but also firmly maintain the morphology and function of the intestine (37, 38). Moreover, SCFAs have also been confirmed to promote glucose intake and metabolism in skeletal muscle, and butyrate can improve the energy metabolism efficiency of muscle fibers (39, 40). Based on the functions of the above bacterial families (fiber fermentation, inflammation mitigation, stress adaptation, and promotion of SCFAs on energy uptake and metabolism in skeletal muscle), it is speculated that these different bacterial families play a positive role in the performance of Thoroughbred horses.

The biomarkers of Mongolian horses belonged to Firmicutes, including Bacilli, Bacillales, Planococcaceae,

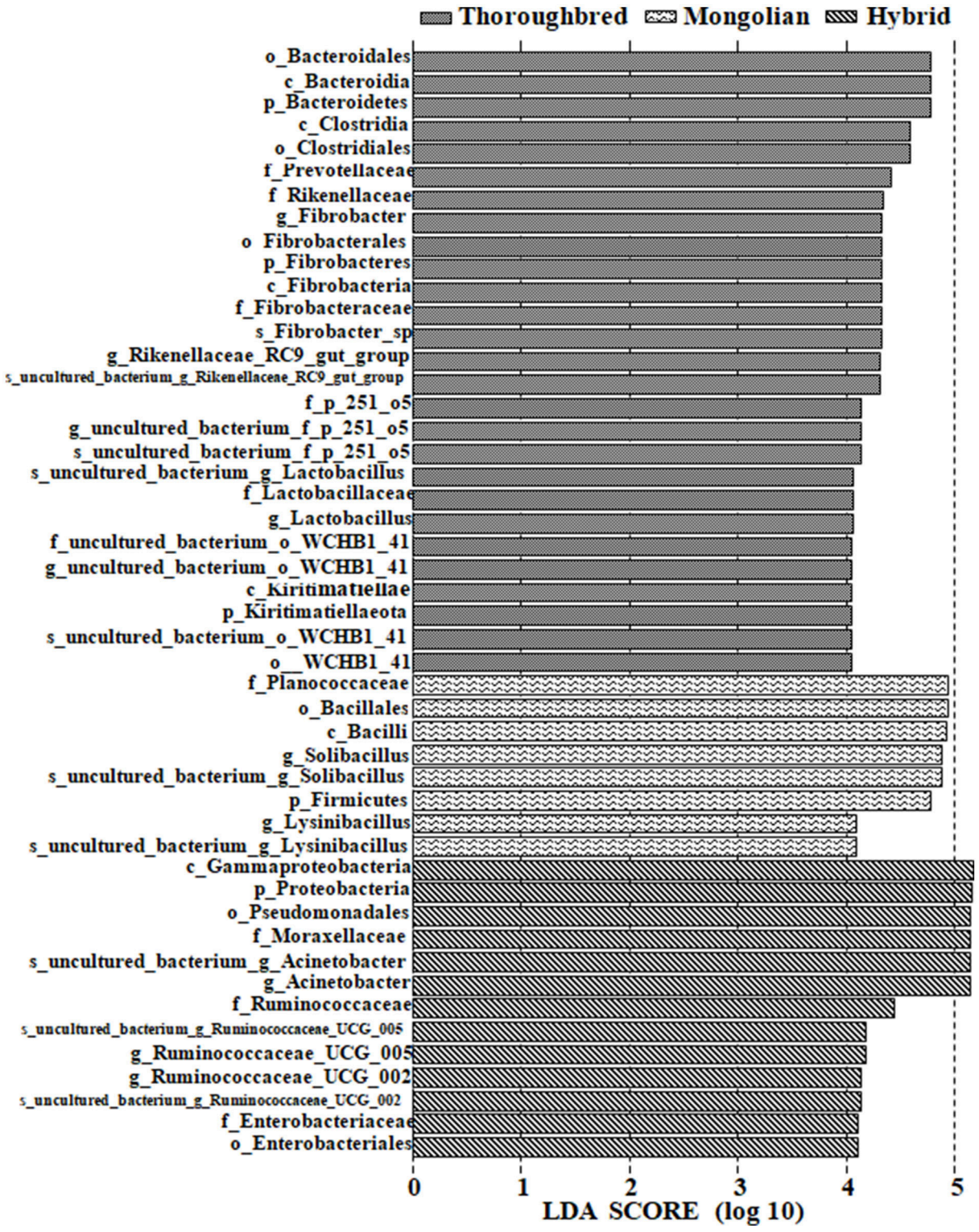

FIGURE 6
LEfSe [linear discriminant analysis (LDA) effect size] analysis of samples between groups (pairwise Wilcoxon test, LDA scores > 4).

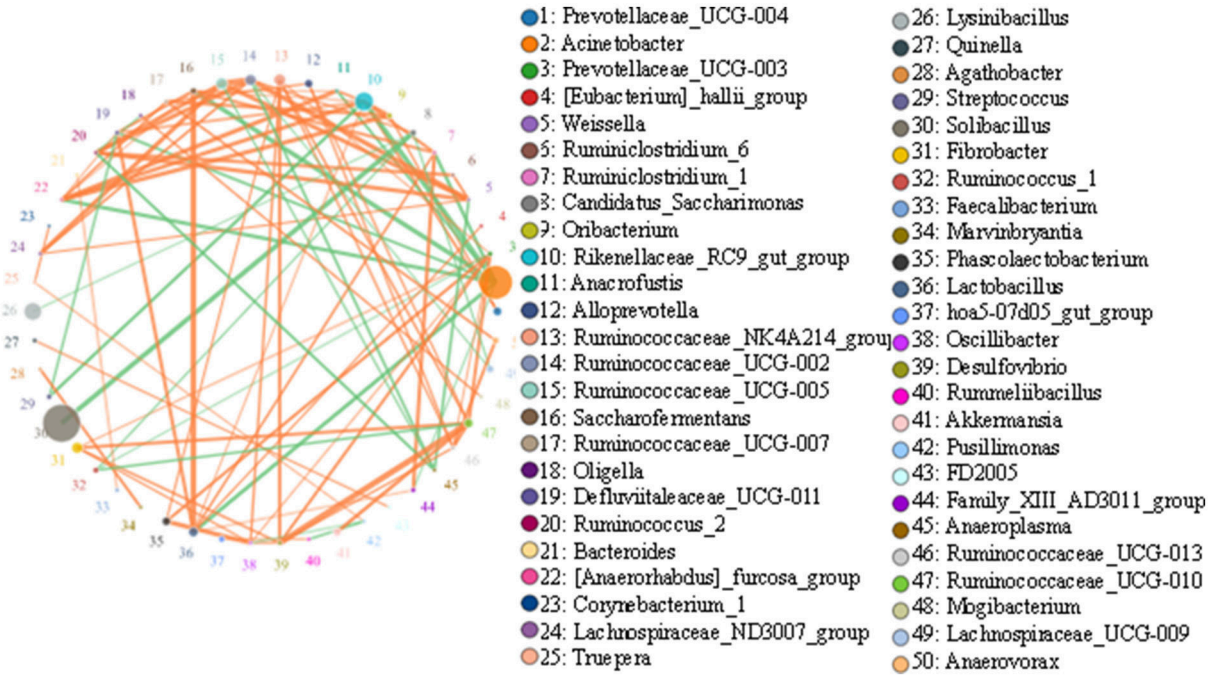

FIGURE 7
Network diagram of each species at the genus level. Circles represent the species, and circle sizes represent the species' average abundance size. Lines represent the correlation between the two species, and the thickness of the lines represents the strength of the correlation. Orange lines represent a positive correlation, and green lines represent a negative correlation.

and two genera (*Solibacillus* and *Lysinibacillus*). In the study of Xiong et al. (41), gut Bacillales and Planococcaceae were found to be negatively associated with the average daily gain and the final weight of pigs at the end of the trial, but positively associated with the height of small intestinal villi and microvilli (41). *Solibacillus* was found to exist as the predominant bacterial genus in the gut of *Macaca munzala* with metabolic disorders (42). It was found that buffaloes grazing in regions lacking pasture had decreased alpha diversity compared with those grazing in pasture-sufficient regions, and the dominant genus was *Solibacillus*. It was speculated that the enrichment of *Solibacillus* in the buffaloes' gut with decreased food intake is an adaptive response to dietary variability (43). *Solibacillus silvestris* and *Lysinibacillus* sp. D060 have been confirmed to contain many bile acid metabolism genes and bile acid biotransformation ability (44). In addition, the functional prediction results showed that the lipid metabolism of the Mongolian horses was significantly higher than that of the other two groups. Therefore, in combination with the above functions of the biomarkers and the prediction results, it can be speculated that the gut microbiota of Mongolian horses has a positive role in maintaining their roughage resistance and stamina.

The differential species in the gut of Hybrid horses included three families (i.e., Moraxellaceae, Enterobacteriaceae, and Ruminococcaceae) and three genera (i.e., *Acinetobacter*, *Ruminococcaceae_UCG_005*, and *Ruminococcaceae_UCG_002*). The genus *Acinetobacter* under the family Moraxellaceae contains many opportunistic pathogens and has been reported to cause multiple diseases in horses, such as respiratory tract infections, foal septicemia, foal abortion (45, 46), meningitis (47), endocarditis (48), wound and skin infections (49), and urogenital tract infections (50). Enterobacteriaceae are widely distributed in nature; have a broad host range; and are parasitic or symbiotic in humans, animals, and plants. Some genera in the family Enterobacteriaceae, such as *Escherichia* (51), *Salmonella* (52), *Shigella* (53), and *Klebsiella* (54), belong to the common opportunistic pathogens. Ruminococcaceae are the main microorganisms that convert primary bile acids into secondary bile acids and are also involved in polysaccharide degradation (55). In addition, the Ruminococcaceae in the horse gut have also been proved to have immunomodulatory and anti-inflammatory effects (56). *Ruminococcaceae_UCG-005* showed a significantly positive correlation with eggshell strength and egg weight, presumably achieved by increasing feed conversion in laying hens (57). *Ruminococcaceae_UCG_005* also has a potent cellulolytic capacity (58). *Ruminococcaceae_UCG-002* can degrade various polysaccharides, and its degradation product SCFAs has anti-inflammatory effects (59). Overall, both Mongolian and Hybrid horses are enriched with opportunistic pathogenic bacteria and important polysaccharide digestion bacteria in the gut, compared with Thoroughbred horses.

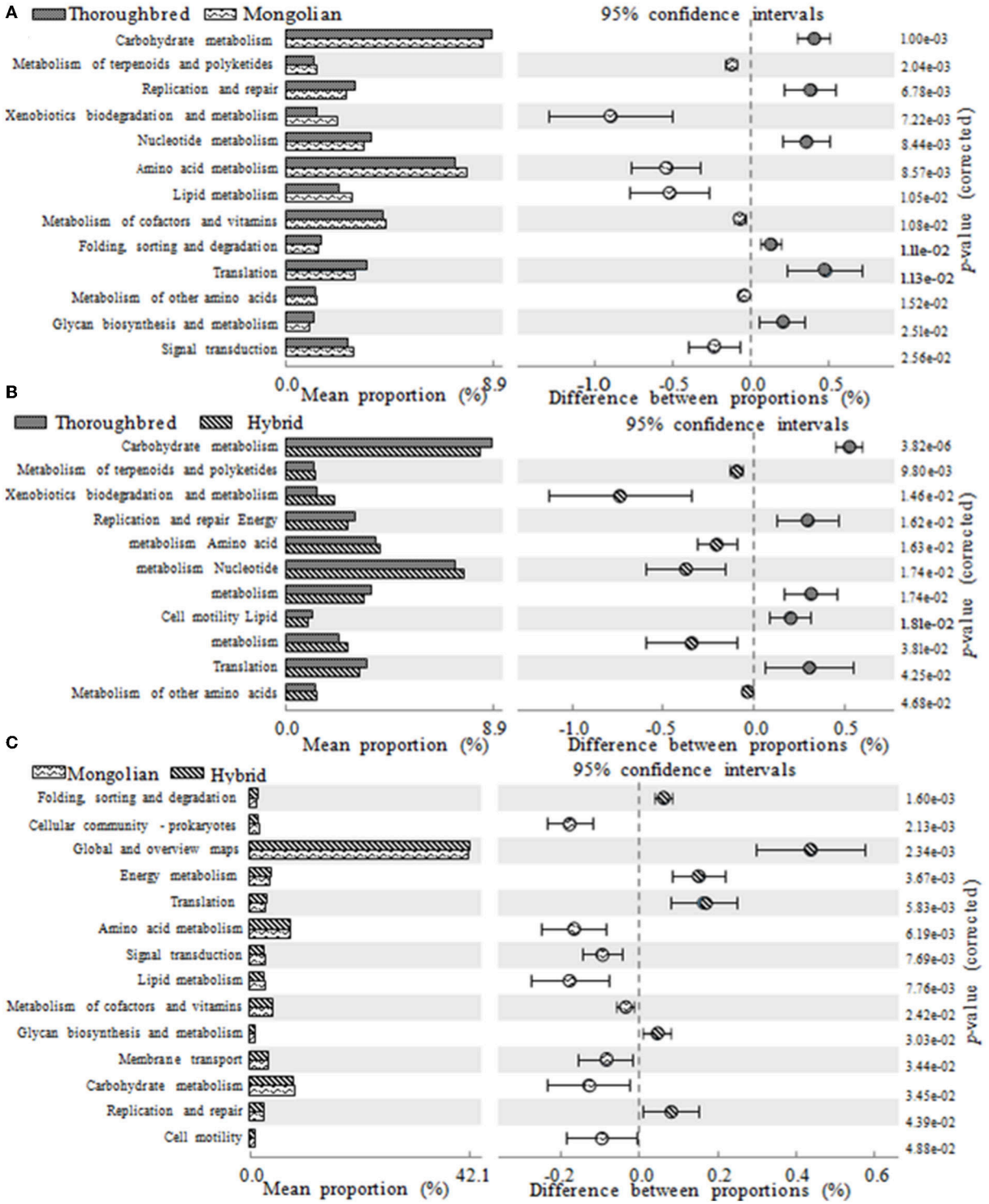

FIGURE 8
Differences in KEGG (Kyoto Encyclopedia of Genes and Genomes) metabolic pathways between groups (one-way ANOVA with Tukey's *post-test*, $P < 0.05$). **(A)** The functional gene differences between Thoroughbred and Mongolian horses. **(B)** The functional gene differences between Thoroughbred and Hybrid horses. **(C)** The functional gene differences between Mongolian and Hybrid horses.

Conclusion

To explore the relationship between horse breeds and gut microbiota, 16S rRNA high-throughput sequencing was used to detect the microbiota in horse fecal samples. The comparison of gut microbial diversity among breeds showed that Thoroughbred horses had higher microbial diversity than Mongolian horses, while Hybrid horses were intermediate between them. Cluster analysis indicated that the similarity of the gut microbiota was higher within groups than between groups, and a higher similarity was found between Mongolian and Hybrid horses. The LEfSe analysis showed a greater enrichment of fibrolytic bacteria in the gut of Thoroughbred horses. Meanwhile, the functional prediction results of the gut microbiota also showed a significantly higher abundance of carbohydrate metabolic pathways in Thoroughbred horses than in Mongolian and Hybrid horses. Compared with Thoroughbred horses, the gut of Mongolian horses and Hybrid horses was rich in opportunistic pathogens and beneficial bacteria that can degrade polysaccharides to produce SCFAs. In conclusion, there is an association between horse breed and gut microbiota. The results of this study could lay a theoretical foundation for further understanding and improving the precision feeding system of horses.

Data availability statement

The datasets presented in this study can be found in online repositories. The names of the repository/repositories and accession number(s) can be found at: https://www.ncbi.nlm.nih.gov/sra/PRJNA812711, PRJNA812711.

Ethics statement

The animal study was reviewed and approved by Ethics Committee of the Shangqiu Normal University.

Author contributions

XW conceived and designed the experiments. SL, DL, CJ, and XZ contributed to sample collection and reagents preparation. QZ and CY analyzed the data. XW wrote the manuscript. LX revised the manuscript. All authors reviewed the manuscript.

Funding

This work was supported by field scientific observation and research of animal diseases in Guangdong Province (Department of Science and Technology of Guangdong Province: 2021B1212050021), Guangdong provincial special fund for modern agriculture industry technology innovation teams (Department of Agriculture and Rural Affairs of Guangdong Province: 2021KJ119), screening and application of anti-foodborne Campylobacter phage (The Education Department of Henan Province: 21B230008), and development and application of feed antibiotic substitute based on immune-antioxidant-gut microecological regulation (Department of Science and Technology of Henan Province: 222102320024).

Conflict of interest

The authors declare that the research was conducted in the absence of any commercial or financial relationships that could be construed as a potential conflict of interest.

Publisher's note

All claims expressed in this article are solely those of the authors and do not necessarily represent those of their affiliated organizations, or those of the publisher, the editors and the reviewers. Any product that may be evaluated in this article, or claim that may be made by its manufacturer, is not guaranteed or endorsed by the publisher.

Supplementary material

The Supplementary Material for this article can be found online at: https://www.frontiersin.org/articles/10.3389/fvets.2022.920080/full#supplementary-material

References

1. Garber A, Hastie P, Murray JA. Factors influencing equine gut microbiota: current knowledge. *J Equine Vet Sci.* (2020) 88:102943. doi: 10.1016/j.jevs.2020.102943

2. Sorensen RJ, Drouillard JS, Douthit TL, Ran Q, Marthaler DG, Kang Q, et al. Effect of hay type on cecal and fecal microbiome and fermentation parameters in horses. *J Anim Sci*. (2021) 99:Skaa407. doi: 10.1093/jas/skaa407

3. Ericsson AC, Johnson PJ, Lopes MA, Perry SC, Lanter HR. A microbiological map of the healthy equine gastrointestinal tract. *PLoS ONE.* (2016) 11:E0166523. doi: 10.1371/journal.pone.0166523

4. Mach N, Ruet A, Clark A, Bars-Cortina D, Ramayo-Caldas Y, Crisci E, et al. Priming for welfare: gut microbiota is associated with

equitation conditions and behavior in horse athletes. *Sci Rep*. (2020) 10:8311. doi: 10.1038/s41598-020-65444-9

5. Arnold CE, Isaiah A, Pilla R, Lidbury J, Coverdale JS, Callaway TR, et al. The cecal and fecal microbiomes and metabolomes of horses before and after metronidazole administration. *PLoS ONE*. (2020) 15:E0232905. doi: 10.1371/journal.pone.0232905

6. Walshe N, Cabrera-Rubio R, Collins R, Puggioni A, Gath V, Crispie F, et al. A multiomic approach to investigate the effects of a weight loss program on the intestinal health of overweight horses. *Front Vet Sci*. (2021) 8:668120. doi: 10.3389/fvets.2021.668120

7. Lara F, Castro R, Thomson P. Changes in the gut microbiome and colic in horses: are they causes or consequences? *Open Vet J*. (2022) 12:242–9. doi: 10.5455/OVJ.2022.v12.i2.12

8. Morrison PK, Newbold CJ, Jones E, Worgan HJ, Grove-White DH, Dugdale AH, et al. The equine gastrointestinal microbiome: impacts of age and obesity. *Front Microbiol*. (2018) 9:3017. doi: 10.3389/fmicb.2018.03017

9. Biddle AS, Tomb JF, Fan Z. Microbiome and blood analyte differences point to community and metabolic signatures in lean and obese horses. *Front Vet Sci*. (2018) 5:225. doi: 10.3389/fvets.2018.00225

10. Garber A, Hastie P, Mcguinness D, Malarange P, Murray JA. Abrupt dietary changes between grass and hay alter faecal microbiota of ponies. *PLoS ONE*. (2020) 15:E0237869. doi: 10.1371/journal.pone.0237869

11. Fernandes KA, Rogers CW, Gee EK, Kittelmann S, Bolwell CF, Bermingham EN, et al. Resilience of faecal microbiota in stabled thoroughbred horses following abrupt dietary transition between freshly cut pasture and three forage-based diets. *Animals*. (2021) 11:2611. doi: 10.3390/ani11092611

12. Destrez A, Grimm P, Julliand V. Dietary-induced modulation of the hindgut microbiota is related to behavioral responses during stressful events in horses. *Physiol Behav*. (2019) 202:94–100. doi: 10.1016/j.physbeh.2019.02.003

13. Hu D, Chao Y, Zhang B, Wang C, Qi Y, Ente M, et al. Effects of gasterophilus pecorum infestation on the intestinal microbiota of the rewilded przewalski's horses in China. *Plos ONE*. (2021) 16:E0251512. doi: 10.1371/journal.pone.0251512

14. Zhao Y, Li B, Bai D, Huang J, Shiraigo W, Yang L, et al. Comparison of fecal microbiota of mongolian and thoroughbred horses by high-throughput sequencing of the V4 region of the 16s rRNA gene. *Asian-Australas J Anim Sci*. (2016) 29:1345–52. doi: 10.5713/ajas.15.0587

15. Park T, Yoon J, Kim A, Unno T, Yun Y. Comparison of the gut microbiota of jeju and thoroughbred horses in Korea. *Vet Sci*. (2021) 8:81. doi: 10.3390/vetsci8050081

16. Massacci FR, Clark A, Ruet A, Lansade L, Costa M, Mach N. Inter-breed diversity and temporal dynamics of the faecal microbiota in healthy horses. *J Anim Breed Genet*. (2020) 137:103–20. doi: 10.1111/jbg.12441

17. Beaumont M, Goodrich JK, Jackson MA, Yet I, Davenport ER, Vieira-Silva S, et al. Heritable components of the human fecal microbiome are associated with visceral fat. *Genome Biol*. (2016) 17:189. doi: 10.1186/s13059-016-1052-7

18. Goodrich JK, Davenport ER, Waters JL, Clark AG, Ley RE. Cross-species comparisons of host genetic associations with the microbiome. *Science*. (2016) 352:532–5. doi: 10.1126/science.aad9379

19. Yang H, Wu J, Huang X, Zhou Y, Zhang Y, Liu M, et al. Abo genotype alters the gut microbiota by regulating galnac levels in pigs. *Nature*. (2022) 606:358–67. doi: 10.1038/s41586-022-04769-z

20. Fan P, Bian B, Teng L, Nelson CD, Driver J, Elzo MA, et al. Host genetic effects upon the early gut microbiota in a bovine model with graduated spectrum of genetic variation. *Isme J*. (2020) 14:302–17. doi: 10.1038/s41396-019-0529-2

21. Han H, Bryan K, Shiraigol W, Bai D, Zhao Y, Bao W, et al. Refinement of global domestic horse biogeography using historic landrace chinese mongolian populations. *J Hered*. (2019) 110:769–81. doi: 10.1093/jhered/esz032

22. Bao T, Han H, Li B, Zhao Y, Bou G, Zhang X, et al. The distinct transcriptomes of fast-twitch and slow-twitch muscles in Mongolian horses. *Comp Biochem Physiol Part D Genomics Proteomics*. (2020) 33:100649. doi: 10.1016/j.cbd.2019.100649

23. Fang J, Zhang D, Cao JW, Zhang L, Liu CX, Xing YP, et al. Pathways involved in pony body size development. *BMC Genomics*. (2021) 22:58. doi: 10.1186/s12864-020-07323-1

24. Mercier Q, Aftalion A. Optimal speed in thoroughbred horse racing. *PLoS ONE*. (2020) 15:E0235024. doi: 10.1371/journal.pone.0235024

25. Hill EW, Mcgivney BA, Rooney MF, Katz LM, Parnell A, Machugh DE. The contribution of myostatin (Mstn) and additional modifying genetic loci to race distance aptitude in thoroughbred horses racing in different geographic regions. *Equine Vet J*. (2019) 51:625–33. doi: 10.1111/evj.13058

26. Moyers BT, Morrell PL, Mckay JK. Genetic costs of domestication and improvement. *J Hered*. (2018) 109:103–16. doi: 10.1093/jhered/esx069

27. Todd ET, Thomson PC, Hamilton NA, Ang RA, Lindgren G, Viklund Å, et al. A Genome-wide scan for candidate lethal variants in thoroughbred horses. *Sci Rep*. (2020) 10:13153. doi: 10.1038/s41598-020-68946-8

28. CCTV7. (2013). Daily Agricultural Economy. Available online at: http://Tv.Cctv.Com/2013/12/05/Vide1409105497642971.Shtml [accessed December 5, 2013].

29. Houtman TA, Eckermann HA, Smidt H, De Weerth C. Gut microbiota and bmi throughout childhood: the role of firmicutes, bacteroidetes, and short-chain fatty acid producers. *Sci Rep*. (2022) 12:3140. doi: 10.1038/s41598-022-07176-6

30. Mao K, Gao J, Wang X, Li X, Geng S, Zhang T. Bifidobacterium animalis subsp. lactis bb-12 has effect against obesity by regulating gut microbiota in two phases in human microbiota-associated rats. *Front Nutr*. (2022) 8:811619. doi: 10.3389/fnut.2021.811619

31. Qiu X, Qin X, Chen L, Chen Z, Hao R, Zhang S. Serum biochemical parameters, rumen fermentation, and rumen bacterial communities are partly driven by the breed and sex of cattle when fed high-grain diet. *Microorganisms*. (2022) 10:323. doi: 10.3390/microorganisms10020323

32. Fan Q, Wanapat M, Hou F. Impacting by herbage grown at different phenological periods on the qinghai-tibet plateau. *Animals*. (2020) 10:1030. doi: 10.3390/ani10061030

33. Cho HM, González-Ortiz G, Melo-Durán D, Heo JM, Cordero G, Bedford MR, et al. Stimbiotic supplementation improved performance and reduced inflammatory response via stimulating fiber fermenting microbiome in weaner pigs housed in a poor sanitary environment and fed an antibiotic-free low zinc oxide diet. *Plos ONE*. (2020) 15:E0240264. doi: 10.1371/journal.pone.0240264

34. Abbas W, Howard JT, Paz HA, Hales KE, Wells JE, Kuehn LA, et al. Influence of host genetics in shaping the rumen bacterial community in beef cattle. *Sci Rep*. (2020) 10:15101. doi: 10.1038/s41598-020-72011-9

35. Park T, Cheong H, Yoon J, Kim A, Yun Y, Unno T. Comparison of the fecal microbiota of horses with intestinal disease and their healthy counterparts. *Vet Sci*. (2021) 8:113. doi: 10.3390/vetsci8060113

36. Guo N, Wu Q, Shi F, Niu J, Zhang T, Degen AA, et al. Seasonal dynamics of diet-gut microbiota interaction in adaptation of yaks to life at high altitude. *NPJ Biofilms Microbiomes*. (2021) 7:38. doi: 10.1038/s41522-021-00207-6

37. Juśkiewicz J, Fotschki B, Jaworska J, Siemieniuch M. Investigations of the maintenance system of the konik polski horse and its effects on fecal microbiota activity during the winter and summer seasons. *Anim Sci J*. (2021) 92:E13603. doi: 10.1111/asj.13603

38. Sallé G, Canlet C, Cortet J, Koch C, Malsa J, Reigner F, et al. Integrative biology defines novel biomarkers of resistance to strongylid infection in horses. *Sci Rep*. (2021) 11:14278. doi: 10.1038/s41598-021-93468-2

39. Frampton J, Murphy KG, Frost G, Chambers ES. Short-chain fatty acids as potential regulators of skeletal muscle metabolism and function. *Nat Metab*. (2020) 2:840–8. doi: 10.1038/s42255-020-0188-7

40. Chen F, Li Q, Chen Y, Wei Y, Liang J, Song Y, et al. Association of the gut microbiota and fecal short-chain fatty acids with skeletal muscle mass and strength in children. *Faseb J*. (2022) 36:E22109. doi: 10.1096/fj.202002697RRR

41. Xiong Y, Cao S, Xiao H, Wu Q, Yi H, Jiang Z, et al. Alterations in intestinal microbiota composition coincide with impaired intestinal morphology and dysfunctional ileal immune response in growing-finishing pigs under constant chronic heat stress. *J Anim Sci Biotechnol*. (2022) 13:1. doi: 10.1186/s40104-021-00651-6

42. Ghosh A, Thakur M, Sharmam LK, Chandra K. Linking gut microbiome with the feeding behavior of the arunachal macaque (macaca munzala). *Sci Rep*. (2021) 11:21926. doi: 10.1038/s41598-021-01316-0

43. Couch CE, Stagaman K, Spaan RS, Combrink HJ, Sharpton TJ, Beechler BR, et al. Diet and gut microbiome enterotype are associated at the population level in african buffalo. *Nat Commun*. (2021) 12:2267. doi: 10.1038/s41467-021-22510-8

44. Yan Q, Zhang S, Li S, Wang G, Zhang A, Jin T, et al. Cultivation and genomic characterization of the bile bacterial species from cholecystitis patients. *Front Microbiol*. (2021) 12:739621. doi: 10.3389/fmicb.2021.739621

45. Van Der Kolk JH, Endimiani A, Graubner C, Gerber V, Perreten V. Acinetobacter in veterinary medicine, with an emphasis on acinetobacter baumannii. *J Glob Antimicrob Resist*. (2019) 16:59–71. doi: 10.1016/j.jgar.2018.08.011

46. Akter R, El-Hage CM, Sansom FM, Carrick J, Devlin JM, Legione AR. Metagenomic investigation of potential abortigenic pathogens in foetal tissues from Australian horses. *BMC Genomics*. (2021) 22:713. doi: 10.1186/s12864-021-08010-5

47. Gutiérrez-Gaitán MP, Montoya-Moncadam AD, Suescún-Vargas JM, Pinzón-Salamanca JY, Aguirre-Borrero BL. Emerging species in pediatrics: a case of acinetobacter johnsonii meningitis. *Bol Med Hosp Infant Mex*. (2022) 79:51–55. doi: 10.24875/BMHIM.21000041

48. Ioannou P, Mavrikakim V, Kofteridis DP. Infective endocarditis by acinetobacter species: a systematic review. *J Chemother*. (2021) 33:203–15. doi: 10.1080/1120009X.2020.1812804

49. Wintachai P, Surachat K, Singkhamanan K. Isolation and characterization of a novel autographiviridae phage and its combined effect with tigecycline in controlling multidrug-resistant acinetobacter baumannii-associated skin and soft tissue infections. *Viruses*. (2022) 14:194. doi: 10.3390/v140 20194

50. Fiester SE, Arivett BA, Schmidt RE, Beckett AC, Ticak T, Carrier MV, et al. Iron-regulated phospholipase c activity contributes to the cytolytic activity and virulence of acinetobacter baumannii. *Plos One*. (2016) 11:E0167068. doi: 10.1371/journal.pone.0167068

51. Tamamura-Andoh Y, Niwa H, Kinoshita Y, Uchida-Fujii E, Arai N, Watanabe-Yanai A, et al. Duplication of blactx-M-1 and a class 1 integron on the chromosome enhances antimicrobial resistance in escherichia coli isolated from racehorses in Japan. *J Glob Antimicrob Resist*. (2021) 27:225–7. doi: 10.1016/j.jgar.2021.10.004

52. Kopper JJ, Willette JA, Kogan CJ, Seguin A, Bolin SR, Schott HCN. Detection of pathogens in blood or feces of adult horses with enteric disease and association with outcome of colitis. *J Vet Intern Med*. (2021) 35:2465–72. doi: 10.1111/jvim.16238

53. Weddle EA, Köseoglu VK, Devasure BA, Agaisse HF. The type three secretion system effector protein ipgb1 promotes shigella flexneri cell-to-cell spread through double-membrane vacuole escape. *PLoS Pathog*. (2022) 18:E1010380. doi: 10.1371/journal.ppat.1010380

54. Thomson K, Eskola K, Eklund M, Suominen K, Määttä M, Junnila J, et al. Characterisation of and risk factors for extended-spectrum β-lactamase producing enterobacterales (Esbl-E) in an equine hospital with a special reference to an outbreak caused by klebsiella pneumoniae St307:Ctx-M-1. *Acta Vet Scand*. (2022) 64:4. doi: 10.1186/s13028-022-00621-6

55. Liu J, Song Y, Zhao Q, Wang Y, Li C, Zou L, et al. Effects of tartary buckwheat protein on gut microbiome and plasma metabolite in rats with high-fat diet. *Foods*. (2021) 10:2457. doi: 10.3390/foods10102457

56. Lindenberg FC, Lützhøft DO, Krych L, Fielden J, Kot W, Frøkiær H, et al. An oligosaccharide rich diet increases akkermansia Spp. bacteria in the equine microbiota. *Front Microbiol*. (2021) 12:666039. doi: 10.3389/fmicb.2021.666039

57. Wan Y, Ma R, Zhang H, Li L, Chai L, Qi R, et al. Different non-cage housing systems alter duodenal and cecal microbiota composition in shendan chickens. *Front Vet Sci*. (2021) 8:728538. doi: 10.3389/fvets.2021.728538

58. Liu W, Wang Q, Song J, Xin J, Zhang S, Lei Y, et al. Comparison of gut microbiota of yaks from different geographical regions. *Front Microbiol*. (2021) 12:666940. doi: 10.3389/fmicb.2021.666940

59. Shang Q, Liu S, Liu H, Mahfuz S, Piao X. Impact of sugar beet pulp and wheat bran on serum biochemical profile, inflammatory responses and gut microbiota in sows during late gestation and lactation. *J Anim Sci Biotechnol*. (2021) 12:54. doi: 10.1186/s40104-021-00573-3

frontiers | Frontiers in Veterinary Science

ORIGINAL RESEARCH
published: 02 August 2022
doi: 10.3389/fvets.2022.840981

The Resistance Mechanism of *Mycoplasma bovis* From Yaks in Tibet to Fluoroquinolones and Aminoglycosides

Jiaqiang Niu, Mingshuai Yan, Jinhua Xu, Yefen Xu, Zhenyu Chang and Suolang Sizhu**

Tibet Agriculture and Animal Husbandry College, Linzhi, China

Mycoplasma bovis (*M. bovis*) is one of the important pathogens for yaks. Aminoglycosides and fluoroquinolones are frequently used medications for the treatment of *M. bovis.* Drug-resistant strains were inevitable with the abuse of antibiotics. The resistance of *M. bovis* to aminoglycosides was related to the base mutations in drug target genes. Amino acid mutations at the quinolone resistance-determining region (QRDR) in gyrA, gyrB, parC, and parE conferred resistance to fluoroquinolones. In order to investigate the resistance mechanism of *M. bovis* from yaks in Tibet to aminoglycosides and fluoroquinolones, six frequently used antibiotics and ten clinical *M. bovis* strains were administered for a drug sensitivity test for *in vitro*-induced highly resistant strains, a drug stable-resistance test, cross-resistance test, and analysis of target gene mutations. The results showed that the clinical strains of *M. bovis* from yaks in Tibet had varying degrees of resistance to fluoroquinolones and aminoglycosides. The mechanism of resistance to fluoroquinolones and aminoglycosides was identified preliminarily for *M. bovis* from yaks: the single-site base mutation mediated the resistance of *M. bovis* from yaks and both base mutations led to highly resistant strains (aminoglycosides: rrs3 and rrs4; fluoroquinolones: gyrA and parC). The active efflux system results of M. bovis showed that there was no active efflux system based on fluoroquinolones and aminoglycosides expressed in *M. bovis* from yaks. The research could provide a reference for clinical treatment of *M. bovis*.

Keywords: fluoroquinolones, resistance mechanism, yak, *Mycoplasma bovis*, aminoglycosides

OPEN ACCESS

Edited by:
Fazul Nabi,
Lasbela University of Agriculture, Water and Marine Sciences, Pakistan

Reviewed by:
Hafiz Ishfaq Ahmad,
University of Veterinary and Animal Sciences, Pakistan
Quratulain Hanif,
Pakistan Institute of Engineering and Applied Sciences, Pakistan

****Correspondence:***
Jiaqiang Niu
lznjq@163.com
Suolang Sizhu
574428982@qq.com

Specialty section:
This article was submitted to Comparative and Clinical Medicine, a section of the journal Frontiers in Veterinary Science

Received: *21 December 2021*
Accepted: *19 April 2022*
Published: *02 August 2022*

Citation:
Niu J, Yan M, Xu J, Xu Y, Chang Z and Sizhu S (2022) The Resistance Mechanism of Mycoplasma bovis From Yaks in Tibet to Fluoroquinolones and Aminoglycosides. Front. Vet. Sci. 9:840981. doi: 10.3389/fvets.2022.840981

INTRODUCTION

Mycoplasma bovis (*M. bovis*) is one of the important pathogens that causes bovine disease syndromes such as pneumonia, mastitis, keratoconjunctivitis, arthritis, genital tract inflammation, miscarriage, and infertility (1). Sick cattle and the respiratory modes of transmission were the main sources and routes of infection (2). *Mycoplasma* was isolated firstly from mastitis milk by Hale et al. (3). It caused huge economic losses to the cattle industry (4).

In China, *M. bovis* was first isolated by Li (5) and proved to be the pathogen of respiratory diseases in cattle until 2008 (5–8). Antibiotics (aminoglycosides and fluoroquinolones) have been used to treat *M. bovis.* Previous research confirmed the resistance to macrolides and fluoroquinolones for *M. bovis* clinically isolated strains (9, 10). In our previous study, we found

that the isolated strains were resistant to macrolides, aminoglycosides, and lincosamides (11). The research was imperative for drug resistance mechanisms (12).

Aminoglycosides and fluoroquinolones are broad-spectrum antibiotics against Gram-negative bacteria (13). The resistance of *M. bovis* to aminoglycosides is related to the base mutations in drug target genes (14). Previous research showed that there was a base mutation in 16S rRNA, but no base mutation was detected in S12 ribosomal protein (15–17). Amino acid mutations at the quinolone resistance-determining region (QRDR) in gyrA, gyrB, parC, and parE conferred resistance to fluoroquinolones (18). The mutation in the QRDR of gyrA contributed to nalidixic acid resistance (19). The amino acid mutation in parC was the leading cause of fluoroquinolones resistance in bacteria (20). The efflux pump mediated the resistance to aminoglycosides by AmrB, MexY, and AcrD genes and to fluoroquinolones by EmrAB، AcrAB، YdhE، AcrEF, and MdfA genes in resistance nodulation cell division (21, 22).

In our study, we performed antibiotic susceptibility testing, drug target gene mutation analysis, and developed a preliminary confirmation of an active drug efflux system on 10 isolates of *M. bovis* from Tibet yaks. It could provide references for the drug-resistant mechanism of *M. bovis*.

MATERIALS AND METHODS

Strains

Ten isolated strains of *M. bovis* from yaks in Tibet (Tibet-1∼10) came from the Key Laboratory of Tibet Plateau Animal Disease Research Autonomous Region (11).

Design and Synthesis of Primers

The DNA of *M. bovis* was extracted by the boiling method (23). The primers were designed as described in a previous research paper (**Table 1**) (17, 18).

Antibiotic Susceptibility Testing

The minimum inhibitory concentration (MIC) of the 10 strains were detected by the microdilution method (17) against SPE (spectinomycin), GEN (gentamicin), KAN (kanamycin), ENR (enrofloxacin), NOR (norfloxacin), and CIP (ciprofloxacin). The drug resistance results referred to the CLSI (Clinical and Laboratory Standards Institute, USA) standards (SPE: MIC≥128 μg/mL; GEN,KAN: MIC≥32 μg/mL; ENR,NOR,CIP: MIC≥4 μg/mL) (24).

Cross-Resistance Test

The highly resistant strains of *M. bovis in vitro* were induced until there was 512 μg/mL of SPE, GEN, KAN, NOR, CIP, and 256 μg/mL of ENR. There were only three highly resistant strains induced successfully (Tibet-1, Tibet-6, and Tibet-8, and named *M. bovis* 1, *M. bovis* 6, and *M. bovis* 8). The highly resistant strains to ENR, NOR, and CIP were tested for cross-resistance for the highly resistant stains to SPE, GEN, and KAN.

Antibiotic Target Mutation Analysis

The DNA was extracted by water-boiling and amplified by PCR for the sensitive, resistant, and *in vitro*-induced strains. The PCR products were recovered using the Gel Extraction Kit (Omega Bio-Tek Co., Ltd., USA) and connected to the pMD18-T. The recombinant plasmid was verified by M13 and sequenced by Shenggong Bioengineering (Shanghai) Co., Ltd. DNAMAN software was used to compare and analyze the sequencing results.

TABLE 1 | Primer sequences.

Gene name	Primer sequence (5′ → 3′)	Tm (°C)	Product length
rrs 3	F: GGATATCTAACGCCGTGTC	50°C	1,857 bp
	R: CGTTCTCGTAGGGATACCT		
rrs 4	F: GAGTTTGATCCTGGCTC	43°C	1,812 bp
	R: GTATTTTCCTATTGTTGTTA		
rps E	F: GCATGGCAGATTTAGAAAACAAGA	51°C	696 bp
	R: CGGTGCTTAACCTAAAAGGTCTTTA		
gyr A	F:GACGAATCATCTAGCGAG	56°C	531 bp
	R:GCCTTCTAGCATCAAAGTAGC		
gyr B	F:CCTTGTTGCCATTGTGTC	56°C	555 bp
	R:CCATCGACATCAGCATCAGTC		
par C	F:GGTACTCCTGAAGCTAAAAGTGC	56°C	488 bp
	R:GAATATGTGCGCCATCAG		
par E	F:GAGCAACAGTTAAACGATTTG	56°C	502 bp
	R:GGCATAACAACTGGCTCTT		

PCR, reaction conditions: 95°C pre-denaturation 3 min, (95°C denaturation 30 s, Tm °C annealing 30 s, 72°C extension 45 s, 30 cycles), extension 10 min at 72°C.

TABLE 2 | The MIC results of the 10 strains (ug/mL).

Strain name	MIC (ug/mL)					
	SPE	GEN	KAN	CIP	ENR	NOR
Tibet-1	64	16	8	8	2	1
Tibet-2	32	8	8	2	2	0.25
Tibet-3	32	8	4	2	1	0.25
Tibet-4	16	2	2	1	0.5	2
Tibet-5	16	2	16	0.5	2	0.5
Tibet-6	128	64	2	4	8	2
Tibet-7	8	8	2	0.5	0.25	4
Tibet-8	128	1	4	4	0.5	1
Tibet-9	4	1	1	1	0.25	4
Tibet-10	4	2	8	0.5	1	0.5

SPE, spectinomycin; GEN, gentamicin; KAN, kanamycin; CIP, ciprofloxacin; ENR, enrofloxacin; NOR, norfloxacin.

Overexpression of the Active Efflux System of *M. bovis*

The MIC of CCCP (carbonyl cyanide m-chlorophenyl hydrazone) and VP (verapamil) was detected for the sensitive, resistant, and *in vitro*-induced strains. The overexpression of the active efflux system was judged to exist when the MIC of antibiotics using CCCP and VP was less than 1/4 of the original MIC value.

TABLE 3 | Test results of cross-resistance induced *in vitro* (ug/mL).

Strain name	Inducing drug concentration μg/mL	MIC (ug/mL)			Inducing drug concentration μg/mL	MIC (ug/mL)		
		CIP	ENR	NOR		SPE	GEN	KAN
M. bovis 1	CIP (512)	512	128	128	SPE (512)	512	128	128
	ENR (256)	128	256	64	GEN (512)	128	512	64
	NOR (512)	64	64	512	KAN (512)	128	64	512
M. bovis 6	CIP (512)	512	64	256	SPE (512)	512	256	64
	ENR (256)	256	256	256	GEN (512)	128	512	32
	NOR (512)	128	32	512	KAN (512)	256	256	512
M. bovis 8	CIP (512)	512	256	256	SPE (512)	512	256	256
	ENR (256)	32	256	128	GEN (512)	128	512	64
	NOR (512)	128	64	512	KAN (512)	128	128	512

SPE, spectinomycin; GEN, gentamicin; KAN, kanamycin; CIP, ciprofloxacin; ENR, enrofloxacin; NOR, norfloxacin. M. bovis 1, M. bovis 6, M. bovis 8: the highly resistant strains induced in vitro.

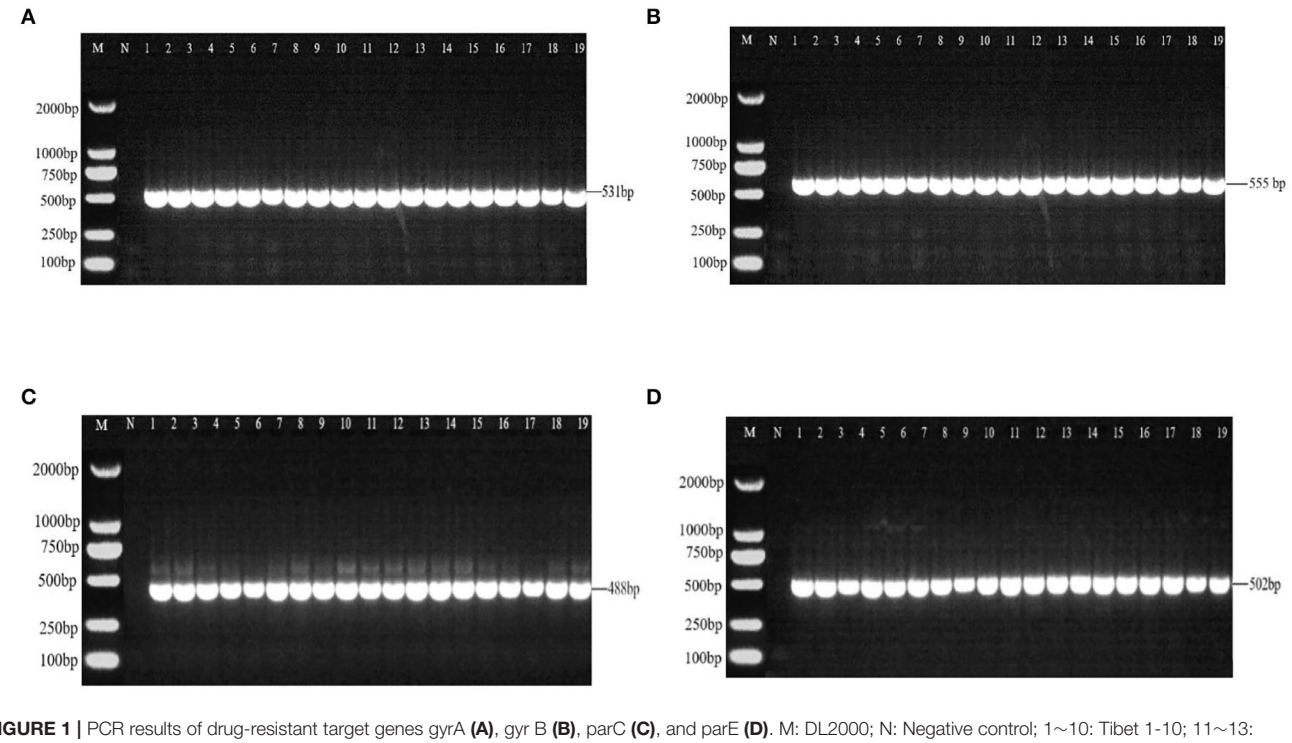

FIGURE 1 | PCR results of drug-resistant target genes gyrA **(A)**, gyr B **(B)**, parC **(C)**, and parE **(D)**. M: DL2000; N: Negative control; 1∼10: Tibet 1-10; 11∼13: CIP-inducible strains; 14∼16: ENR-inducible strains; 17 ∼19: NOR-inducible strains.

RESULTS

Antibiotic Susceptibility Testing

The MIC results of the 10 strains showed that Tibet-1 was resistant to CIP; Tibet-6 was resistant to SPE, GEN, CIP, and ENR; Tibet-7 was resistant to NOR; Tibet-8 was resistant to SPE and CIP; Tibet-9 was resistant to NOR; and other isolates were relatively sensitive to these antibiotics (**Table 2**).

Detection of Cross-Resistance

Three resistant strains to one fluoroquinolone antibiotic were used for cross-resistance to the other fluoroquinolone antibiotics and the same for aminoglycosides. The results showed that there was cross-resistance (**Table 3**).

PCR Results of Target Genes

There were 531 bp, 555 bp, 488 bp, and 502 bp fragments in gyrA, gyrB, parC, and parE genes for the susceptible strains, drug-resistant strains, and *in vitro*-induced strains to fluoroquinolones (**Figure 1**); there were 1,857, 1,812, and 696 bp fragments in rrs3, rrs4, and rpsE genes for the susceptible strains, drug-resistant strains, and *in vitro*-induced strains to aminoglycosides (**Figure 2**).

Analysis of Target Gene Mutations

The mutation analysis of gyrA, gyrB, parC, and parE showed that there was a nonsense mutation in parC (GAC84GAT) of clinically sensitive strains. Mutated amino acids Ser83Phe or Tyr, Ser80Ile or Arg, or Ser81Phe were detected due to base mutations

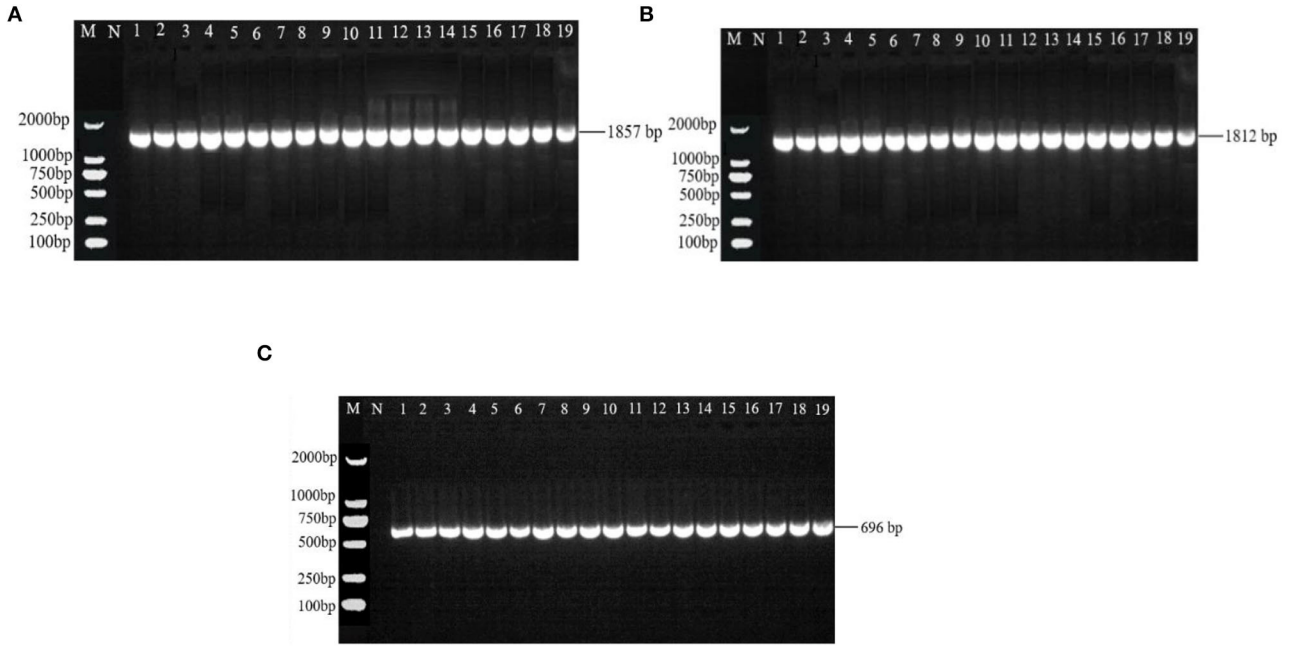

FIGURE 2 | PCR results of drug-resistant target genes rrs3 **(A)**, rrs4 **(B)**, and rpsE **(C)**. M: DL2000; N: Negative control; 1∼10: Tibet 1-10; 11∼13: SPE-inducible strains; 14∼16: GEN-inducible strains; 17∼19: KAN-inducible strains.

TABLE 4 | The QRDR mutations of clinical drug-resistant strains.

Strain name	Gene mutation site situation				
	gyrA	gyrB	parC		parE
	Ser83(TCT)		Ser 80 (AGT)	Ser 81 (TCT)	
Tibet-1 CIP	Phe (TTT)	-	-	-	-
Tibet-6 CIP	-	-	Ile (ATT)	-	-
Tibet-8 CIP	Phe (TTT)	-	-	-	-
Tibet-6 ENR	Tyr (TAT)	-	-	-	-
Tibet-7 NOR	-	-	-	Phe (TTT)	-
Tibet-9 NOR	-	-	Arg (AGA)	-	-

Tibet-1 CIP, The clinical drug-resistant strain to ciprofloxacin; the same for Tibet-6 CIP; Tibet-8 CIP; Tibet-6 ENR; Tibet-7 NOR; Tibet-9 NOR.

TCT83TTT or TAT, AGC80ATT or AGA, or TCT81TTT in gyrA or parC of six clinically resistant strains (**Table 4**). There were multiple base mutations in gyrA and parC of nine strains induced *in vitro*, the strains were highly resistant to fluoroquinolones: the amino acids Gly81Cys, Ser83Phe, and Glu87Asp or Lys were detected to be mutated due to the base mutations of GGT81TGT?TCT83TTT, and GAA87GAT orAAA in gyrA; the amino acids Ser80Ile, Ser81Tyr, and Asp84Asn or Tyr were detected to be mutated with the base mutations of AGT80ATT, TCT81TAT, and GAC84AAT or TAT in parC (**Table 5**).

The mutation analysis of rrs3, rrs4, and rpsE showed that there were no base mutation in clinically sensitive and resistant strains. There were base mutations in rrs3 and rrs4 of nine strains induced *in vitro*: it was a base mutation of A1409T in rrs3 and rrs4 of the highly resistant strain to GEN; there was a base mutation of A1408G in rrs3 and rrs4 of the highly resistant strain to KAN; one highly resistant strain to SPE had a C1192T base mutation in rrs3 and rrs4, and two strains had a C1192T base mutation in rrs3. Sense mutations were not detected in the rpsE-encoding ribosomal protein S5 (**Table 6**).

The Result of the Active Efflux System

The MIC of six antibiotics had no changes after using CCCP and VP, the result showed that there was no active efflux system based on fluoroquinolones and aminoglycosides expressed in *M. bovis* from Tibet yaks (**Tables 7**, **8**).

DISCUSSION

M. bovis is one of the most important pathogens that causes bovine respiratory syndrome (25). Therefore, *M. bovis* depends on drug treatment without a commercial vaccine outside the United States (4). The strain is relatively sensitive to aminoglycosides and fluoroquinolones. However, the large-scale use of antibiotics is contributing to the development of resistance. The action of the drug can be blunted due to drug resistance, thus affecting the health of animals and human (12).

In our study, the antibiotic susceptibility testing showed Tibet-1 was resistant to CIP; Tibet-6 was resistant to SPE, GEN, CIP, and ENR; Tibet-7 was resistant to NOR; Tibet-8 was resistant to SPE and CIP; and Tibet-9 was resistant to NOR. Half of the isolated strains were detected to be drug-resistant and Tibet-6 was resistant to four antibiotics. The drug resistance of *M. bovis* from yaks could not be ignored.

There was limited information about the resistance mechanism of *M. bovis* from yaks. In our research, the

TABLE 5 | The QRDR mutations of strains induced *in vitro* to fluoroquinolones.

Strain name	Gene mutation site situation							
	gyrA			gyrB	parC			parE
	Gly 81 (GGT)	Ser 83 (TCT)	Glu 87 (GAA)		Ser 80 (AGT)	Ser 81 (TCT)	Asp84 (GAC)	
M. bovis 1 CIP		Phe (TTT)		-	Ile (ATT)			-
M. bovis 1 ENR		Phe (TTT)		-		Tyr (TAT)		-
M. bovis 1 NOR		Phe (TTT)		-	Ile (ATT)			-
M. bovis 6 CIP	Cys (TGT)		Asp (GAT)	-	Ile (ATT)			-
M. bovis 6 ENR		Phe (TTT)		-	Ile (ATT)			-
M. bovis 6 NOR		Phe (TTT)		-		Tyr (TAT)		-
M. bovis 8 CIP			Lys (AAA)	-	Ile (ATT)		Asn (AAT)	-
M. bovis 8 ENR			Lys (AAA)	-		Tyr (TAT)		-
M. bovis 8 NOR		Phe (TTT)		-			Tyr (TAT)	-

M. bovis 1 CIP, The high drug-resistant strains induced in vitro to ciprofloxacin; the same for the others.

TABLE 6 | The mutations of target genes in strains induced *in vitro* to aminoglycosides.

Strain name	Gene mutation site situation		
	rrs 3	rrs 4	rps E (S5)
M. bovis 1 GEN	A1409G	A1409G	-
M. bovis 1 KAN	A1408T	A1408T	-
M. bovis 1 SPE	C1192T	C1192T	-
M. bovis 6 GEN	A1409G	A1409G	-
M. bovis 6 KAN	A1408T	A1408T	-
M. bovis 6 SPE	C1192T	-	-
M. bovis 8 GEN	A1409G	A1409G	-
M. bovis 8 KAN	A1408T	A1408T	-
M. bovis 8 SPE	C1192T	-	-

M. bovis 1 GEN, The high drug-resistant strains induced in vitro to gentamicin; the same for the others.

mutation analysis of rrs 3, rrs 4, and rps E showed that there was no base mutation in clinically sensitive and resistant strains to aminoglycosides. There were base mutations in rrs 3 and rrs4 of nine strains induced *in vitro*: there was a base mutation of A1409T in rrs 3 and rrs 4 of the highly resistant strain to GEN; there was a base mutation of A1408G in rrs3 and rrs4 of the highly resistant strain to KAN; and one highly resistant strain to SPE had a C1192T base mutation in rrs3 and rrs4, two strains had a C1192T base mutation in rrs3, and a sense mutation was not detected in the rpsE-encoding ribosomal protein S5. The strains were disrupted with the binding between aminoglycosides and the site in 16S rRNA due to inhibition of polypeptide synthesis (16). Base mutation and the corresponding amino acid mutation have been associated with aminoglycoside resistance. Thus, we concluded that the single base mutation of 16Sr RNA (rrs3 or rrs4) would mediate the resistance of *M. bovis* from yaks to aminoglycosides. The result was the same as that of previous studies and further confirmed the drug-resistance mechanism of *M. bovis* to aminoglycosides (16, 17). The previous research showed that all strains with high resistance to SPE harbored a single mutation the at rrs gene (C1192A in naturally resistant mutants and C1192T mutation in resistant mutants) (26). Meanwhile, there were A1408G and G1488A mutations in 16S rRNA of the Mb218 strain to GEN (27). This was similar to our study.

In our study, a single-site base mutation was detected in gyrA (Ser83Phe) or parC (Ser80Ile) for the clinically resistant strain, both base mutations were found in gyrA (Gly81Cys, Ser83Phe, and Glu87Asp or Lys) and parC (Ser80Ile, Ser81Tyr, and Asp84Asn or Tyr) in the highly resistant strain to fluoroquinolones. DNA gyrase and DNA topoisomerase IV were essential enzymes to fluoroquinolone targeting with two subunits (DNA gyrase: gyrA2gyrB2; DNA topoisomerase IV: parC2parE2). The base mutation in gyrA and parC was the main reason for the resistance to fluoroquinolone compared with that in gyrB and parE (19). The increasing fluoroquinolone resistance was found with both mutations in DNA gyrase and DNA topoisomerase IV (28). For *M. bovis*, the previous research showed that Ser83Phe in gyrA and Asp84Asn in parC point mutation were required for resistance to ENR (18). Japanese researchers found that resistant isolates to fluoroquinolones had a mutation in GyrA (Ser83Leu or Phe) and ParC (Ser81Pro or Ile) (19). The same results were also proved by a French researcher (29).

On the other hand, the previous research showed that the cytoplasmic drug concentrations were decreased by active efflux and reductions in influx. Plasmids were the type of DNA in bacteria and disseminated between cells. Plasmids could help bacteria cope with unfavorable environments by transfer accessory genes (30). The active efflux system results of *M. bovis* showed that there was no active efflux system based on fluoroquinolones and aminoglycosides expressed in *M. bovis* from yaks, and the existence of endogenous plasmids needs further study.

CONCLUSION

The isolated strains of *M. bovis* from yaks in Tibet had varying degrees of resistance to fluoroquinolones and aminoglycosides.

TABLE 7 | The MIC effects of fluoroquinolones by using CCCP and VP.

Strain	MIC (ug/mL)								
	CIP	CCCP	VP	ENR	CCCP	VP	NOR	CCCP	VP
	CIP				ENR	ENR		NOR	NOR
Tibet-1	8	8	8	2	2	2	1	1	1
Tibet-2	2	2	2	2	2	2	0.25	0.25	0.25
Tibet-3	2	2	2	1	1	1	0.25	0.25	0.25
Tibet-4	1	1	1	0.5	0.5	0.5	2	2	2
Tibet-5	0.5	0.5	0.5	2	2	2	0.5	0.5	0.5
Tibet-6	4	4	4	8	8	8	2	2	2
Tibet-7	0.5	0.5	0.5	0.25	0.25	0.25	4	4	4
Tibet-8	4	4	4	0.5	0.5	0.5	1	1	1
Tibet-9	1	1	1	0.25	0.25	0.25	4	4	4
Tibet-10	0.5	0.5	0.5	1	1	1	0.5	0.5	0.5
M. bovis 1	512	512	512	256	256	256	512	512	512
M. bovis 6	512	512	512	256	256	256	512	512	512
M. bovis 8	512	512	512	256	256	256	512	512	512

Tibet 1-10: the clinical strains; M. bovis 1, 6, and 8: the highly resistant strains induced in vitro.

TABLE 8 | The MIC effects of aminoglycosides by using CCCP and VP.

Strain	MIC (ug/mL)								
	SPE	CCCP	VP	GEN	CCCP	VP	KAN	CCCP	VP
		SPE	SPE		GEN	GEN		KAN	KAN
Tibet-1	64	64	64	16	16	16	8	8	8
Tibet-2	32	32	32	8	8	8	8	8	8
Tibet-3	32	32	32	8	8	8	4	4	4
Tibet-4	16	16	16	2	2	2	2	2	2
Tibet-5	16	16	16	2	2	2	16	16	16
Tibet-6	128	128	128	64	64	64	2	2	2
Tibet-7	8	8	8	8	8	8	2	2	2
Tibet-8	128	128	128	1	1	1	4	4	4
Tibet-9	4	4	4	1	1	1	1	1	1
Tibet-10	4	4	4	2	2	2	8	8	8
M. bovis 1	512	512	512	512	512	512	512	512	512
M. bovis 6	512	512	512	512	512	512	512	512	512
M. bovis 8	512	512	512	512	512	512	512	512	512

Tibet 1-10: the clinical strains; M. bovis 1, 6, and 8: the highly resistant strains induced in vitro.

The mechanism of resistance to fluoroquinolones and aminoglycosides was identified preliminarily for *M. bovis* from yaks: the single-site base mutation mediated the resistance of *M. bovis* from yaks and both base mutations led to the highly resistant strain (aminoglycosides: rrs3 and rrs4; fluoroquinolones: gyrA and parC). The research could provide a reference for clinical treatment of *Mycoplasma bovis*.

DATA AVAILABILITY STATEMENT

The original contributions presented in the study are included in the article/supplementary material, further inquiries can be directed to the corresponding authors.

AUTHOR CONTRIBUTIONS

JN and SS conceived and designed the study. JN and MY executed the experiment and analyzed the sera and tissue samples. ZC, JX, and YX analyzed the data. All authors interpreted the data, critically revised the manuscript for important intellectual content, and approved the final version.

FUNDING

This study was supported by the key research and development program of Tibet Autonomous Region (XZ202001ZY0046N) and the Chinese Agricultural Research Service (CARS-37).

REFERENCES

1. Arcangioli MA, Duet A, Meyer G, Dernburg A, Bézille P, Poumarat F. The role of *Mycoplasma bovis* in bovine respiratory disease outbreaks in veal calf feedlots. *Vet J.* (2008) 177:89–93. doi: 10.1016/j.tvjl.2007.03.008
2. Maunsell FP, Woolums AR, Francoz D, Rosenbusch RF, Step DL, Wilson DJ. *Mycoplasma bovis* infections in cattle. *J Vet Internal Med.* (2011) 25:772–83. doi: 10.1111/j.1939-1676.2011.0750.x
3. Hale HH, Helmboldt CF, Plastridge WN, Stula EF. Bovine mastitis caused by Mycoplasma species. *Cornell Vet.* (1962) 52:582–91.
4. Wang HY, Wu H. Effects of different tea extract on milk performance and blood antioxidant index in dairy cows. *China Dairy Cattle.* (2014) 2014:36–41. doi: 10.3969/j.issn.1004-4264.2014.07.011
5. Li JS. Mycotic mastitis in cattle. *Shanghai J Anim Husbandry Vet Med.* (1983) 04:46.
6. Xin JQ, Li Y, Guo D, Song N, Cao P. First isolation of *Mycoplasma bovis* from calf lung with pneumoniae in China. *Chin J Prev Vet Med.* (2008) 30:661–4.
7. Si L, Gong R, Yin ZY. Preliminary diagnosis of cattle infectious *Mycoplasma bovis* pneumonia. *J Huazhong Agric Univer.* (2008) 27:572. doi: 10.13300/j.cnki.hnlkxb.2008.04.020
8. Hu CM, Si L, Gong *R,* Bai Z, Guo ZD, Progress on bovine mycoplasmosis. *Progr Vet Med.* (2009) 30:73–7. doi: 10.16437/j.cnki.1007-5038.2009.08.021
9. Zhang L, Li YP, Li XM, Ni M. Drug sensitivity test of *Mycoplasma bovis*. *Adv Vet Med.* (2012) 33:110–3. doi: 10.16437/j.cnki.1007-5038.2012.02.030
10. Gao D. *Isolation and Identification of Mycoplasma bovis and the Resistance to macrolide Antibiotics*. Jilin: Jilin Agricultural University (2015).
11. Niu J, Wang D, Yan M, Chang Z, Bi DR. Isolation, identification and biological characteristics of *Mycoplasma bovis* in yaks. *Microb Pathog.* (2021) 150:104691. doi: 10.1016/j.micpath.2020.104691
12. Kong LC, Zhang CY, Gao YH, Ma HX. Research progress on drug resistance of *Mycoplasma bovis*. *Chin J Vet Med.* (2013) 47:63–5.
13. Victor TC, Van RA, Jordaan AM. Sequence polymorphism in the rrs gene of *Mycobacterium tuberculosis* is deeply rooted within an evolutionaryclade and is not associated with streptomycin resistance. *J Clin Microbiol.* (2001) 39:4184–6. doi: 10.1128/JCM.39.11.4184-4186.2001
14. Kehrenberg C, Schwarz S. Mutations in 16S rRNA and ribosomal protein s5 associated with high-level spectinomycin resistance in *Pasteurella multocida*. *Antimicrob Agents Chemother.* (2007) 51:2244–6. doi: 10.1128/AAC.00229-07
15. Konigesson MH, Bolske G, Johansson KE. Intraspecific variation in the 16S r RNA genes sequences of *Mycoplasma agalactiae* and *Mycoplasma bovis* strainss. *Vet Microbiol.* (2002) 85:209–20. doi: 10.1016/S0378-1135(01)00517-X
16. Amram E, Mikula I, Schnee C, Ayling RD, Nicholas R, Rosales RS. 16S r RNA gene mutations associated with decreased susceptibility to tetracycline in *Mycoplasma bovis*. *Antimicrob Agents Chemother.* (2015) 59:796–802. doi: 10.1128/AAC.03876-14
17. Jia BY. *Preliminary Study on the Resistance Mechanism of Mycoplasma bovis to Fluoroquinolones and Aminoglycoside Antibiotics*. Jilin: Jilin Agricultural University (2017).
18. Lysnyansky I, Mikula I, Gerchman I, Levisohn S. Rapid detection of a point mutation in the parC Gene associated with decreased susceptibility to fluoroquinolones in *Mycoplasma bovis*. *Antimicrob Agents Chemother.* (2009) 53:4911–4. doi: 10.1128/AAC.00703-09
19. Sato T, Okubo T, Usui M, Higuchi H, Tamura Y. Amino acid substitutions in GyrA and ParC are associated with fluoroquinolone resistance in *Mycoplasma bovis* isolates from Japanese dairy calves. *J Vet Med Sci.* (2013) 75:1063–5. doi: 10.1292/jvms.12-0508
20. Mustafa R, Qi J, Ba X, Chen Y, Hu C, Liu X, et al. *In vitro* quinolones susceptibility analysis of Chinese *Mycoplasma bovis* isolates and their phylogenetic scenarios based upon QRDRs of DNA topoisomerases revealing a unique transition in ParC. *Pak Vet J.* (2013) 33:364–9.
21. Sebastien F, Keith P. Oxidative stress induction of the mex XY multidrug efflux getransporters. *Microbiol Mol Biol Rev.* (2000) 64:672. doi: 10.1128/MMBR.64.4.672-693.2000
22. Jiang XB. *Mechanism Study of Plasmid-Mediated Quinolone Resistance in Escherichia coli*. Guangzhou: South China Unoversity of Technology (2013).
23. Zhai XH. *Establishment of Recombinase Polymerase Amplification (RPA) for Detection of Mycoplasma bovis and the Method for Sample DNA Extraction*. Guangzhou: Chinese Academy of Agricultural Sciences (2019).
24. CLSI. *Performance Standards for Antimicrobial Disk and Dilution Susceptibility Tests for Bacteria Isolated from Animals; Approved Standard-Fourth Edition. CLSI document VET01-A4*. Wayne, PA: Clinical and Laboratory Standards Institute (2015).
25. Nicholas RAJ, Ayling RD. *Mycoplasma bovis*: disease, diagnosis and control. *Res Vet Sci.* (2003) 74:105–12. doi: 10.1016/S0034-5288(02)00155-8
26. Sulyok KM, Kreizinger Z, Wehmann E, Lysnyansk I, Gyuranecz M. Mutations associated with decreased susceptibility to seven antimicrobial families in field and laboratory-derived *Mycoplasma bovis* strains. *Antimicrob Agents Chemother.* (2017) 61:e01983–916. doi: 10.1128/AAC.01983-16
27. Bokma J, Vereecke N, Nauwynck H, Haesebrouck F, Theuns S, Pardon B. Genome-wide association study reveals genetic markers for antimicrobial resistance in *Mycoplasma bovis*. *Microbiol Spectr.* (2021) 9:e0026221. doi: 10.1128/Spectrum.00262-21
28. Veziris N, Chauffour A, Escolano S, Henquet S, Matsuoka M, Jarlier V, et al. Resistance of *M. leprae* to quinolones: a question of relativity? *PLoS Negl Trop Dis.* (2013) 7:e2559. doi: 10.1371/journal.pntd.0002559
29. Khalil D, Becker CA, Tardy F. Alterations in the quinolone resistance-determining regions and fluoroquinolone resistance in clinical isolates and laboratory-derived mutants of *Mycoplasma bovis*: not all genotypes may be equal. *Appl Environ Microbiol.* (2015) 82:1060–8. doi: 10.1128/AEM.03280-15
30. Hernández-Beltrán JCR, San Millán A, Fuentes-Hernández A, Peña-Miller R. Mathematical models of plasmid population dynamics. *Front Microbiol.* (2021) 12:606396. doi: 10.3389/fmicb.2021.606396

Conflict of Interest: The authors declare that the research was conducted in the absence of any commercial or financial relationships that could be construed as a potential conflict of interest.

frontiers | Frontiers in Veterinary Science

TYPE Original Research
PUBLISHED 11 August 2022
DOI 10.3389/fvets.2022.925590

OPEN ACCESS

EDITED BY
Fazul Nabi,
Lasbela University of Agriculture, Water and Marine Sciences, Pakistan

REVIEWED BY
XiuKai Cao,
Yangzhou University, China
Ali Raza Jahejo,
Shanxi Agricultural University, China
Ayman Hassan Abd El-Aziz,
Damanhour University, Egypt

*CORRESPONDENCE
Linsen Zan
zanlinsen@163.com

†These authors have contributed equally to this work

SPECIALTY SECTION
This article was submitted to Comparative and Clinical Medicine, a section of the journal Frontiers in Veterinary Science

RECEIVED 21 April 2022
ACCEPTED 19 July 2022
PUBLISHED 11 August 2022

CITATION
Wang J, Li B, Yang X, Liang C, Raza SHA, Pan Y, Zhang K and Zan L (2022) Integration of RNA-seq and ATAC-seq identifies muscle-regulated hub genes in cattle.
Front. Vet. Sci. 9:925590.
doi: 10.3389/fvets.2022.925590

Integration of RNA-seq and ATAC-seq identifies muscle-regulated hub genes in cattle

Jianfang Wang[1†], Bingzhi Li[1†], Xinran Yang[1], Chengcheng Liang[1], Sayed Haidar Abbas Raza[1], Yueting Pan[1], Ke Zhang[1] and Linsen Zan[1,2*]

[1]College of Animal Science and Technology, Northwest A&F University, Xianyang, China, [2]National Beef Cattle Improvement Center, Northwest A&F University, Xianyang, China

As the main product of livestock, muscle itself plays an irreplaceable role in maintaining animal body movement and regulating metabolism. Therefore, it is of great significance to explore its growth, development and regeneration to improve the meat yield and quality of livestock. In this study, we attempted to use RNA-seq and ATAC-seq techniques to identify differentially expressed genes (DEGs) specifically expressed in bovine skeletal muscle as potential candidates for studying the regulatory mechanisms of muscle development. Microarray data from 8 tissue samples were selected from the GEO database for analysis. First, we obtained gene modules related to each tissue through WGCNA analysis. Through Gene Ontology (GO) functional annotation, the module of lightyellow ($ME_{lightyellow}$) was closely related to muscle development, and 213 hub genes were screened as follow-up research targets. Further, the difference analysis showed that, except for PREB, all other candidate hub genes were up-regulated (muscle group vs. other-group). ATAC-seq analysis showed that muscle-specific accessible chromatin regions were mainly located in promoter of genes related to muscle structure development (GO:0061061), muscle cell development (GO:0055001) and muscle system process (GO:0003012), which were involved in cAMP, CGMP-PKG, MAPK, and other signaling pathways. Next, we integrated the results of RNA-seq and ATAC-seq analysis, and 54 of the 212 candidate hub genes were identified as key regulatory genes in skeletal muscle development. Finally, through motif analysis, 22 of the 54 key genes were found to be potential target genes of transcription factor MEF2C. Including *CAPN3*, *ACTN2*, *MB*, *MYOM3*, *SRL*, *CKM*, *ALPK3*, *MAP3K20*, *UBE2G1*, *NEURL2*, *CAND2*, *DOT1L*, *HRC*, *MAMSTR*, *FSD2*, *LRRC2*, *LSMEM1*, *SLC29A2*, *FHL3*, *KLHL41*, *ATXN7L2*, and *PDRG1*. This provides a potential reference for studying the molecular mechanism of skeletal muscle development in mammals.

KEYWORDS

muscle, RNA-seq, WGCNA, hub genes, ATAC-seq, transcription factor

Introduction

The focus of the adjustment of the new agricultural industrial structure is to develop high-quality and efficient stock husbandry. Compared with pig and poultry breeding, cattle breeding can greatly improve the utilization of straw resources and reduce environmental pollution, so it plays an increasingly important role in the development of animal husbandry. As the largest tissue of cattle organisms, the growth, development and genetic characteristics of skeletal muscle affect and even determine the meat production performance of cattle (1). Many factors are closely related to muscle tenderness and affect meat product quality, such as intramuscular fat content, muscle fiber size, and intramuscular protein content and types (2–5). The growth and development of skeletal muscle is an extremely complex biological process, which is co-regulated by a variety of regulatory factors.

Transcription factors (TFs) are critical in muscle growth and development. Members of the myogenic regulatory factor (MRF) family are typical inducers of skeletal muscle development, including the early myogenic regulatory factors (MYOD, MYF5, MYF6, MRF4, et al.) and the late differentiation marker gene (MyoG) (6). Myocyte enhancer Factor-2 (MEF2) family (MEF2a, MEF2b, MEF2c, and MEF2d) is a kind of key transcription factor discovered after MyoD, which controls the expression of myogenic genes (7). The N-terminal of MEF2 contains a highly conserved MADS-Box domain and its adjacent MEF2 domain. The MADS-Box domain mediates protein dimerization, while the MEF2 domain influences its binding affinity with DNA and its interaction with cofactors (7–9). It has been reported that MEF2s was involved in regulating the proliferation and differentiation of myocyte mainly through participating in Ca^{2+}-calmodulin-dependent protein kinases CaMK-histone deacetylases HDACs, Calconneurin, MAPK and other signaling pathways (10, 11). In addition, with the rise of RNA-seq technology, a large number of genes related to muscle development have been discovered successively, but the signal regulatory networks between genes and genes, transcription factors and target genes, and epistasis and genes are still poorly understood. Moreover, we focused more on finding the few regulators that play a dominant role in the complex regulatory network and exploring their relevant regulatory mechanisms *in vivo*.

As chromatin is the carrier of genes, the activation and silencing of genes will inevitably cause the remodeling of chromatin structure. ATAC-seq is a newly developed technique to study the open regions of genomic chromatin, which helps to elucidate the regulatory mechanisms of genes (12). In recent years, a large number of researchers began to explore the relationship between chromatin open region and gene expression, including domestic animals. A study found a group of highly functionally conserved gene regulatory elements in different tissues by comparing the genomes of three domestic animals (Gallus Galla, Sus Scrofa, Bos Taurus) to human and mouse genomes (13). Furthermore, by comparing chromatin accessibility in muscle, liver and hypothalamus of Bos indicus cattle, learned that MEF2 is the main regulator of muscle-specific open chromatin region (14). Combined with previous studies, we intend to further explore the key regulatory genes involved in skeletal muscle development by comparing the sequencing data of muscle and other tissues, and explore the transcription factors that may be regulated, which will provide some methodological guidance and reference value for the screening and functional research of core genes.

Materials and methods

Data acquisition

The workflow of this study was shown in Figure 1. The data used in this study was from GSE158430 of the GEO database (GEO Accession viewer (nih.gov) (13). GSE158430 is a SuperSeries and has three SubSeries (GSE158412, GSE158414, and GSE158416). GSE158412 dataset contains RNA sequencing data from 8 different tissues (liver, lung, spleen, skeletal muscle, subcutaneous adipose, cerebellum, brain cortex, and hypothalamus) of cattle, pigs, and chickens, with two biological replicates. GSE158414 dataset includes ATAT-seq data from different tissues of cattle and pigs with two biological replicates (except cerebellum tissue in cattle). GSE158416 was CTCF ChIP-seq in 8 different tissues of the above livestock species, which also has two biological replicates. We only downloaded the SRA format data of cattle in GSE158412 and GSE158414 for subsequent analysis (see Supplementary Table 1 for details). The SRA format was then converted to fastq format using sratools' fastq-dump command (15).

Expression matrix pre-processing

To obtain high-quality clean reads, Trimmomatic (v0.36) (16) and FastQC (http://www.bioinformatics.babraham.ac.uk/projects/fastqc/) were used to filter and evaluate the quality of sequencing reads. Clean reads were mapped to cattle (*Bos taurus*) reference genome from Ensembl Genome Browser 104 (http://asia.ensembl.org/index.html) using hisat2 (v2.1.0) (17). SAMtools (v1.7) was used to convert the sam files obtained from mapping to bam files (18). Two important values representing gene expression were tallied: reads count was quantified with featureCounts (v1.6.0) (19), The FPKM (fragments per kilobase of transcript per million fragments mapped) were calculated using StringTie (v2.1.2) (20). Further, the genes were annotated through Ensembl Genome Browser 104 database, and protein-coding genes (PCGs) were screened for WGCNA and Differently Expression analysis (21).

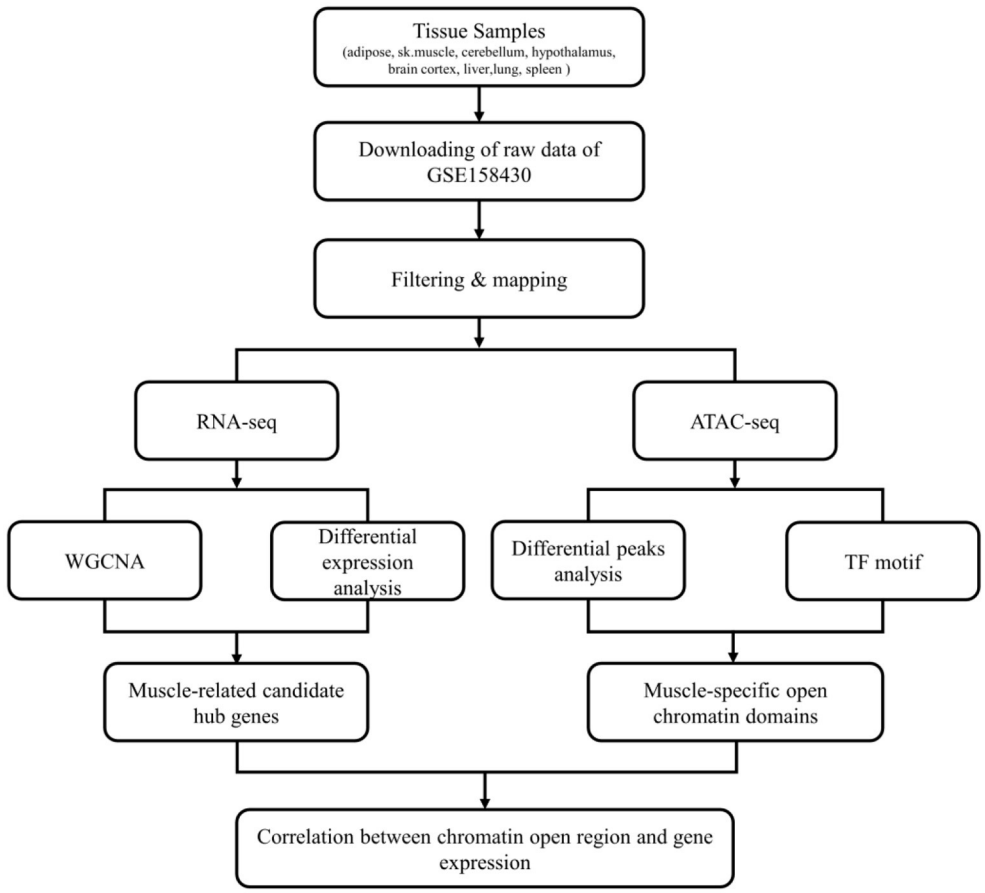

FIGURE 1
The flow chart of whole analysis.

Weighted gene coexpression network analysis

The top 75% of PCGs with the highest median absolute deviation (MAD) were constructed the co-expression network with the value of $\log_2$(FPKM+1) using WGCNA package (v1.70) from Bioconductor in RStudio (v1.2) (http://www.rstudio.org), an integrated development environment for R (v4.0.2). Then, the weighted adjacency matrix of 16 tissue samples was constructed by the formula of the adjacency matrix: amn = |cor(mn)|β (amn, adjacency between m and n; cor(mn), Pearson's correlation between m and n; and β, soft-power threshold) (22). Subsequently, the adjacency matrix was transformed into a topological overlap matrix (TOM) to quantitatively describe the similarity in nodes by comparing the weighted correlation between two nodes and other nodes. Next, hierarchical clustering was used to identify modules according to the TOM matrix with the minModuleSize 100. Similar modules (>75%) were merged (abline = 0.25).

Identification of sample significant modules and hub genes

Module-sample associations were estimated according to TOM ($|cor| > 0.5$, $P < 0.01$). The same module of genes is generally considered to have a higher topological overlap similarity. For each expression profile, gene significance (GS, the correlation between expression profile and each sample) and module membership [MM, the correlation between the module eigengene (ME) and the gene expression profile] were used to identify the Module-sample correlation. Finally, hub genes screened with MM > 0.8 and GS > 0.6 with weighted *P*-value (*P*.weighted) < 0.01.

RNA differential expression analysis

The expression matrix of whole genes was used for further analysis of gene expression differences among different samples by DEseq2 in R software (23). False Discovery Rate (FDR) was

got by adjusting the *P*-value. Genes with fold change > 2 and false discovery rate (FDR) < 0.05 were set as the threshold to be DEGs.

ATAC-seq analysis

First, FastQC was used to detect data quality. The clean reads were obtained by removing low-quality fragments using Fastp (v0.19.4) (24). BWA (Burrows-Wheeler Alignment) (v0.7.17) was used to map clean reads to cattle (Bos taurus) reference genome. Genrich (v0.6.1) was used to calling peaks for each sample (https://github.com/jsh58/Genrich). The different peaks were identified using DiffBind (https://bioconductor.org/packages/release/bioc/html/DiffBind.html) (v2.16.2) with the default parameters (25). ChIPseeker (v1.24.0) (26) was used to annotate the differential peaks according to the Ensembl Genome Browser 104 (http://asia.ensembl.org/index.html) and org.Bt.eg.db (https://bioconductor.org/packages/release/data/annotation/html/org.Bt.eg.db.html). During the genome-wide annotation of peaks, the genome-wide functional regions were divided into promoter, dowstream, exon, intron and distal intergenic regions. The closest gene to each peak can be obtained according to the distance of each binding site to TSS, and their specific distribution of binding sites on the genome can be found out. This study considered the profile of peaks at their ± 3 kb of the transcription start site (TSS) as promoter genes or targets. The motifs were examined using the Multiple EM for Motif Elicitation (MEME) suite (https://meme-suite.org/meme/doc/meme-chip.html?man_type=web). Then, the Motif database scanning algorithm TOMTOM was used to predict transcription factors (TFs) (27). ATACseqQC (v1.12.5) was used for quality detection and motif footprint analysis (28). FIMO was used to scan binding locations of TFs in the promoter regions of DEGs (upstream 2,000 bp and downstream 100 bp) (29).

Gene ontology and kyoto encyclopedia of genes and genomes analysis

To explore the potential biological roles of module genes, Gene Ontology (GO) functional annotation for multiple gene lists was analyzed using clusterProfile (30). And the GO analysis for the Single-gene list was carried out by g:Profiler (https://biit.cs.ut.ee/gprofiler/gost) with the default parameters (31). KEGG pathway analyses were performed using KOBAS (32). We used a significant threshold *P*-value adjusted by Benjamini and Hochberg of 0.05 for KEGG to control the false discovery rate (FDR) and used Fisher's Exact Test as the statistical test method.

Real-time quantitative PCR

The total RNA from bovine tissues or cells was extracted by Trizol reagent kit (Invitrogen, Carlsbad, CA, USA) and then PrimeScript™ RT reagent Kit (Takara, Dalian, China) was used to synthesize cDNA. Real-time quantitative PCR (qRT-PCR) was used to measure the mRNA expression levels (Supplementary Table 2) with TB Green® Premix Ex Taq™ II (Takara, Dalian, China) and CFX Connect Real-Time PCR Detection System. The amplification procedure was as follows: 95°C, 30 s; followed by 40 cycles (95°C, 5 s; 60°C, 30 s) and stored at 4°. Quantitative results were analyzed by the $2^{-\Delta\Delta Ct}$ method for relative expression. All samples contained 3 biological replicates and 3 technical replicates. All data are expressed as Mean ± SD. The unpaired two-tailed Student's *t*-test was used for statistical analysis. In this study, lowercase letters a-g were used to indicate significance ($P < 0.05$).

Results

Construction of co-expression network and identification of muscle-related modules

GSE158412 dataset contains 16 tissue samples of cattle. Before the analysis, we first tested the credibility of biological repetition of the samples by principal component analysis, and the result showed that there was clustering between 2 repeats of 8 tissues (Figure 2A). All samples could be used for analysis. After processing raw data, the gene expression matrix for 10,034 protein-coding genes was obtained. Among them, 7,525 genes (the top 75% of the median absolute deviation) were used to construct the weighted co-expression network. The Pearson's correlation coefficient (PCC) was performed to construct the sample clustering tree (Figure 2B). Then, WGCNA's pickSoftThreshold function was selected to estimate the best value of power (β). In this study, the best value of power was estimated as 9 (β = 9) (scale-free $R^2 = 0.85$) (Figure 2C). The scale-free topology was performed to test the reliability of β = 9 (Figure 2D). Furthermore, the dynamic hierarchical tree cutting algorithm was used to detect common expression modules, and then similar modules (minimum height was set to 0.25) were combined (Figure 2E). Finally, a total of 18 modules were identified (Figures 2E,F). The eigengenes contained in each module was provided in Supplementary Table 3. The correlation between modules and samples was shown in Figure 3A. We found that four modules were highly correlated with muscle tissue, namely ME_{cyan} (cor = 0.74, $P = 0.001$), $ME_{midnightblue}$ (cor = 0.75, P = 8E-04), ME_{grey60} (cor = 0.74, $P = 0.001$) and $ME_{lightyellow}$ (cor = 0.97, P = 1E-09). The adjacency heatmap of the relationship for each model was shown in Figure 3B. In addition, GS and MM were highly correlated (cor

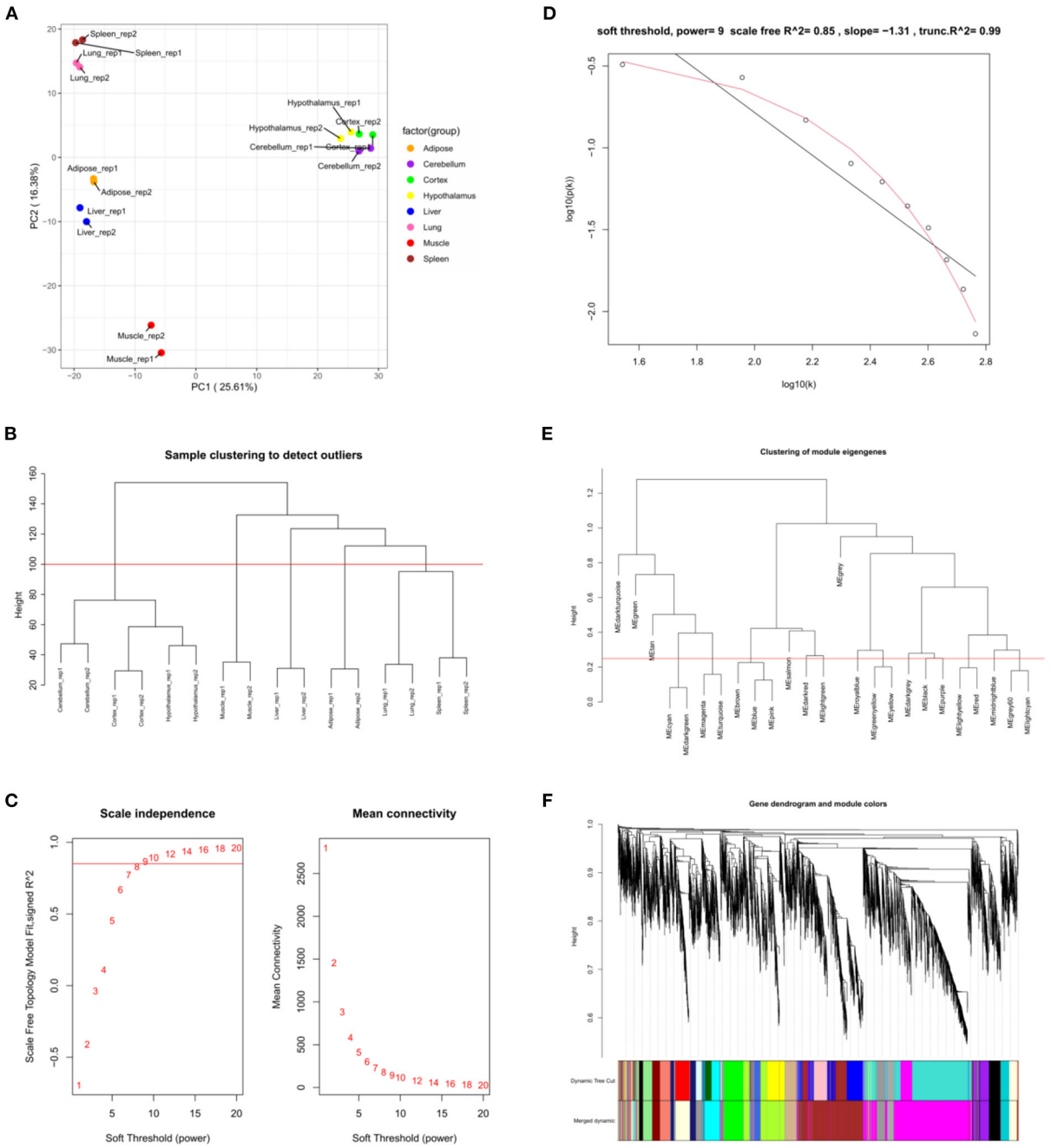

FIGURE 2
Weighted co-expression network analysis. **(A)** Principal component analysis of all samples. **(B)** Sample clustering tree. The red line represents the outlier elimination reference line; **(C)** Soft-threshold powers (β) filtering analysis. The mean connectivity (y-axis) for various soft-threshold powers (x-axis) was showed on the left, and the mean connectivity (y-axis) of different soft-thresholding power (x-axis) was showed on the right; **(D)** Checking the scale-free topology when β = 9. X-axis: the log10 (network connectivity), y-axis: log10 (the corresponding frequency distribution). The distribution approximates a straight line, which is called the approximately scale-free topology; **(E)** The clusting of module eigengenes. The red line represents the reference line for similar module merging; **(F)** The cluster dendrogram of modules.

= 0.89, P =1.8E-178), suggesting that genes that are highly correlated with the characteristics of muscle samples are also the most important (central) elements of modules associated with that sample (Figure 3C). Through roughly performing GO annotation on eigengenes of each module, we found that ME module with the highest correlation to muscle development, including regulation of muscle adaptation and muscle system process, etc. (Figure 3D). Therefore, this study finally extracted

the $ME_{lightyellow}$ module for further analysis. In $ME_{lightyellow}$, 213 out of 519 genes (∼41%) met the screening conditions of hub genes (MM > 0.8, GS > 0.6, *P.weighted* < 0.01) in Supplementary Table 4.

Screening of candidate hub genes with differential expression

In this section, 10,034 protein-coding genes were analyzed to identify muscle-specific DEGs. The result showed that a total of 4,815 DEGs were found, including 1,697 DEGs (up-regulated) in the muscle group and 3,118 DEGs (down-regulated) in the other-group. The analysis profile of DEGs was visualized in Figure 4A. The top 10 up-regulated DEGs were *CKM*, *TNNC1*, *MYOT*, *SLN*, *ACTA1*, *MYL1*, *TNNC2*, *MYLPF*, *MYH2*, and *MYL2*, and the top 10 down-regulated DEGs were *GAD2*, *CLVS2*, *NRXN3*, *CELF3*, *ST8SIA3*, *GRM5*, *GRIN1*, *SCRT1*, *GRIN2A*, and *MYT1* (Table 1; Supplementary Table 5). GO and KEGG results are provided in the supplied materials (Supplementary Tables 6–9). Further analysis found that 212 candidate hub genes (no include PREB) related to muscle development were finally screened by integration difference analysis and WGCNA analysis (Figure 4B). GO analysis was performed on these 212 candidate hub genes with different changes, and the result showed that these genes were also enriched in terms related to muscle development (Figure 4C; Supplementary Table 10), demonstrating the feasibility of integrating differential analysis and WGCNA to obtain muscle-related hub genes.

The landscape of genomic chromatin accessibility

To analyze the influence of chromatin open region on the differential expression of the candidate hub genes, the ATAC-seq technique was applied for further analysis. The raw data of GSE158414 were re-analyzed to obtain the open chromatin region of each sample. Simply, clean reads were first obtained by removing low-quality reads and adaptors, and then mapped to the reference genome (*Bos taurus*). Genrich (https://github.com/jsh58/Genrich) is a new software for analyzing ATAC-seq. It can remove mitochondrial reads, PCR repeats, multiple mapping reads, and multiple biological repeats with just one command. So, Genrich software was used to call peak in this study. The number of peaks for each sample was counted and stored in Supplementary Table 11. To determine whether the sequencing fragments were the open regions of the genome, all samples were selected for the analysis of the distribution of fragment lengths. In all samples analyzed, the 100 bp single-nucleosome fragments in leftmost were found, rather than single or multiple-nucleosome fragments, which indicates that these peaks were from open regions of the genome (Supplementary Figure 1). All results showed the good quality of ATAC-seq. The TSS of genes with active transcription is often open, so the signal profile near TSS is another important factor to identify the quality of ATAC-seq.

The correlative heatmap of tissues was shown significant differences between muscles and other tissues (Figure 5A). Next, through analyzing the differential accessible peaks, 8,963 different peaks were obtained (FDR < 0.05), including 4,564 muscle-affinitive peaks and 4,398 other-affinitive peaks in muscle vs. other. MA-plot of different peaks was shown in Figure 5B, and box-plot of binding affinity was shown in Figure 5C. The annotation result showed that most of the peaks were 10–100 kb away from TSS (Figure 5D). The distribution of these binding sites tends to be at the 3 'end of TSS, which is consistent with the results of previous studies (33). In addition, Figure 5E showed the peak enriched heatmap near TSS. Many peaks enriched near the TSS (±3 kb) of genes, indicating that transcription factors are likely to bind to these chromatin open regions.

To further explore the functional differences between muscle-affinitive peaks and other-affinitive peaks, we performed gene functional region annotation, and found that compared with other-affinitive peaks, muscle-affinitive peaks were enriched in promoter and exon regions significantly. Enrichment of distal intergenic was significantly reduced (Figure 5F). Peaks located in the promoter (called promoter-peaks) are critical to gene expression, so we extracted the genes in the promoter region for GO and KEGG analysis. The GO-BP analysis indicated that muscle-affinitive genes were related to muscle structure development (GO:0061061), muscle cell development (GO:0055001), muscle system process (GO:0003012), and so on (Figure 6A). KEGG analysis found muscle-affinitive genes were involved in cAMP, cGMP-PKG, MAPK, and other related functional pathways (Figure 6B). In addition, we found that several key TFs of muscle development were found to be significantly enriched at these ATAC-seq peaks (Figure 6C), suggesting muscle development may be related to the binding of transcription factors to open regions of chromatin.

Integration analysis of ATAC-seq and RNA-seq

To further determine the relationship between gene expression and open chromatin regions, we overlapped the analysis results from RNA-seq and ATAC-seq, respectively. Fifty-four common muscle-regulated genes were found (Figure 7A). The expression heatmap of these muscle-regulated genes was shown in Figure 7B, and we found these genes have a significant difference between muscle and other tissues. The top 20 genes with high differential expression were shown in

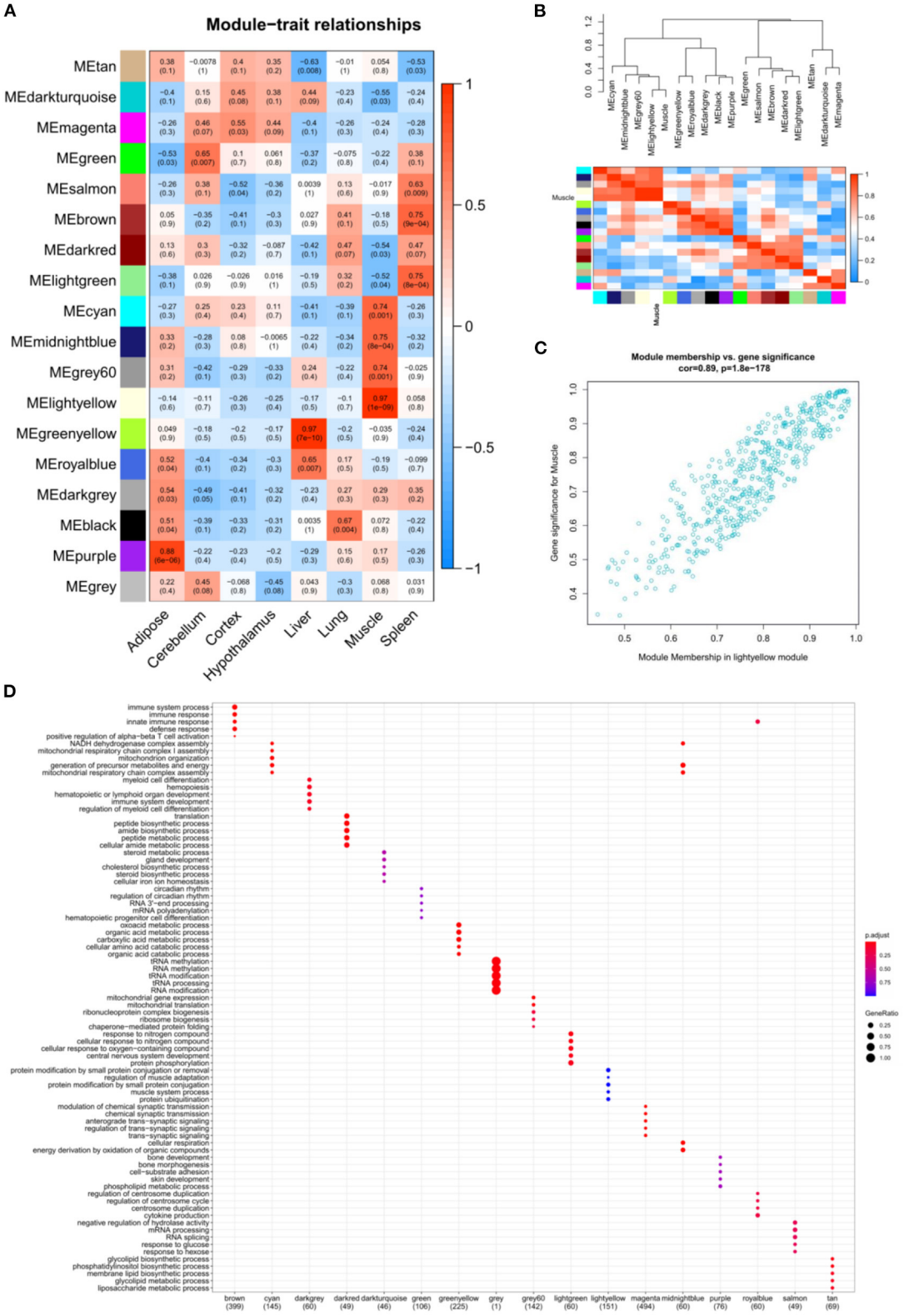

FIGURE 3
The relation analysis between modules and samples. **(A)** Heatmap of the module-sample correlation. Significance (*P*-value) was marked in parentheses. The color bar represented the magnitude of the correlation. Red: positive-correlation, blue: negative-correlation; **(B)** The adjacency heatmap of eigengene, including the module clustering tree (top) and the corresponding module clustering heatmap (below). The color bar represented the magnitude of the correlation. Red: positive-correlation, blue: negative-correlation; **(C)** The scatterplot of GS and MM in MElightyellow module; **(D)** The top 5 significant GO-BP analysis form each module eigengenes.

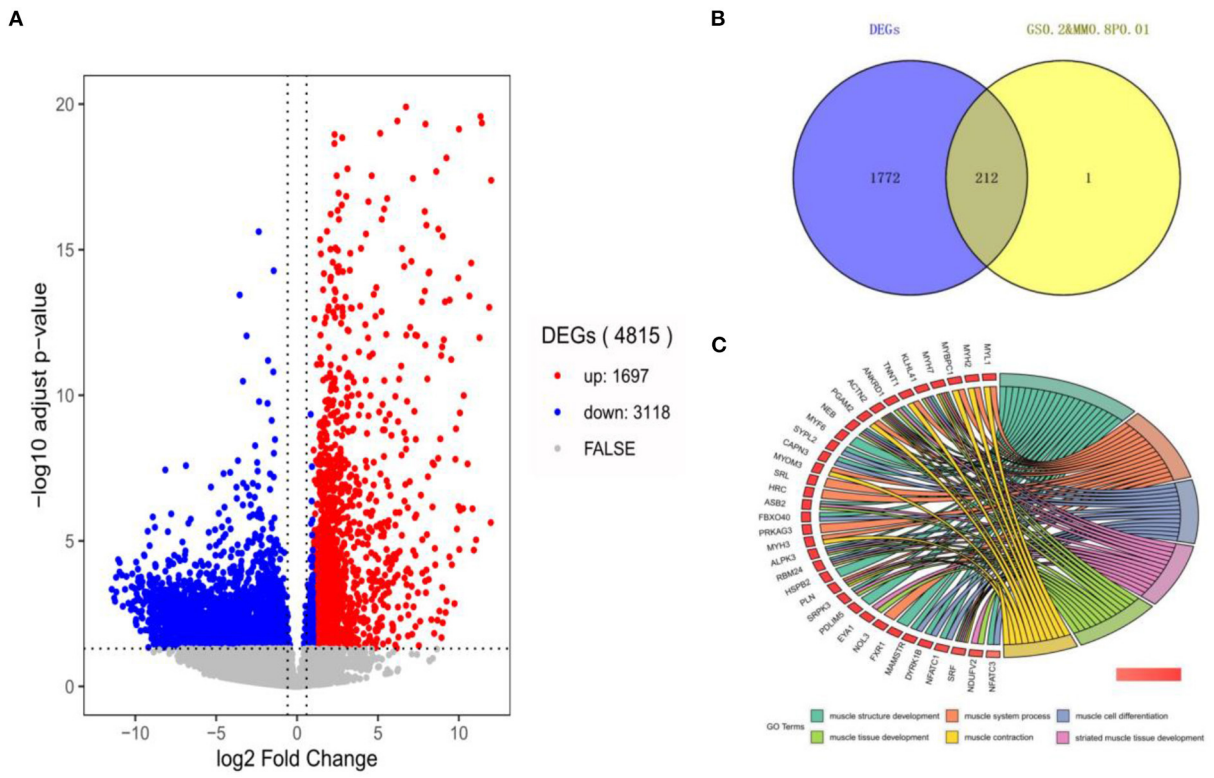

FIGURE 4
The analysis of DEGs by RNA-seq. **(A)** The volcano-plot of DEGs; **(B)** The overlap-plot of DEGs and candidate hub genes in MElightyellow; **(C)** The top 6 GO terms with the high significance of 212 candidate hub genes.

Figure 7C, including *MYOT*, *MYOM3*, Mymyon (*MB*), Kelch Like Family Member 41 (*KLHL41*), Actinin Alpha 2 (*ACTN2*), and *CAPN3* and other muscle-specific expression genes. Again, TF binding analysis was performed on the open chromatin regions corresponding to these 54 genes. The promoter-peaks of 44 of the 54 genes (∼81.48%) were enriched by MEF2C which was the only transcription factor discovered (Figure 7D). The motif footprint analysis of MEF2C was showed in Figure 7E. In addition, we extracted the promoter regions of the 54 genes (upstream 2,000 bp and downstream 100 bp) using bedtools, and analyzed whether the MEF2C promoter is binding in these genes. Twenty-two of 54 hub genes (50%) were found to have MEF2C binding sites ($P < 0.0001$) (Figure 7F). By visually selecting the interaction between these genes and the target genes in $Me_{lightylow}$ with the value of weight > 0.3, MB, HRC, KLHL41, SRL, and ALPK3 was found that occupy important positions in the regulatory network (Figure 7G). They are muscle-specific and muscle-regulated genes, suggesting that the combination of ATAC-seq and RNA-seq make our screening more accurate.

Validate the expression of hub genes

To further confirm our results, 4 high-expression hub genes in muscle, including *CAPN3* and *KLHL41* targeted by MEF2C, and dual specificity tyrosine phosphorylation regulated kinase 1B (*DYRK1B*) and MLX interacting protein (*MLXIP*), were randomly selected for qRT-PCR. The results showed that the expression of these four genes in muscle tissue was significantly higher than that in other tissues, which was highly consistent with the results of RNA-seq (Figure 8A). In addition, we quantified the expression of these four genes in the process of myocyte differentiation, and found that their expression levels increased with the increase of the degree of differentiation of muscle cells, suggesting these genes might also play a crucial role in the differentiation (Figure 8B). Therefore, the screening of muscle-affinitive hub genes through ATAC-seq and RNA-seq can be further studied in the future on the molecular mechanism of muscle proliferation and differentiation.

TABLE 1 Top 10 up- and down-regulated expressed genes.

Genes	Description	log_2FoldChange	*P*value	P_{adj}
CKM	Creatine kinase, M-type	13.45451834	1.41E-209	5.72E-206
TNNC1	Troponin C1	13.45401812	3.51E-128	5.70E-125
MYOT	Myotilin	13.44382896	1.09E-205	2.53E-202
SLN	Sarcolipin	13.39986882	3.53E-86	2.39E-83
ACTA1	Actin alpha 1	13.37281374	1.54E-206	5.00E-203
MYL1	Myosin light chain 1	13.32452561	0	0
TNNC2	Troponin C2	13.31786432	3.10E-134	5.60E-131
MYLPF	Myosin light chain, phosphorylatable	13.31718808	3.82E-80	2.30E-77
MYH2	Myosin heavy chain 2	13.3004601	5.69E-97	4.40E-94
MYL2	Myosin light chain 2	13.28565102	2.31E-110	2.51E-107
GAD2	Glutamate decarboxylase 2	−24.51019661	3.21E-15	2.56E-13
CLVS2	Clavesin 2	−24.45531689	3.28E-15	2.60E-13
NRXN3	Neurexin 3	−24.05692778	3.25E-14	2.34E-12
CELF3	Neurexin 3	−23.93374376	2.20E-14	1.61E-12
ST8SIA3	CUGBP Elav-like family member 3	−23.74276415	2.62E-15	2.11E-13
GRM5	ST8 alpha-N-acetyl-neuraminide alpha-2,8-sialyltransferase 3	−23.70823989	1.38E-11	7.20E-10
GRIN1	Glutamate metabotropic receptor 5	−23.6503701	1.11E-10	5.15E-09
SCRT1	Glutamate ionotropic receptor NMDA type subunit 1	−23.5113897	4.87E-12	2.75E-10
GRIN2A	Scratch family transcriptional repressor 1	−23.46027351	5.45E-12	3.06E-10
MYT1	Glutamate ionotropic receptor NMDA type subunit 2A	−23.25118573	3.92E-15	3.09E-13

Discussion

Different from other tissues, the development of muscle, the main product of beef cattle, directly affects the economic value of beef. To improve beef yield from a genetic perspective, many novel techniques have been applied to explore the mechanism of muscle development in cattle. Among them, bulk RNA-seq has been widely promoted as a routine bulk screening technique for muscle-related genes (34, 35). However, the differentially expressed genes screened by it are often in thousands, and it is still difficult to obtain the core regulatory genes from them. In contrast, weighted gene co-expression network analysis (WGCNA) could be used to characterize correlation patterns between genes and samples (21). Candidate hub genes were identified according to the endogeneity of gene-sets and the association between gene-sets and samples (36). Compared to focusing only on differentially expressed genes, WGCNA is able to use genome-wide information to obtain our gene sets of interest, which not only narrows the screening scope but also makes the analysis more accurate. This technique has been applied extensively to plants, humans, mice, poultry, and livestock (36–41).

In this study, we analyzed the association of genes with different tissues using WGCNA, and obtained 4 module gene-sets with high positive correlation with muscle tissue. Combined with the results of GO functional annotation, we finally targeted $ME_{lightyellow}$ as the study target, from which we screened 213 candidate hub genes (GS > 0.6, MM > 0.8) involved in the positive regulation of muscle development. Compared with other tissues, 212 of 213 (99.53%) candidate hub genes were up-regulated expression in muscle [log2(FC) > 1, FDR < 0.05], which not only verified the robustness of WGCNA analysis, but also provided a reliable collection for the subsequent study.

In eukaryotes, DNA and histones are tightly bound and stored in nucleosomes (chromatin), chromatin structure, nucleosome location and histone modifications affect DNA transcription. Chromatin accessibility is closely related to the binding of regulatory elements or transcription factors, which are particularly important for gene activation and repression. ATAC-seq, an innovative technique for detecting chromatin accessibility, has been increasingly applied to determine the mechanisms of gene expression regulation with RNA-seq (42). In this study, we found that the chromatin open regions of muscle tissue were significantly different from other tissues. The results of functional annotation revealed that muscle-affinitive peaks were more enriched in exons and promoter regions compared to other tissues, suggesting that these chromatin-open regions are associated with gene expression regulation. In addition, we performed GO and KEGG analysis of DEGs around promoter-peaks and found that muscle-affinitive peaks were enriched on the hub genes specifically expressed by muscle as expected. It was involved in the regulation of cAMP, cGMP-PKG, and MAPK signaling pathways. Similar results were obtained in early studies on mouse tissue-specific genes (43).

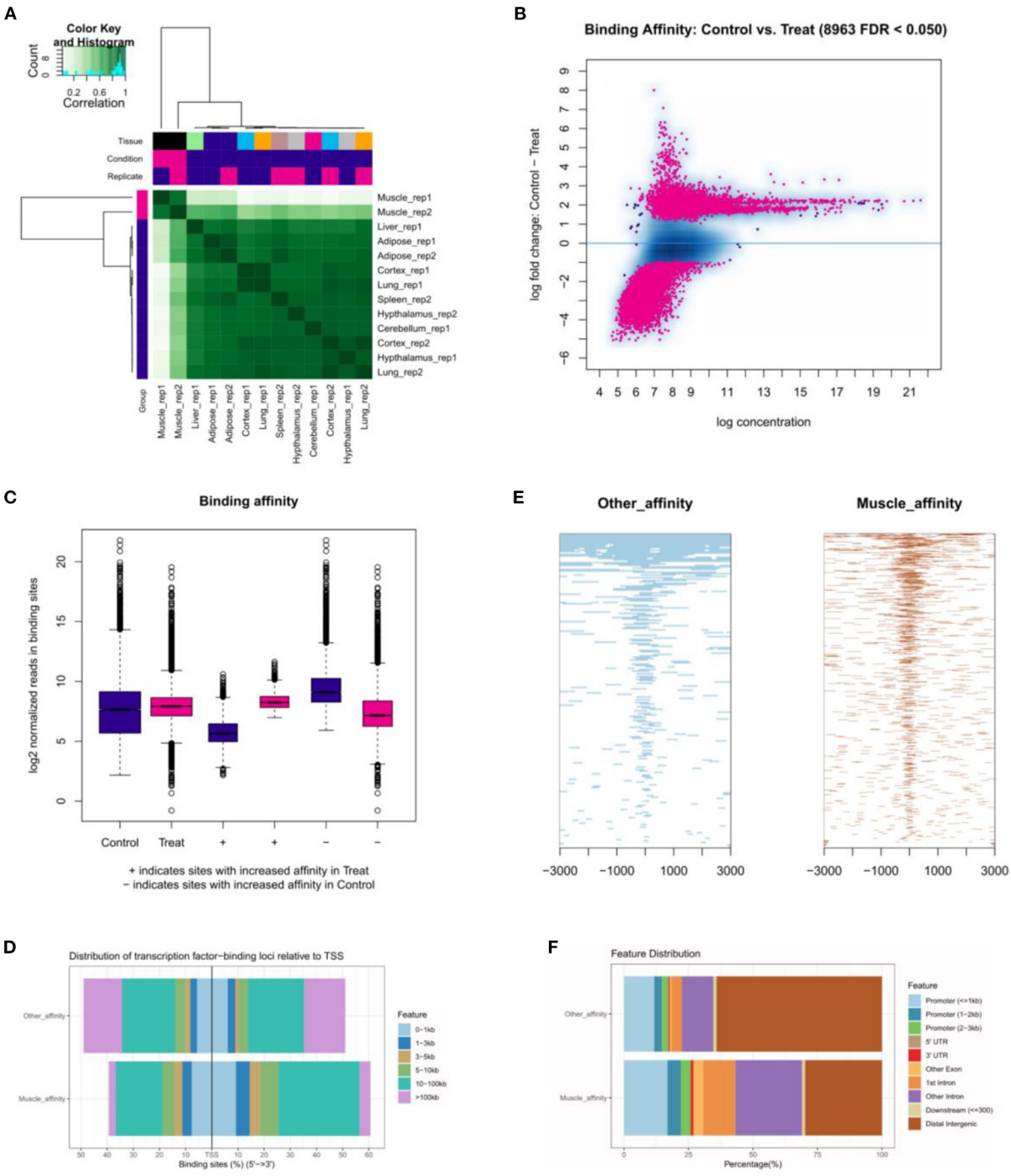

FIGURE 5
The landscape of genomic chromatin accessibility. **(A)** The correlative heatmap of tissues; **(B)** MA plot of difference peaks analysis; **(C)** The box-plot of binding affinity; **(D)** The location distribution of different peaks distance TSS; **(E)** The heatmap of peaks around TSS; **(F)** The distribution of function regions of different peaks.

Among them, MAPK signaling pathway plays a crucial role in in the formation, regeneration, movement and injury repair of skeletal muscle (44–46).

Combined with ATAC-seq, 54 genes with high expression in muscle were identified as muscle-regulated hub genes. To further analyze the regulatory mechanism of these 54 hub genes

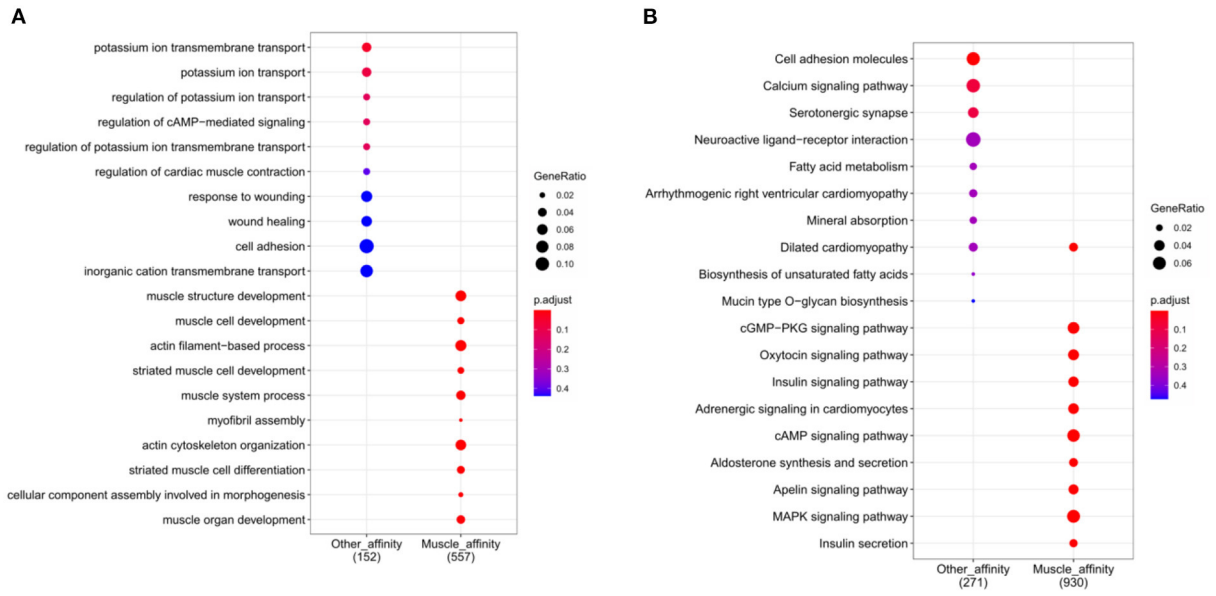

C

Motifs	TFs	E-value
	Ascl2	7.9e-056
	MEF2B	9.8e-046
	SIX1	8.3e-009
	MEF2C	1.20E-05
	SP1	7.8e-005

FIGURE 6
Genomic enrichment analysis. **(A)** GO-BP analysis of different peaks; **(B)** Enrichment analysis of KEGG pathway; **(C)** The top 5 predicted binding known motif in the open chromatin region.

in the development of skeletal muscle, we conducted motif analysis of the chromatin open region fragments. Twenty-two of the 54 genes were predicted to be regulated by MEF2C. This is consistent with earlier tissue analysis in mice (47). MEF2C is a member of the myocyte enhancer factor 2 family, which itself lacks myogenic activity and was initially considered to regulate muscle development by activating the transcriptional activity of bHLH myogen proteins (such as MyoD and MyoG) (48–50). Herein, we analyzed the possible MEF2C involved in downstream target genes, we broadly classified them into 3 major categories: 1. The muscle-specific genes, including *CAPN3*, *ACTN2*, *MB*, *KLHL41*, Cullin associated and neddylation dissociated 2 (*CAND2*), Myomesin 3 (*MYOM3*) and sarcalumenin (*SRL*); 2. The genes of kinases and epigenetic enzymes, including creatine kinase, M-Type (*CKM*), alpha kinase 3 (*ALPK3*), mitogen-activated protein kinase kinase kinase 20 (*MAP3K20*), ubiquitin conjugating enzyme E2 G1 (*UBE2G1*), Neuralized E3 Ubiquitin protein ligase 2 (NEURL2) and DOT1 like Histone lysine methyltransferase (*DOT1L*); 3. other genes with transcriptional regulation functions, including Histidine rich calcium binding protein (*HRC*), MEF2 activating motif and SAP domain containing transcriptional regulator (*MAMSTR*), fibronectin type III and SPRY domain containing 2 (*FSD2*), leucine rich repeat containing 2 (*LRRC2*), leucine rich single-pass membrane protein 1 (*LSMEM1*), solute carrier family 29 member 2 (*SLC29A2*), four and a half LIM domains 3 (*FHL3*), Ataxin 7 like 2 (*ATXN7L2*) and p53 and DNA damage regulated 1 (*PDRG1*).

In this study, some well-known myogenic genes have been reported to be involved in myoblast proliferation and

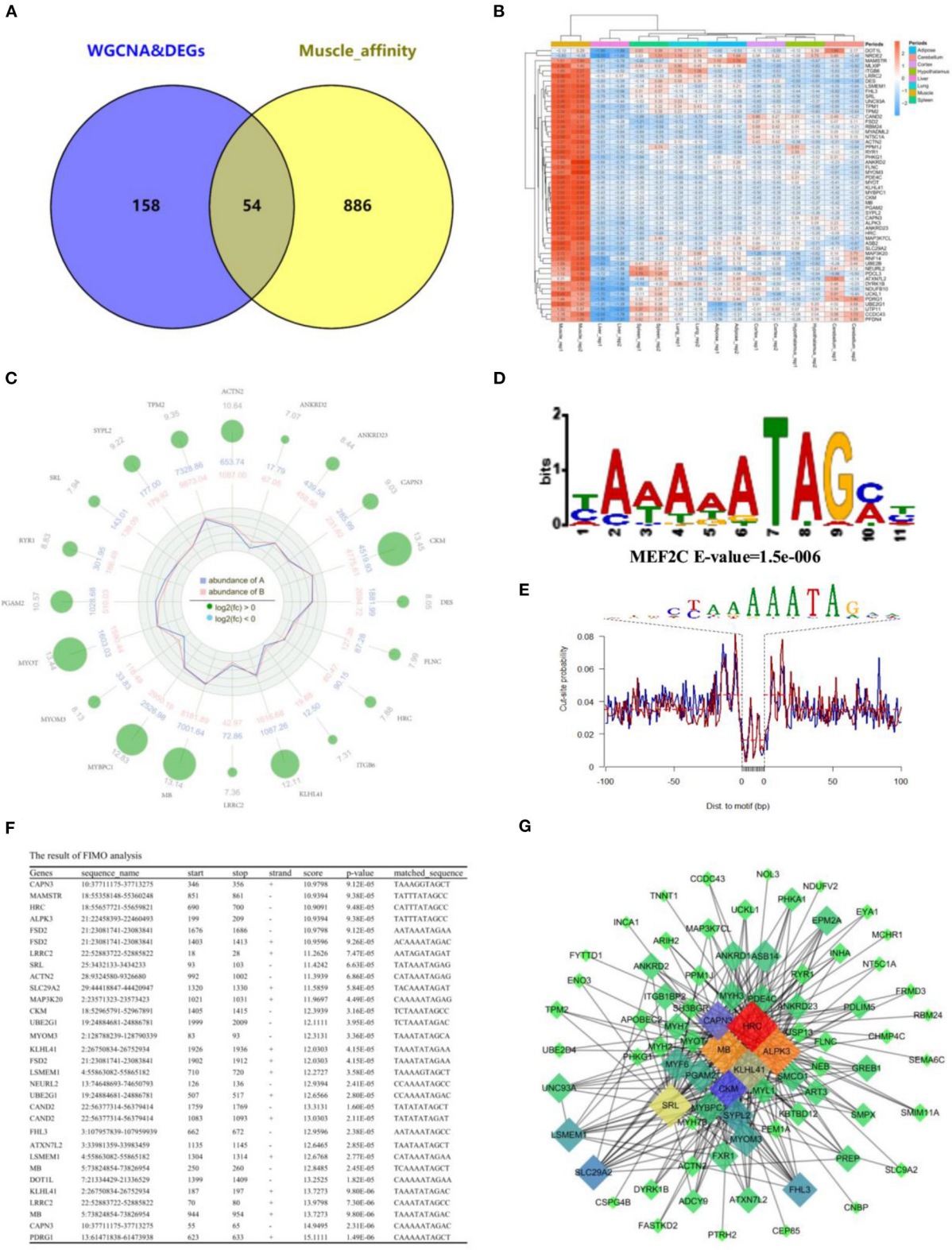

The result of FIMO analysis

Genes	sequence_name	start	stop	strand	score	p-value	matched_sequence
CAPN3	10:37711175-37713275	346	356	+	10.9798	9.12E-05	TAAAGGTAGCT
MAMSTR	18:55358148-55360248	851	861	-	10.9394	9.38E-05	TATTTATAGCC
HRC	18:55657721-55659821	690	700	-	10.9091	9.48E-05	CATTTATAGCC
ALPK3	21:22458393-22460493	199	209	-	10.9394	9.38E-05	TATTTATAGCC
FSD2	21:23081741-23083841	1676	1686	-	10.9798	9.12E-05	AATAAATAGAA
FSD2	21:23081741-23083841	1403	1413	+	10.9596	9.26E-05	ACAAAATAGAC
LRRC2	22:52883722-52885822	18	28	+	11.2626	7.47E-05	AATAGATAGAT
SRL	25:3432133-3434233	93	103	-	11.4242	6.63E-05	TATAAATAGAG
ACTN2	28:9324580-9326680	992	1002	-	11.3939	6.86E-05	CATAAATAGAG
SLC29A2	29:44418847-44420947	1320	1330	+	11.5859	5.84E-05	TACAAATAGAT
MAP3K20	2:23571323-23573423	1021	1031	+	11.9697	4.49E-05	CAAAAATAGAG
CKM	18:52965791-52967891	1405	1415	-	12.3939	3.16E-05	TCTAAATAGCC
UBE2G1	19:24884681-24886781	1999	2009	-	12.1111	3.95E-05	TCTAAATAGAC
MYOM3	2:128788239-128790339	83	93	-	12.3131	3.36E-05	TAAATATAGCA
KLHL41	2:26750834-26752934	1926	1936	+	12.0303	4.15E-05	TAAATATAGAA
FSD2	21:23081741-23083841	1902	1912	+	12.0303	4.15E-05	TAAATATAGAA
LSMEM1	4:55863082-55865182	710	720	+	12.2727	3.58E-05	TAAAAGTAGCT
NEURL2	13:74648693-74650793	126	136	-	12.9394	2.41E-05	CCAAAATAGCC
UBE2G1	19:24884681-24886781	507	517	+	12.6566	2.80E-05	CCAAAATAGAC
CAND2	22:56377314-56379414	1759	1769	-	13.3131	1.60E-05	TATATATAGCT
CAND2	22:56377314-56379414	1083	1093	+	13.0303	2.11E-05	TATATATAGAT
FHL3	3:107957839-107959939	662	672	-	12.9596	2.38E-05	AATAAATAGCC
ATXN7L2	3:33981359-33983459	1135	1145	-	12.6465	2.85E-05	TAATAATAGCT
LSMEM1	4:55863082-55865182	1304	1314	+	12.6768	2.77E-05	CATAAATAGAA
MB	5:73824854-73826954	250	260	-	12.8485	2.45E-05	TCAAAATAGCT
DOT1L	7:21334429-21336529	1399	1409	-	13.2525	1.82E-05	CAAAAATAGAA
KLHL41	2:26750834-26752934	187	197	+	13.7273	9.80E-06	TAAATATAGAC
LRRC2	22:52883722-52885822	70	80	+	13.9798	7.30E-06	CAAATATAGCC
MB	5:73824854-73826954	944	954	+	13.7273	9.80E-06	TAAATATAGAC
CAPN3	10:37711175-37713275	55	65	-	14.9495	2.31E-06	CAAAAATAGAC
PDRG1	13:61471838-61473938	623	633	+	15.1111	1.49E-06	CAAAAATAGCT

FIGURE 7
Integration of RNA-Seq and ATAC-Seq. **(A)** Venn plot of ATAC-seq and RNA-seq, and 54 common genes were found; **(B)** Heatmap plot of common genes; **(C)** Radar plot of the top 20 common genes; **(D)** Motif enrichment analysis of common genes around open chromatin regions. MEF2C was found to be significantly enriched; **(E)** The motif footprint analysis of MEF2C; **(F)** Motif Scanning of MEF2C in promoter region of common gene using FIMO; **(G)** The subregulatory network of 22 predicted MEF2C potential target genes in the ME_{light} module was derived from WGCNA analysis.

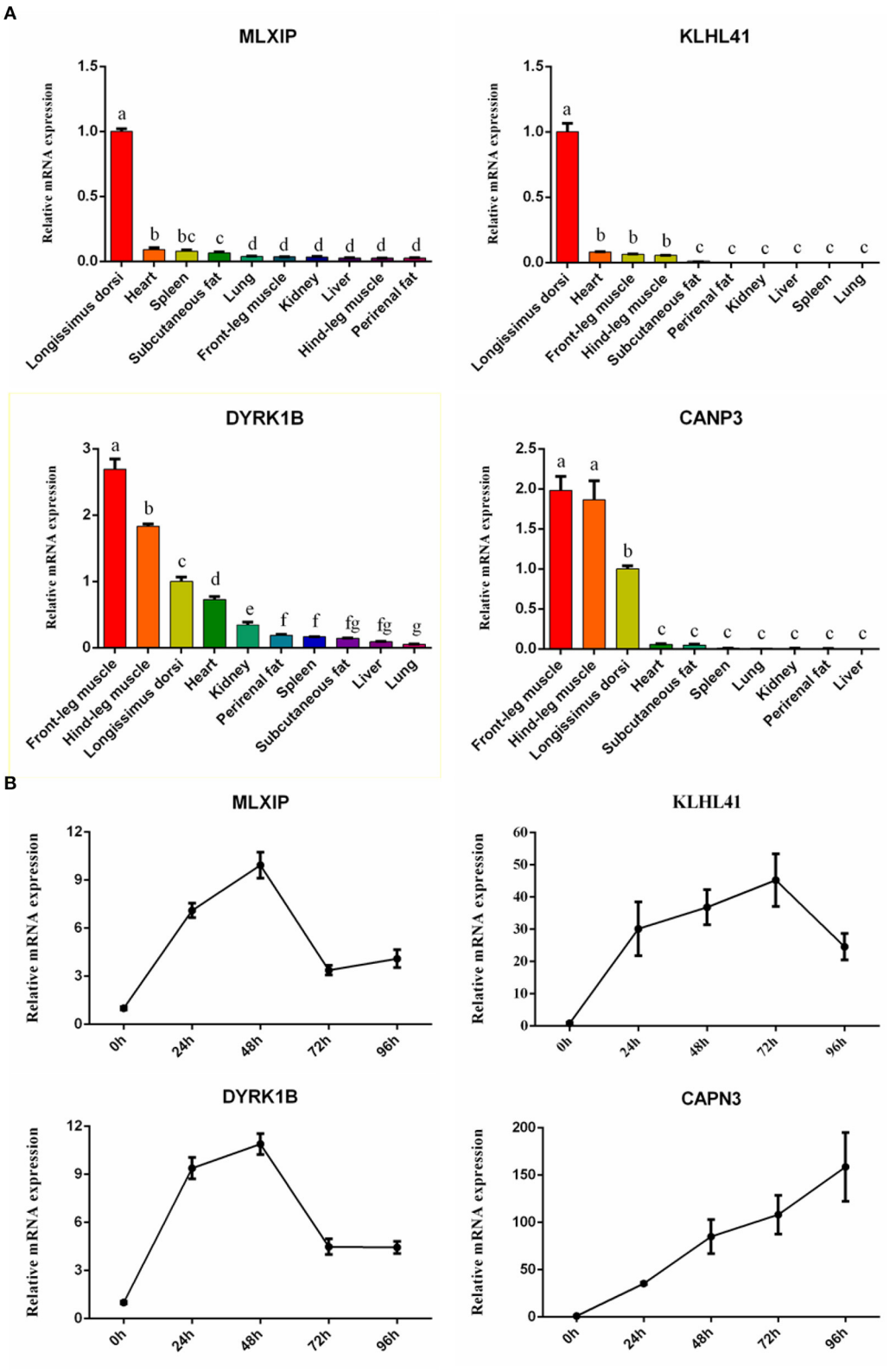

FIGURE 8
The relative expression of hub genes by qRT-PCR. **(A)** The bar plots represented tissue expression profiles. **(B)** The line charts represented myogenic cell differentiation expression profiles.

differentiation dependent on the transcriptional regulation of MEF2, such as *CAPN3*, *MB*, *Myomesin*, and *CKM* (51–54). More interestingly, HRC, a direct target gene of MEF2, encodes histidine-rich calcium-binding protein (HRCBP) involved in the regulation of muscle development mainly in the sarcoplasmic reticulum of cardiac and skeletal muscles and in the calcium bodies of smooth muscle (55, 56). *MASTR*, a coactivator of MEF2, is involved in the regulation of myoblast proliferation and differentiation by encoding a cofactor that stimulates MEF2C (57, 58). These studies confirm the reliability of the results of this study. Other genes have not been reported to interact directly with MEF2C, but many have been reported to be involved in the regulation of muscle. It has been reported that *ACTN2* and its family gene *ACTN3* encode myosin α-actin-2 and α-actin-3 proteins, respectively, which constitute the Z-line in mammalian skeletal muscle fibers (59). SRL is a Ca^{2+}-binding protein localized in the sarcoplasmic reticulum (SR) affecting skeletal muscle movement (60). MAP3K20 is involved in the regulation of the JNK/MAPK signaling pathway, which plays a role in muscle development and regeneration (61). UBE2G1 encodes an E2 ubiquitin-coupled enzyme that functions mainly in the ubiquitin-proteasome system, which is involved in muscle degradation and regeneration (62). NEURL2 is capable of encoding proteins involved in the regulation of myogenic fiber organization and ubiquitin-mediated degradation of β-linked proteins during myogenesis (63). *DOT1L* is a key epigenetic gene that mediates H3K79me2 modifications involved in cardiomyocyte differentiation (64). *LRRC2* is a member of the LRRC family and its role in epigenetic modifications in skeletal muscle has also been reported (65). *KLHL41* is predominantly expressed in skeletal muscle and is essential for the maintenance of skeletal muscle integrity and myogenic fiber formation (66, 67). *FHL3* has been reported to regulate myogenic differentiation and muscle-specific gene expression by acting as a transcriptional co-activator or co-repressor (68). *FSD2* is highly expressed in cardiac and skeletal muscle as a candidate gene affecting sarcomere traits in animals (69). *CAND2* and is a muscle-specific expression gene mediated by mTORC1 that affects cardiac remodeling but not skeletal muscle (70). *ALPK3* has been reported to be closely associated with familial cardiomyopathy, but its role in skeletal muscle has not been reported (71). In this study, *ALPK3* was located at the core of the interaction network of candidate genes with *MB*, *HRC*, *SRL*, and *KLHL41*, so we speculate that it also is irreplaceable for skeletal development. *LSMEM1*, *SLC29A2*, *ATXN7L2*, and *PDRG1* have not been directly reported to be associated with muscle development. In conclusion, these genes are worthy of our attention and their potential regulatory role with transcription factors and their epistatic modifications in muscle development is of great interest to explore.

Notably, this study used other tissues as the background and only contested the analysis of genes with positive regulation with muscle. In fact, there are many more information that can be mined to be further analyzed and verified, such as other tissue-related genes, functional analysis of other modular genes, and joint analysis with other epistatic data.

Data availability statement

The datasets presented in this study can be found in online repositories. The names of the repository/repositories and accession number(s) can be found in the article/Supplementary material.

Ethics statement

The animal study was reviewed and approved by Ethics Committee of Northwest A&F University.

Author contributions

JW, BL, and LZ conceived and designed the experiments. JW wrote the manuscript. XY, CL, SR, YP, and KZ contributed sample collection and reagents preparation, and analyzed the data. JW, BL, XY, CL, SR, YP, KZ, and LZ revised the manuscript. All authors reviewed the manuscript. All authors contributed to the article and approved the submitted version.

Funding

This work was supported by the Natural Science Foundation of China (31972994), Key Research and Development Program of Ningxia Province (2019BEF02004), National Beef and Yak Industrial Technology System (CARS-37), Key Research and Development Program of Shaanxi Province (2022NY-050 and 2022ZDLNY01-01), Transformation Project of Shaanxi Province (NYKJ-2018-LY09) and Special Project for the Central Government to Guide Local Science and Technology Development (2060404-51301).

Conflict of interest

The authors declare that the research was conducted in the absence of any commercial or financial relationships that could be construed as a potential conflict of interest.

Publisher's note

All claims expressed in this article are solely those of the authors and do not necessarily represent those

Supplementary material

The Supplementary Material for this article can be found online at: https://www.frontiersin.org/articles/10.3389/fvets.2022.925590/full#supplementary-material

References

1. Picard B, Berri C, Lefaucheur L, Molette C, Sayd T, Terlouw C. Skeletal muscle proteomics in livestock production. *Brief Funct Genom.* (2010) 9:259–78. doi: 10.1093/bfgp/elq005

2. Zhang Z, Liao Q, Sun Y, Pan T, Liu S, Miao W, et al. Lipidomic and transcriptomic analysis of the longissimus muscle of luchuan and duroc pigs. *Front Nutr.* (2021) 8:667622. doi: 10.3389/fnut.2021.667622

3. Yang XJ, Albrecht E, Ender K, Zhao RQ, Wegner J. Computer image analysis of intramuscular adipocytes and marbling in the longissimus muscle of cattle. *J Anim Sci.* (2006) 84:3251–8. doi: 10.2527/jas.2006-187

4. Huo W, Weng K, Gu T, Zhang Y, Zhang Y, Chen G, et al. Effect of muscle fiber characteristics on meat quality in fast- and slow-growing ducks. *Poult Sci.* (2021) 100:101264. doi: 10.1016/j.psj.2021.101264

5. Ohlendieck K. Skeletal muscle proteomics: current approaches, technical challenges and emerging techniques. *Skeletal Muscle.* (2011) 1:6. doi: 10.1186/2044-5040-1-6

6. Esteves de Lima J, Relaix F. Master regulators of skeletal muscle lineage development and pluripotent stem cells differentiation. *Cell Regen.* (2021) 10:31. doi: 10.1186/s13619-021-00093-5

7. Taylor MV, Hughes SM. Mef2 and the skeletal muscle differentiation program. *Semin Cell Dev Biol.* (2017) 72:33–44. doi: 10.1016/j.semcdb.2017.11.020

8. Molkentin JD, Black BL, Martin JF, Olson EN. Mutational analysis of the DNA binding, dimerization, and transcriptional activation domains of MEF2C. *Mol Cell Biol.* (1996) 16:2627–36. doi: 10.1128/MCB.16.6.2627

9. Black BL, Olson EN. Transcriptional control of muscle development by myocyte enhancer factor-2 (MEF2) proteins. *Ann Rev Cell Dev Biol.* (1998) 14:167–96. doi: 10.1146/annurev.cellbio.14.1.167

10. Schiaffino S, Serrano A. Calcineurin signaling and neural control of skeletal muscle fiber type and size. *Trends Pharmacol Sci.* (2002) 23:569–75. doi: 10.1016/S0165-6147(02)02111-9

11. McKinsey TA, Zhang CL, Olson EN. MEF2: a calcium-dependent regulator of cell division, differentiation and death. *Trends Biochem Sci.* (2002) 27:40–7. doi: 10.1016/S0968-0004(01)02031-X

12. Luo L, Gribskov M, Wang S. Bibliometric review of ATAC-Seq and its application in gene expression. *Brief Bioinform.* (2022) 23:bbac061. doi: 10.1093/bib/bbac061

13. Kern C, Wang Y, Xu X, Pan Z, Halstead M, Chanthavixay G, et al. Functional annotations of three domestic animal genomes provide vital resources for comparative and agricultural research. *Nat Commun.* (2021) 12:1821. doi: 10.1038/s41467-021-22100-8

14. Alexandre PA, Naval-Sánchez M, Menzies M, Nguyen LT, Porto-Neto LR, Fortes MRS, et al. Chromatin accessibility and regulatory vocabulary across indicine cattle tissues. *Genome Biol.* (2021) 22:273. doi: 10.1186/s13059-021-02489-7

15. Leinonen R, Sugawara H, Shumway M, International Nucleotide Sequence Database C. The sequence read archive. *Nucleic Acids Res.* (2011) 39:D19–21. doi: 10.1093/nar/gkq1019

16. Bolger AM, Lohse M, Usadel B. Trimmomatic: a flexible trimmer for illumina sequence data. *Bioinformatics.* (2014) 30:2114–20. doi: 10.1093/bioinformatics/btu170

17. Kim D, Langmead B, Salzberg SL. HISAT: a fast spliced aligner with low memory requirements. *Nat Methods.* (2015) 12:357–60. doi: 10.1038/nmeth.3317

18. Li H, Handsaker B, Wysoker A, Fennell T, Ruan J, Homer N, et al. The sequence alignment/Map format and SAMtools. *Bioinformatics.* (2009) 25:2078–9. doi: 10.1093/bioinformatics/btp352

19. Liao Y, Smyth GK, Shi W. featureCounts: an efficient general purpose program for assigning sequence reads to genomic features. *Bioinformatics.* (2014) 30:923–30. doi: 10.1093/bioinformatics/btt656

20. Pertea M, Pertea GM, Antonescu CM, Chang TC, Mendell JT, Salzberg SL. StringTie enables improved reconstruction of a transcriptome from RNA-seq reads. *Nat Biotechnol.* (2015) 33:290–5. doi: 10.1038/nbt.3122

21. Langfelder P, Horvath S. WGCNA: an R package for weighted correlation network analysis. *BMC Bioinformatics.* (2008) 9:559. doi: 10.1186/1471-2105-9-559

22. Tian Z, He W, Tang J, Liao X, Yang Q, Wu Y, et al. Identification of important modules and biomarkers in breast cancer based on WGCNA. *OncoTargets therapy.* (2020) 13:6805–17. doi: 10.2147/OTT.S258439

23. Love MI, Huber W, Anders S. Moderated estimation of fold change and dispersion for RNA-seq data with DESeq2. *Genome Biol.* (2014) 15:550. doi: 10.1186/s13059-014-0550-8

24. Li H, Durbin R. Fast and accurate short read alignment with Burrows-Wheeler transform. *Bioinformatics.* (2009) 25:1754–60. doi: 10.1093/bioinformatics/btp324

25. Johnston D, Kim J, Taylor JF, Earley B, McCabe MS, Lemon K, et al. ATAC-Seq identifies regions of open chromatin in the bronchial lymph nodes of dairy calves experimentally challenged with bovine respiratory syncytial virus. *BMC Genomics.* (2021) 22:14. doi: 10.1186/s12864-020-07268-5

26. Yu G, Wang L-G, He Q-Y. ChIPseeker: an R/Bioconductor package for ChIP peak annotation, comparison and visualization. *Bioinformatics.* (2015) 31:2382–3. doi: 10.1093/bioinformatics/btv145

27. Bailey TL, Williams N, Misleh C, Li WW. MEME: discovering and analyzing DNA and protein sequence motifs. *Nucleic Acids Res.* (2006) 34:W369–73. doi: 10.1093/nar/gkl198

28. Ou J, Liu H, Yu J, Kelliher MA, Castilla LH, Lawson ND, et al. ATACseqQC: a Bioconductor package for post-alignment quality assessment of ATAC-seq data. *BMC Genomics.* (2018) 19:169. doi: 10.1186/s12864-018-4559-3

29. Grant CE, Bailey TL, Noble WS. FIMO: scanning for occurrences of a given motif. *Bioinformatics.* (2011) 27:1017–8. doi: 10.1093/bioinformatics/btr064

30. Yu G, Wang LG, Han Y, He QY. clusterProfiler: an R package for comparing biological themes among gene clusters. *OMICS.* (2012) 16:284–7. doi: 10.1089/omi.2011.0118

31. Raudvere U, Kolberg L, Kuzmin I, Arak T, Adler P, Peterson H, et al. g:Profiler: a web server for functional enrichment analysis and conversions of gene lists (2019 update). *Nucleic Acids Res.* (2019) 47:W191–8. doi: 10.1093/nar/gkz369

32. Xie C, Mao X, Huang J, Ding Y, Wu J, Dong S, et al. KOBAS 2.0: a web server for annotation and identification of enriched pathways and diseases. *Nucleic Acids Res.* (2011) 39:W316–22. doi: 10.1093/nar/gkr483

33. Yang H, Li G, Qiu G. Bioinformatics analysis using ATAC-seq and RNA-seq for the identification of 15 gene signatures associated with the prediction of prognosis in hepatocellular carcinoma. *Front Oncol.* (2021) 11:726551. doi: 10.3389/fonc.2021.726551

34. Owens NDL, De Domenico E, Gilchrist MJ. An RNA-seq protocol for differential expression analysis. *Cold Spring Harbor Protocols.* (2019) 2019:pdb-rot098368. doi: 10.1101/pdb.prot098368

35. Mortazavi A, Williams BA, McCue K, Schaeffer L, Wold B. Mapping and quantifying mammalian transcriptomes by RNA-Seq. *Nat Methods.* (2008) 5:621–8. doi: 10.1038/nmeth.1226

36. Ding H, Lin Y, Zhang T, Chen L, Zhang G, Wang J, et al. Transcriptome analysis of differentially expressed mRNA related to pigeon muscle development. *Animals.* (2021) 11:2311. doi: 10.3390/ani11082311

37. Yang J, Ren Y, Zhang D, Chen X, Huang J, Xu Y, et al. Transcriptome-based WGCNA analysis reveals regulated metabolite fluxes between floral color and scent in *Narcissus tazetta* flower. *Int J Mol Sci.* (2021) 22:8249. doi: 10.3390/ijms22158249

38. Chen L, Bai J, Li Y. miR-29 mediates exercise-induced skeletal muscle angiogenesis by targeting VEGFA, COL4A1 and COL4A2 via the PI3K/Akt signaling pathway. *Mol Med Rep.* (2020) 22:661–70. doi: 10.3892/mmr.2020.11164

39. Ren K, Wang L, Wang L, Du Q, Cao J, Jin Q, et al. Investigating transcriptional dynamics changes and time-dependent marker gene expression in the early period after skeletal muscle injury in rats. *Front Genet.* (2021) 12:650874. doi: 10.3389/fgene.2021.650874

40. Zhao X, Hu H, Lin H, Wang C, Wang Y, Wang J. Muscle transcriptome analysis reveals potential candidate genes and pathways affecting intramuscular fat content in pigs. *Front Genet.* (2020) 11:877. doi: 10.3389/fgene.2020.00877

41. Bao Q, Zhang X, Bao P, Liang C, Guo X, Chu M, et al. Using weighted gene co-expression network analysis (WGCNA) to identify the hub genes related to hypoxic adaptation in yak (*Bos grunniens*). *Genes Genom.* (2021) 43:1231–46. doi: 10.1007/s13258-021-01137-5

42. Buenrostro JD, Wu B, Chang HY, Greenleaf WJ. ATAC-seq: a method for assaying chromatin accessibility genome-wide. *Curr Protoc Mol Biol.* (2015) 109:21–9. doi: 10.1002/0471142727.mb2129s109

43. Raza SHA, Liang C, Guohua W, Pant SD, Mohammedsaleh ZM, Shater AF, et al. Screening and identification of muscle-specific candidate genes via mouse microarray data analysis. *Front Vet Sci.* (2021) 8:794628. doi: 10.3389/fvets.2021.794628

44. Keren A, Tamir Y, Bengal E. The p38 MAPK signaling pathway: a major regulator of skeletal muscle development. *Mol Cell Endocrinol.* (2006) 252:224–30. doi: 10.1016/j.mce.2006.03.017

45. Tomida T, Adachi-Akahane S. Roles of p38 MAPK signaling in the skeletal muscle formation, regeneration, and pathology. *Nihon yakurigaku zasshi Folia pharmacologica Japonica.* (2020) 155:241–7. doi: 10.1254/fpj20030

46. Kramer HF, Goodyear LJ. Exercise, MAPK, and NF-kappaB signaling in skeletal muscle. *J Appl Physiol.* (2007) 103:388–95. doi: 10.1152/japplphysiol.00085.2007

47. Liu C, Wang M, Wei X, Wu L, Xu J, Dai X, et al. An ATAC-seq atlas of chromatin accessibility in mouse tissues. *Sci Data.* (2019) 6:65. doi: 10.1038/s41597-019-0071-0

48. Molkentin JD, Black BL, Martin JF, Olson EN. Cooperative activation of muscle gene expression by MEF2 and myogenic bHLH proteins. *Cell.* (1995) 83:1125–36. doi: 10.1016/0092-8674(95)90139-6

49. Wang DZ, Valdez MR, McAnally J, Richardson J, Olson EN. The Mef2c gene is a direct transcriptional target of myogenic bHLH and MEF2 proteins during skeletal muscle development. *Development.* (2001) 128:4623–33. doi: 10.1242/dev.128.22.4623

50. Cante-Barrett K, Pieters R, Meijerink JP. Myocyte enhancer factor 2C in hematopoiesis and leukemia. *Oncogene.* (2014) 33:403–10. doi: 10.1038/onc.2013.56

51. Wu R, Wang J, Yao J, Dong Z, Liu Y, Liu M. MEF2A regulates Calpain 3 expression in L6 myoblasts. *Gene.* (2018) 668:204–10. doi: 10.1016/j.gene.2018.05.056

52. Grayson J, Williams RS, Yu YT, Bassel-Duby R. Synergistic interactions between heterologous upstream activation elements and specific TATA sequences in a muscle-specific promoter. *Mol Cell Biol.* (1995) 15:1870–8. doi: 10.1128/MCB.15.4.1870

53. Potthoff MJ, Arnold MA, McAnally J, Richardson JA, Bassel-Duby R, Olson EN. Regulation of skeletal muscle sarcomere integrity and postnatal muscle function by Mef2c. *Mol Cell Biol.* (2007) 27:8143–51. doi: 10.1128/MCB.01187-07

54. Rampalli S, Li L, Mak E, Ge K, Brand M, Tapscott SJ, et al. p38 MAPK signaling regulates recruitment of Ash2L-containing methyltransferase complexes to specific genes during differentiation. *Nat Struct Mol Biol.* (2007) 14:1150–6. doi: 10.1038/nsmb1316

55. Anderson JP, Dodou E, Heidt AB, De Val SJ, Jaehnig EJ, Greene SB, et al. HRC is a direct transcriptional target of MEF2 during cardiac, skeletal, and arterial smooth muscle development *in vivo*. *Mol Cell Biol.* (2004) 24:3757–68. doi: 10.1128/MCB.24.9.3757-3768.2004

56. Lee HG, Kang H, Kim DH, Park WJ. Interaction of HRC (Histidine-rich Ca2+-binding protein) and triadin in the lumen of sarcoplasmic reticulum*. *J Biol Chem.* (2001) 276:39533–8. doi: 10.1074/jbc.M010664200

57. Zhang L, Silva TC, Young JI, Gomez L, Schmidt MA, Hamilton-Nelson KL, et al. Epigenome-wide meta-analysis of DNA methylation differences in prefrontal cortex implicates the immune processes in Alzheimer's disease. *Nat Commun.* (2020) 11:6114. doi: 10.1038/s41467-020-19791-w

58. Creemers EE, Sutherland LB, Oh J, Barbosa AC, Olson EN. Coactivation of MEF2 by the SAP domain proteins myocardin and MASTR. *Mol Cell.* (2006) 23:83–96. doi: 10.1016/j.molcel.2006.05.026

59. Harada N, Gotoda Y, Hatakeyama A, Nakagawa T, Miyatake Y, Kuroda M, et al. Differential regulation of Actn2 and Actn3 expression during unfolded protein response in C2C12 myotubes. *J Muscle Res Cell Motility.* (2020) 41:199–209. doi: 10.1007/s10974-020-09582-7

60. Yoshida M, Minamisawa S, Shimura M, Komazaki S, Kume H, Zhang M, et al. Impaired Ca2+ store functions in skeletal and cardiac muscle cells from sarcalumenin-deficient mice. *J Biol Chem.* (2005) 280:3500–6. doi: 10.1074/jbc.M406618200

61. Yan J, Yang Y, Fan X, Liang G, Wang Z, Li J, et al. circRNAome profiling reveals circFgfr2 regulates myogenesis and muscle regeneration via a feedback loop. *J Cachexia Sarcopenia Muscle.* (2022) 13:696–712. doi: 10.1002/jcsm.12859

62. Santos Silva DBd, Fonseca LFS, Magalhães AFB, Muniz MMM, Baldi F, Ferro JA, et al. Transcriptome profiling of muscle in Nelore cattle phenotypically divergent for the ribeye muscle area. *Genomics.* (2020) 112:1257–63. doi: 10.1016/j.ygeno.2019.07.012

63. Nastasi T, Bongiovanni A, Campos Y, Mann L, Toy JN, Bostrom J, et al. Ozz-E3, a muscle-specific ubiquitin ligase, regulates β-Catenin degradation during myogenesis. *Dev Cell.* (2004) 6:269–82. doi: 10.1016/S1534-5807(04)00020-6

64. Cattaneo P, Kunderfranco P, Greco C, Guffanti A, Stirparo GG, Rusconi F, et al. DOT1L-mediated H3K79me2 modification critically regulates gene expression during cardiomyocyte differentiation. *Cell Death Diff.* (2016) 23:555–64. doi: 10.1038/cdd.2014.199

65. Ehrlich KC, Lacey M, Ehrlich M. Epigenetics of skeletal muscle-associated genes in the ASB, LRRC, TMEM, and OSBPL gene families. *Epigenomes.* (2020) 4:1. doi: 10.3390/epigenomes4010001

66. Pak JH. *KLHL41 in Skeletal Muscle Development*. Boston, MA: Boston University Theses & Dissertations (2019).

67. Ramirez-Martinez A, Cenik BK, Bezprozvannaya S, Chen B, Bassel-Duby R, Liu N, et al. KLHL41 stabilizes skeletal muscle sarcomeres by nonproteolytic ubiquitination. *Elife.* (2017) 6:e26439. doi: 10.7554/eLife.26439

68. Zhang Y, Li W, Zhu M, Li Y, Xu Z, Zuo B. FHL3 differentially regulates the expression of MyHC isoforms through interactions with MyoD and pCREB. *Cell Signal.* (2016) 28:60–73. doi: 10.1016/j.cellsig.2015.10.008

69. Lim K-S, Lee K-T, Lee S-W, Chai H-H, Jang G, Hong K-C, et al. Genomic structure, expression and association study of the porcine FSD2. *Mol Biol Rep.* (2016) 43:1011–8. doi: 10.1007/s11033-016-4029-4

70. Górska AA, Sandmann C, Riechert E, Hofmann C, Malovrh E, Varma E, et al. Muscle-specific Cand2 is translationally upregulated by mTORC1 and promotes adverse cardiac remodeling. *EMBO Rep.* (2021) 22:e52170. doi: 10.15252/embr.202052170

71. Papadopoulos C, Kekou K, Anastasakis A, Svingou M, Malfatti E, Metay C, et al. A novel homozygous ALPK3 variant associated with cardiomyopathy and skeletal muscle involvement. *Muscle Nerve.* (2022) 65:E7–10. doi: 10.1002/mus.27471

frontiers | Frontiers in Veterinary Science

TYPE Original Research
PUBLISHED 02 September 2022
DOI 10.3389/fvets.2022.922623

OPEN ACCESS

EDITED BY
Fazul Nabi,
Lasbela University of Agriculture, Water and Marine Sciences, Pakistan

REVIEWED BY
Ahrar Khan,
Shandong Vocational Animal Science and Veterinary College, China
Xinyu Zhu,
Duke University, United States
Samina Shabbir,
Guangdong Academy of Science (CAS), China

*CORRESPONDENCE
Kun Li
lik2014@sina.com
Zhigang Liu
lzg12021@163.com

†These authors have contributed equally to this work

SPECIALTY SECTION
This article was submitted to Comparative and Clinical Medicine, a section of the journal Frontiers in Veterinary Science

RECEIVED 18 April 2022
ACCEPTED 15 August 2022
PUBLISHED 02 September 2022

CITATION
Liu Z, Ding X, Haider MS, Ali F, Yu H, Chen X, Tan S, Zu Y, Liu W, Ding B, Zheng A, Zheng J, Qian Z, Ashfaq H, Yu D and Li K (2022) A metagenomic insight into the Yangtze finless porpoise virome.
Front. Vet. Sci. 9:922623.
doi: 10.3389/fvets.2022.922623

A metagenomic insight into the Yangtze finless porpoise virome

Zhigang Liu[1,2*†], Xin Ding[1†], Muhammad Shahan Haider[3], Farah Ali[4], Han Yu[1], Xin Chen[1], Shuaishuai Tan[1], Yuan Zu[1], Wenlong Liu[1], Bangzhi Ding[1], Aifang Zheng[1], Jinsong Zheng[5], Zhengyi Qian[6], Hassan Ashfaq[7], Daoping Yu[1,2] and Kun Li[8,9*]

[1]College of Life Science, Anqing Normal University, Anqing, China, [2]Research Center of Aquatic Organism Conservation and Water Ecosystem Restoration in Anhui Province, Anqing Normal University, Anqing, China, [3]Bahria University Medical and Dental College Karachi, Karachi, Pakistan, [4]Department of Theriogenology, Faculty of Veterinary and Animal Sciences, The Islamia University of Bahawalpur, Bahawalpur, Pakistan, [5]Institute of Hydrobiology, Chinese Academy of Sciences, Beijing, China, [6]Hubei Yangtze River Ecological Protection Foundation, Wuhan, China, [7]Institute of Continuing Education and Extension, University of Veterinary Animal Sciences, Lahore, Pakistan, [8]Institute of Traditional Chinese Veterinary Medicine, College of Veterinary Medicine, Nanjing Agricultural University, Nanjing, China, [9]MOE Joint International Research Laboratory of Animal Health and Food Safety, Nanjing Agricultural University, Nanjing, China

The Yangtze finless porpoise (*Neophocaena phocaenoides asiaeorientalis*) inhabiting the Yantze River, China is critically endangered because of the influences of infectious disease, human activity, and water contamination. Viral diseases are one of the crucial factors that threatening the health of Yangtze finless porpoise. However, there are few studies which elaborate the viral diversity of Yangtze finless. Therefore, this study was performed to investigate the viral diversity of Yangtze finless by metagenomics. Results indicated that a total of 12,686,252 high-quality valid sequences were acquired and 2,172 virus reads were recognized. Additionally, we also obtained a total of 10,600 contigs. Phages was the most abundant virus in the samples and the ratio of DNA and RNA viruses were 69.75 and 30.25%, respectively. *Arenaviridae*, *Ackermannviridae* and *Siphoviridae* were the three most predominant families in all the samples. Moreover, the majority of viral genus were *Mammarenavirus*, *Limestonevirus* and *Lambdavirus*. The results of gene prediction indicated that these viruses play vital roles in biological process, cellular component, molecular function, and disease. To the best of our knowledge, this is the first report on the viral diversity of Yangtze finless porpoise, which filled the gaps in its viral information. Meanwhile, this study can also provide a theoretical basis for the establishment of the prevention and protection system for virus disease of Yangtze finless porpoise.

KEYWORDS

Yangtze finless porpoise, diversity, virus, metagenomics, *Arenaviridae*

Introduction

Neophocaena asiaeorientalis ssp. *asiaeorientalis* also known as Yangtze finless porpoises (YFP) are fresh-water mammals that inhabit Yangtze River in People's Republic of China. They are critically endangered

species with an estimated decreasing population of 500–1,800 (1). The survival of Yangtze finless porpoises is affected by multiple factors such as human activities, industrial development, mining, shipping, fishing, dams, water pollution and climate change. Efforts have been put into the research and conservation of this specie by protecting the areas, reserves and *in situ* conservation. Notably, the quantity of Yangtze finless porpoises is still gradually decreasing due to human activities over-fishing and water pollution of the Yangtze River. Water pollution is not only due to imbalance of the Yangtze River ecosystem but also caused the outbreak of viral and bacterial diseases, which posed a serious threat to the survival of Yangtze finless porpoises (2). Statistically, the population of Yangtze finless porpoises is <2,000 and it has been considered as the endangered species by the International Union for Conservation of Nature (IUCN) (3).

Viruses are one of the most abundant biological beings on the earth which are characterized by genomic flexibility, rapid transition, and smaller volume (4, 5). Viral habitat and diversity are important to formulate the prevention, control, and preparedness in case of emergency outbreaks (6). Moreover, this information is important to develop targeted drugs and vaccines against such diseases (6–8). The traditional virus identification/ detection methods include growth on cell culture and electron microscopy, serology, and molecular biology with each having its own benefits and limitations (9, 10). Recently, the high throughput sequencing-based techniques e.g., the metagenomics, has provided an important platform for the large-scale identification of known and novel viruses in a habitat (11, 12). A large amount of known and novel viruses has been identified from the pigs, ducks, turkey, pigeon, and bats by using viral metagenomics (13–17). However, little is known about the viral diversity in Yangtze finless porpoises. Therefore, the objective of this study was to investigate the viral diversity in Yangtze finless porpoise by metagenomics.

Materials and methods

Sample collection and processing

A total of 40 samples including heart, liver, spleen, lung, kidney, pancreas, lymph nodes and skin were collected from the dead Yangtze finless porpoises. The samples were collected from 2017 to 2019. Moreover, these samples were collected from 4 wild finless porpoises inhabiting the Yangtze River, aged 2–5, from the same site. The achieved samples were immediately stored in sterile plastic containers and transported to the laboratory and later stored at −80°C for further processing.

Nucleic acid extraction and library construction

First, the tissue samples were mixed and homogenized and then the debris of the tissues and cells were removed by low-speed centrifugation. Additionally, multiple virologic separation methods including filtration and ultracentrifugation were used for purifying and concentrating the virus-like particle (VLP) in the solution. The nucleic acid of the obtained VLP was extracted by the method of virus DNA (dsDNA, ssDNA) and RNA (ssRNA, dsRNA) co-extraction using viral DNA/RNA extraction kit (Beijing Quanshijin Biotechnology Co., LTD). Afterwards, the genomic libraries were constructed based on viral genome types. The DNA library of dsDNA genome was constructed directly, whereas ssDNA needs to be synthesized into double-stranded DNA before DNA library construction. Prior to the RNA library construction, the RNA genome needs to be converted into double-stranded cDNA through reverse transcription and two-strand synthesis. The total amount and purity of the DNA and RNA were evaluated, and the unqualified nucleic acids need to be re-extracted or undergo whole-genome amplification and purification. The qualified or amplified DNA samples were randomly shattered by an ultrasonic disruptor and the obtained short fragments of DNA were used for sequencing library construction. The final qualified libraries were used for high-throughput sequencing on the Illumina platform at Guangdong Meige Gene Technology Co., Ltd., China.

Bioinformatics analysis

After obtaining the metagenomic sequencing data, the quality of data was evaluated using Soapnuke software to ensure the credibility of subsequent analysis results. The paired reads with adapter and low quality were discarded. Moreover, duplicate reads generated by PCR amplification were also required to be removed. The finally obtained high-quality sequences were used for further data analysis. The clean reads were aligned to the specific host genome to remove the host sequence by using SOAPaligner (v2.0.5) and BWA software's (v0.7.17). Additionally, the high-quality sequences were required to compare with the virus database to obtain the virus composition information in the sample. Meanwhile, the NCBI taxonomy database was used to count the virus taxonomy annotation information. The obtained high-quality reads of each sample were assembled to achieve a longer contigs sequence by using Megahit, Trinity and IDBA software. The quantity, length, and N50 of assembled sequences were counted and the high-quality reads were aligned to the assembled sequence to evaluate the utilization of assembled reads. The reads were compared with the identified viral contigs and the RPKM value of each contig was also calculated. The RPKM value was calculated with

TABLE 1 Statistical analysis of the sequence information.

Sample	Raw-base (G)	Raw-reads (PE)	Clean-base (G)	Clean-reads (PE)	Percent (%)
YFP	14.35	47,824,812	3.81	12,686,252	26.53

TABLE 2 Statistical analysis of the sequence information after removing host sequence.

Sample	Clean_reads (PE)	Rm_rRNA_clean (PE)	Rm_host_clean (PE)
YFP	12,686,252	3,347,258(26.38%)	1,800,277(14.19%)

the following formula: RPKM% = [Contig reads/Total mapped reads × Contig length] × 100%. The MetaGeneMark was used to predict the gene sequences of viral contigs and assess the number and length of the predicted genes. The predicted gene protein sequences were compared with UniProtKB/Swiss-Prot database to obtain functional annotation information.

Results

Sequences analyses

After the filtration of raw data, a total of 12,686,252 high-quality sequences were obtained (Table 1). The obtained high-quality sequences were compared with the ribosomal database (Silva.132) and the host (*Neophocaena asiaeorientalis asiaeorientalis*) database and the corresponding sequences which were <80% of the total length of reads were removed to avoid the influences of ribosome and host sequence on subsequent analysis (Table 2). Additionally, the high-quality sequences were compared with the virus database to quickly obtain the virus composition information in the sample and a total of 2,172 virus reads were found (Supplementary Table S1). The virus classification information was statistically analyzed based on the annotation information of the NCBI taxonomy database. Statistical analysis indicated that *Phages* was the most abundant virus, accounting for approximately 62.94% of the total number of viruses (Supplementary Table S2). Meanwhile, the proportion of DNA and RNA viruses were 69.75% and 30.25%, respectively (Supplementary Table S3). The top 11 preeminent families in the collected samples at the family level are shown in Figure 1A. At the family level, *Arenaviridae*, *Ackermannviridae* and *Siphoviridae* were the three most predominant families, whereas *Inoviridae*, *Myoviridae*, *Podoviridae*, *Herpesviridae*, *Retroviridae*, *Togaviridae*, *Baculoviridae* and *Nairoviridae* were represented with a lower abundance. At the level of genus, *Mammarenavirus*, *Limestonevirus* and *Lambdavirus* were observed as the predominant. Furthermore, other genera including *unclassified_Inoviridae*, *unclassified_Myoviridae*, *unclassified_Podoviridae*, *Muromegalovirus*, *Gammaretrovirus*, *Alphavirus*, *Alphabaculovirus* and *Orthonairovirus* were indicated with a lower abundance (Figure 1B).

Virus sequence identification

After removing the host sequence, 10600 contigs were totally obtained (Table 3) and the length distribution of contigs was displayed in Figure 1C. The obtained contigs were compared with the virus database. After comparison and screening, a total of 25 confirmed viral sequences and 520 suspected viral sequences were found (Table 4). Meanwhile, the percentage of DNA and RNA viral sequences in the total number of confirmed sequences were 56% and 44%, respectively (Supplementary Table S4). On the other hand, the DNA and RNA viral sequences accounted for 46.73% and 53.27% of the total suspected sequences, respectively (Supplementary Table S4). Moreover, the ratio of *Phages* in the confirmed and suspected viruses were 56.00% and 46.73%, respectively (Table 5). However, the identified sequence based on the comparison of the virus database existed some defects, because this method can only identify known viruses and the results may be false positives. Therefore, the variety of databases were increased to further identify viral sequences. Eventually, a total of 42 new viral sequences were identified (Figure 1D). Additionally, *Myoviridae* and *Herpesviridae* possessed the highest contig number at the family level (Figure 2A). The results of virus abundance statistics indicated that Nimaviridae and Whispovirus possessed the highest RPKM values at the family and genus levels, respectively (Figures 2B,C).

Gene prediction and functional analysis

The contigs of virus were genetically predicted using MetaGeneMark (v3.38) software and the sequences of the gene nucleic acid <150 bp was filtered. The results revealed that a total of 52 genes were predicted (Table 6). The protein sequences of genes were compared with the virus sequence of UniProtKB/Swiss-Prot database by using blastp (v2.9.0+)

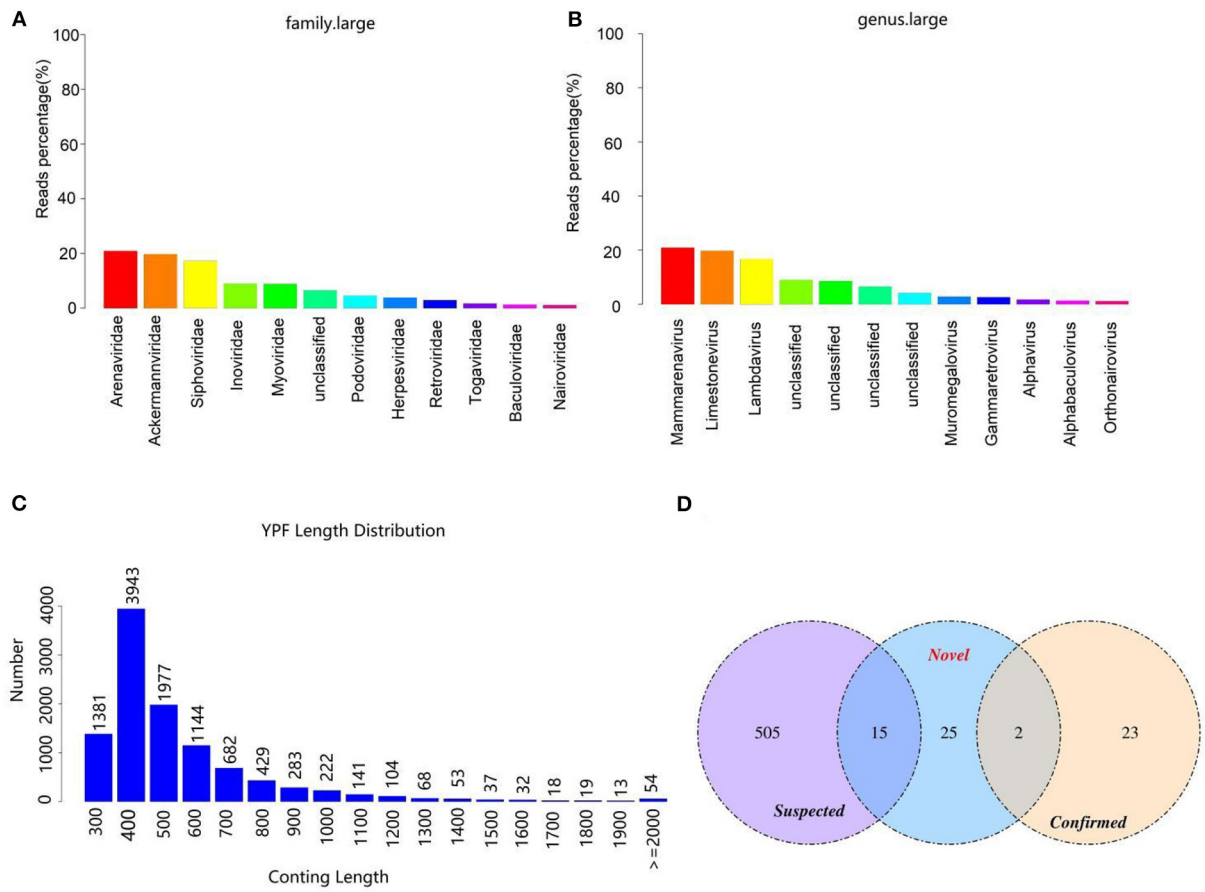

FIGURE 1
Viral composition and the length distribution of contigs. **(A)** The relative abundance of viral composition at the level of family. **(B)** The relative abundance of viral composition at the level of genus. **(C)** The length distribution of contigs. The abscissa represents the length of contigs and the ordinate indicates the number of contigs. **(D)** Comparison of the number of viruses contigs obtained by different methods.

TABLE 3 The information of the obtained contigs.

Sample	Total_base(Mb)	Total_num	Max_len	Min_len	N50	GC (%)
YFP	6.27	10,600	5,879	301	577	50.47

Total_num the number of contigs. Max_lenthe: maximum length of contig; Min_len: the minimum length of contig.

TABLE 4 Statistical analysis of the viral sequence.

Type	Total_base(Mb)	Total_num	Max_len	Min_len	N50	GC (%)
Virus.confirmed	0.03	25	3,963	536	1,253	52.07
Virus.suspected	0.03	520	3,031	355	624	49.61

Total_num: total number; Max_len: maximum length; Min_len: minimum length.

to obtain the functional information of the virus. The results indicated that these genes were closely related to biological process, cellular component, molecular function and disease (Figure 2D).

Discussion

Viral diseases are one of the greatest health challenges in the contemporary world, posing a huge threat to animal

and public health (18, 19). Multiple factors regarding the viral emergence e.g., the climate, population growth, changing diets, human activity and environmental pollution have been demonstrated (20). These factors affect the spread of viruses in humans and animals and may accelerate the emergence of viral epidemics. Consequently, an in-depth investigation of viral diversity is essential to have a base line for the prevention and development of drug strategies against these diseases. Traditional identification methods have certain restrictions mostly based on the lack of corresponding cell lines, antibodies, gene sequences and biosafety facilities (21–24). Metagenomics provide a modern alternative in identifying and discovering novel and existing

TABLE 5 Statistical analysis of viral types in the confirmed and suspected virus.

Type	Total	Phages (%)	Other_virus (%)
Virus.confirmed	25	14 (56.00%)	11 (44.00%)
Virus.suspected	520	243 (46.73%)	277 (53.27%)

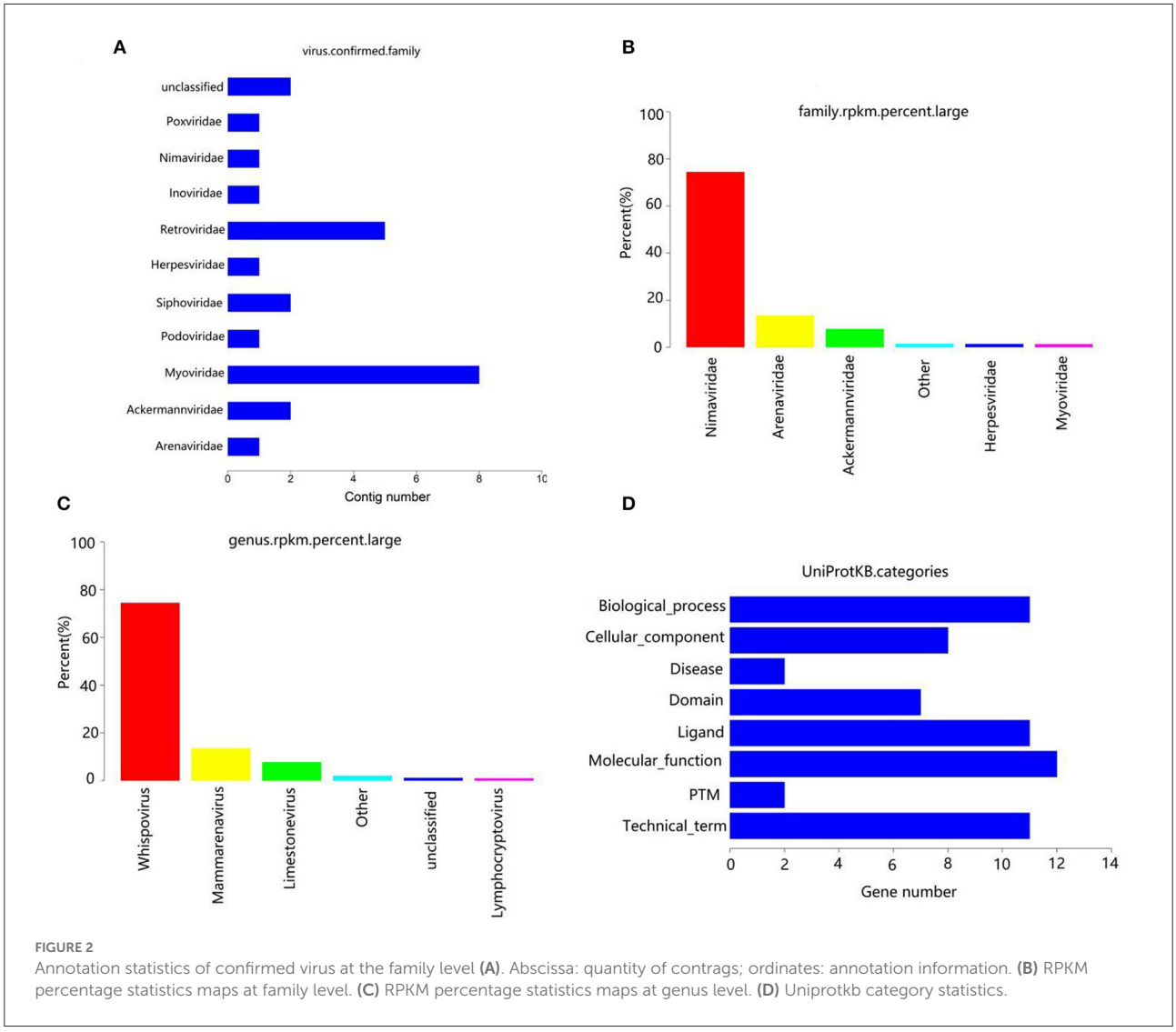

FIGURE 2
Annotation statistics of confirmed virus at the family level **(A)**. Abscissa: quantity of contrags; ordinates: annotation information. **(B)** RPKM percentage statistics maps at family level. **(C)** RPKM percentage statistics maps at genus level. **(D)** Uniprotkb category statistics.

TABLE 6 Statistical analysis of gene prediction results.

Sample	Total_base (Mb)	Total_num	Max_len	Min_len	N50	GC (%)
Viral.contig.gene_nucl	0.03	52	1,275	162	555	48.46

Total_num: total number; Max_len: maximum length; Min_len: minimum length.

microorganisms especially in the samples which was not possible to analyze previously (25). Despite, non-human and environmental samples would need further confirmation and databases (26, 27). Theoretically, metagenomics techniques can perform the genomic characterization and identification of most microorganisms contained in the samples with a generic lab procedure (28). With the popularization and application of metagenomics, the new viruses in mammals have been observed gradually (29, 30).

Bacteriophages are potentially the largest source of gene diversity and are the most abundant biological entities in the ecosphere as well as marine environment (25, 31, 32). Previous research has indicated that temperate phages remain in the host in a latent state, whereas pathogenic phages can infect the bacterium of host and exit the cell by lysis or budding (33). Our results revealed a high abundance of phages in the Yangtze finless porpoise, which was consistent with the previous findings in other animals (34). This may be due to phages which are normally present in higher abundance in marine waters (35). Herpes virus is a DNA virus with envelope and can be divided into four subfamilies (36). Previous studies revealed that herpes virus can infect multiple livestock, poultry and fish and damage their skin, mucosa and nervous tissue (37, 38). Notably, cyprinids are the most susceptible to the herpes virus among aquatic animals. Previous research demonstrated that cyprinids were one of the main foods for the Yangtze finless porpoise (39–43). Moreover, Pei et al. also found herpes virus in the liver of dead Yangtze finless porpoise, which was consistent with our results (44). Therefore, further research is needed to determine whether the Yangtze finless porpoise can infect the herpes virus through the food chain.

The *Poxviridae* is a type of DNA virus with the largest virions generally brick-shaped or elliptic (45). The *Poxviridae* composed of *Orthpoxvirus*, *Parapoxvirus* and *Vaccinia* (46). Previous research revealed that members of the family *Poxviridae* posed a serious threat to the health of pig, poultry, rabbit and ruminant and resulted in skin damage (47). Furthermore, *Poxvirus* can also infect marine mammals such as whales, dolphins, seals, causing ring-shaped, pinhole or tattoo-like skin injury (48).

Retroviruses are spherical RNA viruses with envelopes, including *Tumorigenic virus*, *Lenti virus* and *Foamy virus* (49). Although most members of the *Retroviridae* cannot directly result in diseases, they could induce cancer growth (50, 51). It was reported that *Retroviruses* mainly infect humans and can be transmitted through contaminated water (52). Currently, the water quality of the Yangtze River has seriously degraded due to the discharge of domestic sewage, industrial and agricultural waste (53, 54). However, whether *Retrovirus* could infect Yangtze finless porpoise through polluted water sources remains to be studied.

Early studies indicated that the members of the *Arenaviridae* can cause hemorrhage, meningoencephalitis, hemorrhagic fever and neurological diseases in animal and humans (55, 56). It is still unclear whether members of the family *Arenaviridae* can result in the diseases of Yangtze finless porpoise. *Alphavirus* consists of 27 viruses, all of which are transmitted by vector insects including mosquito, louse, bug and mite (57, 58). The most members of *Alphavirus* can naturally infect birds and rodents (59). Moreover, there have been reports of *Alphavirus* isolated from amphibians and reptiles (60, 61). *Alphavirus* can cause fever, rash, arthralgia and other symptoms in humans and animals and can even lead to death in severe cases (62, 63). Notably, *Alphavirus* was also found in the Yangtze finless porpoise through viral metagenome.

In summary, this study first revealed the viral diversity of the Yangtze finless porpoise by metagenomics. Results indicated that there were many viruses in the Yangtze finless porpoise, such as *Arenaviridae*, *Ackermannviridae* and *Siphoviridae*. Moreover, most of the viruses were reported for the first time in the Yangtze finless porpoise. However, the viral diversity can be influenced by multiple external and internal factors, such as individual biological difference, virus degradation. Considering the restriction of a small number of samples and experiment conditions, we cannot completely remove all the above-mentioned influencing factors. However, our research first attempted to reveal the viral diversity of the Yangtze finless porpoise and supplemented the gap in its virus information. Additionally, our study may provide a theoretical basis for further research on the pathogenic mechanism and prevention and treatment of viral diseases to understand the natural flora in these animals by the use of advanced techniques to know the basis and the possibility of diagnosis and therapy of infectious diseases in these animals.

Data availability statement

The original contributions presented in the study are included in the article/Supplementary material, further inquiries can be directed to the corresponding author/s.

Ethics statement

The animal study was reviewed and approved by Ethics Committee of the Anqing Normal University.

Author contributions

ZL conceived and designed the experiment data curation. ZL and KL contributed sample collection and reagents preparation. MH, FA, ZL, XD, HY, XC, ST, YZ, WL, BD, AZ, JZ, ZQ, HA, and DY revised the manuscript. All the authors reviewed the manuscript. All authors contributed to the article and approved the submitted version.

Funding

This work was supported by the Hubei Yangtze River Ecological Protection Foundation-Dolphin-Vietnam Project, Anqing Normal University High-level Talent Introduction Program (2021), Aquatic Organism Protection and Water Ecological Restoration Project for External Development of Engineering Technology Research Center of Anhui Province Colleges and Universities (2021), and the key project of the Natural Science Foundation of Universities in Anhui Province (KJ2019A0551).

Conflict of interest

The authors declare that the research was conducted in the absence of any commercial or financial relationships that could be construed as a potential conflict of interest.

Publisher's note

All claims expressed in this article are solely those of the authors and do not necessarily represent those of their affiliated organizations, or those of the publisher, the editors and the reviewers. Any product that may be evaluated in this article, or claim that may be made by its manufacturer, is not guaranteed or endorsed by the publisher.

Supplementary material

The Supplementary Material for this article can be found online at: https://www.frontiersin.org/articles/10.3389/fvets.2022.922623/full#supplementary-material

References

1. Liu Z, Li A, Wang Y, Iqbal M, Zheng A, Zhao M, et al. Comparative analysis of microbial community structure between healthy and Aeromonas veronii-infected Yangtze finless porpoise. *Microb Cell Fact.* (2020) 19:123. doi: 10.1186/s12934-020-01383-4

2. Liu ZG, Zheng AF, Chen MM, Lian YX, Zhang XK, Zhang SZ, et al. Isolation and identification of pathogenic Aeromonas veronii from a dead Yangtze finless porpoise. *Dis Aquat Organ.* (2018) 132:13–22. doi: 10.3354/dao03288

3. Wang K, Wang D, Zhang X, Pfluger A, Barrett L. Range-wide Yangtze freshwater dolphin expedition: The last chance to see Baiji? *Environ Sci Pollut Res Int.* (2006) 13:418–24. doi: 10.1065/espr2006.10.350

4. Brussow H, Hendrix RW. Phage genomics: small is beautiful. *Cell.* (2002) 108:13–6. doi: 10.1016/S0092-8674(01)00637-7

5. Angly FE, Felts B, Breitbart M, Salamon P, Edwards RA, Carlson C, et al. The marine viromes of four oceanic regions. *Plos Biol.* (2006) 4:e368. doi: 10.1371/journal.pbio.0040368

6. He B, Li Z, Yang F, Zheng J, Feng Y, Guo H, et al. Virome profiling of bats from Myanmar by metagenomic analysis of tissue samples reveals more novel Mammalian viruses. *PLoS ONE.* (2013) 8:e61950. doi: 10.1371/journal.pone.0061950

7. Yang L, Zhu W, Li X, Bo H, Zhang Y, Zou S, et al. Genesis and dissemination of highly pathogenic H5N6 avian influenza viruses. *J Virol.* (2017) 91:e02199. doi: 10.1128/JVI.02199-16

8. Guo Y, Liu H, Wang Q, Yi S, Niu J, Li D, et al. assessment of the protective efficacy of a feline calicivirus inactivated vaccine using *in vivo* FCV CH-JL2 infection. *Pak Vet J.* (in press). doi: 10.29261/pakvetj/2022.030

9. Paez-Espino D, Eloe-Fadrosh EA, Pavlopoulos GA, Thomas AD, Huntemann M, Mikhailova N, et al. Uncovering earth's virome. *Nature.* (2016) 536:425–30. doi: 10.1038/nature19094

10. Zaheer I, Saleemi MK, Javed MT, Sajjad-ur-Rahman, Abubakar M. Clinical investigation and molecular prevalence of Fowl adenoviruses of commercial poultry from division Faisalabad, Pakistan. *Pak Vet J.* (2022). doi: 10.29261/pakvetj/2022.056

11. Edridge A, Deijs M, van Zeggeren IE, Kinsella CM, Jebbink MF, Bakker M, et al. Viral Metagenomics on Cerebrospinal Fluid. *Genes (Basel).* (2019) 10:e50332. doi: 10.3390/genes10050332

12. Tang P, Chiu C. Metagenomics for the discovery of novel human viruses. *Future Microbiol.* (2010) 5:177–89. doi: 10.2217/fmb.09.120

13. Day JM, Ballard LL, Duke MV, Scheffler BE, Zsak L. Metagenomic analysis of the turkey gut RNA virus community. *Virol J.* (2010) 7:313. doi: 10.1186/1743-422X-7-313

14. Shan T, Li L, Simmonds P, Wang C, Moeser A, Delwart E. The fecal virome of pigs on a high-density farm. *J Virol.* (2011) 85:11697–708. doi: 10.1128/JVI.05217-11

15. Chen GQ, Zhuang QY, Wang KC, Liu S, Shao JZ, Jiang WM, et al. Identification and survey of a novel avian coronavirus in ducks. *PLoS ONE.* (2013) 8:e72918. doi: 10.1371/journal.pone.0072918

16. Phan TG, Vo NP, Boros A, Pankovics P, Reuter G, Li OT, et al. The viruses of wild pigeon droppings. *PLoS ONE.* (2013) 8:e72787. doi: 10.1371/journal.pone.0072787

17. Li L, Victoria JG, Wang C, Jones M, Fellers GM, Kunz TH, et al. Bat guano virome: predominance of dietary viruses from insects and plants plus novel mammalian viruses. *J Virol.* (2010) 84:6955–65. doi: 10.1128/JVI.00501-10

18. Grubaugh ND, Ladner JT, Lemey P, Pybus OG, Rambaut A, Holmes EC, et al. Tracking virus outbreaks in the twenty-first century. *Vat Microbiol.* (2019) 4:10–19. doi: 10.1038/s41564-018-0296-2

19. Hafez H M. Avian adenoviruses infections with special attention to inclusion body hepatitis/hydropericardium syndrome and egg drop syndrome. *Pak Vet J.* (2021) 31:85–92. Available online at: http://www.pvj.com.pk/abstract/31_2/10-110.htm

20. Wolfe ND, Dunavan CP, Diamond J. Origins of major human infectious diseases. *Nature.* (2007) 447:279–83. doi: 10.1038/nature05775

21. Nooij S, Schmitz D, Vennema H, Kroneman A, Koopmans M. Overview of virus metagenomic classification methods and their biological applications. *Front Microbiol.* (2018) 9:749. doi: 10.3389/fmicb.2018.00749

22. Hayes S, Mahony J, Nauta A, van Sinderen D. Metagenomic approaches to assess bacteriophages in various environmental niches. *Viruses.* (2017) 9:e60127. doi: 10.3390/v9060127

23. Yozwiak NL, Skewes-Cox P, Stenglein MD, Balmaseda A, Harris E, DeRisi JL. Virus identification in unknown tropical febrile illness cases using deep sequencing. *PLoS Negl Trop Dis.* (2012) 6:e1485. doi: 10.1371/journal.pntd.0001485

24. Su W, Li Z, He Y, Yan X, Wang L, Peng D. Isolation and identification of a raccoon dog parvovirus and sequence analysis of its VP2 gene. *Pak Vet J.* (2021). doi: 10.29261/pakvetj/2022.027

25. Breitbart M, Salamon P, Andresen B, et al. Genomic analysis of uncultured marine viral communities. *Proc Natl Acad Sci USA.* (2002) 99:14250–5. doi: 10.1073/pnas.202488399

26. Culligan EP, Sleator RD, Marchesi JR, Hill C. Metagenomics and novel gene discovery: promise and potential for novel therapeutics. *Virulence.* (2014) 5:399–412. doi: 10.4161/viru.27208

27. Pallen MJ. Diagnostic metagenomics: potential applications to bacterial, viral and parasitic infections. *Parasitology.* (2014) 141:1856–62. doi: 10.1017/S0031182014000134

28. Wooley JC, Ye Y. Metagenomics: facts and artifacts, and computational challenges*. *J Comput Sci Technol.* (2009) 25:71–81. doi: 10.1007/s11390-010-9306-4

29. Shkoporov AN, Hill C. Bacteriophages of the human gut: the "known unknown" of the microbiome. *Cell Host Microbe.* (2019) 25:195–209. doi: 10.1016/j.chom.2019.01.017

30. Fawaz M, Vijayakumar P, Mishra A, Gandhale PN, Dutta R, Kamble NM, et al. Duck gut viral metagenome analysis captures snapshot of viral diversity. *Gut Pathog.* (2016) 8:30. doi: 10.1186/s13099-016-0113-5

31. Brussow H, Canchaya C, Hardt WD. Phages and the evolution of bacterial pathogens: from genomic rearrangements to lysogenic conversion. *Microbiol Mol Biol Rev.* (2004) 68:560–602. doi: 10.1128/MMBR.68.3.560-602.2004

32. Chibani-Chennoufi S, Bruttin A, Dillmann ML, Brussow H. Phage-host interaction: an ecological perspective. *J Bacteriol.* (2004) 186:3677–86. doi: 10.1128/JB.186.12.3677-3686.2004

33. Lima-Mendez G, Van Helden J, Toussaint A, Leplae R. Reticulate representation of evolutionary and functional relationships between phage genomes. *Mol Biol Evol.* (2008) 25:762–77. doi: 10.1093/molbev/msn023

34. Holmfeldt K, Solonenko N, Shah M, Corrier K, Riemann L, Verberkmoes NC, et al. Twelve previously unknown phage genera are ubiquitous in global oceans. *Proc Natl Acad Sci USA.* (2013) 110:12798–803. doi: 10.1073/pnas.1305956110

35. Bergh B, Rsheim K, Bratbak G, Heldal M. High abundance of viruses found in aquatic environments. *Nature.* (1989) 340:467–46 doi: 10.1038/340467a0

36. Lombardi L, Falanga A, Del GV, Palomba L, Galdiero M, Franci G, et al. A boost to the antiviral activity: Cholesterol tagged peptides derived from glycoprotein B of Herpes Simplex virus type I. *Int J Biol Macromol.* (2020) 162:882–93. doi: 10.1016/j.ijbiomac.2020.06.134

37. Di Lernia V, Mansouri Y. Epstein-Barr virus and skin manifestations in childhood. *Int J Dermatol.* (2013) 52:1177–84. doi: 10.1111/j.1365-4632.2012.05855.x

38. Lin GL, McGinley JP, Drysdale SB, Pollard AJ. Epidemiology and immune pathogenesis of viral sepsis. *Front Immunol.* (2018) 9:2147. doi: 10.3389/fimmu.2018.02147

39. Boutier M, Ronsmans M, Rakus K, Jazowiecka-Rakus J, Vancsok C, Morvan L, et al. Cyprinid herpesvirus 3: an archetype of fish alloherpesviruses. *Adv Virus Res.* (2015) 93:161–256. doi: 10.1016/bs.aivir.2015.03.001

40. Aziz S, Abdullah S, Abbas K, Zia MA. Effects of engineered zinc oxide nanoparticles on freshwater fish, Labeo rohita: Characterization of ZnO nanoparticles, acute toxicity and oxidative stress. *Pak Vet J.* (2020) 40:479–83. doi: 10.29261/pakvetj/2020.030

41. Ghaffar A, Hussain R, Noreen S, Abbas G, Chodhary IR, Khan A, et al. Dose and time-related pathological and genotoxic studies on thiamethoxam in fresh water fish (Labeo rohita) in Pakistan. *Pak Vet J.* (2020) 40(2):151–6. doi: 10.29261/pakvetj/2020.002

42. Aziz S, Abdullah S, Anwar H, Latif F, Mustfa W. Effect of engineered nickel oxide nanoparticles on antioxidant enzymes in fresh water fish, Labeo rohita. *Pak Vet J.* (2021) 41:424–8. doi: 10.29261/pakvetj/2021.044

43. Nabi G, Hao Y, Zeng X, Wang D. Assessment of yangtze finless porpoises (neophocaena asiaorientalis) through biochemical and hematological parameters. *Zool Stud.* (2017) 56:e31. doi: 10.6620/ZS.2017.56-31

44. Pei C, Lei XY, Yuan XP, Wang D, Zhao QZ, Zhang QY. Herpes-like virus infection in Yangtze finless porpoise (Neophocaena phocaenoides): pathology, ultrastructure and molecular analysis. *J Wildl Dis.* (2012) 48:235–7. doi: 10.7589/0090-3558-48.1.235

45. Tuazon KM, Ng E, Al RZ, Pandey P, Ruuls SR, Korner H, et al. TNF deficiency dysregulates inflammatory cytokine production, leading to lung pathology and death during respiratory poxvirus infection. *Proc Natl Acad Sci USA.* (2020) 117:15935–46. doi: 10.1073/pnas.2004615117

46. Fleming SB, Wise LM, Mercer AA. Molecular genetic analysis of orf virus: a poxvirus that has adapted to skin. *Viruses.* (2015) 7:1505–39. doi: 10.3390/v7031505

47. McFadden G. Poxvirus tropism. *Nat Rev Microbiol.* (2005) 3:201–13. doi: 10.1038/nrmicro1099

48. Barnett J, Dastjerdi A, Davison N, Deaville R, Everest D, Peake J, et al. Identification of novel cetacean poxviruses in cetaceans stranded in South West England. *PLoS ONE.* (2015) 10:e0124315. doi: 10.1371/journal.pone.0124315

49. Garcia-Montojo M, Doucet-O'Hare T, Henderson L, Nath A. Human endogenous retrovirus-K (HML-2): a comprehensive review. *Crit Rev Microbiol.* (2018) 44:715–38. doi: 10.1080/1040841X.2018.1501345

50. Premeaux TA, Javandel S, Hosaka K, Greene M, Therrien N, Allen IE, et al. Associations between plasma immunomodulatory and inflammatory mediators with VACS index scores among older HIV-infected adults on antiretroviral therapy. *Front Immunol.* (2020) 11:1321. doi: 10.3389/fimmu.2020.01321

51. Beghin JC, Ruelle J, Goubau P, Van der Linden D. Drug resistance in HIV-infected children living in rural South Africa: Implications of an antiretroviral therapy initiated during the first year of life. *J Clin Virol.* (2020) 129:104547. doi: 10.1016/j.jcv.2020.104547

52. Knight A, Haines J, Stals A, Li D, Uyttendaele M, Knight A, et al. A systematic review of human norovirus survival reveals a greater persistence of human norovirus RT-qPCR signals compared to those of cultivable surrogate viruses. *Int J Food Microbiol.* (2016) 216:40–9. doi: 10.1016/j.ijfoodmicro.2015.08.015

53. Zhang J, Liu L, Zhao Y, Li H, Lian Y, Zhang Z, et al. Development of a high-resolution emission inventory of agricultural machinery with a novel methodology: A case study for Yangtze River Delta region. *Environ Pollut.* (2020) 266:115075. doi: 10.1016/j.envpol.2020.115075

54. Sun J, Jin L, He T, Wei Z, Liu X, Zhu L, et al. Antibiotic resistance genes (ARGs) in agricultural soils from the Yangtze River Delta, China. *Sci Total Environ.* (2020) 740:140001. doi: 10.1016/j.scitotenv.2020.140001

55. Baral P, Pavadai E, Gerstman BS, Chapagain PP. In-silico identification of the vaccine candidate epitopes against the Lassa virus hemorrhagic fever. *Sci Rep.* (2020) 10:7667. doi: 10.1038/s41598-020-63640-1

56. Sudhakar H, Bhate J, Patra AK. Patent landscape of novel technologies for combating category-A Arenavirus infections. *Expert Opin Ther Pat.* (2020) 30:557–65. doi: 10.1080/13543776.2020.1755255

57. Filomatori CV, Merwaiss F, Bardossy ES, Alvarez DE. Impact of alphavirus 3'UTR plasticity on mosquito transmission. *Semin Cell Dev Biol.* (2020) 111:148–55. doi: 10.1016/j.semcdb.2020.07.006

58. Michie A, Ernst T, Chua IJ, Lindsay M, Neville PJ, Nicholson J, et al. Phylogenetic and timescale analysis of Barmah forest virus as inferred from genome sequence analysis. *Viruses.* (2020) 12:E70732. doi: 10.3390/v12070732

59. Nguyen W, Nakayama E, Yan K, Tang B, Le TT, Liu L, et al. Arthritogenic alphavirus vaccines: serogrouping versus cross-protection in mouse models. *Vaccines (Basel).* (2020) 8:e20209. doi: 10.3390/vaccines8020209

60. Aslam ML, Robledo D, Krasnov A, Moghadam HK, Hillestad B, Houston RD, et al. Quantitative trait loci and genes associated with salmonid alphavirus load in Atlantic salmon: implications for pancreas disease resistance and tolerance. *Sci Rep.* (2020) 10:10393. doi: 10.1038/s41598-020-67405-8

61. Jansen MD, Guarracino M, Carson M, Modahl I, Taksdal T, Sindre H, et al. Field evaluation of diagnostic test sensitivity and specificity for salmonid alphavirus (SAV) infection and pancreas disease (PD) in farmed atlantic salmon (Salmo salar L.) in Norway using Bayesian latent class analysis. *Front Vet Sci.* (2019) 6:419. doi: 10.3389/fvets.2019.00419

62. Torres-Ruesta A, Teo TH, Chan YH, Renia L, Ng L. Pathogenic Th1 responses in CHIKV-induced inflammation and their modulation upon Plasmodium parasites co-infection. *Immunol Rev.* (2020) 294:80–91. doi: 10.1111/imr.12825

63. Weger-Lucarelli J, Carrau L, Levi LI, Rezelj V, Vallet T, Blanc H, et al. Host nutritional status affects alphavirus virulence, transmission, and evolution. *PLoS Pathog.* (2019) 15:e1008089. doi: 10.1371/journal.ppat.1008089

Frontiers in Veterinary Science

Transforms how we investigate and improve animal health

The third most-cited veterinary science journal, bridging animal and human health with a comparative approach to medical challenges. It explores innovative biotechnology and therapy for improved health outcomes.

Discover the latest Research Topics

See more →

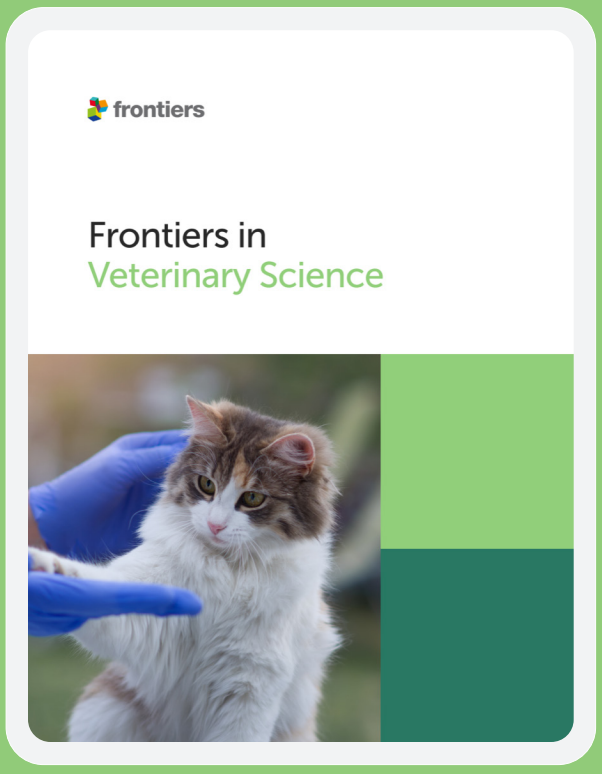

Frontiers

Avenue du Tribunal-Fédéral 34
1005 Lausanne, Switzerland
frontiersin.org

Contact us

+41 (0)21 510 17 00
frontiersin.org/about/contact